Theory and application of optimization strategies for the design of seismically excited structures

HABILITATION

an der Fakultät Bauingenieurwesen

der

BAUHAUS-UNIVERSITÄT WEIMAR

zur Erlangung des akademischen Grades

Doktor-Ingenieur habilitatus (Dr.-Ing. habil.)

vorgelegt von

Dr.-Ing. Rüdiger Weitzmann

aus Erfurt

Weimar 2009

Abstract

The study introduces into the theory and application of optimization strategies in earthquake engineering. The optimization algorithm substitutes the intuitive solution of practical problems done by the engineer in daily practice, providing automatic design tools and numerical means for further exploration of the design space for various extremum states. This requires a mathematical formulation of the design task, that is provided for typical seismic evaluations within this document. Utilizing the natural relation between design and optimization tasks, appropriate mechanical concepts are developed and discussed.

The explanations start with an overview on the mechanical background for continua. Hereby the focus is placed on elasto-plastic structures. The given extremum formulations are treated with help of discretization methods in order to obtain optimization problems. These basics are utilized for derivation of programs for eigenvalue and stability analysis, that are applied in simplified linear analysis for the design of seismically excited structures. Another focus is set on the application in simplified nonlinear design, that uses limit state analyses on the basis of nonlinear problem formulations. Well known concepts as the response and pushover analysis are covered as well as alternative strategies on the basis of shakedown theory or cycle and deformation based evaluations.

Furthermore, the study gives insight into the application of optimization problems in conjunction with nonlinear time history analyses. The solution of step-by-step procedures within optimization algorithms is shown and aspects of dynamic limit state analyses are discussed. For illustration of the great variety of optimization-based concepts in earthquake engineering, several specialized applications are presented, e.g. the generation of artificial ground motions and the determination of reduction coefficients for design spectrum reduction due to viscous and hysteretic damping. As well alternative strategies for the design of base isolated structures with controlled impact are presented. All presented applications are illustrated with help of various examples.

Kurzfassung

Die vorliegende Arbeit führt in die Theorie und Anwendung von Optimiierungsverfahren im Erdbebeningenieurwesen ein. Die vorgestellten Optimierungsalgorithmen ersetzen die typische intuitive Lösung von praktischen Bemessungsaufgaben, mit Bereitstellung von automatischen Methoden und numerischen Mitteln für die Bewertung des Designraumes bezüglich extremer Zustände. Dies erfordert eine geeignete mathematische Formulierung der Bemessungsaufgaben, die für typische Anwendungsfälle bereitgestellt werden. Ausgehend von der engen Beziehung von Bemessungs- und Optimierungsaufgaben werden wesentliche theoretische Grundlagen für die Ableitung praxistauglicher Analysekonzepte entwickelt und diskutiert.

Die Darstellung beginnt mit einem Überblick zum mechanischen Hintergrund. Der Schwerpunkt wird dabei auf die Analyse von elastisch-plastischen Tragwerken gelegt. Die vorgestellten Extremalformulierungen werden mit Methoden der Diskretisierung in Optimierungsprobleme umgeformt. Diese bilden die Grundlage für die Analyse von Eigenwert- und Stabilitätsproblemen im Erdbebeningenierwesen. Weiterhin werden vereinfachte lineare Bemessungsmethoden besprochen. Eine Erweiterung wird duch die Einbeziehung von nichlinearen Aspekten erzielt, die einen wesentlichen Teil der Arbeit ausmachen. Einerseits werden bekannte Konzepte auf der Basis von Antwortspektren und Pushoveranalysen einbezogen, andererseits werden auch alternative Strategien auf der Basis der Einspieltheorie oder zyklen- oder deformationsbasierten Analyse vorgestellt.

Desweiteren werden Anwendungen von Optimierungsverfahren im Zusammenhang mit nichtlinearen Zeitverlaufsmethoden diskutiert. Die Lösung von Zeitverlaufsproblemen in Form von Optimierungsaufgaben wird vorgestellt und Aspekte der Grenzzustandsanalyse für dynamische Probleme behandelt. Die Vielfältigkeit von Optimierungsanwendungen im Erdbebeningenieurwesen wird anhand verschiedener Spezialanwendungen demonstriert wie z.B. die Generierung von künstlichen Erdbebenzeitverläufen und die Modifikation von Bemessungsspektren für die Analyse von nichtlinear beanspruchten Tragwerken mit viskoser und hysteretischer Dämpfung. Darüberhinaus wird eine alternative Methode für die Bemessung von basisisolierten Tragwerken unter Verwendung von kontrollierten Kollisionen vorgestellt. Alle Anwendungen werden in zahlreichen Beispielen näher erläutert.

Contents

1 Introduction **9**
- 1.1 Background 9
- 1.2 Scope 11
- 1.3 Earthquake engineering design strategies 12
- 1.4 Design problem - optimization problem 13
- 1.5 Chapters overview 15

2 Overview optimization problems and formulation strategies **18**
- 2.1 General nonlinear optimization problem 18
- 2.2 Summary of basic relations, conditions and categories 18
- 2.3 Approximation methods 25
- 2.4 Uncertainty and sensitivity of the design 27
- 2.5 Principles for practical derivation of optimization problems in engineering 28
  - 2.5.1 Algorithmic concepts 28
  - 2.5.2 Intuitive derivation of optimization problems 28
  - 2.5.3 Derivation using mechanical principles 31

3 Continuum mechanical background **35**
- 3.1 Hamiltonian principle 35
- 3.2 Quasi-static sub-problems 35
- 3.3 Material point motion 36
- 3.4 Rigid body motion 38
- 3.5 Deformable body motion (line segment example) 38
- 3.6 Deformation gradient (3D-continua) 43
- 3.7 Tensor strain measures 44
- 3.8 Kinematic condition 49
- 3.9 Material law 49
- 3.10 Stresses and Equilibrium 51
- 3.11 Static and geometric boundary conditions 54
- 3.12 Static forces, inertia and damping 54

4 Discrete systems and matrix formulations **56**
- 4.1 Discretization 56
- 4.2 Geometry 56
- 4.3 Displacements 58
- 4.4 Geometric boundary conditions 59
- 4.5 Total strain/displacement relationship 60
- 4.6 Handling of strain components and increments 63
- 4.7 Stresses and internal forces 64
- 4.8 Material law 68
  - 4.8.1 Linear elastic material law 68
  - 4.8.2 Linear plasticity condition 71
  - 4.8.3 von Mises yield criterion 72
  - 4.8.4 Drucker-Prager yield criterion 74
- 4.9 Static boundary conditions 75
- 4.10 Equilibrium condition 76
- 4.11 Forces 78
- 4.12 Geometric nonlinear numerics for material point 78

4.13 Physical nonlinear numerics at material points (elasto-plastic systems) 80
4.14 Gaussian volume integration 82
4.15 Element matrices and vectors 84
4.16 Cross-sectional models for longitudinal force and bending moment problems 88
4.16.1 Separation of the volume integration 88
4.16.2 Direct integration of homogeneous cross sections 90
4.16.3 Polygonally bounded cross sections 92
4.16.4 Layer and fiber models 94
4.16.5 Composite cross sections 95
4.16.6 Segment models 96
4.16.7 Matrix notation for cross section problems 97
4.17 System matrices and vectors of general composite structures 99
4.18 Time integration 102
4.19 Calculation strategies 102

5 Modal and stability analysis 105
5.1 Eigenvalue problems 105
5.2 Special eigenvalue problems 106
5.3 Modal decomposition of undamped systems 108
5.4 Simplified modal decomposition of damped systems 109
5.5 Modal decomposition of damped systems 110
5.6 Solution by optimization strategies 112
5.7 Example dynamic eigenvalue analysis 112
5.8 Classical stability (statics) 113
5.9 Dynamic stability 116
5.9.1 Lyapunov exponent 116
5.10 Simplified stability estimation 117
5.10.1 Method description 117
5.10.2 Example simplified stability analysis 117

6 Simplified linear analysis 122
6.1 Linear response spectrum analysis 122
6.2 Example: Optimization of a tuned mass damper 126
6.3 Example: Retrofitting a frame structure using linear response spectrum analysis 126
6.4 Reduction coefficient/seismic coefficients for inelastic analysis 128
6.5 Example: Reduction coefficient design of a core structure 129
6.6 Equivalent linearization for fixed-base structures 133
6.7 Example: Design of MDOF system as an equivalent linear system 136
6.8 Conventional simplified base-isolation design 136
6.9 Examples: Conventional base isolation design 141
6.10 Improved simplified base-isolation design 144
6.11 Examples: Improved base isolation design 146

7 Simplified nonlinear analysis 148
7.1 Physical nonlinear limit states 148
7.2 Elastic limit state 149
7.2.1 Poisson principle 150
7.2.2 Castigliano principle 151
7.2.3 Lagrange principle 152
7.2.4 Elastic limit load and resistance calculation using mathematical optimization 153
7.2.5 Example: Calculation of elastic limit resistance 158
7.3 Plastic limit state 160
7.3.1 Core principles for elasto-plastic materials 160
7.3.2 Static, kinematic and uniqueness theorem of the plastic limit state for rigid plastic bodies 161

7.3.3 Example 1: Plastic limit load for beam structure 168
7.3.4 Example 2a: Plastic limit load for mixed FEM and EFG model 168
7.3.5 Example 2b: Coupled shear wall system 172
7.4 Shakedown limit state analysis 175
7.4.1 Background 175
7.4.2 Shakedown theorems 177
7.4.3 Load or resistance bounds for the shakedown state of elasto-plastic structures 181
7.4.4 Example shakedown resistance bounds 182
7.4.5 Dissipative energy bounds for the shakedown state of elasto-plastic structures 185
7.4.6 Example dissipative energy bounds 191
7.4.7 Displacement bounds on shakedown state of elasto-plastic structures 191
7.4.8 Example displacement bounds 195
7.4.9 Residual stress bounds on shakedown state of elasto-plastic structures 196
7.4.10 Example residual stress bounds 196
7.4.11 Hardening materials and geometric nonlinear problems 196
7.4.12 Stress and deformation-based conservative limit states 197
7.4.13 Example conservative limit resistance 198
7.5 Cycle-based limit state analysis 199
7.5.1 Introduction 199
7.5.2 General design approach 201
7.5.3 Design based on the elastic limit state 202
7.5.4 Example: Design based on the elastic limit state 203
7.5.5 Design based on the adaptive limit state 205
7.5.6 Design procedures 206
7.5.7 Example Design based on the adaptive limit state 208
7.6 Deformation based limit states 215
7.6.1 Basic concepts 215
7.6.2 Example Deformation based limit state 216
7.7 Capacity-spectrum-based concepts 216

8 Optimization problems on basis of time history approaches 221
8.1 Time discretization and integration 221
8.2 Variational problem formulation 226
8.2.1 Basic concept 226
8.2.2 Implicit Lagrange principle 226
8.2.3 Implicit Castigliano principle 230
8.2.4 Explicit formulations 230
8.3 Contact Problems 230
8.3.1 Mechanical background 230
8.4 Example time history analysis 233
8.5 Dynamic limit state analysis 236
8.5.1 Summary 236
8.5.2 Example limit state analysis 239

9 Special applications 240
9.1 Generation of artificial time histories 240
9.1.1 Classical generation in frequency domain 240
9.1.2 Example: Time history generation in frequency domain 243
9.1.3 Generation of statistically compatible artificial time histories 245
9.1.4 Example: Generation in frequency domain with statistically compatible phase function 245
9.1.5 Generation in time domain 247
9.1.6 Example: Artificial time history generation in time domain 248
9.1.7 Generation of time history sets 250

9.1.8 Example: Artificial time history set generation 250
9.2 Determination of pseudo spectral reduction coefficients 252
9.3 Design of base-isolated structures for low acceleration transmissions 256
9.3.1 Introduction 256
9.3.2 Mechanical model 258
9.3.3 Simplified pounding model 258
9.3.4 Solution Strategy 260
9.3.5 Optimum design strategies for buildings with potential collision 261
9.3.5.1 Strategy I: Prevention of collision 261
9.3.5.2 Example Strategy I 262
9.3.5.3 Strategy II: Acceptance of collision 264
9.3.5.4 Example Pounding SDOF 269
9.3.5.5 Example Pounding 10-DOF 270
9.4 Graphical design of base isolated structures 274
9.4.1 Introduction 274
9.4.2 Base isolation with hysteretic damping 276
9.4.3 Examples for principle usage of maps 281
9.4.4 Base isolation with viscous damping and other device combinations 285

10 Conclusion 286
10.1 Summary 286
10.2 Future work 287

11 Appendices 288
11.1 Appendix A: 3D-Tensor-Matrix transformation operators 288
11.2 Appendix B: Simplified period dependent reduction coefficient for pseudo-acceleration spectra 290
11.3 Appendix C: Period dependent reduction coefficient for total acceleration spectra 294
11.4 Appendix D: Coefficients for modified equivalent linearization in the long period-high damping range 296
11.5 Appendix E: Galerkin Method for solving Poisson differential equation 298
11.6 Appendix F: Kobe ground motion set 299
11.7 Appendix G: SAC-FEMA project Los Angeles 10in50 ground motion set 300
11.8 Appendix H: Conventional ground motion set 301
11.9 Appendix I: Dissipation energy bounds (strategy Atkociunas/Norkus) 302
11.10 Appendix J: Displacement bounds (strategy Ponter) 303
11.11 Appendix K: Residual displacement bounds (strategy Atkociunas/Norkus) 304
11.12 Appendix L: Example parameter maps (hysteretic damping) 305
11.13 Appendix M: Example parameter maps (viscous damping) 308

12 Notations and lists 311
12.1 Notation and abbreviation 311
12.2 Abbreviations 318
12.3 Notation of optimization problems 318
12.3.1 Notation as formulas 318
12.3.2 Tabular notation 319
12.4 List of figures 320
12.5 List of tables 323

13 References 327

Acknowledgement

Main parts of the studies were done during my research and teaching activities as Scientific Assistant at the Institute of Structural Engineering of the Bauhaus-University Weimar. I got the chance to participate in several research projects sponsored by German Research Association (Deutsche Forschungsgemeinschaft, DFG) mainly related to the Collaborative Research Center 524. Additionally, I worked at the Disaster Prevention Research Institute (DPRI) of the Kyoto University Japan for one year. The projects I participated in were mainly related to base isolation design of seismically excited structures.

For the outstanding support and many valuable discussions I would like to thank especially:

Prof. Dr.-Ing. habil. Erich Raue (former Head of Institute of Structural Engineering at Bauhaus-University Weimar)

Prof. Masayoshi Nakashima (PhD) (DPRI, Kyoto University)

I also like to thank all colleagues at the Institutes in Weimar and Kyoto.

Weimar, April 2008

Figure 1-1 Akashi-Keikyo Bridge, Japan

1 Introduction

1.1 Background

Structural deficiencies in the urban environment can cause tremendous casualties in case of earthquake events. Therefore the focus of science and engineering is to assess expectable loading levels and to provide practical engineering measures for appropriate structural resistance. Because of this outstanding and important task, earthquake engineering became one of the most interesting research and application topics. It considers structures in extreme motion, caused by shock-like excitations.

The proof of earthquake resistance is a frequent part in projects, as a certain seismic hazard is present in almost all regions of the world. However, it is still considered as a task for specialists. This is mostly due to the dynamic excitation and the nonlinear response of structures.

Most aspects of seismic design are similar to common engineering. The protection of life remains always the key objective. A given design problem in earthquake engineering could be described as follows: Determine a configuration of the structure, that guarantees the best performance of the structure due to predefined criteria, as load bearing capacity, durability and serviceability, during and after shock, while fulfilling several boundary conditions, e.g. regarding deformations or damage limitations. The objective is to obtain a minimum of remaining risk, with a maximum of economic efficiency. Simply summarized as finding an optimum.

Figure 1-2 Base isolated high rise building at Tokyo Institute of Technology, Japan

Looking closely at engineering practice, it is obvious, that almost all decisions are made with regard to such optimality criteria. It can be stated that "Design is optimization". However, most optimization is still done by experience and intuition. Therefore, it can be beneficial to support planning processes with appropriate mathematical means - the optimization algorithms. The complexity of engineering problems with all involved influences and their solution can be greatly covered by these procedures. Establishing general analysis strategies on basis of mathematical optimization can help finding optimal solutions and automatize design processes.

1.2 Scope

Especially in earthquake engineering, the application of optimization strategies can be advantageous. Nowadays modern structures are not only expected to ensure life safety, but to behave in a predefined manner. This demands complex mechanical models, to obtain best performance and joint operation of structural elements and materials. The subject combines various aspects of nonlinear dynamics, seismology, nonlinear material sciences and involves even social components. Moreover, with the availability of seismic devices, the scientific background reaches far into mechanical engineering. Using this combined knowledge, enables the engineer to reach far beyond traditional limits in the design of structures, as can be seen in Fig. 1-1 and 1-2). Optimization strategies can support realizing such ambitious projects.

In structural optimization, two main types of optimization problems can be distinguished, the shape and topology optimization. Although both are changing the appearance of structures, the first starts with rather few information about the principle shape of the structure. Hereby, the calculation starts with an simply shaped solution space representing a "full" piece of material, that is typically shaped by removement of material. Contrary to this the second method starts with principle information about the appearance and only selected parameters like dimensions or loadings are design variables. As both types show their own methodological characteristics, this study will focus on the second category. It is very practical, as most of the design tasks in earthquake engineering are based on an advanced design level, developed earlier from other criteria, as e.g. aesthetics or resistance due to static excitations.

This study therefore provides a theoretical background and appropriate practical methods for application in earthquake engineering. It gives an introduction to the methodology of optimization in engineering and explains mathematical and algorithmical aspects for the formulation of optimization problems. It can be shown that most applications can be based on known mechanical principles, that need to be transferred into appropriate extremal formulations. All selected aspects are considered with regard to practical earthquake engineering, illustrated with example applications. As well as common design problems are discussed, some specialized applications have been added for demonstration of the great variability of the method.

The basic design philosophy will consider passive structures that′s behavior is designed once according to optimality criteria. The presented methods apply and extend existing design strategies as the Capacity Design Method [15] and Pushover Analysis. Their principles of local and global design can be perfectly implemented at the structural or member scale, improved by optimizing design concepts. As optimization problems directly relate to design problems, the direct translation of design requirements into optimization formulations can be utilized. Many advantages can be derived from the special interface that is provided by optimization algorithms, for the formulation of objectives, equations and inequalities. All contributes to an effective computationally supported design.

1.3 Earthquake engineering design strategies

Mainly three different strategies can be distinguished in earthquake engineering

- elastic design
- plastic design
- isolation

The first category seems to be uneconomical from the first sight. However the applicability depends on the

- seismic hazard
- importance of the structure
- dynamic properties of the structure

Most of large-span light-weight structures, such as bridges, stadiums and halls can be designed to resist elastically, especially if small or moderate earthquake events can be expected. For such structures, the wind load is typically dominating.

Plastic design is popular because of the economic effects, supported by probabilistic scenarios. The resistance of the structure is extended by provision of plastic deformation capacities, that help dissipating the seismic energy in the structure and alter the response due to eigenfrequency changes. This strategy involves nonlinear calculations and careful dimensioning of plastic hinges and elastically remaining parts, that is adjusted in a Capacity Design [15,152].

However, plastic design tolerates certain damage, typically expressed as cracks, spalling and large deformations, that can result in expensive repair or even in the complete loss of the structure. And, more damage is done, if the operability of the structure and the equipment is restricted, e.g. in buildings of the life line infrastructure or hightec industries.

This background is the task in performance based design, that considers explicitly the after shock performance. Special categories have been proposed, as in Tab. 1-1 or e.g. in [9,56], for pre-selection of an acceptable performance (damage) level during design with respect to operability and repair efforts.

Taking these performance based aspects into account, the insulation strategy can be an interesting alternative to plastic design, illustrated in Fig. 1-3. The structure is mounted, typically at the base, on isolation devices that reduce the amplitude of the shock and/or alter the structural frequency. The involved large deformations are concentrated in the isolation layer. This deformation can be combined with viscous or hysteretic damping devices, with passive, semi-active or active control. These technologies can be beneficially used in near-fault regions too [164].

Figure 1-3 Plastic design vs. isolation

1.4 Design problem - optimization problem

Limit state analyses are of essential interest in engineering. They mark critical conditions in structures or structural members, where the structure changes significant mechanical properties. The quantification is done with help of limit state criteria, that can be modeled mathematically as limit state functions. In structural engineering, limit states functions are derived from the bearing capacity, serviceability or technological requirements with respect to safety demands. In codes, recommendations for the choice and formulation of adequate limit state criteria and analysis conditions are given. In special cases, the analysis can be supported by experimental examinations. However, analytical calculations are preferred, using the comparison of the demand S (loads) and supply R (resistance) in the structure. For safe structures the following inequality must be satisfied

$$S \leq R \tag{1-1}$$

in a unique definition space, where S and R are defined with regard of the structural/ environmental and loading properties as well as safety issues

$$R = R(x, t, \sigma_{lim}, \gamma_R, \ldots) \tag{1-2}$$

$$S = S(x, t, f, \Theta, \gamma_S, \ldots) \tag{1-3}$$

Equation (1-1) is a "proof" type formulation. Moreover, the limit state can be used to derive directly "design" formulations

Table 1-1 Basic performance levels according FEMA 356 and associated analysis concepts

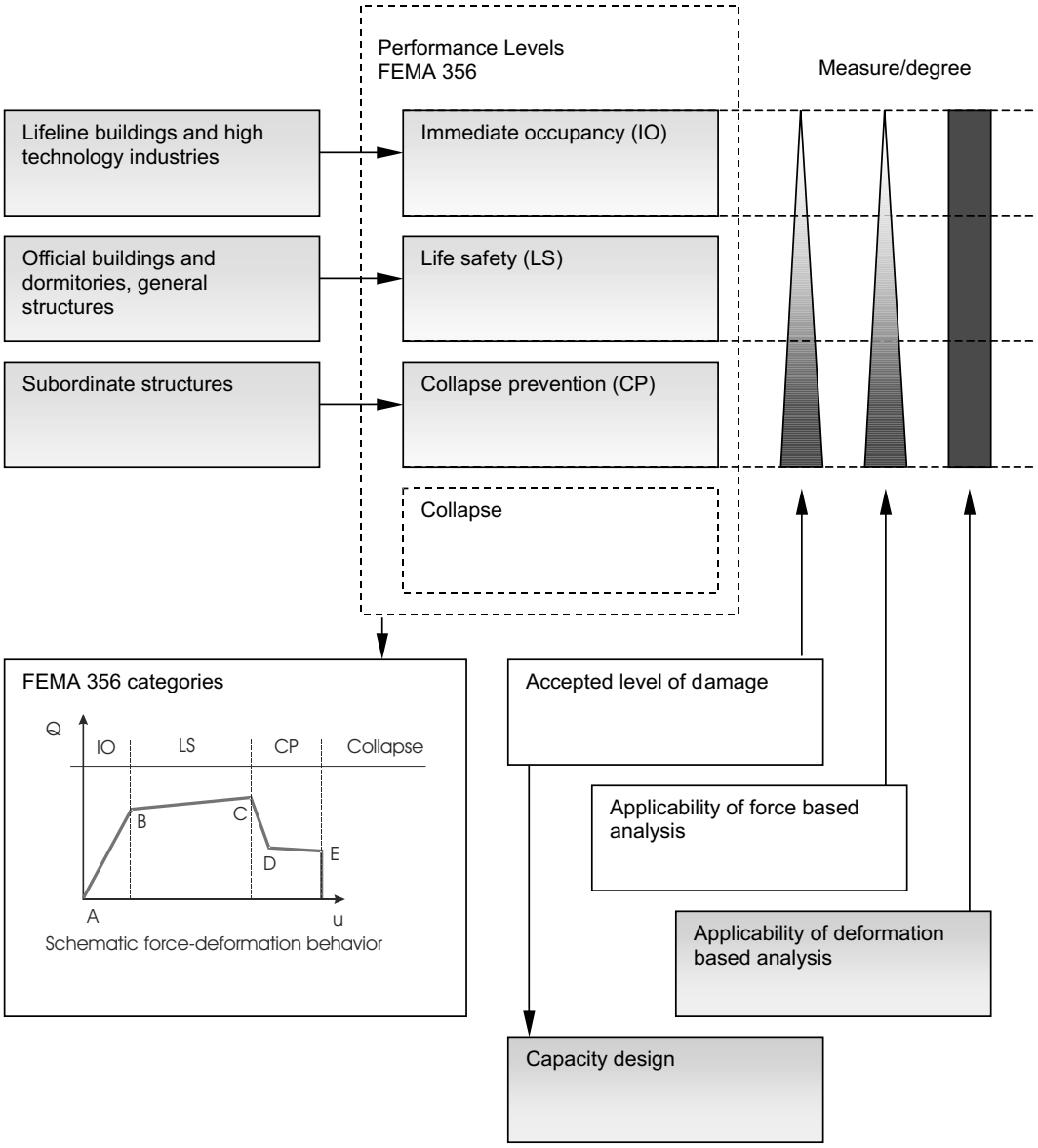

$$S \leq r \cdot R_0 \tag{1-4}$$

that enable the scaling of a predefined basic resistance distribution R_0 with a resistance intensity factor r, or

$$p \cdot S_0 \leq R \tag{1-5}$$

using the reverse methodology, the scaling of a load distribution S_0 with a load intensity factor p.

Economical considerations require the minimum of the structural resistance for a given loading and/or the maximum of the load that can be sustained by a structure, that can be mathematically expressed by

$$r \rightarrow Min \tag{1-6}$$

and

$$p \rightarrow Max \tag{1-7}$$

From a mathematical point of view, the Equations (1-6), (1-2) and (1-4) form an optimization problem, consisting of an objective function and subsidiary conditions. In fact, most engineering design problems can be translated into appropriate optimization problems. This is illustrated in Tab. 1-2. Design problems can be formulated with design parameters. The problem itself is formulated in terms of these parameters, as conditions and restrictions. All design tasks are characterized by the statement of a design objective. With these components, all aspects are given to derive an appropriate optimization problem. The main step is the mathematical description of all conditions and objectives. Some formulations use variational descriptions as they can be directly transformed into optimization problems by application of discretization methods (e.g. Finite element method).

The notation that is used within this study is summarized in Sec. 12.1.

1.5 Chapters overview

Chapter 2 gives an introduction to mathematical optimization. It separates the given strategies of formulation and solution according to several categories often applied in practical engineering. Several solution strategies are shortly noted and described. As well, basic strategies for the derivation and formulation of optimization problems are illustrated.

Chapter 3 provides insight into basic mechanical principles. It uses the Hamiltonian and Poisson principle as the basic variational principles in structural dynamics. Derived from that, general mechanical relations and variational principles for the analysis of rigid and flexible body motions are given for continua.

Directly following the continuum mechanical background, Chapter 4 contains discrete model formulations, that are essential for the application of optimization routines. It con-

Table 1-2 Transformation of a design problem into an optimization problem

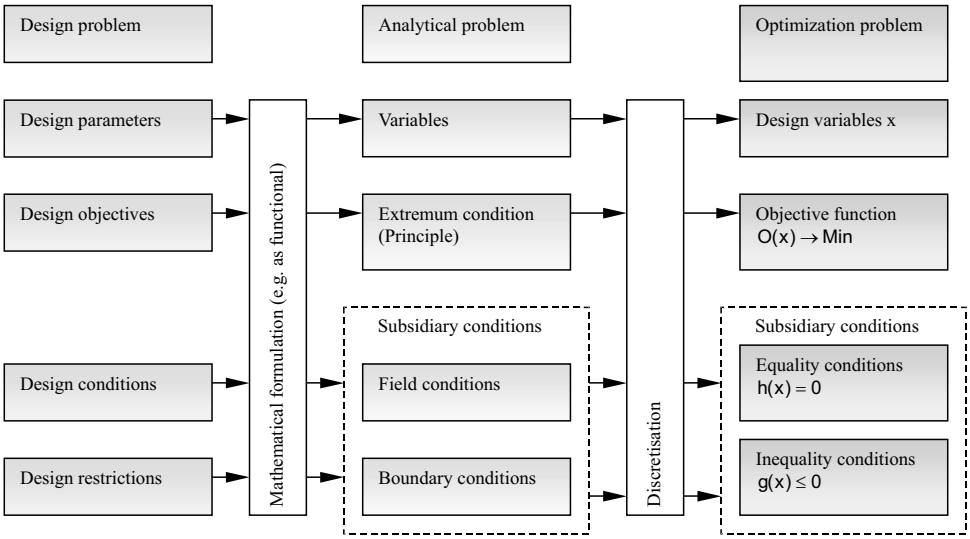

siders the basic mechanical relations for the equation of motion, appropriate kinematics and selected material laws as well as static and geometric boundary conditions. The discretization is done with respect to finite element methods and meshless concepts. The discretization is demonstrated for structural members and cross sectional mechanical models.

Providing basic relations for the modal analysis of seismic exited structures, basic concepts of eigenvalue analysis with help of optimization strategies, for real and complex eigenvalue problems are given in Chapter 5. As well, related problems of structural stability are discussed. Suggestions for practical stability analysis are made.

Chapter 6 relates to the simplified linear analysis concept often applied in practical engineering. It considers several strategies for the formulation of appropriate optimization problems. It provides concepts for the design of conventional and base isolated structures. With help of examples, the given strategies are illustrated.

As one of the most important analysis categories, in Chapter 7 simplified nonlinear analysis methods are discussed. The documentation uses selected limit states for illustration of practical nonlinear design with help of optimization strategies. Beyond classical and advanced principles in limit state analysis, it shows the formulation of known design methods, e.g. the shakedown and capacity spectrum method within optimization tasks. Example applications illustrate the described principles.

As a general analysis concept, the time domain analysis is treated in Chapter 8. The application within optimization strategies is shown, also with help of practical examples. Beyond common time history analysis application in structural optimization, the chapter shows the formulation of dynamic limit state problems.

Finally, Chapter 9 illustrates the huge variety of optimization strategies, practically applicable in earthquake engineering. This chapter provides selected methods for the generation of artificial accelerograms and shows a practical method for the graphical optimization of base isolated structures.

2 Overview optimization problems and formulation strategies

2.1 General nonlinear optimization problem

The most general mathematical description for an optimization problem is given as

$$O_i(x) \rightarrow Min \qquad i = 1 \ldots n_O \tag{2-1}$$

$$G_j(x) \leq 0 \qquad j = 1 \ldots n_G \tag{2-2}$$

with the objective functions $O_i(x)$, requiring their values to become minimum, while respecting the subsidiary conditions $G_j(x)$. Both functions are dependent on the design variables x.

From an early historical development, optimization problems are also called "Programming" problems, as they show abilities of automatic procedures.

In the next sections, the very basics of optimization and several categories of problems and algorithmic solution are shortly acknowledged, without being complete and going into detail. The mentioned algorithms have been selected with respect to possible practical application in earthquake engineering, used throughout this work. For further reading the comprehensive literature is advised, e.g. [101,85,179,211,82,83,189].

2.2 Summary of basic relations, conditions and categories

In practice, not only one general nonlinear algorithm is applied for solution of any optimization problems. Certain sub-categories with special mathematical properties have been separated that provide considerable simplications and therefore a higher effectiveness. Hereby the number of existing approaches is overwhelming, hence the following paragraphs present a selection of optimization problem types and solution strategies appropriate for the topics of this study. Those categories are summarized in Tab. 2-1.

If the design variables x are independent from time the appropriate optimization problems are called "static", otherwise "dynamic" [189]. The design variables x are used as

$$x = [x_1, \ldots, x_{nx}]^T \tag{2-3}$$

For the purposes of this work it is sufficient to have all design variables and functions defined in the real or complex number space. Then the optimization problem is also called "continuous". However, special practical cases, require a design variable solution space consisting of discrete or integer numbers. Such problems can be solved with methods of "Discrete optimization" or "Integer optimization" [120].

Before starting the solution of an optimization problem, a starting vector for the design variables

Table 2-1 Selection of optimization categories

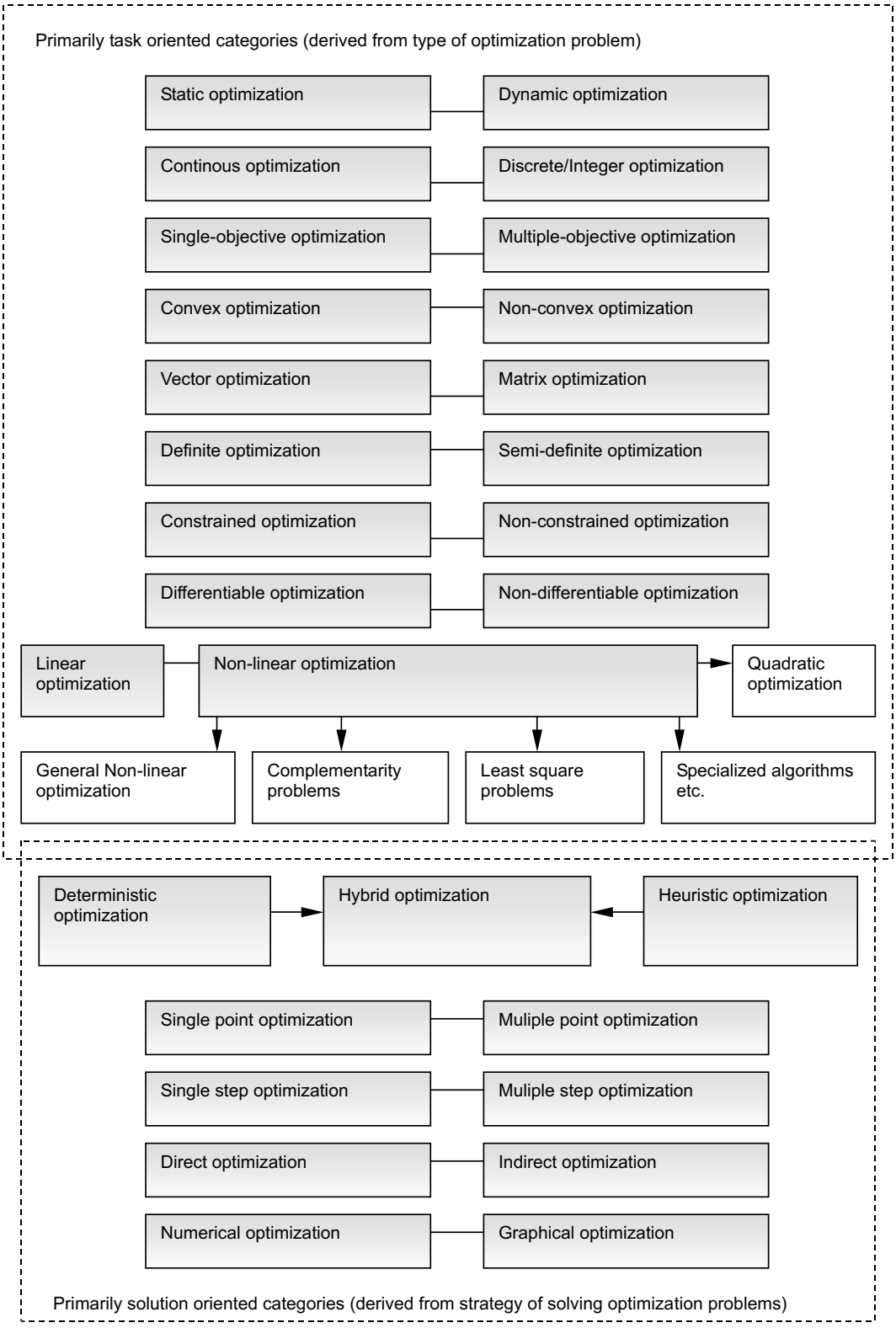

$$x_0 = [x_{0,1}, \ldots, x_{0,n_x}] \tag{2-4}$$

is required. Such starting vectors can have different quality. Some algorithms or applications require just a trivial starting vector, i.e. providing a zero or unity vector. Other algorithms require qualified starting vectors, such as initially feasible vectors, that fulfil the subsidiary conditions from the very beginning. Other quality demands result from the uniqueness of the solution, that might require a starting solution in the neighborhood of the extremum solution, either to ensure solution, simplify solution or distinguish the solution if several extremum points exist in the solution space.

As indicated in Eq. (2-1), optimization problems can contain several objective functions. Such problems are called "multi-objective" or "multi-criterion". Most solutions can be found by defining weights to assign the importance to the functions (sum method, compromise method) in order to transform all objective functions into an appropriate single-objective problem. Others use a transformation into appropriate subsidiary conditions or the separation in several dependent "one-step" optimization problems. Additionally, the functions can be evaluated by taking selected objective functions as constant and perform an evaluation in solution maps (Pareto optimality) [211].

Another category can be derived from the "convexity" of the objective and subsidiary functions. The convexity of a simple function can be defined by application of [39]

$$f(\lambda_1 x_1 + \lambda_2 x_2) = \lambda_1 f(x_1) + \lambda_2 f(x_2) \qquad \lambda_1, \lambda_2 \in (0,1) \qquad \lambda_1 + \lambda_2 = 1 \tag{2-5}$$

If the problem is multidimensional, the (local) convexity of the nonlinear optimization problem is given if the Hesse matrix

$$H(x) = \frac{\partial^2 f(x)}{\partial x_i \partial x_j} \tag{2-6}$$

of the objective function is positive semi-definite

$$\det H(x) \geq 0 \tag{2-7}$$

and the Jacobi-matrix, i.e. the first derivatives of the subsidiary conditions is positive semi-definite.

Closely connected to convexity is the determination of the global minimum in the feasible region Ω

$$O(x_{opt}) \leq O(x) \forall x \in \Omega \tag{2-8}$$

and local minimum

$$O(x_{opt}) \leq O(x) \forall x \in \Omega \qquad \text{with} \quad ||x - x_{opt}|| < \delta \tag{2-9}$$

that is defined as minimum for all x in a small neighborhood of x_{opt}. In convex problems, global and local minima are identical. The existence of a minimum is given by the Weierstrass theorem, that states for $f(x)$ a global minimum if it is continuous and Ω is non-empty, feasible, closed and bounded [7]. Another optimality criterium is given by the Kuhn-Tucker theorem (see later in this section).

Algorithms have been developed for "vector" and "matrix" optimization problems, i.e. the design variables are given as vector or matrix. The matrix formulations commonly respect additional relations between the matrix components, as symmetry and being definite or semi-definite. This also introduces "definite" and "semi-definite" optimization problems. Semi-definite programming (SDP) considers optimization problems with symmetric semidefinite matrix variables with linear objective function and linear constraints, e.g. [226].

Other categories can be stated by evaluation of the subsidiary conditions. The categories "constrained" and "unconstrained" are basic to solution strategies. In preparation of numerical solution strategies it is useful to separate the subsidiary conditions into pure equality conditions and pure inequality conditions [161]

$$h_k(x) = 0 \qquad k = 1 \dots n_h \tag{2-10}$$

$$g_j(x) \leq 0 \qquad j = 1 \dots n_g \tag{2-11}$$

or even highlight simple constraints for all design variables

$$x_{m,min} \leq x_m \leq x_{m,max} \qquad m = 1 \dots n_x \tag{2-12}$$

Any constrained optimization problem , e.g. Eq. (2-1) and (2-2) can be transformed into an simply constrained problem by introduction of Lagrange multipliers λ and slack variables y. In a first step, the inequality conditions are modified with introduction of the slack variables

$$O(x, y) = O(x) \rightarrow Min \tag{2-13}$$

$$G_j(x) - y = 0 \qquad j = 1 \dots n_G \tag{2-14}$$

$$y \leq 0 \tag{2-15}$$

Then, the Lagrange multiplier method is applied to include the original subsidiary conditions into the objective function

$$O(x, \lambda, y) = O(x) + \lambda^T (G(x) - y) \rightarrow Min \tag{2-16}$$

while the non-negativity conditions

$$\lambda \geq 0 \tag{2-17}$$

$$y \geq 0 \tag{2-18}$$

need to be fulfilled. As the new variables λ and y are complementary, the following complementarity condition must be fulfilled

$$\lambda^T y = 0 \tag{2-19}$$

This property will often be utilized in solving algorithms. The necessary conditions for optimality of convex problems are summarized by the "Kuhn-Tucker Theorem" [135] that is given in Tab. 2-2. Hereby the Kuhn-Tucker Theorem is the extension of the Lagrange multiplier method for duality problems with inequality conditions. Herein the "Lagrange function" is describing a saddle point (or max-min) problem, that is characterized by

$$O(x_{1,opt}, x_2) \leq O(x_{1,opt}, x_{2,opt}) \leq O(x_1, x_{2,opt}) \tag{2-20}$$

where several variables show different extremum conditions (either as minimum or maximum) at the optimum point.

From the Kuhn-Tucker conditions the property of duality of optimization problems can be derived. A dual optimization problem

$$o(x, \lambda) \rightarrow max \tag{2-21}$$

$$\frac{\partial O(x, \lambda)}{\partial x} = 0 \tag{2-22}$$

$$\lambda \geq 0 \tag{2-23}$$

is the called "dual" problem to the "primal" problem in Eq. (2-1,2-2), as the results are the same while respecting the same set of Kuhn-Tucker conditions. Such duality properties can be beneficially used in solving optimization problems and for identification of the physical meaning of Lagrange multipliers [225].

Other categories can be separated from the type of applied objective or subsidiary functions. Generally, the functions are considered as linear or nonlinear. The problem with linear objective function and linear constraints, first introduced in [116], are called "Linear optimization" (or Linear programming LP) problems

$$O(x) = Lx \rightarrow Min \tag{2-24}$$

$$Gx + G_0 \leq 0 \tag{2-25}$$

with the coefficient matrices L and G of the objective function and subsidiary conditions. The value G_0 is the constant part of the subsidiary conditions. This type of optimization problem can be solved with

Table 2-2 Lagrange function and Kuhn-Tucker conditions for optimality

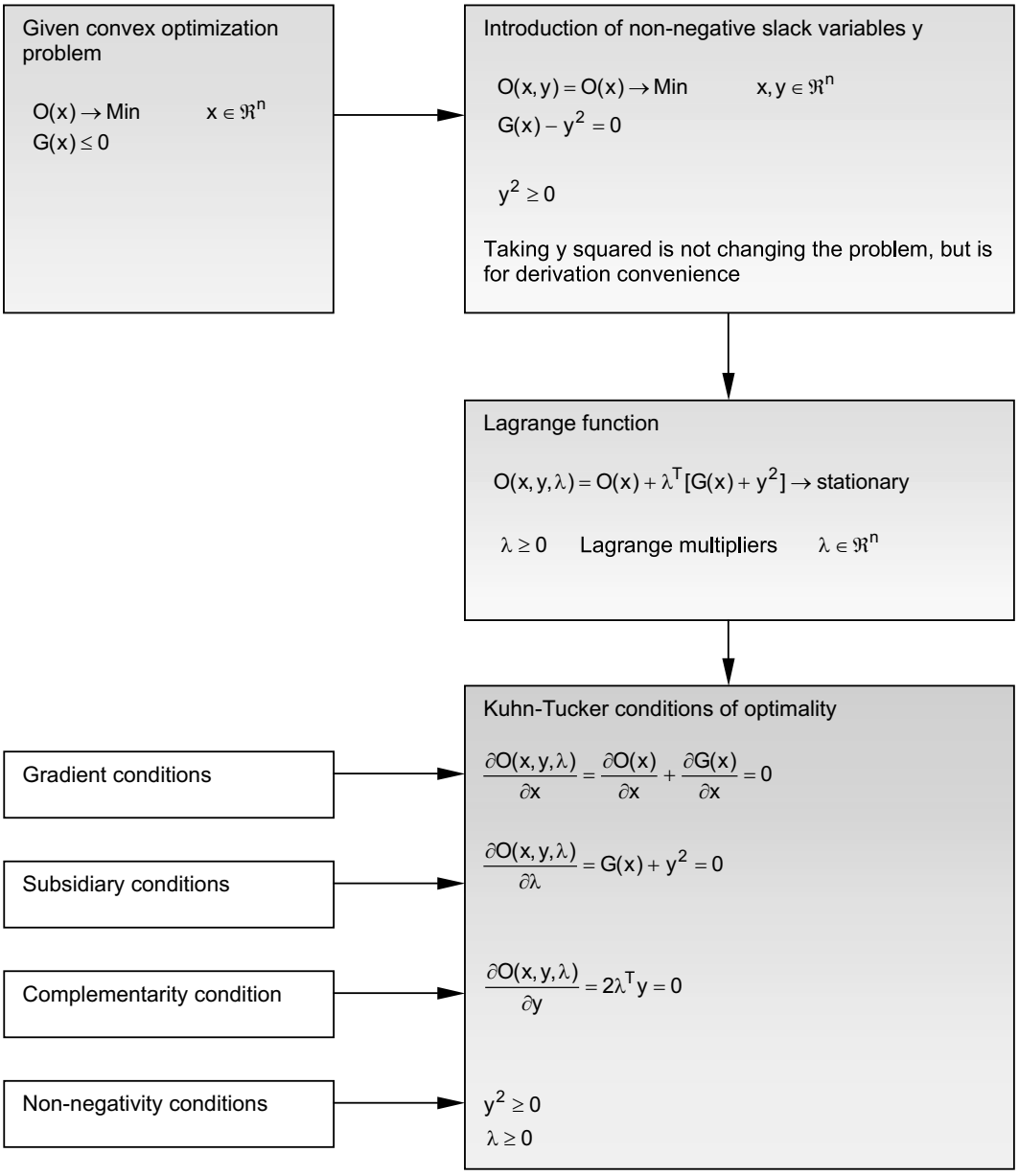

- Simplex algorithm [65]
- Revised simplex algorithm using dual problem properties [157]
- Ellipsoid algorithm [127]
- Projection algorithms [118]

or other concepts, e.g. described in detail in [7,189].

The other group of optimization problems are the "Nonlinear optimization" (or Nonlinear programming NLP) problems, in the general form of (2-1,2-2). These problems are divided into several important subcategories. One important representative is the "Quadratic optimization" (or Quadratic programming QP) problem

$$O(x) = \frac{1}{2}x^T Qx + Lx \rightarrow Min \tag{2-26}$$

$$Gx + G_0 \leq 0 \tag{2-27}$$

that consists of a quadratic objective function and linear subsidiary conditions. Former approaches use simplex type calculation methods, whereas newly concepts involve more strategies known from general convex optimization. Then, as the Hesse matrix $H = Q$ is directly given, the calculations can be very efficient. Popular solving strategies are

- Modified simplex method, e.g. [224]
- Cutting edge method, e.g. [124]
- Potential method, e.g. [79]
- Method of reduced gradients [83]

A special type of nonlinear optimization problems are the "Complementarity problems" (CP). These are characterized by linear subsidiary conditions, except of one quadratic condition

$$O(x, y) \rightarrow Min \tag{2-28}$$

$$G(x, y) + G_0 \leq 0 \tag{2-29}$$

$$x^T y = 0 \tag{2-30}$$

the origin of such problems result from duality problems with dual variables x and y that behave orthogonally. Specialized algorithms are available [78], however most general nonlinear optimization algorithms can be utilized for solution.

Another special case of optimization problems are least square problems

$$O(x, r) = r^T Ir \rightarrow Min \tag{2-31}$$

$$G(x) - G_0 = r \tag{2-32}$$

where r are the residuals, x the coefficients of the fitting function $G(x)$ and G_0 contains the original function. Such problems turn out to be either quadratic or nonlinear optimization problems.

The most general group of optimization algorithms is given by nonlinear optimization, that target either convex or general non-convex optimization problems [5]. Algorithms for convex optimization are described e.g. in [101,85,179,211,82,83,194]. There are mainly two solution categories. First, the "Deterministic programming" algorithms that evolves from a starting solution x_0 to the extremum solution by directly evaluation of the given functions and gradients. Second, the "Heuristic optimization" methods involve certain components of random/stochastic variable modifications [149]. Algorithms belonging to either category are listed in Tab. 2-3. As all algorithms show different advantages and disadvantages, the combination of two or more algorithmic concepts can be beneficial. Such "Hybrid" optimization strategies are often used in non-convex optimization.

Most of the heuristic and deterministic algorithms work at first as "single-point" strategies, i.e. the evaluation is only performed at one single point in the design space. However most concepts can be involved in "multi-point" concepts, where the solution relies on the evaluation of several distinct points in design space, that are provided in parallel. These methods try to combine the information from either point, to improve the extremum search. A popular representative method is the Particle Swarm optimization, that combines methods of evolution algorithms with probabilistic evaluations [126].

All functions in optimization problems could be dependent on results of subordinate optimization problems. These problems are called "multiple-step" problems. Then the optimization problem can be treated by solving several but coupled "one-step" optimization problems. As well, categories can be distinguished regarding the solution strategy. The "direct" methods evaluate a problem in the given form. The "indirect" methods evaluate approximation or substitution problems, that e.g. are defined by simplification, gradient evaluation or dual problem solution.

Finally, the solution can be obtained by graphical or numerical means. However, the graphical version is restricted to very few variables only [211].

Other concepts and categories can be found at [222] and [165].

2.3 Approximation methods

Non-linear optimization problems can show a certain complexity, e.g. resulting from the problem size, the non-convexity or order of the problem. In order to get solutions, or to get them more efficiently, approximation methods are applied to simplify the task. Besides local approximation methods, like Taylor or Binomial series, mainly global approximation methods like the Response Surface or Reduced Basis Methods, or mixed type approximations are applied [130,183].

Table 2-3 Selection of algorithms for deterministic and heuristic optimization

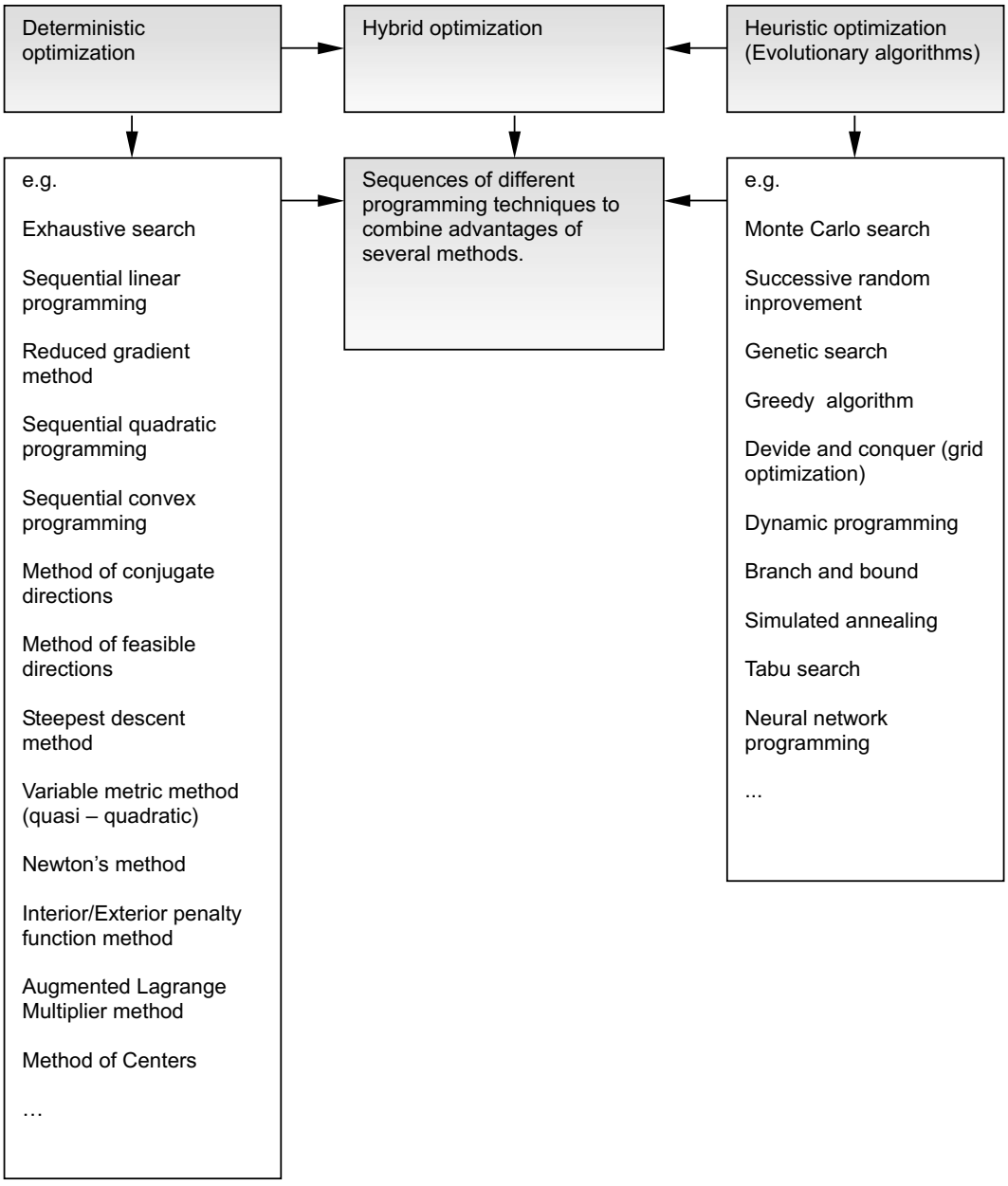

From probabilistics, the Response Surface Method is well known, that replaces the original function by a simpler, but in a given region sufficiently representing function that can be treated more efficiently [49]. The method can be generally used for nonlinear optimization problems as well. Basically, all objective and subsidiary functions can be replaced by a response surface function. For this reason the functions are evaluated at a finite number or selected or randomly chosen supports within a reasonable variable range. The results are used to fit the parameters of a predefined response function, using least square or other regression methods (e.g. neural networks [87]). The response function usually consists of a polynomial of a certain order, that can be adapted by regard of additional response points, by replacement of points with less performance or by increase of the function order. Under appropriate conditions the solution can converge to the exact optimum of the original problem [41].

The simplest response surfaces for the original optimization problem are linear or quadratic functions. This approach is most effective, because the resulting optimization problems can be solved with fast linear or quadratic optimization algorithms. Other than the original problem, the simplified problem is convex and has distinct results. With additional evaluations of the objective function the parameters of the linear or quadratic sub-problem are improved. This is similar to the strategy that is applied in the sequential linear (SLP) or quadratic programming (SQP) methods. An improvement to this method is a piecewise substitution of the original functions with several linear or quadratic approximations. Generally, this procedure can be extended for higher orders [201].

Furthermore, the applied regression methods can be used to condense the problem and therefore to reduce the number of unknowns. This approach is commonly named Reduced Basis Method. However, this concept is not necessarily successful for any application. The properties of the original problems must be carefully explored in order to select an appropriate response surface. The quality of the response surface is dependent on the reasonable selection of the supports (Design of Experiments, [158]). The application is often limited to few design variables. Each calculation should finalize in a verification run with the original problem. Putting less efforts into the adaptation of the response surface, the method is valuable to provide quality starting vectors for other optimization solvers.

2.4 Uncertainty and sensitivity of the design

Practical design often uses only one set of conditions to evaluate the given situation. However, most variables and coefficients cannot be determined to a certain extend, thus they can vary. The inclusion of such effects requires the estimation of the uncertainty of the parameter, given as stochastic moments (e.g. mean values, standard deviation). Such optimization problems can be formally assessed similarly as deterministic parameter problems. Only the design variables will be exchanged by the stochastic parameters.

As well, not only the parameters can vary but the function values as well. So in design, the effects of little changes in the design variables can be of essential interest. This is part

of the sensitivity analysis, that mainly operates by evaluation of the gradient information at the optimum point.

This study will not primarily focus on these types of analyses. Further reading is given e.g. in [43].

2.5 Principles for practical derivation of optimization problems in engineering

2.5.1 Algorithmic concepts

The interface of optimization algorithms is illustrated in the upper scheme in Tab. 2-4. The problem consists of two sides, first the core that provides the problem functions and secondly the optimization algorithm, that evaluates the function values and determines modifications for the design variables in order to get closer to an extremum (or optimal) solution. After a certain amount of iterations, the optimization algorithm provides a solution or error indications.

Regarding the connection of the core function and optimization algorithm, two concepts of algorithmic realization can be distinguished. Most applications in engineering use existing design software, that is externally coupled via an interface with an optimization software. Basically both codes are separated. Either of them can be provided as "gray boxes", the contents is hidden, or known but not changeable. For communication an interface language/protocol need to be specified, e.g. [165]. Such problems use the exterior formulation as indicated in the center part of Tab. 2-4. The advantages of this concept can arise from the availability of problem solvers, that work very effective because of task specific code preparations. However, those programs might not provide all useful information to assist the solution of the optimization problem. Such information can be certain parameter vectors, coefficient matrices and especially gradient information. Some of the algorithms provide approximate gradients by finite differences.

Contrary to this, the second group is dealing with these requirements, as all algorithmic formulations are given in function form, i.e. are open for access and algorithmic handling. Such problems use interior formulations, that give the chance to provide all necessary information for the optimization algorithm. Usually both parts are compiled into one code. This type uses the most flexible interfaces and function formulations for the user. However, all formulations need to be provided, at least as library functions. This concept is illustrated in the lower part of Tab. 2-4.

2.5.2 Intuitive derivation of optimization problems

Some known engineering problems can be directly and intuitively translated into optimization problems, without using additional mathematical preparations. This is demonstrated schematically in Tab. 2-5.

These tasks often deal with simple targets, like the minimum or maximum of a single parameter, optionally combined with some restrictions to this or other parameters. The intuitive derivation bases commonly on exterior optimization problem descriptions (Sec. 2.5.1).

Table 2-4 Algorithmic concepts

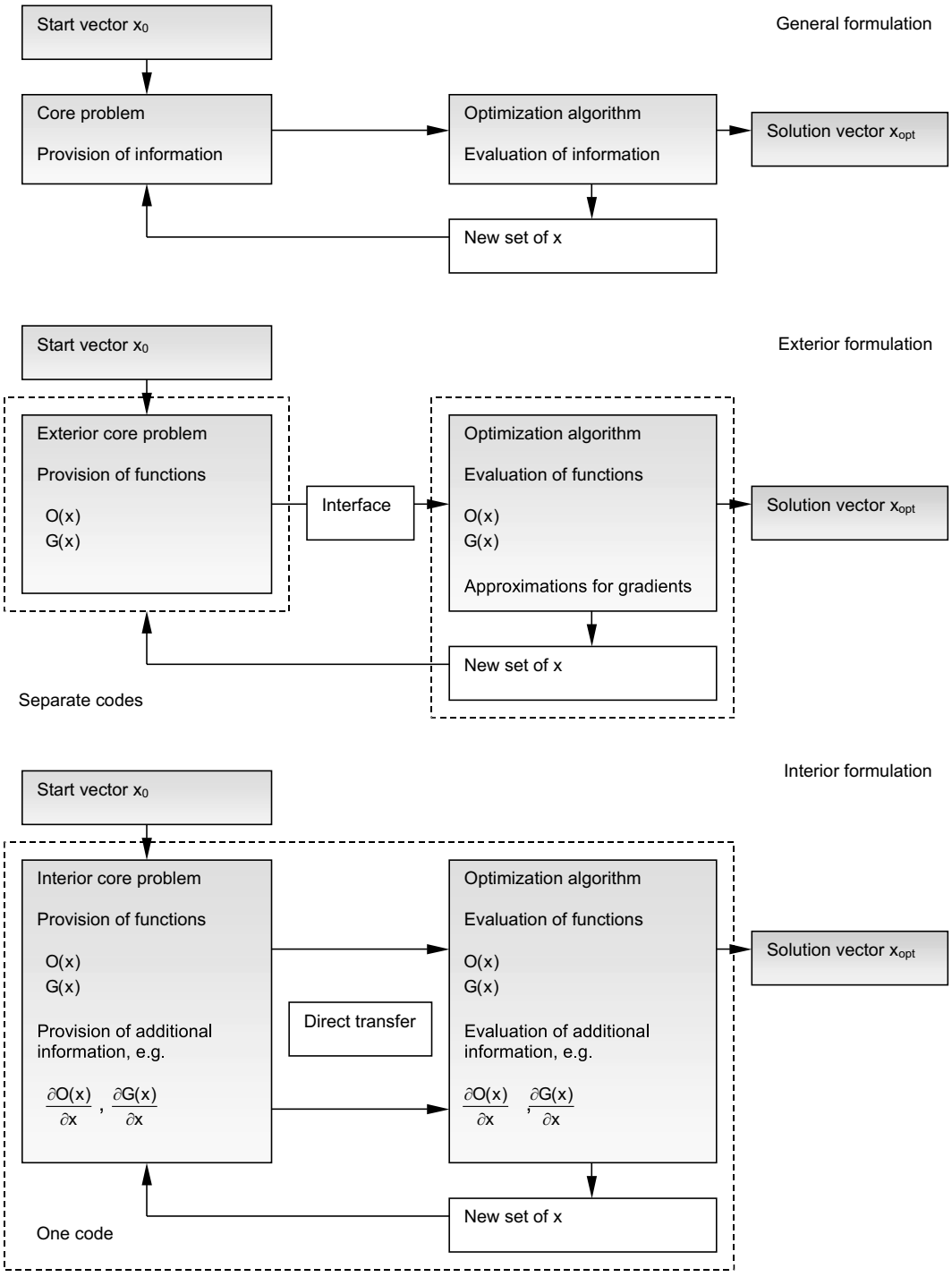

Table 2-5 Scheme of engineering model-optimization algorithm coupling

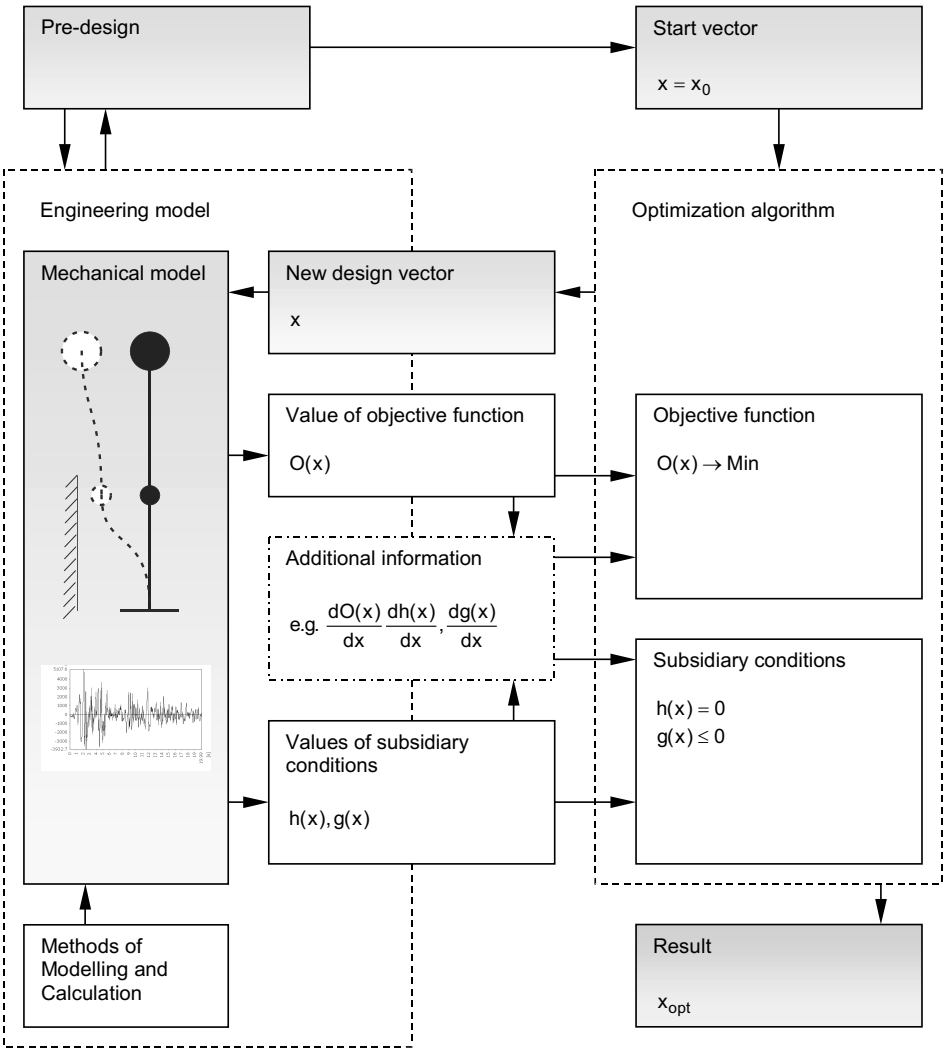

2.5.3 Derivation using mechanical principles

As structural engineering problems base on mechanical principles, they are a natural basis for derivation of appropriate optimization problems. Such principles can be, exemplarily

- Minimum of total energy
- Balance of impulse
- Balance of momentum
- Principle of Hu-Washizu

and conditions e.g.

- Equilibrium
- Material laws
- Kinematic compatibility
- Contact conditions

and much more, that all describe parts or the total behavior of structures.

Mechanical formulations can be described as variational principles, e.g. [214]. Such formulations commonly state an extremum or stationarity condition using an integral term

$$\int V(x)dx -> Ext. \tag{2-33}$$

with respect to several subsidiary conditions, mostly given as differential equations or inequalities.

The traditional concept of transforming variational principles into a set of differential equations is given by the Euler-Lagrange equation [39]. After discretization a system of algebraic equations can be obtained as illustrated in Tab. 2-6. However, the similarity of variational and optimization problems can be directly utilized to derive appropriate optimization formulations. The direct discretization of the variational principle is leading to the appropriate optimization problem. For discretization, known methods can be utilized, e.g. finite difference method, finite element method or meshless representations. With the coupling to variational problems, the powerful means of variational calculus can be utilized to modify and prepare the optimization formulations according to several solving requirements.

The variational principles themselfs can be constructed from their underlying differential equations, such as the Poisson differential equation (see Sec. 3). There are three main representations of a differential problem

- Strong form
- Weak form

Table 2-6 Concepts for solving variational problems

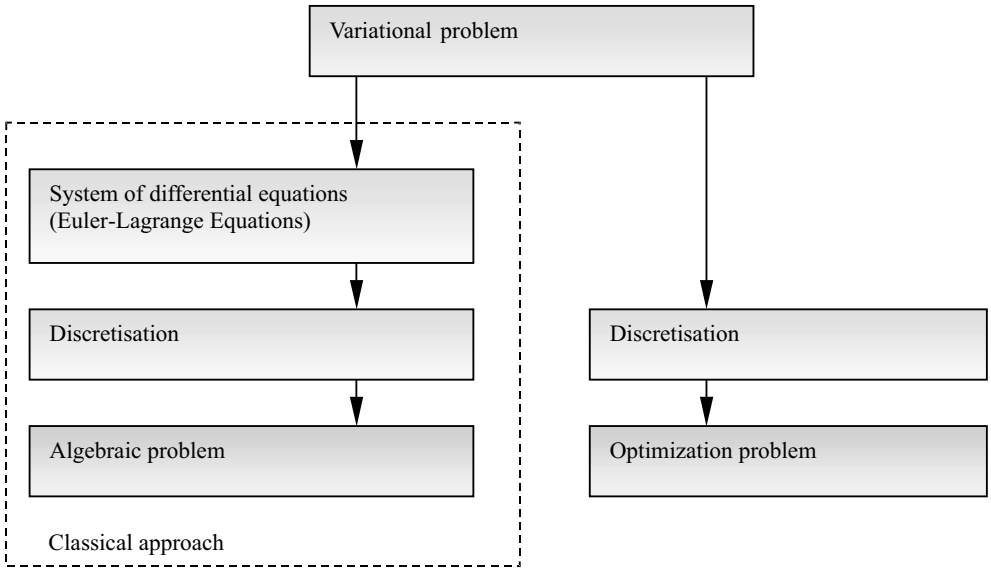

- Variational form

The strong form consists of a system of ordinary or partial differential equations in space and/or time together with a set of boundary conditions. The weak form is a weighted integral equation that relaxes the strong form into a domain-averaging expression. The variational form is a functional, whose stationary conditions generate the weak form and the strong form [214,22]. Thus any of the forms can be transformed into the other. For derivation of appropriate variational formulations the strong form of differential equations can be firstly transformed into a weak form and later to a variational form. This transformation is illustrated schematically in Tab. 2-7 where the differential equations and boundary conditions are considered. Within these transformations the concept of Lagrange multipliers is often utilized to transfer subsidiary conditions into the extremum principle function.

As an example of application, the well known principle of stationary potential (Reissner Principle) for linear elasto-statics is derived in Tab. 2-8. The basis is the differential equations of equilibrium, material law and kinematic conditions, accompanied by the static and geometric boundary conditions. First a coupled weak form of the equilibrium conditions and extended kinematic conditions is established, that is modified by application of the partial integration rule. With introduction of the boundary conditions as variations, the variational equation is obtained. Integrating this expression will provide the extremum principle in the Reissner form.

As this concept of derivation of optimization problems from variational expressions is very practical, other examples are presented in the following sections.

Table 2-7 Principle for derivation of variational formulations from strong form via weak forms approach

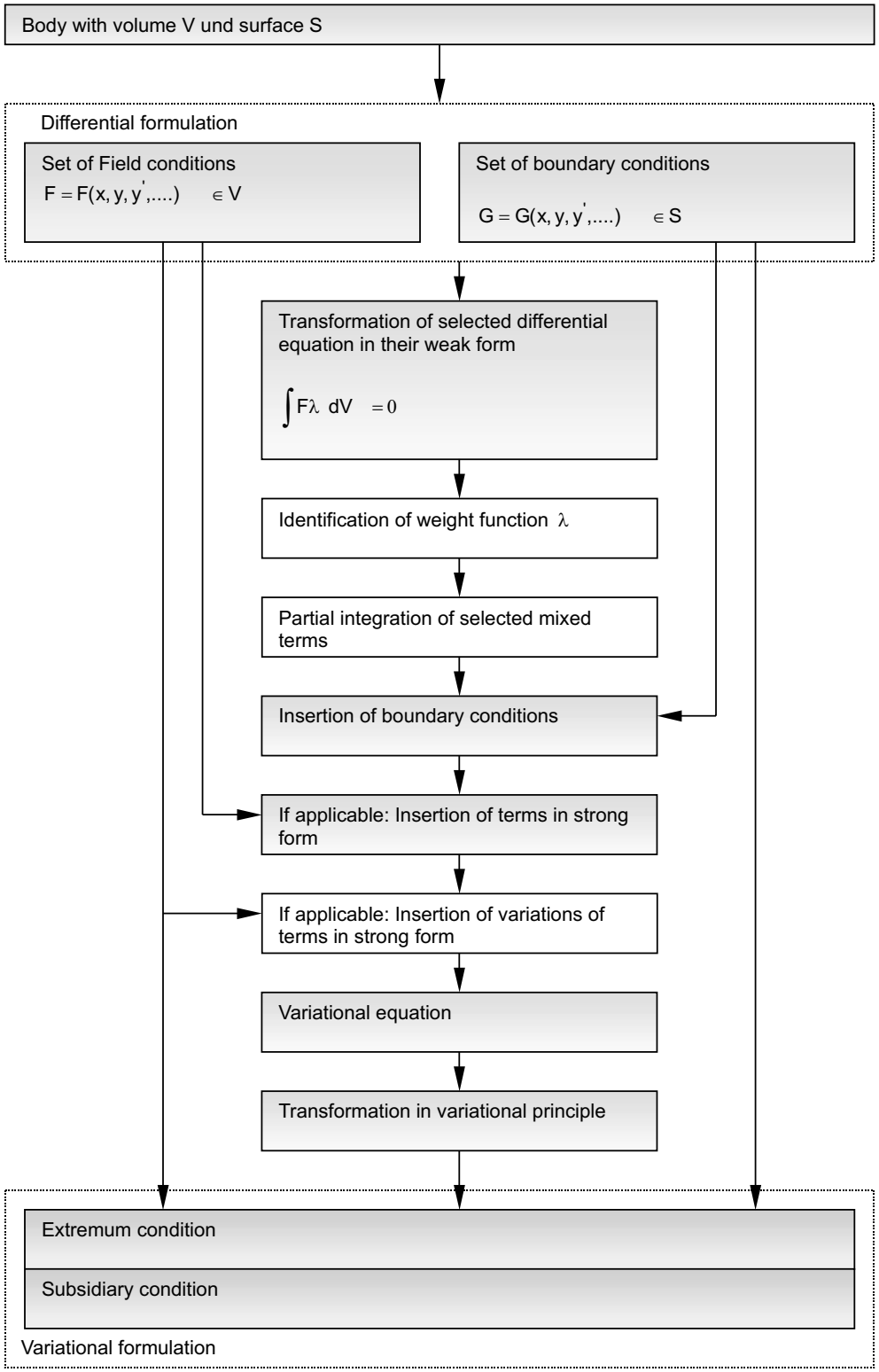

Table 2-8 Derivation for principle of stationary potential with weak forms approach

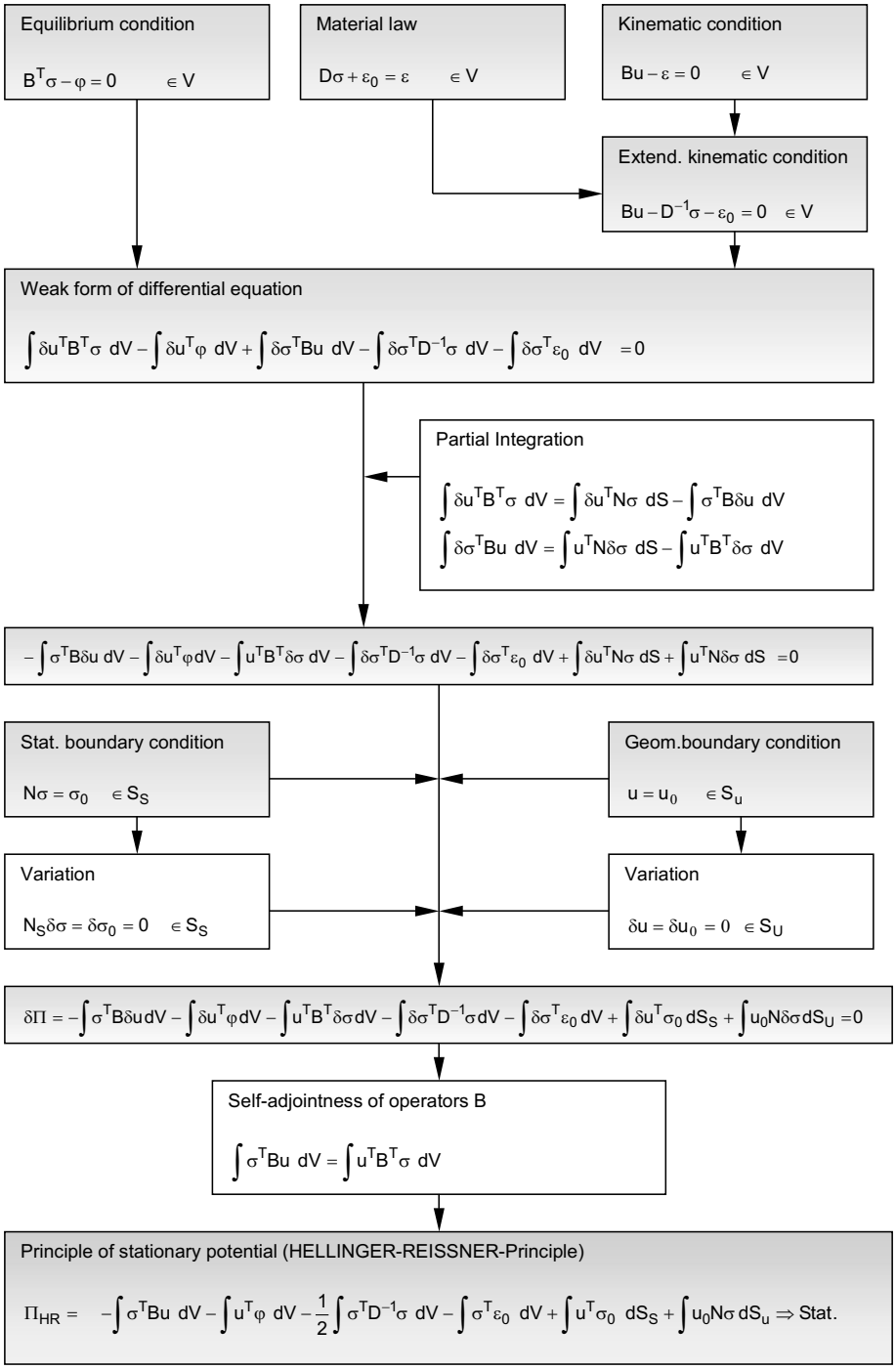

3 Continuum mechanical background

3.1 Hamiltonian principle

Dynamic problems in structural engineering can be solved according to the Hamiltonnian principle

$$J_H = \int \Pi(x,t)dt \rightarrow Min \tag{3-1}$$

with the mechanical potential Π. This potential can be derived from extremum conditions of mechanical principles as the Lagrange and Castigliano principles [214]. Fixing time t, the potential is identical to that from a static problem. As other principles, the Hamiltonian needs to respect given subsidiary conditions defined in time.

From this, the Hamiltonian principle enables that the dynamic problem can be separated into (quasi-) static sub-problems at fixed times, and a superior time integration problem. This separation is the key for almost all numerical solution methods, where single quasi-static problems are solved and integrated separatelly with respect to time. To solve the problems numerically, time and space need to be discretisized.

3.2 Quasi-static sub-problems

Mechanical problems, at discrete times, can be described on the basis of elliptic differential equations. Most problems can be derived from Poisson′s differential equation

$$div\left(\hat{D}\cdot grad\,\hat{u}\right)+\hat{\varphi}=0 \tag{3-2}$$

and it′s special case, the Laplace equation

$$div\left(\hat{D}\cdot grad\,\hat{u}\right)=0 \tag{3-3}$$

Herein, $\hat{\varphi}$ denotes a source that can result e.g. from external forces or damping and inertia forces. The unknown $\hat{u}$ can be identified as the deflections of the material points. The material properties of the system are defined by the constitutive tensor $\hat{D}$.

According to Tab. 3-1 the 2nd order differential equation can be transformed into a set of 1st order differential equaltions by substitution. These functions, consisting of

- equilibrium (or static) conditions, that define the relation of external and internal forces /stresses
- kinematic (or compatibility) conditions, that define the relation of deflections and strains
- material (or constitutive) laws, that define the relation of strains and internal forces/ stresses

determine uniquely the state of a considered material point. On selected material points at the surface of the volume, appropriate boundary conditions can be defined

- static boundary conditions, pre-defining the state of stresses or forces
- geometric (or kinematic) boundary conditions, pre-defining the state of deflections or deformations

The motion of arbitrary three-dimensional solid bodies can be characterized by their position and shape variation in time, within coordinate systems. The motion will be recognised as the states of the body in distinct times. It can be described with help of two considered configurations, firstly, the "reference" (or "initial") configuration ${}^{t}x = x(t)$ and secondly, the "current" (or "end") configuration ${}^{t+\Delta t}x = x(t + \Delta t)$. In general, the body movement can be divided into

- rigid body motion
- relative motion between material points (strain-inducing part).

3.3 Material point motion

According to deterministic formulations in continuum mechanics [223], each material point can be uniquily identified at a given time t. Therefore, the state of the system can be described dependent on the motion of the material points. Such motions can be formulated as mathematical functions in the Euclidian vector space. In this study only orthonormal bases are applied. With the definition of a fixed origin for a Cartesian coordinate system and a Cartesian vector basis, all positions of points (e.g. as part of a considered volume V) can be described uniquely as coordinate tensors $\hat{x}$ at a certain time t in $\mathbb{R}^3$. The movement of material points can be described with help of the "reference" (or "initial") configuration

$${}^{t}\hat{x} = \hat{x}(t) \qquad \in {}^{t}V \tag{3-4}$$

and the "current" (or "recent" or "final") configuration

$${}^{t+\Delta t}\hat{x} = \hat{x}(t + \Delta t) \qquad \in {}^{t+\Delta t}V \tag{3-5}$$

Both configurations can be related as follows:

$${}^{t+\Delta t}\hat{x} = \Xi\left({}^{t}\hat{x}, t, \Delta t\right) \tag{3-6}$$

This is called the "material" or Lagrangian formulation, describing the current configuration as a function $\hat{\Xi}$ of the reference configuration. Stating the truth of bijective mapping, the inverse operation is defined as well, resulting in the "spacial" or Eulerian formulation:

$${}^{t}\hat{x} = \Xi^{-1}\left({}^{t+\Delta t}\hat{x}, t, \Delta t\right) \tag{3-7}$$

describing the reference configuration as a function of the current configuration.

Table 3-1 Structure of general differential equation system (DES)

POISSON's differential equation

$$\nabla^T (\hat{D}\,\nabla\hat{u}) + \hat{\varphi} = 0 \in V$$

$\hat{x}$, t	Cartesian coordinates, time
∇	Nabla differential operator
$\hat{u} = u(\hat{x}, t)$	Solution tensor (deflection)
$\hat{\varphi} = \varphi(\hat{x}, t)$	Source tensor (force)
$\hat{D} = D(\hat{x}, t)$	Constitutive tensor (material)

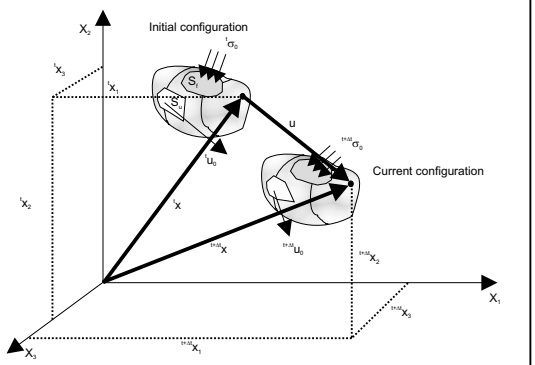

Transformation of DE of 2nd order in DES of 1st order by introduction of a new variable (strains)

$$\hat{\varepsilon} = \nabla\hat{u}$$

Boundary condition

$$\hat{u} = \hat{u}_0 \quad \in S_U$$

$$\nabla^T (\hat{D}\,\hat{\varepsilon}) + \hat{\varphi} = 0 \quad \in V$$
$$\hat{\varepsilon} = \nabla\hat{u} \quad \in V$$

Specification of a constitutive relation (stresses), e.g.

$$\hat{\sigma} = \hat{D}\,\hat{\varepsilon} \quad \in V$$

Boundary condition

$$\hat{\sigma}\hat{n} = \hat{\sigma}_0 \quad \in S_S$$

Field conditions

$\nabla^T \hat{\sigma} + \hat{\varphi} = 0$	Equilibrium condition
$\hat{\varepsilon} = \nabla\hat{u}$	Kinematic condition
$\hat{\sigma} = \hat{D}\,\hat{\varepsilon}$	Material law

Boundary conditions

$\hat{u} = \hat{u}_0$	$\in S_U$	Geometric bound. condition
$\hat{\sigma}\hat{n} = \hat{\sigma}_0$	$\in S_S$	Static boundary condition

The differences in the coordinates can be identified as the deflections $\hat{u}$

$$\hat{u} = {}^{t+\Delta t}\hat{x} - {}^{t}\hat{x} \tag{3-8}$$

Such formulas describe pure flows of material points. Only the knowledge of their position in the reference and in the current position is necessary (only translatory components). In this study, the focus is set on the Lagrangian formulation, as mostly applied in solid mechanics.

3.4 Rigid body motion

Rigid bodies do not have any relative deflections between the points of the body. So only one reference point needs to be observed. Therefore the problem becomes similar to a material point motion. The motion can be uniquely described, in terms of the associated translational and rotational motion components. Figure 3-1 describes the movement of a three dimensional body. The separation of the rotational part of the motion is possible, if both the initial and current states are related to a global basis, as follows:

$${}^{t}\bar{x} = {}^{t}\hat{L}^{T\,t}\hat{x} \tag{3-9}$$

$${}^{t+\Delta t}\bar{x} = {}^{t+\Delta t}\hat{L}^{T\,t+\Delta t}\hat{x} \tag{3-10}$$

with ${}^{t}\hat{L}$ and ${}^{t+\Delta t}\hat{L}$ as left side rotational transformation matrices. These matrices transform the points of the appropriate body from a global coordinate system to local directions.

3.5 Deformable body motion (line segment example)

Solid deformable bodies are characterised by changeable relations between material points. In order to determine the internal deformation state, the rigid body motions need to be excluded from the total motion, similar to Section 3.4. The motion of a differential element of a solid body can be exemplarily illustrated with help of a line segment with length s, as in Fig. 3-2. The effect of rigid body rotations is illustrated in Fig. 3-3 and 3-4.

Whereas the rigid body motion component can be principally determined according to Sec. 3.4, the internal deformation state (length change of the line segment) can be excluded with different strategies:

Method (a) Relation of body segment lengths in the reference and current configuration using Pythagoras′ theorem, e.g.:

$$\frac{{}^{t+\Delta t}s^2}{{}^{t}s^2} = \frac{{}^{t+\Delta t}x_1^2 + {}^{t+\Delta t}x_2^2 + {}^{t+\Delta t}x_3^2}{{}^{t}x_1^2 + {}^{t}x_2^2 + {}^{t}x_3^2} \tag{3-11}$$

Method (b) as (a) but returning to a linear measure

$$\sqrt{\frac{{}^{t+\Delta t}s^2}{{}^{t}s^2}} = \sqrt{\frac{{}^{t+\Delta t}x_1^2 + {}^{t+\Delta t}x_2^2 + {}^{t+\Delta t}x_3^2}{{}^{t}x_1^2 + {}^{t}x_2^2 + {}^{t}x_3^2}} \tag{3-12}$$

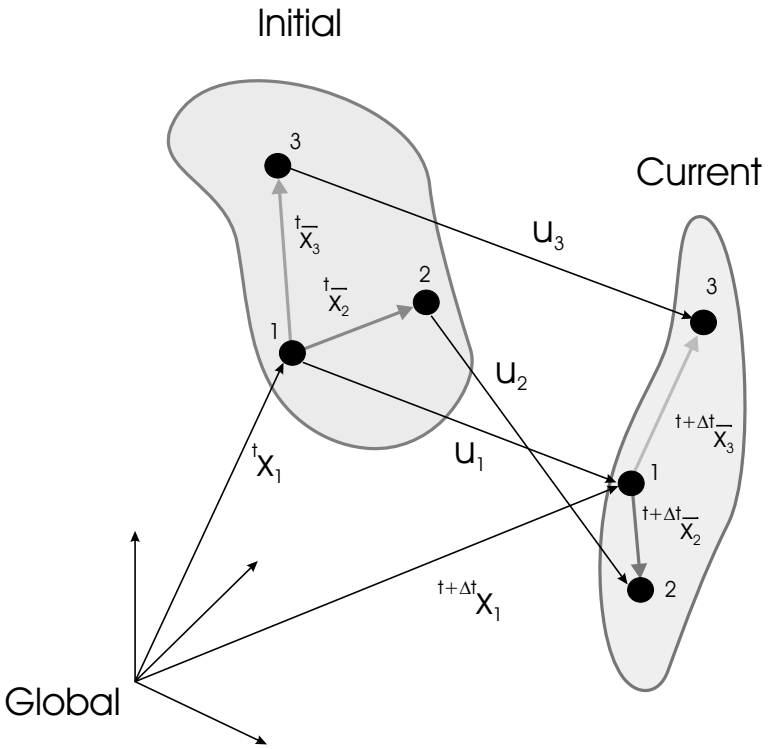

Figure 3-1 General body motion

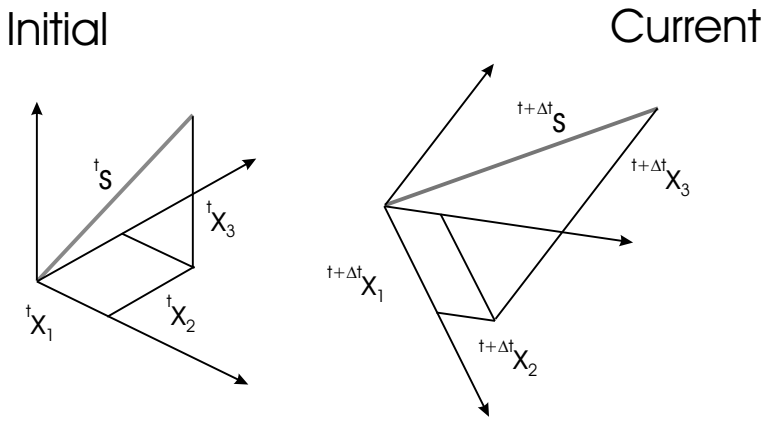

Figure 3-2 Motion of a line segment

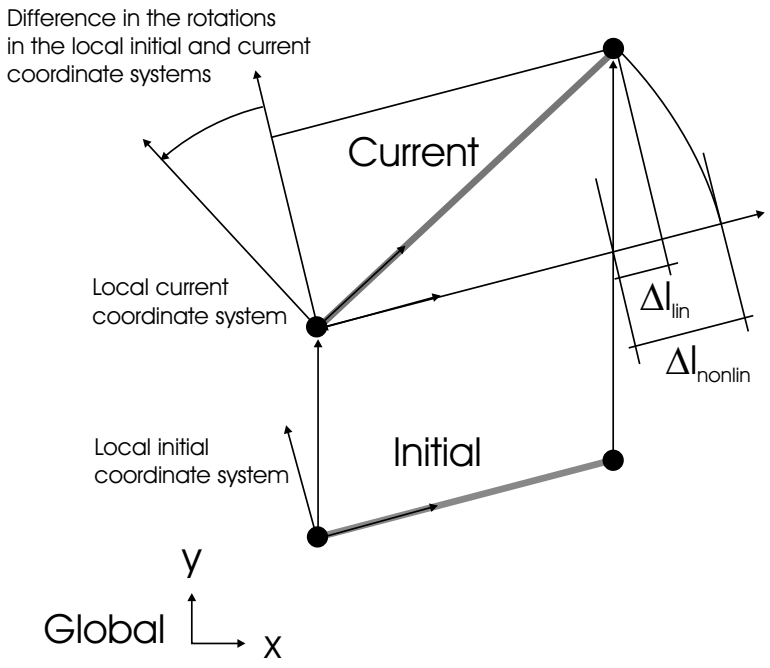

Figure 3-3 Difference in the strain measure in the initial and current system

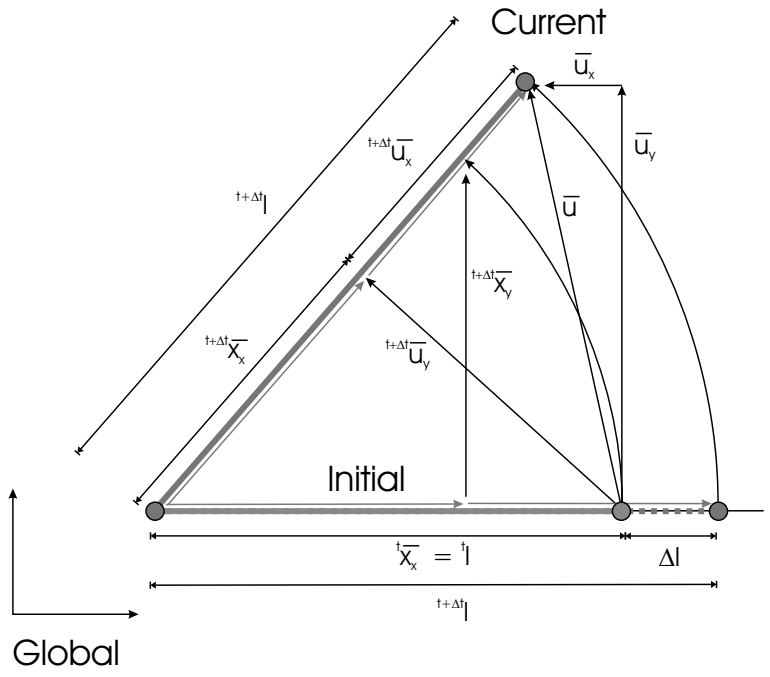

Figure 3-4 Elongation of a line element in current and initial coordinates

Method (c) Relation of body segments in a global coordinate system using orthogonal transformations, e.g.:

$$\frac{{}^{t+\Delta t}s}{{}^{t}s} = \frac{{}^{t+\Delta t}T \cdot \left({}^{t+\Delta t}x, {}^{t+\Delta t}y, {}^{t+\Delta t}z\right)}{{}^{t}T \cdot \left({}^{t}x, {}^{t}y, {}^{t}z\right)} \tag{3-13}$$

Such relations are known as strains or strain measures. They describe the internal deformation state independent from the initial and current geometry of structural elements. In engineering, different strain measures are applied, that describe the relative change of deformable elements.

Within this study, only a selected number of strain measures are considered, that are mostly applied in structural mechanics

- Engineering strains ε_{eng}
- Linear (or Cauchy) strains ε_{C}
- Nominal (or Biot) strains ε_{nom}
- Logarithmic (or Hencky) strains ε_{log}
- Quadratic (or Green-Lagrange) strains ε_{quad}

Other strain measures are discussed in [223].

The engineering strains ignore rigid body rotations, so the strains are measured in the original coordinate system. Thus the coordinates can be treated independently

$$d\varepsilon_{eng} = \frac{dx}{{}^{t}x} \tag{3-14}$$

with dx as the length change in initial coordinate directions. The integrated strains are

$$\varepsilon_{eng} = \int_{{}^{t}x}^{{}^{t+\Delta t}x} \frac{dx}{{}^{t}x} = \frac{{}^{t+\Delta t}x}{{}^{t}x} - 1 \tag{3-15}$$

This provides sufficient approximations for small deformations.

In large deformation theory, the rigid body rotations have to be respected. The nominal strains can be defined with respect to the reference state

$$d\varepsilon_{nom} = \frac{ds}{{}^{t}s} \tag{3-16}$$

including the infinitesimal length difference ds and the initial segment lenght s. The integrated value becomes

$$\varepsilon_{nom} = \int_{{}^{t}s}^{{}^{t+\Delta t}s} \frac{ds}{{}^{t}s} = \frac{{}^{t+\Delta t}s}{{}^{t}s} - 1 \tag{3-17}$$

Similarly the strains can be defined with respect to the current deformation state, as proposed by the Hencky approach

$$d\varepsilon_{log} = \frac{ds}{{}^{t+\Delta t}s} = \frac{ds}{s} \tag{3-18}$$

The appropriate integrated measure is logarithmic

$$\varepsilon_{log} = \int_{{}^{t}s}^{{}^{t+\Delta t}s} \frac{ds}{s} = \ln \frac{{}^{t+\Delta t}s}{{}^{t}s} \tag{3-19}$$

The necessary parameter for the Biot and Hencky strains can be calculated with help of Method (b) or (c). Alternatively, the Green-Lagrange definition corresponds to Method (a), with

$$d\varepsilon_{quad} = \frac{s \cdot ds}{{}^{t}s^2} \tag{3-20}$$

that results for a defined line segment change in

$$\varepsilon_{quad} = \int_{{}^{t}s}^{{}^{t+\Delta t}s} \frac{s}{{}^{t}s^2} ds = \frac{1}{2}\left[\frac{{}^{t+\Delta t}s^2 - {}^{t}s^2}{{}^{t}s^2}\right] = \frac{1}{2}\left[\frac{{}^{t+\Delta t}s^2}{{}^{t}s^2} - 1\right] \tag{3-21}$$

The reason for application of different strain measures is either the simplicity of treatment or the correctness of the superposition of different strain increments. If any increment is calculated with respect to the initial configuration, the superposition of the Biot strains is correct, as

$$\varepsilon_{nom} = \frac{\Delta s_1 + \Delta s_2}{{}^{t}s} \tag{3-22}$$

This is identical to the superposition of the single increments

$$\varepsilon_{nom} = \Delta\varepsilon_{nom,1} + \Delta\varepsilon_{nom,2} = \frac{\Delta s_1}{{}^{t}s} + \frac{\Delta s_2}{{}^{t}s} = \frac{\Delta s_1 + \Delta s_2}{{}^{t}s} \tag{3-23}$$

If the original length of the considered line element cannot be determined, the logarithmic measure should be applied

$$\varepsilon_{log} = \ln \frac{{}^{t}s + \Delta s_1 + \Delta s_2}{{}^{t}s} \tag{3-24}$$

and accordingly for the assembled strain increments

$$\varepsilon_{log} = \Delta\varepsilon_{log,1} + \Delta\varepsilon_{log,2} \tag{3-25}$$

thus

$$\varepsilon_{log} = \ln \frac{{}^{t}s + \Delta s_1}{{}^{t}s} + \ln \frac{{}^{t}s + \Delta s_1 + \Delta s_2}{{}^{t}s + \Delta s_1} = \ln \frac{{}^{t}s + \Delta s_1 + \Delta s_2}{{}^{t}s} \tag{3-26}$$

The calculation of Green-Lagrange strains is relative straighforward, as avoiding transformations. The governing equations require a incremental formulation [22] involving linearizations. Alternatively, a recalculation into Biot or Hencky strains can be considered. All strain measure can be transformed into each other

$$\varepsilon_{log} = \ln(\varepsilon_{nom} + 1) \tag{3-27}$$

$$\varepsilon_{quad} = 0.5(\varepsilon_{nom}^2 + 1) \tag{3-28}$$

Moreover, recalling the differences in the linear and nominal strain measures, a direct link to the Cauchy measure can be established stating a transformation (indicated here as operator T)

$$\varepsilon_{nom} = \frac{^{t+\Delta t}s}{^{t}s} - 1 = T\frac{^{t+\Delta t}x}{^{t}x} - 1 = T(\varepsilon_C + 1) - 1 \tag{3-29}$$

This relation layouts a practical strategy switching from geometric linear to nonlinear calculations.

It should be noted, that other strain measures exist, especially those of the Eulerian formulation type [22]. In structural engineering traditionally Lagrangian formulations and, out of these, the nominal (Biot) measure can be advantageous, because it maintains the affinity between the stress/strain and force/deformation relationship. It is therefore a natural extension to the linear theory. In most practical cases, the required knowledge of the undeformed initial configuration is given.

3.6 Deformation gradient (3D-continua)

In the previous section, the strain definition was illustrated for one dimensional systems. For arbitrary systems, the derivation of the strain/displacement relationship can be generalized with use of the deformation gradient $\hat{X}$. Infinitesimal bodies with $\hat{x}_i$ as it′s local origin and $d\hat{x}_i$ as the extent are considered. For time increments dt the motion is given in Lagrangian formulation

$$^{t+\Delta t}d\hat{x} = \hat{X}\ ^{t}d\hat{x} \tag{3-30}$$

and it′s inverse (Eulerian)

$$^{t}d\hat{x} = \hat{X}^{-1}\ ^{t+\Delta t}d\hat{x} \tag{3-31}$$

related by the deformation gradient $\hat{X}$

$$\hat{X} = \nabla^{t+\Delta t}\hat{x} = \begin{bmatrix} \frac{^{t+\Delta t}\partial x_1}{^{t}\partial x_1} & \frac{^{t+\Delta t}\partial x_1}{^{t}\partial x_2} & \frac{^{t+\Delta t}\partial x_1}{^{t}\partial x_3} \\ \frac{^{t+\Delta t}\partial x_2}{^{t}\partial x_1} & \frac{^{t+\Delta t}\partial x_2}{^{t}\partial x_2} & \frac{^{t+\Delta t}\partial x_2}{^{t}\partial x_3} \\ \frac{^{t+\Delta t}\partial x_3}{^{t}\partial x_1} & \frac{^{t+\Delta t}\partial x_3}{^{t}\partial x_2} & \frac{^{t+\Delta t}\partial x_3}{^{t}\partial x_3} \end{bmatrix} \tag{3-32}$$

This deformation gradient serves as transformation for other quantities too, e.g. as for the normal tensors of surfaces

$$^{t+\Delta t}\hat{n} = \hat{X}^{-T}\,{}^{t}\hat{n} \tag{3-33}$$

The changes in volumes in three dimensional bodies

$$^{t+\Delta t}dV = \det(\hat{X})\,{}^{t}dV \tag{3-34}$$

that are as well appropriate for the special cases of one and two dimensional problems, thus involving lengths and areas. Hence, the mapping of a directed surface element area from the initial to the current configuration is given by the Nanson formula [223]

$$^{t+\Delta t}\hat{n}\,{}^{t+\Delta t}dA = \det(\hat{X})\hat{X}^{-T}\,{}^{t}\hat{n}\,{}^{t}dA \tag{3-35}$$

An associated deflection gradient can be derived from Eq. (3-8) by

$$\nabla\hat{u} = \nabla^{t+\Delta t}\hat{x} - \nabla^{t}\hat{x} = \hat{X} - \hat{X}\hat{X}^{-1} = \hat{X} - \hat{I} \tag{3-36}$$

with $\hat{I}$ as the unity tensor, resulting in

$$\nabla\hat{u} = \begin{bmatrix} \frac{\partial u_1}{^{t}\partial x_1} & \frac{\partial u_1}{^{t}\partial x_2} & \frac{\partial u_1}{^{t}\partial x_3} \\ \frac{\partial u_2}{^{t}\partial x_1} & \frac{\partial u_2}{^{t}\partial x_2} & \frac{\partial u_2}{^{t}\partial x_3} \\ \frac{\partial u_3}{^{t}\partial x_1} & \frac{\partial u_3}{^{t}\partial x_2} & \frac{\partial u_3}{^{t}\partial x_3} \end{bmatrix} \tag{3-37}$$

3.7 Tensor strain measures

As outlined before, the total strains are derived from their relationship to the displacements

$$\hat{\varepsilon}(x) = \varepsilon(\hat{u}(x)) = \begin{bmatrix} \varepsilon_{11} & \varepsilon_{12} & \varepsilon_{13} \\ \varepsilon_{21} & \varepsilon_{22} & \varepsilon_{23} \\ \varepsilon_{31} & \varepsilon_{32} & \varepsilon_{33} \end{bmatrix} \tag{3-38}$$

One appropriate, but more theoretical linear strain measure is the Cauchy strain

$$\hat{\varepsilon}_C = \hat{X} - \hat{I} \tag{3-39}$$

This is more often applied in it′s symmetric form, that is preferred in small deformation mechanics and called engineering strain

$$\hat{\varepsilon}_{eng} = \mathrm{sym}(\hat{\varepsilon}_C) = \frac{1}{2}(\hat{X} + \hat{X}^T) - \hat{I} \tag{3-40}$$

For large deformation compatible strain measures, the properties within the deformation gradient need to be explored. For consideration of rigid body rotations the deformation gradient is splitted using polar decomposition

$$\hat{X} = \hat{L}^T \cdot \hat{U} \tag{3-41}$$

that divides the deformation gradient into a left orthogonal rotation tensor $\hat{L}$ determining the rigid body rotations, and a symmetric tensor $\hat{U}$, known as the stretch tensor. The rotation tensor is identical to the rotational transformation matrix introduced in Eq. (3-9).

Alternatively, the polar decomposition can be expressed in terms of the right rotation tensor $\hat{R}$

$$\hat{X} = \hat{U} \cdot \hat{R}^{-1} \tag{3-42}$$

thus

$$\hat{U} = \hat{X} \cdot \hat{R} \quad \text{with} \quad \hat{R} = \hat{X}^{-1}\hat{L}\hat{X} \tag{3-43}$$

The polar decomposition is commonly calculated from the Cauchy tensor, defined as

$$\hat{C} = \hat{X}^T\hat{X} = \hat{U}^T\hat{L}\hat{L}^T\hat{U} = \hat{U}^T\hat{U} \tag{3-44}$$

It can be seen that this tensor is insensitive to rotations. According to this approach (Tab. 3-2), the stretch tensor can be calculated from the eigenvectors $\hat{T}_C$ of the Cauchy tensor

$$\hat{U} = \hat{T}_C\hat{\Lambda}\hat{T}_C^T \tag{3-45}$$

with the principal stretch tensor

$$\hat{\Lambda} = \left(\hat{T}_C^T\hat{C}\hat{T}_C\right)^{\frac{1}{2}} \tag{3-46}$$

Alternatively, the transformation matrices $\hat{L}$ and $\hat{R}$ can be directly calculated from the geometry gradient $\hat{X}$, as it is illustrated in Tab. 3-3. For three-dimensional problems the procedure is iterative. In practice, only a small number of iterations is required to gain sufficent accuracy. The method is extremely fast for two dimensional deformation gradients, as no iterations are necessary. The procedure is summarized in Tab. 3-4.

In order to avoid square root operations during strain determinations (as discussed for Method (a) in Sec. 3.5), modifications of the Cauchy strains are often directly used as

Table 3-2 Polar decomposition of deformation gradient (regular approach)

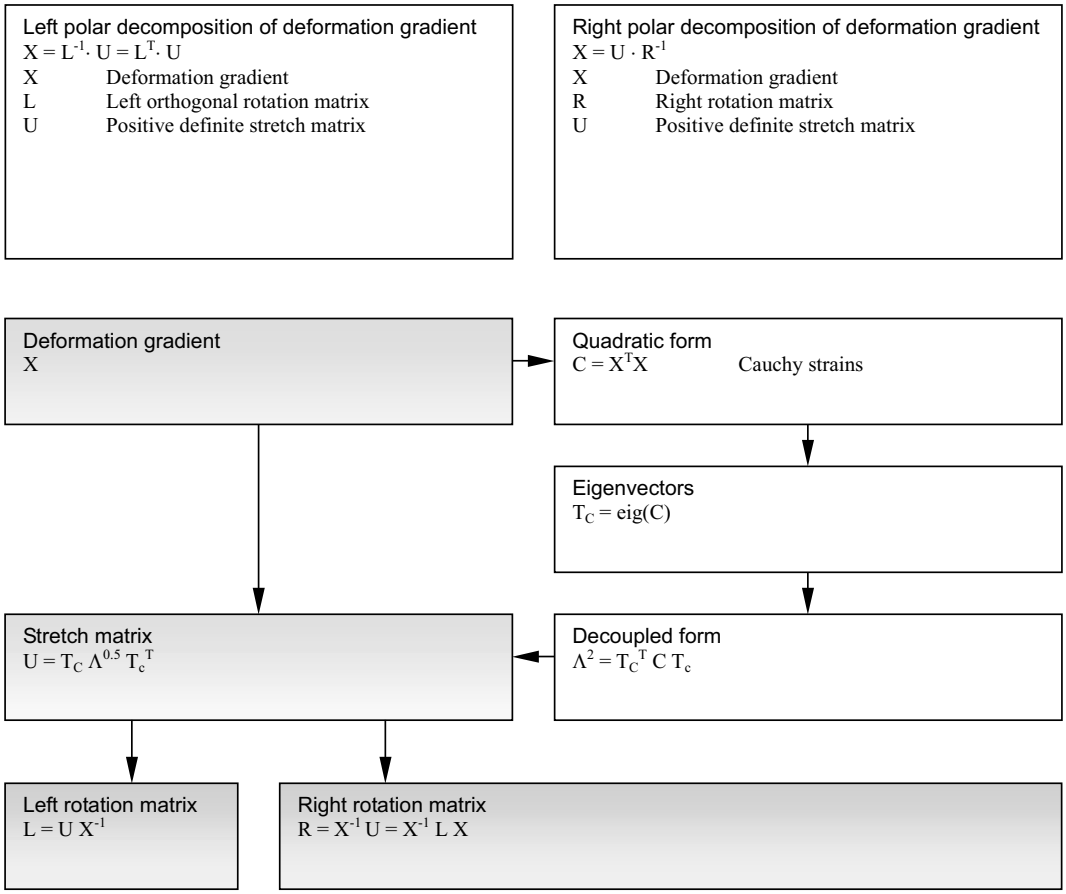

strain measures [22,223]. For example, the Cauchy strains are the basis for the Green-Lagrangian tensor

$$\hat{\varepsilon}_{quad} = \frac{1}{2}\left(\hat{X}^T\hat{X} - \hat{I}\right) = \frac{1}{2}\left(\hat{C} - \hat{I}\right) \tag{3-47}$$

The advantage is the simplicity of the derived mechanical relations. The Hencky strains (3-19) are calculated as

$$\hat{\varepsilon}_{log} = \ln \hat{U} \tag{3-48}$$

For practical purposes, nominal measures according to Eq. (3-17) are often preferred, generalized in three dimensions:

$$\hat{\varepsilon}_{nom} = \hat{U} - \hat{I} \tag{3-49}$$

Contradictory to engineering measures, this formulation avoids the influence of the rigid body motion and has the advantage of material compatiblity to linear strains.

Table 3-3 Polar decomposition of geometry gradient (Orthogonal transformation approach)

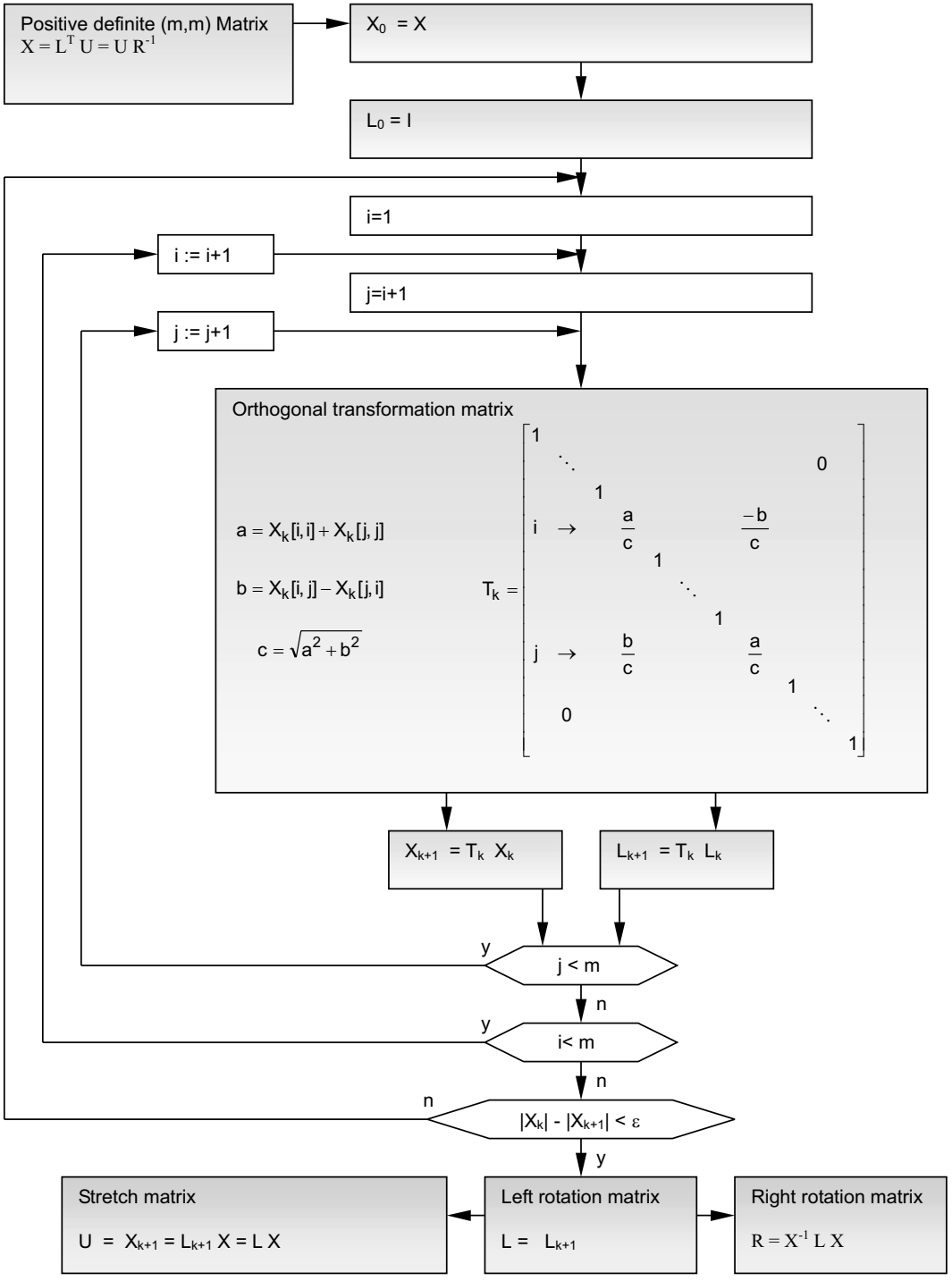

Table 3-4 Polar decomposition of 2D-geometry gradient (Orthogonal transformation approach)

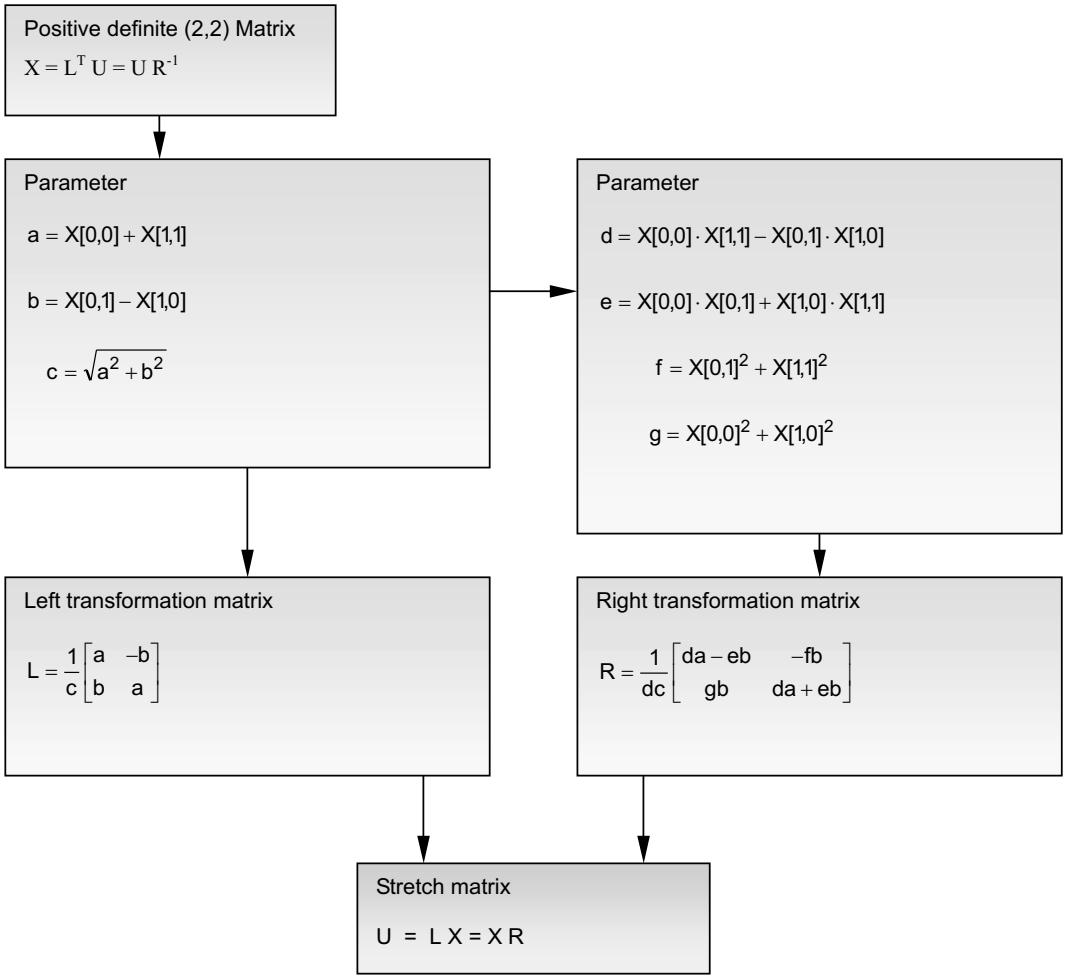

Generalizing, a common form of strain calculations can be declared. It is convenient to understand the large strain theory as an extension to the linear theory. Then, any strain calculation can be stated in a linear form

$$\hat{\varepsilon} = \hat{X} \cdot \hat{T}_u - \hat{I} \tag{3-50}$$

with $\hat{T}_u$ as the transformation tensor of the kinematic conditions, that contains strain measure transformations and rigid body rotations. The tensor is calculated, if ε is exchanged by any appropriate strain measure. It is obvious, that for Cauchy strains $\hat{T}_u = \hat{I}$ and for nominal strains $\hat{T}_u = \hat{R}$.

3.8 Kinematic condition

The kinematic condition relates the internal to the external strain configuration. Combining different internal components, the total strains can be assembled from several parts e.g. from elastic, plastic and predefinded parts, thus

$$d\varepsilon = d\varepsilon_{total} - (d\varepsilon_e + d\varepsilon_p + d\varepsilon_0 + \ldots) \tag{3-51}$$

This is true if all components are defined on the same strain measure basis. Otherwise, transformations to a reference measure must be conducted. Finally, the kinematic condition reads

$$d\varepsilon = 0 \qquad \in V \tag{3-52}$$

3.9 Material law

The material relation is either given as a function of strains

$$\hat{\sigma} = \sigma(\hat{\varepsilon}) \tag{3-53}$$

or as it′s reverse

$$\hat{\varepsilon} = \varepsilon(\hat{\sigma}) \tag{3-54}$$

An often applied differential stress-strain relationship is the special case of elastic material, the relation between strains and stresses is defined by Hook′s law

$$\hat{\varepsilon}_e = \hat{D}\hat{\sigma} \tag{3-55}$$

with $\hat{D}$ as a forth order constitutive tensor. In practical cases, $\hat{D}$ often simplifies due to symmetric properties, e.g. of isotropic or orthotropic materials. The determination of the material tensor $\hat{D}$ is dependend on the selected measures for the stresses and strains. The use of work-conjugated pairs of strains and stresses is often applied. Transformations between different stress measures can be considered in the eqilibrium condition. Changing strain measures is conducted in the kinematic condition. Hence, the energy balance may require a modification in the material tensors $\hat{D}$ as well. An example is given in Fig. 3-5. Very often, hyper-elastic material laws are considered in software codes using the large deformation theory [1,6].

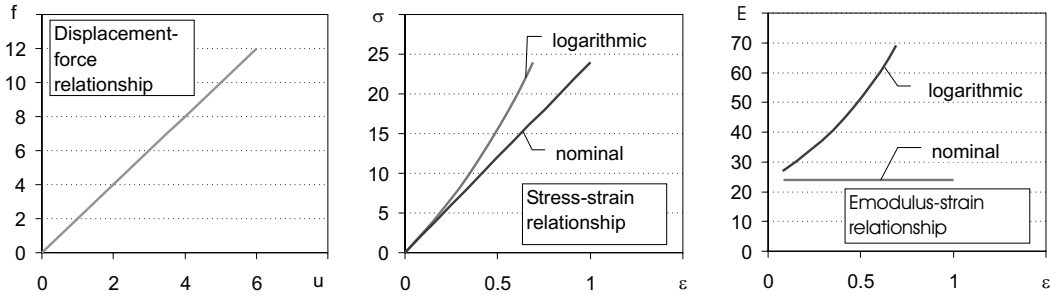

Figure 3-5 Differences in nominal and logarithmic strain measures for a linear force/ displacement relationship

In order to determine the appropriate components of the material tensor, multi-axial tests can be conducted. In these tests, the initial and current geometry can be monitored for a given load intensity. After loading, the deformation gradient X can be calculated directly from the geometry changes. This is the basis to determine the strains ε, dependend on the selected measure, e.g. with Eq. (3-47-3-49). On the other hand, the force is used to determine the stresses, e.g. the Cauchy stresses in the direction i

$$\sigma_i = \frac{f_i}{{}^{t+\Delta t}A_i} \tag{3-56}$$

From this, transformations into selected stress measures can be calculated. The selection of appropriate stress-strain pairs is mostly done with a view to effective handling in calculation. In material science the combination of Green-Lagrangian strains with 2nd Piola-Kirchhoff stresses is preferred. In structural engineering, most material laws are given for nominal stress-strain parameters, that can be adopted from the geometrically linear theory.

Plastic deformations ε_p can develop if a yield function Y is fulfilled:

$$Y(\varepsilon) = 0 \tag{3-57}$$

Within this study, Y is always assumed to be a convex function. A formulation in terms of stresses σ is more often preferred, leading to an expression for perfect plasticity

$$Y_{YF}(\sigma) = 0 \tag{3-58}$$

The appropriate plastic strains are calculated from

$$d\varepsilon_p = d\lambda \frac{\partial Y_{PS}}{\partial \sigma} \tag{3-59}$$

with the plastic multiplier λ, having the property of non-negativity

$$\lambda \geq 0 \tag{3-60}$$

The multiplier is a general unknown of the augmented Lagrange problem and can be calculated by introduction of the extended kinematic condition into the yield function.

Beyond perfect plasticity, as in Eq. (3-58), real materials develop hardening effects, thus the yield function can be extended, e.g. in dependency to the plastic multipiers

$$Y_{YF}(\sigma, \lambda) = 0 \tag{3-61}$$

In compliance with the Drucker stability postulate [71], the product of the stress and plastic deformations rate is positive

$$d\sigma d\varepsilon_p \geq 0 \tag{3-62}$$

The yield law is called "associated" if the derivatives of the yield condition in the yield function Eq. (3-58) and plastic strain condtion Eq. (3-59) are identical

$$\frac{\partial Y_{PS}}{\partial \sigma} = \frac{\partial Y_{YF}}{\partial \sigma} = \frac{\partial Y}{\partial \sigma} \tag{3-63}$$

Large strain problems often raise questions about the volumetric behavior of the considered body during extreme excitation. The rate in volume change can be described as a function of the current deformation state and time

$$dV = V({}^{t+dt}dx, dt) \tag{3-64}$$

or even as a inequality condition

$$dV \leq V({}^{t+dt}dx, dt) \tag{3-65}$$

A special case is the isochoric behavior, where

$$dV = 0 \tag{3-66}$$

The change in volume within the time step dt can be evaluated with the change of the geometric gradient

$$dV = \frac{\det({}^{t+dt}\hat{X})}{\det({}^{t}\hat{X})} \tag{3-67}$$

3.10 Stresses and Equilibrium

The equlibrium ensures the equivalence of all forces in the system. Within this context it provides a relation between the external forces and stresses (internal forces) in the body. Generally for an infinitesimal volume, the internal stresses are

$$\hat{\tau} = -\frac{{}^{t+\Delta t}d\hat{\phi}}{{}^{t+\Delta t}dA} \tag{3-68}$$

for the current area ${}^{t+\Delta t}dA$ loaded by external forces ${}^{t+\Delta t}d\hat{\phi}$. All parameters are given in the current configuration and same direction ${}^{t+\Delta t}\hat{n}$, that describes the orientation of the loaded surface within the coordinate system.

The equilibrium requires the sum of all internal forces to vanish. The equation can be directly obtained from Eq. (3-68), integrating over the appropriate regions

$$\hat{\tau}\,{}^{t+\Delta t}dA + {}^{t+\Delta t}d\hat{\phi} = 0 \tag{3-69}$$

The transformation between surface-oriented stresses $\hat{\tau}$ and volumetric-oriented Cauchy stresses $\hat{\sigma}_C$ can be formulated as

$$\hat{\tau} = \hat{\sigma}_C\,{}^{t+\Delta t}\hat{n} \tag{3-70}$$

with the vector of direction cosines ${}^{t+\Delta t}\hat{n}$ of the normal to the plane on which the forces act. The Cauchy stresses can be assigned to three coordinate directions to form a 2nd order tensor

$$\hat{\sigma}_C = \begin{bmatrix} \sigma_{11} & \sigma_{12} & \sigma_{13} \\ \sigma_{21} & \sigma_{22} & \sigma_{23} \\ \sigma_{31} & \sigma_{32} & \sigma_{33} \end{bmatrix} \tag{3-71}$$

With substitution of Eq. (3-70) into Eq. (3-69), the equilibrium reads

$$\hat{\sigma}_C\,{}^{t+\Delta t}\hat{n}\,{}^{t+\Delta t}dA + {}^{t+\Delta t}d\hat{\phi} = 0 \tag{3-72}$$

Furthermore, the stresses in the current configuration of an infinitesimal volume can be related to the surface in the initial configuration by application of Eq. (3-35), thus giving

$$\hat{\sigma}_C\ \det(\hat{X})\hat{X}^{-T}\,{}^{t}\hat{n}\,{}^{t}dA + {}^{t+\Delta t}d\hat{\phi} = 0 \tag{3-73}$$

Here another stress measure can be defined by the 1st Piola-Kirchhoff stress tensor

$$\sigma_P = \hat{\sigma}_C\ \det(\hat{X})\hat{X}^{-T} \tag{3-74}$$

thus the equilibrium is

$$\hat{\sigma}_P\,{}^{t}\hat{n}\,{}^{t}dA + {}^{t+\Delta t}d\hat{\phi} = 0 \tag{3-75}$$

Using the Gauss/Ostrogradski theorem [39]

$$\hat{\sigma}_P\,{}^{t}\hat{n}{}^{t}dA = \frac{\partial}{\partial x}\hat{\sigma}_P\,{}^{t}dV \tag{3-76}$$

leads to

$$\frac{\partial}{\partial x}\hat{\sigma}_P\, {}^t dV + {}^{t+\Delta t}d\hat{\phi} = 0 \tag{3-77}$$

This is the most common applied form of equilibrium conditions. It can be modified to fit for other stress measures. To provide a general form that is not dependent on the applied stress definition, the equilibrium conditions can be witten as

$$\frac{\partial}{\partial x}\hat{\sigma}\ \ T_s\, {}^t dV + {}^{t+\Delta t}d\hat{\phi} = 0 \tag{3-78}$$

Herein σ is the selected stress and $\hat{T}_s$ is the appropriate transformation tensor of the equilibrium conditions, governing the stress measure switches and rigid body transformations.

For instance, some implementations of the Hencky type theory use, e.g. [6]

$$\sigma T_s = \sigma_{log}\ \det(\hat{X})\hat{X}^{-T} \tag{3-79}$$

As the nominal (Biot) stresses are

$$\sigma_{nom} = L\sigma_P \tag{3-80}$$

the implementation is as follows

$$\sigma T_s = \sigma_{nom} L^T \tag{3-81}$$

If the forces are given in the initial configuration, the following transformation holds

$${}^t d\hat{\phi} = X^{-1}\ \ {}^{t+\Delta t}d\hat{\phi} \tag{3-82}$$

Then, the equilibrium is as follows

$$\frac{\partial}{\partial x}\hat{\sigma}_P\, {}^t dV + \hat{X}\, {}^t d\hat{\phi} = 0 \tag{3-83}$$

or re-arranged

$$\frac{\partial}{\partial x}\hat{X}^{-1}\hat{\sigma}_P\, {}^t dV + {}^t d\hat{\phi} = 0 \tag{3-84}$$

and with introduction of the 2st Piola-Kirchhoff stress

$$\hat{\sigma}_{quad} = \hat{X}^{-1}\,\hat{\sigma}_C\ \det(\hat{X})\hat{X}^{-T} = \hat{X}^{-1}\,\hat{\sigma}_P \tag{3-85}$$

a special form of the equilibrium conditions is obtained

$$\frac{\partial}{\partial x}\hat{\sigma}_{quad}\, {}^t dV + {}^t d\hat{\phi} = 0 \tag{3-86}$$

The stress measures can be exchanged by other measures. These basics are intensively shown throughout the literature, e.g. [22,14,32,170].

Generally, pairs of strain and stress measures can almost arbitrarely be selected. However, reasonable combinations are only obtained, if the pairs of strains ε and stresses σ have the same configuration basis and being "work-conjugate". They can be directly used to express the internal work rate

$$dW_{intern} = \sigma d\varepsilon \tag{3-87}$$

that is typically derrived by transformations from the reference pair Cauchy stresses σ_C and tensor of deformation velocity D, as in [168]

$$dW_{intern} = \sigma d\varepsilon = \sigma_C D \tag{3-88}$$

for pairs in the current configuration and

$$dW_{intern} = \sigma d\varepsilon = \sigma_C D \det X \tag{3-89}$$

for pairs in the initial configuration, involving the volumetric change in the transformation.

3.11 Static and geometric boundary conditions

The static boundary condition provides an equation, that specifies the stresses at the surface S_s of the considered volume

$$\hat{\sigma}\hat{n}_s - \hat{\sigma}_0 = 0 \qquad \in S_s \tag{3-90}$$

It is obvious, that this formulation is formally similar to Eq. (3-70).

The geometric boundary condition relates the deflections $\hat{u}$ of material points at the surface S_u to given deflections $\hat{u}_0$

$$\hat{u}\hat{n}_u - \hat{u}_0 = 0 \qquad \in S_u \tag{3-91}$$

The direction cosines are given with the tensors $\hat{n}_s$ and $\hat{n}_u$.

3.12 Static forces, inertia and damping

Forces within the structure can be of different origin. In structural dynamics, according to d′Alemberts principle, the forces can be separated due to static effects $\hat{d\phi}_{Stat}$, inertia $\hat{d\phi}_M$ and damping $\hat{d\phi}_C$, and so on:

$$\hat{d\phi} = \hat{d\phi}_M + \hat{d\phi}_C + \hat{d\phi}_{Stat} + \dots \tag{3-92}$$

The static forces are distributed throughout the volume V, or along a surface S or as concentrated forces

$$\hat{d\phi}_{Stat} = \hat{\varphi}_V dV + \hat{\varphi}_S dS_f + f_j \tag{3-93}$$

The inertia forces are dependent on the density ρ, and the acceleration $\hat{\ddot{u}}$ within the body

$$d\hat{\phi}_M = \hat{\rho}\hat{\ddot{u}}dV \tag{3-94}$$

The damping can be given similarely, introducing the damping density ν and the velocity $\hat{\dot{u}}$

$$\hat{d}\phi_C = \hat{\nu}\hat{\dot{u}}dV \tag{3-95}$$

It should be noted, that all of these quantities can change throughout motion and deformations. The appropriate transformations need to be applied, typically volumetric adaptions as in Eq. (3-34).

4 Discrete systems and matrix formulations

4.1 Discretization

For numerical evaluation only a finite set of parameters needs to be considered. For the necessary approximation of continuum mechanical problems, discretization procedures for time and space are applied. Subspaces (elements) or time steps are selected, that behave less complex as the overall system and therefore can be simplified. In the resulting meshes, the governing functions of the discrete problem are expressed with respect to a limited number of reasonable selected times or positions. Besides others, often used discretization methods for solving boundary value problems in structural dynamics are:

- Finite Element Method (FEM) [22,230]
- Element Free Galerkin method (EFG) [27,28,29]

that are considered within this study. The concepts apply different discretization strategies. In the traditional FEM and EFG, the time discretization is done with help of finite differences, whereas trial functions are applied for volume discretization (Tab. 4-1). In the following sections the basic approaches are summarized.

For numerical calculations it is necessary to derive a matrix/vector form of the governing equations and inequalities. Appropriate tensor-matrix transformation operators need to be defined. In the appendix Sec. 11.1, examples for three-dimensional operators are provided.

Table 4-1 Discretization categories in structural dynamics

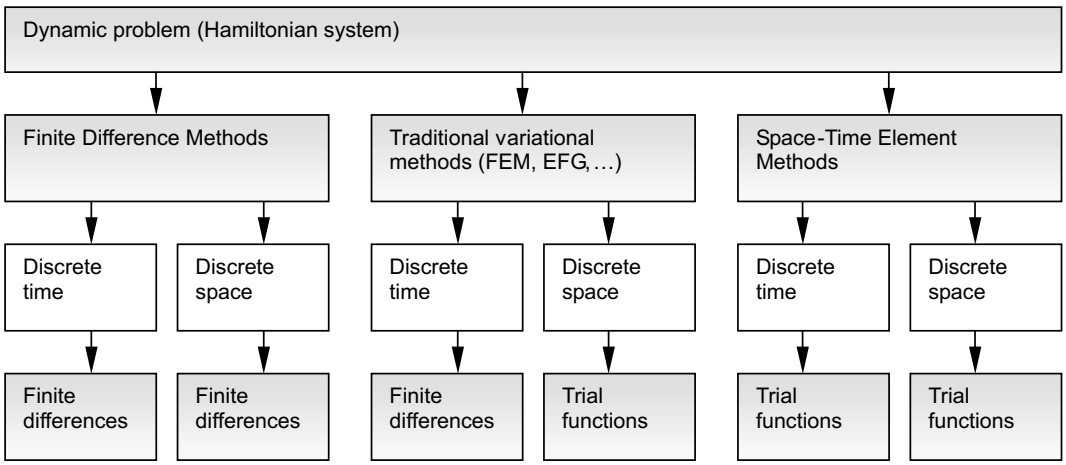

4.2 Geometry

The behavior of the element is expressed as functions of the parameters given in a grid of discrete points (nodes, times). The nodes can be identified at a discrete time t in a Cartesian coordinate system by the location matrix

$$ {}^t\hat{x}_N = diag\left[{}^tx_1, {}^tx_2, {}^tx_3\right]^T \qquad \in V \tag{4-1} $$

The directions are independent, so a vector form

$$ {}^tx_N = {}^t\hat{x}_N \cdot I \tag{4-2} $$

with I as the unity vector is often used as well. After a time step Δt the same node is characterized by

$$ {}^{t+\Delta t}\hat{x}_N = diag\left[{}^{t+\Delta t}x_1, {}^{t+\Delta t}x_2, {}^{t+\Delta t}x_3\right]^T \qquad \in V \tag{4-3} $$

The subspaces considered as elements (e.g. in FDM, FEM) or supports (e.g. in EFG) are defined by associated nodes. The node coordinates, belonging to one element, can be assembled, independent from the considered time

$$ x_E = \left[x_{N1}^T, \ldots, x_{Nn}^T\right]^T \tag{4-4} $$

Any point within the element can be addressed by geometric field equations

$$ x = H_g(x) \cdot x_E \tag{4-5} $$

that consists of the interpolation matrix H_g

$$ H_g(x) = P_g(x) \cdot G_g(x_E)^{-1} \tag{4-6} $$

The matrix P_g is the polynomial interpolation function, commonly consisting of complete polynomials of the linear Lagrange type. The appropriate coefficients are provided with the inverse of the nodal polynomial function

$$ G_g(x_E) = \left[P_g(x_{N1}), \ldots, P_g(x_{Nn})\right]^T \tag{4-7} $$

Coordinates in different times can be assessed by implementing directly

$$ {}^{t+\Delta t}x = H_g({}^tx) \cdot {}^{t+\Delta t}x_E \tag{4-8} $$

where the shape matrix can be defined for a reference system (time t). The derivative relation at different times was introduced in Eq. (3-30) with the geometry gradient

$$ \hat{X}_g = {}^{t+\Delta t}\hat{x}_E \cdot \frac{\partial H_g({}^t\hat{x})}{\partial x} \tag{4-9} $$

For different times the derivatives can be directly calculated from:

$$\frac{\partial H_g({}^{t+\Delta t}\hat{x})}{\partial x} = \frac{\partial H_g({}^{t}\hat{x})}{\partial x} \cdot \hat{X}_g^{-1} \tag{4-10}$$

4.3 Displacements

The difference in coordinate positions through time is the displacement u

$$\hat{u}_N = {}^{t+\Delta t}x_N - {}^{t}x_N = diag\,[u_1, u_2, u_3]^T \qquad \in V \tag{4-11}$$

The element′s nodal displacements can be assembled as

$$\hat{u}_E = \left[\hat{u}_{N1}^T, \ldots, \hat{u}_{Nn}^T\right]^T \tag{4-12}$$

The displacement behavior between the nodes of a subregion is described by shape (or trial) functions, that are usually formed from polynomials with potentials from x and appropriate coefficients a_u

$$\hat{u}(x) = \hat{P}_u(x) \cdot \hat{a}_u \tag{4-13}$$

The polynomial matrix of the displacements $\hat{P}_u(x)$ is preselected in FEM, according to the order of the selected shape function. The coefficient matrix a_u can be calculated from the node values

$$\hat{u}_E = \hat{G}_u \cdot \hat{a}_u \tag{4-14}$$

with

$$\hat{G}_u = [P_u(\hat{x}_{N1}), \ldots, P_u(\hat{x}_{Nn})]^T \tag{4-15}$$

If the number of unknowns in the element and the number of shape functions as well as the shape function order are compatible, the matrix G_u is invertible, then

$$\hat{a}_u = \hat{G}_u^{-1} \cdot \hat{u}_E \tag{4-16}$$

Combining Eq. (4-13) and (4-16) leads to

$$\hat{u}(x) = \hat{P}_u(x)\hat{G}_u^{-1} \cdot \hat{u}_E \tag{4-17}$$

thus any material point in the considered subregion can be addressed. The direct invertibility of G_u is requested in FEM. In other methods, like the Element Free Galerkin method, the matrix G_u is non-quadratic, from over-determination. This can be eliminated by interpolation methods. Besides others concepts [156], most popular in this context is the Moving Least Square method [136]. The method first constructs a non-singular quadratic matrix

$$\hat{\Gamma}_1 = \hat{w}_{EFG} \cdot \hat{G}_{EFG} \hat{G}_{EFG}^T \tag{4-18}$$

where G_{EFG} is constructed similar to (4-15), but is in general non-quadratic. Additionally a weight vector w_{EFG} is introduced that evaluates the contribution of the considered node to the result at the considered point x. Often spline type functions are used e.g. the cubic spline interpolation function with radius r around the considered point x [27]

$$w(r) = \begin{cases} \frac{2}{3} - 4r^2 + 4r^3 & for\, r \leq 0.5 \\ \frac{4}{3} - 4r + 4r^2 & for\, 0.5 < r \leq 1.0 \\ 0 & for\, r > 1.0 \end{cases} \tag{4-19}$$

An example is given in Fig. 4-1. A second matrix is defined

$$\hat{\Gamma}_2 = \hat{w}_{EFG} \cdot \hat{G}_{EFG} \tag{4-20}$$

that together with Eq. (4-18) gives finally

$$\hat{G}_u^{-1} = \hat{\Gamma}_1^{-1} \hat{\Gamma}_2 \tag{4-21}$$

so that Eq. (4-17) can be used similarly to the FEM concept. Equation (4-17) is commonly shortened to

$$\hat{u}(x) = \hat{H}_u(x) \cdot \hat{u}_E \tag{4-22}$$

with $\hat{H}_u(x)$ as the matrix of the displacement shape function. In case that $\hat{H}_u(x)$ is identical with the interpolation matrix of the geometry $\hat{H}_g(x)$ from Eq. (4-5), the formed element is called ′isoparametric′.

The nodal deformations can be expressed in vector form as

$$u_N = \hat{u}_N \cdot I \tag{4-23}$$

Accordingly, the element displacements are

$$u_E = \left[u_{N1}^T, \ldots, u_{Nn}^T\right]^T \tag{4-24}$$

4.4 Geometric boundary conditions

The geometric boundary conditions relate the displacements on the surface of a body to a set of pre-defined displacements. In discretized systems, continuous boundary definitions are transformed into discrete formulations by application of form functions, e.g. in a linear formulation the geometric boundary condition reads

$$\begin{aligned} &N_u(x) H_u(x) u_E - u_0(x) = N_u(x) H_u(x) u_E - H_u(x) u_0(x_E) \\ &= N_u(x) u_E - u_0(x_E) = 0 \qquad \in S_u \end{aligned} \tag{4-25}$$

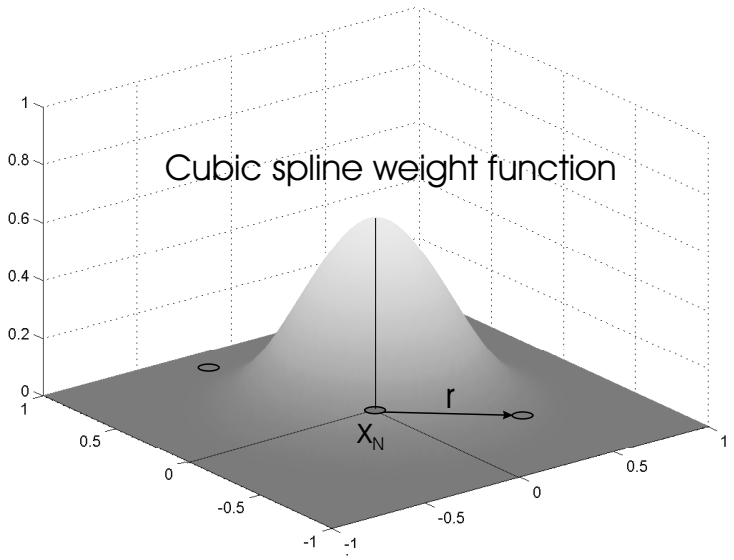

Figure 4-1 Example weight function

The matrix N_u is the direction matrix, that additionally identifies a material point to be a part of the geometrically predetermined boundary S_u. Any applied kinematic boundary condition induces a resisting support force c_s as a dual parameter.

A special case of geometric boundary conditions are contact problems. They can be mathematically formulated as inequality conditions

$$N_u(x)u_E - u_0(x_E) \leq 0 \tag{4-26}$$

Whereas the consideration of contact conditions in traditional finite element calculations involves the organization of an iterative calculation strategy. The consideration of such inequality conditions within optimization problems is straightforward.

4.5 Total strain/displacement relationship

As sketched in Sec. 3.7, the strain measures for large deformations can be interpreted as an extension of the linear (Cauchy) theory. The basic derivation of the linear coefficient matrices from continuum mechanics is illustrated in Tab. 4-2 including the engineering simplifications. The linear strains can be derived from the symmetric part of the displacement derivatives

$$\hat{B}_u(x) = \left(\frac{\partial}{\partial x}\right) \tag{4-27}$$

The ignorance of the antimetric part, that contains the rotational components, is characteristic for linear approximations.

Table 4-2 Derivation of engineering operator matrix of kinematic conditions

Position change of a material point

$$^{t+\Delta t}\hat{x} = {}^{t}\hat{x} + \hat{u}$$

Strain tensor separation

$$\hat{\varepsilon} = \nabla\hat{u} = \frac{\partial u_i}{\partial x_j} = \underbrace{\frac{1}{2}\left(\frac{\partial u_i}{\partial x_j} + \frac{\partial u_j}{\partial x_i}\right)}_{\text{symmetric}} + \underbrace{\frac{1}{2}\left(\frac{\partial u_i}{\partial x_j} - \frac{\partial u_j}{\partial x_i}\right)}_{\text{antimetric } \overset{!}{=} 0 \text{ (engineering model)}}$$

Strain tensor (symmetric part)

$$\hat{\varepsilon} = \frac{1}{2}\left(\frac{\partial u_i}{\partial x_j} + \frac{\partial u_j}{\partial x_i}\right) = \begin{bmatrix} \frac{\partial u_1}{\partial x_1} & \frac{1}{2}\left(\frac{\partial u_1}{\partial x_2} + \frac{\partial u_2}{\partial x_1}\right) & \frac{1}{2}\left(\frac{\partial u_1}{\partial x_3} + \frac{\partial u_3}{\partial x_1}\right) \\ & \frac{\partial u_2}{\partial x_2} & \frac{1}{2}\left(\frac{\partial u_2}{\partial x_3} + \frac{\partial u_3}{\partial x_2}\right) \\ \text{symm.} & & \frac{\partial u_3}{\partial x_3} \end{bmatrix}$$

Transformation into vector/matrix formulation

Strain vector and operator matrix (engineering model)

$$\varepsilon = \begin{bmatrix} \varepsilon_{11} \\ \varepsilon_{22} \\ \varepsilon_{33} \\ 2\gamma_{12} \\ 2\gamma_{23} \\ 2\gamma_{13} \end{bmatrix} = \begin{bmatrix} \frac{\partial u_1}{\partial x_1} \\ \frac{\partial u_2}{\partial x_2} \\ \frac{\partial u_3}{\partial x_3} \\ \frac{\partial u_1}{\partial x_2} + \frac{\partial u_2}{\partial x_1} \\ \frac{\partial u_2}{\partial x_3} + \frac{\partial u_3}{\partial x_2} \\ \frac{\partial u_1}{\partial x_3} + \frac{\partial u_3}{\partial x_1} \end{bmatrix} = B_u u = \begin{bmatrix} \frac{\partial}{\partial x_1} & & \\ & \frac{\partial}{\partial x_2} & \\ & & \frac{\partial}{\partial x_3} \\ \frac{\partial}{\partial x_2} & \frac{\partial}{\partial x_1} & \\ & \frac{\partial}{\partial x_3} & \frac{\partial}{\partial x_2} \\ \frac{\partial}{\partial x_3} & & \frac{\partial}{\partial x_1} \end{bmatrix} \cdot \begin{bmatrix} u_1 \\ u_2 \\ u_3 \end{bmatrix}$$

The derivative matrix of the displacement field with respect to element shape functions can be directly calculated from the shape functions Eq. (4-22)

$$\left(\frac{\partial \hat{P}_u(x) \cdot \hat{G}_u^{-1}}{\partial x} \right) = \hat{B}_u(x) \hat{H}_u(x) \tag{4-28}$$

In Sec. 3.7 a general form of the kinematic condition was proposed, that can be stated independently from the selected strain measure. The general transformation tensor $\hat{T}_u$ is within the kinematic condition

$${}^{t+\Delta t}\hat{\varepsilon}(x) = {}^{t+\Delta t}\hat{T}_u(x) \hat{B}_u(x) \hat{H}_u(x) {}^{t+\Delta t}x_E - \hat{I} \tag{4-29}$$

As known from Sec. 3, the strain measures can be derived from the deformation gradient X_u

$${}^{t+\Delta t}\hat{X}_u(x) = \hat{B}_u(x) \hat{H}_u(x) {}^{t+\Delta t}x_E \tag{4-30}$$

thus

$${}^{t+\Delta t}\hat{\varepsilon}(x) = {}^{t+\Delta t}\hat{T}_u(x) {}^{t+\Delta t}\hat{X}_u(x) - \hat{I} \tag{4-31}$$

The transformation tensor ${}^{t+\Delta t}\hat{T}_u(x)$ is dependent on the selected strain measure and can be generally calculated from reversing Eq. (4-31), thus

$${}^{t+\Delta t}\hat{T}_u(x) = ({}^{t+\Delta t}\hat{\varepsilon}(x) - \hat{I}) {}^{t+\Delta t}\hat{X}_u^{-1}(x) \tag{4-32}$$

while replacing the strains ${}^{t+\Delta t}\hat{\varepsilon}(x)$, e.g. with either of

$${}^{t+\Delta t}\hat{\varepsilon}_C(x) = {}^{t+\Delta t}\hat{X}_u(x) - \hat{I} \tag{4-33}$$

$${}^{t+\Delta t}\hat{\varepsilon}_{nom}(x) = {}^{t+\Delta t}\hat{L} {}^{t+\Delta t}\hat{X}_u(x) - \hat{I} = \hat{U} - \hat{I} \tag{4-34}$$

$${}^{t+\Delta t}\hat{\varepsilon}_{log}(x) = \ln({}^{t+\Delta t}\hat{L} {}^{t+\Delta t}\hat{X}_u(x)) = \ln \hat{U} \tag{4-35}$$

$${}^{t+\Delta t}\hat{\varepsilon}_{quad}(x) = 0.5 * ({}^{t+\Delta t}\hat{X}_u^T(x) {}^{t+\Delta t}\hat{X}_u(x) - \hat{I}) = 0.5(\hat{C} - \hat{I}) \tag{4-36}$$

Now with Eq. (4-32) and (4-33) any of the strain measures can be written as a function of the Cauchy strains

$${}^{t+\Delta t}\hat{\varepsilon}(x) = {}^{t+\Delta t}\hat{T}_u(x) {}^{t+\Delta t}\hat{\varepsilon}_C(x) \tag{4-37}$$

Such strains can evolve from previous strain states, thus Eq. (4-29) can be written as

$${}^{t+\Delta t}\hat{\varepsilon}(x) = \hat{T}_u(x) \hat{B}_u(x) \hat{H}_u(x) ({}^t x_E + u_E) - \hat{I} \tag{4-38}$$

Separating an initial strain condition for time t

$$\hat{\varepsilon}_0 = {}^t\hat{\varepsilon}_C = \hat{B}_u(x)\hat{H}_u(x)^t x_E - \hat{I} \tag{4-39}$$

that itself needs to be a valid Cauchy strain, the equation turns to

$${}^{t+\Delta t}\hat{\varepsilon}(x) = {}^{t+\Delta t}\hat{T}_u(x)(\hat{\varepsilon}_0 + \hat{I} + \hat{B}_u(x)\hat{H}_u(x)u_E) - \hat{I} \tag{4-40}$$

The coefficients of the deformations u_E are simplified, using

$$\hat{A}_u(x) = {}^{t+\Delta t}\hat{T}_u(x)\hat{B}_u(x)\hat{H}_u(x) \tag{4-41}$$

and transformed

$$A_u(x) = \mathrm{spr}(\hat{A}_u(x)) \tag{4-42}$$

with spr as the transcription operator that shifts the tensor form into an equivalent matrix appearance (Sec. 11.1). Accordingly, the transformation tensor ${}^{t+\Delta t}\hat{T}_u(x)$ of the initial strains reads in matrix form

$$T_u(x) = \mathrm{arr}({}^{t+\Delta t}\hat{T}_u(x)) \tag{4-43}$$

And, the vector forms of the strains and initial strains read

$$\varepsilon(x) = \mathrm{vec}({}^{t+\Delta t}\varepsilon(x)) \tag{4-44}$$

$$\varepsilon_0(x) = \mathrm{vec}({}^t\hat{\varepsilon}_C(x)) = \mathrm{vec}(\hat{\varepsilon}_0(x)) \tag{4-45}$$

If static boundary conditions are defined (see Sec. 4.9), the dual support displacements c_u need consideration within the kinematic conditions. Summarizing the matrix form of the kinematic conditions, the following expression is derived

$$\varepsilon = A_u(x)u_E + T_u(x)(\varepsilon_0 + I) - I + N_s^T(x)c_u(x) \tag{4-46}$$

The calculation of all matrices simplifies, if isoparametric elements are applied. Then the shape functions of geometry and displacements are identical and therefore

$$\hat{X}_g(x) = \hat{X}_u(x) = \hat{X}(x) \tag{4-47}$$

4.6 Handling of strain components and increments

As defined in Sec. 3 it is assumed that in linear theory the total strains can be calculated from different strain components e.g.

$$\varepsilon_C = \int d\varepsilon_C = \sum_i \Delta\varepsilon_{C,i} \tag{4-48}$$

e.g as a combination of elastic and plastic contributions.

In nonlinear theory this concept can be adopted almost similarly. As $\hat{\varepsilon}_0$ in Eq. (4-40) could be considered as the sum of different Cauchy strain components, the following equation can be stated

$$^{t+\Delta t}\hat{\varepsilon}(x) = {}^{t+\Delta t}\hat{T}_u(x)\left(\sum_i(\hat{\varepsilon}_{C,i}) + I + \hat{B}_u(x)\hat{H}_u(x)u_E\right) - I \tag{4-49}$$

Either component must be given in a compatible strain measure. Difference in measures A and B can be expressed using the matrix equation

$$\hat{T}_{\varepsilon,A-B} = (\hat{\varepsilon}_A + \hat{I})(\hat{\varepsilon}_B + \hat{I})^{-1} \tag{4-50}$$

and used for strain transformations. For the transformation of material laws, a useful direct transformation formula is

$$\hat{T}_{D,A-B} = \hat{\varepsilon}_A\hat{\varepsilon}_B^{-1} \tag{4-51}$$

provided that $\hat{\varepsilon}_B$ is not evaluated at the zero point. As indicated, the transformation is generally strain dependent. Therefore the transformed material tensor is

$$D_A(\hat{\varepsilon}_A) = \hat{T}_{D,A-B}D_B(\hat{\varepsilon}_B) \tag{4-52}$$

Mostly, the available solid mechanics software is based on persistent nonlinear approaches as symbolized in Tab. 4-4. Alternatively, interfaces between measures (e.g. nonlinear and linear) can be installed at any position as it is illustrated in Tabs. 4-4-4-6, involving strains, stresses or forces separately within the nonlinear measure range. Most compatibility with traditional engineering approaches is obtained, if the nominal strain approach is used throughout any calculation or if the transformations are organized as indicated in Tab. 4-6.

However, the tasks in finite element analysis are widely spreaded, that′s why given finite element programs select one or more strain measures and material descriptions that in combination fits best for the intended situation. To be consistent with most of the applications, tools for least square fittings for determination of appropriate material constants have to be provided e.g. [1].

4.7 Stresses and internal forces

With introduction of appropriate stress shape functions, all stresses within an element can be expressed as functions of the nodal stress values $\hat{\sigma}_N$.

$$\hat{\sigma}_N = \begin{bmatrix} \sigma_{11} & \sigma_{12} & \sigma_{13} \\ \sigma_{21} & \sigma_{22} & \sigma_{23} \\ \sigma_{31} & \sigma_{32} & \sigma_{33} \end{bmatrix} \tag{4-53}$$

All nodal stresses within an element can be summarized within a matrix

Table 4-3 Linear/nominal strain measures

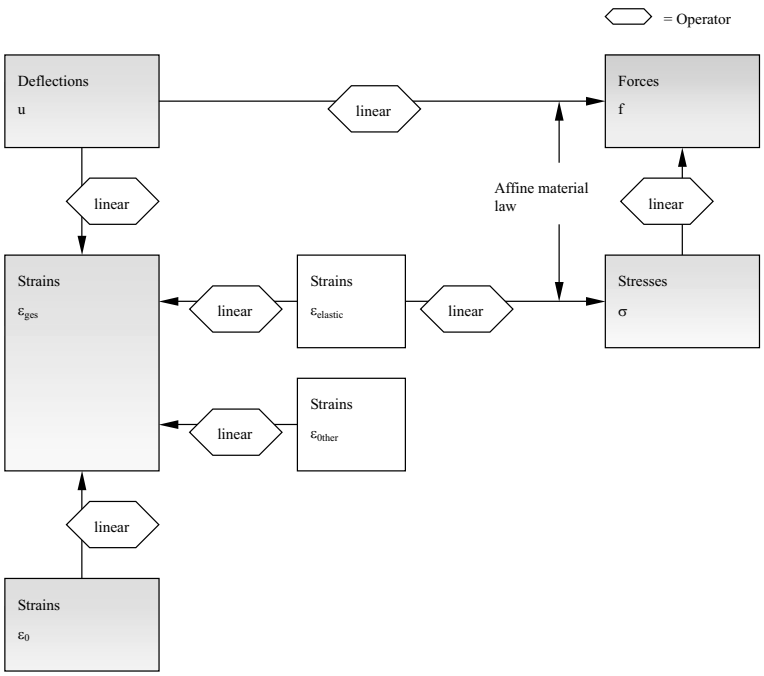

Table 4-4 Use of nonlinear strain measures (nonlinear strains, stresses and forces)

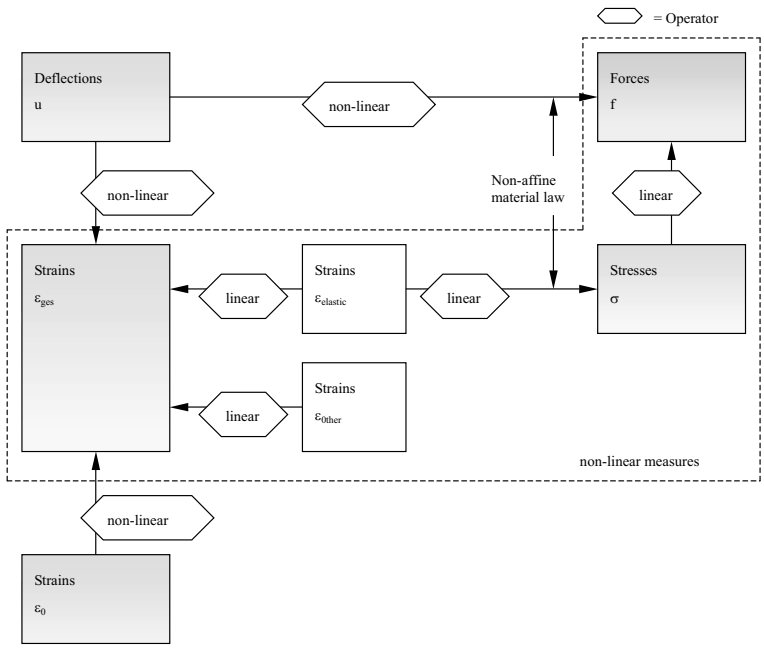

Table 4-5 Use of nonlinear strain measures (nonlinear strains and stresses)

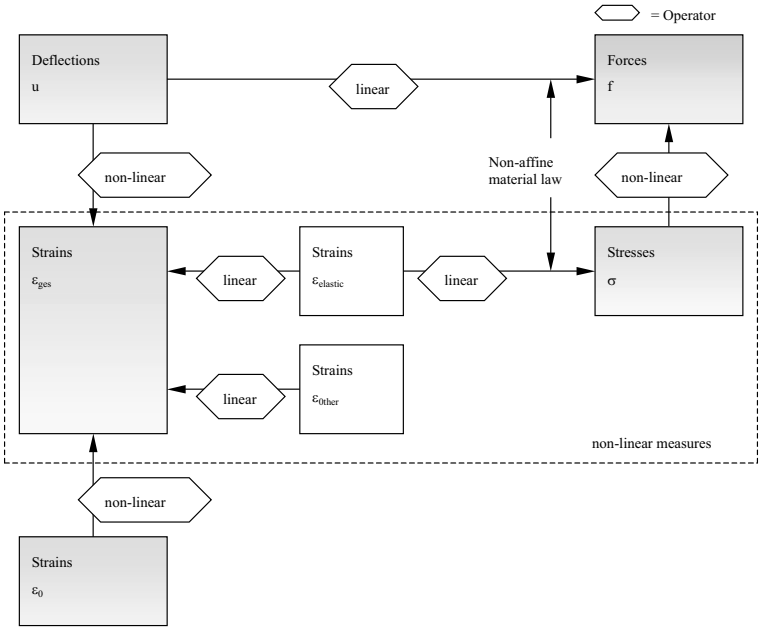

Table 4-6 Use of nonlinear strain measures (nonlinear strains)

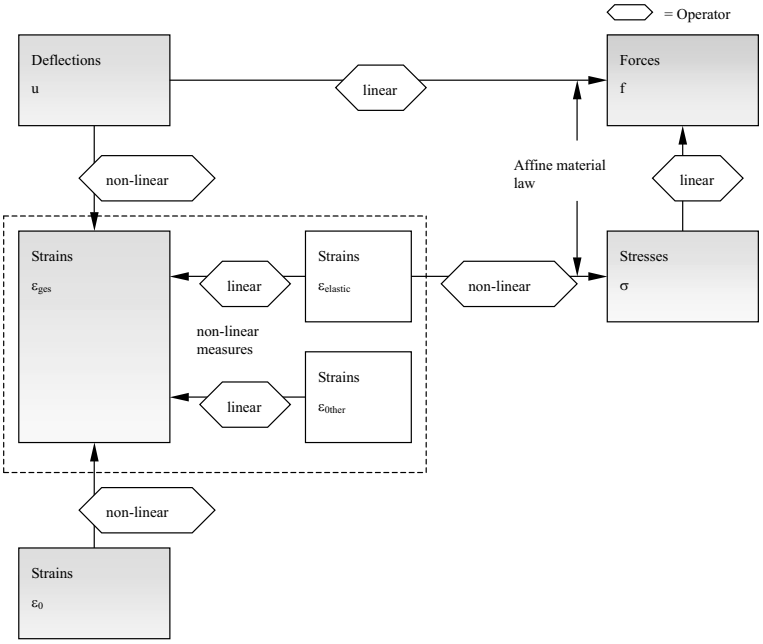

$$\hat{\sigma}_E = \left[\sigma_N 1^T, \ldots, \sigma_N n^T\right]^T \tag{4-54}$$

The shape functions, are commonly formed from polynomials with potentials from x and appropriate coefficients $\hat{a}_s$

$$\hat{\sigma}(x) = \hat{P}_s(x) \cdot \hat{a}_s \tag{4-55}$$

with $\hat{P}_s$ as the matrix of basis functions. The coefficient matrix $\hat{a}_s$ can be calculated from the node values

$$\hat{\sigma}_E = \hat{G}_s \cdot \hat{a}_s \tag{4-56}$$

with

$$\hat{G}_s = \left[\hat{P}_s^T(x_{N1}), \ldots, \hat{P}_s^T(x_{Nn})\right]^T \tag{4-57}$$

If the number of unknowns in the element and the number of shape functions as well as the shape function order are compatible, the matrix $\hat{G}_s$ is invertible, then

$$\hat{a}_s = \hat{G}_s^{-1} \cdot \hat{\sigma}_E \tag{4-58}$$

Combining Eq. (4-55) and (4-58) leads to

$$\hat{\sigma}(x) = \hat{P}_s(x)\hat{G}_s^{-1} \cdot \hat{u}_E \tag{4-59}$$

Approaches for the Element Free Galerkin method are formally possible, similar to the approaches of Eq. (4-18-4-22). Equation (4-59) can be shortened to

$$\hat{\sigma}(x) = \hat{H}_s(x) \cdot \hat{\sigma}_E \tag{4-60}$$

with $\hat{H}_s(x)$ the matrix of the stress shape function.

Dependent on the problem, it is sometimes useful to use partly integrated stresses (stress resultants or internal forces) in order to reduce the dimension of the problem (longitudinal forces, transversal forces, moments). These parameters are derived by introduction of cross-sections with e.g. area, moment of inertia and height, and integration with respect to the stresses in such cross-sections. They are mostly used to simplify the calculation of such structural elements, whose dimensions have been reduced in the mechanical model, e.g. beams, plates and shells. As an example, the calculation of a bending moment in a simple beam element is given

$$\hat{M}_x = \int \hat{y}\hat{\sigma}(x, y)dxdy \tag{4-61}$$

As internal forces are just integral parameters directly dependent on the stresses, the mechanics in terms of internal forces is not different from that in terms of stresses. For generalizing the mathematical treatment of stresses and internal forces within mechanical

procedures of this study, a superior variable s is introduced, that represents either stresses or internal forces. The assignment to the appropriate variable is then dependent on the selected element formulation.

The stresses, and internal forces respectively, can be expressed in vector form

$$\sigma(x) = \mathrm{vec}(\hat{\sigma}(x)) \tag{4-62}$$

4.8 Material law

In a general material law the stresses are defined as the function of the strains or vice versa, as mentioned in Sec. 3. The number of available material laws is overwhelming. In this study, only two material law types are selected for detailed consideration

- Linear elastic material law
- Linear elastic - plastic material law

that have a major practical relevancy for seismic design purposes.

4.8.1 Linear elastic material law

For linear elastic materials, or elastic parts of strain components, the relationship is

$$\hat{\sigma}(x) = \hat{D}(x)\hat{\varepsilon}_e(x) \tag{4-63}$$

determined by the elasticity tensor $\hat{D}(x)$. The derivation of $\hat{D}(x)$ out of continuum mechanical considerations is illustrated in Tab. 4-7. With application of symmetry conditions, the important isotropic and orthotropic cases can be derived. Two dimensional special cases are discussed in Tab. 4-8. The transformation into matrix form is generally given by the operation

$$D(x) = \mathrm{mat}(\tilde{D}(x)) \tag{4-64}$$

with the 2nd order pseudo-tensor $\tilde{D}(x)$, that have been condensed for orthotropic elastic material out of the 4th order tensor $\hat{D}(x)$.

Equation (4-60) can be directly used to replace the volume stresses $\hat{\sigma}(x)$ in the elastic material law Eq. (4-63) by the element′s nodal stresses $\hat{\sigma}_E$

$$\hat{\varepsilon}_e = \hat{D}(x)^{-1}\hat{H}_s(x) \cdot \hat{\sigma}_E \tag{4-65}$$

If the strains are also to be calculated at the nodes of elements the following expression can be applied

$$\hat{\varepsilon}_{E,e} = \hat{H}_s^T(x)\hat{D}(x)^{-1}\hat{H}_s(x) \cdot \hat{\sigma}_E \tag{4-66}$$

With

Table 4-7 Elastic material matrix D

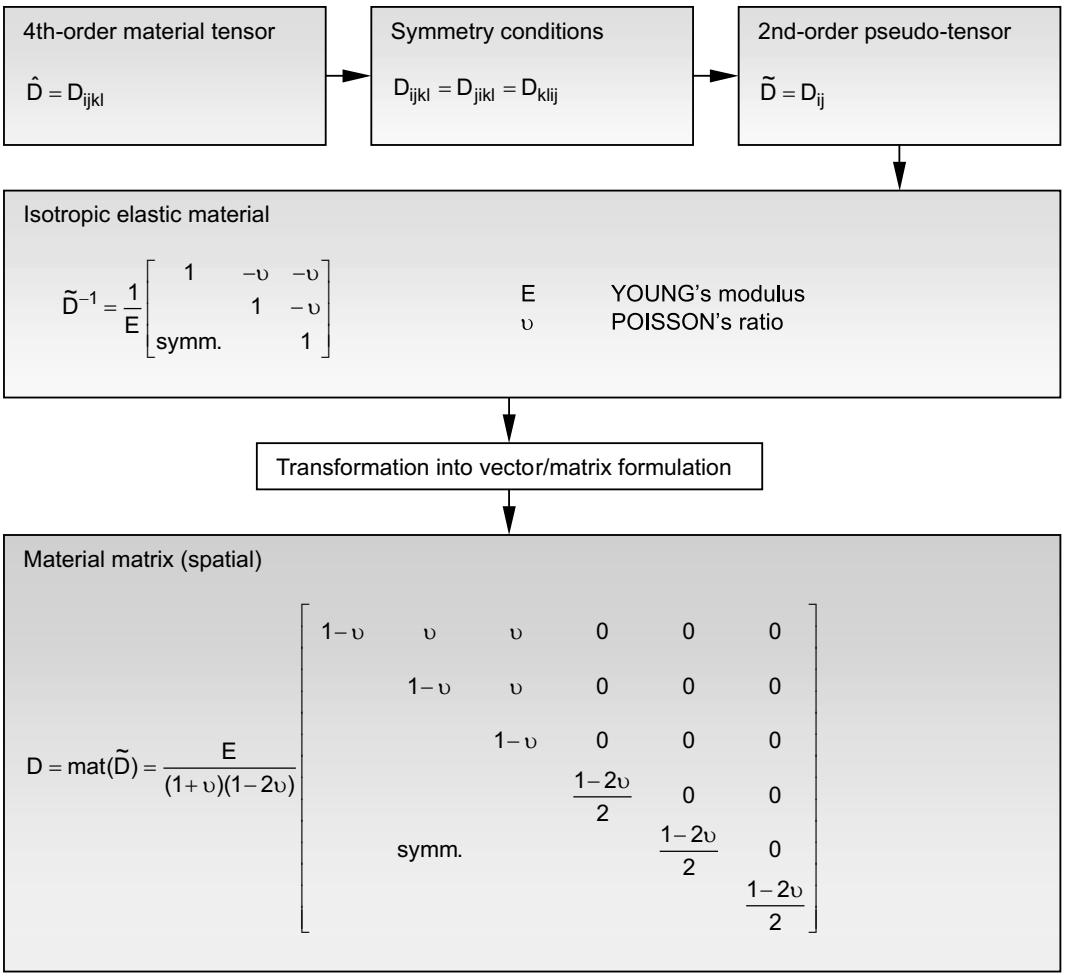

$$\hat{Q}(x) = \hat{H}_s^T(x)\hat{D}(x)^{-1}\hat{H}_s(x) \tag{4-67}$$

the equation simplifies to

$$\hat{\varepsilon}_{E,e} = \hat{Q}(x) \cdot \hat{\sigma}_E \tag{4-68}$$

The handling of compressible/incompressible material can be organized by substitution of Eq. (4-9) into (3-67), that leads to a nonlinear matrix function. It can be directly introduced as a subsidiary condition of an optimization problem.

The formulation of elasto-plastic material behavior as inequality conditions of an optimization problem makes the implementation very convenient. The commonly applied procedures of prediction and correction of the stress state as in classical incremental approaches need not explicitly be performed. The problem is solved as a nonlinear problem. The necessary iterations need not to be organized by the user, they are part of the optimization algorithm.

Table 4-8 Elastic isotropic material matrix D (plane special cases)

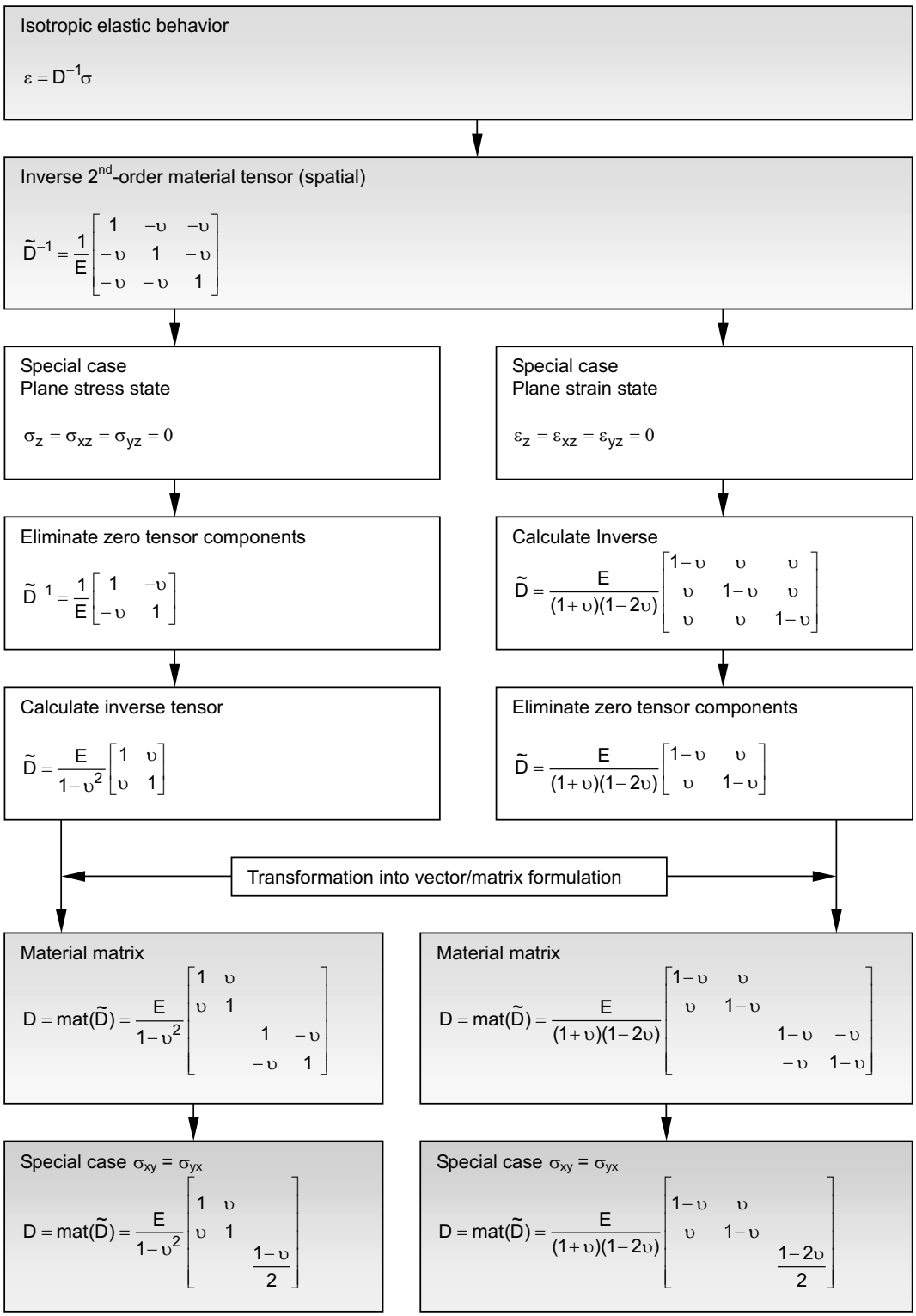

Elastic-plastic material laws commonly apply the superposition approach, starting from an elastic basis and adding plastic components

$$d\hat{\varepsilon} = d\hat{\varepsilon}_e + d\hat{\varepsilon}_p \tag{4-69}$$

Except for pure linear elasticity, the total strains within a body are generally history dependent. Those material laws will be usually combined with a yield hinge assumption, where the plastic strains are concentrated in discrete points or lines, as introduced in Sec. 3.9.

Following, the derivation of matrix notations for selected elasto-plastic material laws are exemplarily demonstrated. The matrix forms allow for convenient numerical treatment for the yield condition as well as for gradient determinations. Only the case of "associated" yield rules is illustrated. It should be noted, that the selected material laws are appropriate for most design purposes. Dependent on the considered problem, analysis tasks may require more complex descriptions [22,223].

4.8.2 Linear plasticity condition

The yield condition is a linear function, given as

$$\hat{Y}_L(x) = L_{p,L}^T(x)\hat{\sigma}(x) - \hat{\sigma}_{lim}(x) = 0 \qquad \in V_p \tag{4-70}$$

The linear coefficients $L_{p,L}(x)$ read

$$L_{p,L}^T(x) = [\ L_{p,1} \quad \cdots \quad L_{p,n_s}\ ] \tag{4-71}$$

with the number of interacting stress components n_S at the plasticize volume part V_p. The constant part of the equation is $\hat{\sigma}_{lim}$.

Equation (4-70) can be extended for the case of hardening materials, here given as a function of the plastic strains

$$\hat{Y}_L = \hat{Y}(\sigma, \varepsilon_p) \tag{4-72}$$

The hardening can be incorparated in Eq. (4-70) as follows

$$L_{p,L}^T(\hat{\sigma}(x) - A_h(\lambda(x))) - \hat{\sigma}_{lim}(x) = 0 \qquad \in V_p \tag{4-73}$$

with the hardening function A_h, that is dependent on the plastic multipliers or plastic deformation. For example, it can be defined as a polygonal approach, i.e. as a function of the plastic strains

$$A_h(\hat{\varepsilon}_p(x)) = \sum_{i=1}^{n_h} h_i(x)\varepsilon_p^i(x) \tag{4-74}$$

with n_h as the polynomial degree. Examples are shown in Fig. 4-2.

The plastic strain components are calculated from

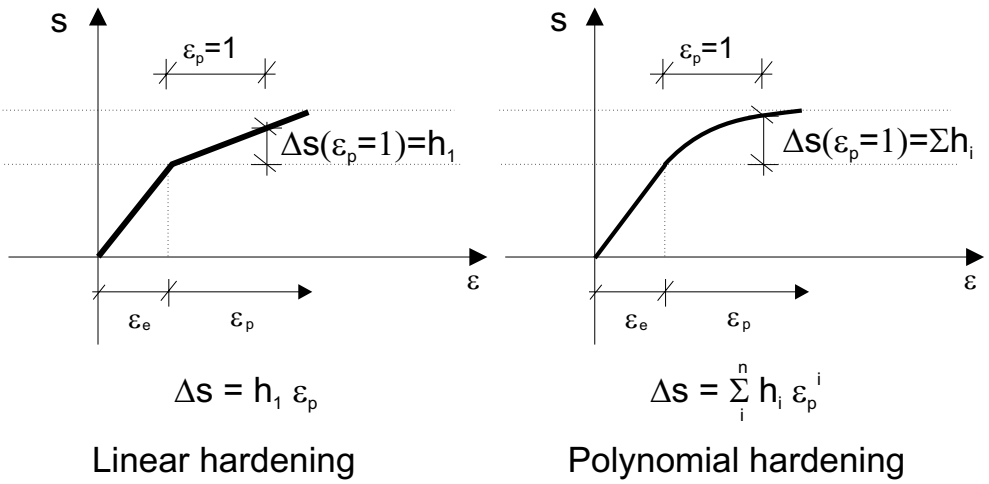

Figure 4-2 Hardening concepts

$$\hat{\varepsilon}_p(x) = L_{p,L}^T(x) \cdot \lambda(x) \qquad \in V_p \tag{4-75}$$

More generally, for linear hardening, the corresponding relation can be given in matrix form

$$A_h(\lambda(x)) = A_h(x)\lambda(x) \tag{4-76}$$

In the correspondent isotropic hardening rule, matrix A_h is computable at point x from

$$A_{h,iso}(x) = h\hat{\sigma}_{lim}(x)^T\sigma_{lim}(x) \tag{4-77}$$

As well, Prager′s kinematic hardening approach reads

$$A_{h,kin}(x) = h\, L_{p,L}^T L_{p,L} \tag{4-78}$$

with h as the hardening modulus [133]. Koiter′s hardening is stating the independence of the hardening modes with the implementation of a pure diagonal hardening matrix [61].

Linear plasticity is numerically effective to express a yield function. If possible, nonlinear problems should be linearized, as can be seen in the example of Fig. 4-3. Here an interaction condition of two stress/internal force components is implemented as a linear condition. The coefficient L_p,L contains the yield plane parameters a_{ij} and σ_{lim} is the distance b_i.

4.8.3 von Mises yield criterion

The von Mises yield criterion [153] is given at a material point as a function of the second stress deviator invariant J_2

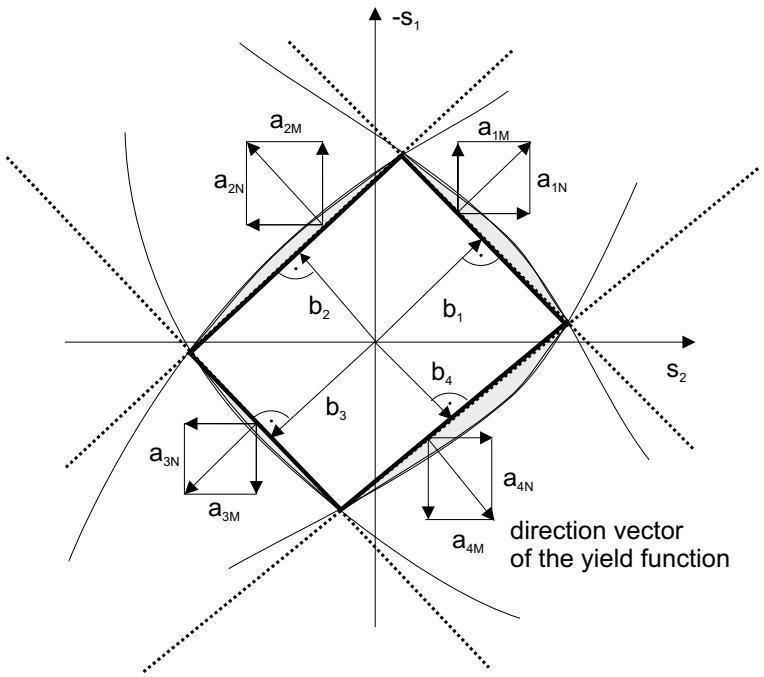

Figure 4-3 Linearization of plasticity conditions

$$\hat{Y}_{vM}(\hat{\sigma}(x)) = \sqrt{J_2(x)} - \hat{\sigma}_{lim,vM}(x) \leq 0 \qquad \in V_p \tag{4-79}$$

As in Eq. 4.8.2, the condition can be extended for hardening materials.

The invariant is in three dimensions

$$J_2(x) = \frac{1}{6}\left[(\sigma_{11} - \sigma_{22})^2 + (\sigma_{11} - \sigma_{33})^2 + (\sigma_{22} - \sigma_{33})^2\right] + \sigma_{12}^2 + \sigma_{23}^2 + \sigma_{31}^2 \tag{4-80}$$

and is always a positive number. From the inequality (4-79) it is obvious, that the von Mises limit stress $\sigma_{lim,vM}(x)$ is always greater or equal to $\sqrt{J_2(x)}$, hence it is also positive. Thus the condition still holds for the squares

$$J_2(x) \leq \hat{\sigma}_{lim,vM}^2(x) \tag{4-81}$$

The invariant $J_2(x)$ can be expressed in matrix form

$$J_2(x) = \frac{1}{2}\sigma^T(x) Q_{p,vM} \sigma(x) \tag{4-82}$$

where $\sigma(x)$ is the stress component vector and $Q_{p,vM}$ is a constant coefficient matrix

$$Q_{p,vM} = \begin{bmatrix} \frac{2}{3} & -\frac{1}{3} & -\frac{1}{3} & & & \\ -\frac{1}{3} & \frac{2}{3} & -\frac{1}{3} & & & \\ -\frac{1}{3} & -\frac{1}{3} & \frac{2}{3} & & & \\ & & & 2 & & \\ & & & & 2 & \\ & & & & & 2 \end{bmatrix} \tag{4-83}$$

Thus the von Mises yield criterion becomes finally a quadratic inequality

$$\frac{1}{2}\sigma^T(x)Q_{p,vM}\sigma(x) - \sigma^2_{lim,vM}(x) \leq 0 \tag{4-84}$$

4.8.4 Drucker-Prager yield criterion

The Drucker-Prager yield criterion [72] is an extension to the von Mises approach, given as a function of the first stress invariant I_1 and the second stress deviator invariant J_2

$$Y_{DP}(\sigma(x)) = \alpha_{DP}I_1(x) + \sqrt{J_2(x)} - \tau_{DP} \leq 0 \qquad \in V_p \tag{4-85}$$

The parameter α_{DP} is a friction coefficient, that estimates the influence of pressure on the yield limit, important for materials with cohesive frictional properties such as concrete. The parameter τ_{DP} is the limit yield stress under pure shear loading. The parameters α_{DP} and τ_{DP} are commonly calculated from the friction angle ϕ and the cohesion c

$$\alpha_{DP} = \frac{6\sin(\phi)}{\sqrt{3}(3 - sin(\phi))} \tag{4-86}$$

$$\tau_{DP} = \frac{6c\cos(\phi)}{\sqrt{3}(3 - sin(\phi))} \tag{4-87}$$

With rearrangement of (4-85)

$$\sqrt{J_2(x)} \leq \tau_{DP} - \alpha_{DP}I_1(x) \tag{4-88}$$

it is obvious, that from the non-negativity of $\sqrt{J_2(x)}$ follows the non-negativity of the right side of the inequality. Thus the condition is equal to it′s quadratic form

$$J_2(x) \leq (\tau_{DP} - \alpha_{DP}I_1(x))^2 \tag{4-89}$$

or

$$J_2(x) \leq \tau^2_{DP} - 2\tau_{DP}\alpha_{DP}I_1(x) + \alpha^2_{DP}I^2_1(x) \tag{4-90}$$

The third term is given as:

$$2\tau_{DP}\alpha_{DP}I_1(x) = 2\tau_{DP}\alpha_{DP}\frac{1}{3}\left(\sigma_{11}+\sigma_{22}+\sigma_{33}\right) \tag{4-91}$$

that is in matrix notation

$$2\tau_{DP}\alpha_{DP}I_1(x) = L_{p,DP}^T\sigma(x) \tag{4-92}$$

with the vector

$$L_{p,DP} = \begin{bmatrix} \frac{2\tau_{DP}\alpha_{DP}}{3} & \frac{2\tau_{DP}\alpha_{DP}}{3} & \frac{2\tau_{DP}\alpha_{DP}}{3} & 0 & 0 & 0 \end{bmatrix}^T \tag{4-93}$$

Accordingly, the forth term of (4-90) is in matrix notation

$$\alpha_{DP}^2 I_1^2(x) = \frac{1}{2}\sigma^T(x)Q_{p,2}\sigma \tag{4-94}$$

with

$$Q_{p,2} = \frac{2\alpha^2}{9}\begin{bmatrix} 1 & 1 & 1 & & & \\ 1 & 1 & 1 & & & \\ 1 & 1 & 1 & & & \\ & & & 0 & & \\ & & & & 0 & \\ & & & & & 0 \end{bmatrix} \tag{4-95}$$

Including Eq. (4-82), the yield criterion is

$$\frac{1}{2}\sigma^T(x)Q_{p,vM}\sigma(x) - \frac{1}{2}\sigma^T(x)Q_{p,2}\sigma(x) + L_{p,DP}^T\sigma(x) \leq \tau_{DP}^2 \tag{4-96}$$

or combined, in a quadratic form

$$\frac{1}{2}\sigma^T(x)Q_{p,DP}\sigma(x) + L_{p,DP}^T\sigma(x) \leq \tau_{DP}^2 \tag{4-97}$$

with

$$Q_{p,DP} = \frac{2}{9}\begin{bmatrix} 3-\alpha^2 & -0.5\left(3+\alpha^2\right) & -0.5\left(3+\alpha^2\right) & & & \\ -0.5\left(3+\alpha^2\right) & 3-\alpha^2 & -0.5\left(3+\alpha^2\right) & & & \\ -0.5\left(3+\alpha^2\right) & -0.5\left(3+\alpha^2\right) & 3-\alpha^2 & & & \\ & & & 9 & & \\ & & & & 9 & \\ & & & & & 9 \end{bmatrix} \tag{4-98}$$

Respectively, the condition can be extended for hardening materials.

4.9 Static boundary conditions

Static boundary conditions relate the stresses on the surface of a body to a set of predefined stresses. As well as for the kinematic boundary conditions, continous boundary definitions are transformed into discrete formulations by application of form functions, e.g. in a linear formulation the static boundary condition reads

$$N_s(x)H_s(x)\sigma_E - \sigma_0(x) = N_s(x)H_s(x)\sigma_E - H_s(x)\sigma_0(x_E) = N_s(x)\sigma_E - \sigma_0(x_E) = 0 \qquad \in S_s \tag{4-99}$$

The matrix N_s is the direction matrix, that additionally identifies a material point to be a part of the statically predetermined boundary S_s. Similarly to stresses, the static boundary conditions can be defined for internla force values. Any applied static boundary condition induces a support displacement c_u as a dual parameter.

4.10 Equilibrium condition

The equilibrium condition connects the external with the internal forces/stresses. Generally, the equilibrium condition can be formulated

$$\hat{B}_s(x)\hat{T}_s(x)\hat{\sigma}(x) + \hat{\varphi}(x) = 0 \qquad \in V \tag{4-100}$$

where $\hat{B}_s(x)$ is a derivative tensor. Table 4-9 is illustrating the derivation of the appropriate linear derivative matrix B_s from continuum mechanics. In comparison with the operator matrix of the kinematic conditions B_u it becomes obvious, that B_s is the transpose of B_u. Thus, because the problem is formulated in the reel number space, the operators fulfill the property of self-adjointness.

Using the stress shape functions defined in Sec. 4.7, the equilibrium condition (4-100) can be defined as

$$\hat{B}_s(x)\hat{T}_s(x)\hat{H}_s(x)\hat{\sigma}_E + \hat{\varphi}(x) = 0 \tag{4-101}$$

Similarly to the strain/displacement conditions, the coefficients can be assembled in one operator

$$\hat{A}_s(x) = \hat{B}_s(x)\hat{T}_s(x)\hat{H}_s(x) \tag{4-102}$$

Then Eq. (4-100) is shorter

$$\hat{A}_s(x)\hat{\sigma}_E + \hat{\varphi}(x) = 0 \tag{4-103}$$

The matrix formulation is obtained by application of tensor-matrix transformations

$$A_s(x)^T = \mathrm{spr}(\hat{A}_s(x)^T) \tag{4-104}$$

If the motion of the material point is restricted by geometric boundary conditions, the resulting reaction forces c_s are considered within the equilibrium conditions. The equilibrium condition in matrix notation is

$$A_s(x)\sigma_E + N_u^T c_s + \varphi(x) = 0 \tag{4-105}$$

Table 4-9 Derivation of operator matrix of equilibrium conditions

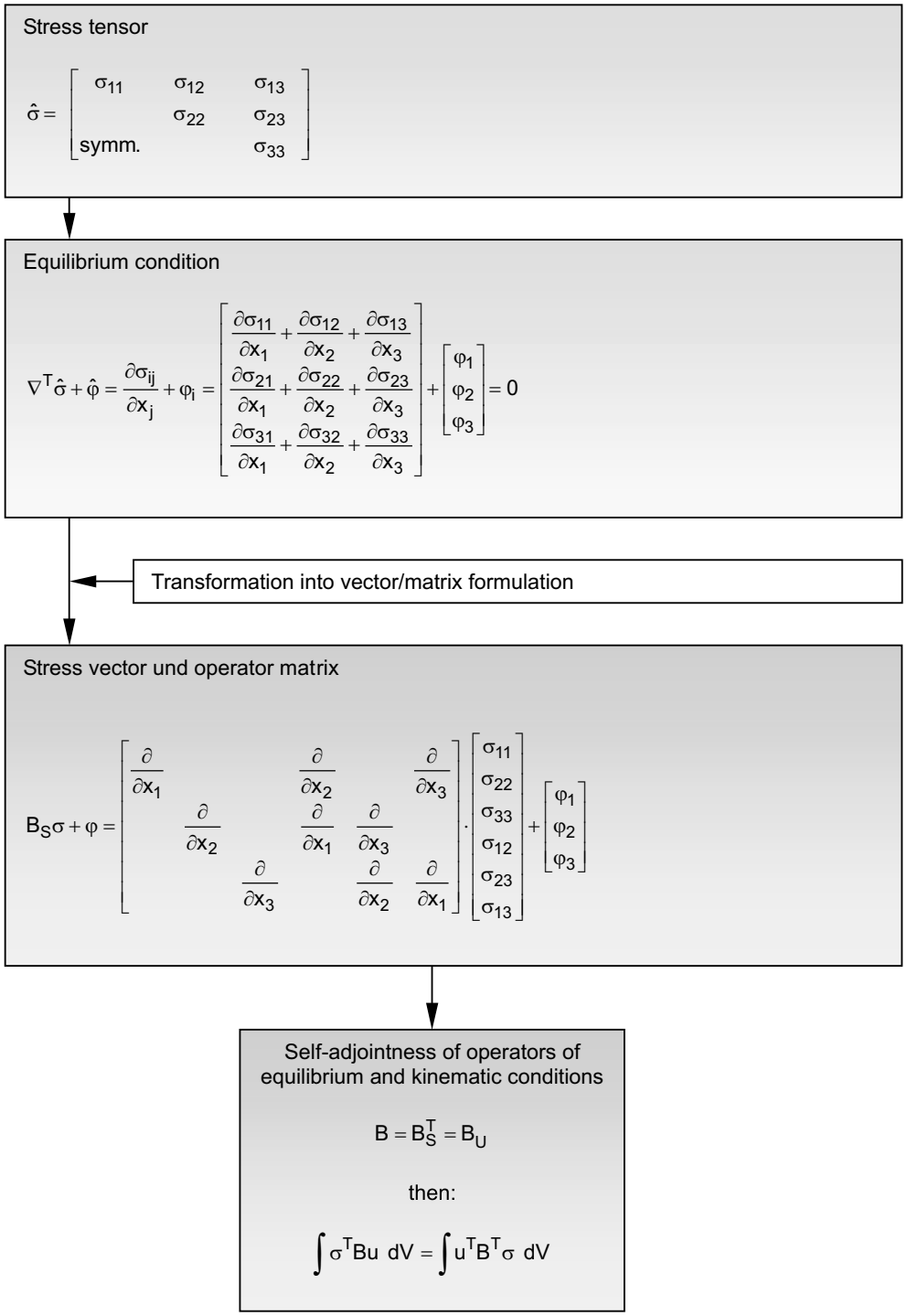

4.11 Forces

As well, external forces are discretized, while assuming conservative loads within this study. The function of the forces can be given as a shape functions H_φ. Following the procedure in Sec. 4.3 and 4.7, the shape function can be derived

$$\varphi(x) = H_\varphi(x) \cdot \varphi_E \tag{4-106}$$

dependent on the nodal forces φ_{Ni} within the element

$$\varphi_E = [\varphi_{N1}, \ldots, \varphi_{Nn}]^T \tag{4-107}$$

According to d′Alembert′s principle, inertia and damping forces are superposed as already indicated in Eq. (3-92). For these components, discrete descriptions can be provided as well. The mass is dependent on the mass density ρ and the distribution in the vicinity of x, given by the shape functions H_m

$$\varphi_M(x) = \rho(x)\ddot{u}(x) = {}^{t+\Delta t}H_m(x)\rho_E{}^{t+\Delta t}H_u^T(x)\ddot{u}_E \tag{4-108}$$

With respect to the change of the material direction, during deformations the relation turns to

$$\varphi_M(x) = H_m(x)L(x)\rho_E L^T(x)H_u^T(x)\ddot{u}_E \tag{4-109}$$

The damping is mostly treated separately, dependent on the stiffness and masses (Rayleigh approach). Nevertheless a general formula with the damping density ν and the damping distribution function H_c can be given

$$\varphi_C(x) = \nu(x)\dot{u}(x) = H_c(x)L(x)\nu_E L^T(x)H_u^T(x)\dot{u}_E \tag{4-110}$$

4.12 Geometric nonlinear numerics for material point

The relations derived in the last section can be implemented for the numerical solution of tasks in engineering. The appropriate governing equations are as follows for physical linearity:

Equilibrium condition:

$$A_s(x)\sigma_E + H_\varphi(x)\varphi_E = 0 \qquad \in V \tag{4-111}$$

Kinematic condition:

$$A_u(x)u_E + T_u(x)(\varepsilon_0(x) + I) - I = \varepsilon(x) \qquad \in V \tag{4-112}$$

Linear elastic material law:

$$\sigma_E = Q^{-1}(x)\varepsilon(x) \qquad \in V \tag{4-113}$$

and the geometric and static boundary conditions

$$N_u(x)u_E - u_0(x_E) = 0 \qquad \in V \tag{4-114}$$

$$N_s(x)\sigma_E - \sigma_0(x_E) = 0 \qquad \in V \tag{4-115}$$

Equations (4-111-4-113) can be combined to

$$K_{NL}(x)u_E + \varphi_{geo}(x) = -H_\varphi(x)\varphi_E \tag{4-116}$$

with

$$K_{NL}(x) = A_s(x)Q^{-1}(x)A_u(x) \tag{4-117}$$

$$\varphi_{geo} = A_s(x)Q^{-1}(x)\left(T_u(x)(\varepsilon_0(x) + I) - I\right) \tag{4-118}$$

In dynamics, φ contains inertia and damping forces. Then Eq. (4-116) is known as the ′equation of motion′, i.e. for elastic problems

$$K_{NL}(x)u_E + \varphi_{geo}(x) + \varphi_{Stat}(x) = -\varphi_M(x) - \varphi_C(x) \tag{4-119}$$

The boundary conditions can be included according to the preceding sections. The engineering simplifications are given if

$$T_u = I \tag{4-120}$$

and

$$A_s = A_u^T \tag{4-121}$$

If the structure is subjected to large deformations, considerable differences in geometric linear and nonlinear calculation can be expected, as illustrated in the example of Fig. 4-4.

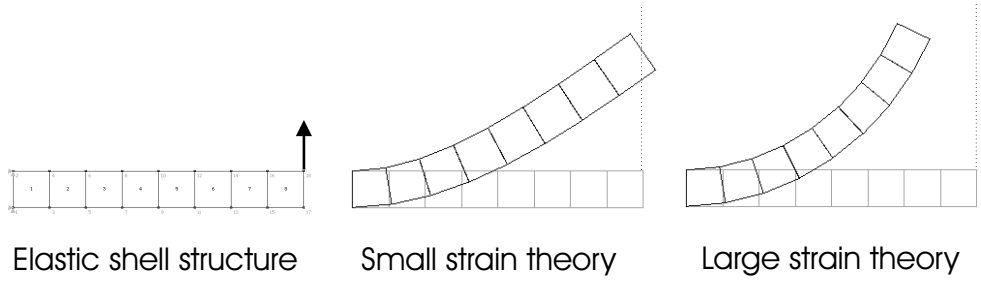

Figure 4-4 Comparison of geometric linear and nonlinear calculation of an extremely loaded shell structure

4.13 Physical nonlinear numerics at material points (elasto-plastic systems)

Generalizing all physical nonlinear matrix equations and equalities, a basic condition scheme can be provided with Tab. 4-10. Here the conditions are summarized for linear yield functions and linear boundary conditions. It contains all governing functions with respect to a primal variable set, specified at the top of the scheme. Associated to any function, a dual variable at the very left of the table is given. Such dual variables are identical to the associated Lagrange multipliers of the function, that are often given as part of the results of nonlinear optimization problems. The condition system is complete, because the scheme is symmetric and can be rotated by 90 degree and the primal variables become the dual and vice versa. Within the system the inequality conditions of the yield conditions are eliminated by introduction of the dual slack variables λ and y. Such slack variables are generally non-negative (non-negativity conditions in the dual formulations).

If appropriate in practical calculations, this general scheme can be simplified. Some equations can be used to substitute variables, as the material law can be introduced in the kinematic condition. In such a case the strains can be eliminated, as demonstrated in Tab. 4-11. Furthermore, symmetric schemes can be transformed into non-symmetric, if conditions are only substituted in the primal system. An example is given in Tab. 4-12, where the slack variables are eliminate and the boundary conditions are included in the equilibrium and extended kinematic condition.

A purely kinematic formulation is given in Tab. 4-13, where only kinematic parameters, the displacement u and the Lagrange multipliers of the plasticity conditions λ (related to the plastic strains) are the remaining unknowns of the mechanical system. Such schemes are often applicable in structural optimization, because most structural conditions (such as the material law) can be defined as a function of kinematic parameters.

In such schemes, all mechanical properties are provided. Such schemes are perfectly suited as a set of subsidiary conditions in nonlinear optimization. The advantage of the reduced schemes is the reduced number of unknowns. Because of the arbitrary objective

Table 4-10 Detailed relation scheme of mechanical quantities for elastic-plastic structures

Primal variables		Dual variables													
		σ^T	σ^T	σ^T	σ^T	c_u^T	c_s^T	u^T	y^T	λ^T	ε_e	ε_p	ε		
σ	σ	σ	σ	c_u	c_s	u	y	λ	ε_e	ε_p	ε				
$-D^{-1}$									1					Elastic material law	=0
										L_P		1		Associates yield law	=0
											-1	-1	1	Elastic-plastic material law	$=\varepsilon_0$
				N_S				B					-1	Kinematic field condition	=0
			N_S^T											Static boundary condition	$=\sigma_0$
						N_U								Geometric boundary condition	$=u_0$
		B^T			N_U^T									Equilibrium condition	$=-\varphi$
									1					Non-negativity condition	≥ 0
	L_P^T									1				Yield condition	$=-\sigma_{lim}$
	1										-1			Equivalence condition	=0
											-1	1		Equivalence condition	=0
-1											1			Equivalence condition	=0
=0	=0	=0	=0	$=\sigma_0$	$=u_0$	=-f	≥ 0	$=-\sigma_{lim}$	=0	=0	=0	=0	=0	Complementarity condition	$\lambda^T y = 0$

Table 4-11 Reduced relation scheme of mechanical quantities for elastic-plastic structures (Strains eliminated)

		Primal variable								
		σ	c_u	c_s	u	λ	y	1		
Dual variables	σ^T	$-D^{-1}$	N_S		B	$-L_P$			$=\varepsilon_0$	Ext. kinematic condition
	c_u^T	N_S^T							$=\sigma_0$	Static boundary condition
	c_s^T				N_U				$=u_0$	Geom. boundary condition
	u^T	B^T		N_U^T					$=-\varphi$	Equilibrium
	λ^T	$-L_P^T$					1		$=-\sigma_{lim}$	Plasticity condition
	y^T					1			≥ 0	Non-negativity
								$\lambda^T Y$	$=0$	Complementarity

function, a variety of different optimization task can be solves, e.g. the calculation of the deformation based limit state.

4.14 Gaussian volume integration

The governing system equations, described in the previous sections, are formulated for material points within elements/supports. The assessment of the entire body needs integration of the functions $p(x)$ over the given volume.

$$y = \int p(x) dV \tag{4-122}$$

The integration can be simplified, because the volume is divided in several elements and the single contribution to the parameter is summarized

$$y = \sum_{i=1}^{n_E} y_i = \sum_{i=1}^{n_E} \int p(x_{E,i}) dV_i \tag{4-123}$$

Within elements,all parameters are described in terms of nodal parameters and definition of shape functions for all parameters. The numerical integration within elements is easily done by Gauss integration [22]. The integral is exchange by a sum of weighted function values at n_G distinct points x_G (integration or Gauss points)

Table 4-12 Simplified relation scheme of mechanical quantities for elastic-plastic structures (Strains, slack variables eliminated, boundary conditions introduced)

		Primal variables								
			σ		u	λ	1			
Dual variables										
	σ^T			$-D^{-1}$		B	$-L_P$		$=\varepsilon_0$	Ext. kinematic condition
	u^T			B^T					$=\varphi$	Equilibrium
	λ^T			$-L_P^T$				σ_{lim}	≥ 0	Plasticity condition
	y^T						1		≥ 0	Non-negativity
		$\lambda^T ($		$-L_P^T$				σ_{lim}	$) = 0$	Complementarity

$$y_i \approx \sum_{j=1}^{n_G} w_j(x_{G,j}) p(x_{G,j}) \tag{4-124}$$

For standard finite elements, especially for isoparametric types, the Gaussian parameters, the position of the integration points within the element x_G and the associated weights $w_i(x_G)$, are provided in tables [22].

For numerical calculation of Gauss integration parameters, a nonlinear optimization problem can be solved. The procedure is illustrated in Tab. 4-14 for a trapezoid area. For arbitrary elements, the integration value can than be assembled from the values of a group of trapezoid areas, as illustrated in Tab. 4-15. The elements edges are forming several trapezoid areas, defined by the lines between nodes. The integrals are calculated for these partial area according Tab. 4-14. The resulting values are positive or negative, depending on the direction of the trapezoidal boundary lines. The direction of the lines is defined by the numbering of the nodes. A continuous, clock wise numbering of the nodes is ensuring a positive value of the integral.

For integrals of linear matrix functions $p(x) = P \cdot x$,

$$y_i = \int P \cdot x \, dx \tag{4-125}$$

Table 4-13 Simplified relation scheme of mechanical quantities for elastic-plastic structures (Stresses and strains eliminated, boundary conditions introduced)

			Primal variables				
			u	λ	1		
Dual variables	u^T		$B^T D B$	$-B^T D L_P$		$= \varphi$	Ext. Equilibrium
	λ^T		$-L_P^T D B$	$L_p^T D L_p$	σ_{lim}	≥ 0	Plasticity condition
	y^T			1			Non-negativity
		$\lambda^T ($	$-L_P^T D B$	$L_p^T D L_p$	σ_{lim}	$) = 0$	Complementarity

the Gauss integration can be formally expressed as a matrix multiplication. The integration matrix W contains the weights of the Gaussian points as diagonal values. The associated coefficient matrix P_G of the linear function $p(x)$ is a vector of submatrices, that have been built with respect to all n_G Gaussian points within an element i. The integration becomes

$$y_i = P_G \cdot W \cdot x_G = \begin{bmatrix} p_1 & \cdots & p_{n_G} \end{bmatrix} \begin{bmatrix} w_1 & & 0 \\ & \ddots & \\ 0 & & w_{n_G} \end{bmatrix} \cdot \begin{bmatrix} x_1 \\ \vdots \\ x_{n_G} \end{bmatrix} \tag{4-126}$$

4.15 Element matrices and vectors

As described in the previous sections, finite element concepts divide the considered bodies into several subregions (elements), that′s behavior can be described with help of simpler approximations. Those approximations are the shape functions, that are provided for all governing parameters. The appropriate system equations require the integration of the volume of the body or of the surfaces for boundary conditions. With help of numerical integration, the governing equations can be transformed into matrix/vector formulations for effective numerical treatment. Following, the main concepts for derivation of important system matrices are discussed.

Table 4-14 Gauss integration parameter derivation (2D example, trapezoidal object)

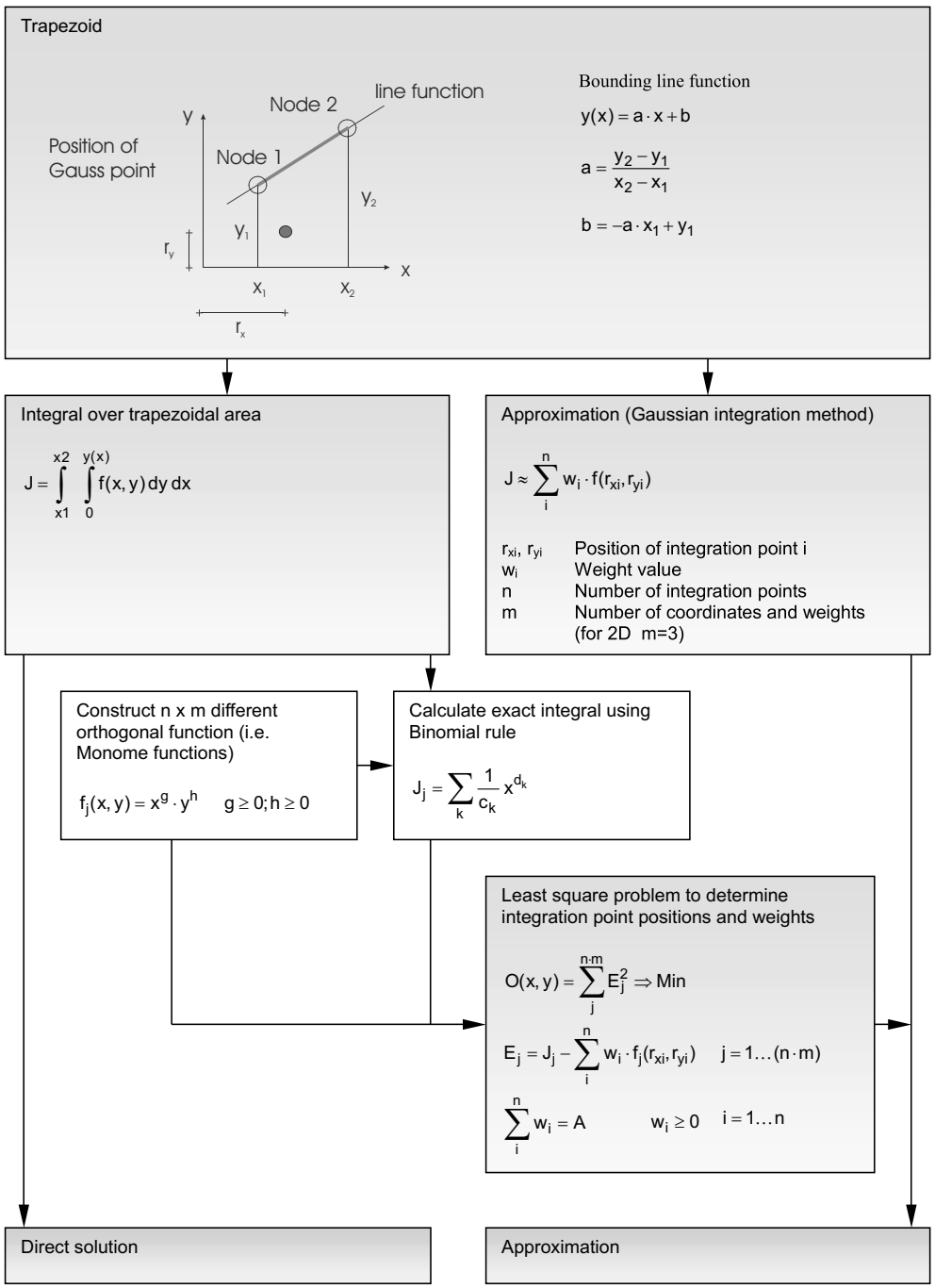

Table 4-15 Integration of arbitrary volumes (2D example)

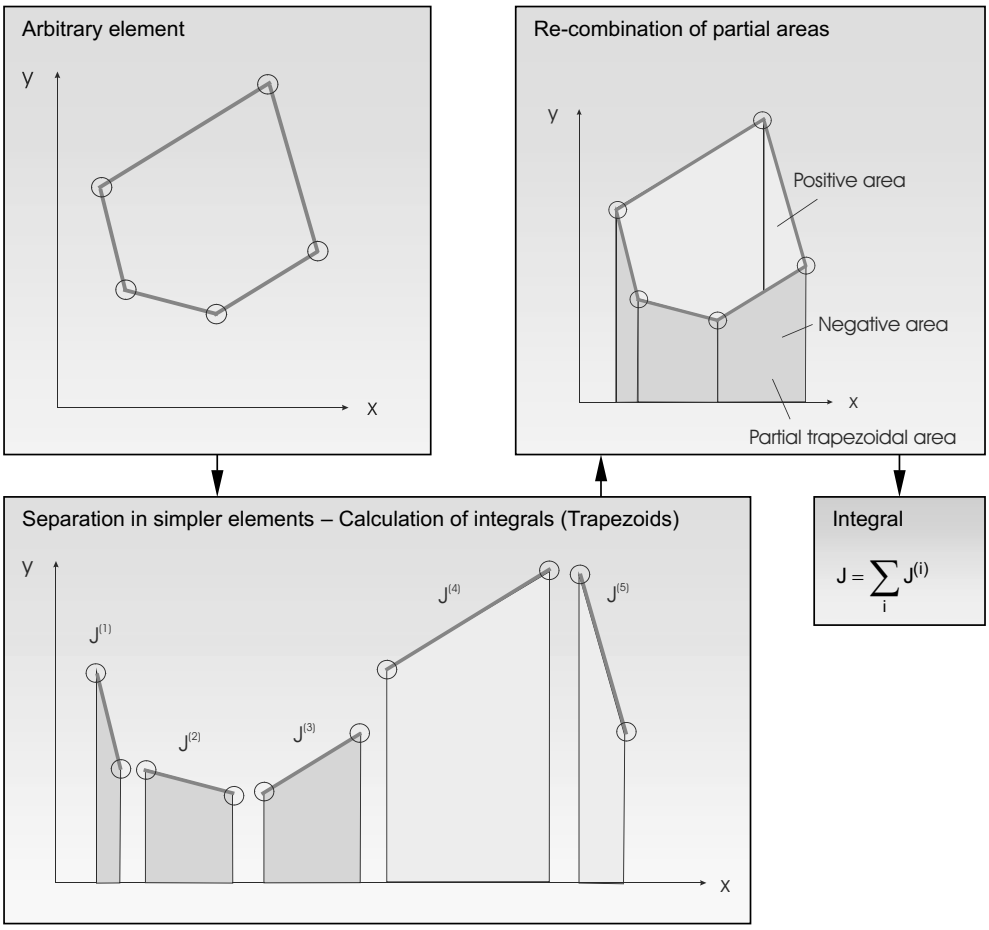

The concept covers the provision of the vectors of the external state variables, the forces f_E and displacements u_E, at the nodes of the element. The appropriate values within the element are calculated with help of shape functions. The internal state variable vectors are denoted by the internal forces s and deformations e. These notations are introduced for generalization, to provide unique variable names for different types of internal parameters. For instance for continuum elements is $s = \sigma$ the stresses and $e = \varepsilon$ are the strains, for non-continuum elements, like beams and plates, the variable s denotes integrated stresses (stress resultants) $F_x, F_y, M_z, \ldots$ and e is the vector of displacement differences $\Delta u_x, \Delta u_y, \Delta \phi_z, \ldots$.

At the integration points, the vectors of deformations e_G and internal forces s_G are calculated, that are the basis for the integration over the body volume. From this, the static term of the equilibrium condition is in matrix notation

$$\int B_s(x) T_s(x) s(x) dV = B_s(x_G) T_s(x_G) W s_G \tag{4-127}$$

The external forces need to be known at the nodes, thus distributed forces must be integrated over the loaded region, here shown for volumetric forces

$$f_E = \int \varphi(x) dV = H_f^T(x_{G,f}) W \varphi(x_{G,f}) = H_f^T(x_{G,f}) W H_\phi(x_{G,f}) \varphi(x_E) \tag{4-128}$$

with H_f as the distribution function of the forces. For integration, the Gauss approach is applied as well. The used integration points $x_{G,f}$ are dependent on the complexity of the shape function H_ϕ. Accordingly, the mass and damping terms are provided

$$\begin{aligned} &\int H_m(x) L(x) \rho_E L^T(x) H_u^T(x) \ddot{u}_E dV \\ &= H_m(x_{G,m}) L(x_{G,m}) \rho_E W L^T(x_{G,u}) H_u^T(x_{G,u}) \ddot{u}_E \\ &= M \ddot{u}_E \end{aligned} \tag{4-129}$$

$$\begin{aligned} &\int H_c(x) L(x) \nu_E L^T(x) H_u^T(x) \dot{u}_E dV \\ &= H_c(x_{G,c}) L(x_G) \nu_E L^T(x_{G,u}) W H_u^T(x_{G,u}) \dot{u}_E \\ &= C \dot{u}_E \end{aligned} \tag{4-130}$$

Within the kinematic conditions, the total strains are calculated at the integration points

$$e_G = \int T_u(x) B_u(x) u(x) dV = W T_u(x_G) B_u(x_G) u_E \tag{4-131}$$

Accordingly, the linear elastic strains are

$$e_{G,e} = \int D(x) s(x) dV = D(x_G) W s_G \tag{4-132}$$

Following the concept of yield hinges, the plastic conditions are described at distinct points, typically at the integration points where the stresses are known. Thus the plastic strains are derived from

$$e_{G,p} = A_p(x_G) \lambda \tag{4-133}$$

with the vector λ, that contains the plastic multipliers of n_p plasticity conditions

$$\lambda = \begin{bmatrix} \lambda_1 & \cdots & \lambda_{n_p} \end{bmatrix}^T \geq 0 \tag{4-134}$$

The matrix A_p is the coefficient matrix of the linear plasticity condition

$$A_p^T s_G - s_{G,lim} \leq 0 \tag{4-135}$$

incorporating several yield conditions at integration points with

$$A_p = \begin{bmatrix} {}_{p,1}(x_G) & \cdots & {}_{p,n_p}(x_G) \end{bmatrix}^T \tag{4-136}$$

The constant part is a vector

$$s_{G,lim} = \begin{bmatrix} \sigma_{lim,1} & \cdots & \sigma_{lim,n_p} \end{bmatrix}^T \tag{4-137}$$

Accordingly, all boundary conditions are formulated at the element nodes or integration points

$$N_u u_E = u_{E,0} \tag{4-138}$$

$$N_s s_G = s_{G,0} \tag{4-139}$$

In this concept, the knowledge of shape functions for the stresses/strains is not necessary. However, as shown with Eq. (4-103) the strains and stresses can be made dependable from the nodal strains and stresses by application of stress shape functions. Then all system equations can be summarized, e.g. for elastic material

$$A_s s_E + N_u^T c_{E,s} + M\ddot{u}_E + C\dot{u}_E + f_E = 0 \tag{4-140}$$

$$A_u u_E - Q s_E - A_p \lambda + N_s^T c_{E,u} = e_{E,0} \tag{4-141}$$

$$N_u u_E = u_{E,0} \tag{4-142}$$

$$N_s s_E = s_{E,0} \tag{4-143}$$

$$A_p^T s_E \leq s_{E,lim} \tag{4-144}$$

$$\lambda \geq 0 \tag{4-145}$$

4.16 Cross-sectional models for longitudinal force and bending moment problems

4.16.1 Separation of the volume integration

As mentioned in Sec. 4.7, for certain types of structures it is convenient to separate the integration of the entire volume into a structural part and a cross-sectional part. The resulting problems become simpler, as the number of integration dimensions is decreased in either analysis. For instance, the considered dimension of a beam element reduces to one in the structural model and down to two in the cross-sectional part. If the dimensions of the cross section are small compared to the dimensions in the structural model, some simplifications can be applied to summarize the behavior of the entire cross section with a few number of parameters. As well, this strategy requires integrated loads or excitations, compatible with their internal counterparts.

The properties of the cross-section are expressed in terms of areas, moments of inertia and internal forces. These parameters are traditionally applied, e.g. for elastic materials to derive longitudinal forces in a beam, that are the integrated stresses, parallel to the main structural dimension x

$$N = \int \sigma_x(x,y,z)\, dydz = \int E(x,y,z)\varepsilon_x(x,y,z)\, dydz \tag{4-146}$$

The integration is simplified by introduction of the area

$$A(x) = \int_{z_a}^{z_e} \int_{y_a}^{y_e} dydz \tag{4-147}$$

and the assumption of an average material in the cross section

$$E(x) = E(x, y, z) \tag{4-148}$$

and the average strain calculated by the mean value theorem

$$\bar{\varepsilon}(x) = \frac{1}{(z_e - z_a)(y_e - y_a)} \int_{z_a}^{z_e} \int_{y_a}^{y_e} \varepsilon_x(x, y, z) dydz \tag{4-149}$$

This expression simplifies with the introduction of the Bernoulli hypothesis. Hereafter plane cross sections remain plane after deformation. The resulting strain plane (Bernoulli plane) is completely defined by three parameters, e.g. with the strain values at three distinct points, not lying on one line. More often the parameter triple consist of one representative strain ε_m at a reference point m and two curvature values κ_y and κ_z, that are the rotation angles of the Bernoulli plane in the coordinate system (y, z). The strains at point i can be calculated with the equations

$$\varepsilon_i(x) = \varepsilon_m(x) + \kappa_y(z_i - z_m) + \kappa_z(y_i - y_m) \tag{4-150}$$

It should be noted, that the reference point m is not necessarily the center of gravity of the cross section. However this is often preferred, because the strain at the center of gravity is the mean strain, given as a property of the Bernoulli plane for homogeneous materials. The mean strain in turn can be used for determination of the appropriate longitudinal force

$$N(x) = E(x)A(x)\bar{\varepsilon}(x) \tag{4-151}$$

However, the governing equations can be formulated at any point m, provided that any mechanical parameter can be transferred to be compatible to the conditions at m.

The moments M_y and M_z can be similarly defined. The dependent strain components are the curvatures κ_y and κ_z

$$M_y(x) = E(x)I_y(x)\kappa_y \tag{4-152}$$

$$M_z(x) = E(x)I_z(x)\kappa_z \tag{4-153}$$

with application of the moments of inertia I_y and I_z.

All made assumptions qualify this approach for the treatment of elastic or linearized materials. However, if physically nonlinear behavior or hybrid structures are considered, the necessary averaging of parameters over the entire cross section can be complex. Fur-

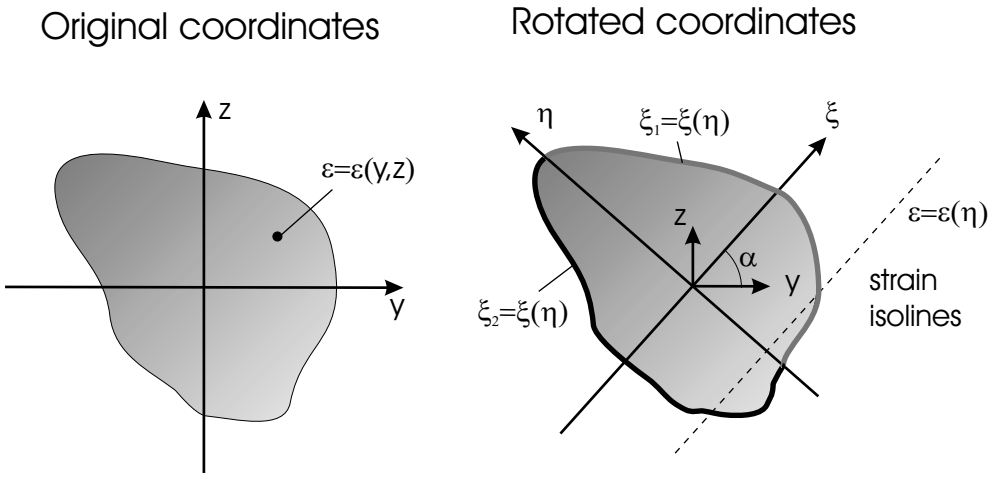

Figure 4-5 Integration over bounds using coordinate rotations into the Bernoulli-plane

thermore, the obtained values may not sufficiently represent the real behavior anymore. Alternatives are described in the following sections.

4.16.2 Direct integration of homogeneous cross sections

The analytical integration over the area of the cross section in order to determine the internal parameters is a practical opportunity, if the material law and kinematic condition are mathematically simple. For this purpose, the boundary of the cross section is discretized in several parts, so that the integration can be calculated with respect to the area under these curves. Such a strategy is comparable to the finite element method, in forming fragments (elements) that can be treated simpler than the overall region. Thus, the internal forces of the entire cross section are determined from the sum of the results obtained from the segments

$$N(x) = \sum_i N_i = \sum_i \int_{z_i}^{z_{i+1}} \int_0^{y(z)} \sigma(y,z)\, dydz \tag{4-154}$$

$$M_y(x) = \sum_i M_{y,i} = \sum_i \int_{z_i}^{z_{i+1}} \int_0^{y(z)} \sigma(y,z) z\, dydz \tag{4-155}$$

$$M_z(x) = \sum_i M_{z,i} = \sum_i \int_{z_i}^{z_{i+1}} \int_0^{y(z)} \sigma(y,z) y\, dydz \tag{4-156}$$

With application of the Bernoulli hypothesis, the integration simplifies considerable for homogeneous cross sections. The stain state is dependent on three parameters ε_m, κ_y and κ_z (see [81,187]). In the coordinate system (y, z) all parameters are generally a function

of two directions. However, the properties of the Bernoulli plane allow for an additional simplification. For a given loading state and if the curvature in the cross section is different from zero, a unique distribution of isolines can be determined, where strains and stresses remain constant. Their direction is given as the angle α in the original coordinate system (y, z). As the strains are constant, the appropriate orthogonal curvature is zero.

Transforming the problem into this direction, gives the new coordinate system (ξ, η) that is defined at the same origin as the original system, but is rotated so that the ξ direction is parallel to the strain isolines in the Bernoulli plane (see Fig. 4-5). Now the set of unknowns is ε_m, $\kappa = \kappa_\xi$ and α. The coordinates transform according to

$$\xi_i = y_i \cos(\alpha) + z_i \sin(\alpha) \tag{4-157}$$

$$\eta_i = z_i \cos(\alpha) - y_i \sin(\alpha) \tag{4-158}$$

Then the strains and stresses are a function of the orthogonal coordinates η only

$$\varepsilon(\eta) = \varepsilon_m + \kappa\eta \tag{4-159}$$

$$\sigma(\eta) = \sigma(\varepsilon(\eta)) \tag{4-160}$$

Consequently, the discretization of the boundary and determination of the internal forces is done in the same coordinate system

$$N(x) = \sum_i N_i = \sum_i \int_{\eta_i}^{\eta_{i+1}} \int_0^{\xi(\eta)} \sigma(\eta)\, d\xi d\eta \tag{4-161}$$

$$M_\xi(x) = \sum_i M_{\xi,i} = \sum_i \int_{\eta_i}^{\eta_{i+1}} \int_0^{\xi(\eta)} \sigma(\eta)\eta\, d\xi d\eta \tag{4-162}$$

$$M_\eta(x) = \sum_i M_{\eta,i} = \sum_i \int_{\eta_i}^{\eta_{i+1}} \int_0^{\xi(\eta)} \sigma(\eta)\xi\, d\xi d\eta \tag{4-163}$$

The back-transformed internal forces at the origin of the (x, y) coordinate system are

$$M_x(x) = M_\xi(x) \cos(\alpha) - M_\eta(x) \sin(\alpha) \tag{4-164}$$

$$M_y(x) = M_\eta(x) \cos(\alpha) + M_\xi(x) \sin(\alpha) \tag{4-165}$$

that must be equivalent to the external forces at this point.

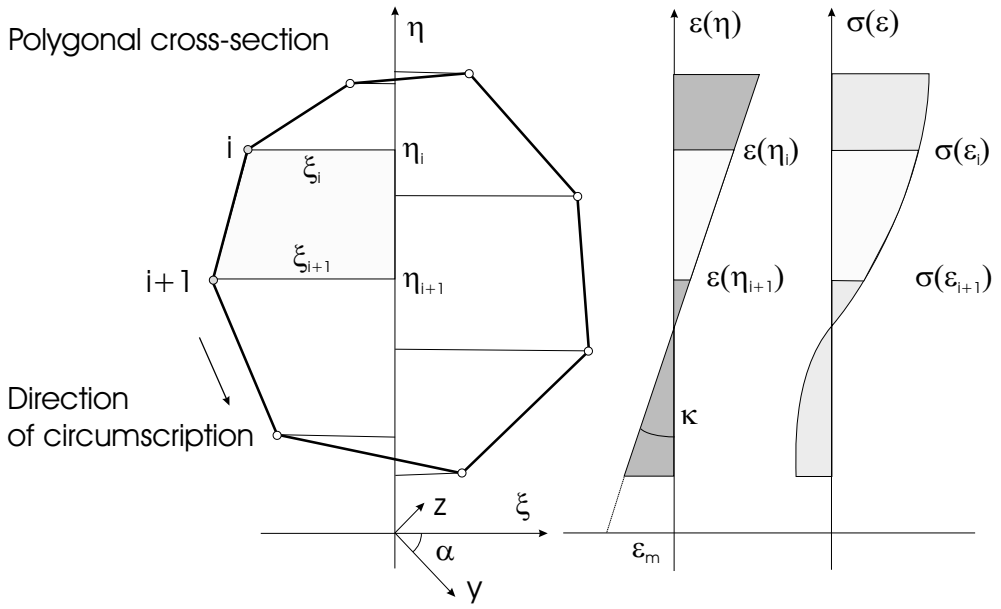

Figure 4-6 Model of a polygonally bounded cross section

4.16.3 Polygonally bounded cross sections

The application of the direct integration model from Section 4.16.2 within numerical programs, requires the boundary functions $\xi(\eta)$ to be relatively simple. An efficient strategy uses the approximation of an arbitrary boundary with piecewise linear functions [81]

$$\xi(\eta) = m_1(\eta - \eta_i) + \xi_i = m_1\eta - m_0 \tag{4-166}$$

which are evaluated in the interval between adjacent boundary points i and $i+1$, thus forming altogether a polygon. Here m_1 is the gradient

$$m_1 = \begin{cases} \dfrac{\xi_{i+1} - \xi_i}{\eta_{i+1} - \eta_i} & for \quad \eta_{i+1} \neq \eta_i \\ 0 & for \quad \eta_{i+1} = \eta_i \end{cases} \tag{4-167}$$

and m_0 represents the constant part of the line equation

$$m_0 = \begin{cases} m_0\eta_i - \xi_i & for \quad \eta_{i+1} \neq \eta_i \\ 0 & for \quad \eta_{i+1} = \eta_i \end{cases} \tag{4-168}$$

with the conditions for vanishing integration regions ($\eta_{i+1} = \eta_i$).

The obtained integration regions are trapezoids (similar to elements), as illustrated in Fig. 4-6. Here is indicated, that for the proper integration, all line functions of the trape-

zoids are to be defined following the same direction of circumscription. The internal force components, as defined in Eq. (4-161-4-163) for one trapezoid are

$$N_i(x) = \int_{\eta_i}^{\eta_{i+1}} \int_{0}^{m_1\eta - m_0} \sigma(\eta) d\xi d\eta = m_1 \Delta y_1 - m_0 \Delta y_0 \tag{4-169}$$

$$M_{\xi,i}(x) = \int_{\eta_i}^{\eta_{i+1}} \int_{0}^{m_1\eta - m_0} \sigma(\eta) \eta d\xi d\eta = m_1 \Delta y_2 - m_0 \Delta y_1 \tag{4-170}$$

$$M_{\eta,i}(x) = \int_{\eta_i}^{\eta_{i+1}} \int_{0}^{m_1\eta - m_0} \sigma(\eta) \xi d\xi d\eta = m_1^2 \Delta y_2 - 2 m_1 m_0 \Delta y_1 + m_0^2 \Delta y_0 \tag{4-171}$$

The functions Δy_n of order n are integrals with respect to η

$$\Delta y_n = y_n(\eta_{i+1}) - y_n(\eta_i) = \int_{\eta_i}^{\eta_{i+1}} \sigma(\eta) \eta^n d\eta \tag{4-172}$$

If possible, the integrals can be solved in the present form, or can be transformed for $\kappa \neq 0$ into a relation dependent on strains by application of Eq. (4-159)

$$y_n(\eta) = y_n(\varepsilon) = \frac{1}{\kappa^{n+1}} \int \sigma(\varepsilon) (\varepsilon - \varepsilon_m)^n d\varepsilon \tag{4-173}$$

Furthermore, dependent on the applied material law, integration by parts can lead to more convenient forms, as suggested in [187]. Then the integrals read

$$y_0(\varepsilon) = \frac{1}{\kappa} \psi_0 \tag{4-174}$$

$$y_1(\varepsilon) = \frac{1}{\kappa^2} \left[(\varepsilon - \varepsilon_m) \psi_0 - \psi_1 \right] \tag{4-175}$$

$$y_2(\varepsilon) = \frac{1}{\kappa^3} \left[(\varepsilon - \varepsilon_m)^2 \psi_0 - 2 (\varepsilon - \varepsilon_m) \psi_1 + 2 \psi_2 \right] \tag{4-176}$$

with

$$\psi_0(\varepsilon) = \int \sigma(\varepsilon) d\varepsilon \tag{4-177}$$

$$\psi_1(\varepsilon) = \int \psi_0(\varepsilon) d\varepsilon \tag{4-178}$$

$$\psi_2(\varepsilon) = \int \psi_1(\varepsilon) d\varepsilon \tag{4-179}$$

As in [187], all integrals can be provided for non-smooth or composed material laws too.

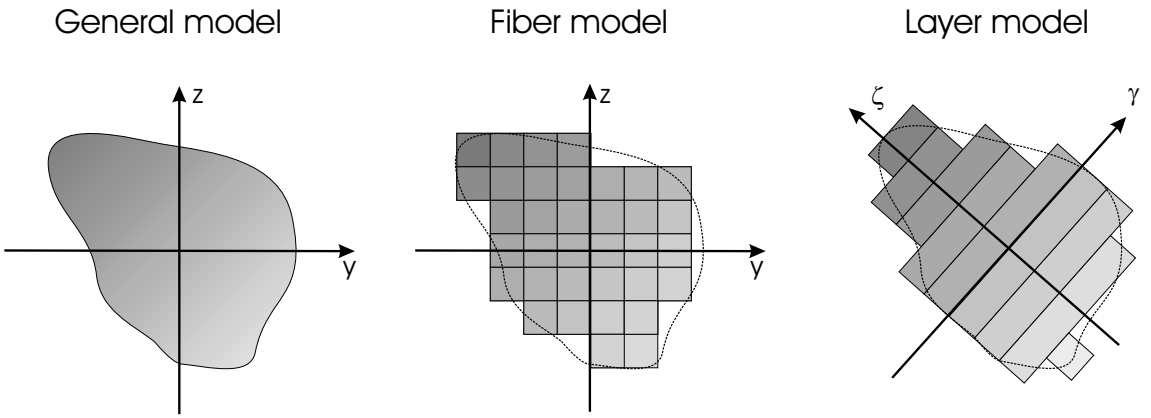

Figure 4-7 Illustration of cross section discretization as a fiber or layer model, using rectangular shapes and averaged material properties

4.16.4 Layer and fiber models

The previously described polygonally bounded cross sections are characterized by the discretization of the cross section into relatively few elements with complex material laws. With layer and fiber models, a contrary strategy is pursuited. The cross section is discretized into a relatively large number of fibers (elements) with simple geometry (like rectangles), while each of the fibers can behave differently but according to a relatively simple material law (preferentially linear or constant). This on the one hand increases the number of unknowns in the problem but decreases considerable the efforts for integration.

Principally, one fiber is treated like one cross section in Sec. 4.16.1, with the averaging over the fiber area. If the discretization is fine enough, the before-mentioned simplifications can be applied without greater loss of accuracy. The problem simplifies to a layer model, if the material properties and strains in a cross section are constant in a unique direction, denoted as coordinate directions (γ, ζ) in Fig. 4-7.

The basic assumption for this type of models is again the Bernoulli hypothesis, hence Eq. (4-150) applies as well. In any fiber the stress and internal force state can be calculated separately. In the equilibrium condition, all internal force and moment contributions from the fibers are summarized

$$N(x) = \sum_j N_j(x) \tag{4-180}$$

$$M_z(x) = \sum_j M_{z,j}(x) \approx \sum_j N_j(x) y_j \tag{4-181}$$

$$M_y(x) = \sum_j M_{y,j}(x) \approx \sum_j N_j(x) z_j \tag{4-182}$$

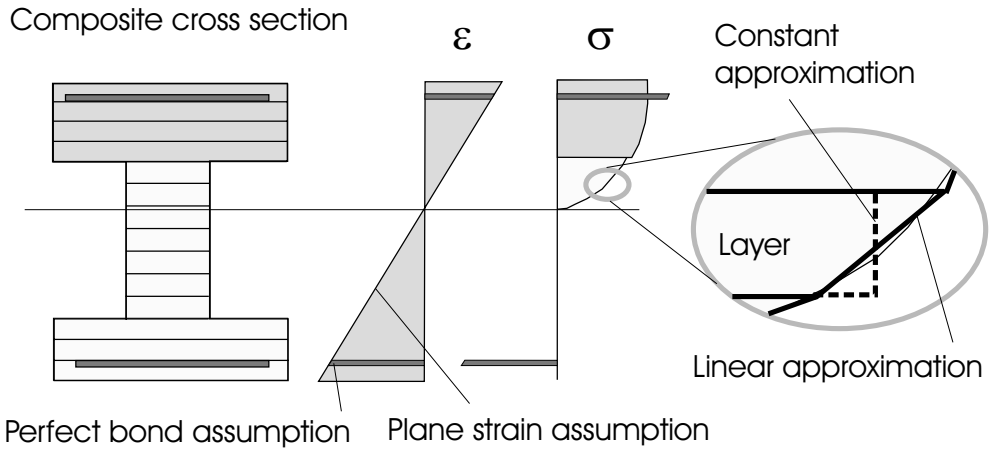

Figure 4-8 Example: Application of nonlinear material laws in layer models of composite cross sections

using the distances y_j and z_j from a reference point m to the centers of gravity of the fibers or layers j.

The application of nonlinear material behaviors is quite easy, because the nonlinear material functions can be applied separately to each fiber. For example, a simple elasto-plastic material law is

$$\sigma_i = \sigma(\varepsilon_i) \leq \sigma_{lim} \tag{4-183}$$

in form of a inequality condition. Although the stresses in the fibers are linear or constant, the resulting stress distribution in the cross section is nonlinear, as illustrated in Fig. 4-8.

4.16.5 Composite cross sections

Composite cross sections combine several parts with different properties. The strains in the components are related to each other, according to compatibility conditions, that specify the overall contribution of the part to the load transfer, or as bond conditions, describing the states at contact surfaces. Hereby cross sections need not necessarily be compact. If such conditions are given as mathematical equations or inequalities, they can be introduced as subsidiary conditions in optimization problems.

In structural engineering, most problems exhibit small deformations, thus the assumption of plane strains is appropriate. This already includes the assumption of perfect bond between the components. As can be seen in Fig. 4-8, fiber and layer models are naturally qualified for the analysis of composite cross sections. More details on the general treatment of composite structures are discussed later in Sec. 4.17.

4.16.6 Segment models

In the before-mentioned cross section models, the plane strain state has been assumed. This is appropriate for thin cross sections. An extension are segment models for the analysis of divided cross sections. The main characteristic is, that the Bernoulli hypothesis is not applied to the overall cross section, but locally for distinct segments. This is useful also for cross sections with non-perfect bond conditions between components.

The bond between the segments is organized either by the assumption of a deformation relation (e.g. rigid membrane effects) or definition of connection force functions (shear connections) at coupling points. Hereby the deformations and coupling forces serve as dual variables of the same problem. The definition with shear forces is often preferred, as the integration of specialized bond rules can be easily conducted, e.g. to implement an elasto-plastic behavior in the joints. Besides for member sections, segment models are often applied for the analysis of cross sections if an entire structures is cutted horizontally at the floor levels. Then the bearing walls form an appropriate cross section.

In order to describe the state of a structure between two components of a system, new variables can be introduced according to the methods of sections in mechanics. It is necessary to define appropriate coupling locations and parameters. In a kinematic formulation, the displacements or rotations between two segments are related by a coupling function. As dual variables, the coupling forces are derived. On the other hand, a static formulation relates the forces in both components, triggering appropriate deformations as dual parameters.

Any segment can be discretized in fibers (Sec, 4.16.4), or modeled as a polygonally bounded cross section (Sec. 4.16.3) or by forming an equivalent beam model according to (Sec. 4.16.1). Some methods are illustrated in Fig. 4-9. The equivalent beam model is very effective, because of the small number of unknowns. It is often used in the engineering practice to simulate low and high-rise panel buildings [2,75]. Because all walls are simulated as equivalent beams, given structural software can be applied. The necessary coupling conditions need to be specified, e.g. as in Fig. 4-10. Then the connection nodes are related to the beam nodes in a small deformation theory

$$u_{xk} = u_{xm} \tag{4-184}$$

$$u_{yk} = u_{ym} - \frac{\kappa_m b}{2} \tag{4-185}$$

$$\kappa_k = \kappa_m \tag{4-186}$$

stating the membrane, shear and local Bernoulli condition for the displacements u and plane rotations κ, given at the reference point m of the wall and the coupling point k.

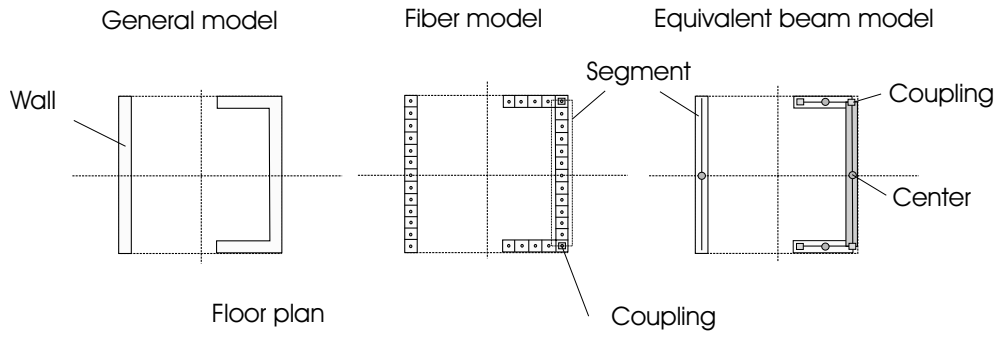

Figure 4-9 Derivation of segment models, using fiber or equivalent beam discretizations

Accordingly to this kinematic condition, the relation can be formulated in a static (equilibrium) formulation

$$t_{xk} = N_m + f_N \tag{4-187}$$

$$t_{yk} = V_m + f_V \tag{4-188}$$

$$t_{\phi k} = M_m - \frac{t_{yk} b}{2} + f_M \tag{4-189}$$

for the joint forces t and beam internal forces N , V, M and the external forces f. The segments are connected by joint functions between two nodal parameters. An elastic-perfectly plastic behavior in joints can be implemented with a inequality condition

$$t_k \leq t_{lim} \tag{4-190}$$

The behavior of continuously connected walls is analysed with help of the shear flow between two walls, e.g. with a linear distribution

$$\tau_k = \frac{t_{k,B} - t_{k,A}}{h} \tag{4-191}$$

4.16.7 Matrix notation for cross section problems

As well as for structural problems, cross section calculations can be formulated in matrix notation. Independent from the discretization method, cross sectional problem are characterized by internal parameters, as internal forces and strains in the discretized parts, e.g.

$$s = [N_j, M_{y,j}, \ldots,] \tag{4-192}$$

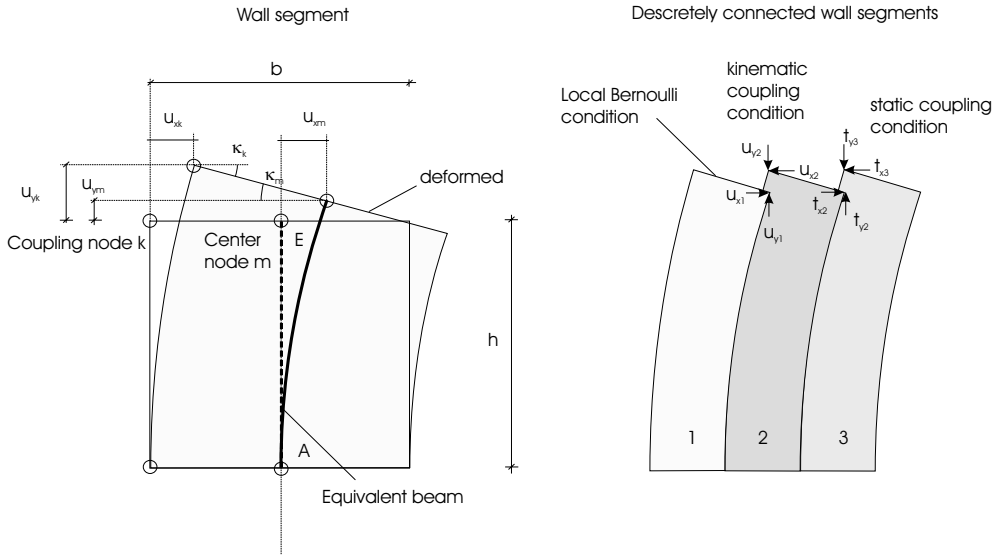

Figure 4-10 Equivalent beam model for the analysis of wall structures

$$e = [\varepsilon_j, \kappa_{y,j}, \ldots,] \tag{4-193}$$

The external parameters are discrete (integrated) external loads, such as longitudinal forces and moments, and the deformations that are the parameters of the Bernoulli plane, e.g.

$$f = [N, M_y, M_z] \tag{4-194}$$

$$u = [\varepsilon_m, \kappa_y, \kappa_z] \tag{4-195}$$

Then, for a fixed strain state the following form of the governing equations, including all necessary transformations, can be derived, with the kinematic condition

$$A_u u - e_0 = e \tag{4-196}$$

the material law

$$Q(e)s = e \tag{4-197}$$

and the equilibrium condition

$$A_s s + f = 0 \tag{4-198}$$

In comparison with the definition of structural problems in Sec. 4.15 it is obvious, that the basic formulation of both the cross sectional and structural problems is identical. There-

fore in the following, both problems are treated similarly, in the derivation of extremum and optimization problems.

4.17 System matrices and vectors of general composite structures

The assembly of structural components consisting of

- Components derived by discretization (e.g. finite elements, meshless discretized regions, fibers)
- Structural components (e.g. reinforcement, concrete)
- Structural members (e.g. girders, plates)
- Partial structures (e.g. main building and extensions)

into a global model is required for analysis. Such components are characterized by different

- Loading (concentrated, distributed)
- Material behavior (material type, rheology dependent,temperature dependent,...)
- Pre-states (pre-strain, pre-stress,...)

Hereby the parameters of the components are related by definition of coupling conditions. Basically two models for coupling can be distinguished.

Firstly, the "direct coupling" of parameters p_1 of the component 1 and p_2 of component 2 states a functional relation like

$$p_1 = p(p_2) \tag{4-199}$$

or as an inequality condition

$$p_1 \leq p(p_2) \tag{4-200}$$

The relation is "explicit" if it is applied as an additional subsidiary condition. The variables belonging to the interface are still part of their origin models, thus the number of unknowns in the problem remains constant. If on the other hand the relation is used to eliminate the connected variable from the system, thus reducing the number of problem unknowns, the coupling becomes "implicit". Then the interface variables (Index $_{int}$) are shared variables. In Tab. 4-16 the two forms of direct coupling are illustrated for the Poisson scheme of two elastic systems. The displacements u are implicitly coupled, whereas for the internal forces s the coupling is explicit.

As an application example, direct coupling is used to connect different parts of a structure, that have been discretized with different discretization methods, having the linked parameters be incompatible. This is given, e.g. if FEM and EFG models are coupled. Because of the applied interpolation methods, the displacement variables u_{EFG} of the EFG model are not the real displacements at the nodes of the problem. However, the node displace-

Table 4-16 Direct coupling of systems with different pre-deformation state (elastic example)

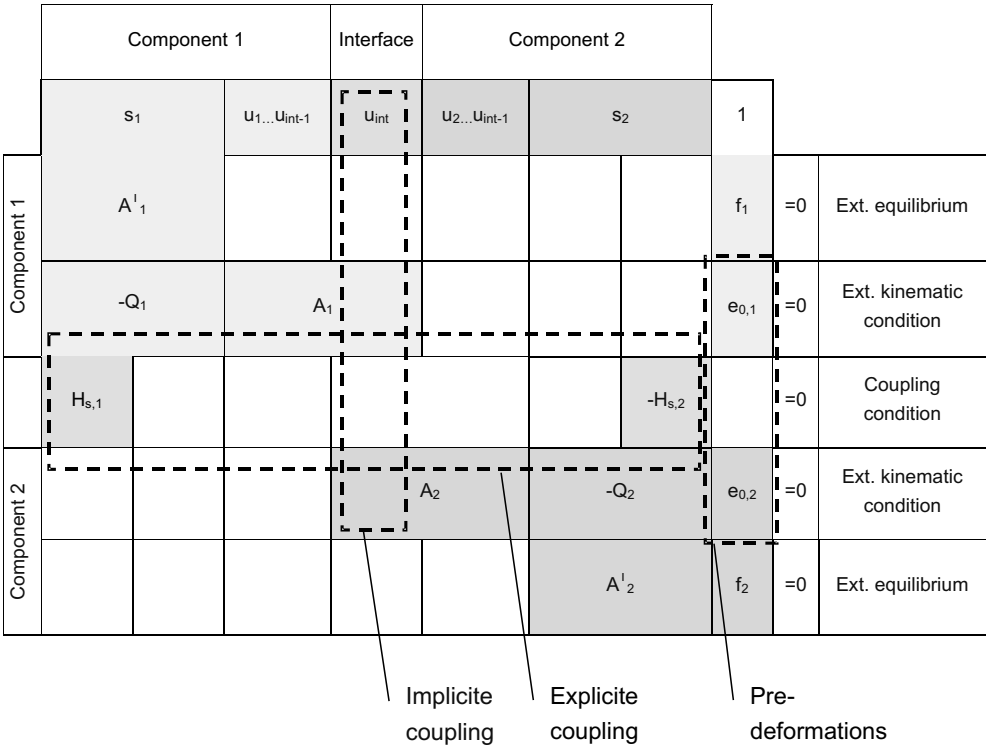

ments can be calculated from the shape function Eq. (4-22). Hence a possible coupling condition can be

$$H_{u,FEM} u_{FEM} - H_{u,EFG} u_{EFG} = 0 \tag{4-201}$$

commonly formulated explicitly as additional coupling conditions within optimization problems. Examples are given in Sec. 7.3.4 and 7.3.5.

Another interesting application is the coupling of models from different model categories. For instance, it can be used to connect a structural model with the appropriate cross section problems. The structural model part typically consist of simple elements, such as beams. At the predominant parts of the structure it is sufficient to state the material behavior of the beams with simple moment-curvature relations. Only at selected points a connection to a cross section model is established. This is useful, if extreme nonlinear responses are anticipated, that can be more efficiently or realistically estimated with help of cross section models. The application is especially advisable, if the interaction of internal forces needs to be considered [92,188].

Table 4-17 Indirect coupling of systems with different pre-deformation state (elastic example)

	Component 1				Interface		Component 2						
	s_1		u_1		u_{int}	t_{int}	u_2		s_2		1		
Component 1	$A^l{}_1$										f_1	=0	Ext. equil.
	$-Q_1$		A_1								$e_{0,1}$	=0	Ext. kinematic. condition
Interface				$N_{u,1}$	$-N_{u,int1}$							=0	Kinematic Coupling condition
					$-N_{u,int2}$			$N_{u,2}$				=0	
	$N_{s,1}$					$-N_{s,int1}$						=0	Static Coupling condition
						$-N_{s,int2}$				$N_{s,2}$		=0	
Component 2							A_2		$-Q_2$		$e_{0,2}$	=0	Ext. kinematic condition
									$A^l{}_2$		f_2	=0	Ext. equil.

Secondly, as already practiced for linking segment models in Sec. 4.16.6, it is sometimes useful to introduce additional variables, that itself can now be better related to further conditions. Then the coupling functions become, for the additional interface parameter p_{int}

$$p_{int} = p(p_1) \tag{4-202}$$

$$p_{int} = p(p_2) \tag{4-203}$$

to state an "indirect" connection. Respectively, the condition can be expressed as an inequality condition. Furthermore, as $p(p_1)$ and $p(p_2)$ can be arbitrary functions, the variable p_inT has not necessarily the same mechanical meaning as the connected variables. Table 4-17 illustrates the indirect coupling for two elastic systems.

All coupling functions must establish the compatibility of the involved parameters. This applies especially for the parameter transformation of different components into the same

(often global) coordinate system direction. For continuum elements, the transformation matrices L and R (obtained by polar decomposition according Sec. 3.7) already contain the transformations from local to global directions. Using the engineering simplifications for the strain calculation, the transformation from local into global directions must be explicitly provided. Then the matrices are $L = T$ and $R = T^T$ as the appropriate transformation matrices.

A special case of composite structures are hybrid structures. Hybrid structures are characterized by the connection of at least two structural components, that alone can fulfill the structural task. As for all composite structures, the advantages of the involved components can be emphasized, while the disadvantages can be compensated to a certain extend.

Figure 4-11 is illustrating the coupling of composite and hybrid structures. Generally, from this section it is obvious, that the treatment of coupling problem is generally straightforward within mathematical optimization.

4.18 Time integration

Following the Hamiltonian principle, the integration over time can be separated from the calculation of quasi-static problems. For time discretization, the application of the Finite Difference Method is often applied. Hereby the solution can be achieved with information of the past (explicit methods), as well as current and past information (implicit methods). Depending on the number of considered events in the past, the methods are called one- or multi-step methods. Beyond traditional methods, as in [166], a comprehensive summary about general treatment of linear multi-step time integration is given in [80]. A detailed discussion of time integration within optimization problems is provided in Sec 8.

4.19 Calculation strategies

For analysis and design in earthquake engineering the following calculation strategies are applied

- Modal decomposition analysis
- Simplified analysis
- Time history analysis

Modal decomposition methods evaluate the behavior of the structure without considering the loading. The structure is modeled linearly. Using eigenvalue analysis, the problem is transformed into the frequency domain. This information is valuable to estimate basic motion forms in the structure and the vulnerability to excitation frequencies. It is part of all simplified analysis methods. Furthermore, mainly due to complex eigenvalue analysis, the dynamic stability of a structure can be characterized. The application of modal analysis concepts on the basis of optimization algorithms is discussed in Sec. 5.

Simplified analysis methods avoid direct time history calculations of the structure. They use modal decomposition in order to derive decoupled differential equations. For the ge-

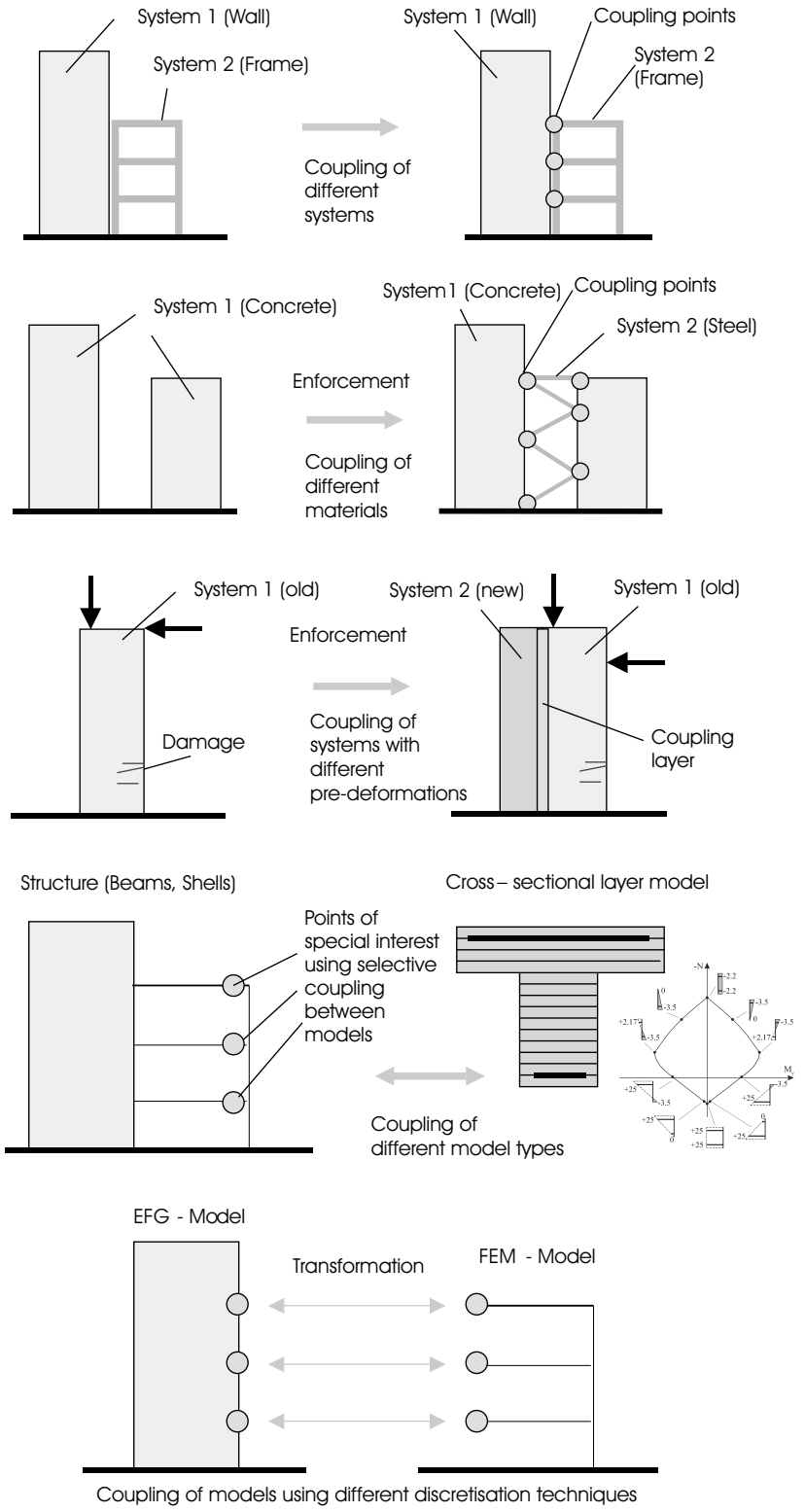

Figure 4-11 Examples for composite structures

nerated SDOF systems, the time history analysis is performed. This information can be gathered in advance and independent from the actual structure and is typically provided as response spectra, that contain the maximum responses of several SDOF calculations with varying eigenfrequencies. The main principle of simplified analysis is the transformation of the dynamic problem into an equivalent static problem, that exhibits approximately the same extreme reactions as the original problem. The following concepts can be distinguished:

- Simplified linear analysis
- Simplified nonlinear analysis

The first group is often called "force based design" whereas the second is called "displacement based design" [35], although in either method forces and displacements are evaluated. The main difference is, that linear methods base on linearizations and linear calculations, even if nonlinear structures are designed. The nonlinear methods however involve nonlinear relation directly in the calculation concept. Both design concepts are popular in codes, e.g. [24,105,73] and are herein discussed in Sec. 6 and 7.

Time history methods solve the dynamic problem directly by application of time integration methods. The solution is obtained at distinct times, commonly calculated in a step-by step strategy. Time history analysis is considered to be the most precise calculation concept. However it requires more information and numerical efforts. This complicates optimization strategies, where the time history analysis is repeatedly performed in order to monitor the effects of modified parameters. Furthermore, time history calculations for design purposes require the consideration of several earthquake records, in order to obtain a representative average solution. Examples for earthquake sets are given in the Appendix Secs. 11.6 and 11.7. Strategies based on time history analysis are presented in Sec. 8.

As all types of analysis are known to have their limits and benefits, for structures of a certain complexity a typical analysis requires mixed concepts. The simplified methods are quick and conceptive and are therefore perfect means for pre-design and basic configuration. Furthermore, in some countries the analysis based on spectra interpretation is considered to be the basis of defining a minimum safety level [104,105,73]. The time history analysis is applied to check the performance of the chosen design, to refine the concept and to decide necessary changes.

5 Modal and stability analysis

5.1 Eigenvalue problems

Exploring limit states is the main tasks in structural engineering in order to optimize the behavior according to given criteria. Herein one analysis type deals with the evaluation of the system performance, that can be defined by mathematical solvability limits. For instance, the static problem

$$Ku = f \tag{5-1}$$

can only be uniquely determined (i.e. is solvable), if the determinant of the system matrix is greater than zero

$$\det K > 0 \tag{5-2}$$

In this case, the matrix is positive determinant or definite. Hence, in structural mechanics, the investigation of $zero$-determinant conditions, generated as

$$\det(K - \ldots) = 0 \tag{5-3}$$

becomes of practical interest, as they mark limit states of the structure, e.g. regarding stability or resonance. Such problems are called eigenvalue problems as they describe important properties of the system without regard of external influences.

The evaluation of eigenproblems can be simplified, if the problems (5-3) can be transformed into a set of decoupled equations, thus providing only diagonal elements in the matrices. Such forms can be obtained if appropriate orthogonal transformations can be found.

For the simple case

$$\det(K - I\lambda) = 0 \tag{5-4}$$

where I is the unity matrix and λ a scalar value, it is sufficient to find the diagonal matrix K^* with application of the orthogonal transformation matrix Φ

$$K^* = \Phi^T K \Phi \tag{5-5}$$

The elements of the matrix K^* can be separated by stating

$$K^* = \Lambda I \tag{5-6}$$

introducing the vector

$$\Lambda = diag\,(K^*) \tag{5-7}$$

Then Eq. (5-5) is written

$$\Phi^T K \Phi - \Lambda I = 0 \tag{5-8}$$

As Φ is orthogonal, the following condition holds

$$\Phi^{-1} = \Phi^T \tag{5-9}$$

Therefore Eq. (5-5) can be rewritten

$$K\Phi - I\Phi\Lambda = 0 \tag{5-10}$$

As Φ has the ability of decoupling in Eq. (5-5), this relation can be shortened for distinct vectors of Φ

$$\Phi = [u_1, \ldots, u_i, \ldots, u_n]^T \tag{5-11}$$

and scalar components of Λ

$$\Lambda = [\lambda_1, \ldots, \lambda_i, \ldots \lambda_n]^T \tag{5-12}$$

thus giving

$$Ku_i - Iu_i\lambda_i = 0 \tag{5-13}$$

This formulation is called a real special eigenvalue problem and is identical to solving problem (5-4). In general, this relation holds for 1 to n (dimension of matrix K) components of Φ and Λ. The values λ_i,u_i and Φ are called the eigenvalue, eigenvector and modal matrix of the problem. The task is to find non-trivial solutions for λ_i and u_i.

5.2 Special eigenvalue problems

For the solution of Eq. (5-13) specialized algorithms can be provided. As well, optimization strategies can be utilized. They can be directly derived from the properties of eigenvalue problems:

- matrix Φ is orthogonal
- as for orthogonal transformations, the problem is independent from the scaling of matrix Φ
- matrix K is positive definite, thus orthogonal transformations with Φ lead to a decoupled problem
- the eigenvalues can be sorted, generating $\lambda_i \leq \lambda_{i+1}$. The index 1 is used for the smallest eigenvalue in the following sections.

Summarizing, the following optimization problem for determination of the smallest eigenvalue and it′s associated eigenvector can be stated

$$O(u_1, \lambda_1) = \lambda_1 \rightarrow Min \tag{5-14}$$

$$Ku_1 - Iu_1\lambda_1 = 0 \tag{5-15}$$

$$u_1^T u_1 = 1 \tag{5-16}$$

The last subsidiary condition regards for the scaling of the eigenvector, and can be almost arbitrarily modified.

Different from other eigenvalue problem solvers, in the optimization version additional possibilities of calculation control are offered, e.g. the calculation of the smallest eigenvalue that is beyond a certain limit $\lambda_{lim}.This will lead to the following task$

$$O(u_i, \lambda_i) = \lambda_i \rightarrow Min \tag{5-17}$$

$$Ku_i - Iu_i\lambda_i = 0 \tag{5-18}$$

$$u_i^T u_i = 1 \tag{5-19}$$

$$\lambda_i < \lambda_{lim} \tag{5-20}$$

This form also offers a strategy to calculate successively all eigenvalues of matrix K.

Furthermore, the scaling condition itself, given in the form of Eq. (5-16) can be applied for deriving an equivalent problem. Condition (5-15) can be multiplied with the eigenvector, so

$$u_1^T Ku_1 - u_1^T Iu_1\lambda_1 = 0 \tag{5-21}$$

With knowledge of Eq. (5-16) it becomes

$$u_1^T Ku_1 = \lambda_1 \tag{5-22}$$

This relation can be introduced in the objective function Eq. (5-14), thus this subsidiary condition and one variable are eliminated, leading to the following optimization problem

$$O(u_1) = u_1^T Ku_1 = \lambda_i \rightarrow Min \tag{5-23}$$

$$u_1^T u_1 = 1 \tag{5-24}$$

For determination of the next eigenvalue λ_2 and the associated eigenvector u_2, the orthogonality condition can be used

$$u_2^T u_1 = 0 \tag{5-25}$$

by using the previous solution u_1. Generalizing, the following optimization problem can be stated

$$O(u_{i+1}) = u_{i+1}^T K u_{i+1} = \lambda_{i+1} \rightarrow Min \tag{5-26}$$

$$u_{i+1}^T u_{i+1} = 1 \tag{5-27}$$

$$u_{i+1}^T \Phi_i = 0 \tag{5-28}$$

As indicated, all eigenvalue/eigenvector pairs can now be determined, starting with the smallest value and successively calculating the next. In the matrix Φ_i the vectors $u_1, \ldots, u_i$ of previous calculation steps are collected.

5.3 Modal decomposition of undamped systems

Similar strategies are adopted for the analysis of dynamic systems, here first given by neglecting the damping

$$Ku + M\ddot{u} = f(t) \tag{5-29}$$

that for itself is a linear differential relation. Such linear problems can be solved by modal decomposition, i.e. providing a set of basic solutions of a homogeneous problem

$$Ku + M\ddot{u} = 0 \tag{5-30}$$

that afterwards can be appropriately superposed in order to get the final solution. The first step is the substitution of the unknown displacement by a basic function

$$u = e^{i\omega t} \tag{5-31}$$

then providing the derivatives with respect to t

$$\dot{u} = i\omega e^{i\omega t} = i\omega u \tag{5-32}$$

$$\ddot{u} = -\omega^2 e^{i\omega t} = -\omega^2 u = -\lambda u \tag{5-33}$$

Equation (5-33) is now introduced into the homogeneous system Eq. (5-30)

$$Ku - Mu\lambda = 0 \tag{5-34}$$

thus giving the characteristic equation. As can be seen, this is a similar problem as Eq. (5-13) and can be therefore solved with means of eigenvalue analysis.

Utilizing again an optimization approach, the problem can be stated as

$$O(u_{i+1}) = u_{i+1}^T K u_{i+1} = \lambda_{i+1} \rightarrow Min \tag{5-35}$$

$$u_{i+1}^T M u_{i+1} = 1 \tag{5-36}$$

$$u_{i+1}^T M \Phi_i = 0 \tag{5-37}$$

providing the eigenvalues λ and eigenvectors u of the system. As before, the purpose of Equation (5-36) is to provide a fixed scaling for the eigenvectors, e.g. here given as a mass proportional norm.

The values $\omega_i = \sqrt{\lambda_i}$ are the circle frequencies of the system, indicating important resonance frequencies of the structure. If the system is harmonically excited exactly at these frequencies, the system is responding with the deformation shape given by the eigenvector u_i, known in dynamics also as modes, collected in the modal matrix Φ.

Despite neglecting the (practically small) damping in this kind of calculation, the knowledge of the eigenvectors and eigenfrequencies is essential for earthquake engineering as they help to position the structural behavior against the frequencies of the earthquake excitation. They help estimating the possible vulnerability of systems.

After determination of the modal matrix, the decomposition can be finished in a second step, by application of the modal matrix Φ, introducing a set of generalized coordinates v

$$u = \Phi v \tag{5-38}$$

Now Eq. (5-29) is given as

$$K \Phi v + M \Phi \ddot{v} = f(t) \tag{5-39}$$

With multiplication of the transposed modal matrix

$$\Phi^T K \Phi v + \Phi^T M \Phi \ddot{v} = \Phi^T f(t) \tag{5-40}$$

only diagonal matrices are left

$$K^* v + M^* \ddot{v} = f^*(t) \tag{5-41}$$

Thus the problem decouples into a set of simple equations

$$K_i^* y_i + M_i^* \ddot{y}_i = f_i^*(t) \tag{5-42}$$

that can be solved e.g. by Duhamel integral or numerically by a step-by-step solving approach. The application of the modal decoupling is shown in Sec. 6

5.4 Simplified modal decomposition of damped systems

A simplification for the modal decomposition of damped systems

$$Ku + C\dot{u} + M\ddot{u} = f(t) \tag{5-43}$$

can be established in structural engineering, as the relatively small damping is not significantly influencing the quantity of eigenvalues and eigenvectors. First the eigenproblem

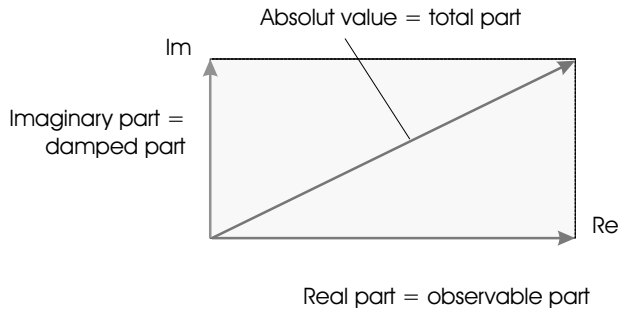

Figure 5-1 Real and imaginary parts of complex modes

is solved without acknowledgement of damping. Secondly, the decomposition regards the damping

$$\Phi^T K \Phi y_i + \Phi^T C \Phi \dot{y}_i + \Phi^T M \Phi \ddot{y}_i = f_i^*(t) \tag{5-44}$$

or shorter

$$K^* v + C^* \dot{v} + M^* \ddot{v} = f^*(t) \tag{5-45}$$

The matrix C^* is not necessarily diagonal. However, using the Rayleigh approach that compiles damping as

$$C = \beta_K K + \beta_M M \tag{5-46}$$

results in a mass or stiffness proportional representation for what β_M and β_K are appropriate scalar values. Using this or similar approaches, e.g. from [22], the generalized matrix C^* is diagonal as well. The resulting decoupled equations can be solved in the known manner.

5.5 Modal decomposition of damped systems

The simplicity of the undamped or simplified analysis strategies described in the previous section is given because the eigenvalue problems have only real solutions. This also means that damping effects are not considered in the modal analysis. This will change to complex solutions, if damping is directly involved. The contents and meaning of complex modes is illustrated in Fig. 5-1 where it is obvious, that the real part of the system energy is transformed into motion whereas the imaginary part is dissipated through damping.

Solving strategies based on mathematical optimization can be principally derived in the same manner as in the previous sections. The homogeneous equation

$$Ku + C\dot{u} + M\ddot{u} = 0 \tag{5-47}$$

is transferred into the characteristic equation

$$Ku + Cui\omega - Mu\omega^2 = 0 \tag{5-48}$$

by application of the basic functions Eq. (5-31-5-33). As the eigenvector u needs normalization, the following mass-proportional norm is stated

$$uMu = 1 + 0i \tag{5-49}$$

thus giving a first form of an optimization problem

$$O(u, \omega) = \omega^2 \rightarrow Min \tag{5-50}$$

$$Ku + Cui\omega - Mu\omega^2 = 0 \tag{5-51}$$

$$uMu = 1 \tag{5-52}$$

This form of optimization problem requires for solving not necessarily special algorithms that are prepared for complex analysis. Conventional real solvers can be utilized too. Complex calculations are only necessary before entering the interfaces of the optimization algorithm. For computation, just the real and imaginary parts of complex numbers are treated as separate variables. Hence, the eigenvector u is a real vector, but containing the complex number components

$$u = \left[u_1^{real}, u_1^{imag}, \ldots, u_n^{real}, u_n^{imag}\right]^T \tag{5-53}$$

Thus the amount of unknowns and subsidiary conditions is typically doubled compared with the appropriate real problem.

As described in Sec. 5.2, the equation is multiplied by the eigenvector u, giving

$$uKu + uCui\omega - uMu\omega^2 = 0 \tag{5-54}$$

With application of the norm Eq. (5-49), the optimization problem can be simplified

$$O(u, \omega) = \omega^2 = uKu + uCui\omega \rightarrow Min \tag{5-55}$$

$$uMu = 1 \tag{5-56}$$

The result is the smallest eigenvalue and the appropriate eigenform. By assembling the eigenvectors in a complex modal matrix Φ the successive calculation of higher modes can be performed

$$O(u_{i+1}, \omega_{i+1}) = \omega_{i+1}^2 = Ku_{i+1} + Cu_{i+1}i\omega_{i+1} \rightarrow Min \tag{5-57}$$

$$u_{i+1}Mu_{i+1} = 1 \tag{5-58}$$

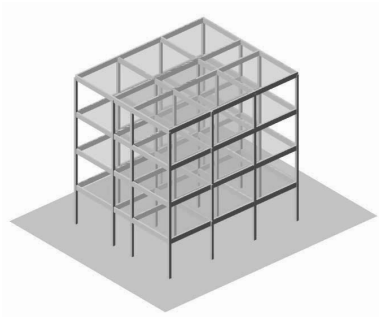

Figure 5-2 Example eigenvalue analysis (spatial model)

$$\Phi_i M u_{i+1} = 0 \tag{5-59}$$

with the orthogonality condition Eq. (5-59).

5.6 Solution by optimization strategies

All optimization problems for analysis of the previously described set of eigenvalue problems are quadratic complementarity problems, as they consists of quadratic objective functions, linear subsidiary conditions except for the orthogonality condition that is quadratic. They can be solved with specialized algorithms or ordinary nonlinear optimization strategies, as in Sec. 2.

The solution of the real problem is typically non-problematic, as those problems are convex, thus leading to an unique solution. However the complex problem as given in Sec. 5.5 is generally non-convex, resulting in the necessity of suitable starting vector provisions. As the damping in structural engineering is typically small, the solutions of damped and undamped problems are close and the real eigenvalue problem can provide these starting vectors. Then, a positive side effect is, that the solution duration is decreased for the complex system, as the algorithm needs only to search within the vicinity of the given start solution.

5.7 Example dynamic eigenvalue analysis

The following example is demonstrating the analysis methods given in the previous chapters. The structure of Fig. 5-2 is applied. For simplicity only a plane substructure is analysed as given in Fig. 5-3.

First, real and complex eigenvalue analyses are performed simultaneously. The results for the eigenvalues are listed in Tab. 5-1. This example uses mass proportional damping. As the mass is uniquely distributed in this example, the real part is constant for different modes. In Tab. 5-2 a stiffness proportional version is shown for comparison. Here the influence of the changing stiffness of columns and beams can be studied. For all cases,

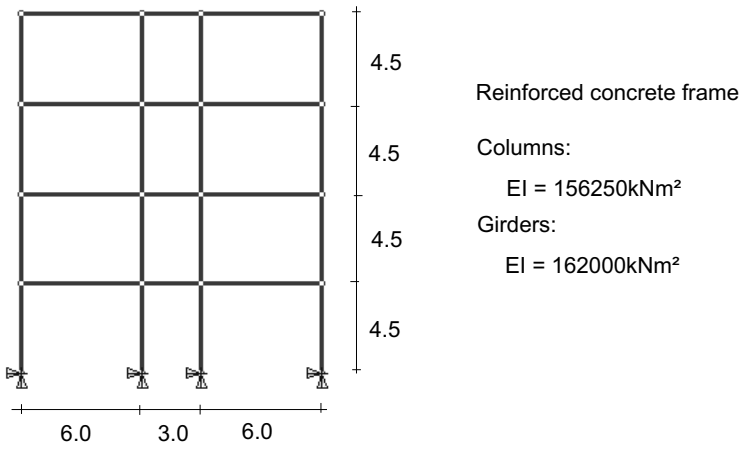

Figure 5-3 Example eigenvalue analysis (plane frame)

the eigenforms are given in Tabs. 5-3, 5-4 and 5-5. Here also, the influence of damping is obvious.

Table 5-1 Example: Real and complex eigenfrequencies using mass proportional damping

No. Eigenvalue	Real	Complex real part	Complex imag part
1	8.1793	-0.326250	8.172686
2	25.492	-0.326250	25.489321

Table 5-2 Example: Real and complex eigenfrequencies using stiffness proportional damping

No. Eigenvalue	Real	Complex real part	Complex imag part
1	8.1793	-0.511073	8.163213
2	25.492	-4.964206	25.003372

5.8 Classical stability (statics)

The classical stability (or buckling) analysis tries to determine a multiplier for the applied forces that exactly describes the stability limit state. Often this principle is exchanged for a multiplier for the internal forces or stresses in the structure. Then, two different stiffness parts are distinguished, a linear part K_{lin} and a geometric nonlinear part K_{geo} that is dependent on the internal force situation

$$u + f = 0 \tag{5-60}$$

Characterizing the solvability of the problem, the following eigenvalue problem can be stated

Table 5-3 Example: Real modes

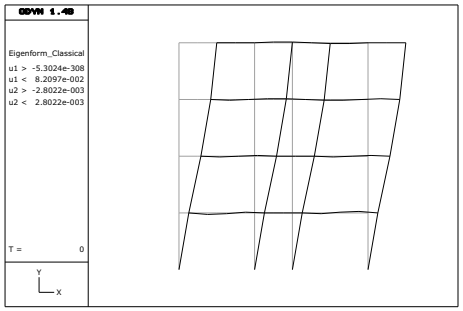

Eigenform 1

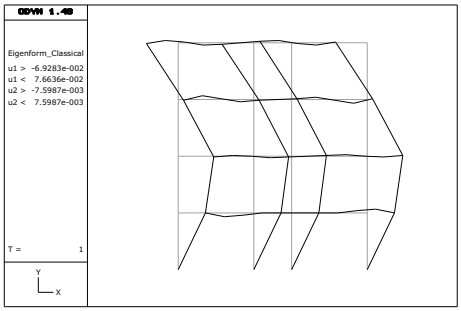

Eigenform 2

Table 5-4 Example: Complex modes mass proportional damping

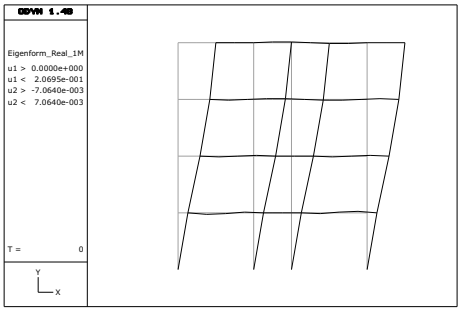

Eigenform 1 real part

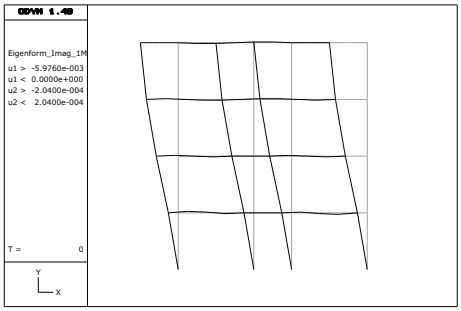

Eigenform 1 imaginary part

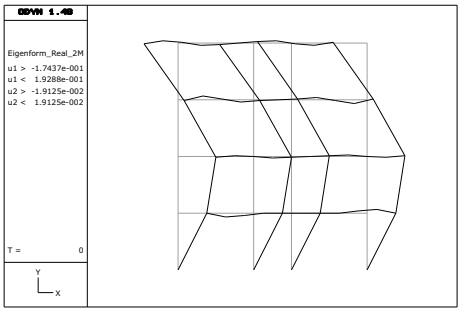

Eigenform 2 real part

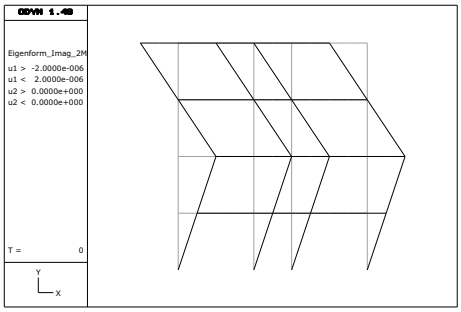

Eigenform 2 imaginary part

Table 5-5 Example: Complex modes stiffness proportional damping

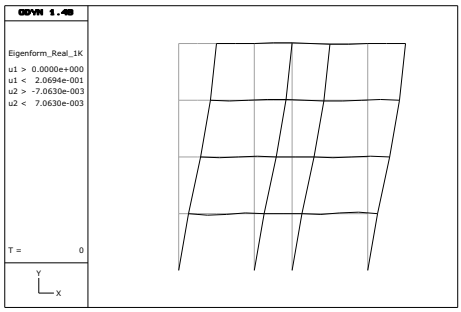

Eigenform 1 real part

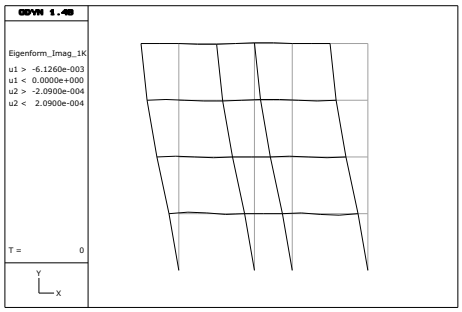

Eigenform 1 imaginary part

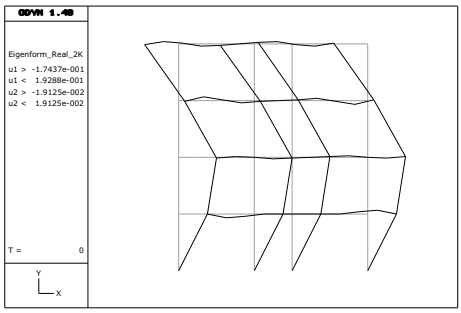

Eigenform 2 real part

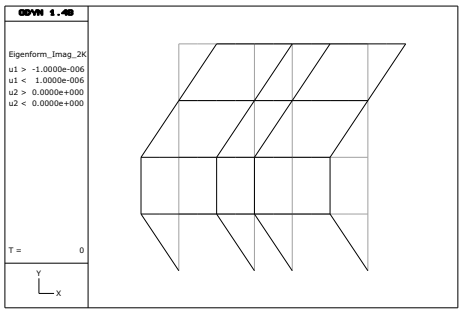

Eigenform 2 imaginary part

$$u = 0 \tag{5-61}$$

The eigenvalue λ can serve as the required limit state multiplier. Two aspects need to be fulfilled for the correctness of such a limit state problem. First, the pre-deformation state necessary for the determination of the internal force state must be linearly dependent on the force application. Secondly, the geometric stiffness matrix K_{geo} needs to be independent on the strain state. Such a prerequisite is only given, if the systems are linear, that′s why this theory is called linear stability analysis.

In order to evaluate the stability of a general system, the situation near to the bifurcation point need to be assessed. Or, the claim of determination of a multiplier will be abandoned. Then the solvability of a given system under given excitations need to be assessed. The situation is as follows, using the notation from Sec. 4

$$K_{NL}\, u + \varphi_{geo} + f = 0 \tag{5-62}$$

The definiteness of the problem is now only dependent on the properties of the nonlinear stiffness matrix, thus can be solved with methods of Sec. 5.2.

5.9 Dynamic stability

5.9.1 Lyapunov exponent

The dynamic stability analysis evaluates the behavior of dynamic systems in time. Hereby a system can have the following basic states:

- The system is asymptotically stable (or dissipative). The solution has an attractor where most of the motion is concentrated. The phase space is contracting.
- The system is conservative (non dissipative) if the volume of a phase space remains constant around a trajectory.
- The system behaves chaotic, i.e. small changes in excitation can result in extreme responses.

The most general measure to distinguish between these three states is the Lyapunov exponent, that is determined for a dynamic function $y(t, x, x_0)$ as

$$\lambda = \lim_{t\to\infty} \frac{1}{t} \ln \left| \frac{dy(t, x, x_0)}{dx} \right| \tag{5-63}$$

This exponent is positive if chaotic, zero for conservative systems and negative for asymptotically stable systems. The more negative the exponent, the greater the stability. As can be seen, the Lyapunov exponent is basically a statistical parameter, being a mean value for a dynamic process.

For multi-dimensional problems, the exponent is given as a spectrum of values

$$\lambda = [\lambda_1, \cdots, \lambda_i] \tag{5-64}$$

that are the eigenvalues for the Jacobian matrix of the function y

$$J = \frac{dy(t, x, x_0)}{dx} \tag{5-65}$$

calculated by the eigenforms of the quadratic form

$$T_J = \mathrm{eig}(JJ^T) \tag{5-66}$$

resulting in

$$\lambda = \ln \left[(T_J^T J J^T T_J)^{0.5} \right] \tag{5-67}$$

Usually, the evaluation of the maximum value is taken for system characterization. The basics on that topic are provided e.g. in [212,173]

Theoretically, the determination of the Lyapunov exponent seams to be a convenient concept of stability analysis, that can be also used for design of systems. The following opti-

mization problem can be stated, here noted in dependency on the general system parameter x

$$O(x) = \lambda(x) \rightarrow Min \tag{5-68}$$

$$y(x) = 0 \tag{5-69}$$

$$x <= x_{lim} \tag{5-70}$$

containing a general description of the structure in the function $y(x)$ and restrictions. However, the calculation of $\lambda(x)$ is quite costly, as it involves a huge number of times t with a representative amount of excitations.

5.10 Simplified stability estimation

5.10.1 Method description

The dynamic stability of a dynamically excited structure can be determined by

- the geometric stability (buckling)
- the physical stability (kinematic chain)

or combined effects. In static calculations without inertia forces, these instabilities are easily detected, because no equilibrium can be found. In dynamic calculations, such effects are complex and hard to detect.

However, for practical reasons in earthquake engineering, a simple eigenvalue analysis can be helpful. As known, eigenvalue analyses are limited to linear problems. That′s why the analysis can only be performed, if the time and system properties are linearized and therefore all coefficients are constant. This simplification is possible to apply at distinct times, if all nonlinear influences are introduced in the coefficient matrices, including geometric and physical nonlinear effects, e.g. deformations and damages contained in the structure. Then the method given in Tab. 5-6 can be applied. Compared with the Lyapunov exponent, the procedure generates conservative but practically useful results.

5.10.2 Example simplified stability analysis

The above described method is illustrated with help of an example. The structure is given in Fig. 5-4. The cross-sectional material behavior of the system is linear elastic - perfectly plastic, i.e. the admissible moments in all beams ends are restricted to be greater than -150 kNm. The structure is excited by an artificial earthquake (Fig. 5-5). For discussion of results one beam end has been selected.

In a first calculation a linear and a nonlinear time history analysis is performed. The bending moment result for the selected beam end is illustrated in Fig. 5-6. The redistribution effect of the moment is well visible.

Secondly, the structure is loaded at two load intensity levels:

Table 5-6 Principle of a simplified stability estimation

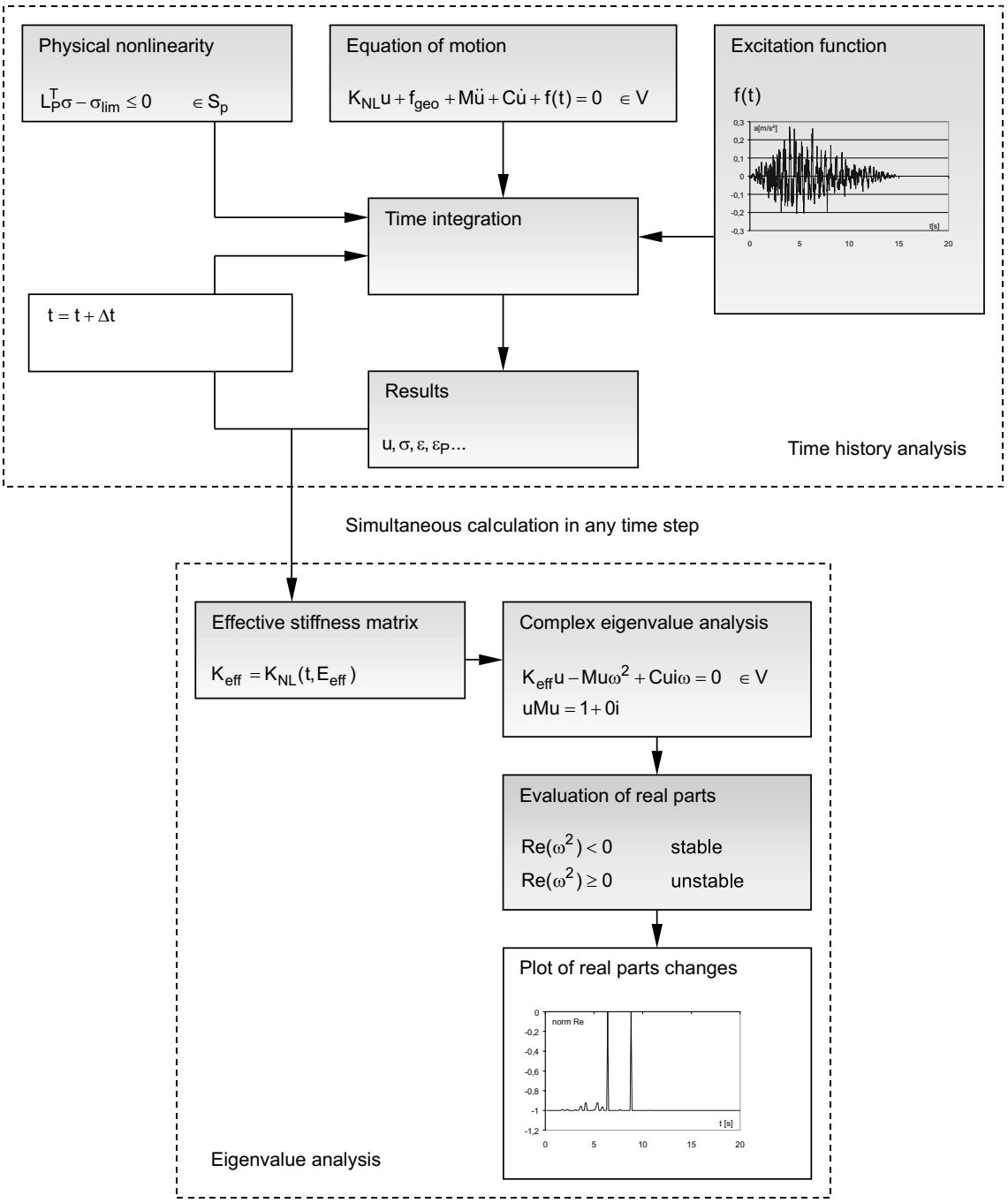

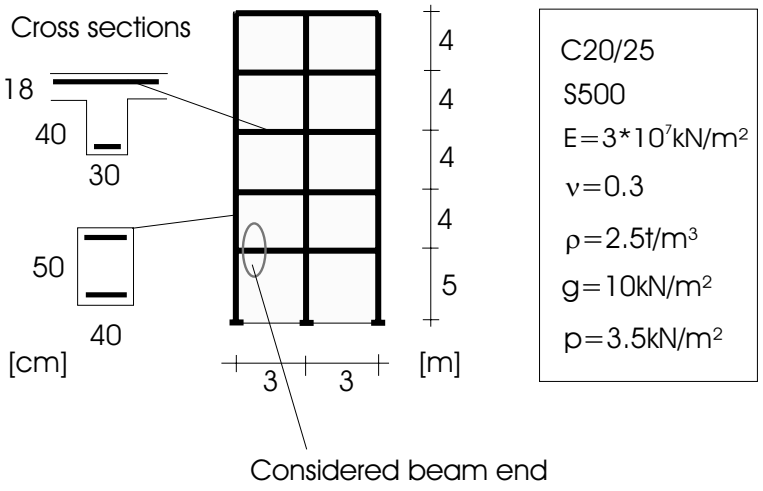

Figure 5-4 Example: Structural configuration

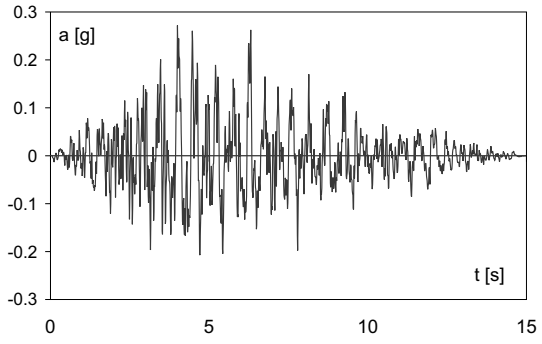

Figure 5-5 Example: Artificial accelerograms

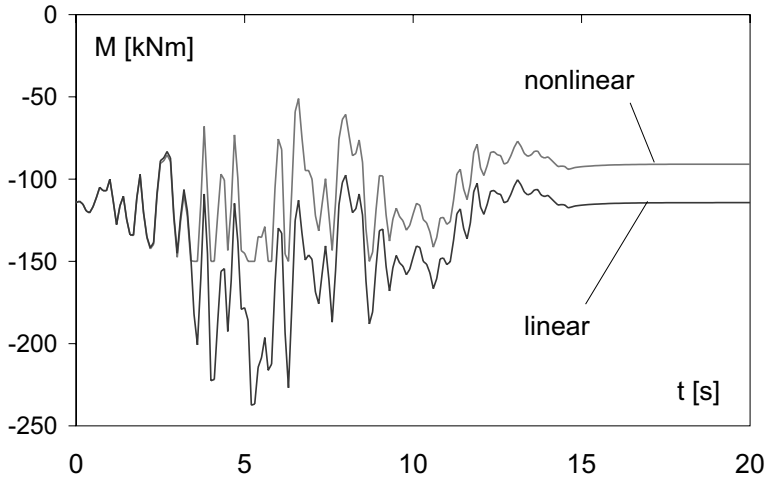

Figure 5-6 Example: Differences in moment development calculated in a linear and nonlinear analysis at Load level 1

Table 5-7 Example: Comparison of real part eigenvalue differences

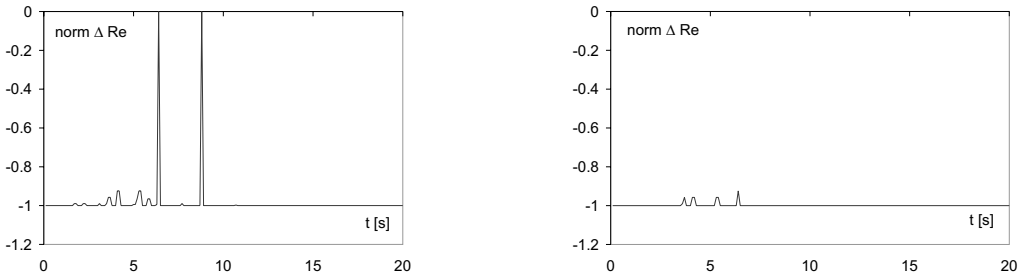

Load level 1 Load level 2

- Load level 1: Given load path effects in plastic hinges are not considered during design. The applied accelerogram intensity is 1.0.
- Load level 2: The structure is designed according to the shakedown limit state (see Sec. 7.4), therefore the development of plastic hinges during excitation is controlled. The appropriate accelerogram intensity is 0.71.

For both levels, the analysis steps given in Tab. 5-6 are performed. The appropriate results for the real parts of first complex eigenvalues over time can be compared in Tab. 5-7. As can be seen for Load level 1, the system becomes kinematic during the excitation. This behavior was not directly discovered in the time history analysis, but in the simultaneously performed complex eigenvalue analysis.

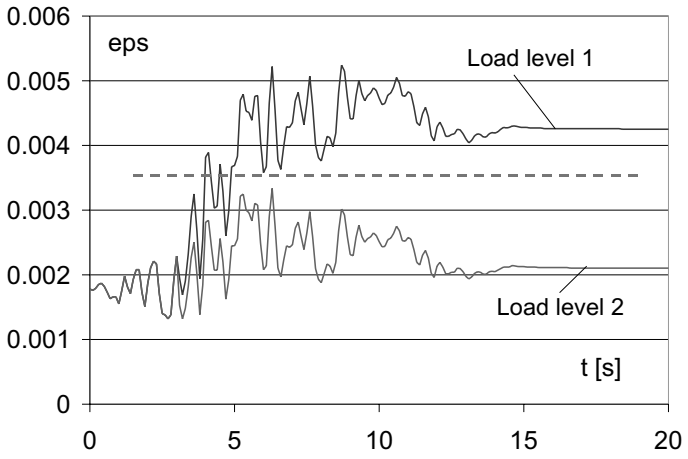

Figure 5-7 Example: Development of concrete strains in the considered beam end

In Load level 2, these problems vanish, as the adaptive limit state analysis avoids the development of a kinematic chain. In Fig. 5-7 the total deformations are given for the considered beam end. As can be seen, also for Load level 2 a more conservative behavior is obtained, by showing lower strains in the concrete as the limit of 0.0035.

6 Simplified linear analysis

Simplified linear methods base the analysis of nonlinear structures on linear models in order to utilize the computational advantages. For this purpose, nonlinear problems are transformed into equivalent linear models, that show approximately the same response characteristics as the original problem. Load reduction coefficient concepts and equivalent linearization strategies are applied.

6.1 Linear response spectrum analysis

The method uses modal decomposition of a discrete linear dynamic problem with n_{DOF} degrees of freedoms

$$M\ddot{u} + C\dot{u} + Ku + f(t) = 0 \tag{6-1}$$

with the excitation , commonly given as a function of the ground acceleration value $\ddot{u}_g$

$$f(t) = MI_{inf}\ddot{u}_g \tag{6-2}$$

where I_{inf} is the influence vector. This multi degree of freedom system (MDOF) is transformed into a set of single degree of freedom systems (SDOF) by using orthogonal transformations with help of $n_{Mode} \leq n_{DOF}$ eigenforms, given in the modal matrix Φ and generalized coordinates v [51]. With the substitution

$$u = \Phi v \tag{6-3}$$

in Eq. (6-1) and multiplication with Φ^T the following form is achieved

$$\Phi^T M\Phi\ddot{v} + \Phi^T C\Phi\dot{v} + \Phi^T K\Phi v + \Phi^T MI_{inf}\ddot{u}_g = 0 \tag{6-4}$$

that is, because of the orthogonality, identical with the solution of n_{Mode} decoupled equations

$$\Phi_i^T M\Phi_i\ddot{v}_i + \Phi_i^T C\Phi_i\dot{v}_i + \Phi_i^T K\Phi_i v_i + \Phi_i^T MI_{inf}\ddot{u}_g = 0 \tag{6-5}$$

Or simplified, if the modal mass $m_i = \Phi_i^T M\Phi_i$ is not vanishing, the equation reads

$$\ddot{v}_i + 2\xi_i\omega_i\dot{v}_i + \omega_i^2 v_i + \Gamma_i\ddot{u}_g = 0 \tag{6-6}$$

with the angular frequency

$$\omega_i = \sqrt{\frac{\Phi_i^T K\Phi_i}{\Phi_i^T M\Phi_i}} = \sqrt{\frac{k_i}{m_i}} \tag{6-7}$$

the damping rate

$$\xi_i = \frac{\Phi_i^T C \Phi_i}{2\Phi_i^T K \Phi_i} = \frac{c_i}{2\omega_i m_i} \tag{6-8}$$

and the participation factor

$$\Gamma_i = \frac{\Phi_i^T M I_{inf}}{\Phi_i^T M \Phi_i} = \frac{\Phi_i^T M I_{inf}}{m_i} \tag{6-9}$$

For non-vanishing participation, Eq. (6-6) can be written as

$$Sa_i + 2\xi_i \omega_i Sv_i + \omega_i^2 Sd_i + \ddot{u}_g = 0 \tag{6-10}$$

so that the obtained relation represents an SDOF system, that is only dependent on the damping ratio, the natural frequency and the ground acceleration. Hence, the values Sa, Sv, Sd can be provided in advance as response spectra, for a fixed damping ratio, a particular ground acceleration and a given interval of frequencies. An response spectrum is defined as the extreme absolute response of an SDOF system with defined natural angular frequency ω to a particular dynamic acceleration signal $\ddot{u}_g$ with a fixed duration $t = t_0 \dots t_n$, under a fixed rate of damping ξ, e.g. for the deformations

$$Sd(\omega, \xi, \ddot{u}_g(t)) = \max |Sd(\omega, \xi, \ddot{u}_g(t), t)| \tag{6-11}$$

The spectrum is commonly provided as a plot of (T,S(T)) pairs, if the natural period $T = 2\pi/\omega$ of the SDOF is stepwise altered within an interval. The necessary time integration is done e.g. by solving Duhamel′s integral, here given for the deformations

$$Sd(\omega, \xi, \ddot{u}_g(t), t) = \frac{1}{\omega} \int_0^t \ddot{u}_g \exp\left[\xi\omega\left(t-\tau\right)\right] \sin\left[\omega\left(t-\tau\right)\right] d\tau \tag{6-12}$$

or by application of a step-by-step numerical integration scheme (see Sec. 8). In the calculation of fixed-base structures, the damping ratio is relatively small. In this case, the explicit calculation of the modal acceleration and velocity is approximately

$$Sv \approx PSv = Sd\omega \tag{6-13}$$

$$Sa \approx PSa = PSv\omega = Sd\omega^2 \tag{6-14}$$

thus the spectral values are replaced by pseudo spectral values.

The classical procedure in Tab. 6-1 neglects the damping for the eigenvalue analysis (real eigenvalues)

$$(K - \bar{\omega}^2 M)\bar{\Phi} = 0 \tag{6-15}$$

whereas in the spectrum the damping is considered. For decoupling of the differential equation system Eq. (6-1), the damping matrix needs to have the property

$$\bar{\Phi}^T C \bar{\Phi} = diag(c_i) \tag{6-16}$$

that is e.g. provided by a linear combination of the mass and stiffness matrix (Rayleigh approach)

$$C = \alpha_M M + \alpha_K K \tag{6-17}$$

Furthermore, the classical procedure consequently applies the pseudo spectral simplifications. After determination, the spectral values are re-transformed into the time domain, applying the participation and eigenvectors. The procedure is repeated for all selected modes. Finally all modal results can be superposed to get the response of the structure. The application of a superposition rule is necessary, because spectral values itself are always positive and the sign of the mode shapes is not definite. The most commonly applied superposition rules are

- Sum of absolute peak values
- Square root of the sum of squares (SRSS)
- Complete quadratic combination (CQC)

For design purposes, spectra are provided in codes. Such "design spectra" are calculated from several ground motions and are treated by statistical means. They are simplified for practical use. Typically, codes provide a basic spectrum ("elastic spectrum") that considers a global viscous damping of 5%. The basic spectral values are then modified by seismic coefficients, e.g. for coverage of a different damping ratio or local soil characteristics, as described in the following sections.

The response spectrum analysis can be solved as an optimization problem (Sec. 5). Depending on a design parameter p and for a given acceleration spectra Sa, a typical design task in earthquake engineering is

$$p \rightarrow Min \tag{6-18}$$

with the subsidiary conditions

$$u = \sqrt{\sum_{i=0}^{n_{Mode}} u_i^2} \qquad (SRSS) \tag{6-19}$$

$$u_i = \Gamma_i Sa_i(\omega_i(p))\Phi_i(p) \tag{6-20}$$

$$\Gamma_i = \frac{\Phi_i^T(p) M(p) I_{inf}}{\Phi_i^T(p) M(p) \Phi_i(p)} \tag{6-21}$$

$$u \leq u_{lim} \tag{6-22}$$

Table 6-1 Classical response spectrum analysis

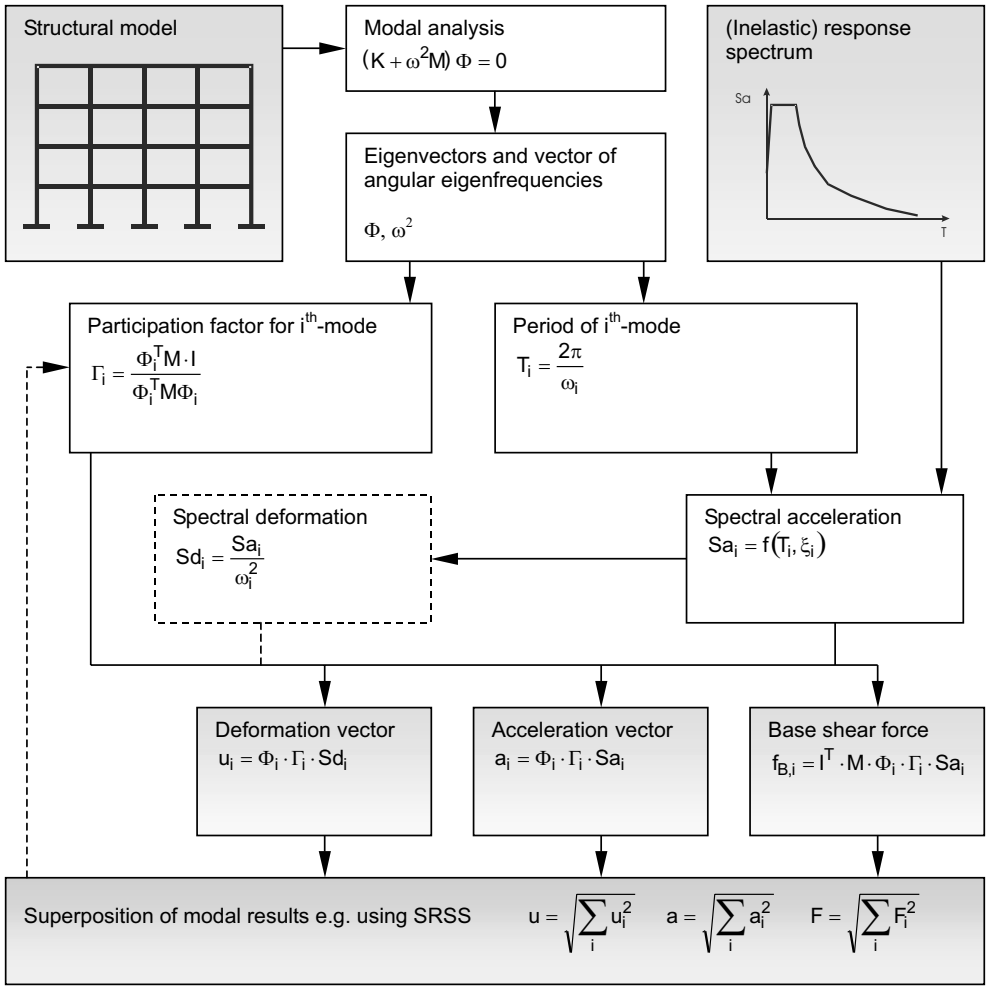

The last inequality contains the limit condition, for that p is adjusted. The values $\Phi_i$and ω_i are derived from a reel eigenvalue problem , e.g. with help of an embedded optimization problem from Sec. 5

$$\Phi_i(p), \omega_i(p) = \left\{ \begin{array}{l} \Phi_i^T K(p) \Phi_i = \omega_i^2 \rightarrow Min \\ \Phi_i^T M(p) \Phi_i = 1 \\ \Phi_{1,\ldots,i-1}^T M(p) \Phi_i = 0 \end{array} \right\} \tag{6-23}$$

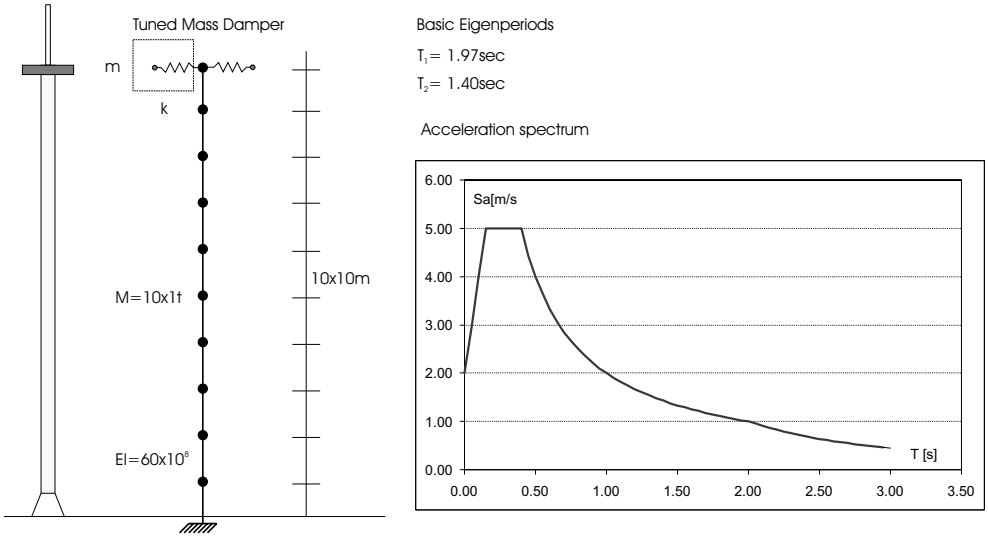

Figure 6-1 Example: Tuned mass damper

6.2 Example: Optimization of a tuned mass damper

The tower given in Fig. 6-1 can be simplified to a cantilever MDOF system. At the top of the building, a tuned mass damper should be installed. This device is modeled as a combination of spring and additional mass. The effect is illustrated in Fig. 6-2 where for a grid of mass damper properties the maximum accelerations are given. The typical minimum point can be seen, that can be as well determined by means of mathematical optimization, using gradient solvers. For this example, the acceleration was reduced down to 43%.

6.3 Example: Retrofitting a frame structure using linear response spectrum analysis

The two-story frame structure in Fig. 6-3 is to be retrofitted in order to reduce the interstory drift. The structure is loaded by the displayed ground acceleration. The limit state is defined by the admissible interstory drift, that is set to 1%. For retrofit, additional cable braces should be installed and appropriately designed for each story. The design variable is a scaling factor for the area of the cables A_{cab}. For analysis, the classical linear response spectrum method is applied. The structure is to remain elastic.

First the original structure is analysed ($p = A_{cab} = 0$). The first natural period is $T_1 = 1.39s$. The calculation is done with help of nonlinear optimization, using a gradient solver. For the eigenvalue analysis, the first three natural modes of the structure are included in the calculations. From this, the maximum interstory drift for the non-modified structure is 4.75% that is not sufficient.

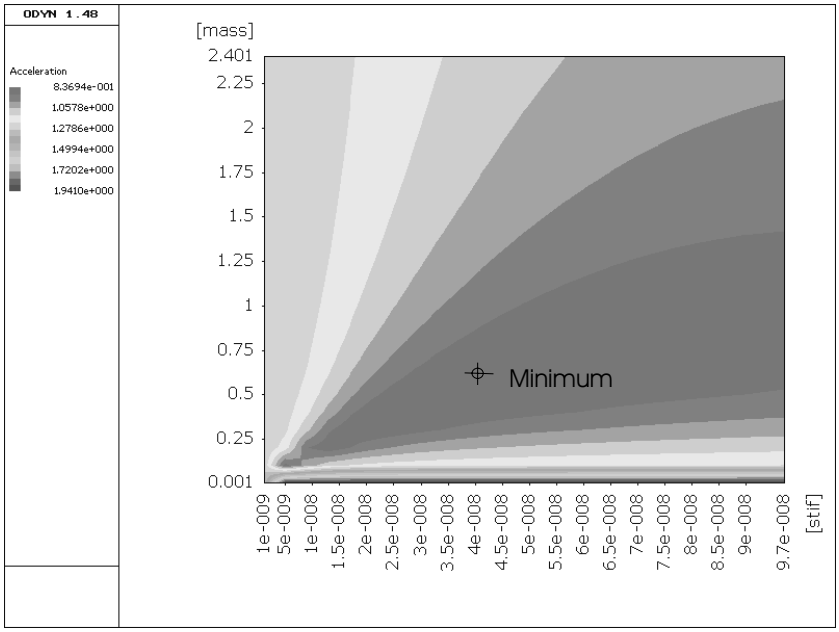

Figure 6-2 Example: Tuned mass damper, Illustration of design space, minimum point

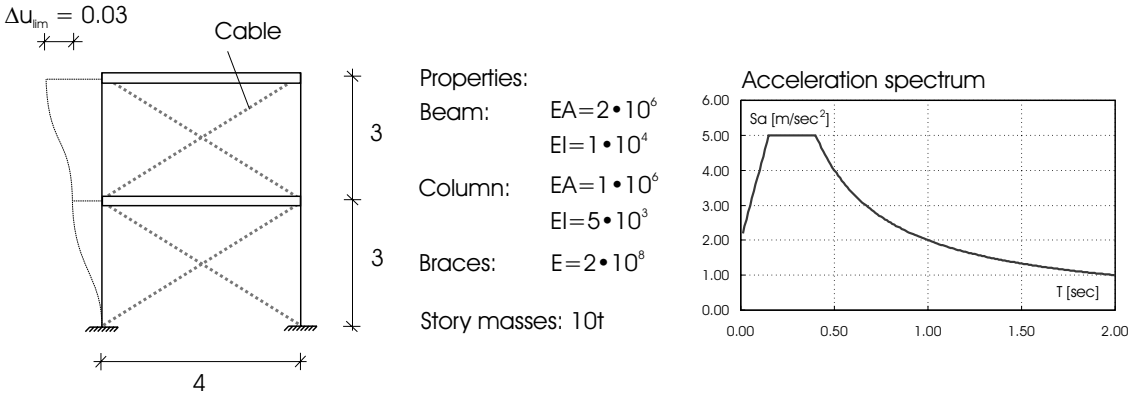

Figure 6-3 Example: Application of response spectrum method for the retrofit with cable braces

Second, the cables are installed. From solving the optimization problem (6-18-6-23), a minimum area of 1.5 cm^2 for each steel cable is required to guarantee the ultimate interstory drift. As the effect of the stiffening, the first natural period is decreased to $T_1 = 0.99sec.$

6.4 Reduction coefficient/seismic coefficients for inelastic analysis

The classical response spectrum method was developed for the analysis of linear elastic structures. Because of the energy dissipation during inelastic deformations, the internal forces of the structure can be significantly decreased. Approximately, this effect can be simulated in a linear response spectrum analysis, if the seismic loads are reduced. This strategy utilizes spectral reduction coefficients R in order to reduce the spectral excitation values Sa or Sd to a level, where the ultimate forces in the linear (substitute) system and nonlinear system are identical. Assuming a linear elastic - perfectly plastic behavior, the level of excitations in a system is then defined by

$$f_e = f_{nl} = \frac{1}{R} f \tag{6-24}$$

However, the appropriate deformations are much higher than in the fictitious elastic system. For calculation of ultimate displacements of the inelastic system u_u, equivalent displacement approaches or equivalent energy approaches are proposed according to Fig. 6-4 [51]. It becomes clear, that the reduction factor depends directly on the ductility, given as the ratio between the ultimate and yield deformation

$$\mu = u_u / u_e \tag{6-25}$$

The reduction coefficient concept is widely used among seismic design recommendations [73,69,105]. Codes provide rules to determine fixed reduction coefficients R (or sometimes called as structural system coefficients [208], or behavior factors with $q = 1/R$ [73]) or seismic coefficients c_s.

The coefficient R is applied in order to reduce the loading, e.g. acceleration spectra

$$Sa_{red} = \frac{Sa}{R} \tag{6-26}$$

The seismic coefficient is a factor to calculate the base shear force

$$f_B = c_s \cdot W \tag{6-27}$$

from the total weight W of the structure. Both concepts can include considerations of the

- Importance of the structure
- Regularity and rigidity of the structure
- Material, structural system, ductility supply
- Site effects, distance from the epicenter

In modern seismic codes, these criteria can be additionally combined with a performance factor, that accounts for an intended post-seismic performance [73,105,77]. Problematic is

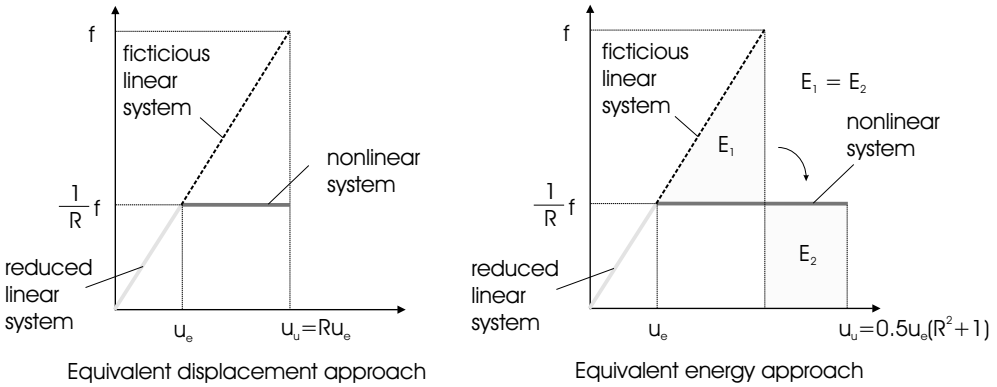

Figure 6-4 Comparison of equivalent displacement and energy approaches for the derivation of the reduction factor

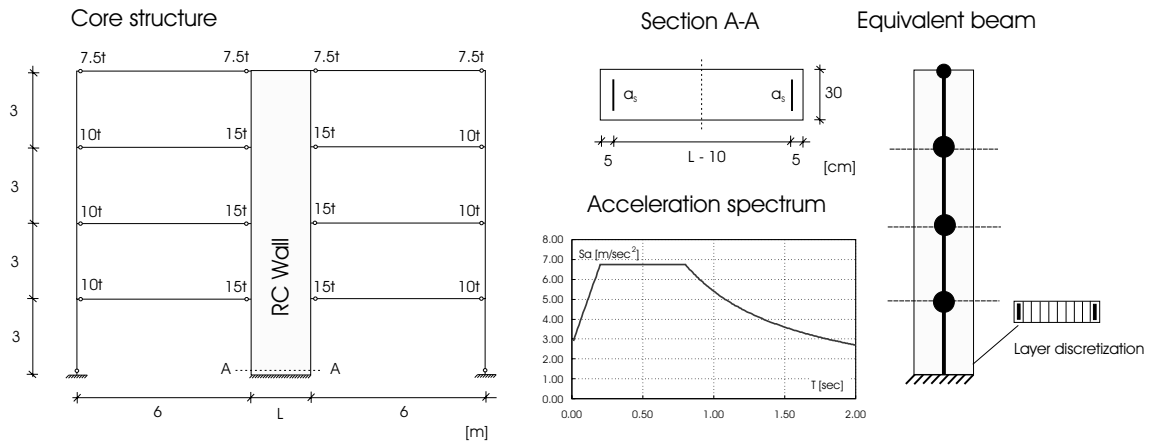

Figure 6-5 Example: Application of the reduction coefficient method

the appropriate determination of effective material parameters and the missing sensitivity to internal force re-distributions during nonlinear excitations.

6.5 Example: Reduction coefficient design of a core structure

The bending capacity of the reinforced concrete core structure in Fig. 6-5 is to be dimensioned. The length of the wall as well as the reinforcement is to be adjusted. Except for the length of the wall, all other geometric parameters are fixed. The loading is according to the acceleration spectrum in Fig. 6-5. The reduction coefficient is given with $R = 2.0$. The necessary area for the wall reinforcement in cross section A-A need to be calculated.

The calculation is performed in two steps. It starts with a pre-design of the wall length L. The design criterion is a limit interstory drift of 1%. The necessary effective stiffness

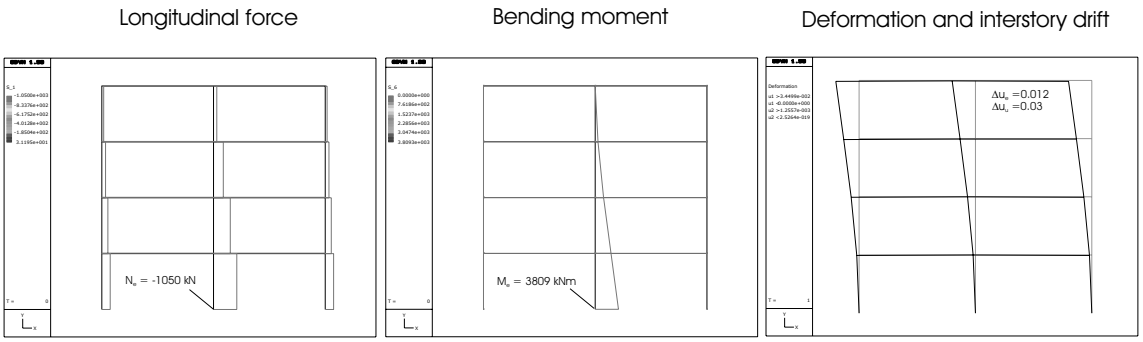

Figure 6-6 Example: Results from linear calculation obtained with spectrum reduction (R=2.0)

of the wall is determined from solving an elastic response spectrum analysis according to Model (6-18) - (6-23). The spectrum is reduced by application of R. In this calculation, the inelastic deformation is estimated with the equal energy approach (Fig. 6-4). The optimum value is an effective stiffness of

$$O(L) = EI_{eff} \rightarrow Min \tag{6-28}$$

that is calculated to 465660 kNm^2. From this, the appropriate length of the wall is calculated with the assumption of a 70% ratio of the stiffness of cracked to uncracked cross section. The necessary length is $L = 2.07m$. The plots of the appropriate deformation state, longitudinal force and bending moment distribution in the structure is shown in Fig. 6-6.

In a second step, a minimum optimization problem is solved to dimension the reinforcement of the structure to match the elastic longitudinal force N_e and the elastic moment of M_e. For analysis, the core is treated as an equivalent beam model according to Sec. 4.16.6, using a layer discretization for the cross section problem. The objective function is to provide a minimum reinforcement a_s, that is identically used in the tension and pressure zone of the cross section

$$O(a_s) = a_s \rightarrow Min \tag{6-29}$$

The subsidiary conditions contain the equilibrium condition, dependent on the stresses at the layer boundaries σ

$$A^T \sigma = f \tag{6-30}$$

with the loads f at the same points. The kinematic condition is

$$Au - \varepsilon = 0 \tag{6-31}$$

connecting the strains at the layer boundaries ε with the appropriate deformation. The following material law for concrete within cross section models is taken

$$\sigma = \begin{cases} -f_{cd} & for \quad \varepsilon_{c2} \geq \varepsilon \geq \varepsilon_{c2u} \\ -f_{cd}\left(1 - \left(1 - \frac{\varepsilon}{\varepsilon_{c2}}\right)^n\right) & for \quad 0 \geq \varepsilon \geq \varepsilon_{c2} \\ 0 & for \quad \varepsilon \geq 0 \end{cases} \tag{6-32}$$

with $n = 2$, $f_{cd} = 1.13$, and $\varepsilon_{c2} = -0.002$ for C20/25 [68]. The steel behaves linear elastic until the yield limit f_{yd} is reached. After yielding, the material is perfectly plastic. As the yield limit of the steel is determining the yield moment of the cross section, the following criterion is added

$$\sigma_s \leq f_{yd} \tag{6-33}$$

The problem is mainly determined by the boundary condition. This is Bernoulli′s hypothesis, stating that any deformation in the cross section is dependent on the deformation at an selected point m, beeing a plane cross section, thus

$$u = A_b u_m \tag{6-34}$$

with

$$A_b = \begin{bmatrix} 1 & y_j \\ 0 & 1 \\ \vdots & \vdots \end{bmatrix} \tag{6-35}$$

as the appropriate coefficient matrix (2D excitation). The matrix A_b connects the deformations at the point j with those at point m (see definition in Sec. 4.16). The deformation state is identically described with

$$u_m = [\varepsilon_m, \kappa_y] \tag{6-36}$$

The matrix A_b is identical with those that can be used to summarize the internal force state in the cross section at point m

$$f_m = A_b^T f \tag{6-37}$$

Hence, the Eqs. (6-34) and (6-37) can be used to substitute the layer parameters f and u by the parameters f_m and u_m, thus

$$A_b^T A^T \sigma = f_m \tag{6-38}$$

$$A A_b u_m - \varepsilon = 0 \tag{6-39}$$

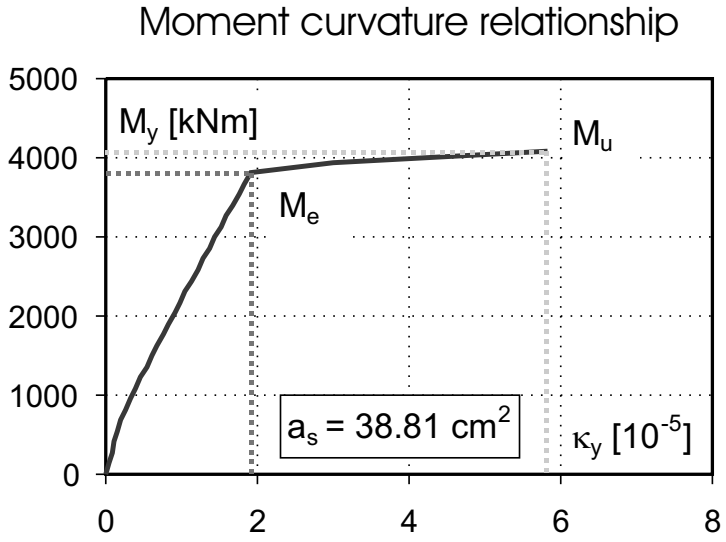

Figure 6-7 Example: Cross-section behavior for a fixed reinforcement

that is considerably reducing the dimension of the matrices. For this example, the following excitation is applied

$$f = [N_e = 1050kN, M_e = 3809kNm] \tag{6-40}$$

containing the elastic internal forces from the equivalent beam modes at the wall bottom.

Using this optimization problem, the reinforcement can be calculated. The result is $a_s = 38.81cm^2$ for either side of the cross section. For this reinforcement,the elastic curvature of the cross section is $\kappa_{v,e} = 1.91 \cdot 10^{-5}$, readable from the moment-curvature relationship in Fig. 6-7. The ultimate capacity is $M_u = 407979kNm$ while the appropriate maximum curvature is $\kappa_{v,u} = 5.83 \cdot 10^{-5}$. At this point a limit concrete strain of -0.0035 is reached.

For control, the ductility

$$\mu = \kappa_{v,u}/\kappa_{v,u} = 3.05 \tag{6-41}$$

is determined. Therefore it is obvious, that the reduction factor $R = 2.0$ was selected with enough safety margin, as the ultimate ductility in the equal energy approach is

$$\mu_u = 0.5(R^2 + 1) = 2.5 \tag{6-42}$$

It should be mentioned, that the effects of interaction of longitudinal force and bending moment is disregarded for the sake of simplicity in this example. However, in real design it is imperative to check for the effects of changing longitudinal forces.

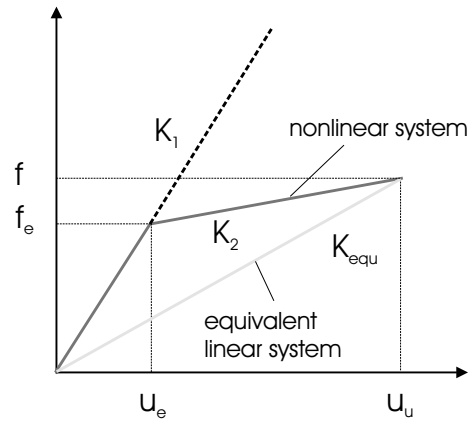

Figure 6-8 Definition of equivalent stiffness

6.6 Equivalent linearization for fixed-base structures

Besides spectrum reduction, a second strategy for application of the response spectrum procedure from Sec. 6.1 for inelastic systems is possible. It uses the transformation of the system into an equivalent linear system. One basic assumption in equivalent linearization is the comparability of the responses due to hysteretic and viscous damping. The generally nonlinear material law in hysteretic damping will be replaced by an equivalent linear elastic system with relatively high viscous damping. For that purpose an appropriate combination of equivalent stiffness and damping has to be provided. This topic was intensively studied in the last decades, e.g. in [106,107,110], and is already utilized in several design concepts. Because of observed analysis deficits in different fields of application, many adjustments and modifications have been proposed, mainly for fixed base design e.g. [52,53,106,22], or for base isolation designs, e.g. [115,103].

The fundamental approaches in equivalent linearization will be summarized as follows. To calculate the stiffness of the equivalent linear system the maximum structural forces f_u at the maximum deformations u_u in the viscous and elasto-plastic models are equated. As illustrated in Fig. 6-8 this will lead to the following expression for the equivalent stiffness

$$K_{equ} = \frac{f_u}{u_u} = K_1 \frac{(1 + \mu\gamma - \gamma)}{\mu} \tag{6-43}$$

dependent on the initial stiffness K_1, the ratio between the first and second slope stiffness $\gamma = K_2/K_1$ and the ductility μ. Since the masses in both systems are identical, the corresponding equivalent period is given by

$$T_{equ} = T_1 \left(\frac{\mu}{1 + \mu\gamma - \gamma} \right)^{\frac{1}{2}} \tag{6-44}$$

Hereby T_1 denotes the period of the elastic structure. The basic concept to derive the appropriate equivalent damping is, firstly, to assume a steady state response (sinusoidal) and, secondly, to assume that at maximum deformations one complete cycle in the response will be observed. Those two issues play a major role for the accuracy of the method especially if applied to real earthquake records.

Thus, for the derivation of the equivalent damping coefficient ξ_{equ} the equal dissipated energy rule will be applied. Both energies are schematically shown in Fig. 6-9. The dissipated energy of the hysteretic model is given by

$$E_h = 4 \cdot K_1 u_e (u - u_e)(1 - \gamma) = 4 \cdot K_1 {u_e}^2 (\mu - 1)(1 - \gamma) \tag{6-45}$$

The corresponding viscous energy is

$$E_v = \pi c \omega u^2 \tag{6-46}$$

is dependent on the square of the deformations u, the damping coefficient c and the circle frequency of excitation ω. Using an expression dependent on the damping ratio ξ will incorporate the parameters of the equivalent system

$$E_v = 2\pi \xi_{equ} K_{equ} u^2 \frac{\omega}{\omega_{equ}} \tag{6-47}$$

Equating both energies Eq. (6-45) and Eq. (6-47)

$$E_h = E_v \tag{6-48}$$

leads to the following original expression for the equivalent damping ratio

$$\xi_{equ,orig} = \frac{2(\mu - 1)(1 - \gamma)}{\pi \mu^2} \frac{T_{equ} T}{T_1^2} \tag{6-49}$$

A review of existing concepts showed that the frequency dependency of the damping is often simplified applying

$$T = T_{equ} \tag{6-50}$$

so that

$$\xi_{equ} = \frac{2(\mu - 1)(1 - \gamma)}{\pi \mu (1 + \mu \gamma - \gamma)} \tag{6-51}$$

The definitions in Eqn. (6-44) and (6-50) are widely accepted and used in earthquake engineering, e.g. as a basic part of the capacity spectrum method described in ATC40 [9]. Fig. 6-10 shows the effect of ductility change on the damping ratio ξ with respect to different stiffness ratios γ.

Finally the inelastic spectral value can be derived from reduced spectra, that can be calculated by time history analysis applying the appropriate viscous damping ξ_{equ}.

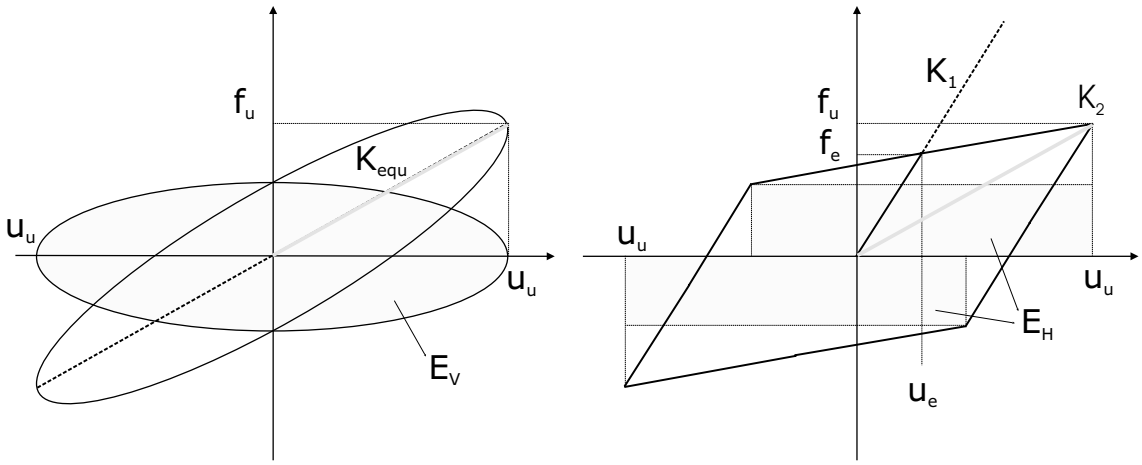

Figure 6-9 Equivalence of responses in viscously and hysteretically damped systems

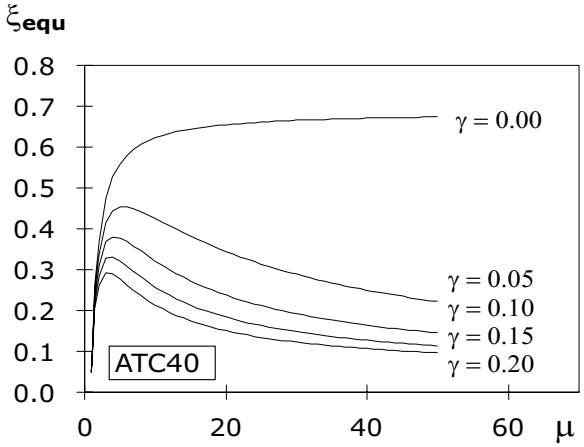

Figure 6-10 Dependency of equivalent damping on ductility and stiffness ratio

$$Sa \approx f(T_{equ}, \xi_{equ}) \tag{6-52}$$

It should be noted, that the application of the linear equivalent model requires the knowledge of the maximum deformations u, since the stiffness and damping are directly dependent. As those are mostly not available in practical cases, all calculations are basically iterative.

The method is qualified as a design strategy. The application is illustrated in Tab. 6-2. The procedure consists of two iteration loops. First, the appropriate damping ratio ξ is determined from the displacement of an substitute SDOF system. Otherwise a complex eigenvalue analysis can be alternatively performed. Second, the resistance parameter p is calculated that is the ratio between the elastic stiffness K_1 and equivalent stiffness K_{equ} in the plastic hinge zones. The design is finished if all deformation limits ε_{lim} are fulfilled or matched. For example, possible deformation criteria can be formulated depending on the cross-section curvatures or the interstory drift.

The control of the analysis can be organized as an optimization problem. Here the resistance factor p and the SDOF ductility parameter μ are the design parameters. The problem is illustrated in Tab. 6-3. The minimum of p is required in the objective function. The analysis is finished if the minimum parameter is found for that the subsidiary conditions are fulfilled. The calculation stops, if one kinematic parameter ε_{max} reaches it′s limit criterion ε_{lim}.

6.7 Example: Design of MDOF system as an equivalent linear system

The structure in Fig. 6-11 is to be designed for the shown earthquake excitation. Only the marked beam sections are selected to develop plastic hinges. The analysis is done according Tab. 6-3 with application of a nonlinear optimization algorithm. For equivalent linearization, the stiffness in the plastic zones is modified with a factor p, that can be modified between 0.0 and 1.0. As the design criterion, the maximum affordable total curvature in the beams must not exceed $\kappa_{lim} = 0.01$. The result of the analysis is $p = 0.14$, then the limit curvature is reached at the first story beam. Fig. 6-12 contains a comparison of the bending moments for the initial elastic and inelastic system. From this, the moments are reduced by a force reduction coefficient of $R = 382/231 = 1.65$.

As the optimization problem is only dependent on the parameter p, the solution space can be graphically illustrated. This is done in Fig 6-13, where the local curvature in the first-story beam and the global ductility μ are given in dependency from the stiffness modification factor p. From this it is obvious, that the solution space near the solution is relatively smooth and convex. Thus, the application of gradient optimization solvers is advisable for most solving efficiency.

6.8 Conventional simplified base-isolation design

The concept of base isolation effects two mayor modifications in the structural configuration.

Table 6-2 Iterative analysis of MDOF systems using equivalent linearization

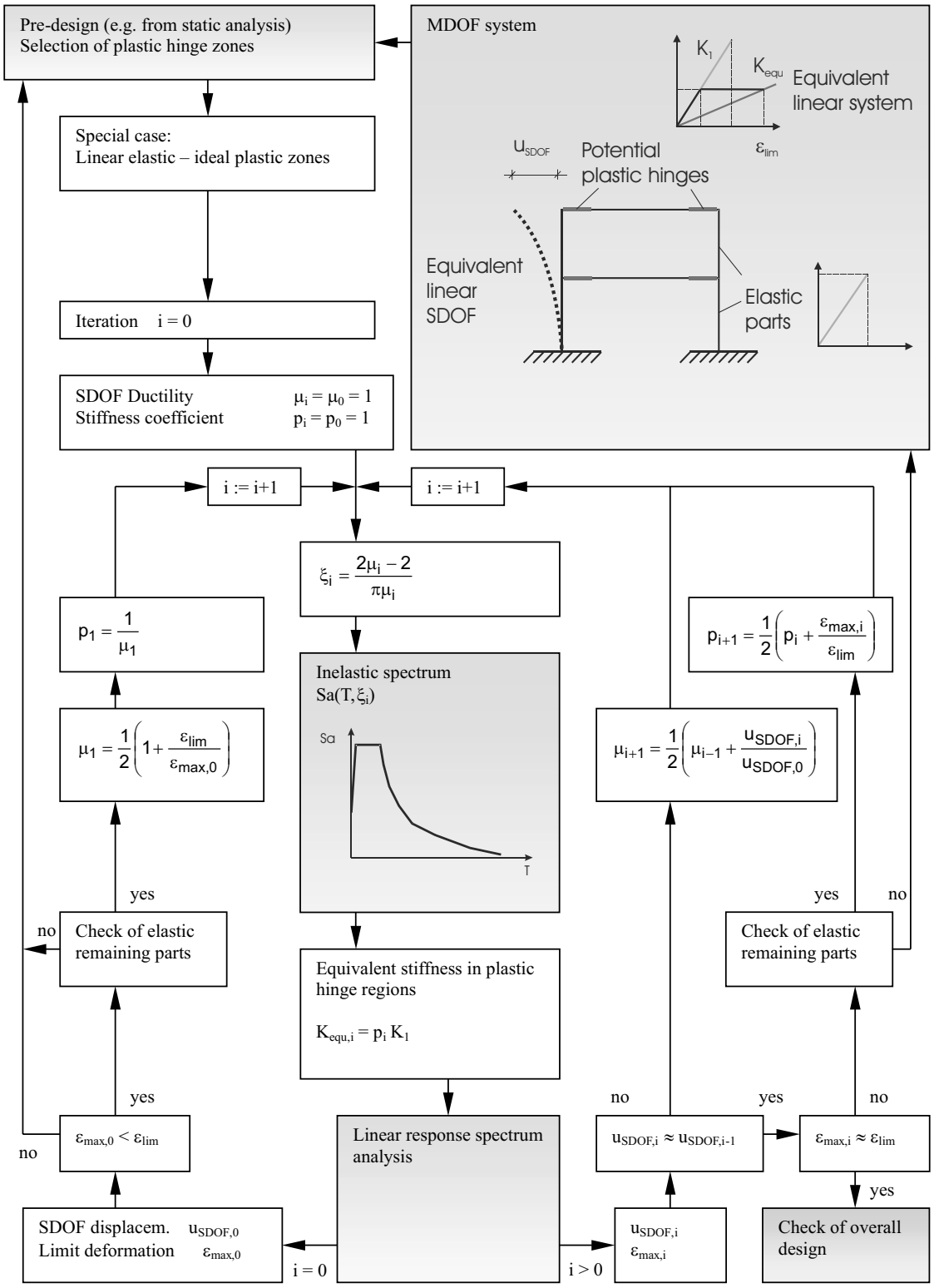

Table 6-3 Analysis of MDOF systems using equivalent linearization and nonlinear optimization

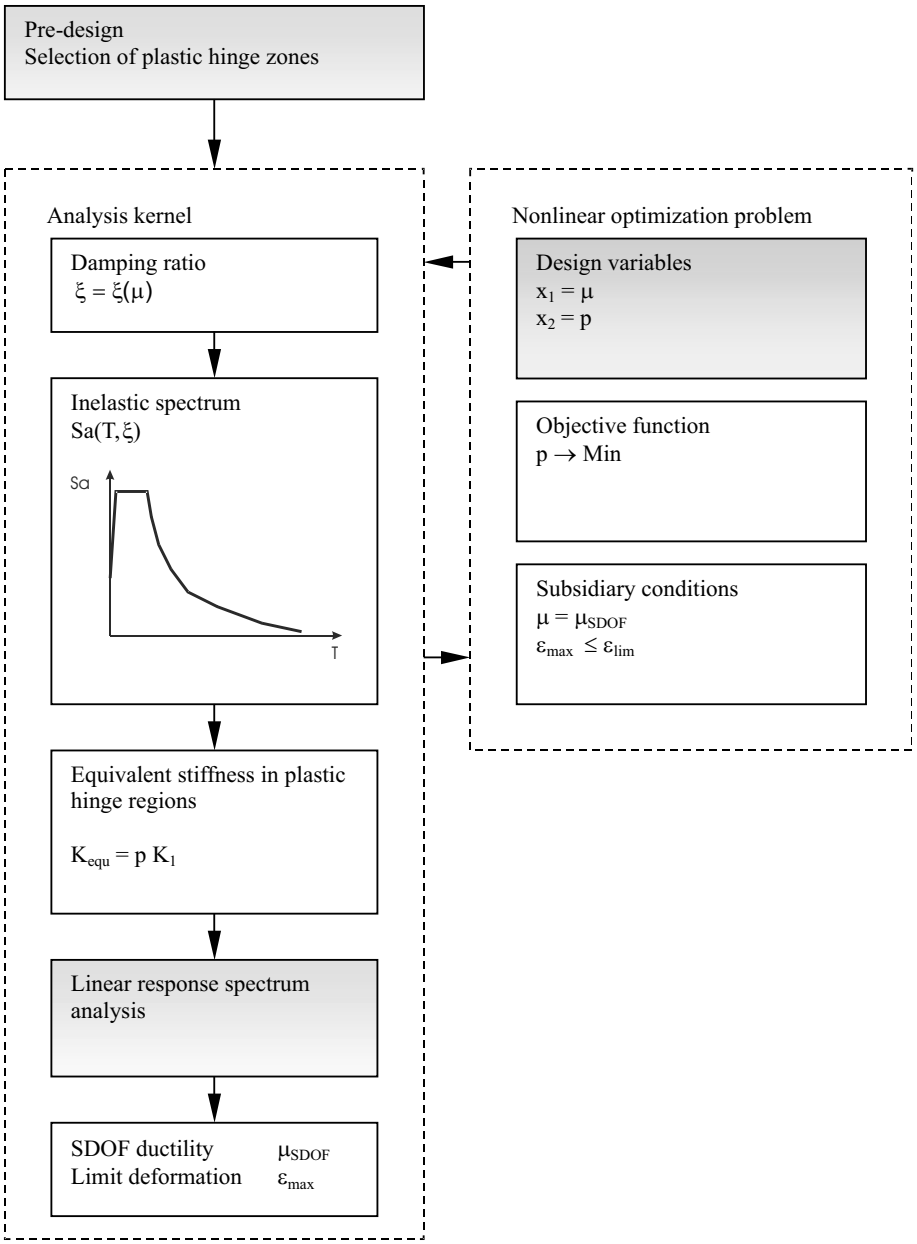

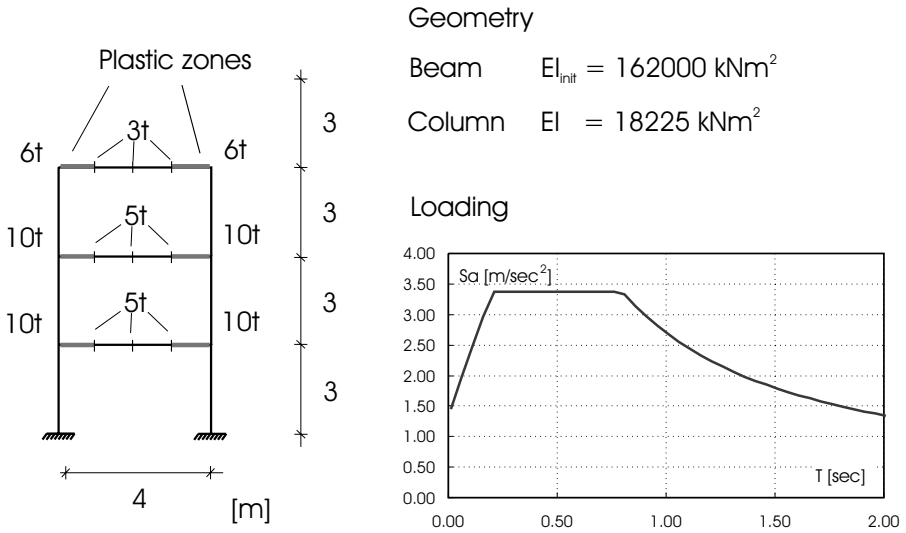

Figure 6-11 Example: Design of MDOF structure using equivalent linearization

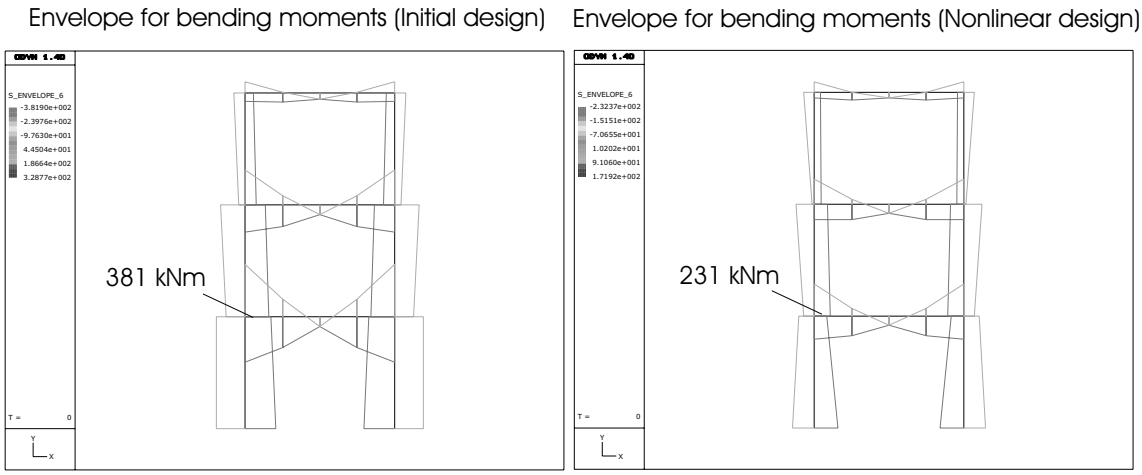

Figure 6-12 Example: Moment envelope for the elastic and inelastic systems

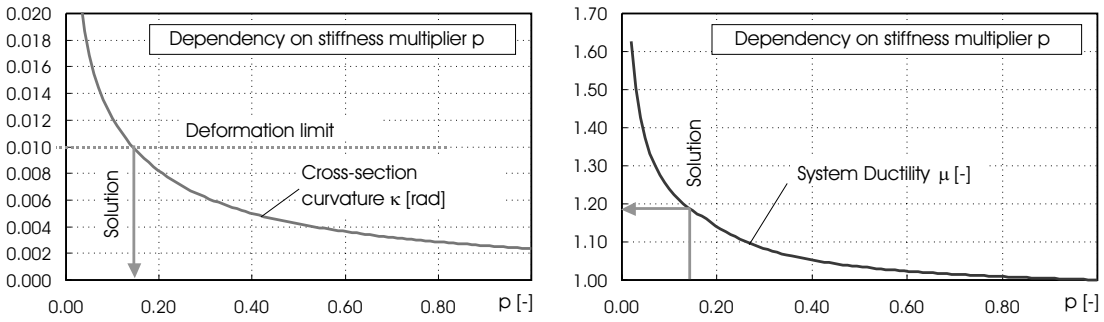

Figure 6-13 Example: Solution space; Dependency of the curvature and system ductility on the stiffness multiplier

Firstly: Providing a story with reduced stiffness commonly applied next to the base. Rubber bearing devices and sliding systems are combined in order to adjust the stiffness [171]. Dependent on the device configuration, the structural periods are shifted into long and very long range. Periods far beyond three seconds can be obtained [227,163]. This will result in greatly reduced super-structural forces and accelerations. Naturally, this has practical limits mainly because of the gradually growing flexibility. Limits given by isolation device characteristics, the disposable clearance to neighboring facilities as well as desired self-centering capabilities will determine the design.

Secondly: Instead of purely adjusting the stiffness, a combination with damping devices can be considered. This adds dissipative capacities to the system and reduces deformations due to an increase in the effective stiffness. This can be advantageous up to a certain point from that on additional damping will lead again to an increase in the loading of the superstructure [125]. Finding a beneficial balance of the stiffness and damping contribution to the structural behavior and the appropriate selection of suitable device combinations is a challenging task in design. The application of optimization strategies can be beneficial in the planning process.

Figure 6-14 shows basic device types and the typical composite reaction. The changes in the structural configuration require special precautions, especially for large deformations, to prevent impacts against surrounding facilities and to maintain the operability and stability of isolation devices. Additional interest arises for the accelerations in the superstructure. This parameter mainly determines the operability within the superstructure. Limit values are e.g. given in order to maintain sensitive equipment or to ensure the well being of patients in hospitals.

For analysis and design, simplified and time history methods are commonly utilized together. The former is quick and conceptive and is therefore a perfect mean for pre-design and device configuration. Furthermore, simplified analysis is often considered to be the

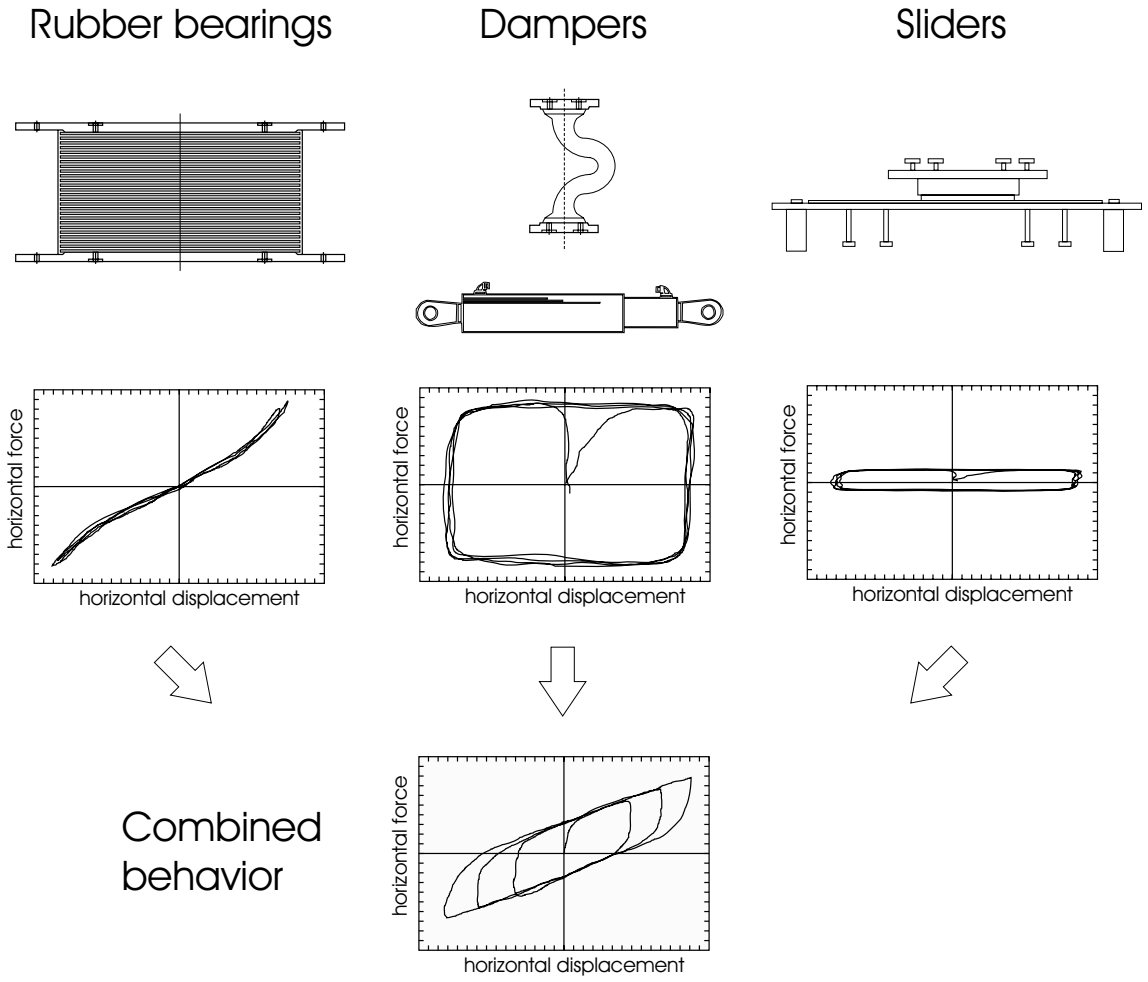

Figure 6-14 Base isolation basic devices and combined reaction

basis to define a minimum safety level [105,73]. Time history analysis will be applied to check the performance of the chosen design and to refine the concept.

The classical simplified design concepts base on equivalent linear models, as described in Sec. 6.6. They are used to replace the nonlinear behavior of the isolating layer. Generating a soft story, the superstructure motion is close to a rigid body motion for low- and midrise buildings. Therefore SDOF or 2-DOF systems are mostly sufficient. Highrise buildings show more flexibility, thus the application of MDOF shear-models can be necessary. Figure 6-15 illustrates often applied model variants. As can be seen from Fig. 6-14, the hysteretic behavior of an isolation layer is close to a linear-elastic-plastic system. Therefore the model can be simplified, as shown in Fig. 6-16.

6.9 Examples: Conventional base isolation design

The application of the linear simplified method for base isolation design has been explored for two examples.

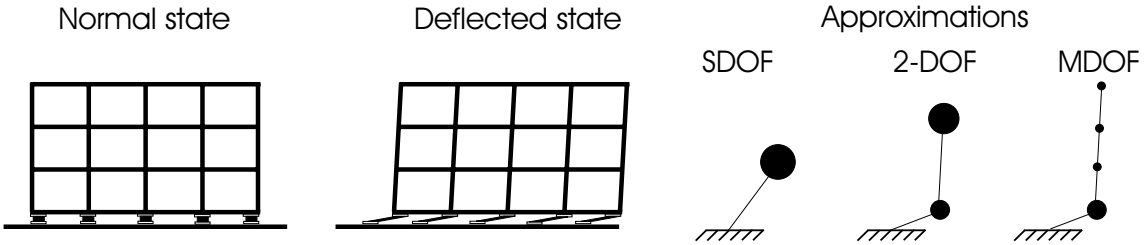

Figure 6-15 Typical base isolation model assumptions

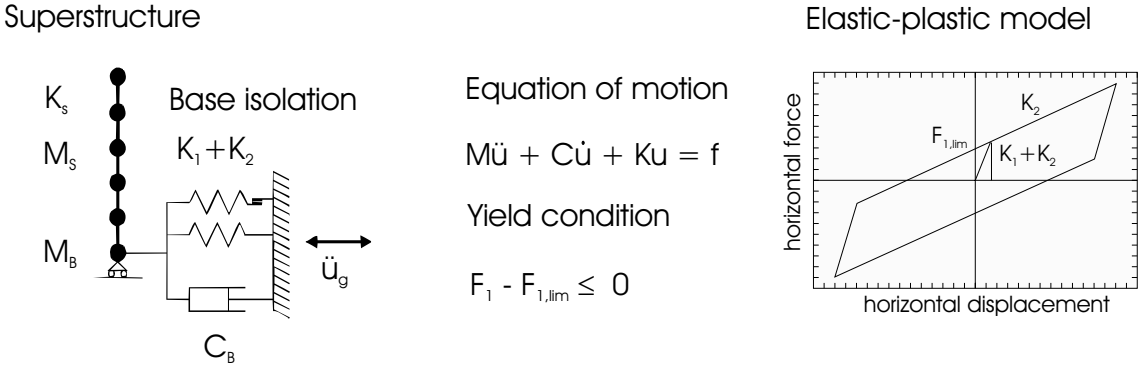

Figure 6-16 Elasto plastic analysis model for base isolated structures

Example a.): A SDOF model for a base-isolated structure is examined. The mass is set to 1000t. The stiffness K_2 (e.g. provided by natural rubber bearings) was chosen to provide a period of 4 seconds. The yield force $F_{1,v}$ (e.g. determined by hysteretic dampers) was adjusted to resist elastically a horizontal load of 10% weight of the structure. This device combination was altered for a parameter study in the range of equivalent periods from around 2 to 8 seconds. The structure is subjected to a mean spectrum from the Kobe near fault set (Appendix 11.6). The calculation algorithm corresponds to Tab. 6-3. For comparison, the effects from different well known spectral reduction concepts are investigated, using [73,122,24,167]. The applied reduction concepts do not respect influences from the structural period and are described in Appendix 11.2. As the damping induced by the isolation devices can be considerable, the deviations in the coefficients may cause significant impact on the results.

For reference the appropriate time history solution is calculated as well. In Fig. 6-17 the displacement and acceleration is shown for the chosen period range. As well, the relative errors are given with respect to the appropriate time history solution. It can be seen that spread results are obtained. The use of the relations given by BCJ 2000 and Newmark-Hall within this procedure seems to be generally inappropriate. They give evidence that

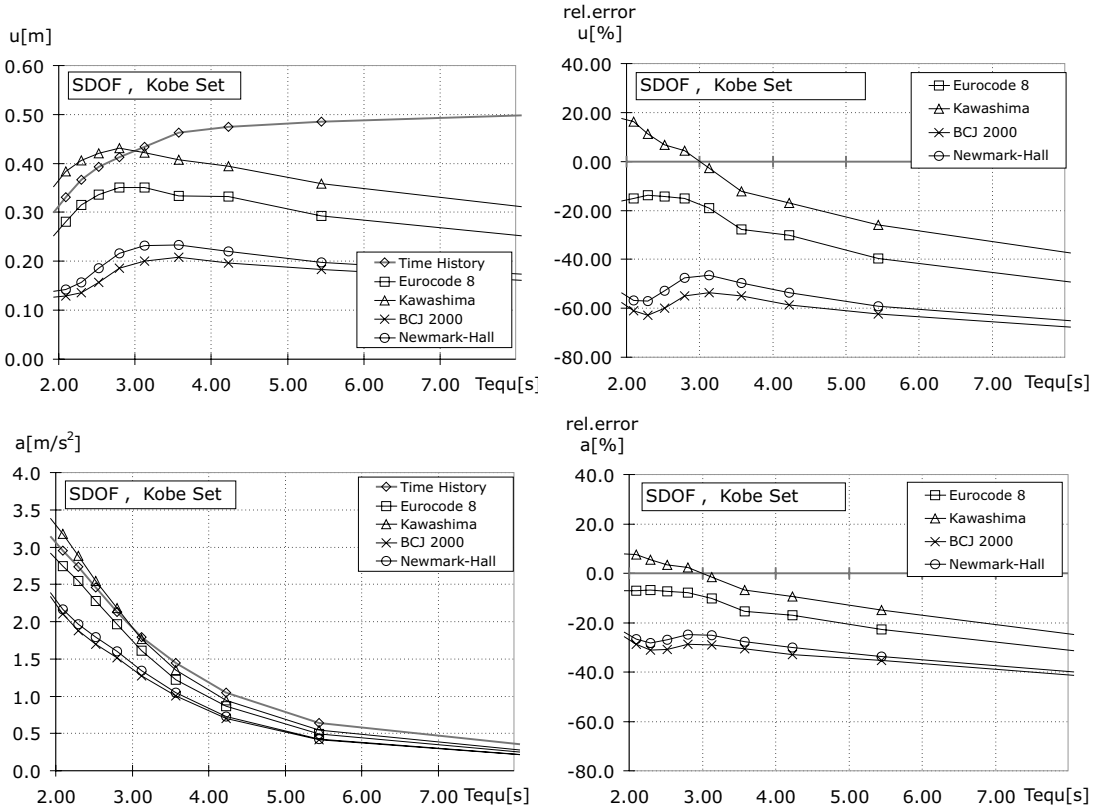

Figure 6-17 Example: Comparison of maximum deformations and accelerations for SDOF obtained by time history analysis and simplified linear analysis, utilizing period-independent spectrum reduction coefficients

an uncontrolled extrapolation of formulas out of their original context can be problematic. Within a first view only the simplified Kawashima/Aizawa and EC8 relationships seem to be capable of deriving acceptable approximations, but only for structures with equivalent periods less than 3 to 4 seconds. It should be mentioned, that the Kawashima/Aizawa-relationship was originally derived to reflect reductions of total acceleration spectra, rather than pseudo-accelerations. This will explain the tendency of overestimation in the short period range. The observed percentage of deviations in this range corresponds with observations from conventional design [55,56]. However, all models gradually fail in higher period ranges.

Example b.): Generally the same behavior can be stated for MDOF structures. In Fig. 6-18 selected results for a 10-story stick model with lumped 1000t story masses, 2000t baselevel-mass and 1.3 seconds fixed base period are given. Whereas the maximum deformations in the superstructure u_s and at base level u_b are qualitatively behaving like the SDOF solution in Example a), the accelerations a_s and a_b are dramatically underestimated.

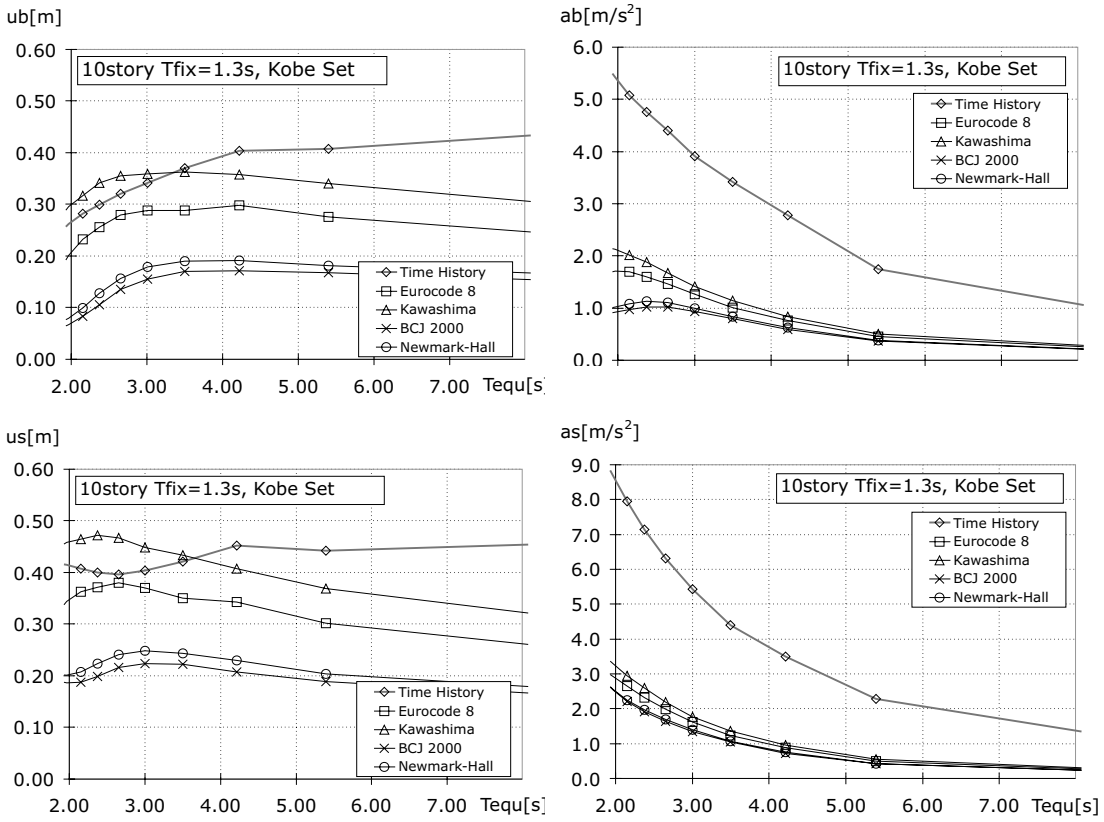

Figure 6-18 Example: Maximum deformations and accelerations for 10-DOF obtained by time history analysis and simplified linear analysis, utilizing period-independent spectrum reduction coefficients

6.10 Improved simplified base-isolation design

As obtained in the previous sections, contrary to fixed-base design, simplified methods show less accuracy in the design of base isolated structures. This is unexpected, because base isolation makes the structural behavior simpler and facilitates simple calculation methods [159]. In [221] it has been shown, that the reasons for errors arise from unconditional extrapolation of concepts known from fixed-base design. The period elongation and the introduction of high damping requires special modifications in the analysis concepts. This is mainly the appropriate use of reduction formulas dependent on the period, the modified estimation of the damping in the structure and an appropriate relation between maximum accelerations and maximum deformations.

A considerable part of the observed deviations are caused by the use of the reduction formulas given in Appendix 11.2. These relations are constant with respect to the periods of vibration. For small damping ratios and small periods these models give sufficient appro-

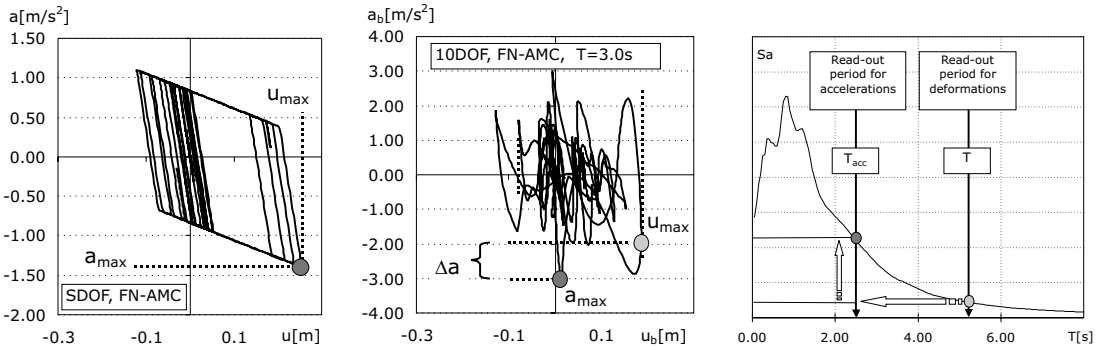

Figure 6-19 Deformation-acceleration relationship at isolation level for:
SDOF, MDOF example and principle of period shift

ximations. However, in all other cases the differences can be significant. This applies for the differences in pseudo and total spectral accelerations that become more significant in the long period range. This effect is strongly dependent on the amount of involved damping. For this purpose, the appendices 11.2 and 11.3 provide period-dependent spectral reduction concepts from [221] appropriate for the long period-large damping range.

Additionally, the equivalent linearization procedures require adoption to longer periods and higher damping ratio. From the examples it is obvious that the deviations in the deformations rise for longer periods. Obviously in this part of the spectrum, the assessed damping is too high and needs to be lowered continuously. A period-dependent modification of the damping can be easily established, because the simplification Eq. (6-50) in the damping ratio assessment Eq. (6-49) is not appropriate in the long period range. Therefore the formula (6-51) from engineering practice can be modified as

$$\xi_{mod} = \xi_{equ}\nu_1\nu_2 \tag{6-53}$$

with the damping modification factors ν_1 and ν_2 that are in detail described in Appendix Sec. 11.4.

Following the response spectrum approach in Tab. 6-1, the spectral deformations are evaluated at their corresponding natural periods. On the other side, the accelerations given at this period are only acceptable for SDOF solutions, because then the acceleration history is directly linked to the history of the deformations, as illustrated in the deformation-acceleration plot of Fig 6-19.

For MDOF systems the situation changes significantly. In the example of Fig. 6-19 it can be seen that the peak in the acceleration record occurs not at the same time as the deformation peak. The acceleration, corresponding to the maximum deformation, as determined by response spectrum approach, can be significantly different from the real maximum value. This effect can be approximately considered within simplified procedures by shif-

ting the read-out period in the spectrum (Fig. 6-19). The estimation of such a shift due to specific single ground motions is difficult, but average predictions for motion sets can be determined. Hereby the acceleration increase corresponds approximately to the ratio of the base- and super-structural initial periods. This observation is utilized for shifting the read-out period for the accelerations

$$T_{acc} \approx T \frac{T_0}{T_{0,s}} \qquad with\, T_{0,s} = 2\pi \sqrt{\frac{m}{f_{b,v}/u_y}} \tag{6-54}$$

Here, $T_{0,s}$ is the initial period, evaluated for the overall mass m with the elastic limit base shear $f_{b,v}$ and the elastic limit deformation u_y at the top of the structure. This formulation includes, that very stiff MDOF structures behave almost like SDOF.

All modifications fit now in the procedures of linear equivalent design using optimization strategies as described before.

6.11 Examples: Improved base isolation design

The examples a) and b) from Sec. 6.9 are again calculated with respect to the modifications for the long period range. In Fig. 6-20 the results for the deformations and accelerations are given. From this it is obvious, that the modifications greatly contribute to a better assessment of the dynamic behavior of either SDOF and MDOF structures. For reference, the time history calculation and the non-modified model based on the EC8 spectral reduction coefficient are plotted again.

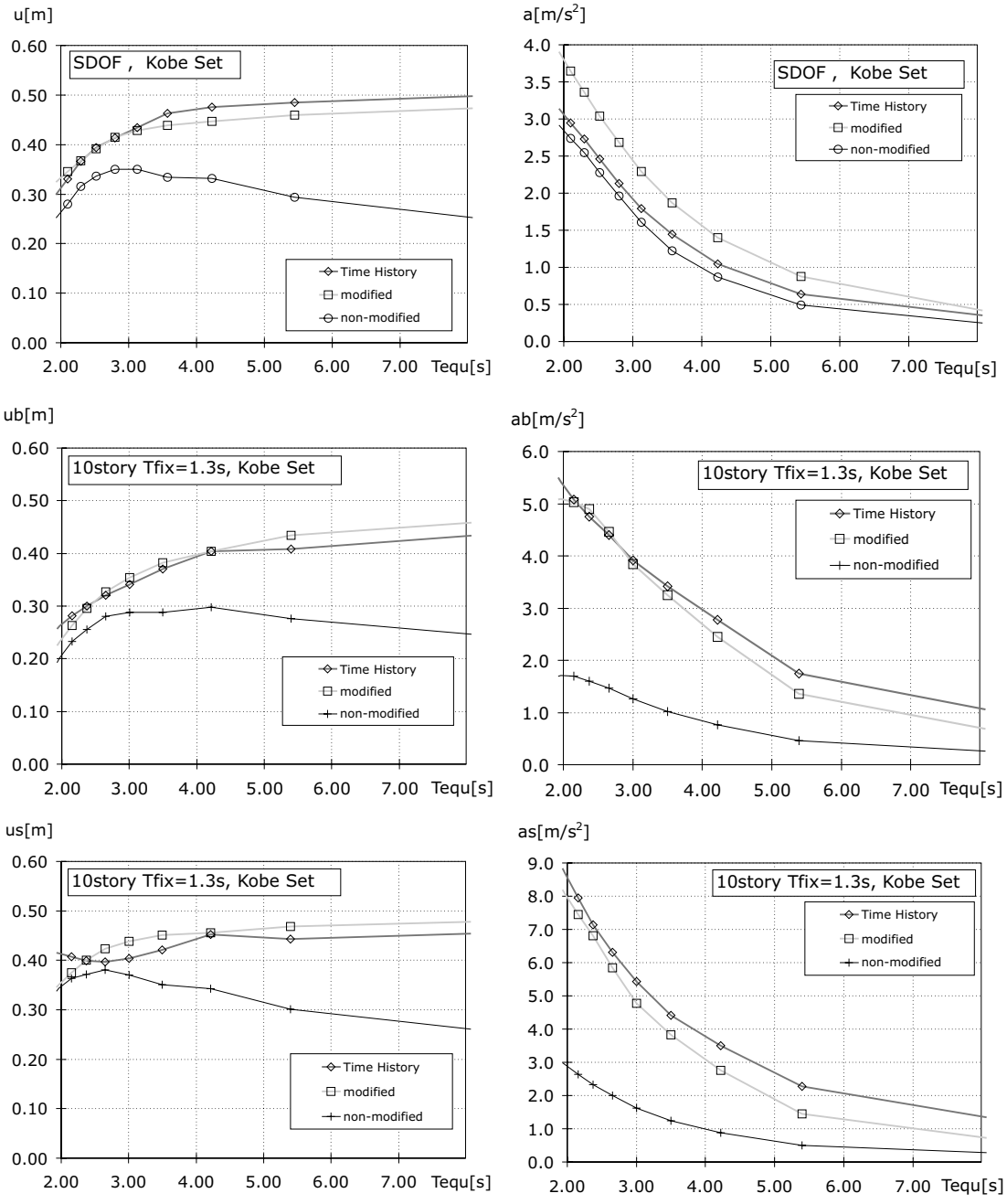

Figure 6-20 Example: Comparison of deformations and accelerations for SDOF and MDOF structure

7 Simplified nonlinear analysis

7.1 Physical nonlinear limit states

Different from the simplified linear methods in Sec. 6, simplified nonlinear methods solve nonlinear governing equations in calculations, without explicit consideration of time effects. In seismic design, especially the evaluation of the physical nonlinear capacities gain importance, as the utilization of the energy dissipation by plastic deformation is the most applied concept in seismic design. Those solutions are preferred, that exhibit sufficient ductility, while maintaining enough capacity in cross sections during plastic excitations.

Although real elasto-plastic materials or material combinations show general nonlinear behavior, the transition from elastic to plastic behavior is often visible as a distinct break in material laws. This enables approximations of the material law as piecewise linear, especially if the integral cross section behavior is considered. For most practical design cases, a bilinear simplification can be sufficient, mostly due to the steel behavior or participation of steel. For instance in reinforced concrete structures, the concrete itself shows negligible ductility. However, if properly designed, the reinforcement dominates the limit state behavior, thus obtaining a quasi-ductility on the cross section level. The same applies for timber structures. Typically, the timber parts are elastically designed, whereas the steel connections add yielding capabilities. For this reason, most practical calculation strategies, especially those proposed in codes, base on bilinear material laws. Also the considerations in the following sections will focus on this approximation.

As mentioned before in Sec. 1.3, besides failure prevention, the definition and design of the structural performance after impacts becomes more and more important. From a mechanical point of view, the following basic limit criteria can be distinguished to determine the extend of inelastic excitation in structures with bilinear materials

- Elastic limit
- Plastic limit
- Conservative limit
- Adaptive limit
- Deformation based limit

It is the advantage of design concepts based on optimization algorithms, that they already contain an interface for formulation of limit states - the inequality conditions. Furthermore, the possibility to pursue design objectives enables the engineer to utilize the limit criteria to find economic solutions. All simplified nonlinear analysis methods base on one of the mentioned limit state evaluations. The different strategies are examined in detail in the following sections.

7.2 Elastic limit state

The elastic limit state is defined as the maximum load intensity or minimum resistance configuration, for that plastic limits are reached, but no plastic deformations or failure or any other kind of damage is observed. The definition allows for different interpretations, dependent on the level of the considerations, e.g. whether it is a structural (global) or a cross-sectional (local) problem. The limit states are generally different in the stress space or internal force space or external force space. While having a linear material law and ignoring geometric nonlinear effects, the elastic limit state and all states below this limit can be calculated from superposition of load cases and by linear scaling. If the structure or member is unloaded, no residual stresses/forces are maintained.

For mechanical formulation, the following types of extremum principles are often applied in the calculation of elastic structures:

1.) Poisson principle

2.) Stationary principles (Hellinger-Reissner, Hu-Washizu)

3.) Castigliano principle (Principle of conjugated potential)

4.) Lagrange principle (Principle of total potential)

5.) Mixed type principles

As all principles generally represent the same mechanical background, all obtained solutions are identical. They can be transformed out of each other by using methods of variational calculus (Sec 2). Thus the selection of a certain principle is only due to effectiveness of the problem formulation and numerical treatment. In the traditional forms, geometrical linear behavior and small strains are assumed (Sec. 4.5).

The principles of the Poisson category contain all mechanical relations as equalities or inequalities and are free of extremum conditions. In this form, the mechanical governing relations are just "listed" in the subsidiary conditions and are therefore easily formulated. The free extremum condition can be utilized conveniently for design tasks.

Contrary to this, the second category is a pure extremum condition, free of subsidiary conditions. It forms saddle point problems with different extremum conditions (maximum and minimum) for different types of unknowns. Such problem formulations are seldomly applied in practical calculations and are not further considered.

The third and fourth types are special among extremum principles, because of their dependency on one group of unknowns only and therefore their resulting simplicity. Whereas the Castigliano principle bases on internal forces or stresses, the Lagrange principle is based on kinematic values only. They are an important basis for the formulation of force based or deformation based calculation concepts in mechanics.

The fifth category contains all intermediate principles, that are obtained during variational transformations. They usually contain several subsidiary conditions and are typically dependent on a larger number of variables.

Because of the importance of the Poisson, Castigliano and Lagrange principles for the formulation of simplified analysis methods, the derivation is illustrated in the following subsections. The principles serve as a basis for optimization problems, because they can be directly transformed into linear or quadratic optimization problems. Moreover, they are often applied as core relations for others than elastic calculations.

7.2.1 Poisson principle

In terms of variational calculus, the Poisson principle consists only of subsidiary conditions, describing all governing relations of mechanics (equilibrium, kinematic condition, material law, boundary conditions) as introduced in general in Secs. 3 and 4. Dependent on the stresses σ and displacements u, the equations can be summarized as follows

$$B_s\sigma - N_u^T c_s + \varphi = 0 \qquad \in V \tag{7-1}$$

$$B_u u - N_s^T c_u - \varepsilon = 0 \qquad \in V \tag{7-2}$$

$$D^{-1}\sigma + \varepsilon_0 - \varepsilon = 0 \qquad \in V \tag{7-3}$$

$$-N_u u = u_0 \qquad \in S_u \tag{7-4}$$

$$N_s\sigma = s_0 \qquad \in S_s \tag{7-5}$$

specified at one material point. An extremum condition is initially not specified, but can be conveniently used to define design objectives. It is therefore not a typical variational principle, but is of practical relevance and the basis to derive other formulations.

A numerically effective form of the Poisson principle can be obtained, if the stresses σ and strains ε are eliminated. For this purpose the material law Eq. (7-3) is incorporated into the kinematic condition Eq. (7-2) to eliminate the strains ε, to form an extended kinematic condition

$$B_u u - N_s^T c_u - D^{-1}\sigma - \varepsilon_0 = 0 \qquad \in V \tag{7-6}$$

This equation can be re-arranged

$$\sigma = DB_u u - DN_s^T c_u - D\varepsilon_0 \tag{7-7}$$

to separate σ. This expression is introduced into Eq. (7-1)

$$B_s DB_u u - B_s DN_s^T c_u - B_s D\varepsilon_0 - N_u^T c_s + \varphi = 0 \qquad \in V \tag{7-8}$$

Under the condition $B_s = B_u^T = B$, Eq. (7-8) simplifies to

$$B^T DBu - B^T DN_s^T c_u - B^T D\varepsilon_0 - N_u^T c_s + \varphi = 0 \qquad \in V \tag{7-9}$$

that have to be solved, with respect to the boundary conditions (7-4,7-5). Herein the term

$$B^T DB = K \tag{7-10}$$

is known as the linear stiffness matrix. The Poisson principle (in the given traditional form) can be directly transformed into a linear optimization problem, by application of discretization methods. The resulting problem contains of linear subsidiary conditions. The value of the objective function is left free and can be arbitrarily chosen.

7.2.2 Castigliano principle

The Castigliano principle is derivable from the Poisson principle using the weak form approach in Tab. 2-7. The weak expression is obtained for one material point out of the extended kinematic condition Eq. (7-6), resulting in

$$\int \delta\sigma^T Bu\, dV - \int \delta\sigma^T N_s^T c_u\, dS_s - \int \delta\sigma^T Q\sigma\, dV - \int \delta\sigma^T \varepsilon_0\, dV = 0 \tag{7-11}$$

The first term can be partially integrated

$$\int \delta\sigma^T Bu\, dV = \int u^T N_s \delta\sigma\, dS - \int u^T B^T \delta\sigma\, dV \tag{7-12}$$

where the surface S can be splitted into one part S_s, where the static boundary conditions are applied and a second part S_u, where the geometric boundary conditions are applied, therefore

$$\int u^T N\delta\sigma\, dS = \int c_u^T N_s \delta\sigma\, dS_s + \int u^T N_u^T \delta c_s\, dS_u \tag{7-13}$$

On the other hand, the equilibrium condition Eq. (7-6) is varied

$$B_s \cdot \delta\sigma = 0 \tag{7-14}$$

The Eqs. (7-13-7-14) are introduced into (7-11), thus giving the principle of virtual stresses

$$\int c_u^T N_u \delta c_s\, dS_u - \int \delta\sigma^T D^{-1}\sigma\, dV - \int \delta\sigma^T \varepsilon_0\, dV = 0 \tag{7-15}$$

Including the geometric and static boundary conditions Eqs. (7-4,7-5) and integrating with respect to σ gives the principle of conjugated potential, or Castigliano principle

$$\Pi_C = -\tfrac{1}{2} \int \sigma^T D^{-1}\sigma\, dV - \int u_0 c_s\, dS_U + \int u_0^T N_s \sigma\, dS_u - \int \sigma^T e_0\, dV \to Max \tag{7-16}$$

$$B_s \cdot \delta\sigma - N_u^T c_s + \delta\varphi = 0 \qquad \in V \tag{7-17}$$

$$N_s\sigma = \delta s_0 \qquad \in S_s \tag{7-18}$$

that contains the equilibrium and static boundary conditions as subsidiary conditions. This principle can be directly transformed into an optimization problem, by application of discretization methods. The resulting problem is quadratic, containing a quadratic objective function and several linear equality subsidiary conditions.

7.2.3 Lagrange principle

The Lagrange principle can be derived with the dual method of variation according Tab. 2-7. Here the equilibrium condition (7-1) is transformed into it′s weak form

$$\int \delta u^T B^T \sigma \, dV - \int \delta u^T N_u c_s \, dS_u + \int \delta u^T \varphi \, dV = 0 \tag{7-19}$$

The first term is integrated by parts

$$\int \delta u^T B^T \sigma \, dV = \int \delta u^T N_s \sigma \, dS - \int \sigma^T B \delta u \, dV \tag{7-20}$$

The surface S is divided according to Eq. (7-13), so obtaining

$$\delta\Pi = \int \delta c_u^T N_s \sigma \, dS_s - \int \sigma^T B \delta u \, dV + \int \delta u^T \varphi \, dV = 0 \tag{7-21}$$

as the principle of virtual deformations. In this equation, the static boundary condition Eq. (7-5) is applied, as well as the transformed extended kinematic condition Eq. (7-7), resulting in

$$-\int \delta c_u^T \sigma_0 \, dS_s - \int \left(DBu - DN_s^T c_u - D\varepsilon_0\right)^T B \delta u \, dV + \int \delta u^T \varphi \, dV = 0 \tag{7-22}$$

Integrating with respect to u, leads to the principle of total work or Lagrange principle

$$\Pi_L = -\tfrac{1}{2} \int u^T B^T DBu \, dV + \int c_u^T N_s DBu \, dV + \int \varepsilon_0 DBu \, dV - \int c_u^T s_0 \, dS + \int u^T \varphi \, dV \rightarrow Max \tag{7-23}$$

together with the geometric boundary conditions

$$-N_u u = u_0 \qquad \in S_u \tag{7-24}$$

With this principle the deformations in a structure can be calculated. The appropriate stresses or internal forces are calculated from Eq. (7-7). This principle forms a quadratic optimization problem if discretization methods are applied.

7.2.4 Elastic limit load and resistance calculation using mathematical optimization

With help of the Poisson, Castigliano and Lagrange principles, serving as core principles, the elastic limit load of a structure can be calculated. Because of the special form of the Poisson principle, the free objective function can be directly used to search for the maximum of the applicable load (limit load). A simple and practical form is a one parameter optimization problem, that is maximizing a multiplier p for a given load pattern $\bar{f}$

$$p \rightarrow Max \tag{7-25}$$

The force pattern $\bar{f}$ is containing a quasi-static representation of the dynamic excitation and can be given as a "unity" force distribution that is scaled by p.

Alternatively, multi-parametrical limit state problems can be declared. Herein, the force distribution f itself is altered in the optimization problem, this means, that a maximal force function for the structure is in demand

$$p(f) \rightarrow Max \tag{7-26}$$

However, such problems are very rare in earthquake engineering, because the essential distribution of the forces is commonly predetermined by the ground excitation and the structural assembly.

Using the one-parametrical form Eq. (7-25), an eigenform solution is often utilized as force distribution $\bar{f}$ in order to approximate the dynamic load. The Poisson principle is applied e.g. in the shortened matrix form

$$Ku - A^T Q^{-1} N_s^T c_u - A^T Q^{-1} \varepsilon_0 - N_u^T c_s + p\bar{f} = 0 \qquad \in V \tag{7-27}$$

$$-N_u u = u_0 \qquad \in S_u \tag{7-28}$$

$$N_s \left(Q^{-1} A_u u - Q^{-1} N_s^T c_u - Q^{-1} \varepsilon_0 \right) = s_0 \qquad \in S_s \tag{7-29}$$

with the scaled unity force. The limit criteria of the elastic limit state can be added in form of a yield criterion of a plastic material law

$$L_p^T \left(Q^{-1} A_u u - Q^{-1} N_s^T c_u - Q^{-1} \varepsilon_0 \right) \leq s_{lim} \tag{7-30}$$

as discussed in Sec. 4.8.

A corresponding design problem is the limit resistance factor calculation, that reads

$$r \rightarrow Min \tag{7-31}$$

with the resistance limit factor r that is a multiplier of a unit resistance distribution $\bar{s}_{lim}$. Then the appropriate subsidiary conditions are

$$Ku - A^T Q^{-1} N_s^T c_u - A^T Q^{-1} \varepsilon_0 - N_u^T c_s + f = 0 \qquad \in V \tag{7-32}$$

$$-N_u u = u_0 \qquad \in S_u \tag{7-33}$$

$$N_s \left(Q^{-1} A_u u - Q^{-1} N_s^T c_u - Q^{-1} \varepsilon_0 \right) = s_0 \qquad \in S_s \tag{7-34}$$

$$L_p^T \left(Q^{-1} A_u u - Q^{-1} N_s^T c_u - Q^{-1} \varepsilon_0 \right) \leq r \bar{s}_{lim} \tag{7-35}$$

For both forms of elastic limit state calculation, the one-parametrical optimization schemes are illustrated in Tab. 7-1 for the case, that only simple boundary conditions $-N_u u = 0$ and $N_s s = 0$ are applied and the assigned unknowns in the vectors u and s are eliminated.

The application of the Poisson principle results in a one-step optimization procedure for the calculation of the elastic limit state. Contrary, the Castigliano and Lagrange principles demand for two-step strategies in the calculation of the elastic limit state. In a first step a base answer $\bar{s}$ is calculated by application of the principles from Sec. 7.2.2 and 7.2.3. Then, in a next step, the appropriate limit state factor p or r is calculated under the conditions

$$\bar{s} \leq r s_{lim} \tag{7-36}$$

or

$$p \bar{s} \leq s_{lim} \tag{7-37}$$

that are linear optimization problems. For the limit load calculations $\bar{s}$ can be even a normalized answer e.g. due to unity forces. In Tabs. 7-2-7-1 the optimization problems are illustrated as optimization schemes, assuming simple boundary conditions. The multi-step character of the calculation is indicated.

As for the limit load problem, a multi-parametrical form for the resistance calculation can be established. Herein the resistance distribution s_{lim} is not fixed, but is itself an unknown of the problem

$$r(s_{lim}) \rightarrow Min \tag{7-38}$$

In practice, only a selected part of the s_{lim} vector needs to be made variable. The function $r(s_{lim})$ is commonly a normative type of function, to obtain a single objective function, e.g.

$$r = |s_{lim}| \tag{7-39}$$

or simply

$$r = \sum s_{lim}^2 \tag{7-40}$$

Table 7-1 Determination of elastic limit resistance and limit load factor (Poisson formulation)

Linear optimization

		Primal variables				
		u	r	1		
			1		→ Min	Objective function
Dual variables	u^T	$A^T Q^{-1} A$		-f	= 0	Equilibrium condition
	$c_S{}^T$	$-N_U$			=0	Static boundary condition
	λ^T	$-L_P Q^{-1} A$	s_{lim}		≥ 0	Plasticity condition

Linear optimization

		Primal variables				
		u	p	1		
			1		→ Max	Objective function
Dual variables	u^T	$A^I Q^{-1} A$	-f		= 0	Equilibrium condition
	$c_S{}^T$	$-N_U$			=0	Static boundary condition
	λ^T	$-L_P Q^{-1} A$		s_{lim}	≥ 0	Plasticity condition

Table 7-2 Steps for determination of elastic limit load factor (Lagrange formulation)

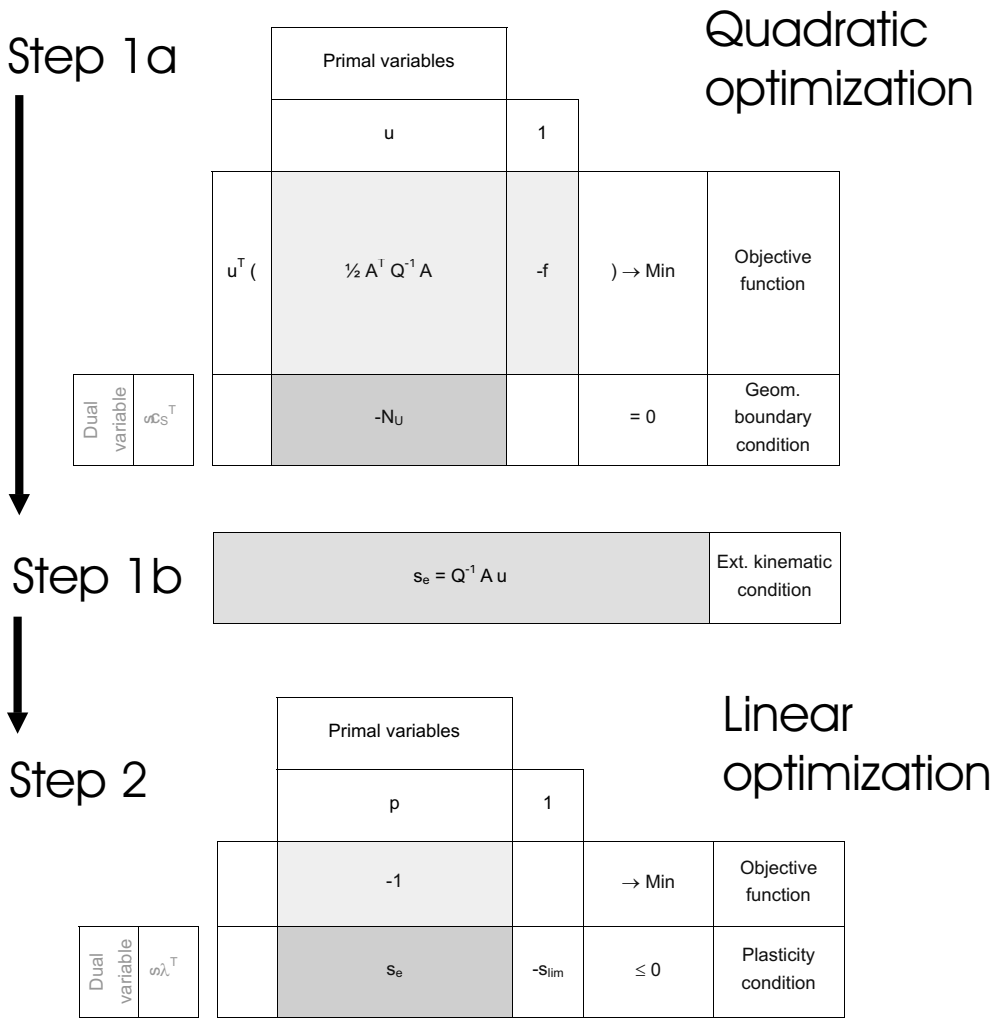

Table 7-3 Steps for determination of elastic limit resistance factor (Castigliano formulation)

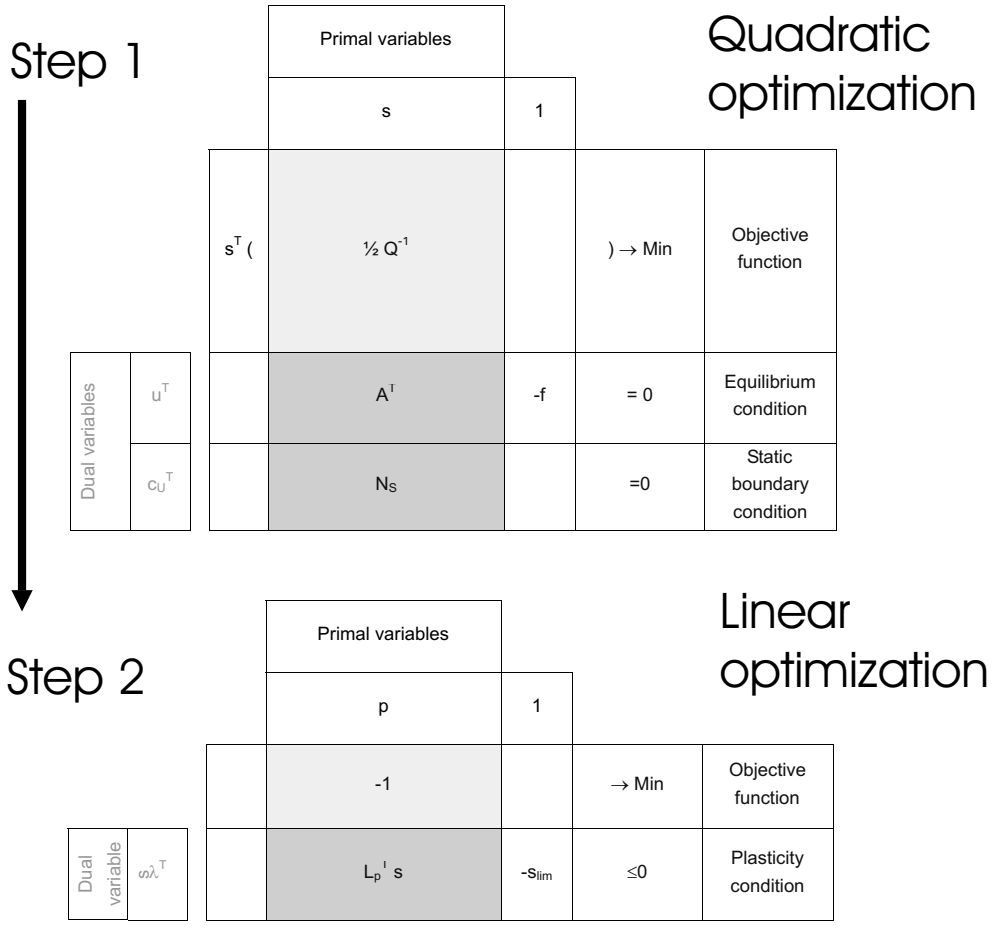

With this type of formulations, particularly economical solutions can be obtained. However, it should be noted, that the solution of such problems is computationally intensive and the solution space is commonly non-convex. Specialized algorithms (Sec. 2) must be applied. Furthermore such formulations require additional restrictions, in order to obtain technologically meaningful solutions.

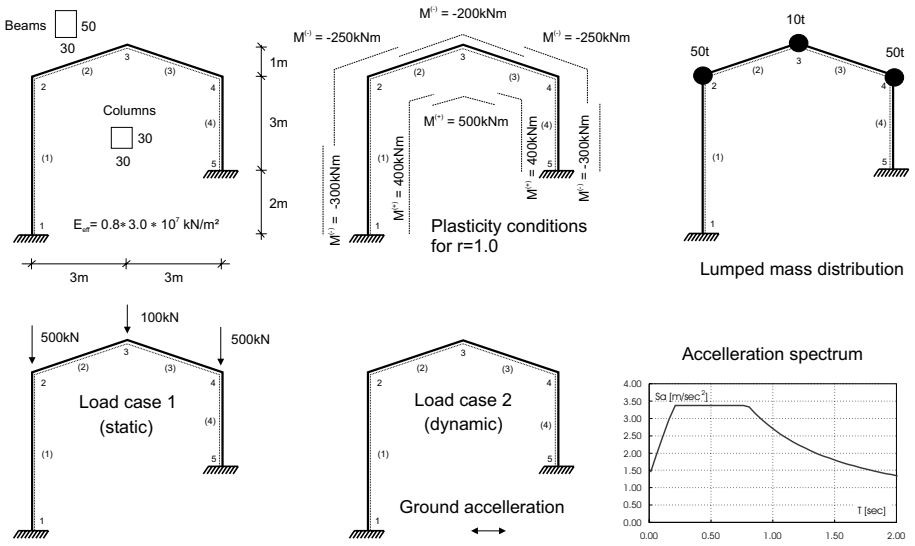

Figure 7-1 Example: System and initial conditions

7.2.5 Example: *Calculation of elastic limit resistance*

For demonstration of a design according to limit loads, the following example is introduced. In the following sections, this example will be concluded for other limit criteria. The mechanical system of an unsymmetrical frame structure and the appropriate geometrical and material conditions are summarized in Fig. 7-1. All cross sections are assumed to behave elastic perfectly plastic. The stiffness was manipulated by a factor of 0.8, simulating a drop of the section capacity due to possible inelasticity or predamage. A limit moment distribution is noted, symbolizing the load bearing capacity of the cross sections. The frame is loaded by static and seismic loads. The seismic load is given in form of a response spectrum. For analysis, it is assumed to have a lumped mass distribution.

For this configuration, the quasi-static substitution loads are calculated first via modal decomposition and response spectrum application. For simplicity, the calculation is restricted to only the first modal period. The first modal shape is given in Tab. 7-4. The first natural period is $T = 0.806s$. The quasi-static substitution load case is calculated with means of modal decomposition (Sec. 6.1). The structure can be loaded by two possible load combinations

- Combination I (LC I): Load case 1 + Load case 2
- Combination II (LC II): Load case 1 - Load case 2

The one-parametric elastic limit resistance factor r is calculated using the model in Tab. 7-3. The resistance factor for load combination I is $r = 1.575$ and for load combination II $r = 1.529$. Therefore the resulting elastic resistance factor is the maximum of all load

Table 7-4 Example: First natural mode and quasi-static substitution load cases

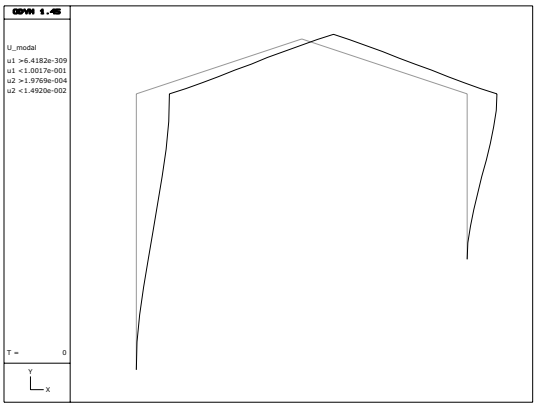

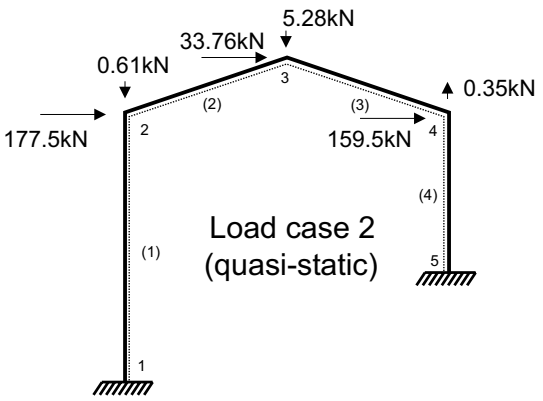

Table 7-5 Example: Moment distribution (Elastic limit resistance)

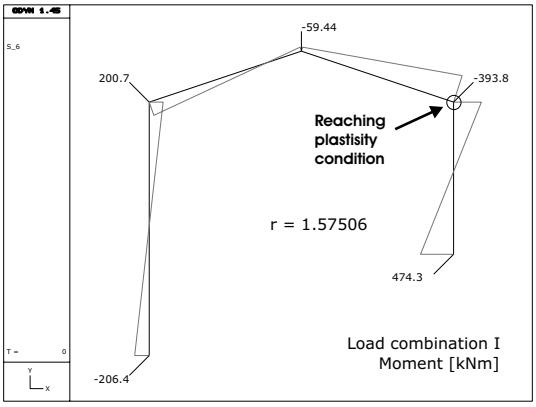

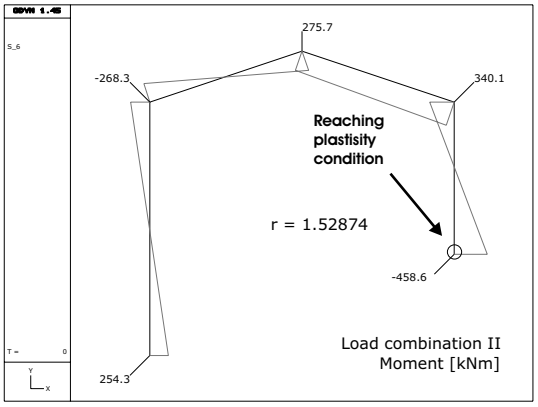

combinations $r_e = 1.575$. The obtained moment distribution is given in Tab. 7-5. Only at distinct points the plasticity conditions are reached, without loading beyond. Thus, the residual moment distributions for both load combinations are vanishing (Tab. 7-6). As indicated in this table, non of the load combinations are inducing residual moments, as accepted for elastic load cases.

Table 7-6 Example: Residual moment distribution (Elastic limit resistance)

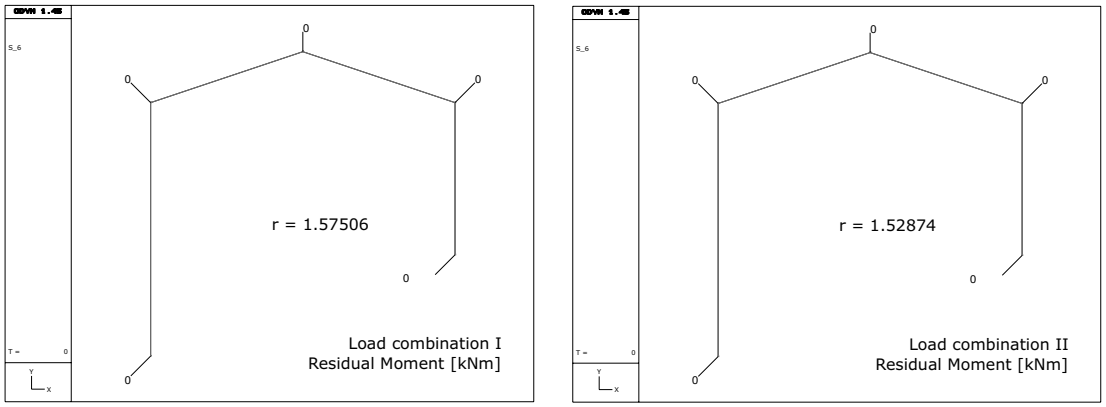

7.3 Plastic limit state

Statically undetermined structures can contain additional bearing capacities, when reaching the elastic limit. These reserves can be utilized by accepting plastic deformations and internal force redistributions. Those structures demands for a sufficient ductile behavior. Most materials or material combinations exhibit a certain amount of plastic deformability. In codes, the utilization of plastic reserves is generally permitted, under predefined circumstances. In earthquake engineering, the use of the inelastic capacities became the most important strategy in the design of seismic resistant structures. The occurring dissipation of energy during plastic deformations leads to a significant reduction of the structural impact.

Different to elastic limit state calculations (Sec. 7.2), the load and resistance limit factors p and r cannot be simply calculated using superposition rules. However, the limit state problems can be altered according to the plasticity theory. The concepts have been originally developed for statically excited structures. However, the theorems can be applied to quasi-static simplifications, as discussed in this section. The basic theorems have been stated for structures with rigid perfectly plastic materials. They can be derived from the mechanical properties of plastic bodies, assembled in matrix form in Tab. 7-7. From this, it is obvious that the kinematic and static parameters are decoupled. Therefore two basic forms of limit load calculations can be derived. They are the basis for the classical theorems of plasticity [86,181], the kinematic, static and uniqueness theorem of the limit load [37,64,141].

7.3.1 Core principles for elasto-plastic materials

Generally, the principles presented in Sec. 7.2 can be altered to meet the requirements of the elasto-plastic analysis. The only difference to elastic structures is the changes in the material law, as discussed in Sec. 4.8

Table 7-7 Relation scheme for analysis of rigid plastic bodies (simple boundaries)

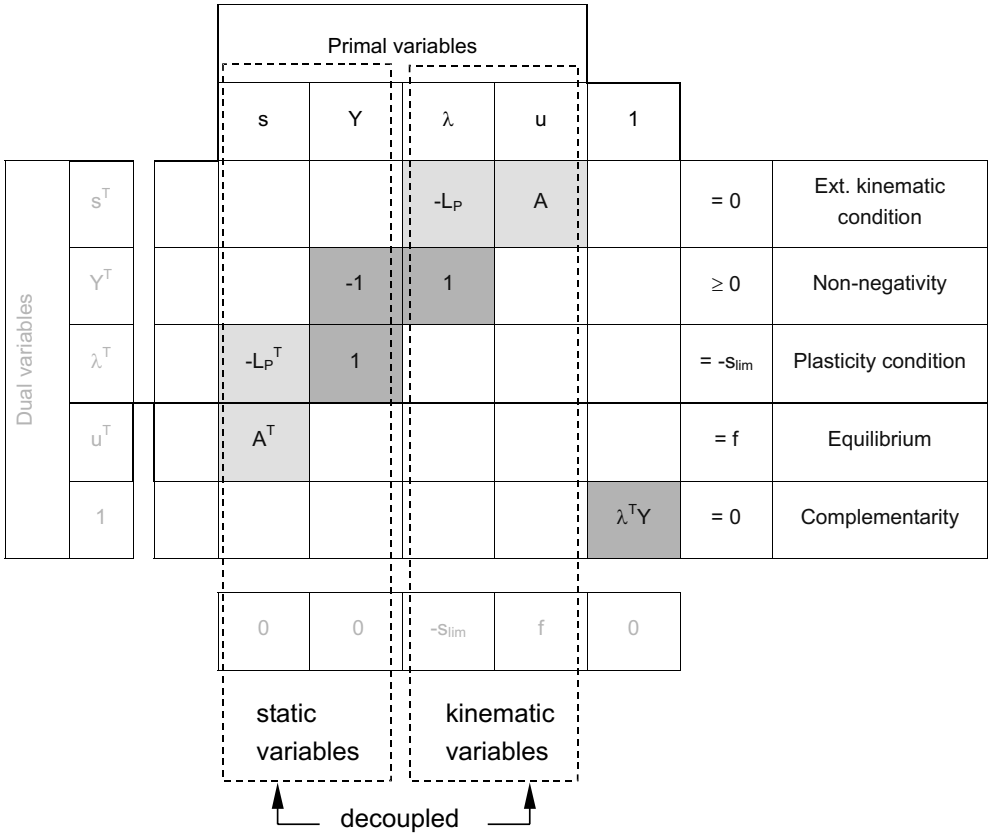

$$Qs + \varepsilon_p + \varepsilon_0 - \varepsilon = 0 \qquad \in V \tag{7-41}$$

$$\varepsilon_p = L_p \cdot \lambda \qquad \in V \tag{7-42}$$

$$L_p^T s - s_{lim} \leq 0 \qquad \in V \tag{7-43}$$

It contains additional plastic strains and, here exemplarily, linear plasticity conditions. The derivation of appropriate extremum principles can be done similar to Sec. 7.2. The variational derivation of Castigliano and Lagrange extremum principles for linear elastic-perfectly plastic structures are summarized in the Tabs. 7-8-7-10.

7.3.2 Static, kinematic and uniqueness theorem of the plastic limit state for rigid plastic bodies

The static theorem is giving a lower bound on the solution of the limit load of a structure:

> **Theorem 1**: *The structure is kinematically stable if a statically admissible internal force state can be found.*

Table 7-8 Derivation of the principle of conjugated potential (elasto-plastic material)

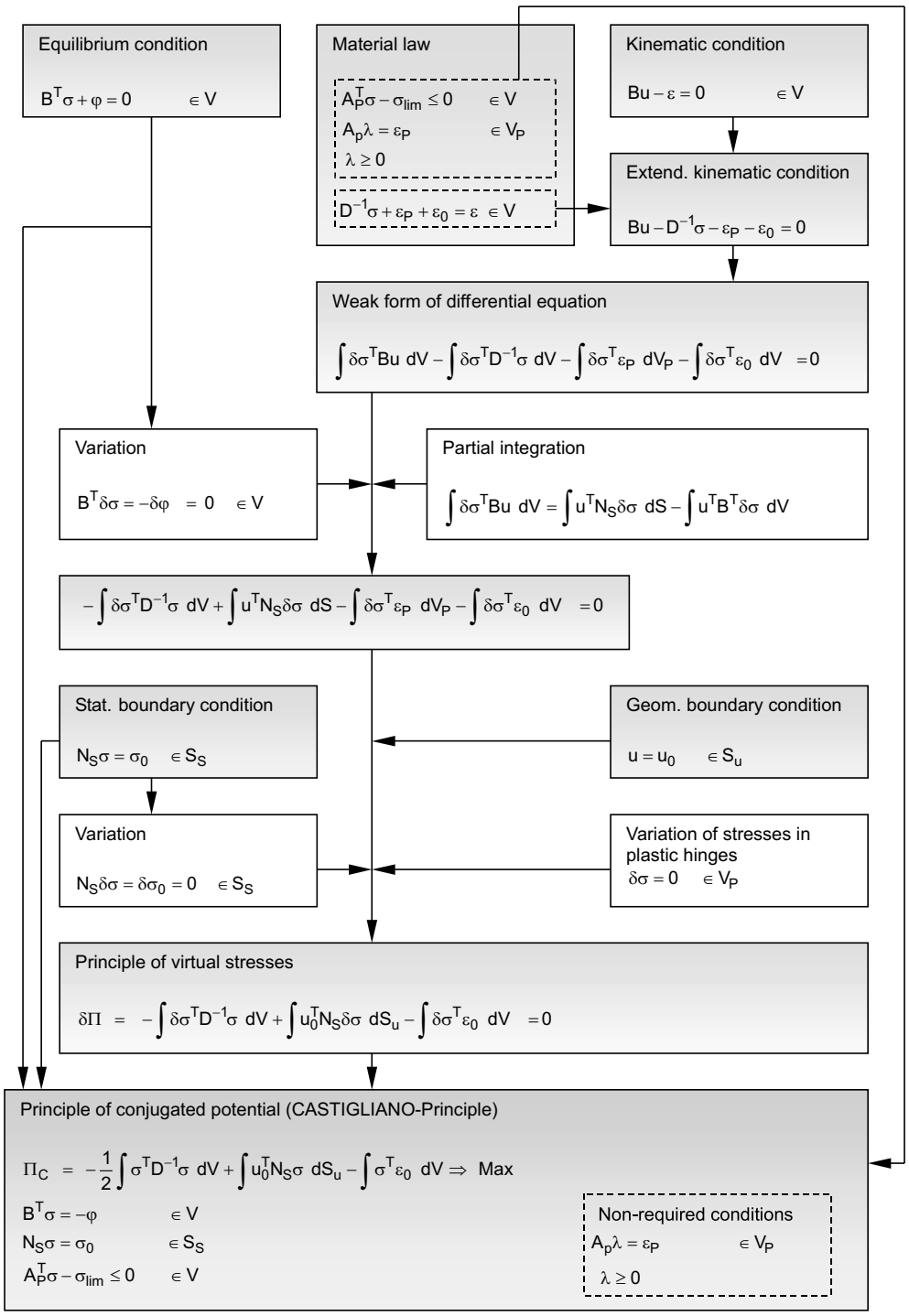

Table 7-9 Derivation of the principle of total potential (elasto-plastic material)

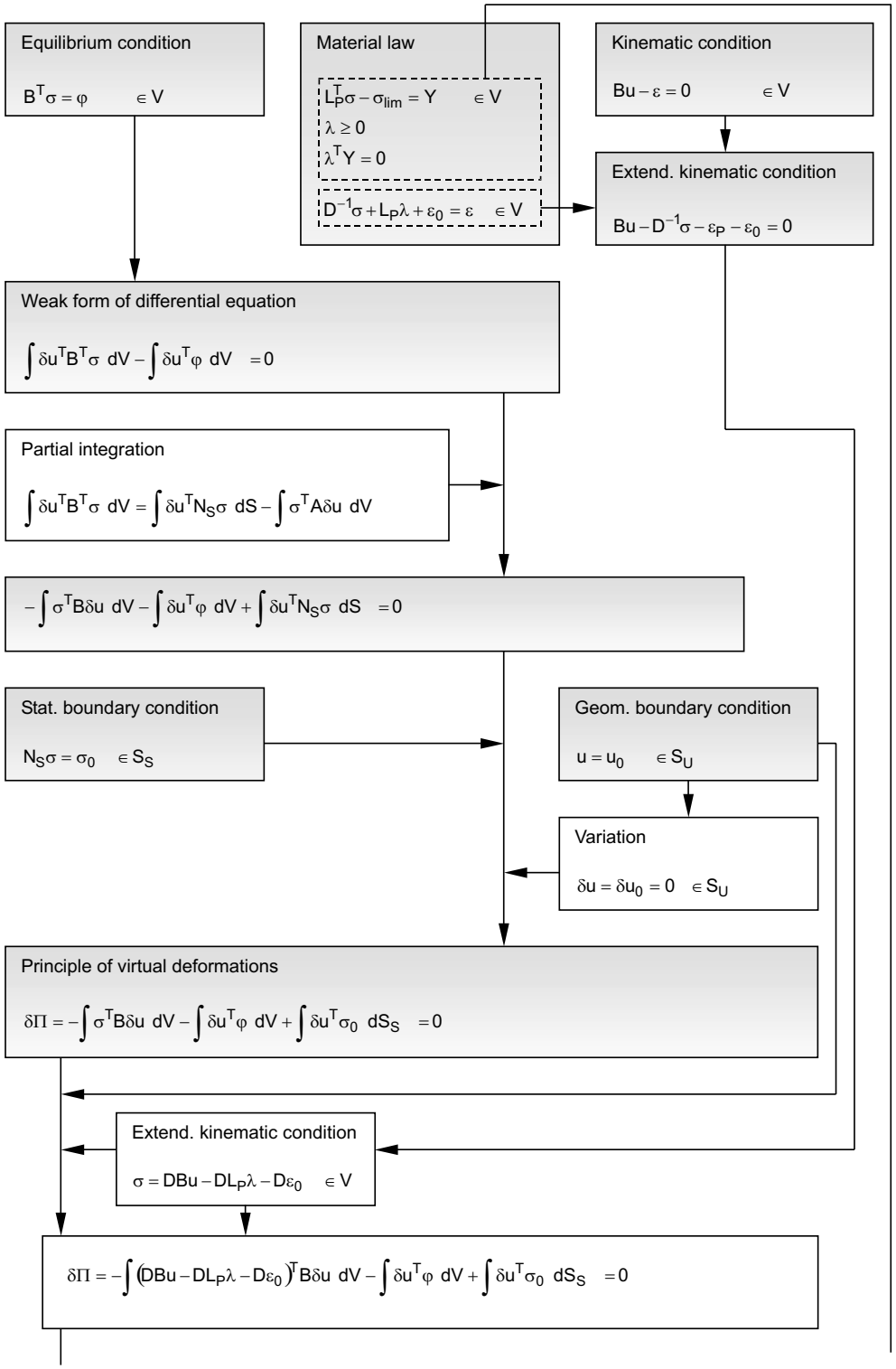

Table 7-10 Derivation of the principle of total potential (elasto-plastic material); continued

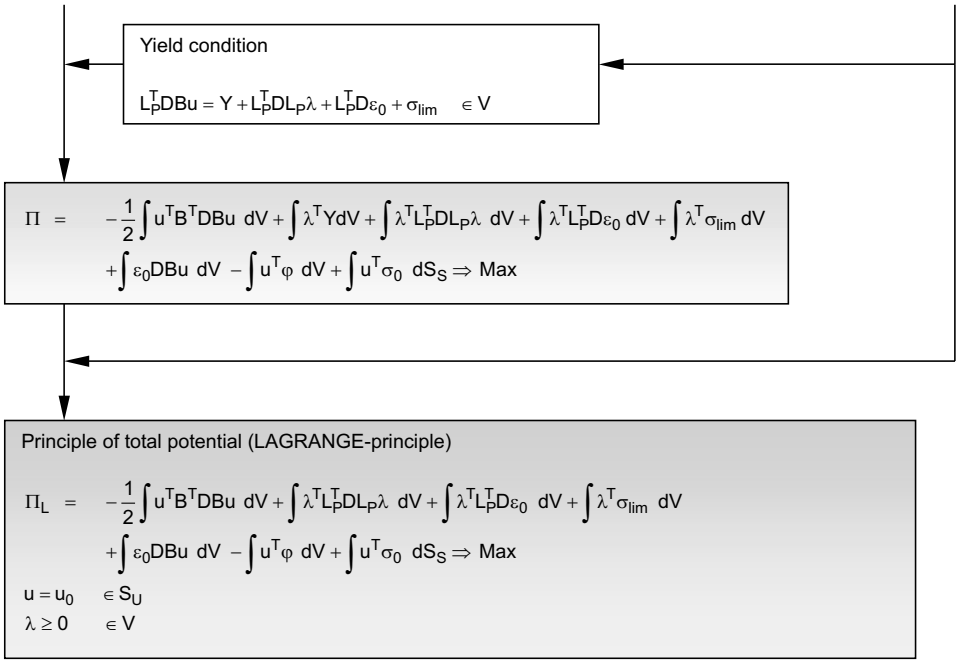

An internal force state is admissible, if the equilibrium conditions, the static boundary conditions and the appropriate yield conditions are fulfilled. The plastic limit load can be calculated on basis of the static theorem as indicated in Tab. 7-11. The relations have been simply derived from Tab. 7-7, by meaningful scaling of the decoupled kinematic parameter part of the scheme. Then some of the variables and conditions can be left out. It must be noted, that for rigid plastic bodies the obtained internal forces s are undetermined in the local regions with non-plastic behavior. Because the internal forces and displacements are not coupled in the kinematic condition, the appropriate displacement state is undetermined as well.

The kinematic theorem states

> **Theorem 2**: *A structure is statically stable, if a kinematically admissible displacement state can be found.*

A displacement state is kinematically admissible, if the appropriate kinematic conditions, the kinematic boundary conditions and plasticity conditions are fulfilled. This theorem can be used to calculate a limit load of the structure.

$$p \rightarrow Max \tag{7-44}$$

$$Au - L_p\lambda = 0 \qquad \in V \tag{7-45}$$

Table 7-11 Optimization scheme for limit load analysis of rigid plastic structures (Static formulation)

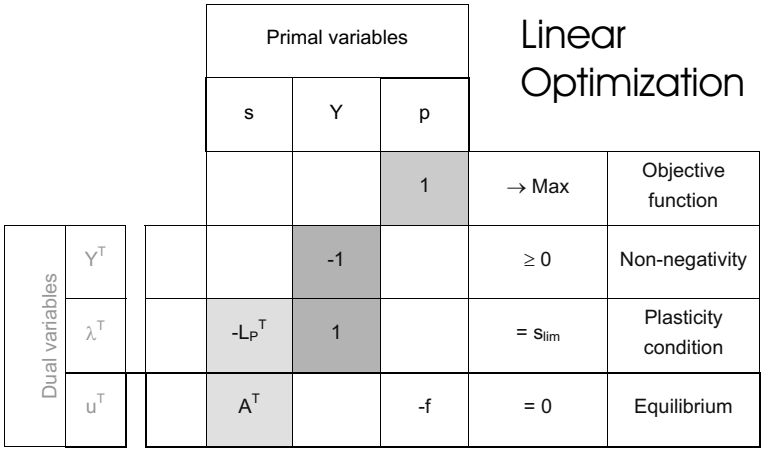

$$A^T s = p\hat{f} \qquad \in V \tag{7-46}$$

$$L_p^T s + s_{lim} \leq 0 \tag{7-47}$$

$$u = u_0 \qquad \in S_u \tag{7-48}$$

$$\lambda \geq 0 \tag{7-49}$$

This complete set of conditions is required, as the equilibrium condition (containing the force with the scaling factor p) needs to be respected

$$A^T s = \hat{f} p \qquad \in V \tag{7-50}$$

However, this condition can be multiplied with the displacement u

$$u^T A^T s = u^T \hat{f} p \qquad \in V \tag{7-51}$$

With the insertion of the kinematic condition Eq. (7-45)

$$\lambda^T L_p^T s = u^T \hat{f} p \qquad \in V \tag{7-52}$$

and substitution of the plasticity condition, the equation reads

$$\lambda^T s_{lim} = u^T \hat{f} p \qquad \in V \tag{7-53}$$

Table 7-12 Nonlinear optimization scheme for limit load analysis of rigid plastic structures (Kinematic formulation)

			Primal variables			Nonlinear Optimization	
			u	λ	p		
					1	→ Min	Objective function
Dual variables	s^T		A	$-L_p$		=0	Ext. kinematic condition
	y^T			1		≥ 0	Non-negativity
	1		$-p f^T$	s_{lim}^T		= 0	Energy condition

This is similar to an energy condition, relating the external energy to the plastic energy of the structure. Then the limit load task can be written

$$p \rightarrow Max \tag{7-54}$$

$$\lambda^T s_{lim} = u^T \hat{f} p \qquad \in V \tag{7-55}$$

$$Au - L_p \lambda = 0 \qquad \in V \tag{7-56}$$

$$u = u_0 \qquad \in S_u \tag{7-57}$$

$$\lambda \geq 0 \tag{7-58}$$

The appropriate nonlinear optimization scheme is given in Tab. 7-12. In this form, only kinematic quantities are left as structural variables.

For further simplification of the problem, the nonlinearity in the calculation can be eliminated by introducing a scaling

$$u^T f = -1 \tag{7-59}$$

Hence, the problem is as given in Tab. 7-13.

Theoretically, pure kinematic formulations of the limit load problem can be defined. Then the loading of the structure is given as deformations. Accordingly, the stress based formu-

Table 7-13 Linear optimization scheme for limit load analysis of rigid plastic structures (Kinematic formulation)

			Primal variables		Linear Optimization	
			u	λ		
				s_{lim}^T	→ Min	Objective function
Dual variables	s^T		A	$-L_p$	=0	Ext. kinematic condition
	y^T			1	≥ 0	Non-negativity
	1		f^T		= - 1	Scaling condition

lation of the yield criterion needs to be transformed into a deformation based form. Then the appropriate extremum principle is

$$p \rightarrow Max \tag{7-60}$$

$$A_u u - N_s^T c_u - p\hat{\varepsilon} = 0 \qquad \in V \tag{7-61}$$

$$-N_u u = u_0 \qquad \in S_u \tag{7-62}$$

$$A_{p,\varepsilon}^T \varepsilon - \varepsilon_{lim} \leq 0 \qquad \in V \tag{7-63}$$

The plastic limit load is determined by application of the uniqueness theorem. It states

> **Theorem 3**: *If a load can be found for a kinematically admissible mechanism and a statically admissible internal force state, then this load is the plastic limit load of the structure.*

It states that solutions due to static and kinematic formulations of the limit state analysis must be identical.

As in Sec. 7.2, the limit state can be alternatively described in terms of a limit resistance intensity$r$ rather than a limit load intensity p. Furthermore, the previously introduced optimization problems are one-parameter formulations, because only the scalar value of p is altered. Alternative formulations can consist more parameters or a completely decoupled

modification of loading or resistance parameters, e.g. the objective function in Eq. (7-44) can be changed to

$$f \rightarrow Max \tag{7-64}$$

Such formulations result in non-convex problems, thus global optimization methods must be adopted for solution. The calculations can be relatively costly.

7.3.3 Example 1: Plastic limit load for beam structure

In continuation of the example from Sec. 7.2.5, the frame structure is analyzed regarding the plastic limit resistance. The optimization scheme of Tab. 7-11 is applied, slightly changed for derivation of a scalar limit resistance factor. Then the following optimization scheme can be applied (static formulation)

$$O(r, s) = r \rightarrow Min \tag{7-65}$$

$$A^T s = \hat{f} \qquad \in V \tag{7-66}$$

$$L_p^T s + r s_{lim} \leq 0 \tag{7-67}$$

Furthermore, in comparison with Tab. 7-11, the slack variable y has been eliminated by transformation of the plasticity condition to a inequality condition.

For this example, both load combinations are applied. For LC I, the resistance factor is $r = 1.040$ and for LC II $r = 1.020$, hence the plastic limit resistance factor considering all possible load combinations is the maximum value, hence $r_P = 1.04$. The moment distribution is illustrated in Tab. 7-14. Three plastic hinges are developed and at one additional position the plasticity condition is touched. Thus an infinitesimal increase of the loading will result in the failure of the structure.

Residual moments can be observed, if the structure is completely unloaded. The distribution is given in Tab. 7-15. It can be seen, that the position of plastic hinges and the residual moment distribution of both load combinations are different.

7.3.4 Example 2a: Plastic limit load for mixed FEM and EFG model

In this example the Finite Element Method (FEM) and Element Free Galerkin (EFG) method are applied for simplified seismic analysis according to the previously discussed limit load approaches. The mechanical background has been introduced in Sec. 4.3 and 4.17. While considering hybrid structures it can be necessary to decompose the structure into different model domains that can be discretized alternatively:

- Single domain models (either FEM or EFG) or
- Mixed domain models (FEM and EFG).

Table 7-14 Example: Moment distribution (Plastic limit resistance)

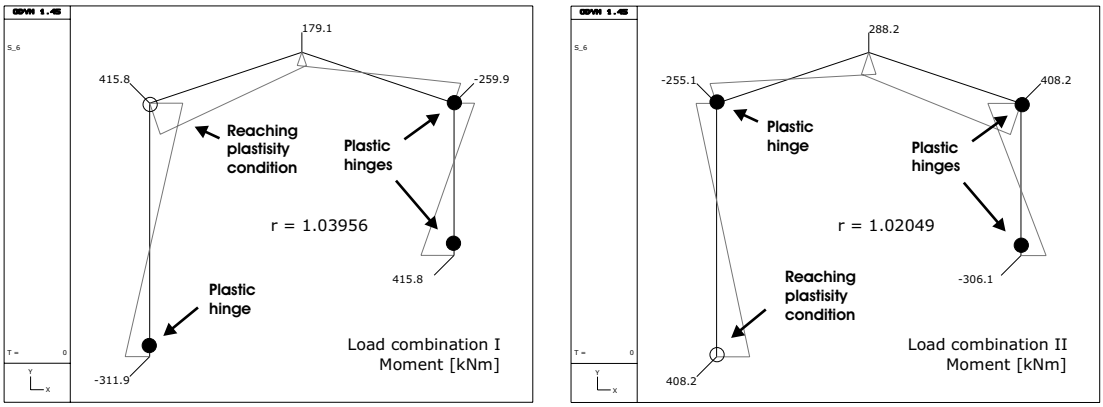

Table 7-15 Example: Residual moment distribution (Plastic limit resistance)

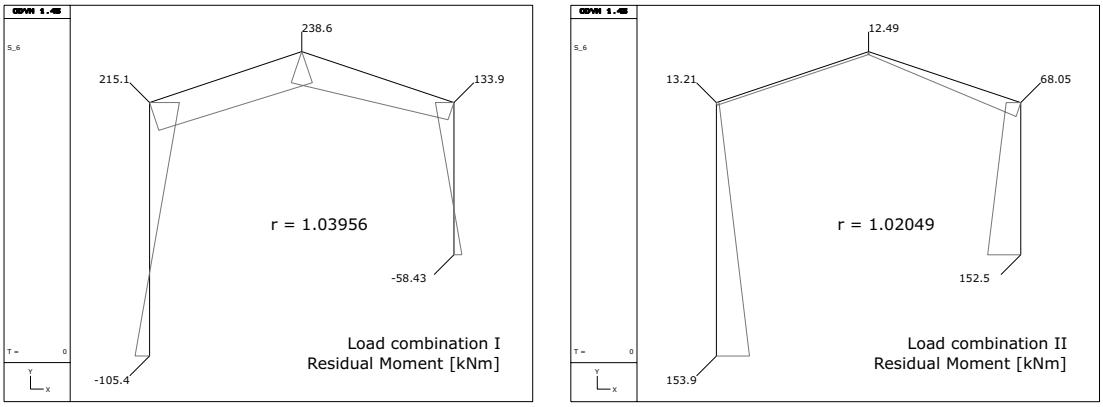

Table 7-16 Optimization scheme for plastic limit load analysis for different domains EFG and FEM

Design variables	s_{EFG}	s_{FEM}	$c_{s,EFG}$	$c_{s,FEM}$	f_c	p	1		
Objective function						-1		$\rightarrow$	Min
Equilibrium cond.	A_{EFG}^T		$N_{u,EFG}$		H_{EFG}^I	$-f_{m,1}$	$-f_{d,EFG}$	=	0
		A_{FEM}^T		$N_{u,FEM}$	$-H_{FEM}^I$	$-f_{m,2}$	$-f_{d,FEM}$	=	0
Static bnd. conditions	$N_{S,EFG}^T$						$-s_{0,EFG}$	=	0
		$N_{S,FEM}^T$					$-s_{0,FEM}$	=	0
Plasticity condition	$L_{P,EFG}^T$						$-s_{lim,EFG}$	$\leq$	0
		$L_{P,FEM}^T$					$-s_{lim,FEM}$	$\leq$	0

Because of the non-direct compatibility between the unknowns u_{EFG} of the meshless model and the nodal deformations u_{FEM} of the FEM solution it is necessary to provide a interface or transformation relation. It can be easily done by utilize the displacement interpolation (shape) functions matrices $H_{u,FEM}$ and $H_{u,EFG}$. Equating both conditions leads to Eq. (4-201) that can be directly applied for all interface points between two domains.

In Tab. 7-16 an optimization scheme for solving the plastic limit load problem according to the Castigliano approach is given. The number of unknowns will increase with the vector of coupling forces f_c along the domain interface. As in this example scheme, the objective function and all subsidiary conditions are linear, the problem can be solved by linear optimization.

For comparability of the solutions derived with single and mixed domain models for both FEM and EFG, the same configuration of the mesh and Gaussian quadrature is chosen. This results in models with identical number of unknowns. For the modeling of shear walls, a standard 4-nodes finite element with bilinear shape function is used. For the EFG part, a bilinear basis and circular support function is applied.

In Fig. 7-2 a hybrid beam-column-shear wall structures is given. The structure is loaded by dead loads and a seismic horizontal load. In this structure, two different types of models are connected. For the wall structure part the EFG method is used, whereas for the beam and columns common FE beam elements are applied. Because of the pure quality of EFG results for beam structures this decomposition is always recommended. Fig. 7-3 shows the discretization of the two domains and the interface points. The mesh in the EFG part is for domain integration only and can be chosen for convenience.

The following state and limit state analysis cases will be discussed:

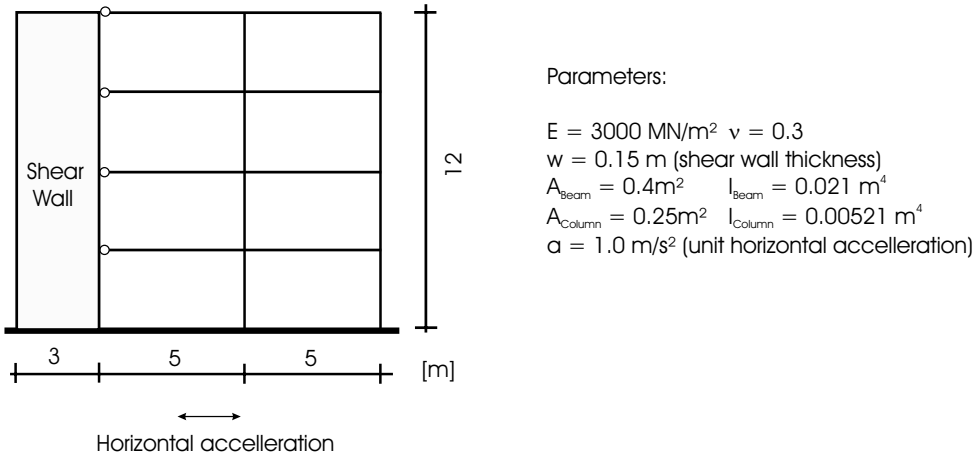

Figure 7-2 Example EFG-FEM: Structural system and parameters

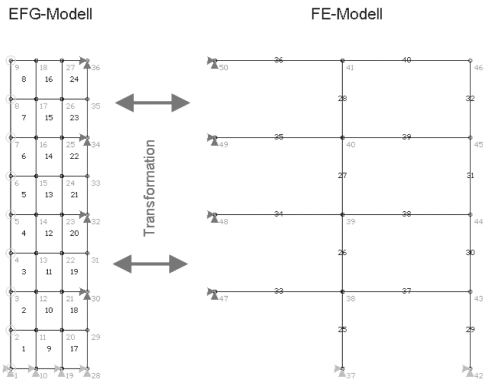

Figure 7-3 Example EFG-FEM: Domains of different discretization

Table 7-17 Example EFG-FEM: Results of analysis

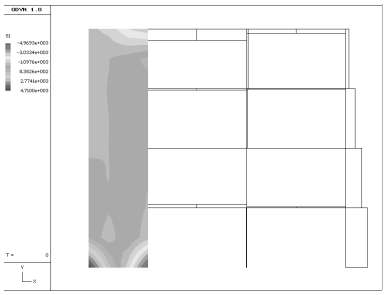

Elastic Response σ_x (case 1)

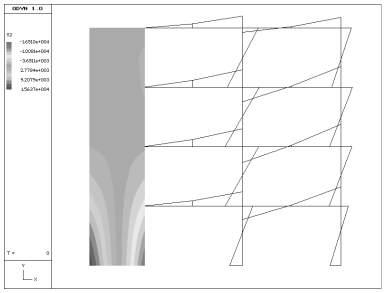

Elastic Response σ_y (case 1)

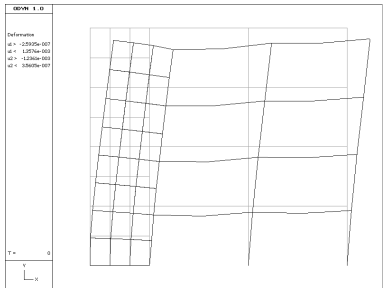

Plastic Deformation (case 3)

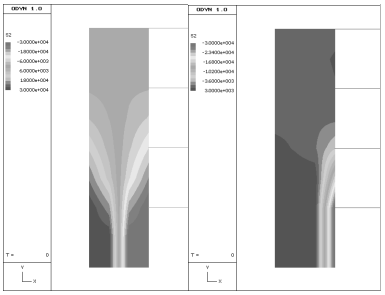

Plastic Response σ_y (case 2,3)

1.) Elastic state with load intensity p = 1.0

2.) Plastic limit state with equal yield limitations in both tension and pressure direction

3.) Plastic limit state with different yield limitations in tension and pressure direction

In this example, simple non-interacting uniaxial plasticity conditions for the stresses and internal forces are used. Selected results of the calculation are given in Tab. 7-17 The plastic limit load is 2.85. This result can now be compared to the seismic loading applied to the structure. Despite the relatively coarse mesh in the wall section the resulting stress distribution is continuous. This applies also for the linear and nonlinear stress distributions.

7.3.5 Example 2b: Coupled shear wall system

The analysis in mixed EFG-FEM domains is demonstrated for a coupled wall system according to Tab. 7-18. The appropriate system discretization and selected deformation figures are given in Tab. 7-19

For examination purposes three cases will be considered:

1.) Both walls are FEM-discretized

2.) Wall 1 will be EFG and wall 2 FEM modeled

Table 7-18 Example: Coupled shear wall: Structural system and parameters

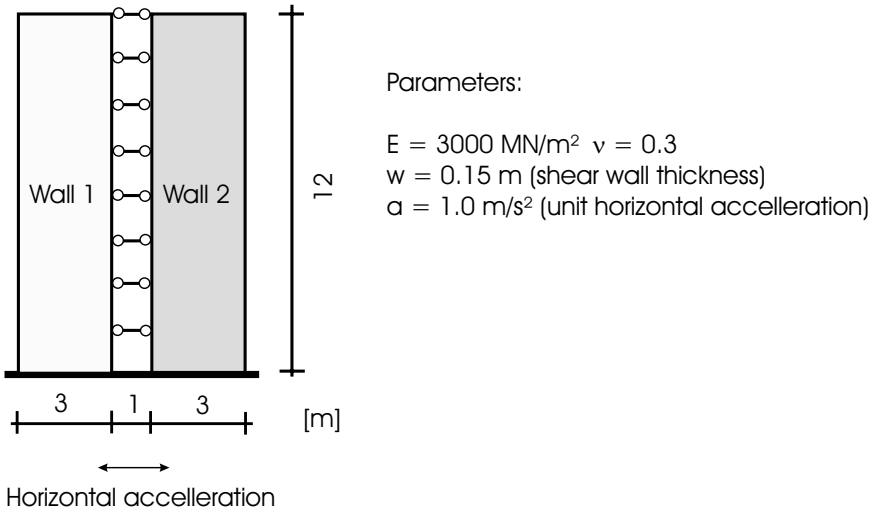

3.) Both walls will have an EFG discretization

For all cases an elastic state and plastic limit state analysis will be performed. The results are listed in Tab. 7-20. As visible in the mixed structure results (Tab 7-21 and 7-22) the EFG-discretization has an advantage in representing the stress distribution in the structure. In limit state analysis the difference in modeling is not so important for the determination of the ultimate limit load itself. But it is essential for the approximation of the resulting stresses and deformations. It should be stated that the FE solution can be approved by refining the mesh or using better element formulations.

The investigations show a good adaptability of the meshless methods to the design of hybrid structures by using optimization strategies. As well as single domain models, mixed domain models can be used. With this method, the advantages of both finite element and meshless methods can be utilized most suitable. With the property of a minimum amount of unknowns by maintaining an adequate quality of the results the application of mixed finite element and meshless methods can be an alternative to traditional methods in structural analysis and optimization.

Table 7-19 Example coupled shear walls: System and deformation for case 2 elastic p= 1.0 and case 2 elasto-plastic p=1.835

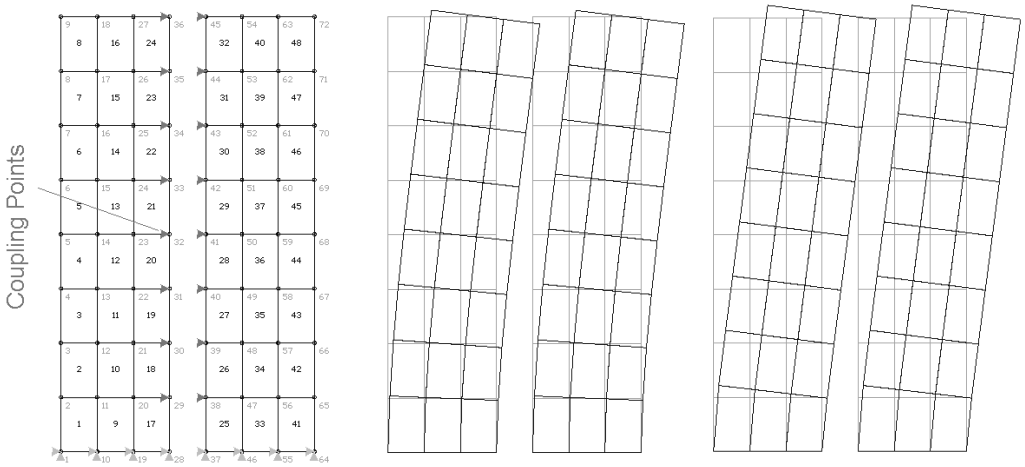

Table 7-20 Example coupled shear walls: Summary of results

Modell			Elastic calculation		Elastic-Plastic calculation			
case	wall 1	wall2	Intensity factor	max u [mm]	Intensity factor	max u [mm]	Intensity factor	max. u [mm]
1	FEM	FEM	p=1.0	3.0	p=1.0	3.2	1.835	18.0
2	EFG	FEM	p=1.0	3.1	p=1.0	3.3	1.835	28.5
3	EFG	EFG	p=1.0	3.2	p=1.0	3.4	1.835	196.2

Table 7-21 Example coupled shear walls: Elasto-Plastic Response (case 2, p=1.0)

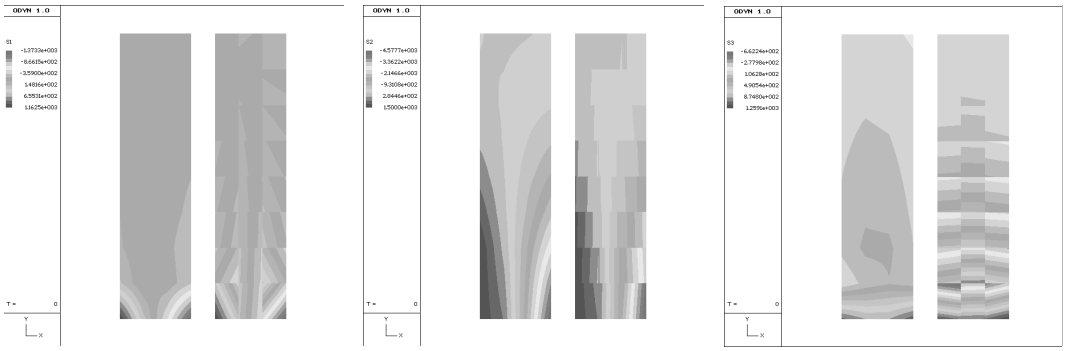

Table 7-22 Example coupled shear walls: Elasto-Plastic Response (case 2, p=1.853)

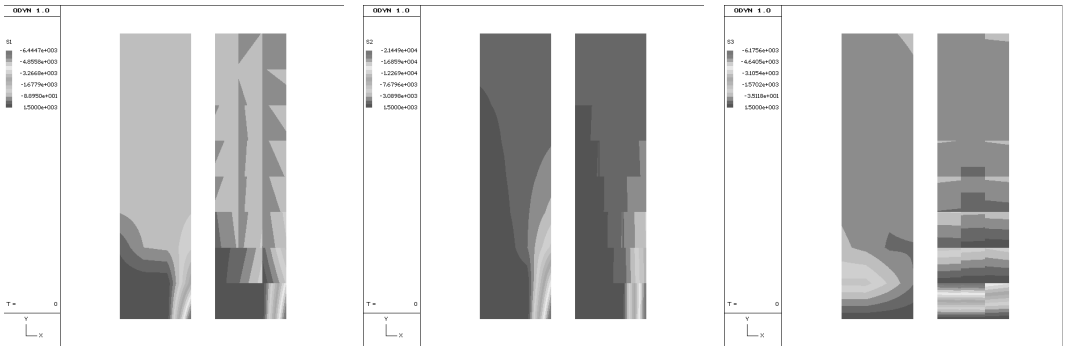

7.4 Shakedown limit state analysis

7.4.1 Background

The application of the theorems in Sec. 7.3 actually requires monotonically increasing plasticity histories. In reality the structure exhibits several changes in the plastification. An unconditional application of quasi-static loads within the plasticity theory can be critical. The sequence of loading needs to be considered in order to monitor alternating or progressive plasticity effects. Such plastifications are often experienced as damage, that can be accumulated in time. In [90] an observation was described, that if the intensity of loading is limited to a certain level, the structure first shows a limited number of plastification and afterwards only elastic responses, always if the load program is repeated. This state is called shakedown or adaptation state. This state is characterized by a stable residual parameter distribution in the structure. Basic relations for a theoretical assessment of the phenomenon have been formulated in [25,147,148,134] for perfectly plastic materials.

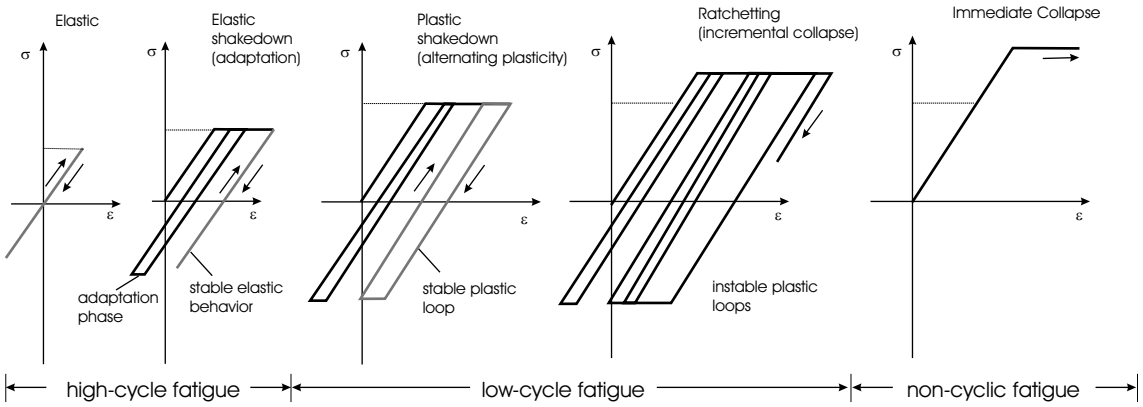

Figure 7-4 Behavior characteristics due to different load intensities of elastic-plastic structures

Later on, shakedown of structures under various conditions have been widely investigated, e.g. [216,217,132,143,144,175,176,177,36,113]. The following general categories of structural behavior are distinguished for cyclic loaded elasto plastic structures (geometric linear):

1.) Elastic response: The structure is loaded below all yield limits, any response is elastic.

2.) Elastic shakedown: After a limited number of inelastic deformations a stable residual state will be constituted, all further behavior is elastic (adaptation).

3.) Plastic shakedown: The plastic cycles stabilize to closed loops of plastic deformations (alternating plasticity).

4.) Ratchetting (incremental collapse): Unlimited plastic deformation until failure.

5.) Immediate failure (plastic collapse): The structure fails immediately due to the development of a kinematic mechanism.

They are illustrated in Fig. 7-4, here exemplarily with perfectly plastic branches in the material law. Looking for the first three categories, for practical purposes only the limitation below the elastic limit or elastic shakedown limit state are reasonable to adopt for design. Even if the application of higher load intensities within seismic designs seems to be theoretically possible because of the limited amount of expected cycles, plastic shakedown is difficult to establish and to control for real materials. Therefore following, the elastic shakedown is further considered, abbreviated next just as shakedown or adaptation.

Special aspects of dynamic shakedown have been highlighted in [48,60,61,102,186]. In seismic design, as specified in [197,219], the shakedown state denotes an appropriate performance level for structures with limited damage levels. Utilizing the shakedown state in structural design ensures the usage of plastic reserves for energy dissipation, but the

avoidance of infinite damage accumulations (low cycle fatigue) and therefore a limitation of plastic deformations. It is most interesting in performance based design because of the assurance of full operability at the same safety level (after-shock resistance).

Shakedown of structures can be characterized as the bounding of plastic deformations in time. This can be expressed in terms of plastic multipliers

$$\lim_{t\to\infty} \lambda(t) < \infty \tag{7-68}$$

Conditions for shakedown have been mostly explored for elastic plastic structures. In general, the test of all possible load histories, will give proof for the existence of shakedown and respectively the true bounds for all considered structural parameters. This procedure can be extremely costly even if only for a fixed load intensity the shakedown of a structure has to be proven. The efforts are even increased, if the appropriate shakedown limit state is to be identified.

The great value of shakedown analysis for seismic design is the option to mainly ignore the actual characteristic of the seismic response of a particular earthquake. The response to such a record is rather hypothetical, as the loading is uncertain. Instead of performing a probabilistic analysis, shakedown analysis tries to evaluate extremum responses without considering any possible load sequence. Contrary to time history analysis methods, shakedown analysis needs only the information about the intensity of elastic response in form of an elastic result envelope. This intensity information can be determined simpler than defining a significant ground acceleration. This envelope information can be determined either by simplified elastic analysis according to Sec. 6 or by application of linear elastic time history analyses (Sec. 8).

7.4.2 Shakedown theorems

The total response of a structure is assumed to be dividable into an elastic (subscript e) and a residual part (subscript r) , e.g. for stresses, strains and displacements

$$\sigma(x,t) = \sigma_e(x,t) + \sigma_r(x) \tag{7-69}$$

$$\varepsilon(x,t) = \varepsilon_e(x,t) + \varepsilon_r(x) \tag{7-70}$$

$$u(x,t) = u_e(x,t) + u_r(x) \tag{7-71}$$

thus both parts are regarded separately and can be superposed. As can be seen in Fig. 7-5, this assumption is realistic for elastic plastic structures because such structures behave linear elastic in the first stage even if a certain inelastic deformation history was attended. However, this assumption requires sufficient independence of the elastic response from the residual state. Otherwise iterative concepts need to be applied.

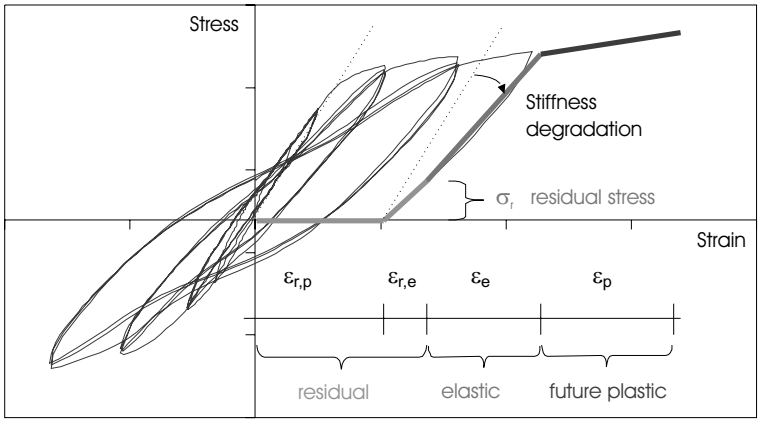

Figure 7-5 Elastic behavior after certain amount of plastic cycles

The residual state itself consists of an elastic and plastic part. The stresses represent only the elastic components according to the material law, whereas the residual strains are composed of an elastic an the total plastic part.

$$\sigma_r(x,t) = \sigma_{r,e}(x,t) \tag{7-72}$$

$$\varepsilon_r(x,t) = \varepsilon_{r,e}(x,t) + \varepsilon_P(x) \tag{7-73}$$

In simplified design, tracking of the exact damage history is omitted, however the assessment of magnitudes is intended. Therefore the elastic part $\sigma_e(x,t)$ in Eq. (7-69) is typically simplified by representation as an envelope response at any location x

$$Y_{YF}(\sigma_e(x)) = \max\left(Y_{YF}(\sigma_e(x,t))\right) \qquad \forall t \tag{7-74}$$

analyzed with respect to the yield function Y_{YF}. The elastic (dynamic) response $\sigma_e(x,t)$ has to be calculated with the same structural assumptions, with the applied actual loading (given load pool), but with purely elastic material. The elastic envelope can be calculated by methods of linear elastic analysis, e.g. time history or simplified linear analysis. However, with the obtained envelope response, any further dependency of time is neglected. Therefore the elastic envelope solution is sometimes also called fictitious or quasi-static. The meaning of the compound solution defined in Eq. (7-69) is illustrated further in Fig. 7-6. It can be seen, that the residual state σ_r is leading the actual response σ of the structure back into the elastic envelope range of the yield function Y. The same case is illustrated for nonlinear yield conditions in Fig. 7-7. Here the definition of an convex envelope polyhedron for the elastic response in general three dimensional case is illustrated. This polyhedron reduces the entire elastic response to only some representatives at the polyhedron edges. This concept is useful for yielding conditions that form a convex domain of admissible elastic responses in order to reduce the size of the vector σ_e in calculations.

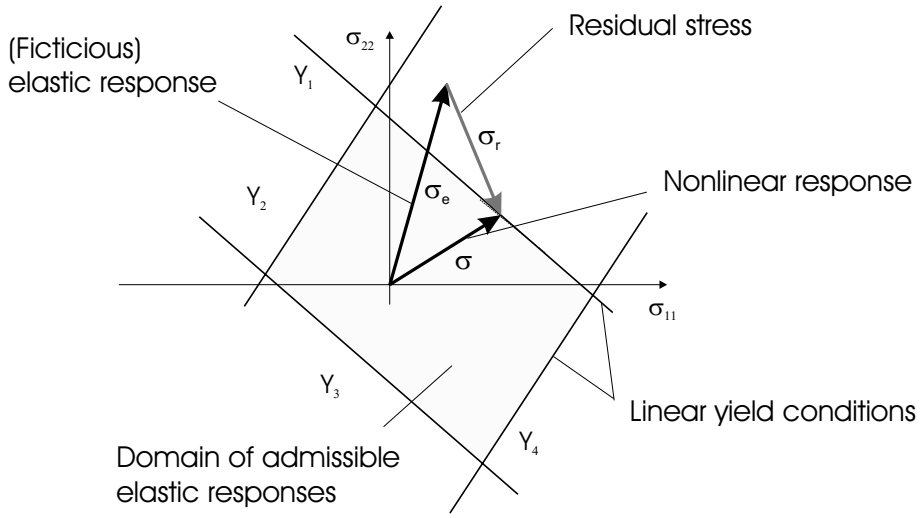

Figure 7-6 Principle of superposition of elastic and residual response components

In addition the application within a limit load analysis and a limit resistance analysis is demonstrated.

Under these conditions, the static theorem of shakedown (Bleich-Melan theorem [147]) states

> **Theorem 4**: *Shakedown occurs, if for a given elastic envelope response σ_e a self-equilibrated residual stress field σ_r can be found, and the superposition of σ_e and σ_r is fulfilling the plasticity conditions.*

This theorem can be provided in mathematical form. The equilibrium condition for the residual stresses is

$$A_s^T \sigma_r = 0 \tag{7-75}$$

and the plasticity condition reads

$$Y_{YF}(\sigma_r + p_{sta} \cdot \sigma_e, \lambda) \leq 0 \tag{7-76}$$

The corresponding load intensity for the elastic envelope p_{sta} is giving a lower bound on the shakedown limit load p_a

$$p_{sta} \leq p_a \tag{7-77}$$

The appropriate kinematic theorem (Koiter theorem [134]) is

> **Theorem 5**: *Shakedown cannot occur, if for a given elastic envelope response $p_{kin} \cdot \sigma_e$ the power of the elastic envelope on the plastic deformations exceeds the general dissipation power capacity of the system in time.*

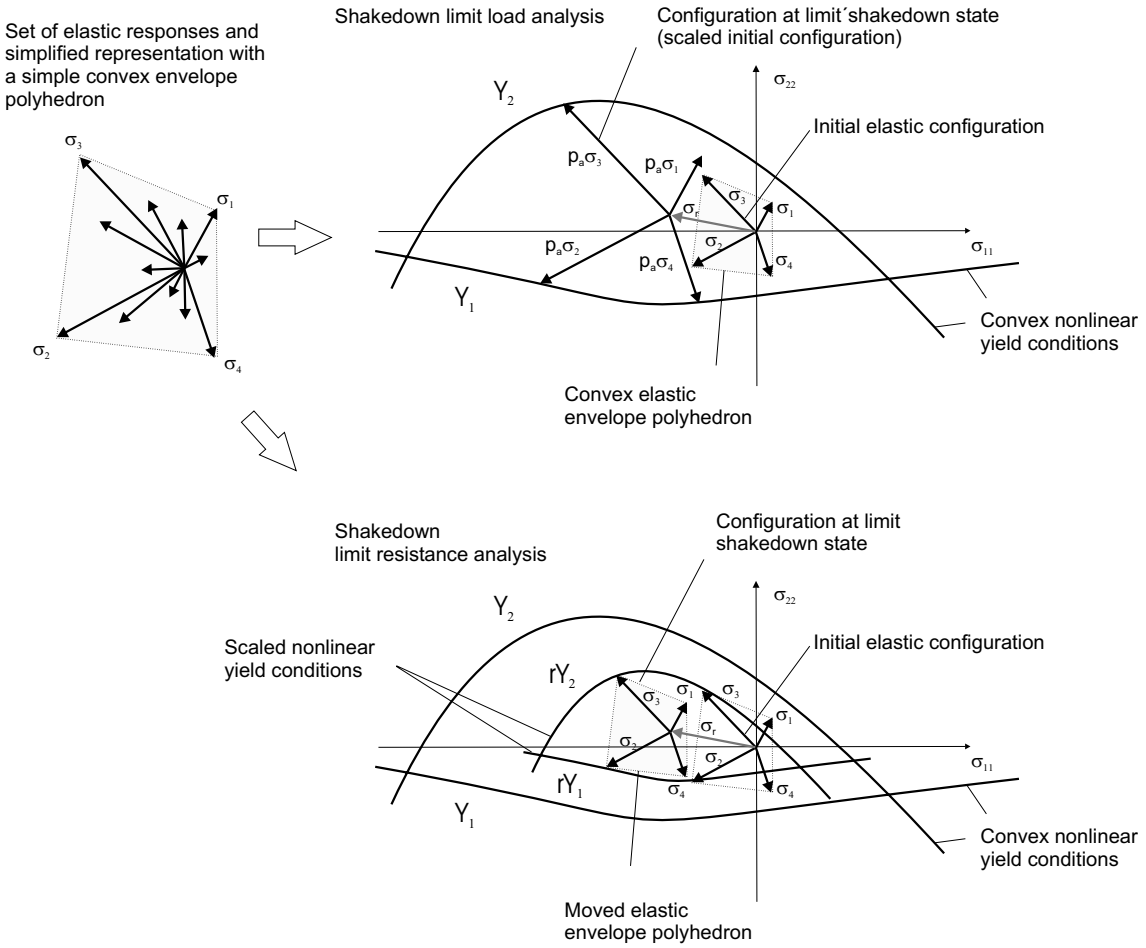

Figure 7-7 Determination of the elastic envelope response for nonlinear yield conditions and simplification by polyhedron envelope

In mathematical form the theorem can be written as

$$\int_0^t \int_V s_{lim}^T \lambda - p_{kin} \cdot \sigma_e \dot{\varepsilon}_p dV dt \leq 0 \tag{7-78}$$

Herein $s_{lim}\lambda$ is denoting the plastic dissipation capacity with s_{lim} as the constant part of the plasticity condition. The condition holds for plastic strain fields that are compatible with the residual displacements u_r in the system, e.g. for perfectly plastic material

$$\varepsilon_p = A_u u_r \tag{7-79}$$

The kinematic theorem is an inadaptation theorem, giving an upper bound on the shakedown limit load intensity

$$p_a \leq p_{kin} \tag{7-80}$$

The shakedown limit load is defined with the uniqueness theorem

> **Theorem 6**: *The load intensity is the shakedown limit, if all conditions of the static and kinematic theorem are fulfilled.*

Shakedown analysis only considers the knowledge of the envelope response $\sigma_e(x)$, without reflections on the actual process $\sigma_e(x,t)$. This means firstly, that although the magnitude of all loads in the given load pool remains constant, their sequence must be considered to be variable, with infinite number of repetition of any load of the pool. This fact limits possibilities to test in practice any possible situation. Secondly, the analysis is implicitly considering load situations that are not part of the original load pool, but are producing responses that fit the given elastic envelope as well. This property inherits a special suitability of the method for seismic design, where the specifics of the response history are mainly unknown, except for an estimation of the magnitude. It is an easy concept to take the stochastic character of the seismic loading into account, without explicit probabilistic calculations.

7.4.3 Load or resistance bounds for the shakedown state of elasto-plastic structures

Simplified analysis methods have been developed for special types of structures. For seismic design, simple linear elastic - plastic model assumptions are often appropriate. The stiffness degradation has to be regarded. The necessary cross-sectional parameters can be determined in a pre-phase with use of simple fiber models (push over analysis for the cross section). Conditions for the shakedown of linear elastic-plastic materials with linear plasticity and hardening have been derived, e.g. in [59,133]. According to this, a structure will shake down if

$$L_p(\sigma_r + \sigma_e) - A_h\lambda - s_{lim} \leq 0 \tag{7-81}$$

Except for the plasticity condition (7-81) and self-equilibrium condition (7-75) for the residual stresses, any other mechanical relationship remains unchanged. Thus the core relations from Sec. 7.3 are only minimally altered to fit the requirements of shakedown analysis. Then the appropriate extremum principle, in either Castigliano, Lagrange and Poisson formulation, can be formally derived. The calculation of the limit load intensity with means of optimization can be adopted. The appropriate formulation is given Tab. 7-23 for the calculation of the limit load intensity p_a or the resistance limit r_a. As the kinematic and material conditions have not been respected, the obtained vector s_r is independent from the displacement field. In Tab. 7-24 the optimization scheme for the calculation of the appropriate residual state for linear elastic perfectly plastic material is given. Both given forms are derived by modification of the Castigliano and Lagrange principles introduced in Tabs. 7-8 and 7-9.

Table 7-23 Optimization schemes for shakedown limit state analysis of rigid plastic structures (Static formulation)

		Primal variables			Linear Optimization	
		s_r	y	p		
				1	→ Max	Objective function
Dual variables	y^T		-1		≥ 0	Non-negativity
	λ^T	$-L_p^T$	1	$-L_p^T s_e$	$= s_{lim}$	Plasticity condition
	u_r^T	A^T			= 0	Equilibrium

Limit load

		Primal variables			Linear Optimization	
		s_r	y	r		
				1	→ Min	Objective function
Dual variables	y^T		-1		≥ 0	Non-negativity
	λ^T	$-L_p^T$	1	- s_{lim}	$= L_p^T s_e$	Plasticity condition
	u_r^T	A^T			= 0	Equilibrium

Limit resistance

Table 7-24 Optimization scheme for shakedown state analysis of elasto plastic structures (Static formulation)

		Primal variables		Quadratic Optimization	
		s_r	y		
	s_r^T	Q		→ Min	Objective function
Dual variables	y^T		-1	≥ 0	Non-negativity
	λ^T	$-L_p^T$	1	$= r\, s_{lim} + p\, L_p^T s_e$	Plasticity condition
	u_r^T	A^T		= 0	Equilibrium

7.4.4 Example shakedown resistance bounds

This is the continuation of the example in Sec. 7.3.3. For simulating time effects, the following load sequences are defined, that are composed of the previously defined load combinations LC I and LC II

- Sequence A : LC S, R, LC I, R, LC II, R, LC I, R, ...
- Sequence B : LC S, R, LC II, R, LC I, R, LC II, R, ...

consisting in total of four complete cycles. Both sequences start with load case "LC S", that is a pure static load case, "R" is symbolizing a zero load step with total unloading of the structure in order to analyse the residual state after load applications. This analysis can be performed with methods of Sec. 8, ignoring the mass and damping in the system. It should be noted, that the simplicity of the sequences is a property of this particular

Table 7-25 Example: Cyclic behavior for plastic strains at plastic limit state for Load Sequence A and B

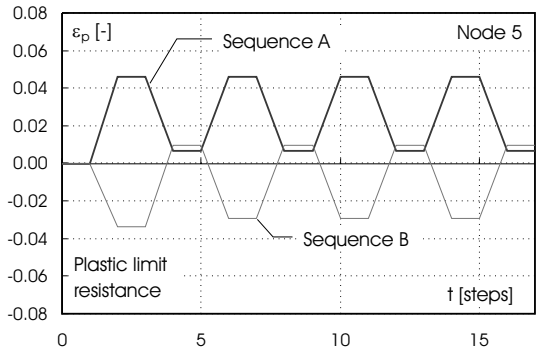

example. In other examples, more than two load combinations might be considered. Then combinatorical rules need to be applied to develop all possible load sequences, so the calculational efforts rise exponentially with the number of load combinations.

From Sec. 7.2.5 it is clear, that a structure with the capacity due to the elastic limit resistance ($r_e = 1.575$) will withstand all sequences without developing any plastic deformation. Therefore the elastic behavior is preferred for structures that necessarily need to survive any seismic impact without any damage, because the importance is eminent and a repair is too costly. The efforts to build such structures can be tremendous and are therefore mostly applied in regions of lower seismicity.

Alternatively to the elastic design, the plastic resistance level, calculated in Sec. 7.2.5, can be made a criteria for design (Plastic limit resistance factor $r_p = 1.04$). From the definitions of plastic limit, it seems to be perfect for structures with low importance. However, just preventing the kinematic chain can be dangerous as the structure is experiencing several plastic cycles. Such cyclic behavior is disregarded in the concept of plastic limit design. At node 5 of this example, the plastic deformations develop according to Tab. 7-25. It is visible, that the plastic deformations due to the load sequences develop differently and without stabilization. This means, that nearly any cycle is introducing new damage to the structure. This can also be observed from the bending moment plots in Tab. 7-26. The residual moments of either load sequence are permanently alternating.

The plastic limit state seems to be non-adequate for higher numbers of cycles. Taking the effects of cyclic behavior into account, the design according to the shakedown limit can mitigate the effects of plastification. Using the static shakedown theorem, the following optimization problem can be solved in order to calculate the limit resistance factor

$$O(r, s_r) = r \rightarrow Min \tag{7-82}$$

$$A^T s_r = 0 \qquad \in V \tag{7-83}$$

Table 7-26 Example: Cyclic behavior for bending moments at plastic limit state for Load Sequence A and B

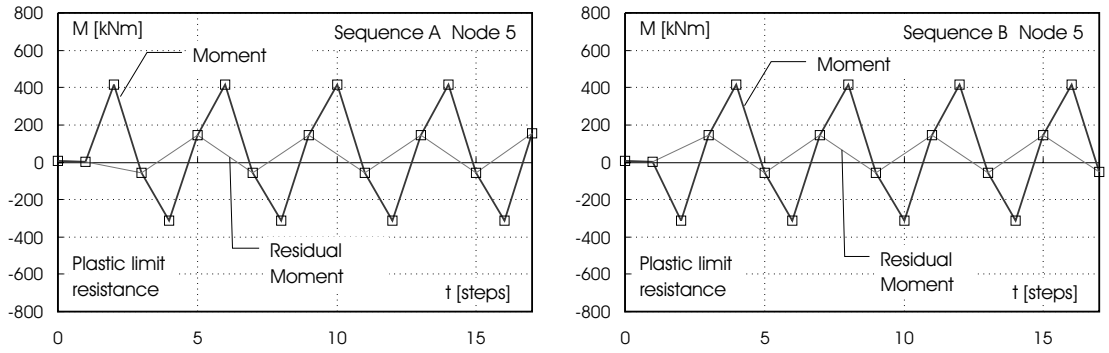

$$L_p^T s_r + s_e + r s_{lim} \leq 0 \tag{7-84}$$

Herein s_e is the envelope function for all elastic results $s_{e,i}$ for all n_{LC} considered load combinations

$$s_e = \max_{i=1}^{n_{LC}} \left(L_p^T s_{e,i} \right) \tag{7-85}$$

The envelope function is given in Tab. 7-27. The calculation of the limit resistance factor gives $r_a = 1.333$. The appropriate residual moment distribution is drawn in Tab. 7-27. If this residual moment distribution is obtained, all following load impacts from each of the load combinations cannot change the residual state again. As well the expected positions for plastic hinges are indicated. For the two load combinations, the appropriate superposed moment distributions are given in Tab. 7-28.

The experiment is continued by testing the effect of the single load cases at the shakedown limit resistance level. The residual moment distributions left in the structure after loading and complete unloading are given in Tab. 7-29. As expected, no load combination is leaving exactly the same plot as calculated previously (Tab. T. Example shakedown envelope). Only at plastic hinge points the values coincide or at least are not exceeding those of the calculated shakedown state. This gives intentions to analyse the uniqueness of the shakedown results more in detail.

The analysis is continued with a load sequence analysis using the sequences defined in Sec. 7.3.3. In this analysis, the sequence is applied and all predeformation effects resulting from plastifications caused in the previous load steps are considered. Tab. 7-30 and 7-31 illustrate the effect of shakedown. Contrary to the plastic limit state, the plastic strains and the residual moments will stabilize after a limited number of load impacts. It can be concluded, that the calculated resistance level is able to prevent alternating or progressive plastifications. However, the calculated internal forces and deformations are only approximations. The approximation is sufficient to be used in design tasks of seismic engineering.

Table 7-27 Example: a.) Envelope function b.) Residual moment distribution

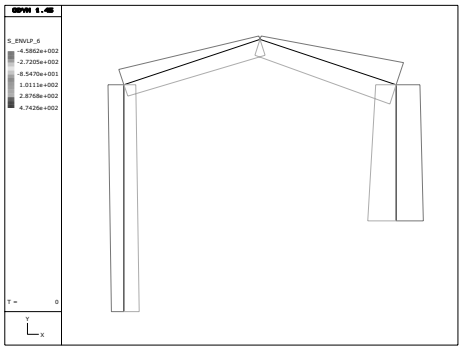

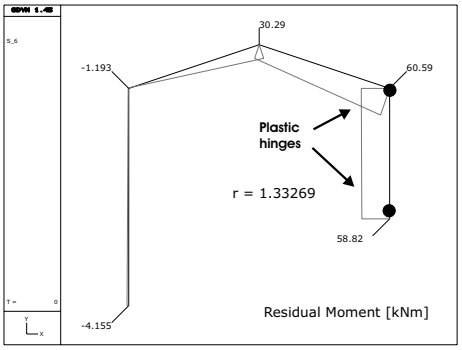

Table 7-28 Example: Moment distribution for load combinations (Shakedown limit resistance)

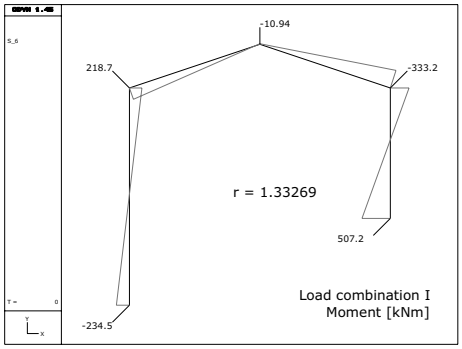

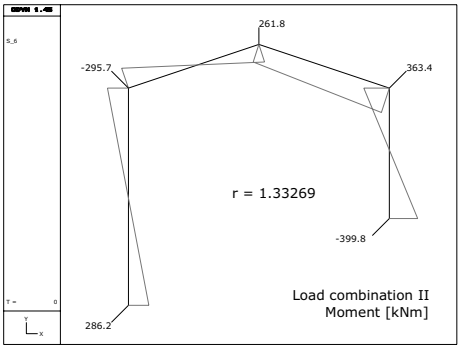

Table 7-29 Example: Residual moment distribution for load combinations (Shakedown limit resistance)

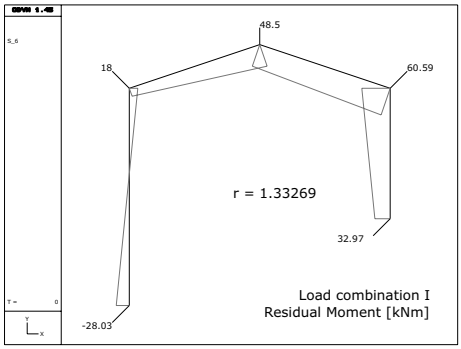

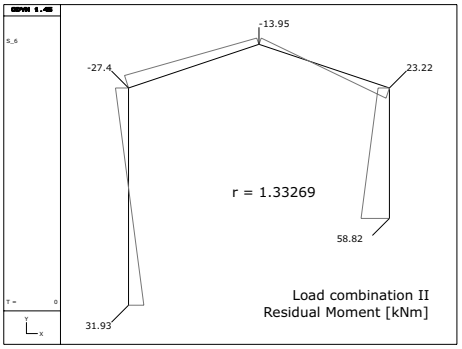

Table 7-30 Example: Cyclic behavior for shakedown strains at plastic limit state for Load Sequence A and B

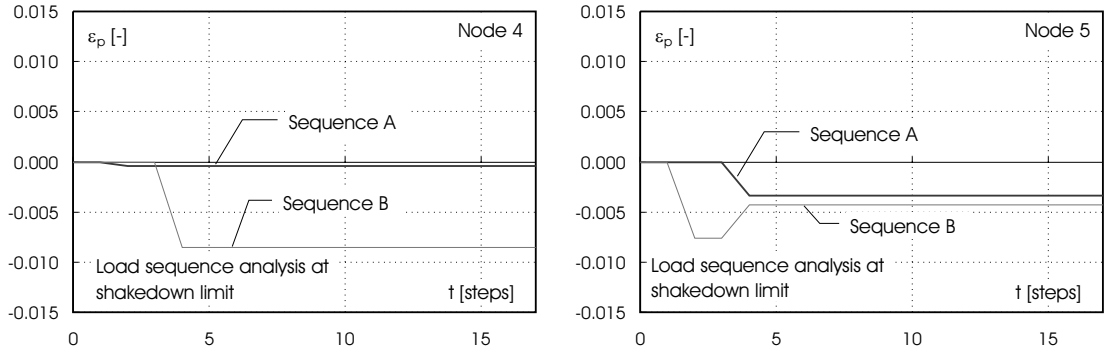

Table 7-31 Example: Cyclic behavior for moments at shakedown limit state for Load Sequence A and B

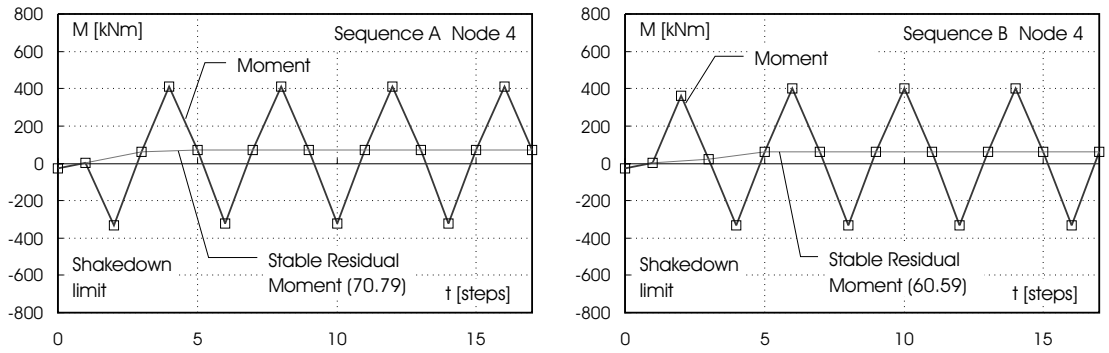

If a detailed load sequence analysis is performed, the final residual moment distribution is as in Tab. 7-32.

7.4.5 Dissipative energy bounds for the shakedown state of elasto-plastic structures

Another characterization of the shakedown process is the estimation of the lower and upper bounds of the dissipative energy (plastic potential). With these bounds the amount of damage in the structure can be assessed, or controlled. Classical shakedown theorems as in Sec. 7.4.3 can be used to calculate the lower limit. The derivation of the appropriate calculation schemes is given in Tab. 7-33. As can be seen, the classical concepts, following the Castigiano and Lagrange type of problem derivation, are both supporting the minimum calculation. This is due to the minimum energy properties of the classical theorems.

The estimation of the upper dissipative energy bound is much more complicated, as actually for a correct analysis, all possible load histories must be considered. This is often not efficient, therefore other concepts are proposed. Most given concepts simply manipu-

Table 7-32 Example: Residual moment distribution after load sequence application (Shakedown limit resistance)

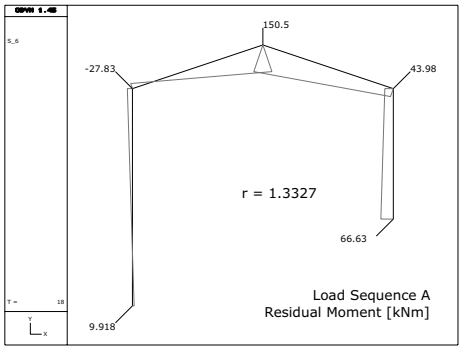

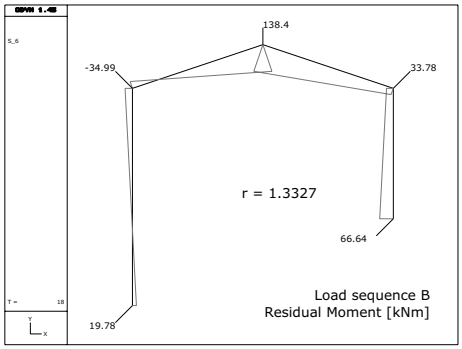

late the classical theorems, by neglected or altering one or more of the subsidiary conditions. For an increase of the plastic potential

$$E_p = s_{lim}^T \lambda \tag{7-86}$$

either the number of active plasticity conditions must rise and/or the values of plastic multipliers λ are increased and/or the plasticity conditions (e.g. the constant part s_{lim} or indirectly the elastic envelope s_e) are altered. As one representative concept, in [12] the plasticity conditions are changed to

$$s_{lim}^* = \max \left[L_p^{T-} s_r + s_e^-; L_p^{T+} s_r + s_e^+ \right] \tag{7-87}$$

at one cross section in the structure, having both minimum and maximum elastic envelope values s_e^- and s_e^+. Afterwards, the elastic envelope is changed as well to the value s_e^* leading to the maximum result in Eq. (7-87). The size of the coefficient matrices and vectors in the plasticity condition reduces accordingly. The entire derivation of the proposed concept is outlined in Appendix Sec. 11.9. As can be seen, the formulation presumes the constancy of the elastic energy in the shakedown state, although the obtained value of the dissipative energy might be larger.

However, the mechanical background of the applied manipulation is not explained in detail. Furthermore, this proposed problem formulation has the disadvantage of being non-convex, thus the result is dependent on the starting vector. For the calculation, a special quadratic programming algorithm is required that is working without a positive definite Hesse-matrix, or a general nonlinear optimization algorithm needs to be applied. Therefore, an alternative, result compatible, but simpler formulation, based on a Castigliano derivation, is given as well. This alternative, either used to calculate the lower or upper bound of the dissipative energy show better performance and calculation stability.

Alternatively a successive deactivation strategy can be used for assessment of the upper bound of the dissipative energy for a given load pool. The background for the derivation

Table 7-33 Classical optimization problems for determination of the lower bound for dissipation energy

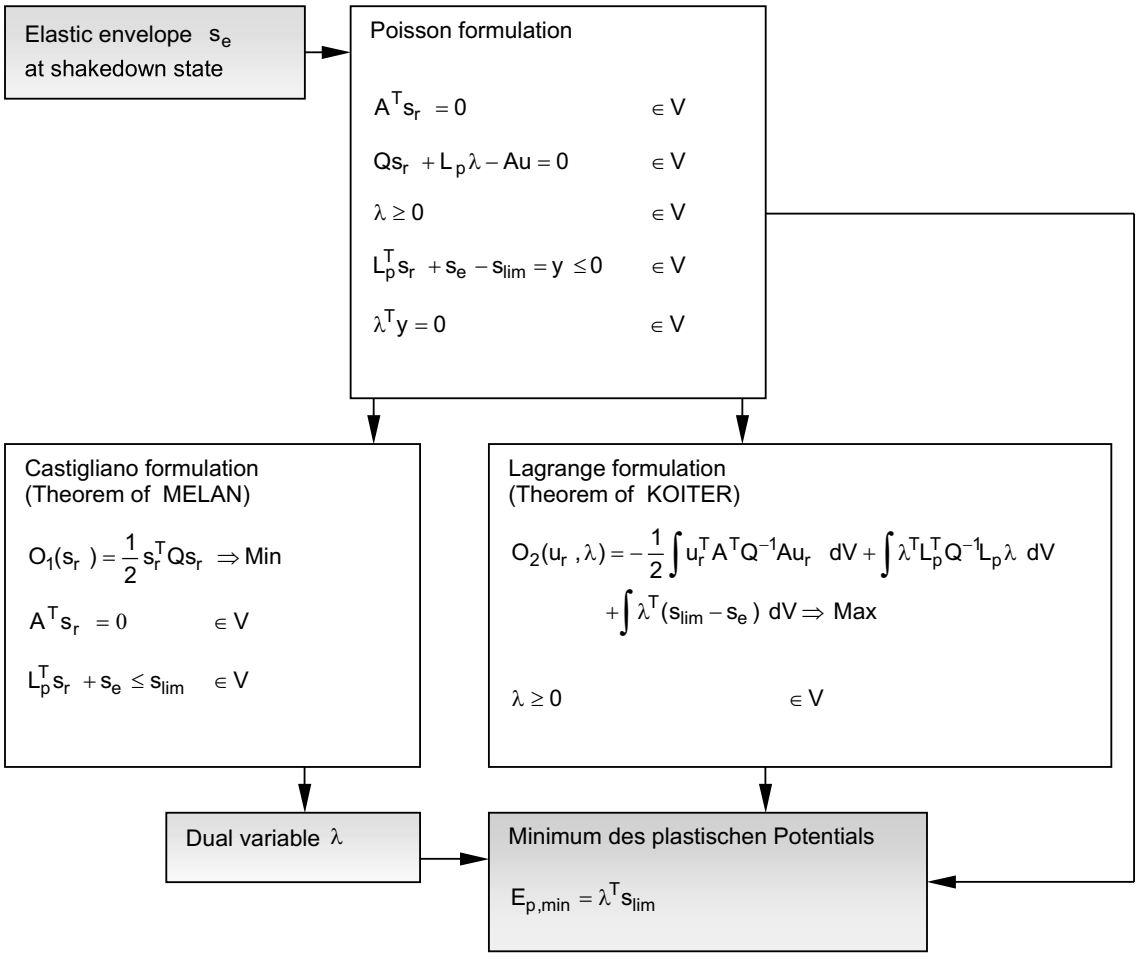

is illustrated in Fig. 7-8. Here the reasons for different plastic states in a structure are explained with help of an example. The elastic envelope can consist of different parts, that are initiated by different load cases. Then the sequence of the load cases can considerable alter the residual state in the structure and therefore the bounds of the dissipative energy.

An alternative strategy therefore proposes a systematic deactivation of plasticity conditions at different locations, in order to favor load case results, that otherwise will be predominated by larger events. In this way the activation of different plasticity conditions may be obtained, other than activated with the calculation in Sec. 7.4.3. Thus a broader distribution of possible plastifications is represented. In additional steps the newly obtained plastic strain states are used as pre-deformation in an classical shakedown analysis. From this, the maximum plastic energy can be assessed. This principle procedure can be altered in general using different and multiple deactivations and plastic strain superpositions combinations. If all possible combinations are analysed, the maximum plastic energy can be obtained.

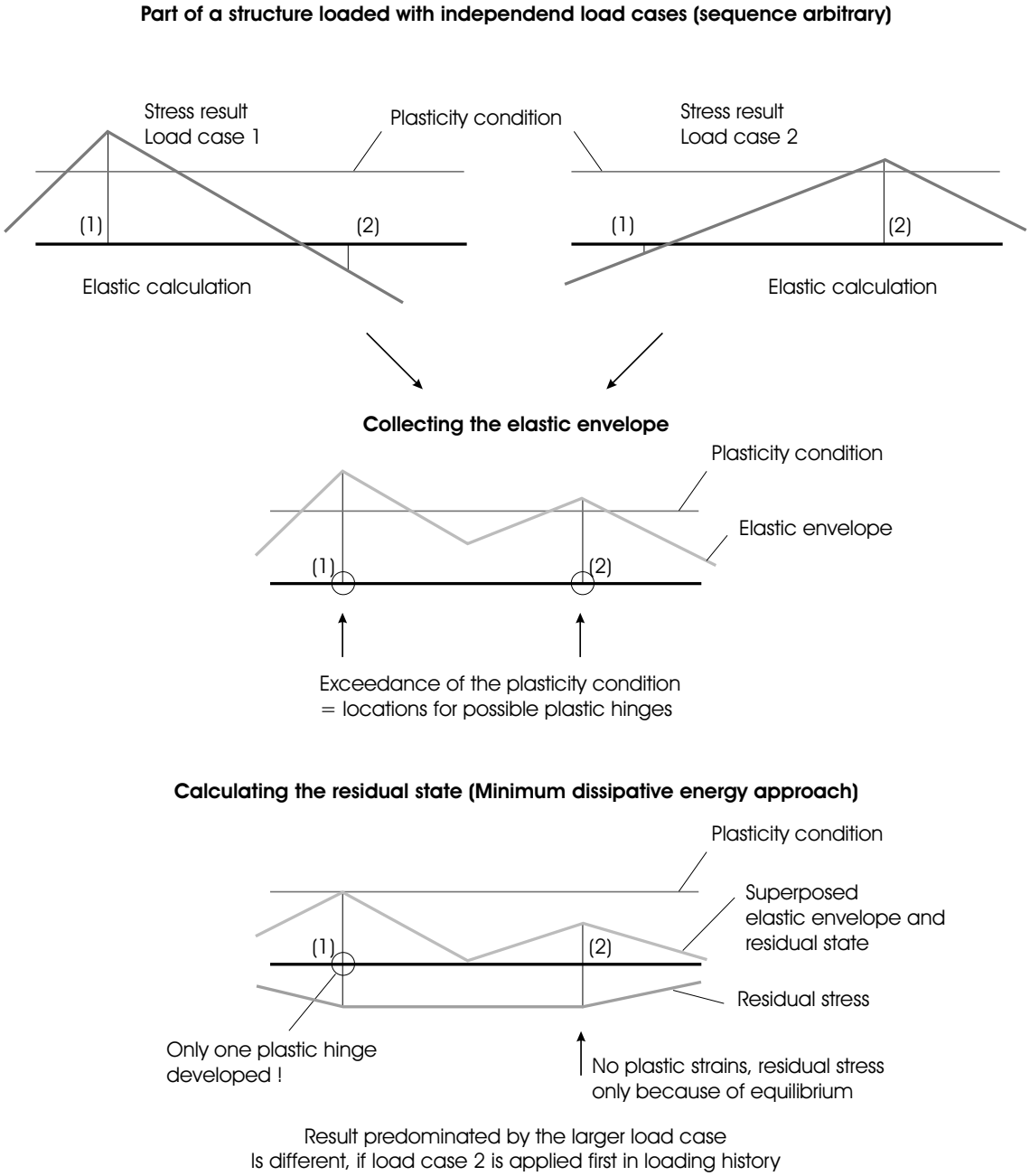

Figure 7-8 Illustration of possible differences in the residual state

For most practical purposes, a two step strategy is sufficient as provided in Tab. 7-34. Here the plasticity conditions are successively deactivated in the order of hinge activation. The plastic strains calculated in this step are applied to the classical shakedown calculation (e.g. Melan′s theorem), but with predeformations triggered in the first step. This procedure simulates the case that the "smaller" load case is acting first, followed again by the "dominating" load case. In that way, other strain distributions are obtained. Then the maximum energy can be calculated. Contrary to expectations, the method is not capable to calculate the residual displacements or residual internal forces bounds. This is because the applied analysis steps are based on a minimum energy approach too.

In comparison to the classical shakedown analysis, this strategy needs several calculations steps. But contrary to load sequence analysis problems, for that the number of possible sequences is dependent on the number of considered load cases or combinations, the number of steps is dependent on the number of locations with possible plastic hinges that are commonly relatively low. Using this strategy can considerably reduce the computational efforts.

7.4.6 Example dissipative energy bounds

Continuing the example of Sec. 7.3.3, the dissipative energy bounds of the system loaded with the possible load sequences A and B are derived. First, a load sequence analysis is performed in order to determine the "real" energy bounds. The progress is given in Tab. 7-35. As well the minimum dissipative energy level is indicated, that can be calculated from classical shakedown analysis, e.g. from Tab. 7-33. It can be seen, that each load sequence exceeds the minimum level.

If the successive deactivation strategy of Tab. 7-34 is applied, the maximum value of $E_p = 7.67kNm$ (calculated previously in the load sequence analysis) is confirmed. Due to the fact that in this example only two plasticity conditions are possible to be activated by the elastic envelope, only two analysis loops have to be performed. This effort is less than necessary for the appropriate load sequence calculations. It becomes even more effective, if the amount of considered load cases is rising.

7.4.7 Displacement bounds on shakedown state of elasto-plastic structures

The formulations used in Sec. 7.4.3 can be applied for the estimation of the residual displacements in the structure that are associated to the minimum of plastic stain energy in a shakedown process. These residual displacements are not uniquely determined, if the loading pool consisting of different load cases is applied to the structure. As the loading sequence can be arbitrary, the resulting residual displacement state u_r, e.g. calculated with Tab. 7-24, can be different for any tested sequence.

Only if all possible sequences are calculated, appropriate values for upper and lower bounds for the residual deformations can be obtained. However, as already mentioned, this is rather theoretical, as a detailed testing is in most cases impossible because of the combinatorical increase of the number of sequences with increasing amount of load ca-

Table 7-34 Two step strategy for estimation of the upper bound of dissipative energy at shakedown state (Successive activation strategy)

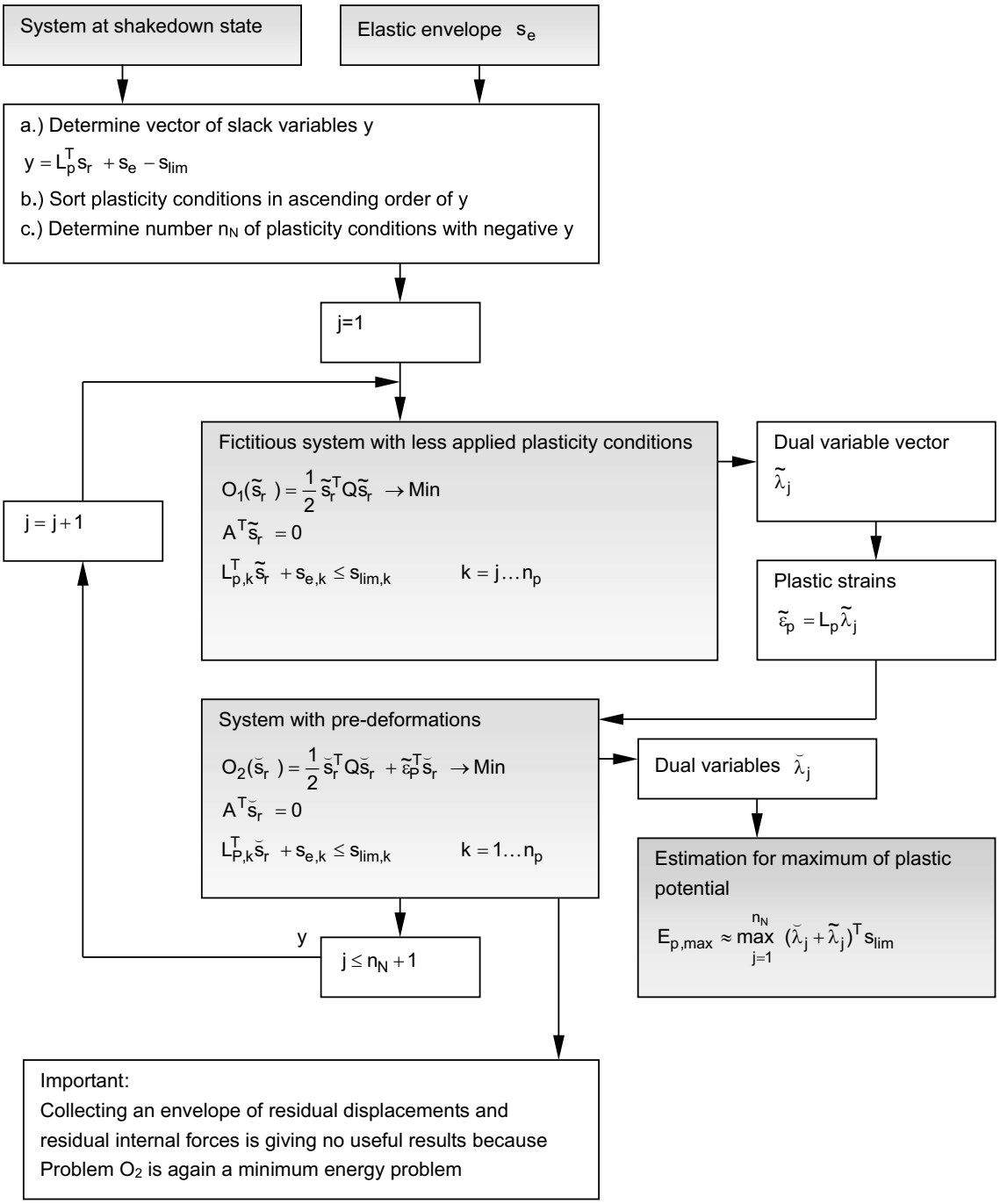

Table 7-35 Example: Load sequence analysis of dissipative energy at shakedown limit

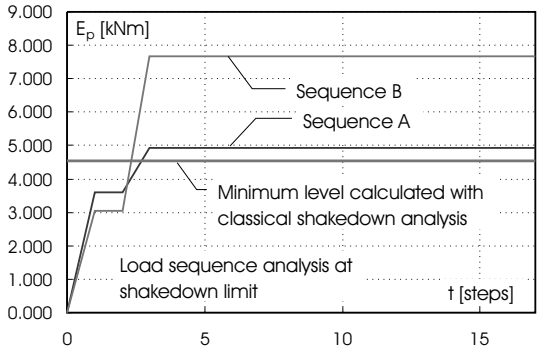

ses in the considered load pool. Following the concept of shakedown analysis, everything should be evaluated with respect solely to the elastic envelope solution.

Specialized bounding principles have been developed by several authors, e.g. [174,178] or [213,137,138,205,44,45,63,70,10,11,12,13]. Generally two major strategies in bound estimation can be distinguished:

1.) Bounds based on principle of virtual energy (e.g. [178,213,205,137,70])

2.) Bounds based on maximum plastic energy estimation (e.g. [10,11,12,13])

The first category mainly bases on the Castigliano (static) formulation of the shakedown problem. The residual state is superposed with a virtual load case, consisting of a single load at the position where the extremum displacement is to be calculated. According to the principle of virtual energy the external energy of the virtual load developed on the residual displacements must be equal to the internal energy of the residual state. Then the extremum displacement can be calculated. This procedure must be repeated for all locations where the extremum residual displacements need to be determined.

In [138] several concepts for upper and lower displacement estimations are compared. According to this, the best results are obtained from the approach of Ponter [178]. The appropriate derivation of the Ponter formulation is given in Appendix Sec. 11.10. The associated optimization problem is nonlinear. Another disadvantage is that the problem often is singular for the shakedown limit state.

Alternatively, the virtual load superposition concept can be divided into several steps. These steps are illustrated in Tab. 7-36. First the lower bound on the resistance needs to be calculated with help of a linear optimization problem (similar to Tab. 7-23). Next the necessary limit load factor for the virtual load is calculated solving another linear optimization problem. In a last step the lower or upper bound on the displacement can be calculated with help of a quadratic optimization problem. This concept has the advantage over the existing displacement bounding methods because it produces limited and improved bounds, even directly at shakedown limit.

Table 7-36 Strategy for estimation of the upper and lower bound of residual displacements at shakedown state using virtual loads

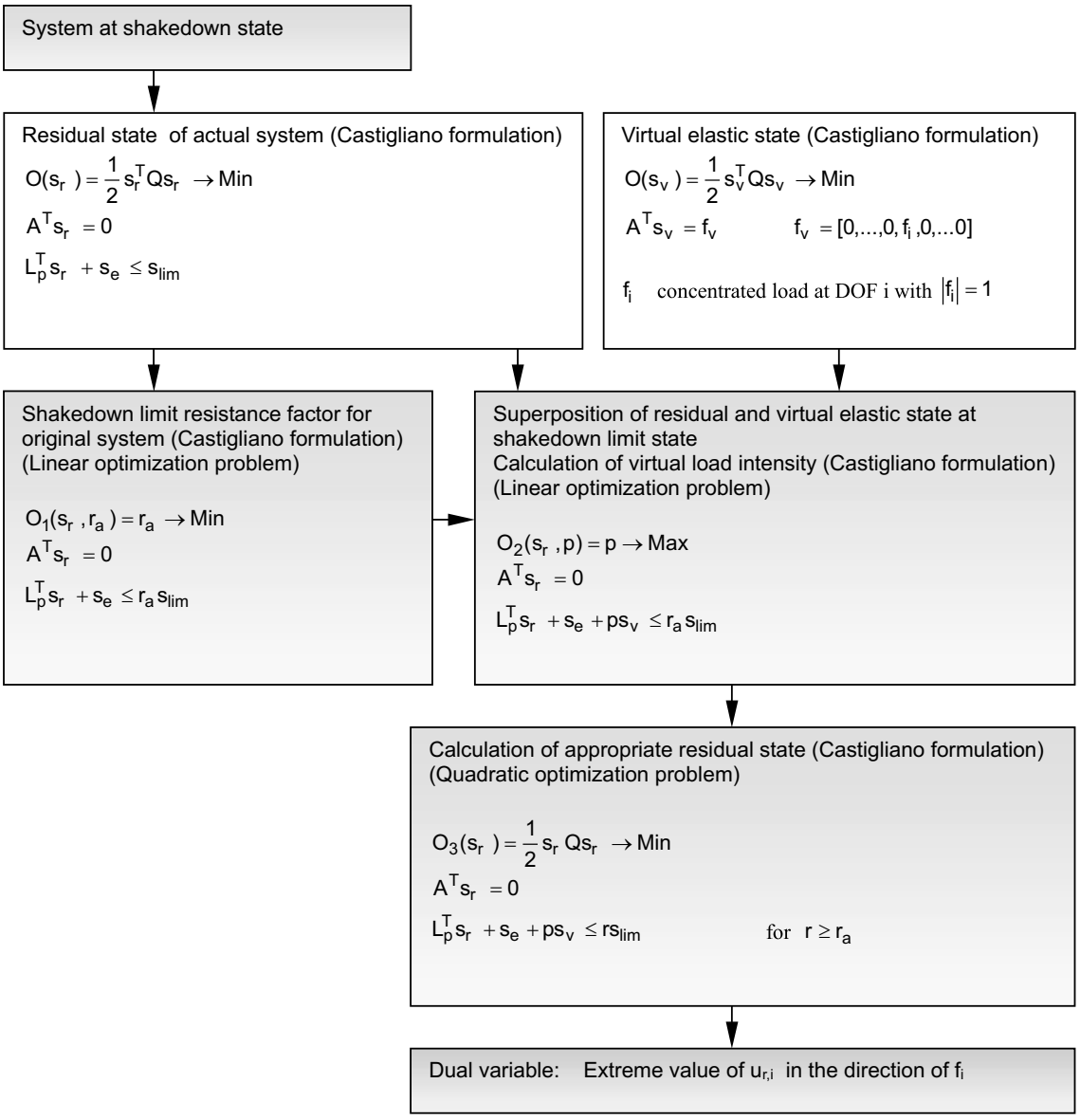

The second category of residual displacements bounding strategies uses estimations for the maximum expectable dissipation energy. The dissipative energy bounds $E_{p,max}$, e.g. obtained from Appendix Sec. 11.9 can be applied. The procedure is described e.g. in [12] and is summarized in Appendix Sec. 11.11. Two different strategies of implementation are discussed. The first version replaces the plasticity condition in the Poisson formulation with the energy condition

$$\lambda^T s_{lim} \leq E_{P,max} \tag{7-88}$$

Table 7-37 Strategy for estimation of the upper and lower bounds of residual displacements and stresses at shakedown state using dissipative energy bounds

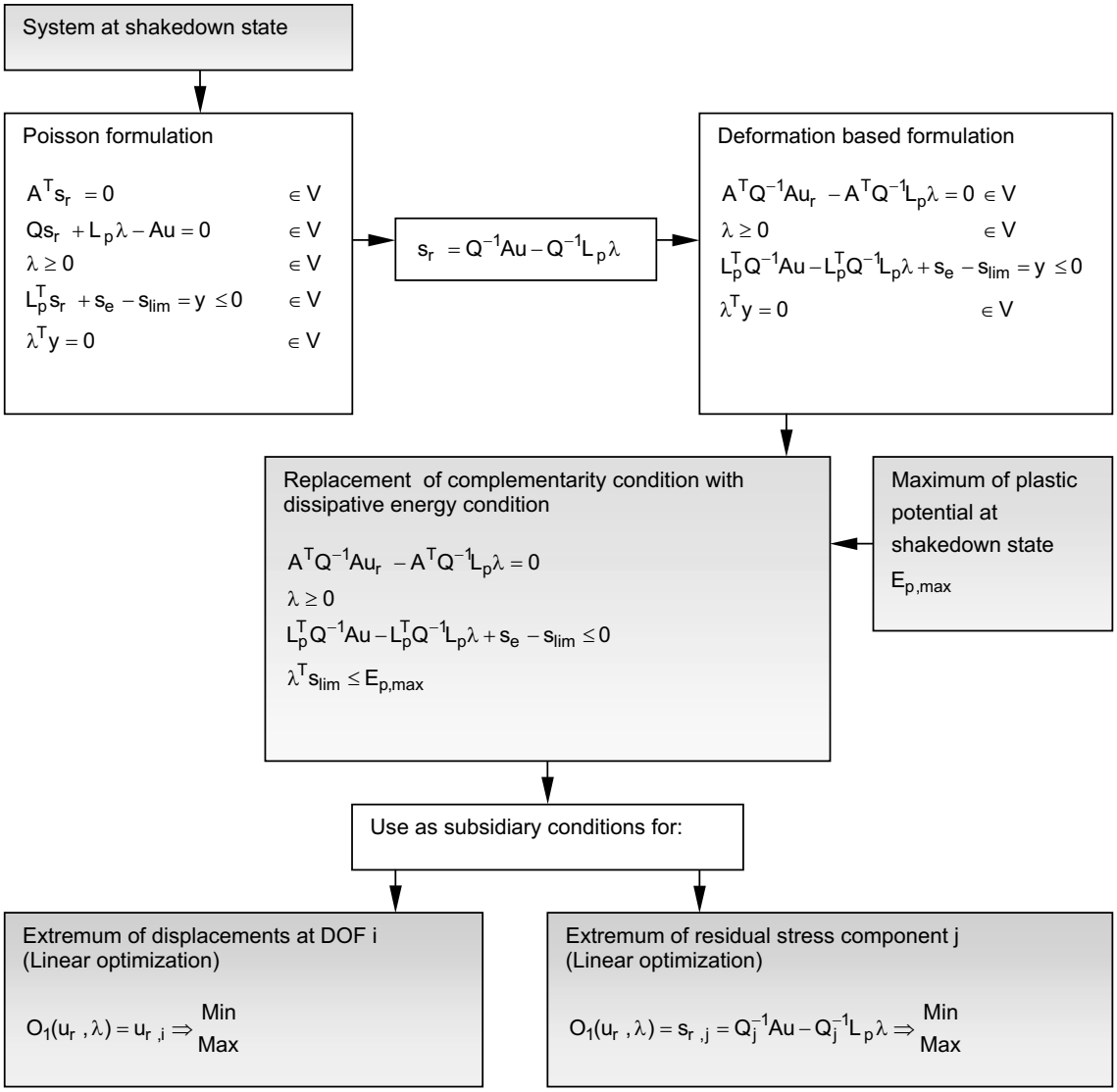

while searching for the extremum of the displacements. On the other hand, the second version favors a replacement of the extended kinematic condition with the energy condition (7-88). Several modifications of the governing equations have been introduced for either version in order to reduce the number of unknowns.

Alternatively the bounds can be explored with releasing the complementarity in the original Poisson principle. Thus also at different positions plasticity conditions can be activated. The appropriate concept is summarize in Tab. 7-37.

Table 7-38 Example: Load sequence analysis of residual horizontal displacement (shakedown limit state)

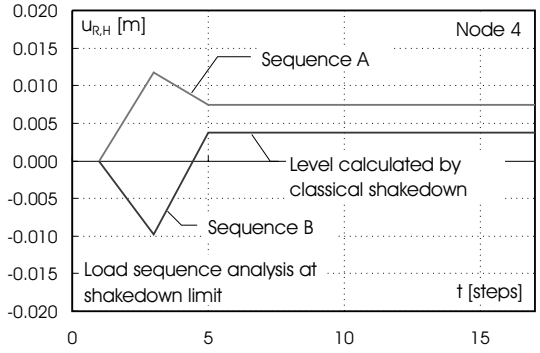

7.4.8 Example displacement bounds

Continuing the example of Sec. 7.3.3, the upper and lower bounds for the residual displacements are calculated. For verification reasons, the appropriate load sequence analysis result is calculated firstly. The result for the horizontal displacement at node 4 is illustrated in Tab. 7-38 for either load sequence A and B. It can be seen that the load sequences produce different residual displacements. The classical shakedown analysis is calculating just the lower value.

The application of the virtual loads strategy of [178] gives a minimum value of $u_{r,min} = -0.0198288m$ (positive direction is indicated by the vector from node 1 to 5). However, only an infinite value for the upper displacement bound can be calculated directly at shakedown limit. For meaningful application, the resistance factor must be increased.

By application of the method in Tab. 7-36 the extremum horizontal displacements at node 4 are determined to $-0.11m \leq u_r \leq 0.18m$. Secondly the dissipative energy base method of Tab. 7-37 is applied using the previously determined maximum plastic energy from Sec. 7.4.6. The determined bounds are $-0.0179347m \leq u_r = \leq 0.0245203m$. Both methods have shown that they are capable of estimating safe upper and lower bounds for the problem. While evaluating the results it should be mentioned, that the deviations from the sequence calculations are acceptable, because the method is not referring to the original load sequences, but only to the envelope response, that theoretically can contain an infinite number of different load cases. Commonly, as can be seen also in this example, the dissipative energy method has advantages, because the value of the maximum plastic energy is calculated with "pseudo sequences" if the successive deactivation strategy of Sec. 7.4.5 is applied.

7.4.9 Residual stress bounds on shakedown state of elasto-plastic structures

As well as the dissipative energy and the residual displacements, the residual stresses are not necessarily unique for a given pool of loads, applied in arbitrary load sequences. According to [12], the residual stresses are only unique if the maximum and minimum dissipative energies of a systems are equal

$$E_{p,min} = E_{p,max} \tag{7-89}$$

In all other cases, the residual stresses e.g. obtained with an optimization problem in Tab. 7-24 are only approximations. The real bounds can be estimated using bounding techniques. Most of the previously discussed bounding principles can be used for combined calculations of the appropriate residual stress state as well. In Tab. 7-37 one concept is indicated, on the basis of the maximum plastic energy estimation. It is mostly identical with the displacement bound principle introduced in Sec. 7.4.7, so that upper bounds for displacements and internal forces can be calculated on the same basis.

7.4.10 Example residual stress bounds

Again, the example of Sec. 7.3.3 is continued. The lower and upper bounds for the residual moment calculated with Tab. 7-37 are determined. At node 4 the bounds are $-128.88 \leq M_r \leq 60.59$ and at node 5 it is $-58.82 \leq M_r \leq 58.82$. In comparison with the load sequence results previously presented in Tab. 7-29, the calculated bounds are practically useful.

7.4.11 Hardening materials and geometric nonlinear problems

The previously described concepts rely on materials with perfectly plastic branches in the stress-strain relationship. The presence of hardening may significantly affect the shakedown limit state. Kinematic hardening (see Sec. 4.8.2) can lead to alternating plasticity (plastic shakedown). On the other hand, the structure will shake down under any load intensity if the hardening matrix A_h (see Eq. (4-76) is positive semi-definite (as for Koiter′s hardening concept) [133].

Specialized theorems regarding geometric nonlinear problems have been studied e.g. in [66,62]. Ignoring the influence of plasticity on the geometric nonlinear effects, both problems of elastic envelope calculation and shakedown state calculation can be adapted separately with terms for geometric nonlinear effects (see Sec. 4). If the effects are not negligible, an iterative strategy can be applied according to [197]. This feedback strategy is illustrated in Tab. 7-39 for a shakedown limit load calculation and in Tab. 7-40 for the appropriate shakedown limit resistance calculation. The limit load analysis requires additional modifications for the load intensity in the elastic envelope calculation. From these illustrations it is obvious, that the appropriate calculations can be costly. A general alternative to this procedure is discussed in Sec. 7.6.

Table 7-39 Iterative calculation for geometrical nonlinear shakedown analysis (Limit load analysis)

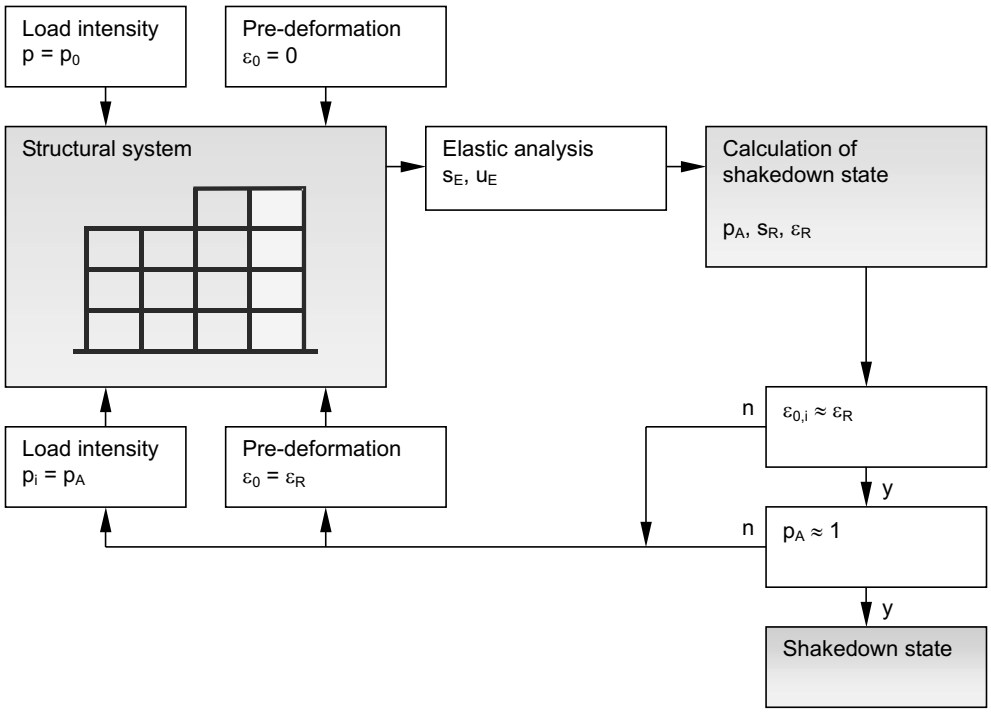

7.4.12 Stress and deformation-based conservative limit states

As described in Sec. 7.4.7 and 7.4.9 the residual displacements and stresses are stable but not necessarily unique for arbitrary load sequences from a fixes load pool, if the load intensity is below the shakedown limit. In practical cases, the exact knowledge of the response might be of interest and an undetermined stress or deformation state is inadmissible. The load sequence independence can be reached by further limitation of the load intensity to the level of the conservative limit load. The basis of all calculations is again an elastic envelope response derived from load case calculations. As an extension to the definitions in [218], two types of conservative limit states can be distinguished. First, the stress-based conservative limit load is defined as follows

> **Theorem 7**: *If for any possible load sequence, consisting of all possible load cases, the resulting residual stress state is unique, the loading intensity is below the stress-based conservative limit load.*

Energetic conditions can be utilized for numeric calculation of this limit state. The strategy can be deducted from Sec. 7.4.9. If the residual stress state is unique, the minimum and maximum plastic energy bounds are identical (see Eq. (7-89)). This condition, in conjunction with the method in Tabs. 7-33 and 7-34 can be applied within optimization procedures in order to calculate the stress-based conservative limit state.

Table 7-40 Iterative calculation for geometrical nonlinear shakedown analysis (Limit resistance analysis)

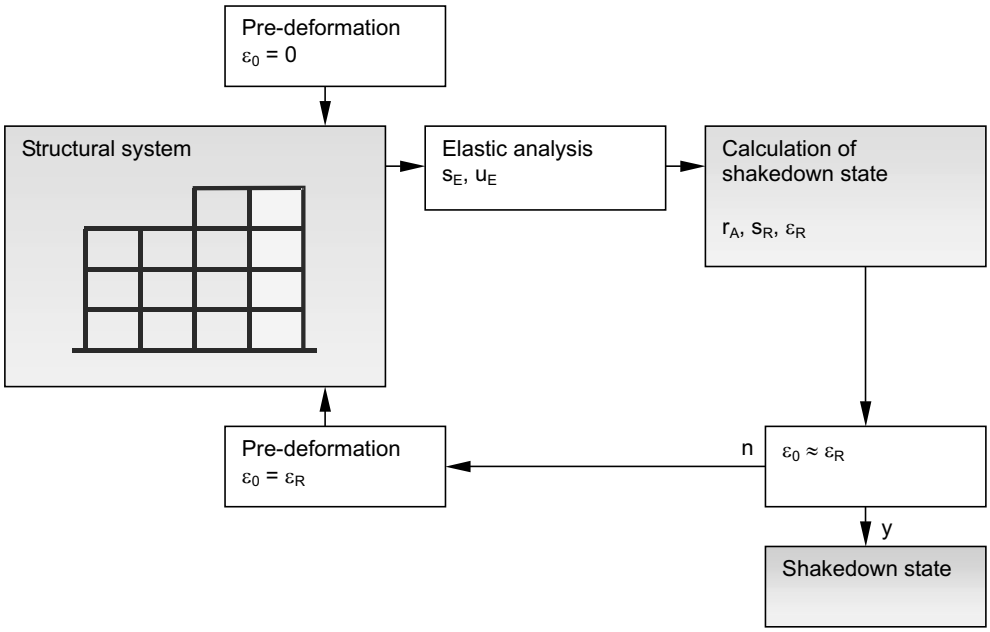

Accordingly, a deformation-based variant can be stated

> **Theorem 8**: *If for any possible load sequence, consisting of all possible load cases, the resulting residual deformation state is unique, the loading intensity is below the deformation-based conservative limit load.*

This condition is always fulfilled if only one load case or impulse can trigger plastic deformations in the structure. Regarding the classical limit state definitions the following relation can be stated for the resistance factors r and limit load factors p

$$r_e \geq r_{cd} \geq r_{cs} \geq r_a \geq r_p \qquad p_e \leq pcd \leq p_{cs} \leq p_a \leq p_p \tag{7-90}$$

relating the elastic (e), deformation-based conservative (cd), stress-based conservative (cs), shakedown (a) and plastic (p) limit states.

7.4.13 Example conservative limit resistance

The conservative limit states for the example of Sec. 7.3.3 are calculated. The appropriate stress-based resistance factor is $r_{cs} = 1.5289$. The appropriate residual moment distribution as well as the development in Node 4 is described in Tab. 7-41. Contrary to the shakedown limit load results from Sec. 7.4.4, the residual stress level is unique for either load sequence (Tab. 7-41).

Table 7-41 Example: Residual moment distribution after load sequence application (Stress-based conservative limit resistance)

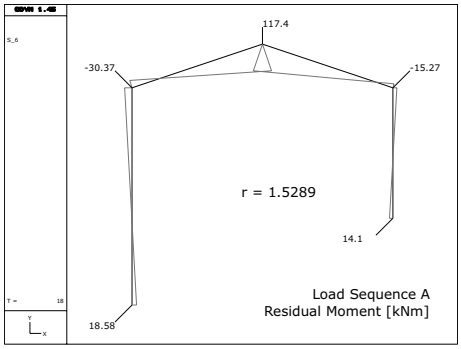

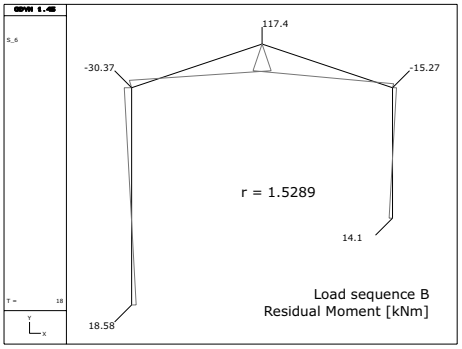

Table 7-42 Example: Residual plastic strain distribution after load sequence application (Deformation-based conservative limit resistance)

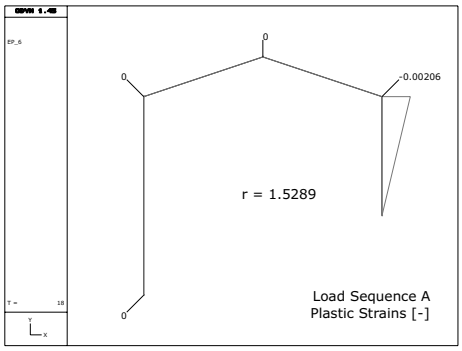

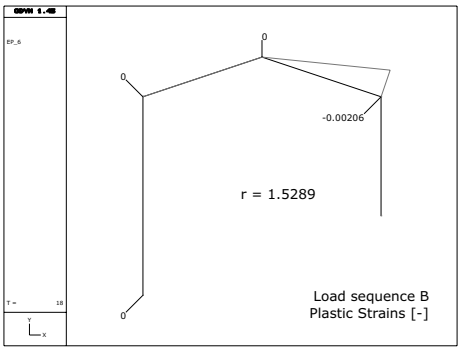

For this example the deformation-based and stress-based conservative resistance factors are identical $r_{cd} = r_{cs}$, thus the plastic deformation state is stable and unique as illustrated in Tab. 7-42.

7.5 Cycle-based limit state analysis

7.5.1 Introduction

For structures facing cyclic excitation, e.g. in seismic regions, the demand for non-degrading or limited-degrading structures with ductile behavior is rising. Samples are buildings of lifeline and high technology industries that have to maintain their operability during and after the event. Furthermore, it is required to restrict the amount of accepted damage to limit repair efforts. These requirements define a minimum performance or capacity level that have to be maintained after excitation. In these cases the application of isolation technologies is not always appropriate and necessary. Structural dissipating strategies can be applied as well, if a performance level can be adjusted that utilizes plastic reserves for energy dissipation, while assuring a predefined damage limit [9,3,52].

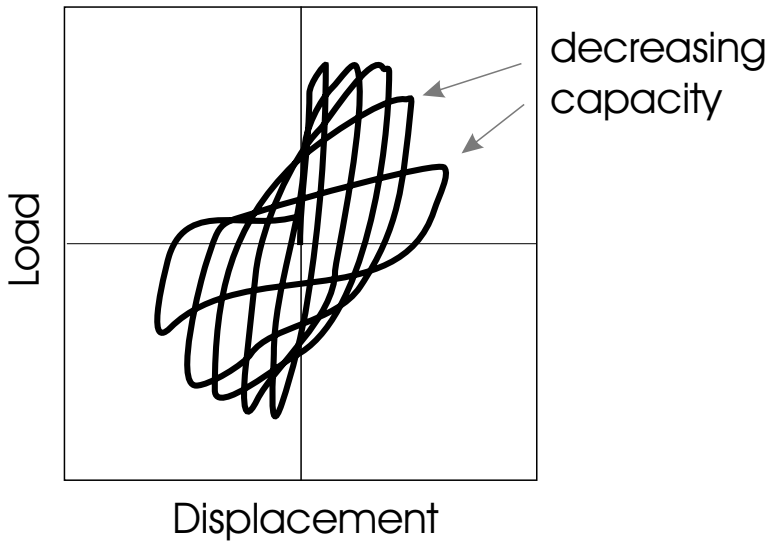

Figure 7-9 Decreasing capacity due to cyclic action

Problems arise if the capacity of the members decreases rapidly after some cycles with damaging (plastic) potential, as illustrated in Fig 7-9. Hereby, substantial damage is caused from several re-plastifications. This can be critical for cross-sections with limited ductility, such as in reinforced concrete members. Besides failure prevention, high degrading levels are often not acceptable, e.g. for life-line structures. They demand for limited damage extends, in order to ensure operability and quick repair. Requirements can reach from a purely elastic behavior to higher but limited damage levels that can be characterized by maximum plastic excitations and the number of plastic cycles or re-plastifications.

In the following sections, a simplified performance-based design procedure is described that considers the following circumstances and objectives:

- Planned application for performance levels operability and immediate occupancy
- Application for structures with elasto-plastic cross sectional behavior (at plastic hinges) like r/c-, src-, steel- or mixed type structures
- Avoidance of equivalent replacement systems, use of all kind FE structural models, especially of models proposed by codes
- No a-priori necessity for regular systems
- No modification of loads by global reduction factors
- Including a response abstracting step (relying on the statistical character of earthquake excitations, no direct dependency to a specific time history like in nonlinear dynamic analysis)
- Reduction of responses considering acceptable deformations and numbers of replastifications

- Individual scalability for each point of the structure
- Capacity validation and design at local points, including estimation of global behavior
- Reflection of cross sectional behavior including force interactions
- Direct verification of performance, direct feedback of design decisions to the structural behavior
- Direct support and application of capacity design principles
- Use of simple and fast calculation algorithms (mainly on a linear basis even if the analysis is nonlinear itself, manual approaches should be considered for simple structures)
- Evaluation of effects caused by damping or isolation devices
- Optionally: direct design improvement by application of optimization technologies

7.5.2 General design approach

The design method is derived from signal evaluation methods that consider amounts of re-plastifications caused by a sequence of plastic cycles. They are used to reduce the elastic response of the structure for the design, due to the utilization of plastic dissipation.

The enhancement in the approach is the implementation of signal reduction procedures considering the number of re-plastifications. The principle is almost similar to approaches that reduce spectra data on a cycle basis. These approaches were originally specified to support the application of linear response spectrum methods for nonlinear structures [121,91]. The idea is to reduce the resistance of the structure to a certain level, from that only a predefined amount of load peaks effect hysteretic behavior. With the choice of the parameter n as "number of re-plastifications" a simple method to scale and influence the perspective damage can be established.

However, the application within this study provides a main difference. Contrary to the mentioned methods, the reduction procedure refers not to the loads but to the linear structural response in the member cross-sections. Thus a linear time history analysis or response spectrum analysis has to be performed. Commonly this is not a problem because physically linear analysis is well established, and theoretically clear.

It is the convention herein, to refer not on complete cycles (complete hysteresis) but on the number of re-plastifications n, as the number of altering inelastic deformations. The purely elastic case will be referred as a special case with $n = 0$. Starting with $n = 1$, the cross-section performs plastic deformations, but only one-directional. The first cycle of inelastic deformation is characterized by $n = 2$ and so forth.

The reduced response can be used within two concepts of limit state analysis:

- Elastic limit state analysis (Elastic basis)
- Adaptive limit state analysis (Adaptive basis)

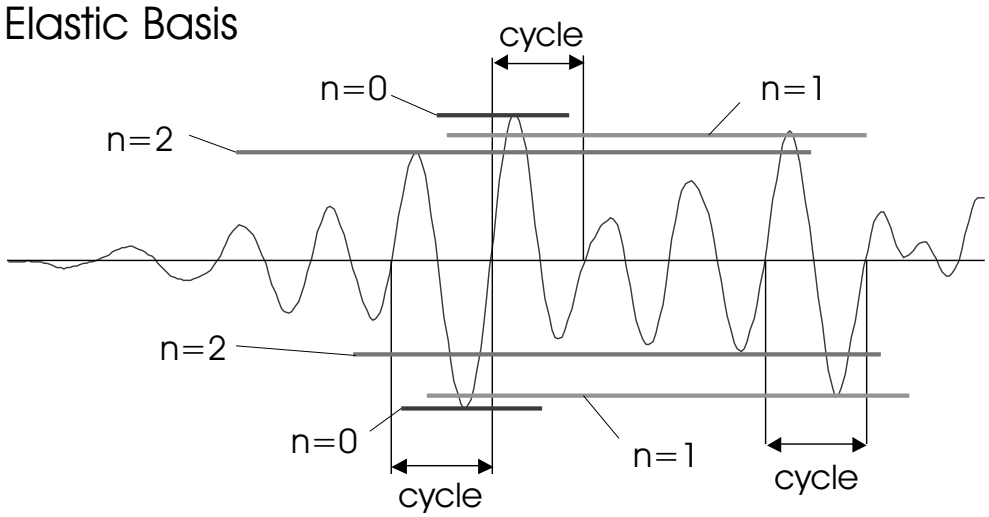

Figure 7-10 Principle of signal reduction corresponding to the number of re-plastifications n

The two concepts are discussed in the following sections.

7.5.3 Design based on the elastic limit state

The simplest concept is to assume, that if the elastic limit is exceeded, cyclic behavior can be obtained. The elastic limit (or reduction of the elastic response) is defined, according to the pre-defined number of re-plastifications. The main principle of reducing the maximum amplitude of internal forces by cycle approaches is illustrated in Fig. 7-10. All peaks that exceed the elastic limit are potential candidates to trigger plastic deformations. If the reduction is done for the positive and negative values respectively, a cyclic behavior can be expected. The disregard of the dissipation effects of the plastic hinging is responsible, that this approach is conservative. This means that the relation between the "really observed" number n_{cal} and the previously intended number of re-plastification n_{design} of the design is

$$\frac{n_{cal}}{n_{design}} <= 1 \tag{7-91}$$

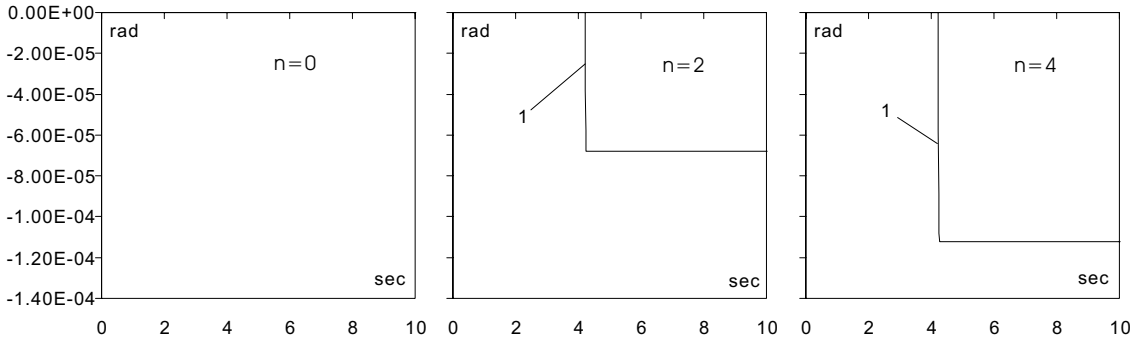

Figure 7-11 Example: Plastic rotations development for the design procedure based on the elastic limit load for $n = 0, 2, 4$

7.5.4 Example: Design based on the elastic limit state

This assumption is proofed with help of the example of Fig. 7-14. The structure is again designed for plastic hinging at the ends of the horizontal beams only. The initial distribution of the limit moments in all hinges is $-50kN <= M <= 50kN$. At the beginning of the considered beam (Point 3), the elastic moment according to Fig. 7-12 is obtained. In this figure, the reductions of the response for three numbers of re-plastifications $n = 0, 2, 4$ are marked. If these reductions are used to perform the design of the structure, the plastic deformations ε_p at beam 5 will develop according Fig. 7-11. They are calculated with nonlinear time history analysis. This step is not part of the procedure but to test the effects caused by this approach. Additionally, the reduction factors r, as the multiplier of the plastic limit distribution, are given in Tab. 7-43, as well as the comparison of the previously intended number of re-plastification n_{design} and the observed number n_{cal}.

From these results, it will be obvious, that the approach is able to activate plastic reserves in the structure, if $n >= 1$. However, the post-elastic behavior complies not to the intended cyclic behavior if the number is $n >= 2$. In this example, even a value of $n_design = 4$ is only resulting in $n_cal = 1$. This behavior is conservative, but to a relatively large extend. The reason is the initial shakedown of the structure in the first plastic cycles. Taking this effect into account, an improved concept can be derived, that is presented in the following section.

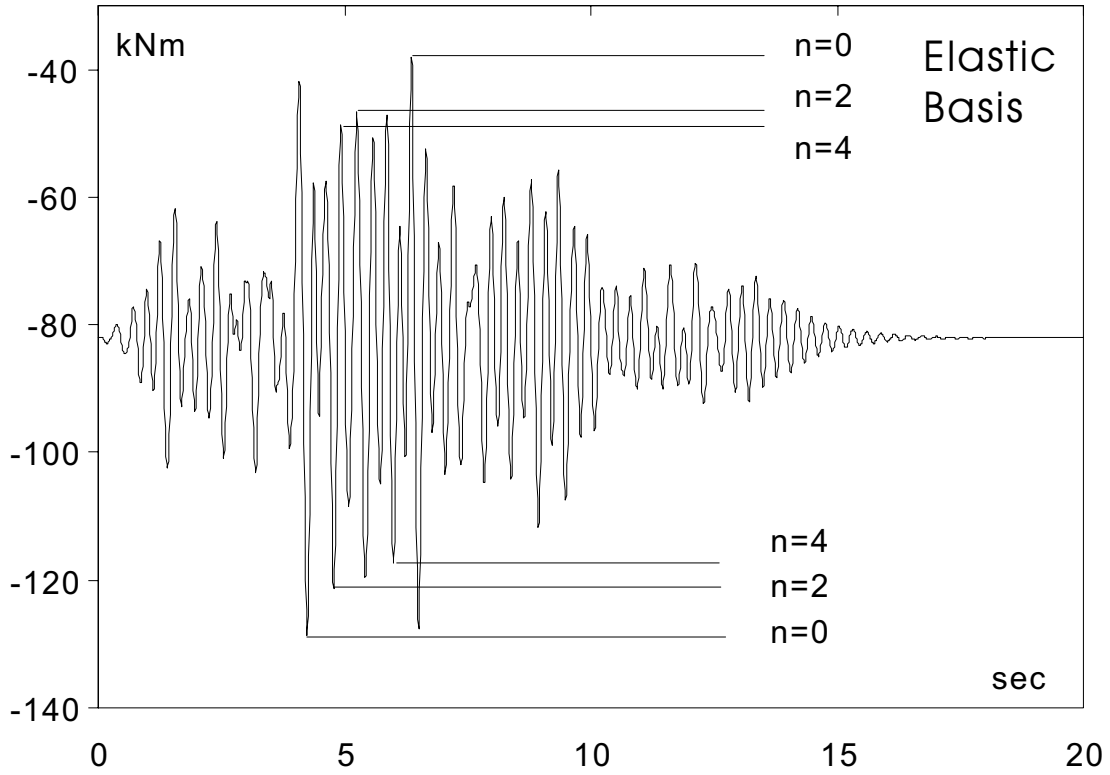

Figure 7-12 Example: Elastic moments at beam 5 and levels of reduction according to $n = 0, 2, 4$ for an elastic basis

Table 7-43 Example: Resistance factors r for intended numbers of re-plastifications n_{design} and the obtained numbers n_{cal} (on basis of elastic limit state)

n_{design}	n_{cal}	r	% of elastic limit
0	0	2.57	100.0
2	1	2.42	94.2
4	1	2.34	91.0

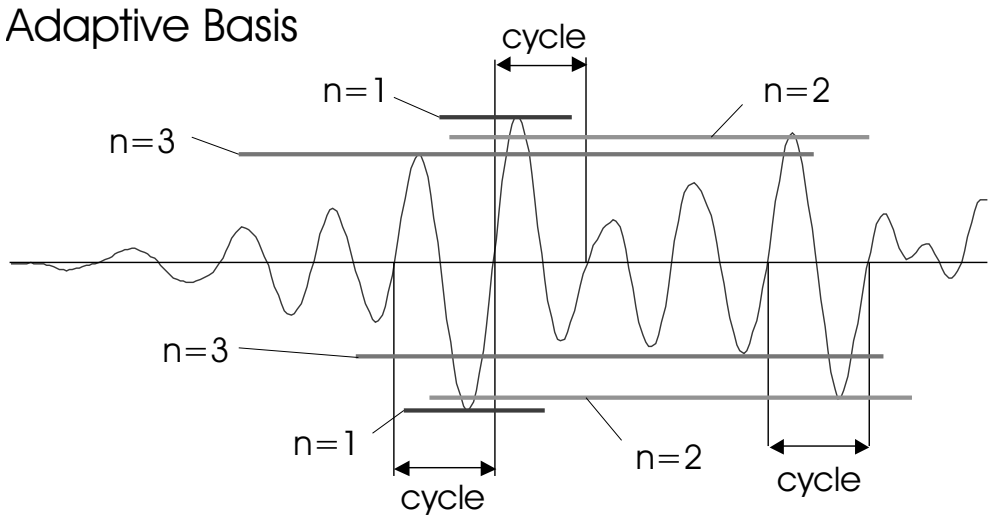

Figure 7-13 Principle of signal reduction corresponding to the number of re-plastifications n

7.5.5 Design based on the adaptive limit state

This concept was already introduced for the design of seismic excited structures in Sec. 7.4. The application of shakedown theory leads to conservative solutions compared with other design strategies, that accept plastic hysteretic behavior. It determines the limit from where altering or unlimited progressive plasticity have to be expected. Starting from this limit, load impacts beyond the shakedown limit level can result in inelastic hysteretic behavior combined with re-plastification cycles in plastic hinges. Because of this, the adaptive limit state is therefore a better basis to derive a cycle based design procedure than the elastic basis.

Maintaining the original definition, the number of re-plastifications $n = 0$ is indicating the pure elastic behavior. The pure shakedown state is indicated by $n = 1$. A complete cycle of inelastic deformation is characterized by $n = 2$ and so forth. This differs slightly from the definition with elastic basis. Having an adaptive basis, the maximum peak already is associated to $n = 1$. The principle to derive the reduction levels on an adaptive basis is illustrated in Fig. 7-13.

7.5.6 Design procedures

Both concepts, the elastic and adaptive basis, can be used within a common design procedure. Short chart descriptions can be found in Tab. 7-44 and 7-45. The first strategy (designated as strategy V) is conceived regarding structural verification. The mechanical system, the loads and masses are determined traditionally. According to this, the complete detailing has to be provided. Important is the determination of regions for potential plastification, according to Capacity Design rules. Out of this, the resistance (supply) of the structure can be calculated. After calculating the elastic response (either with time history or simplified analysis), the derived envelope will be reduced due to the targeted number of re-plastifications. In a limit state analysis, the resistance factor r and the residual state are derived. The factor scales linearly the resistance parameters of a pre-defined cross-sectional resistance distribution, e.g. for reinforced concrete structures, this can be interpreted as changing the reinforcement. The resulting behavior has to be evaluated with respect to the plastic hinge distribution and loading. For structural safety, the resistance factor r must be greater than 1.0.

The second strategy follows a design and dimensioning objective (noted as strategy D). The core sequences are almost similar to procedure V. However, the advantage is the shorter pre-design, that requires only an assessment of the structural stiffness distribution. The calculation of the elastic envelope is according to procedure V. This is the basis to determine an appropriate kinematic mechanism, by placing limit conditions to the potential hinge regions. After this, the appropriate resistance factor is calculated, with the elastic limit state analysis according to Sec. 7.2 or with the adaptive limit analysis (Sec. 7.4). The appropriate residual states are fictitious, and represent the behavior for the reduced excitation for $n > 1$. On an elastic basis the residual states are always zero, independent from n. The superposition of the residual results and the elastic envelope can be used as design relevant internal forces. The hinge distribution has to be evaluated and the detailing can take place. In a last step, the previously made stiffness assumptions should be compared with the design. The calculation should be repeated in an iterative process in case of great differences as indicated in Tab. 1 and 2.

In Tabs. 7-46 and 7-47 two options for the derivation of the elastic envelope solution in the design procedures are presented in more detail. The derivation of the elastic envelope is illustrated in Tab. 7-46 for the strategy that utilizes linear time history responses. For respectation of the statistical distribution of the response parameters, sets of time history data should be evaluated. For any of this the elastic responses are calculated for the structure. In the traditional procedure, the maximum and minimum response peaks are determined at each point of the structure (Strategy I). In an advanced procedure (Strategy II), the response can be selected at the plastic hinge regions with respect to the number of re-plastifications n. For all other points, that are supposed to remain elastic during the excitation, the envelope calculation can omitted or the envelope is simply determined for $n = 1$. Consequently, a reduced envelope response is derived. The calculation has to be

Table 7-44 Design procedure "Verification"

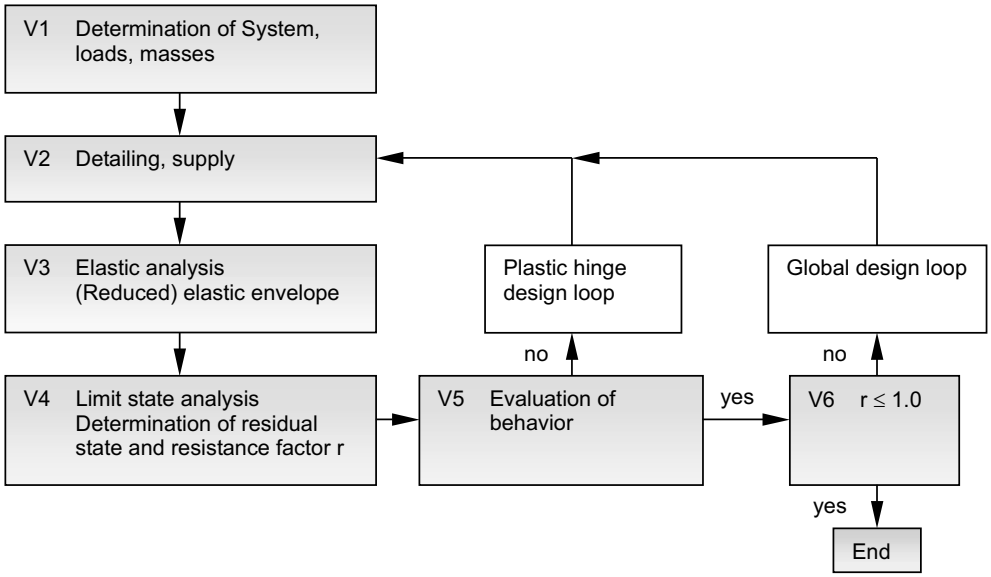

repeated for all selected sets of time history loads. Then the elastic envelope consists of extreme results for all time history sets.

In Tab. 7-47 a method is sketched for utilizing cycle based response spectra data for calculating the elastic envelope. The calculation of the spectral values must be altered, so that the extreme responses are selected with respect to the cycles in the linear response. This step mainly corresponds to the time history evaluation method given in Tab. 7-46, but for SDOF systems only. If the procedure is repeated for different structural periods in the SDOF, the corresponding response values are collected to form a reduced spectrum. This spectrum is the basis to calculate the elastic response of the entire structure to the selected excitation, to calculate the envelope solution. Also in this procedure, several sets of excitations can be beneficially included.

In Tab. 7-48 the sequence of calculating the limit state and the appropriate residual state is presented. The shown approach bases on optimization technologies. The procedure consists of two separate steps. First, the calculation of the adaptive resistance factor r, that scales the resistance parameters in the cross sections. This value is used to scale the resistance (here indicated exemplarily as the constant part of the plasticity conditions s_{lim}). Secondly, the appropriate residual stress distribution can be calculated with help of a quadratic optimization approach. This calculation can be done with the reduced elastic envelope $s_{e,n}$ that gives an approximate average plastic performance overview. Using the non-reduced envelope $s_{e,1}$ (for $n = 1$) instead is adequate to indicate the extreme results for the plastic deformations. The use of the residual state information within the design procedures V and D are sketched shortly within Tab. 7-48.

Table 7-45 Design procedure "Dimensioning"

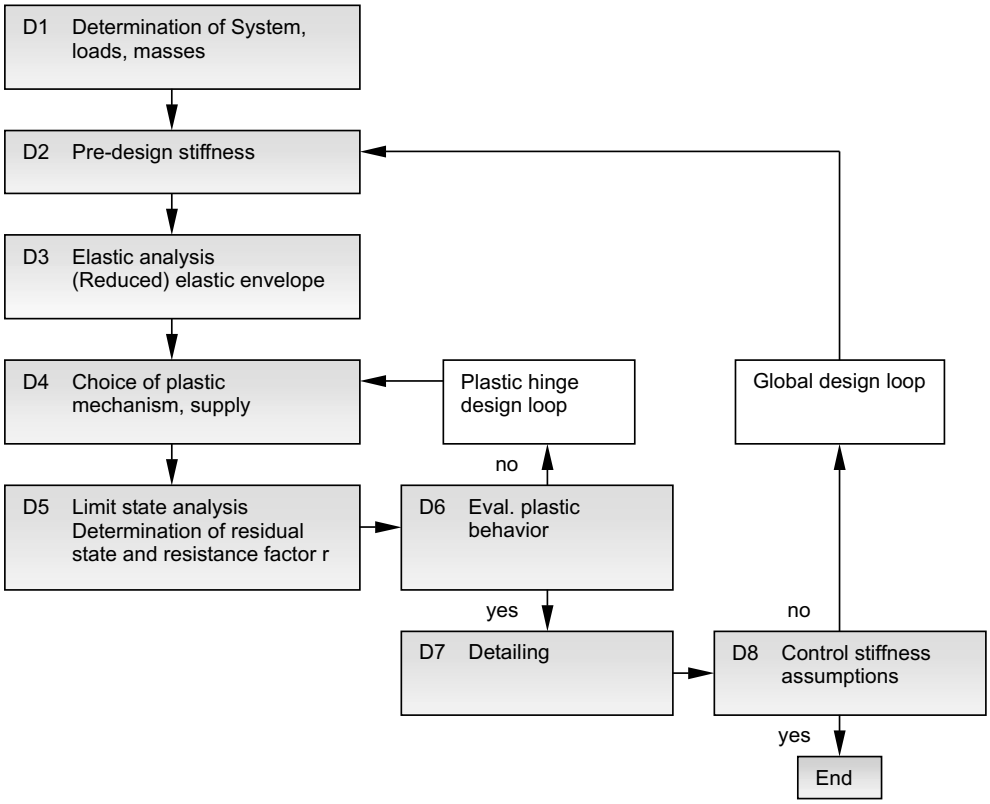

The results obtained by this procedures are conservative. That means, that the indicated number of re-plastifications is an upper bound that will never be exceeded. The real responses due to single dynamic events can be smaller than calculated within this procedure. This is due to simplification that are made to neglect time effects and therefore to reduce the response to their envelope values. The effects can be caused by plastic dissipation that takes place prior to the actually considered extreme events in the time history. Such plastic dissipation reduces the amplitudes of the subsequent response peaks, so that the caused plastic deformations can be smaller than those calculated with the elastic envelope simplification. However, the maximum expectable plastic deformations can be assessed conveniently.

For extension of the given procedure further approaches can consider a probabilistic treatment for reducing the elastic envelope.

7.5.7 Example Design based on the adaptive limit state

A simple beam-column structure is given in Fig. 7-14, excited by an artificial ground acceleration. For simplicity the usually recommended load case studies are not performed, thus excitations only from one time history and only from one direction are considered.

Table 7-46 Elastic analysis and derivation of the reduced envelope for strategy based on time history analysis

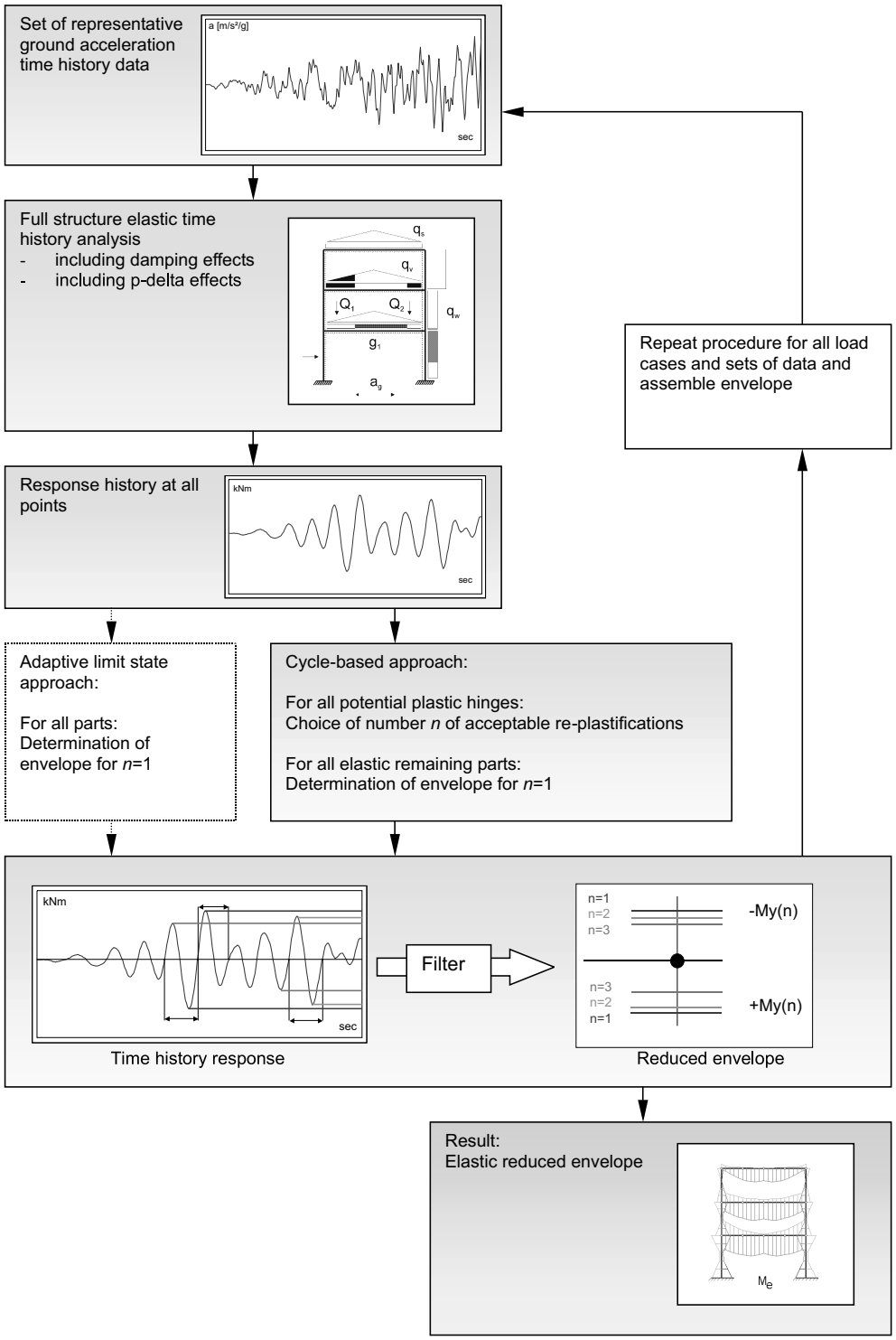

Table 7-47 Elastic analysis and derivation of the reduced envelope for strategy based on response spectrum analysis

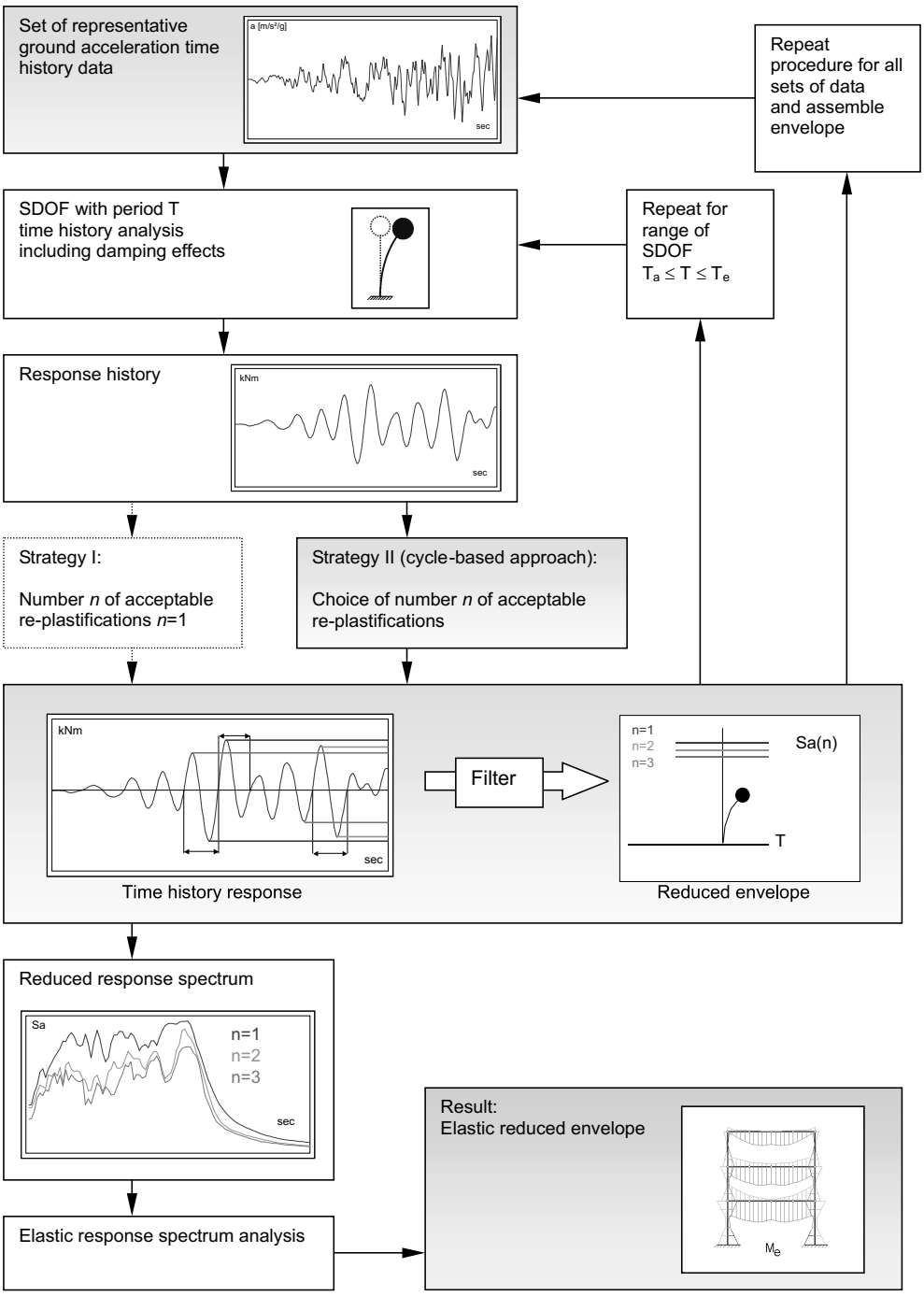

Table 7-48 Limit state analysis

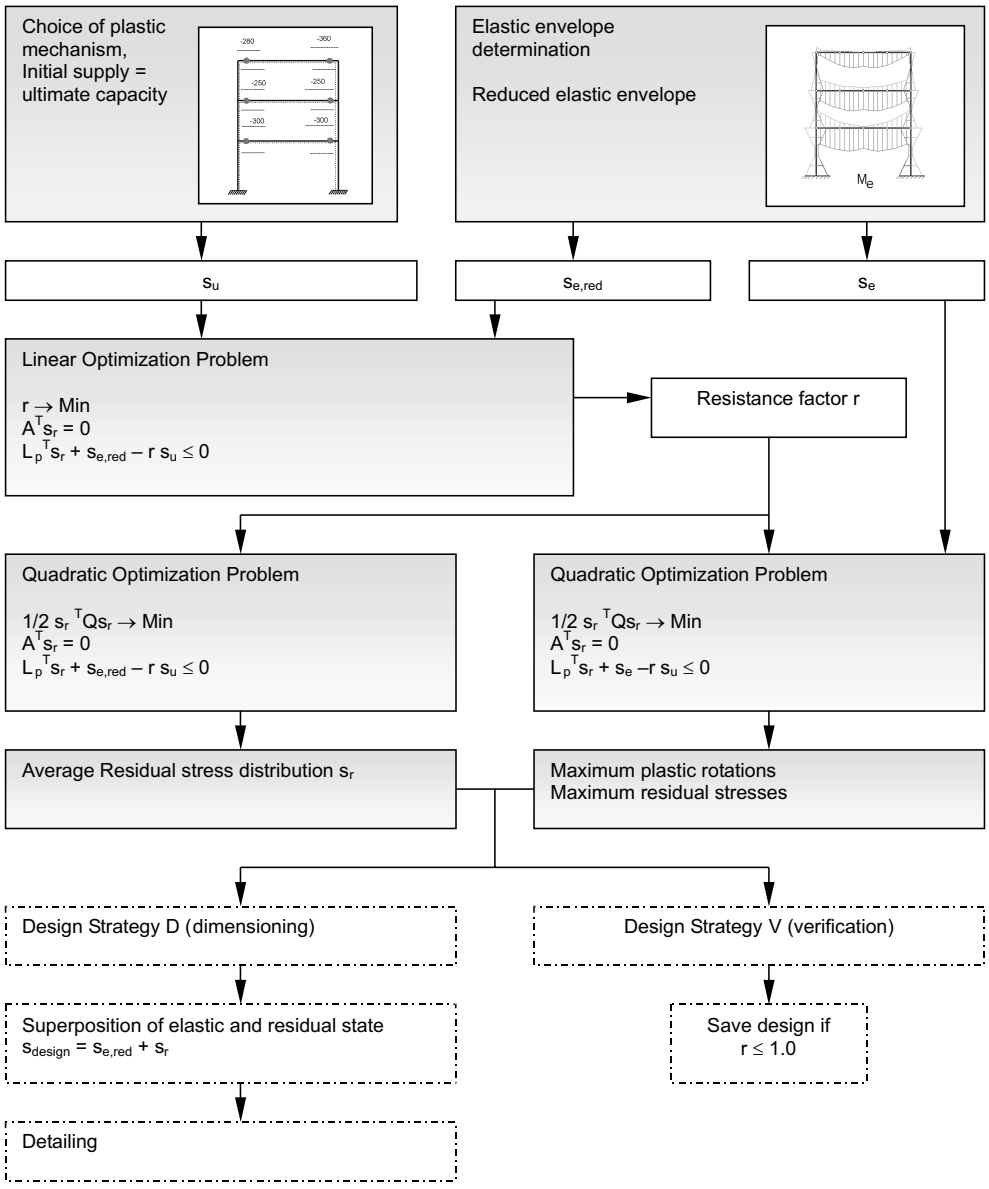

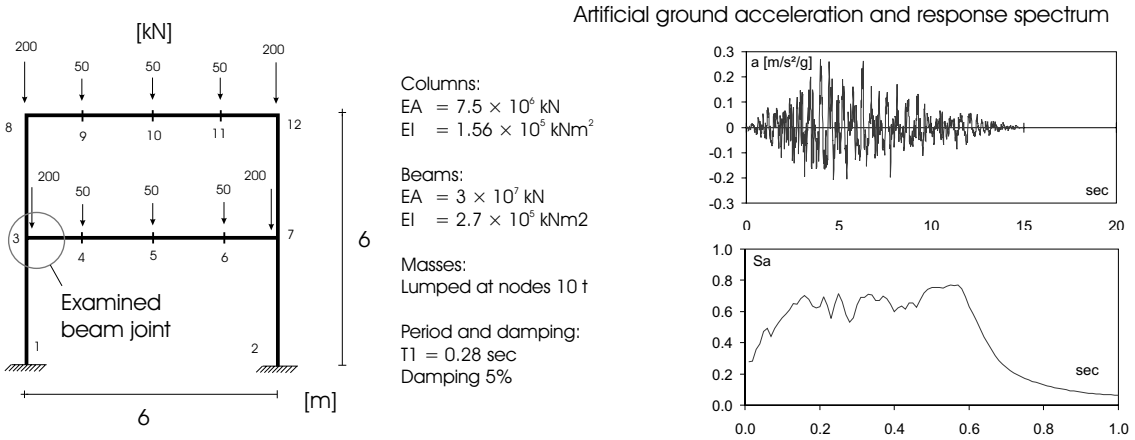

Figure 7-14 Example: System, loads, masses, pre-design of stiffness

The application of Design Procedure D (according to Tab. 7-45) is demonstrated for the Example of Fig. 7-14. For result discussion, the behavior at the end of the beam in the first floor (Beam 5, Node 3) is focused most. After performing an elastic time history analysis the elastic envelope is calculated.

The response values will be used to assemble the elastic envelope solution according to the sequence in Tab. 7-46. After choosing the plastic mechanism the reduced envelope values can be filtered. For demonstration in this example three different numbers of re-plastification (1,3 and 5) are chosen (Fig. 7-15). The position of the potential plastic hinges and the initial values of the moment capacities are given.

The reduced elastic envelope is used to calculate the resistance factors. In Tab. 7-49 the resistance factors r according to their appropriate numbers of re-plastification n are shown. The theoretical case of total elastic behavior ($n = 0$) is given for comparison. The residual forces are calculated as well.

Table 7-49 Example: Resistance factors r for intended numbers of re-plastifications n_{design} and the obtained numbers n_{cal} (on basis of adaptive limit state)

n_{design}	n_{cal}	r	% of elastic limit
0	0	2.57	100.0
1	1	0.90	35.0
3	3	0.75	29.2
5	5	0.68	26.5

For better distribution of plastic deformations within the structure, a simple loop back to step D4 can be done to rearrange the initial moment capacity distribution and calculate the limit state again without considering the time history again. In computer implementations an automatic procedure for finding the optimal distribution with help of a programming

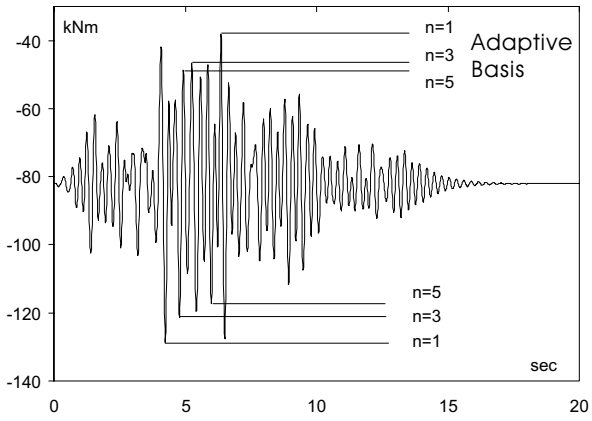

D3 Elastic analysis, elastic envelope

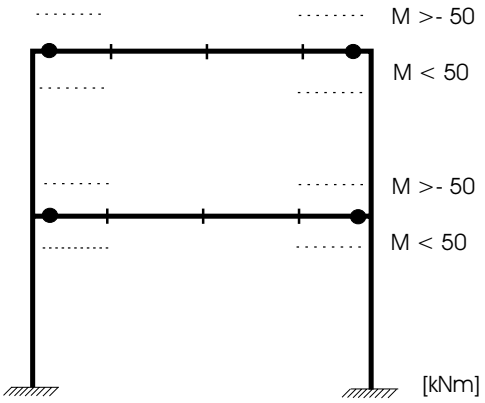

D4 Choice of plastic mechanism and supply

Figure 7-15 Example: Design steps D3/D4.

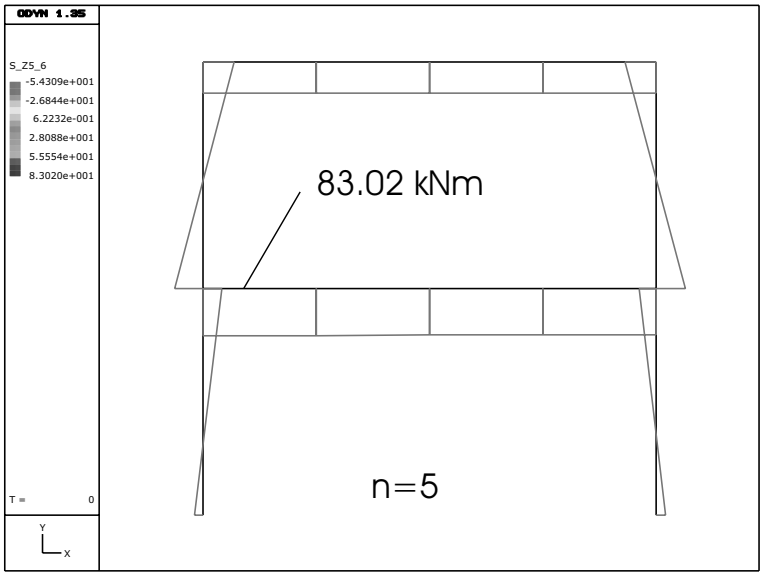

Figure 7-16 Example: Design steps D5/D6. Calculation of limit state: Fictitious residual state

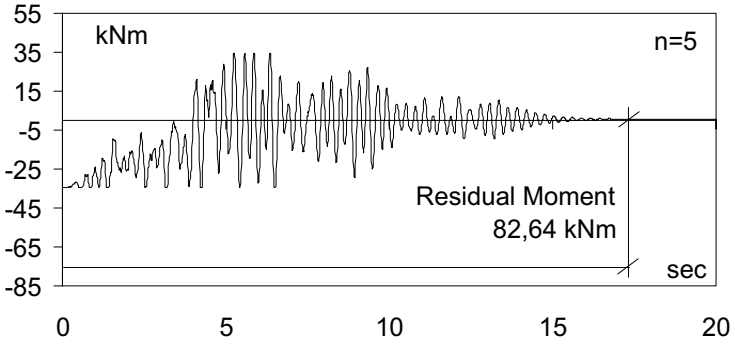

Figure 7-17 Bending moment at point 3 for n=5

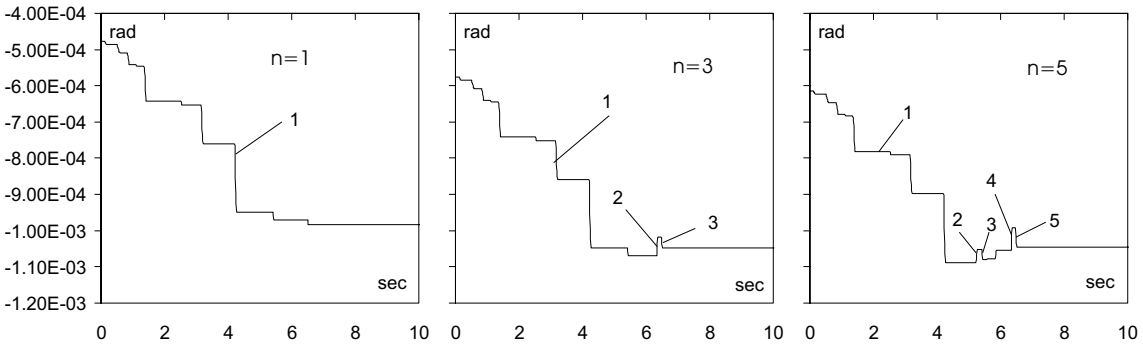

Figure 7-18 Plastic beam rotations at point 3 for n = 1,3 and 5; Marked: changes in plasticity direction

approach can be included easily. Having an acceptable behavior, the procedure can be finished by superposing the residual state and the elastic envelope for the derivation of the design forces. The detailing can now be established according to Capacity Design rules.

To control how this design will perform during an earthquake, a comparison with a non-linear dynamic analysis is provided here. It should be noted, that this step is not part of the design routine. The given ground acceleration of Tab. 7-14 is used as excitation. In Tab. 7-17 the bending moment history for n=5 and the plastic part of the rotations at the considered beam end (Point 3) are shown for different numbers of re-plastification. It can be outlined, that according to the design objective all accounts of re-plastification will stay below it′s projected values. For this specific example the ultimate number of re-plastification is adjusted. This is not necessarily and always the case. The procedure just guarantees, that the ultimate number is not exceeded. As expected the maximum plastic rotations calculated by the limit state analysis is not exceeded at the observed point

(Fig. 7-18) . The calculated value of residual moment is almost as calculated by the simplified approach.

7.6 Deformation based limit states

7.6.1 Basic concepts

The previously discussed limit state concepts commonly assume sufficient plastic deformability. However, even if the level of plastification is limited as for shakedown, the associated state may be not acceptable due to large deformations. Restricting limit state problems with respect to deformations is leading to deformation based limit state problems. They are especially developed for direct consideration of the large increase of deformations in plastic zones or due to geometric nonlinearities, that can cause local failure before developing kinematic chains. These problems are discussed in detail in [218] also for seismically excited structures and are summarized shortly in the following.

Three main concepts of simplified calculation can be distinguished:

1.) Calculation without consideration of load sequence problems

2.) Calculation with consideration of load sequence problems according to the concept of superposed residual state

3.) Calculation with consideration of load sequence problems according to the concept of shared plastic response

All concepts are schematically explained in Tab. 7-50. The first concept mainly conforms to the simplified method given in Sec. 7.3. However, it commonly bases exclusively on the Poisson or Lagrange type of formulation. This is because the unknowns contain deformations. In these formulations just additive inequality conditions for solving the appropriate optimization problems can be applied in order to integrate deformation limit criteria, e.g.

$$u \leq u_{lim} \tag{7-92}$$

The second method is mainly related to the shakedown state analysis given in Sec. 7.4, especially using deformation unknowns. The influence of time is neglected as well. This allows to consider not only a single given seismic load but a class of excitations. As before the deformation criteria can be added simply by introducing an additional inequality.

The third concept integrates all load combinations into one optimization scheme for the limit state analysis. The unknowns are the deformations resulting from the appropriate load combinations that are superposed to a shared plastic response. One example for an optimization problem is given in Tab. 7-51. The difference is, that no elastic envelope needs to be calculated. The advantage of this model is the extension of the analysis for geometrically nonlinear calculations, as the unknown displacements are total displacements, without superposition with an elastic envelope part.

Using deformation based limit analysis, all limit criteria can be applied in one universal format. So by application of deformation criteria and scaling the load or resistance factors,

Table 7-50 Concepts for deformation based limit state analysis

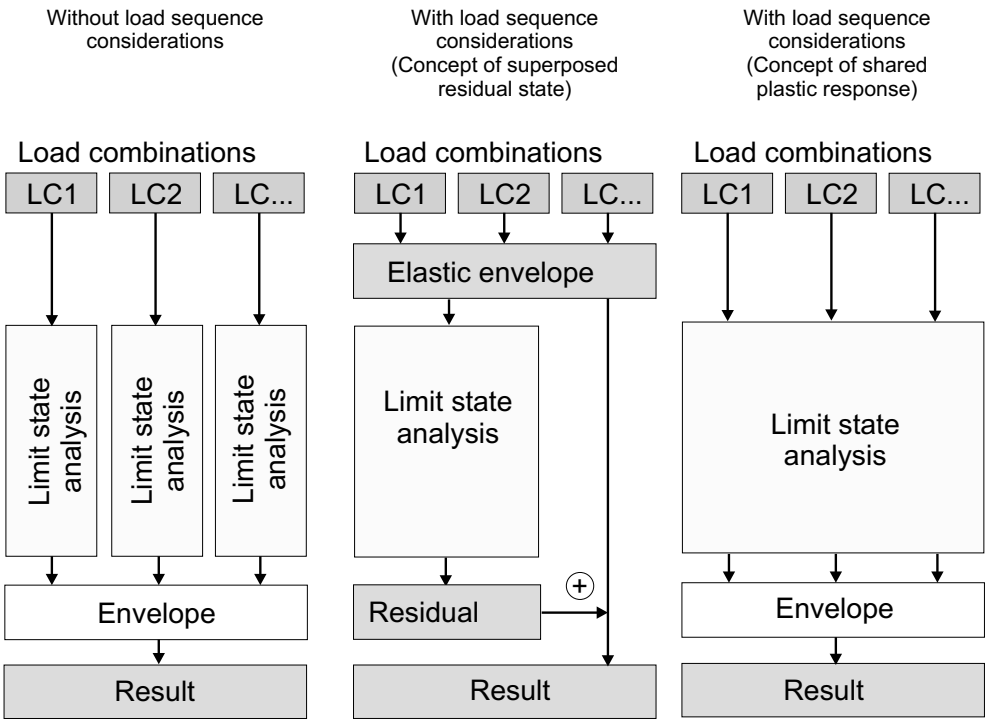

arbitrary conditions can be introduced, e.g. limit bearing or serviceability conditions. One major application in seismic engineering is the limitation of displacements and ductility demands.

7.6.2 Example Deformation based limit state

The concept of Tab. 7-51 is applied to the example from Sec. 7.3.3. In Tab. 7-52 the deformations at the plastic limit state ($r_p = 1.039$) are compared to the displacement bound of $u_{lim} = 10mm$ at Node 4. It can be seen, that for both load sequences, the limit displacement is lower than the applied bound. The appropriate limit resistance factor is $r_d = 1.125$. From this it is obvious, that the resistance factor is between the plastic and adaptive limit factor calculated in Sec. 7.4.4).

7.7 Capacity-spectrum-based concepts

The application of capacity spectrum methods recently gained popularity in the evaluation of nonlinear structures. The differences to the linear methods previously described arise mainly from the substitution of the eigenform by a pushover curve derived by nonlinear static analysis. In combination with the capacity spectrum method, that provides concepts to transform these data as well as response spectra into a capacity-demand spectrum format. This is done on the basis of equivalent linear modeling. In a visible way the structural supplies can be assessed [9,52].

Table 7-51 Optimization scheme for calculation of deformation based limit state according to the concept of shared plastic response

			Primal variables						
			u_1	⋯	u_n	λ	r		
							1	→	Min
Dual variables	u_1^T		$A^I Q^{-1} A$	⋱		$-A^I Q^{-1} L_P$		$= f_1$	Ext. Equilibrium
	⋮					⋮		⋮	
	u_n^T				$A^I Q^{-1} A$	$-A^I Q^{-1} L_P$		$= f_n$	
	λ^T		$-L_P{}^I Q^{-1} A$			$L_p{}^T Q^{-1} L_p$	s_{lim}	≥ 0	Plasticity condition
	⋮			⋱		⋮	⋮	⋮	
	λ^T				$-L_P{}^I Q^{-1} A$	$L_p{}^T Q^{-1} L_p$	s_{lim}	≥ 0	
	y^T					1		≥ 0	Non-negativity
	λ^T (		$-L_P{}^I Q^{-1} A$			$L_p{}^T Q^{-1} L_p$	s_{lim}	) = 0	Complementarity
	⋮					⋮	⋮	⋮	
	λ^T (				$-L_P{}^I Q^{-1} A$	$L_p{}^T Q^{-1} L_p$	s_{lim}	) = 0	
			$-N_u$					$\geq u_{lim}$	Deformation limit
	⋮					⋮	⋮	⋮	
					$-N_u$			$\geq u_{lim}$	

Table 7-52 Example: Limitation of the total horizontal deformations using deformation based optimization strategies

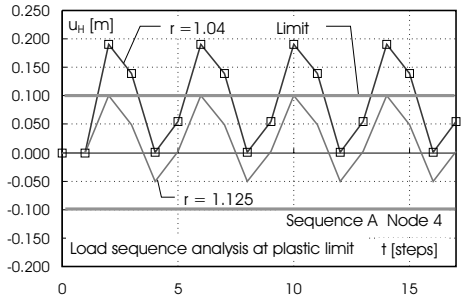

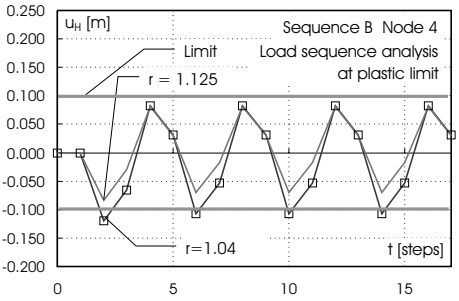

It is known from conventional design, that the simplified linear analysis method for the assessment of a nonlinear behavior is performing less accurate than the methods based on pushover curves. The main reason for that is the non-appropriate estimation of the nonlinear structural behavior observed during transient excitation on the basis of eigenvectors.

The basic assumptions regarding equivalent linearization are generally the same as outlined in Sec. 6.6. Exceptionally is the fact that the equivalent stiffness is not calculated explicitly during the iterations because it is an inherent part of the capacity curve. As in the original procedure the period dependency of the damping ratio is neglected as well, so Eq. (7-93) is commonly applied [9]. For simplicity the explicit calculation of the ductility and stiffness ratio is bypassed. Instead, the identical form expressed in terms of directly readable yield and maximum spectral accelerations and deformations is used

$$\xi_{equ} = \frac{2\left(Sa_e \cdot Sd_u - Sd_e \cdot Sa_u\right)}{\pi \cdot Sa_u \cdot Sd_u} \tag{7-93}$$

The capacity curve is dependent on the load pattern chosen for the pushover. It has been found that the traditional load distribution, conform with the product from modal shape and mass is appropriate for this purpose. Following the suggestions given for conventional design the deformations are traced at the very top and the shear forces at the bottom of the structure in order to derive the pushover curve.

As illustrated in Tab. 7-53 the following analysis steps are performed, mainly following ATC40 [9]. As the equivalent damping is dependent on the knowledge of the deformation and acceleration, the calculation is iterative.

First, the structure is modeled with nonlinear characteristics. The eigenvalue analysis is done with the initial material parameters. As a result, the eigenvectors Y, eigenvalues λ and participation factors Γ are obtained. The mass distribution is multiplied with a selected eigenvector to form a load pattern. This load pattern is used to perform a stepwise nonlinear static analysis (pushover analysis). The maximum deformation (measured typically at the roof of the structure) and the appropriate base shear force is traced throughout the steps and are both assembled in the "pushover curve". This curve is transformed into a

"capacity spectrum" and relates to the behavior of an equivalent SDOF, showing the same maximum deformation and base shear force as the original structure. This approximation is sufficient for regular systems.

Secondly, for the loading, an elastic mean spectrum (calculated from time history sets) or code spectrum must be selected. In the first iteration loop, a damping ratio ξ is estimated. The damping ratio is used to calculate the inelastic spectrum Eq. (6-26). This reduced spectrum is transformed into the "demand spectrum". Both, the capacity and demand spectrum are intersected in one diagram. The intersection point is the "performance point", giving the ultimate spectral deformation Sd_u and acceleration Sa_u for the structure. These values are used to calculate the damping ratio Eq. (7-93). This damping ratio is compared to the previously assumed value. If the difference is too big (>5% difference) the calculation of the demand spectrum must be repeated while using the newly calculated damping ratio. The iteration is stopped if the changes in the result will be within reasonable limits. In the end, spectral values Sd and Sa have to be retransformed into real deformations and accelerations.

This procedure can be used as analytical kernels in optimization problems. An example for an appropriate optimization scheme is

$$O(r) = r \rightarrow Min \tag{7-94}$$

$$u(x_i) \leq 0 \tag{7-95}$$

$$\ddot{u}(x_k) \leq 0 \tag{7-96}$$

where $u(x_i)$ and $\ddot{u}(x_j)$ are responses calculated by the capacity design method. Any previously discussed limit state can be reproduced.

Table 7-53 Principle of capacity spectrum analysis

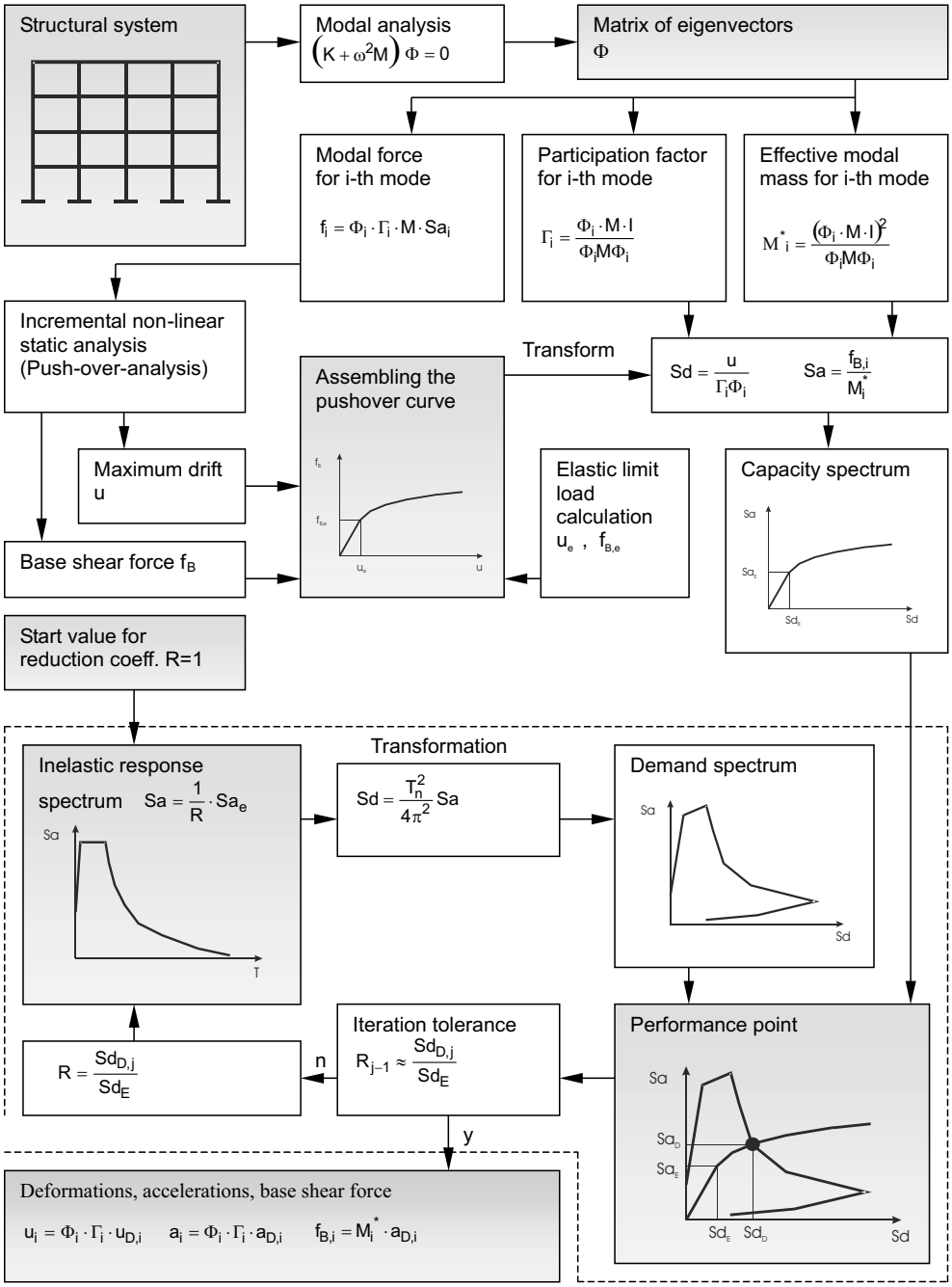

8 Optimization problems on basis of time history approaches

8.1 Time discretization and integration

Time domain problems are initial value problems, that can be transformed from time-space continuum to discrete problems by application of discretization methods. As already discussed in Sec. 3.1, the dynamic problem can be divided into quasi-static subproblems (at fixed times) using a superior integration with respect to discrete times. This separation leads to a considerable simplification for the numerical treatment. For this purpose, several time integration methods are known, e.g. described in [22,230]. The most popular are named in Tab. 8-1.

In time discretization methods, the knowledge of results at discrete times is utilized in order to calculate the integral behavior. According to d′Alemberts principle, the sum of all forces must be zero at all times. Then the internal, external, inertia and damping forces can be added in the equilibrium condition, that can be transformed, together with the kinematic and material conditions (Eq. (4-119)) into the equation of motion for the time t, e.g. as a linear function

$$K^t u = -M^t \ddot{u} - C^t \dot{u} - {}^t f_R \tag{8-1}$$

In the following, as indicated herein, only proportional (viscous) damping is considered, that is commonly composed according to the Rayleigh assumption

$$C = \alpha_M M + \alpha_K K \tag{8-2}$$

Results at successive times, are used to replace the temporal derivatives, according to Taylor series substitutions (e.g. Runge-Kutta, Leap Frog, Newmark) or finite difference approaches (e.g. Central Difference). Depending on the selected information, the following integration categories are distinguished

- explicit
- implicit
- semi-implicit

that can be formulated as one- or multi-step methods. In explicit time integration only information from the past are involved (p is here symbolizing an arbitrary time dependent parameter)

$${}^{t+\Delta t}p = f({}^t p, {}^t\dot{p}, {}^t\ddot{p}, {}^{t-\Delta t}p, \ldots) \tag{8-3}$$

By application of the Central Difference Method, the derivatives of the displacements are

$${}^t\ddot{u} = \frac{1}{\Delta t^2}\left({}^{t-\Delta t}u - 2^t u + {}^{t+\Delta t}u\right) \tag{8-4}$$

Table 8-1 Selection of time integration methods in structural engineering

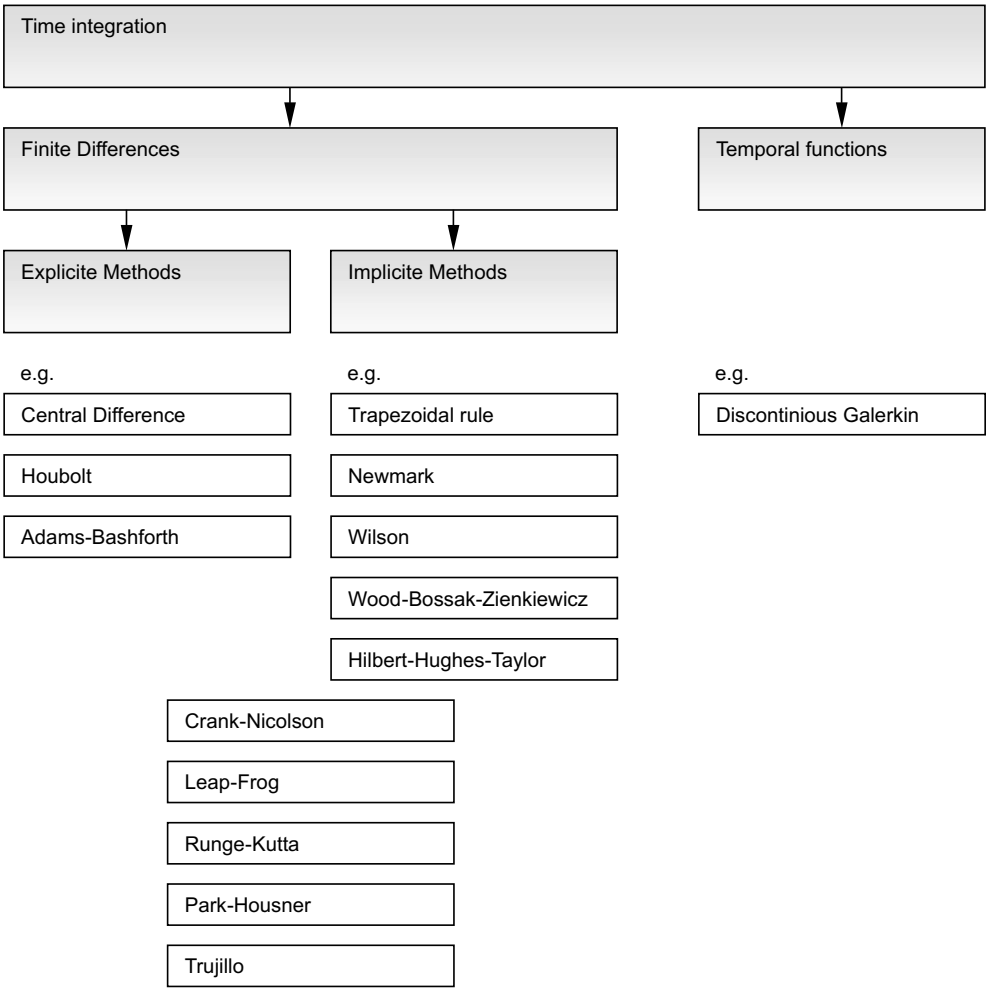

and

$$ {}^{t}\dot{u} = \frac{1}{2\Delta t}\left({}^{t+\Delta t}u - {}^{t-\Delta t}u\right) \tag{8-5} $$

The resulting problem is

$$ \left(\frac{1}{\Delta t^2}M + \frac{1}{2\Delta t}C\right) {}^{t+\Delta t}u = {}^{t}_{t-\Delta t}R \tag{8-6} $$

where R contains all terms related to the times t and $t - \Delta t$.

In implicit time integration, parameters at time $t + \Delta t$ are calculated with parameters at all times

$$ {}^{t+\Delta t}p = f({}^{t+\Delta t}p, {}^{t+\Delta t}\dot{p}, {}^{t+\Delta t}\ddot{p}, {}^{t}p, \ldots) \tag{8-7} $$

The application of implicit methods is common in structural engineering. Especially implicit one-step methods (Newmark-Wilson type procedures) are often applied. Table 8-2 explains the basic procedures of derivative substitution within such methods. One special case is the Newmark scheme, most popular in engineering software. It is exemplified in Tab. 8-3. The classical choice of the coefficients $\delta = 1/4$ and $\gamma = 1/2$ corresponds to a constant acceleration. For this, the solution is unconditional stable. A linear acceleration is achieved for $\delta = 1/6$ and $\gamma = 1/2$, that is conditional stable. The conditionally stable method of finite differences is represented by $\delta = 0$ and $\gamma = 1/2$.

Semi-implicit methods combine implicit and explicit features. They use weighted information from current and past time steps

$$^{t+\Delta t}p = f(\alpha_0{}^{t+\Delta t}p, \alpha_1{}^{t+\Delta t}\dot{p}, \alpha_2{}^{t+\Delta t}\ddot{p}, \beta_0{}^{t}p, \ldots) \tag{8-8}$$

The selection of appropriate time integration schemes is dependent on the consistency, stability, accuracy and efficiency of the method in the intended application. The consistency describes the ability of the method to reduce the numerical error with reduced time steps. The class of consistency is given by the exponent of time in the error term. The numerical stability describes the ability to prevent accumulation of errors in the solution, in order to stay sufficiently close to the actual solution. The stability of a method can be tested by analysis of the amplification function of the dynamic problem

$$^{t+\Delta t}X = \Xi{}^{t}X + {}^{t+\Delta t}f \tag{8-9}$$

by calculation of the eigenvalue problem

$$(\Xi - \lambda_x I) = 0 \tag{8-10}$$

with the complex eigenvalues

$$\lambda_{x,1,2} = a_{real} \pm a_{imag} \tag{8-11}$$

and evaluation of the spectral radius

$$\rho = \sqrt{a_{real}^2 + a_{imag}^2} \tag{8-12}$$

Whether or not being dependent on the time step size, the method is called conditional or unconditional stable. With $\rho \leq 0$ the problem is non-conditional stable. The expected numerical damping is

$$\xi_{num} = \frac{1}{2\arctan(\frac{b}{a})} \ln(a_{real}^2 + a_{imag}^2) \tag{8-13}$$

Adjusting the numerical damping is a general mean to control stability.

Table 8-2 Time integration scheme for implicit one-step methods

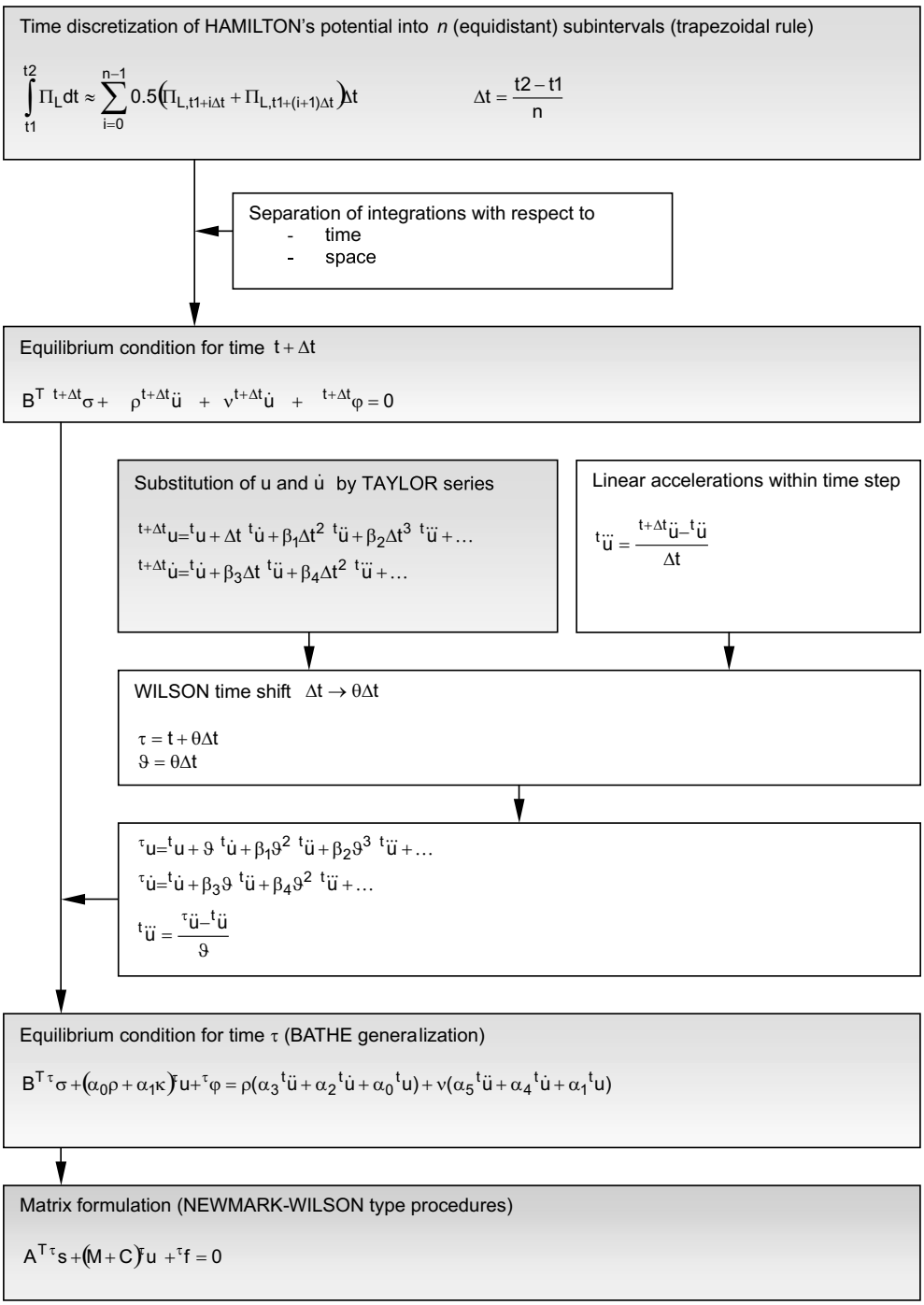

Table 8-3 Newmark time integration scheme

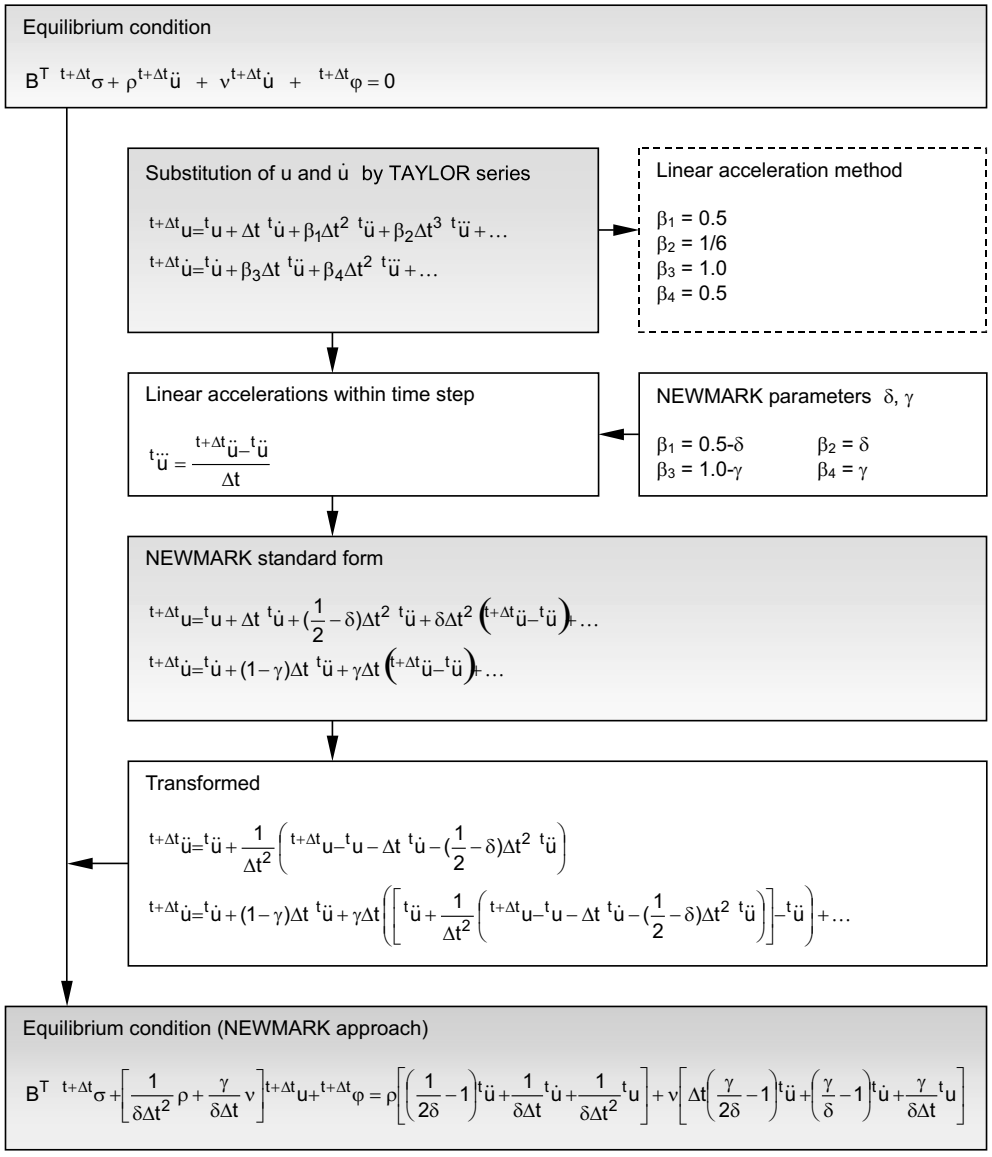

Closely related is the accuracy of the numerical solution, that evaluates the relation of the numeric to the exact results due to the governing differential equations. Finally, the efficiency relates costs and benefits of the numerical treatment.

Further reading on time integration methods is provided e.g. in [8,22,230,166] or [38,100,207,172].

8.2 Variational problem formulation

8.2.1 Basic concept

Time domain analysis can be applied for structural optimization. For the derivation of appropriate tasks to solve nonlinear dynamic problems, modifications of traditional principles can be used, that have been originally formulated for static problems. Everything can be based on the Poisson principle (Sec. 7.2.1). More often appropriate are the smaller Lagrange and Castigliano extremum principles (Sec. 7.2.2 and 7.2.3), that pursue either a deformation based (Lagrange) or force based (Castigliano) assessment of the mechanical system.

These principles can be used as quasi-static cores Π for dynamic calculations. This is possible according to the Hamiltonian principle

$$J_H = \int \Pi(x,t)dt \rightarrow Min \tag{8-14}$$

respecting given subsidiary conditions. The introduction of the Lagrange and Castigliano principles is illustrated next.

8.2.2 Implicit Lagrange principle

Traditionally, the Lagrange principle Π_L serves as core principle. This principle is formulated for dynamic behavior similar to Sec. 7. The difference is, that an extended equilibrium condition, consisting of static, inertia and damping force components, must be considered. As for static problems, the principle is assembled from separate system equations. If necessary, physical and geometric nonlinearities can be introduced within the core, similar to Sec. 4.12 and 4.13. If an implicit integration scheme is applied, e.g. Newmark approach, one considerable advantage of this approach is obtained because the number of unknowns is identical to the quasi-static formulations known from Sec. 7.2.3. Thus relatively little modifications need to be introduced for the dynamic extensions.

In general, the Lagrange potential for dynamic systems states the balance between the kinetic and potential energy

$$\Pi_L = W(u,\dot{u},\ddot{u}) - V(u) \tag{8-15}$$

This potential is integrated into the Hamiltonian principle (or action integral) in Eq. (8-14). By means of discretization, the extremum principle can be transformed into an optimization problem. Using the implicit Newmark-Wilson time integration approach, the appropriate optimization scheme is given in Tab. 8-4 and 8-5. Here already an elasto-plastic material is considered. If the problem is geometrically linear and the plasticity

Table 8-4 Optimization problem for implicit time integration (Lagrange approach, elasto-plastic material)

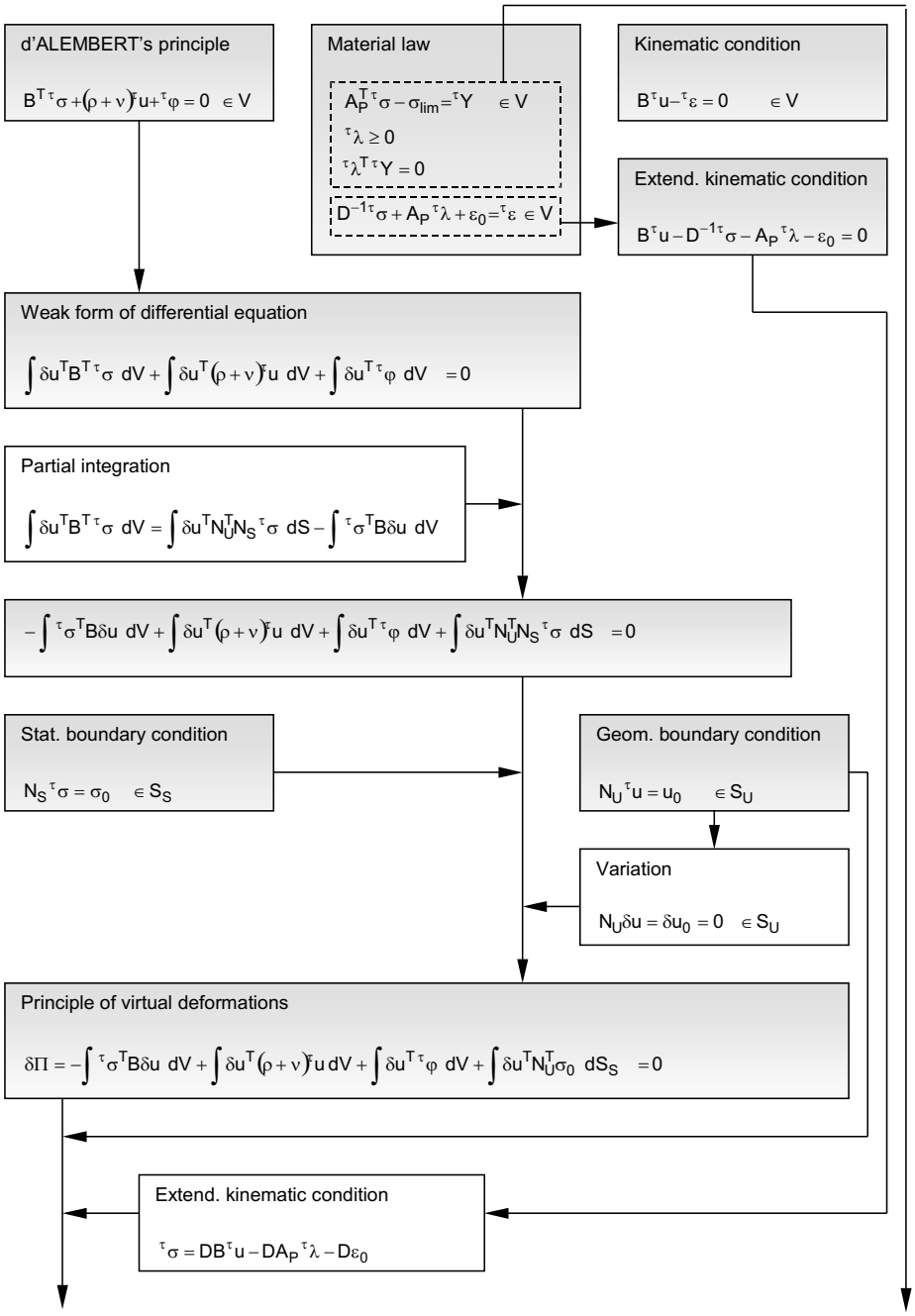

conditions are linear, the optimization problem can be solved with means of quadratic optimization.

Table 8-5 Optimization problem for implicit time integration (Lagrange approach, continued)

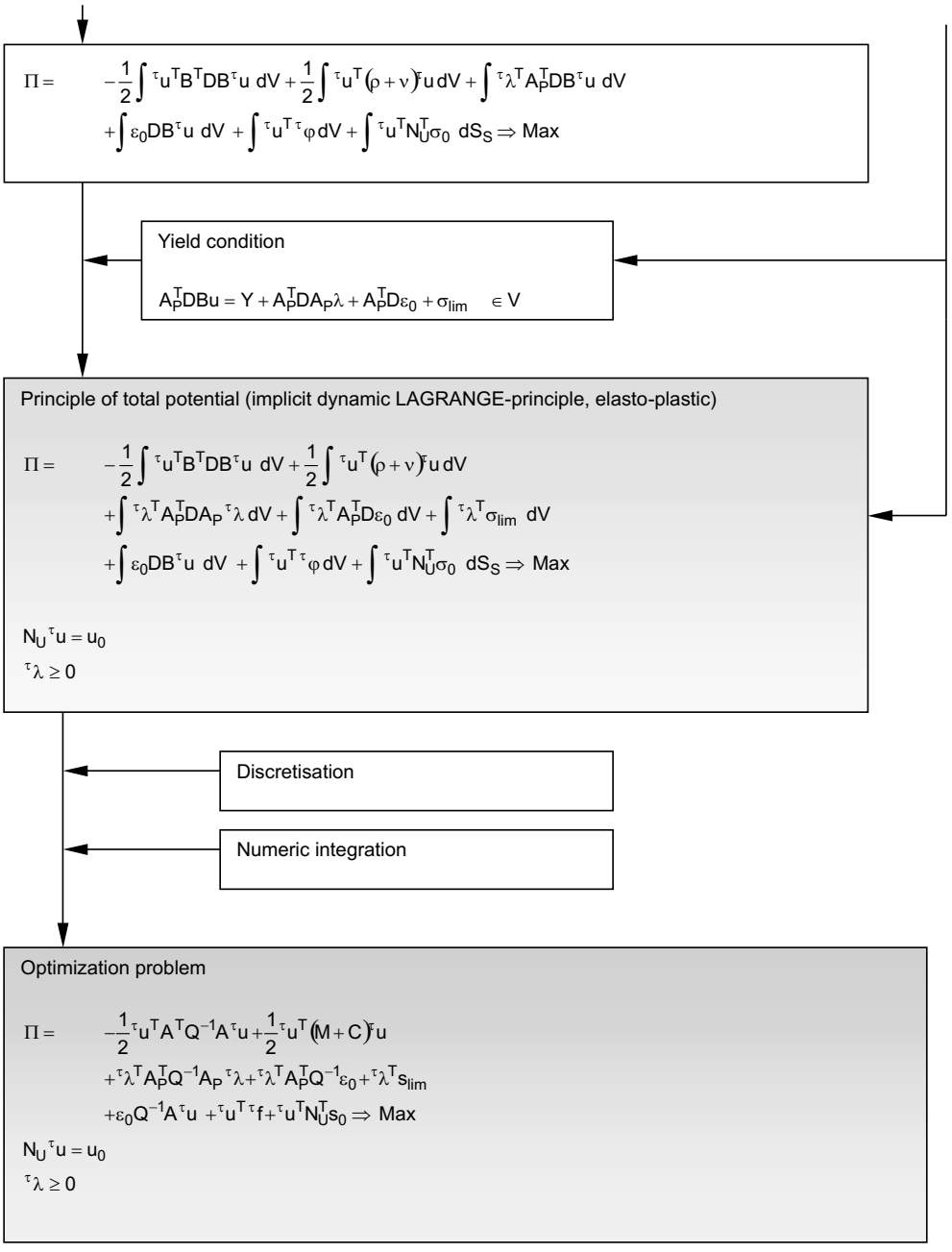

Table 8-6 Quadratic optimization scheme for step-by-step analysis of elasto-plastic structures (implicit dynamic Lagrange formulation)

		Primal variables					
		u	λ	c_U	1		
	$u^T($	$\frac{1}{2}A^TQ^{-1}A - \frac{1}{2}(M+C)$		$\frac{1}{2}(N_SQ^{-1}A)^T$	$A^TQ^{-1}\varepsilon_0 - f$)		
	$\lambda^T($		$-A_P^TQ^{-1}A_P$		$A_P^TQ^{-1}\varepsilon_0 - s_{lim}$)	$\Rightarrow$ Min	Objective function
	$c_U^T($	$\frac{1}{2}N_SQ^{-1}A$			$-s_0$)		
Dual variables	c_s^T	N_U			u_0	= 0	Geometric boundary condition
Dual variables	Y^T		-1			≤ 0	Non-negativity condition

Thus, the optimization problem is (as a core algorithm) solved in any time step. It requires a pre-calculation of the Bathe parameters (Tab. 8-2) from the previous time step. After determination of the displacements ${}^{t+\Delta t}u$ by optimization, the appropriate velocities, accelerations and stresses can be calculated in a post-calculation step.

In case of plastic deformation, the plastic strains are calculated from the Lagrange multipliers λ. They need to be accumulated over time and serve as predeformations in the successive time steps

$${}^{t+\Delta t}\varepsilon_0 = \sum_{ti=t0}^{t} {}^{ti}\varepsilon_p \tag{8-16}$$

The appropriate translation into a quadratic optimization scheme is given in Tab. 8-6, considering constant geometric and static boundary conditions and linear yield conditions.

8.2.3 Implicit Castigliano principle

As the "force-based" counterpart to the Lagrange principle, the preparation of the Castigliano principle for dynamic calculations is demonstrated in Tabs. 8-7 and 8-8. Also here, only the equilibrium condition is changed for consideration of additional inertia and damping forces. Contrary to the quasi-static Castigliano principle, the dynamic version contains stresses and displacements as well, so the number of unknowns is increased.

The application of this core within a step-by-step calculation procedure is demonstrated for the dynamic Castigliano principle in Tab. 8-9. As time integration method the implicit Newmark-Wilson scheme 8-2 is applied.

8.2.4 Explicit formulations

Similar to the implicit derivation schemes, explicit forms of time integration procedures can be implemented. As the unknowns of the problem are only dependent on the previous time step results, the explicit schemes simply evaluate the equilibrium condition. As exemplarily seen for the Central difference method in Tab. 8-10 and 8-11, the explicit Lagrange and Castigliano principles are easily derived and are related directly by the Lagrange multiplier method. Within the Castigliano principle, the extremum principle is arbitrary and can be set constant. Thus the problem can be solved with linear algebraic solvers. On the other hand, the Lagrange form is a quadratic optimization problem with constant boundaries. For both forms, dependent on the number of pre-steps in the explicit time integration method, the necessary starting solutions due to previous time steps can be calculated, e.g. with help of implicit calculations.

8.3 Contact Problems

8.3.1 Mechanical background

Traditional numerical concepts base on the transformation of nonlinear problems into linear algebraic approximations, that are assembled and solved in an iterative manner. The most difference of optimization algorithms is the supply of an interface for the formulation of an objective function and inequality conditions additionally to the equality conditions. The encapsulation of the iterative processes from the user is characteristic. Especially the inequality conditions provide various chances for the formulation of limit conditions, such as contact conditions. Usually, the treatment of contact conditions require permanent monitoring of the deformations, and if the contact condition applies, the solution has to be traced back to the limit condition and an additional equation needs to be introduced temporarily. If several conditions apply simultaneously, the organization of an effective procedure can be costly. Contrary to this procedure, the application of an optimization algorithm needs only the addition of an inequality condition, e.g.

$$u(x,t) \leq u_{lim,x} \tag{8-17}$$

Table 8-7 Optimization problem for implicit time integration (Castigliano approach)

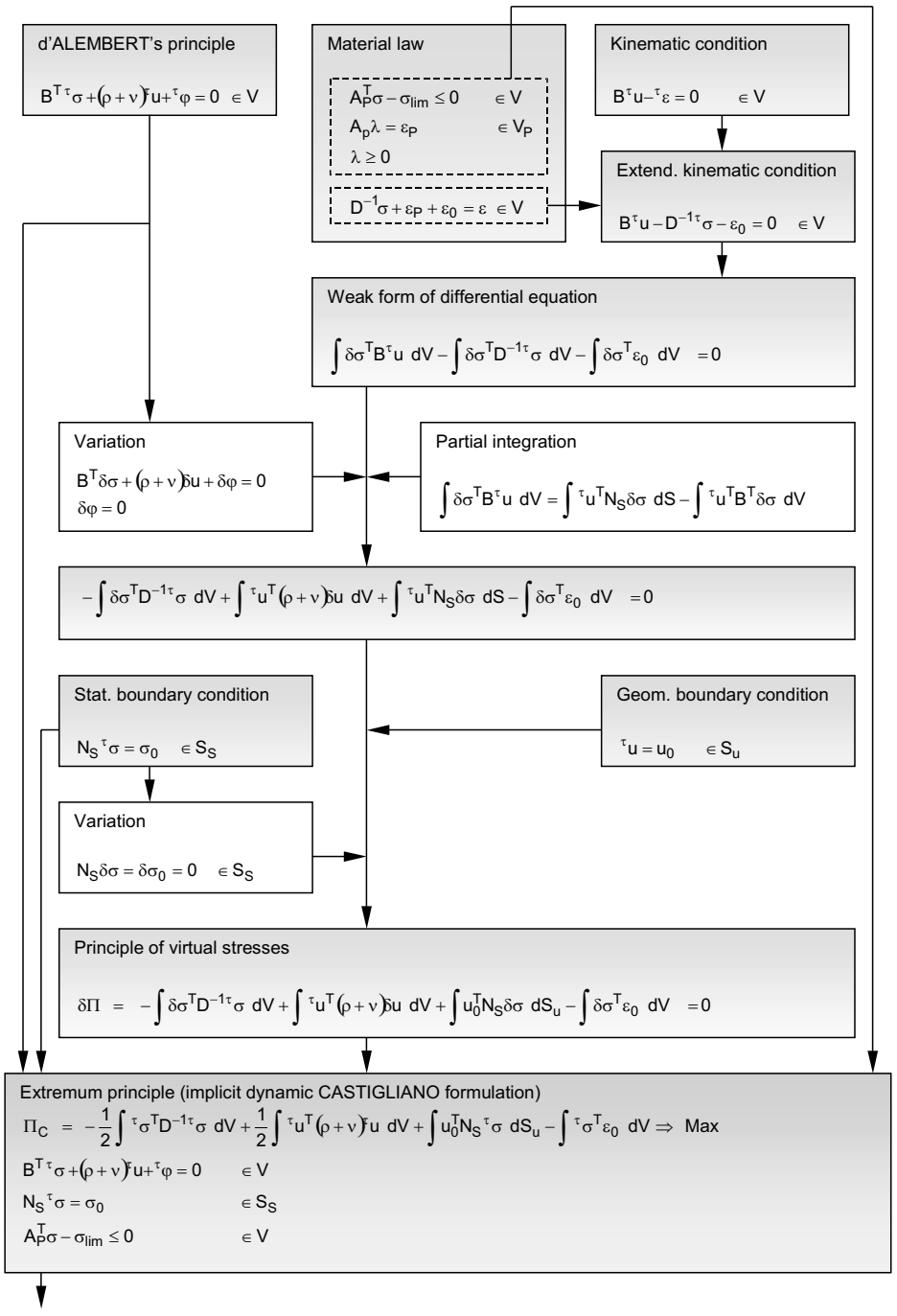

Table 8-8 Optimization problem for implicit time integration (Castigliano approach, continued)

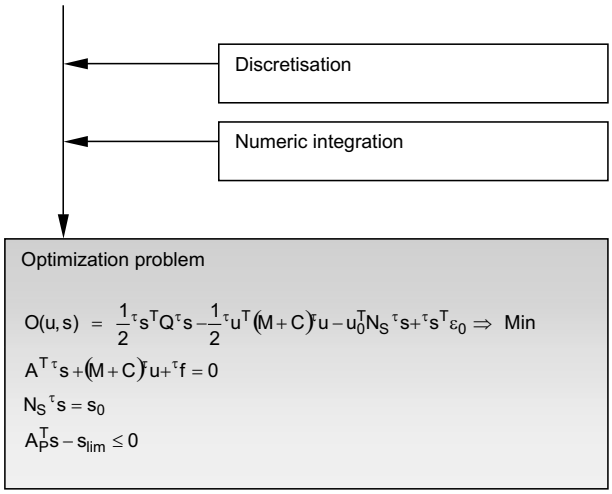

Here a contact to a fixed support is simulated. As well, contact conditions between degrees of freedom can be stated accordingly, e.g.

$$l_1 u(x_1,t) + l_2 u(x_2,t) \le u_{lim,1,2} \tag{8-18}$$

or in general matrix formulation

$$L_u^T u(t) \le u_{lim} \tag{8-19}$$

Mathematical programming is known to be an efficient calculation strategy for contact problem, with or without involvement of friction and pressure problems [131,228,229] or [111,54,142,128,26,169,182]. However, the duality of parameters is not always properly respected in any approach.

The treatment of contact conditions is similar to those of the plasticity conditions introduced in Sec. 4.8.2. With introduction of a slack variable y_u the inequality condition can be given as

$$L_u^T u(t) - u_{lim} = y_u \tag{8-20}$$

The appropriate dual variable is the Lagrange multiplier λ_u that is connected with y_u as a complementary couple

$$\lambda_u \ge 0 \tag{8-21}$$

$$y_u \ge 0 \tag{8-22}$$

$$\lambda_u^T y_u = 0 \tag{8-23}$$

Table 8-9 Quadratic optimization scheme for step-by-step analysis of elasto-plastic structures (implicit dynamic Castigliano formulation)

		Primal variables					
		s	u	c_S	1		
	$s^T($	$\frac{1}{2}Q$			$\varepsilon_0)$	$\Rightarrow$ Min	Objective function
	$u^T($		$-\frac{1}{2}(M+C)$		$)$		
	$c_S^T($				$-u_0)$		
Dual variables	u^T	A^T	$(M+C)$	N_U^T		= 0	Equilibrium condition
	λ^T	$A_p{}'$			$-s_{lim}$	≤ 0	Plasticity condition
	c_U^T	N_S			s_0	= 0	Static boundary condition

The appropriate parameter system for the continuum, is illustrated in the relation scheme Tab. 8-12. The duality must be fulfilled, hence obtaining always a symmetric relation scheme. It is obvious, that besides the contact condition an additional term must be considered in the equilibrium condition (equation of motion). The parameter λ_u can be identified as the Lagrange multiplier that is related to the support or linking force in case of contact

$$c_c = L_u \lambda_u \tag{8-24}$$

All these conditions can be similarly considered in all discussed mechanical principles, e.g. the Poisson, Lagrange and Castigliano principles used before.

8.4 Example time history analysis

The following simple example illustrates the application of optimization strategies together with time integration methods. The structure is given in Fig. 8-1 as well as the excitations. The eigenperiod is appropriately high as for a shear wall structure with 0.25s.

Table 8-10 Optimization problem for explicit time integration (Lagrange formulation)

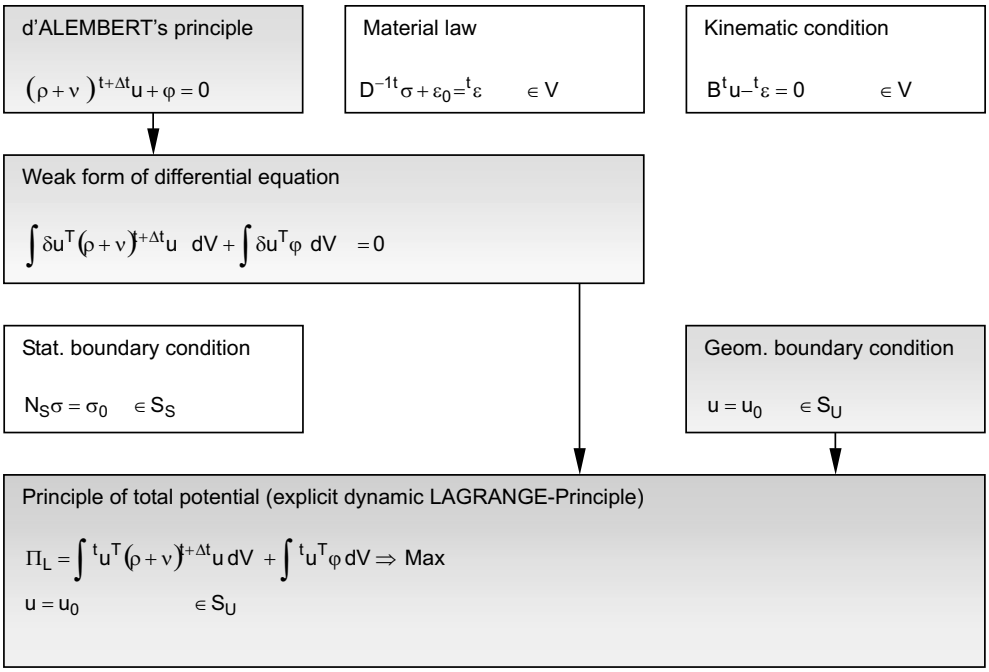

Table 8-11 Optimization problem for explicit time integration (Castigliano formulation)

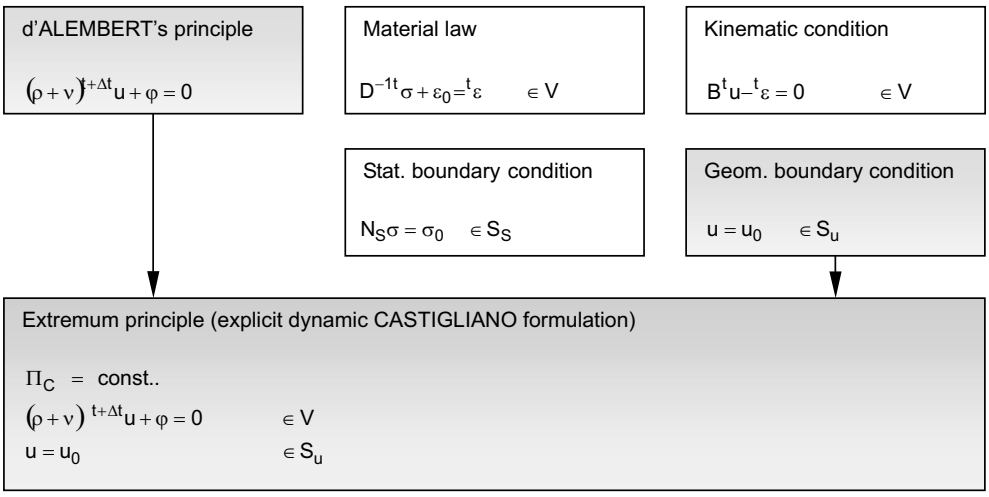

The structure is firstly subjected to an impulse load (Case 1) applied at the bottom of the structure. The appropriate time history of the deformation and equivalent stress, assuming a pure elastic behavior is given in Tab. 8-13. The introduction of high frequency components in the signal from impulsive loading can be seen in the stress plot.

Secondly the analysis is repeated, using an elastic perfectly plastic material law, assuming a limit of equivalent stress of 20MPa in the wall. The analysis results are summarized in Tab. 8-14. The limit of the stress can be observed, as well as the development of plastic strains. In this case, only with few plastic steps the final plastic strain state is reached. And, only one directional plastification is obtained.

Thirdly, the analysis is performed for the given seismic (transient) loading. The results for the points A and B are documented in Tab. 8-15 and 8-16. It can be seen, that in case of the plastic analysis (again with 20MPa yield limit for the stresses) the stress plot is shifted, showing the residual part of the stresses remaining in the structure, also after all excitation is over. As well, the appropriate displacement is enlarged compared with the elastic results. And, in this example, the plastic strains show the replastifications that occur at the given load level.

Table 8-12 Relation scheme of mechanical quantities for contact problems

			Primal variable								
			σ	c_u	c_s	u	λ_U	y_U	1		
Dual variables	σ^T		$-D^{-1}$	N_S		B				$=\varepsilon_0$	Ext. kinematic condition
	c_u^T		N_S^I							$=\sigma_0$	Static boundary condition
	c_s^T					N_U				$=u_0$	Geom. boundary condition
	u^T		B^I		N_U^I		$-L_U$			$=\varphi_R$	Equation of motion
	λ_U^T					$-L_U^T$		1		$=-u_{lim}$	Contact condition
	y_U^T						1	-1		≥ 0	Non-negativity
									$\lambda_U^T y_U$	$=0$	Complementarity

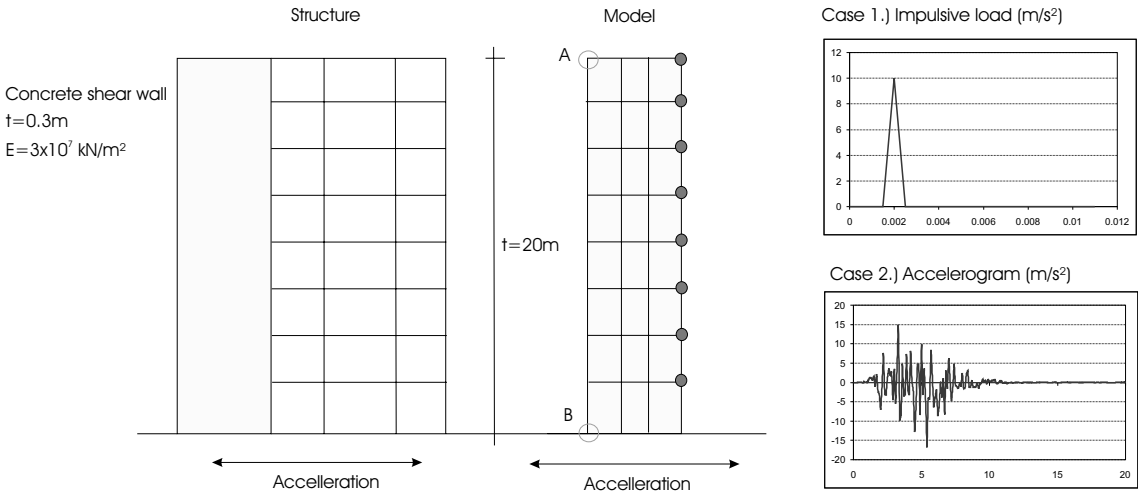

Figure 8-1 Example: Time history analysis, case 1.) impulsive load, case 2.) transient (seismic) load

Table 8-13 Example: Case 1.) Impulsive load at elastic structure

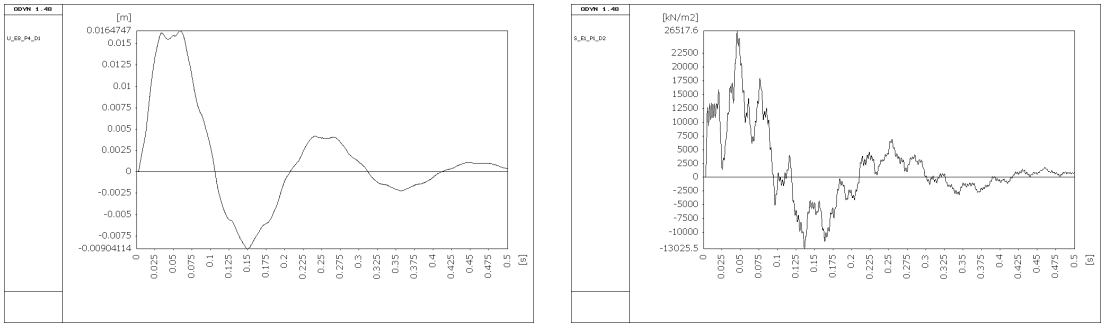

Deformation at point A

Equivalent stress at point B

8.5 Dynamic limit state analysis

8.5.1 Summary

A dynamic limit state analysis can be performed similarly to the quasi-static procedures already discussed in Sec. 7. Thus in this section only the main statements need to be repeated and adopted for time histories.

The elastic limit state can be calculated with help of the following optimization problem, here for elastic perfectly plastic material, similar to the procedure of Sec. 7.2.4.

$$O(p) = p \rightarrow Max \tag{8-25}$$

Table 8-14 Example: Case 1.) Example: Impulsive load at elastic-plastic structure

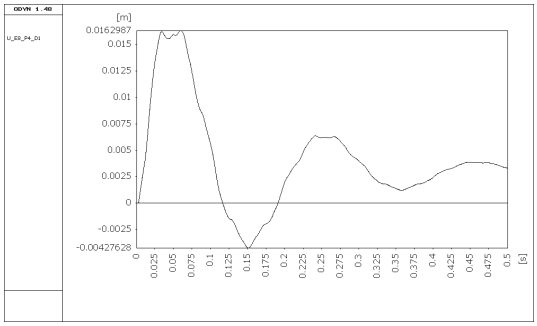

Deformation at point A

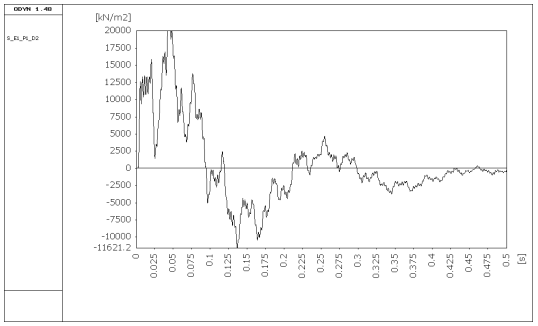

Equivalent stress at point B

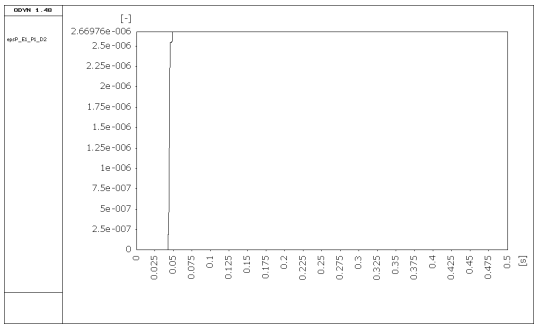

Plastic strain at point B

Table 8-15 Example: Case 1.) Seismic load at elastic structure

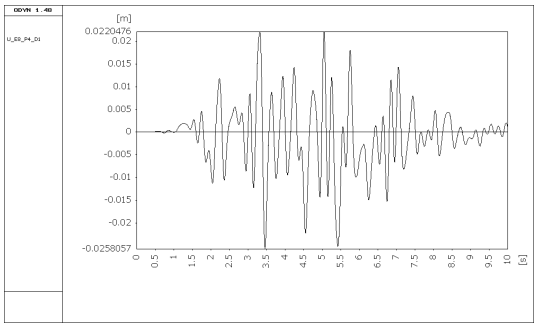

Deformation at point A

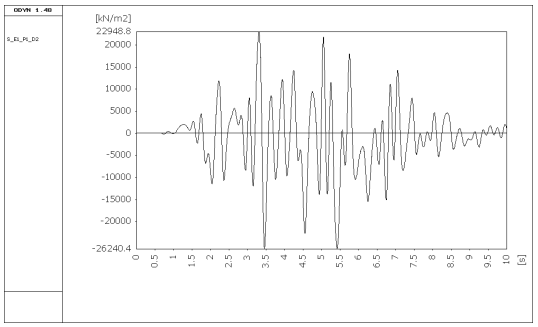

Equivalent stress at point B

Table 8-16 Example: Case 1.) Example: Seismic load at elastic-plastic structure

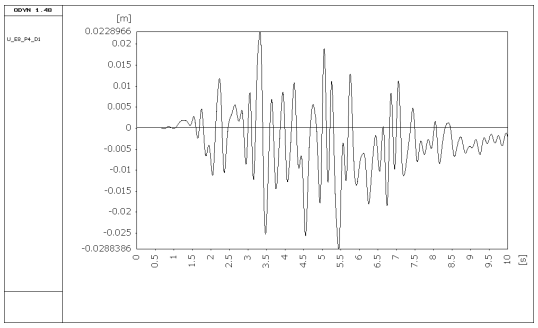

Deformation at point A

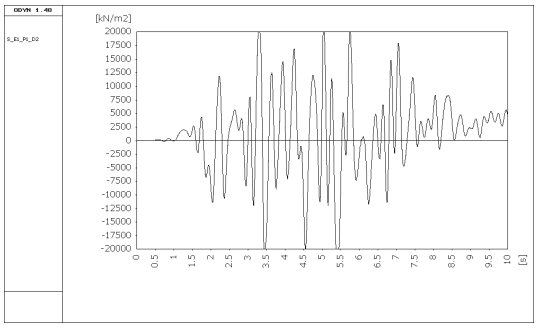

Equivalent stress at point B

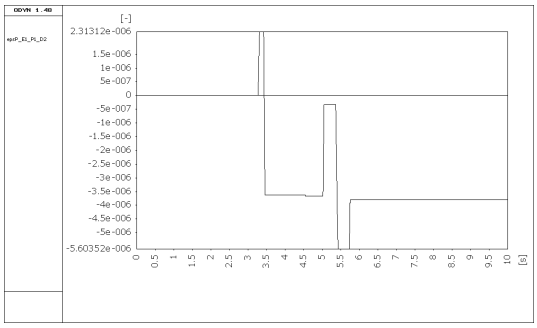

Plastic strain at point B

$$A^T Q A u(t) - A^T Q L_p \lambda(t) + C\dot{u}(t) + M\ddot{u}(t) = pf(t) \tag{8-26}$$

$$\Phi = L_p^T Q A u(t) - L_p^T Q L_p \lambda(t) - s_{lim} \leq 0 \tag{8-27}$$

$$\lambda^T(t)\Phi = 0 \tag{8-28}$$

The difference is the dependency of the problem on time. This can be interpretet as the performance of all steps of the time integration in one optimization problem. This method is quite costly. On the other hand, one simple calculation with a unity force $f(t)$ (taken $p = 1$) can be performed and the results of the extremum stresses s_e can be scaled accordingly

$$O(p) = p \rightarrow Max \tag{8-29}$$

$$ps_e \leq s_{lim} \tag{8-30}$$

The plastic limit state can be determined as already given in Sec. 5.10. As well, the shakedown, cycle based and deformation based limit state can be obtained as described in

Sec. 7.4, 7.5 and 7.6, exchanging the static load sequences by dynamic loading, applied in steps.

8.5.2 Example limit state analysis

The example of Sec. 8.4 is concluded. In Tab. 8-17 the results for the elastic, plastic and adaptive limit state are listed. All factors are related to the basic load intensity ($p = 1$) for the seismic load given in Fig. 8-1. For the elastic limit state, all plastifications are avoided. The plastic limit state is determined by the complex eigenvalue analysis procedure, determining the kinematic chain behavior. The given value is naturally high for wall structures. The shakedown limit ensures that only one-directional plastification occur in all parts of the structure.

Table 8-17 Example: Dynamic limit load intensity factors

Limit state	Load intensity factor p
Given load level	1.00
Elastic limit state	0.73
Plastic limit state	3.78
Shakedown limit state	0.89

9 Special applications

Within this section, special applications for optimization strategies are discussed. They are selected from a wide range of design tasks, in order to demonstrate the universality of optimization strategies.

9.1 Generation of artificial time histories

Time history analyses in seismic design commonly require several input ground motions in order to assess the structural response behavior sufficiently. Only sets of time histories provide the statistically representative frequency content and amplitude. The number of required time histories is dependent on the selected code, e.g. three in [73] and seven in [105].

For this purpose, ground motion sets have been proposed, e.g. in [200,164], to match the requirements of local regions. For some seismically active regions in the world, the sets can be composed out of recorded accelerograms. As far as these ground motion sets cannot be obtained or transformed for other locations, artificially generated ground motions are applied that match design spectra provided in codes. Two groups of generation concepts can be distinguished, the generation in the frequency domain (indirectly) and in the time domain (direct method). All methods can be supported by application of optimization strategies. First applications of genetic algorithms for ground motion selection and scaling has been published in [160].

9.1.1 Classical generation in frequency domain

This version follows the traditional concept for derivation of artificial time history records. The method utilizes the similarities of Fourier and response spectra to achieve an approximation for the time history plot matching a given response spectrum. Among several methods, the method proposed in [109,84] is commonly applied. The method bases on a reverse Fourier transformation approach. It states, that any periodic function can be decomposed into a series of trigonometric functions, e.g. a sinusoidal representation for the acceleration time history

$$\ddot{u}_0(t,a) = I(t) \sum_{i=1}^{n} a_i \sin(\omega_i t + \Phi_i) \tag{9-1}$$

depending on the number of series n, the representation will be more or less approximate. In numerical calculations, the acceleration is determined for a number of discrete times from $t = t_0 \ldots t_{end}$ and discrete angular frequencies ω_i. The acceleration history is dependent on the vector a_i and Φ_i containing the amplitudes and phase angles of the ith component. The envelope function $I(t)$ is to assign the appearance of a real earthquake consisting of initialization, strong motion and phase-out periods. In Fig. 9-1 the most often applied envelopes are illustrated according to [210].

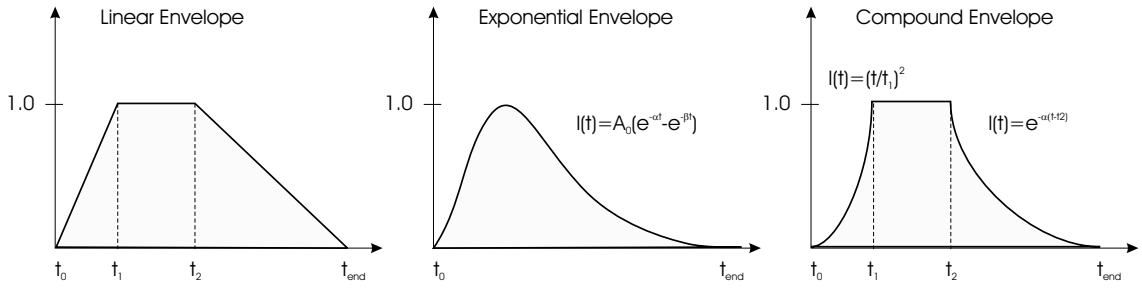

Figure 9-1 Shape functions for artificially generated time history plots

The corresponding response spectrum is calculated from time history analysis, with the previously generated acceleration function $\ddot{u}_0(t, a)$ that is dependent on the amplitude vector

$$Sa(\omega_i, \xi, \ddot{u}(t, a)) = \max |\ddot{u}(\omega, \xi, \ddot{u}_0(t, a), t)| \tag{9-2}$$

with Sa as the maximum response of an SDOF system over time $t_0 - t_{end}$, having the eigen angular frequency ω_i and considering the damping ratio ξ.

The phase angle field Φ must be pre-selected, either arbitrarily or calculated from a given time history that has comparable properties. In the classical procedure, the appropriate amplitudes are calculated in an iterative procedure. Starting with a constant vector other than zero, the amplitudes are improved according to the assumption that the ratio of the Fourier spectrum between the current a_i and target values $a_{T,i}$ behave approximately like the ratio in the response spectrum between the current Sa_i and target spectrum $Sa_{T,i}$ for a given eigenfrequency

$$\frac{a_{T,i}}{a_i} \approx \left(\frac{Sa_{T,i}}{Sa_i} \right)^{1...2} \tag{9-3}$$

This relation is used for iteration control, with $a_{i,new} = a_{T,i}$. The entire procedure is documented in Tab. 9-1. The iteration uses the newly obtained amplitudes for improvement of the approximation. The iteration stops if no further improvement is achieved. This particular form of iteration control has the disadvantage that the sign of the amplitude cannot change because the fraction term in Eq. (9-3) is always positive. A correction of deficiencies in the phase function is not possible. A change in the iteration control might be helpful.

The previously described strategy is numerically effective. However, the method often results in relatively large deviation errors in the approximation of the target response spectrum. Then the recommendation is to repeat the calculation with a new random phase function. Alternatively, the accuracy can be improved if the update of the amplitudes is performed with help of a nonlinear optimization routine. The design variables are the

Table 9-1 Classical artificial time history determination

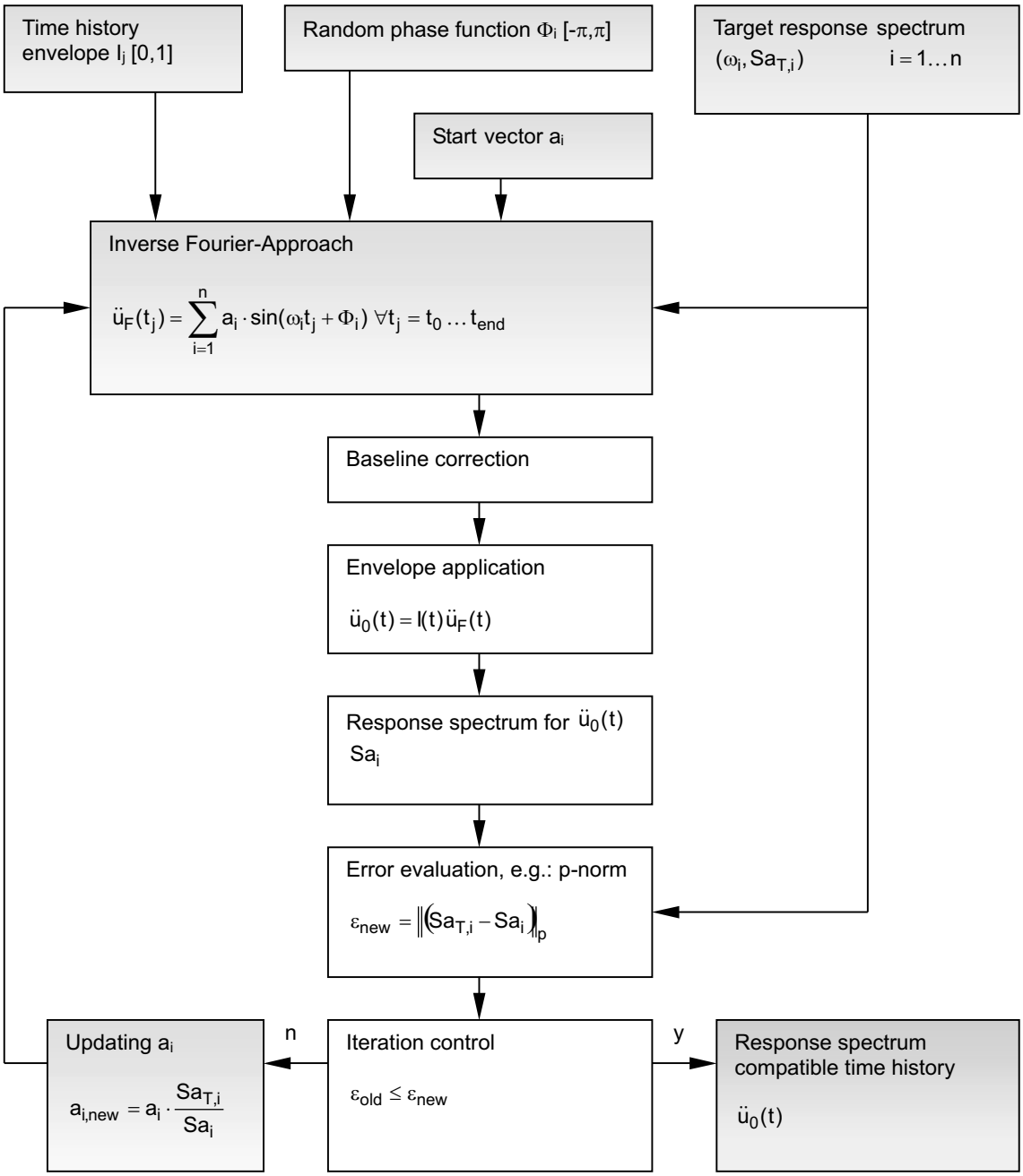

amplitudes a_i for which a minimum of the deviation from the target spectrum is to be found. The objective function is

$$O(a) = \|Sa_{T,i} - Sa_i(a)\| \rightarrow Min \tag{9-4}$$

with a baseline correction as a conditional subsidiary condition

$$\sum_t \ddot{u}_0(t,a) = 0 \tag{9-5}$$

Furthermore, the baseline correction can be even managed within the nonlinear objective function, thus a unconstrained nonlinear optimization problem is obtained. Those nonlinear optimization problems can be solved with help of gradient solvers. The accuracy is comparable or higher than in the classical iteration method. The accuracy can be further improved, if non-convex solving strategies, like successive search or genetic algorithm solvers (see Sec. 2) are applied. Most effective regarding the accuracy is a combination of non-convex and convex solving strategies.

The following advantages of optimization strategies compared to classical iterations can be noted:

- higher independence from chosen phase function
- improved solution control
- option for multi-stage improvement strategies

9.1.2 Example: Time history generation in frequency domain

The generation of artificial ground motions by modification of parameters in the frequency domain is demonstrated in the following example. A typical design acceleration spectrum is selected as target. The simulation of such spectra can be challenging because of the constant peak acceleration and the overall smooth spectrum characteristics.

The target spectrum, derived from Eurocode 8 [73], for spectrum type 1 and soil condition C, is applied for time history generation. The spectrum should be mapped in a period range from $0.05s$ up to $3s$. The damping is fixed at $\xi = 0.05$. The peak spectral acceleration is defined by $250cm/s^2$. The spectrum is drawn in Tab. 9-2.

The length of the desired time history is predefined by 20 seconds. A compound envelope function according to Fig. 9-2 is chosen. The calculation of the artificial data is done either by the classical approach according to Tab. 9-1 or alternatively by using the optimization approach Eq. (9-4,9-5). For start conditions, the amplitudes vector is selected as constant $Sa_i = 100cm/s^2$ and the phase function is randomly preselected (uniform distribution) in the range $-\pi \leq \Phi_i \leq \pi$.

The obtained result data are illustrated in Tab. 9-3. For comparison with the target response spectrum, the corresponding response spectra are introduced in Tab. 9-2. Whereas the results given by the classical approach show the typical peak-like deviations, the optimiza-

Table 9-2 Example: Time history generation in frequency domain

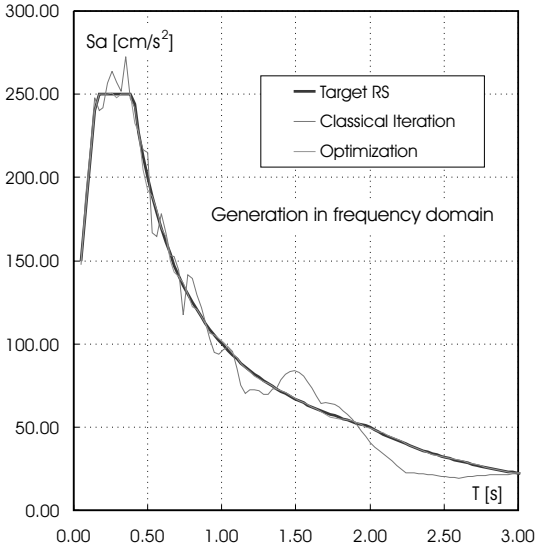

Target spectrum and result spectra from artificial time history generation

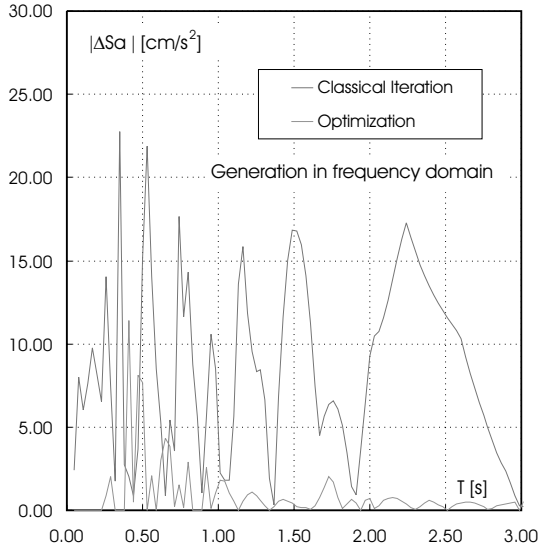

Absolute errors

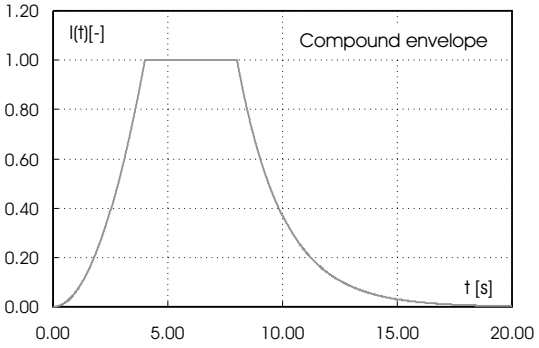

Figure 9-2 Example: Compound envelope function

tion routine produces almost a smooth spectrum. From the deviations plot the differences can be estimated for both calculation strategies. It should be noted, that these results can be improved, however for the classical method just by accident, finding a better fitting random phase function.

Table 9-3 Example: Artificial time history results obtained by modification of the spectrum amplitudes

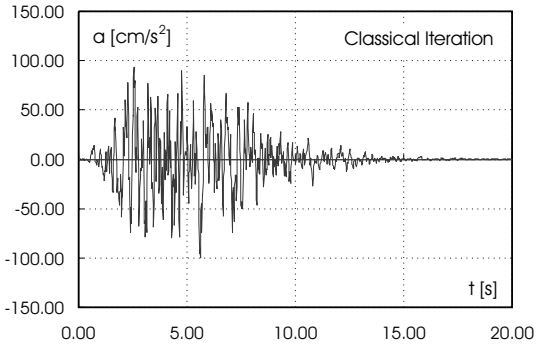

Generated by classical iteration method

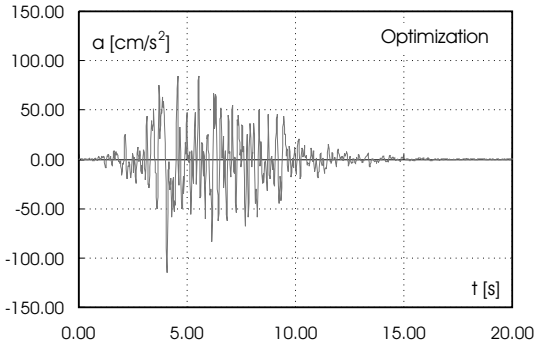

Generated by optimization method

9.1.3 Generation of statistically compatible artificial time histories

There are some suspicions about the level of reality of the ground motions generated with methods from the Sec. 9.1.1. The most obvious deviation to natural records is the obtained unrealistic high number of cycles in the time history. To mitigate this problem, there are several chances of correlating the problem to natural events, e.g. [210]. One alternative strategy is to affect the randomly chosen phase function Φ_i.

In Tab. 9-4, one strategy to derive improved phase angles estimates is sketched. The method uses real earthquake input. The motion record is treated with Fourier analysis, to calculate the phase function. For this function, the progress of phase differences are

$$\Delta\Phi_i = \Phi_i - \Phi_{i-1} \tag{9-6}$$

For this difference function, a cumulative density function is calculated to analyse the statistical distribution of the phase angle differences in the signal. This plot is used to generate randomly a new set of phase differences, showing the same cumulative density function as the natural event. Finally the differences are reassembled in order to obtain the new phase function. This phase function can now be used within the procedures of Sec. 9.1.1.

9.1.4 Example: Generation in frequency domain with statistically compatible phase function

The example from Sec. 9.1.2 is repeated with the same conditions, but for the case of statistically compatible phase functions. The selected original time history is given in Tab. 9-5 together with the appropriate cumulative density function of the phase differences. From this the new phase function is calculated according to the strategy of Tab. 9-4. The time history result is given in Tab. 9-6. As well, a randomly generated phase function is plotted for comparison. It is obvious, that the compatible phase angles behave more periodic.

Table 9-4 Statistically compatible phase function generation

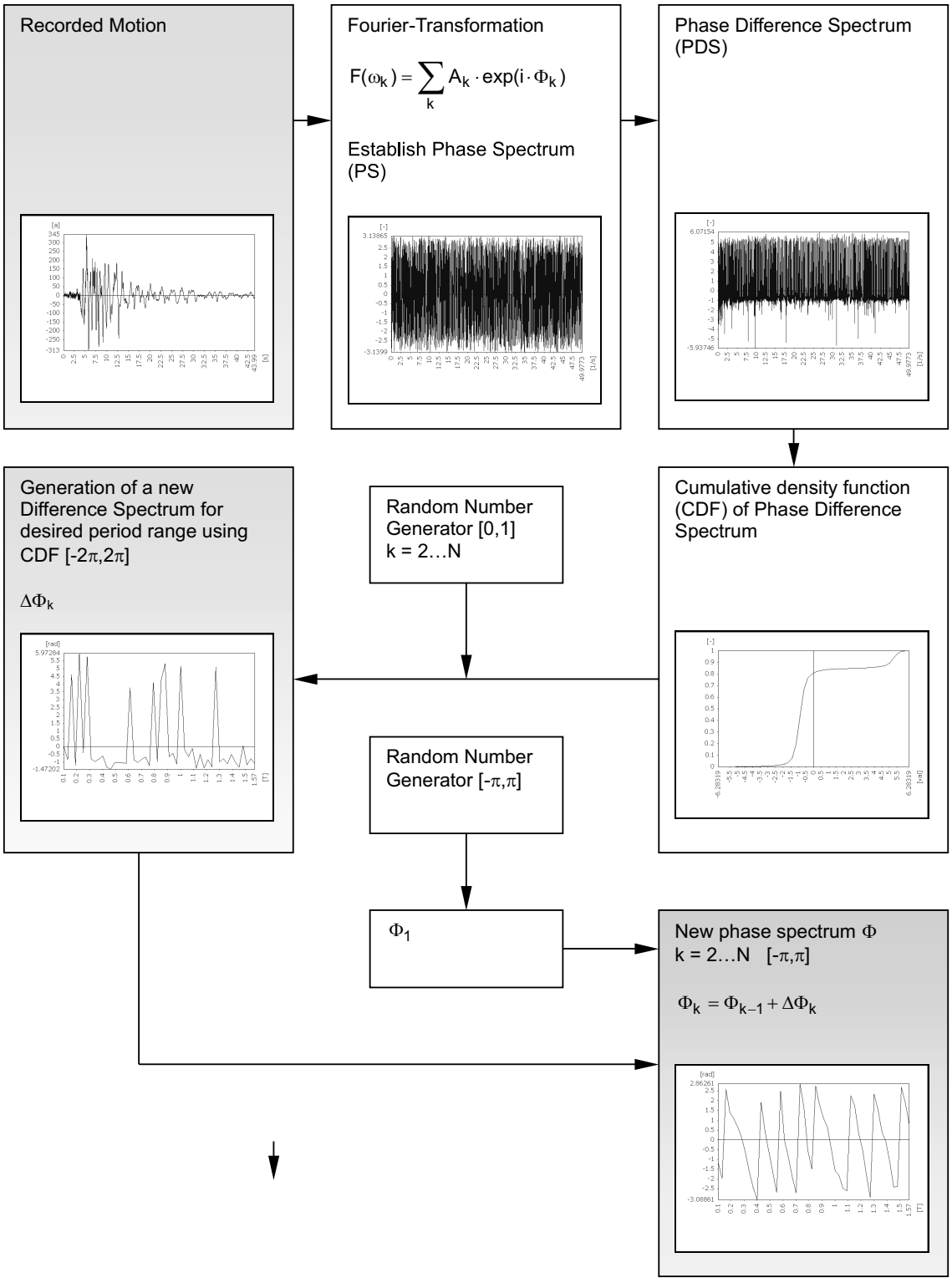

Table 9-5 Example: Input time history

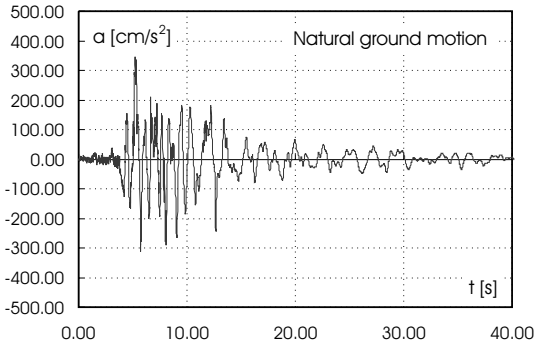

Acceleration record

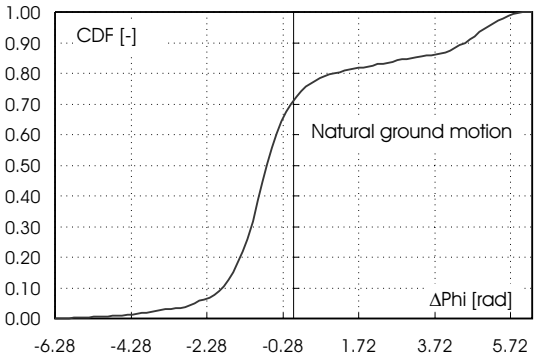

Cumulative density function of phase differences

Table 9-6 Example: Phase function generation

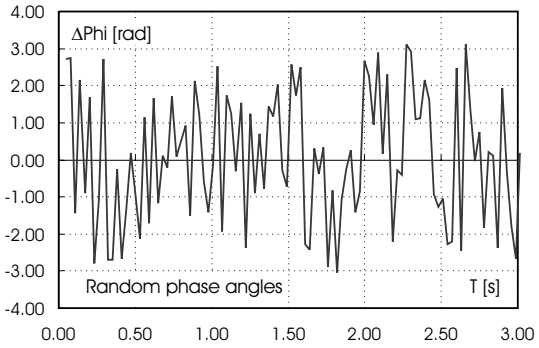

Randomly generated

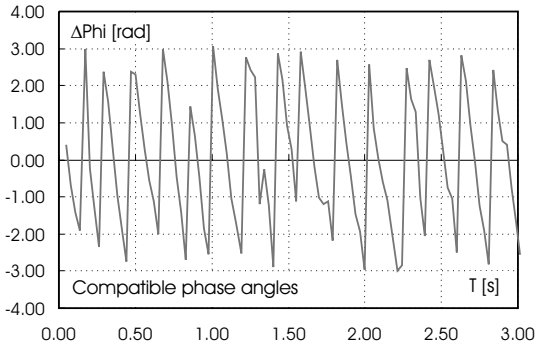

Statistically compatible

This phase function is applied in the generation of the artificial ground motion. The ground motion result is plotted in Tab. 9-7 as well as the appropriate acceleration spectrum.

9.1.5 Generation in time domain

Using the advantages of optimization approaches, the question is, why the generation of artificial time histories should be performed in the frequency domain, as proposed in the traditional methods. The generation in the time domain contains several options to include specific time effects as e.g.

- influence time characteristics (change of frequency content in time)
- influence number of cycles
- influence number, time and amplitude of extreme peaks.

Table 9-7 Example: Artificial ground motion

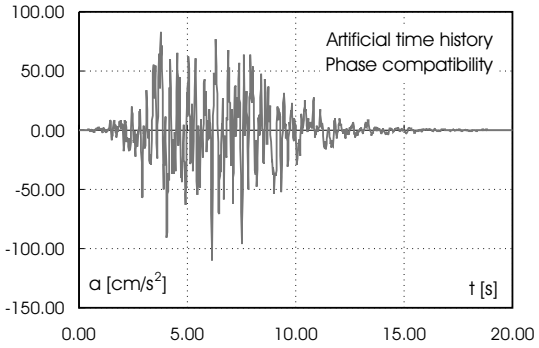

Acceleration plot

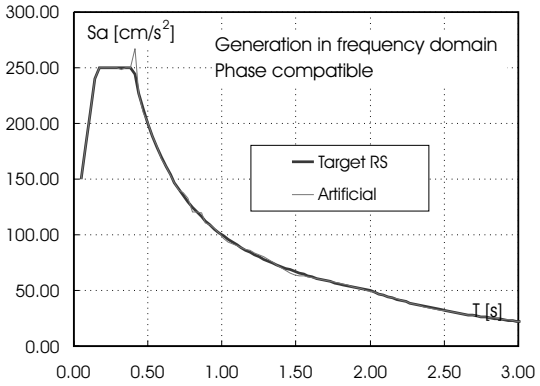

Acceleration spectrum in comparison to the target spectrum

The appropriate problem can be solved with optimization algorithms. The following objective

$$O(\ddot{u}_0(t)) = \|Sa_{T,i} - Sa_i(\ddot{u}_0(t))\| \rightarrow Min \tag{9-7}$$

can be stated, subjected to a baseline correction

$$\sum_t \ddot{u}_0(t) = 0 \tag{9-8}$$

In contrast to the problem (9-4-9-5), the time history itself is the design variable. The objective function is evaluating the generated history in comparison to the target spectrum. However, the number of unknowns is usually increased, if an appropriate time increment and length of the ground motion has to be obtained.

Modifications on the artificial time history can be introduced in two ways:

- formulating additional subsidiary conditions
- using specified start vectors.

The last way is preferable, as the main characteristics of the starting vector is mostly preserved during the calculation. And the problem size and therefore the numerical efficiency is not changed.

9.1.6 Example: Artificial time history generation in time domain

The generation method in the time domain is illustrated in an example. The target spectrum from Sec. 9.1.2 is applied in the same period range. The method is applied for two cases
(a) Generation with random start vector
(b) Generation with a superposition of 50% random and 50% sinusoidal content

Table 9-8 Example: Generation in time domain using random start vector

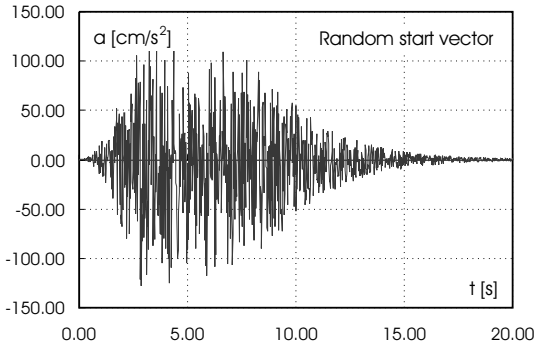

Table 9-9 Example: Generation in time domain

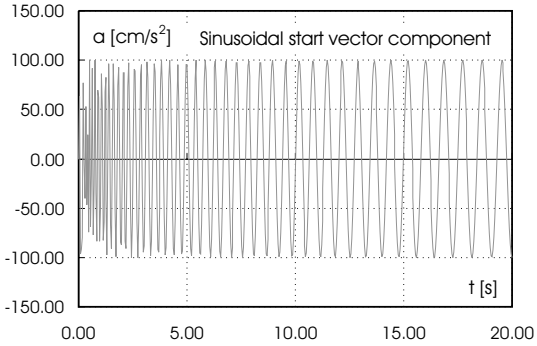

Sinus function for superposition

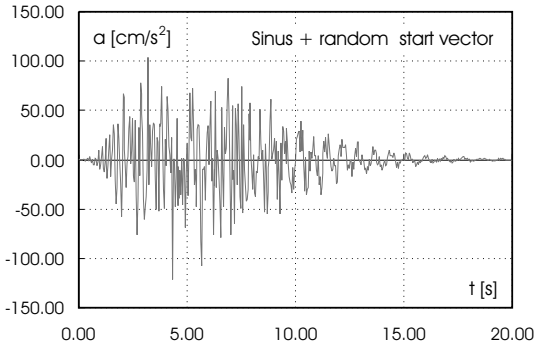

Time history generated using sinusoidal and random start vector

In the first case the components of the start vector are randomly generated with a uniform distribution in the range of $-200cm/s^2 \leq \ddot{u}_0(t) \leq 200cm/s^2$. The obtained vector is multiplied by the compound envelope function of Fig. 9-2. The result is given in Tab. 9-8. It is visible that the number of cycles is relatively high.

The conditions for the second case are similar, however the start vector contains the sum of a uniform randomly generated part and a sinusoidal function, both in the range of $-100cm/s^2 \leq \ddot{u}_0(t) \leq 100cm/s^2$. The sinusoidal function is a swelling function, simulating the fact that the long period content in real earthquakes is increasing with time. The sinusoidal function is illustrated in Tab. 9-9.

Table 9-10 Example: Spectra for random and sinusoidal+random case

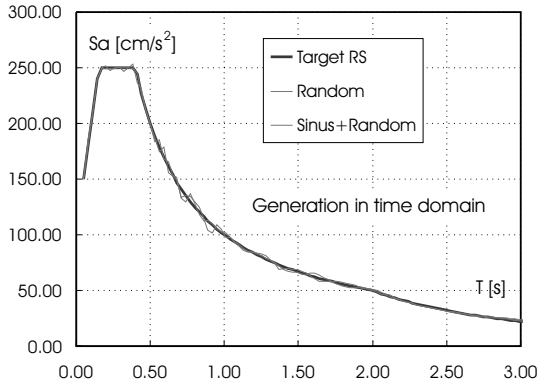

9.1.7 Generation of time history sets

The application of single time histories is not advisable in the design of structures. Several calculations with different time histories must be conducted. This applies also to artificially generated ground motions. It is possible to generate sets that fulfill statistical requirements. In general, both the generation in the frequency and time domain can be utilized for this task. According to the selected number of earthquakes $j = 1 \dots n_{EQ}$ the following optimization task can be solved

$$O(\ddot{u}_{0,1}(t) \dots u_{0,n_{EQ}}(t)) = \left\| Sa_{T,i} - \frac{1}{n_{EQ}} \sum_{j=1} n_{EQ} Sa_i(\ddot{u}_0(t,j)) \right\| \rightarrow Min \tag{9-9}$$

subjected to n_{EQ} subsidiary conditions for managing the baseline correction

$$\sum_t \ddot{u}_0(t,j) = 0 \tag{9-10}$$

This form is an example for a generation in time domain. The appropriate frequency domain model can be formulated similarly. In addition to the mean calculation, the objective function can be completed by the evaluation of the standard deviation. This is demonstrated in the following example.

9.1.8 Example: Artificial time history set generation

The combined generation of 10 time history sets is demonstrated in this example. The objective is to have a set with a mean spectrum according to the example of Sec. 9.1.2 and with a target standard deviation of $\sigma_T = 40 cm/s^2$ in the entire period range. For variety, the envelope functions are changed for any member of the set. The following optimization problem is solved

Table 9-11 Example: Generation of time history set

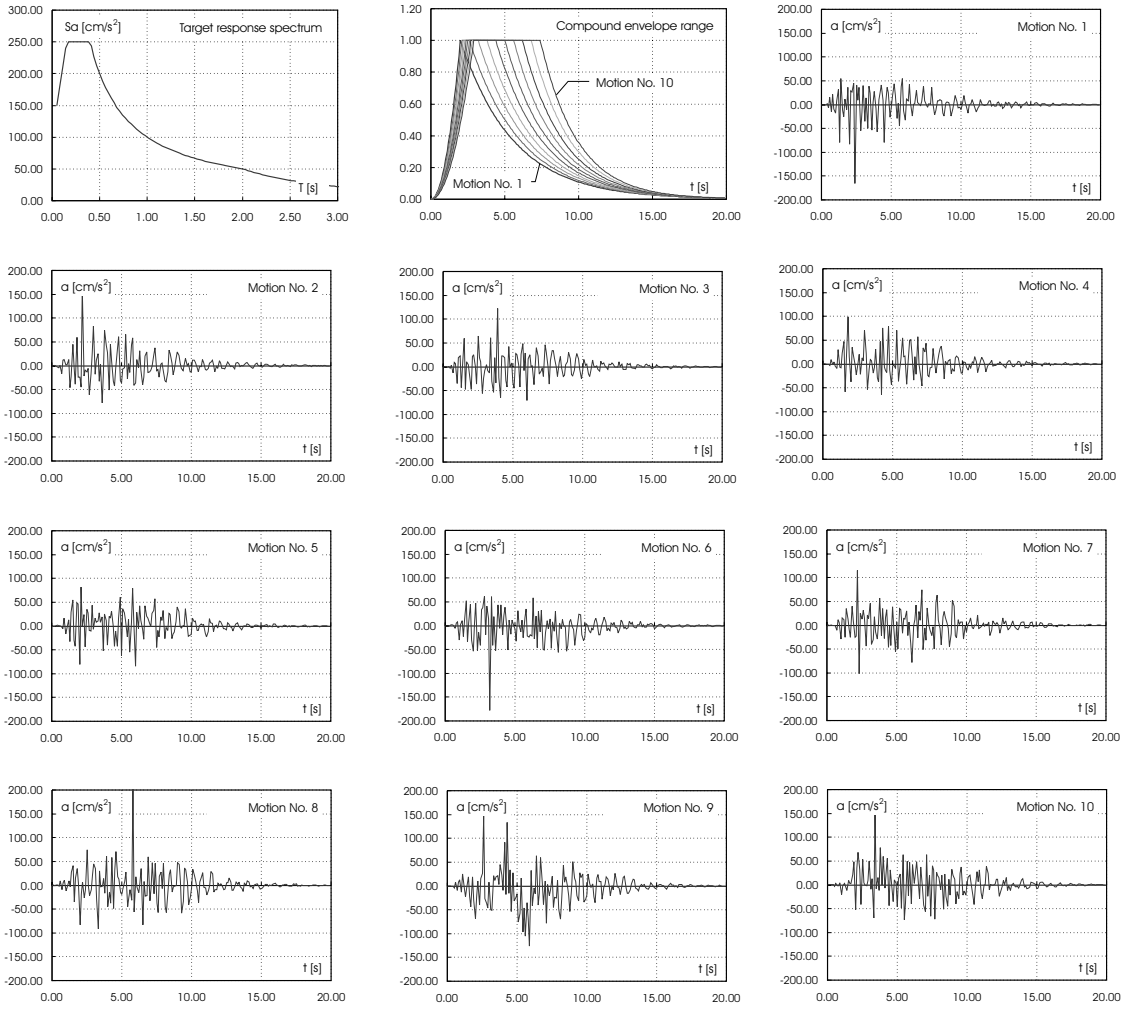

$$\left\| Sa_{T,i} - \frac{1}{n_{EQ}} \sum_{j=1}^{n_{EQ}} Sa_i(\ddot{u}_0(t,j)) \right\| + \|\sigma_{T,i} - \sigma_i(\ddot{u}_0(t, j = 1 \ldots n_{EQ}))\| \rightarrow Min \qquad (9\text{-}11)$$

subjected to Eq. (9-10).

For special importance weighting of either the mean or the standard deviation some weight factors can be introduced for the terms in Eq. (9-11). The target spectrum, the envelope and the generated ground motions are given in Tab. 9-11. The resulting spectra for all single time histories and the statistical evaluation is plotted in Tab. 9-12.

Table 9-12 Example: Spectra of ground motion sets

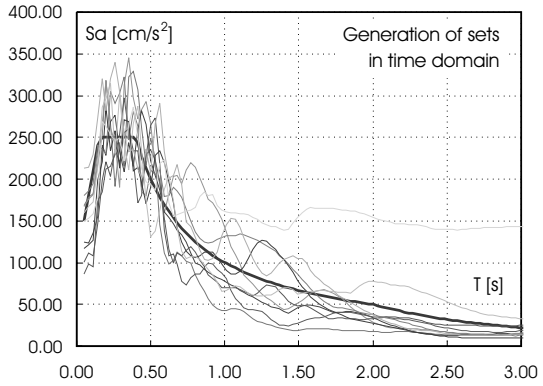

All spectra

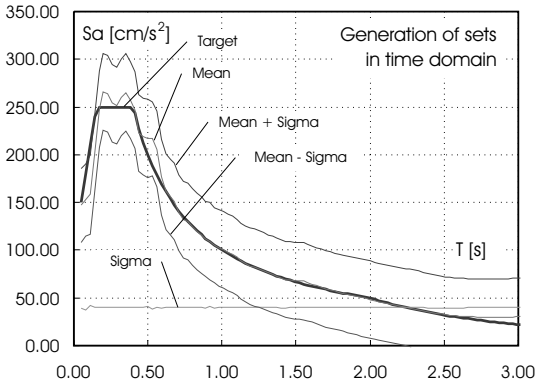

Mean and standard deviation

9.2 Determination of pseudo spectral reduction coefficients

In simplified analysis according to Secs. 6 or 7, maximum structural deformations are traditionally calculated from pseudo-accelerations PSa_ξ. Examples of spectra, calculated by time history analysis are given in Tab. 9-13. Instead of calculating all spectral values for damping ratios ξ directly by time-history analysis, PSa_ξ is derived from pseudo-acceleration spectra with fixed-damping ratios (typically 5%) by utilizing reduction coefficients R

$$R = \frac{PSa_{5\%}}{PSa_\xi} \tag{9-12}$$

In Tab. 9-14 an example is given for the reduction coefficient, that can be calculated via time history analysis.

Among others, easy-to-use expressions such as the reduction formula given in [73], based on investigations in [34,35] are often applied

$$R_{EC8} = \left(\frac{10}{100\xi + 5}\right)^{-0.5} \tag{9-13}$$

Alternatively, according to the Japanese code [24]

$$R_{BCJ} = \left(\frac{1.5}{10\xi + 1}\right)^{-1} \tag{9-14}$$

or according to Kawashima/Aizawa [122]

$$R_{KA} = \left(\frac{1.5}{40\xi + 1} + 0.5\right)^{-1} \tag{9-15}$$

Table 9-13 Mean acceleration spectra of ground motion sets with applied damping

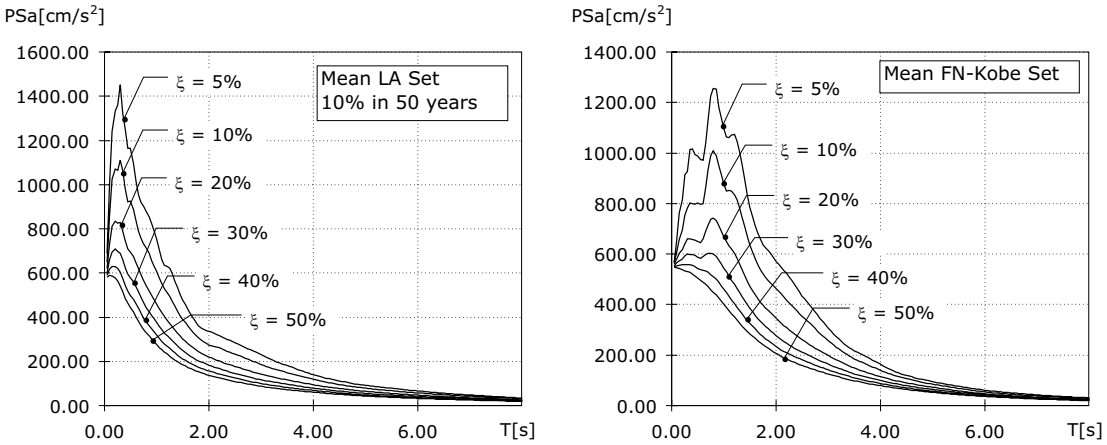

Table 9-14 Reduction coefficients calculated by time-history analysis

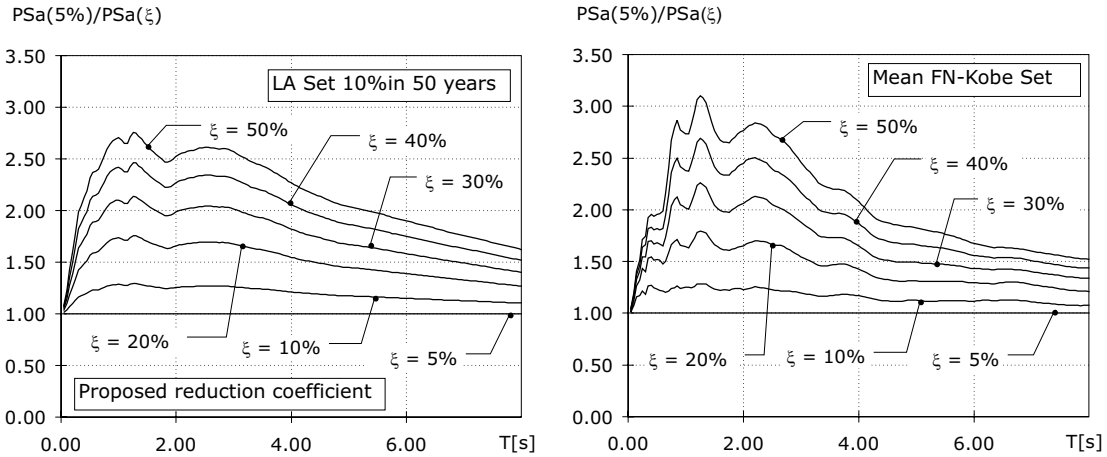

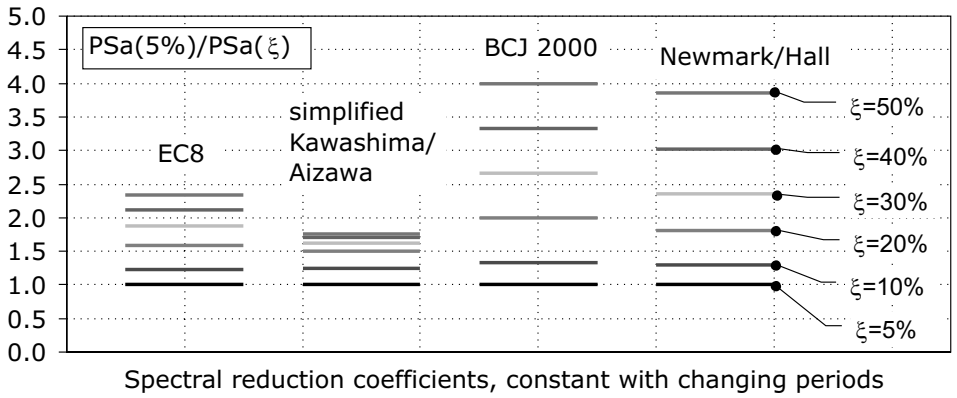

Figure 9-3 Comparison of different period-independent reduction coefficients

or following Newmark-Hall [167]

$$R_{NH} = \left(\frac{3.21 - 0.68 \ln(100\xi)}{2.12} \right)^{-1} \tag{9-16}$$

It should be noted that these formulas are originally derived with specific background and intension and therefore, as illustrated in Fig. 9-3, are leading to significant differences in the reduction. Nevertheless they are often found to be recommended unchanged for use in extended fields of application, as for seismic isolation design e.g. [8,30]. Further comparison of the concepts is given in Fig. 9-4.

Considerable deviations have been observed in [221], that are caused if the formula is applied independently from the period of vibration. As illustrated in Tab. 9-14, the actual relationships are highly nonlinear with respect to the natural period. Furthermore, they are dependent on the specific time-history. To include this attribute in the reduction concept, a period-dependent modification is proposed. As viscous damping is related to velocity (see similarity between the coefficient in Tab. 9-14 and the 5% damped pseudo-velocity spectrum $PSv_{5\%}$ in Tab. 9-15, the reduction of the pseudo-acceleration spectrum due to different damping ratios can be established with help of a velocity-based coefficient

$$R_{mod} = 1 + (R_\xi - 1)\frac{1}{\eta_1} PSv_{5\%} \tag{9-17}$$

Herein R_ξ denotes a reduction coefficient, dependent only on the damping ratio. The last term includes the period dependency. Principally, this concept adds a period dependency to any period-independent reduction formula, hence R_ξ can be replaced, e.g. by R_{EC8} in Eq. (9-13). The coefficient η_1 is constant for each specific ground motion or ground motion set and can be determined by means of mathematical optimization.

The following nonlinear optimization problem can be solved

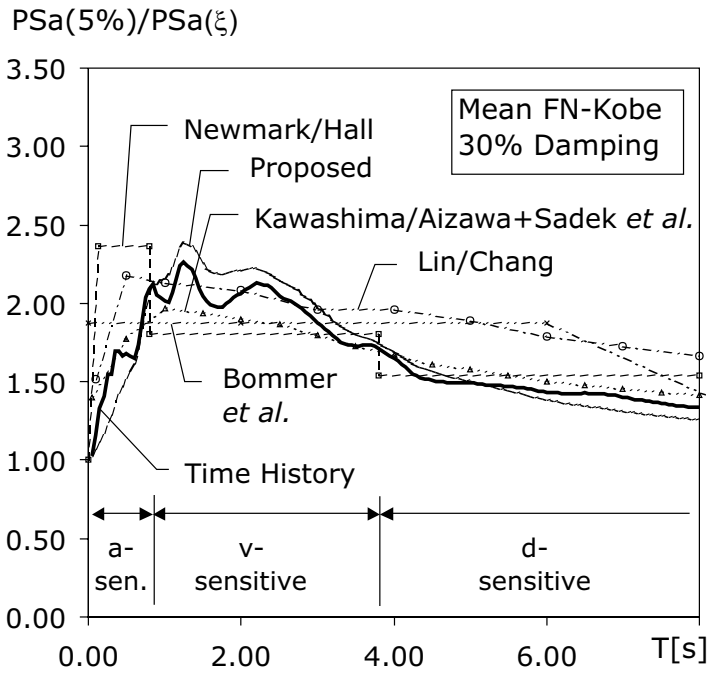

Figure 9-4 Comparison of reduction concepts for damping ratio of 30%

Table 9-15 Pseudo velocity spectra

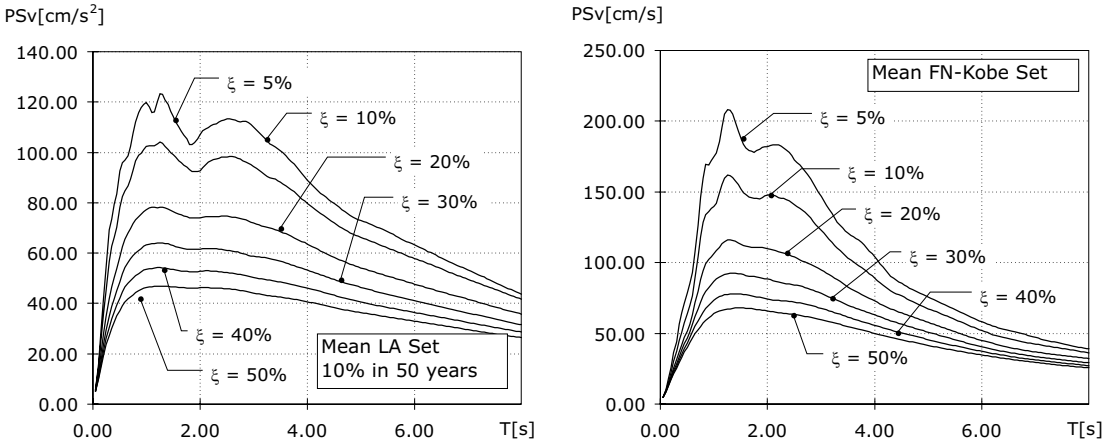

Table 9-16 Proposed approximation

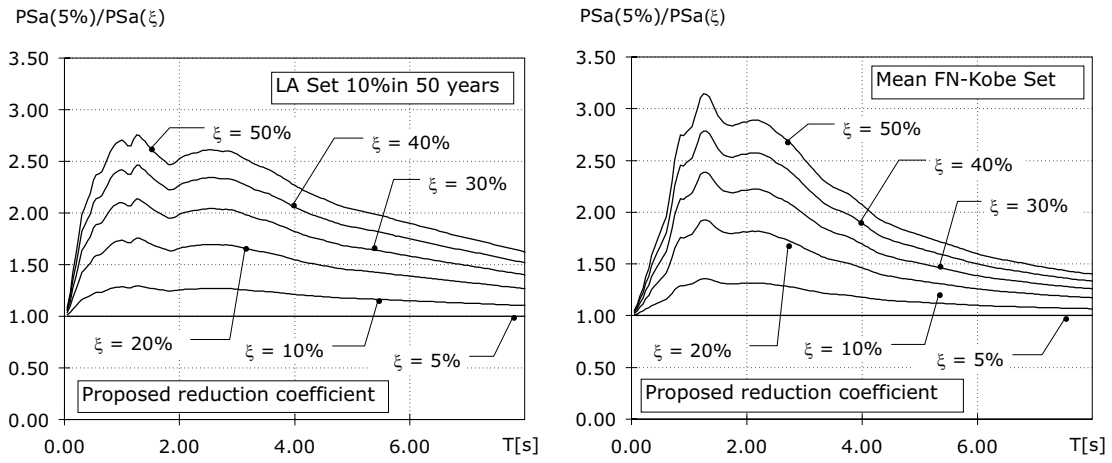

$$O(\eta_1) = \|PSa(eta_1, \xi) - PSa_{TH}(\xi)\| \rightarrow min \tag{9-18}$$

in order to determine the optimum value for η_1, matching several levels of damping (e.g. $\xi = 5 \ldots 50\%$). $PSa(eta_1, \xi)$ is the mean pseudo acceleration spectrum generated by a standard 5% spectrum reduced by multiplication of $R_{mod}(\eta_1)$ (Eq. (9-17)). $PSa_{TH}(\xi)$ is the mean pseudo acceleration spectrum calculated by time history analysis. This task can be solved by gradient solvers for unconstrained problems. For example, the value of eta_1 is 1.31m/s for the Kobe near fault set (Sec. 11.6) and 0.95m/s for the LA10in50 set of SAC/FEMA Project (Sec. 11.7). The example result for the Kobe and LA set is given in Tab. 9-16. The good agreement to the time history results in Tab. 9-14 is obvious.

As published in [221], the determination of the parameter η_1 can be further simplified. The procedure is documented in Appendix Sec. 11.2. According to Appendix Sec. 11.3 the appropriate conversation between pseudo to total acceleration values can be achieved.

9.3 Design of base-isolated structures for low acceleration transmissions

9.3.1 Introduction

Recent seismic events triggered the introduction of special near-field regulations in most codes [105,24,73] this results in modifications for the design motion level. This applies also for base isolated structures. Those codes propose the avoidance of collisions due to ultimate seismic excitations. In order to achieve this objective, the design has to consider either larger or stiffer, highly damping devices, resulting in increased super-structural responses also in lower excitation levels. The costs are rising and the benefits gained from the isolation effects are reduced. This is contradictory to the fact that such events are rather seldom. So dependent on the local conditions, alternative design strategies that consider explicitly collisions, can be an economic compromise 9-17. This also includes cases where less clearance to surrounding facilities can be provided as in urban areas.

Table 9-17 Pounding problem

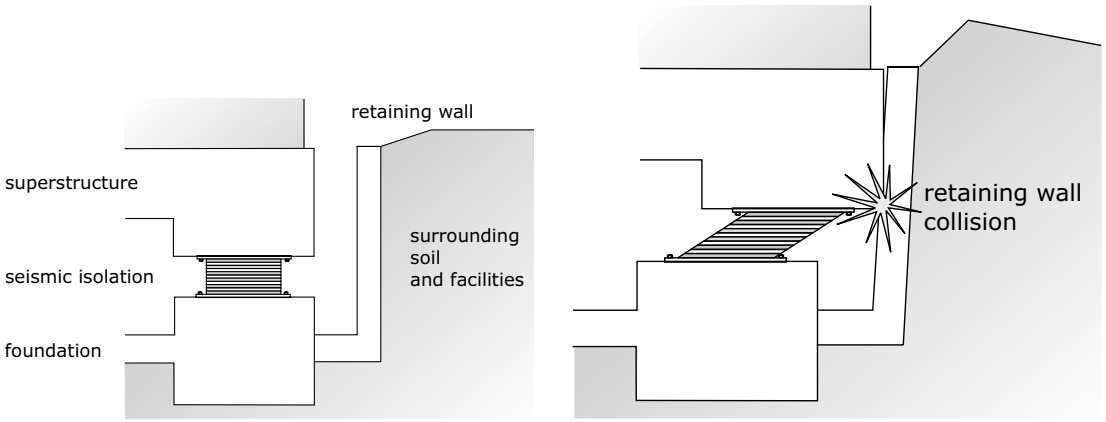

This section concentrates on passively isolated structures. The collision of structures has been discussed in [50]. Kawashima et al. [139,123,191,192,215] investigated colliding bridge decks, wave propagation and appropriate retrofit measures. DesRoches and Muthukumar analyzed multiple-frame bridges [67]. Unjoh et al. mentioned a utilization of collisions as a possible energy dissipation option [209]. Kashiwa et al. [119] explored the influences of different retaining wall characteristics on the inter-story drifts during crashes of base-isolated structures.

Already for the design without collision according to classical perceptions, the configuration of a base isolation layer is challenging, because an appropriate device combination has to be selected that respects different influences, risks and constraints. The device configuration needs to be balanced for a generally stochastic excitation considering safety and serviceability demands. Involving extreme changes of the device parameters in the considerations as well as collisions against device stops or surrounding facilities will dramatically increase the efforts during design.

A general approach for solving multi-parameter-multi-constraint design problems is given by the mathematical optimization. This approach provides a general interface for the definition of mechanical problems and combines it with effective computational treatment. The existence of optimum parameter combinations for base-isolated structures has been explored by Jangid [108]. Sinha and Li [199] presented a design strategy involving additional absorbers . Constantinou and Tadjbakish [57,58] developed a general design strategy for base isolated structures based on optimization routines, involving a probabilistic approach . Baratta and Corbi [19] examined soil-structure interactions within their optimization models based on energy approaches . Kaplan and Seireg as well as Moreschi and Sing [117,155] describe design procedures for specific isolation systems . Takewaki [203] quantifies influences of stiffness and damping within optimum designs . Kitagawa et al. [204,114] presented a selection strategy for isolation devices with help of genetic/simulated annealing algorithms.

9.3.2 Mechanical model

In order to reflect the nonlinear behavior in base isolated structures and the nonlinear behavior of the retaining wall, a multi-linear model is applied. This model is assembled by superposition of n linear-elastic perfectly-plastic bodies. Each body is defined by the deformation u_0 describing the starting point of linear excitations, the deformation u_y denoting the deformation at the yield limit and the yield force f. In order to determine the ultimate shear force F_u in the isolation interface, the ultimate deformation u_u in the structure the number n_e of elastically remaining bodies and the number n_p of in-elastically deformed bodies has to be known. Then the ultimate force can be calculated by

$$F_u = \sum_{i=1}^{np} f_i + \sum_{j=1}^{ne} f_j \frac{u_u - u_{0,j}}{u_{y,j} - u_{0,j}} \tag{9-19}$$

The underlying concept is additionally illustrated in Fig. 9-5. Equation (9-19) can be conveniently used in time history approaches. However in some countries, the exclusive use of time history approaches for design is not permitted. According to the codes [105,73], the design has to be based on (or at least accompanied by) simplified considerations using response spectra. Furthermore, time history approaches can be computationally expensive within optimization processes, especially if several ground motion out of motion sets need to be evaluated. Simplifications can be beneficially used in the pre-design phase to provide starting vectors for further optimization.

In order to utilize the hardening options specified in the material law Eq. (9-19) only the application of simplified nonlinear methods can cover all possible combinations. The adaptation of a special procedure derived for base isolated structures described in Sec. 7.7 consisting of a combined pushover and capacity spectrum approach is suggested.

9.3.3 Simplified pounding model

The response due to a collision event is dependent on the characteristics of the retaining wall - soil interaction and the velocity of the structure prior to the collision. After the collision the structure, retaining wall and system behaves like a coupled system. The behavior of this system can be simplified by stating a linear equivalent system. If the superstructure can be assumed to be rigid, the structural system can be simplified as a single mass M. The appropriate stiffness consists of the stiffness $K_{b,equ}$ of the structure and $K_{w,equ}$ of the wall/soil compound according to Fig. a.) in Tab. 9-18. Both values are dependent on the deformation u or on Δu, describing the intrusion depth of the superstructure.

The velocity and the acceleration of the structure at the wall $\dot{u}_w$ and $\ddot{u}_w$ can be approximately determined from the responses of a non-colliding system $\ddot{u}_{free}$, u_{free} and $\dot{u}_{free}$ by

$$\dot{u}_w = \dot{u}_{free} \cos\left(\frac{u_w}{u_{free}}\right) \tag{9-20}$$

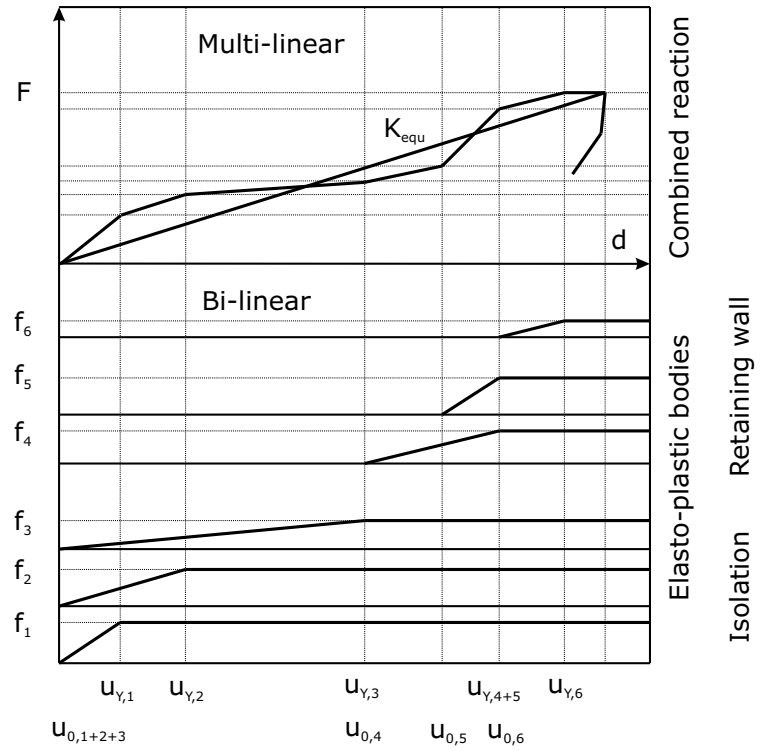

Figure 9-5 Composition of multi-linear material law out of several elastic perfectly-plastic bodies

Table 9-18 Simplified pounding analysis

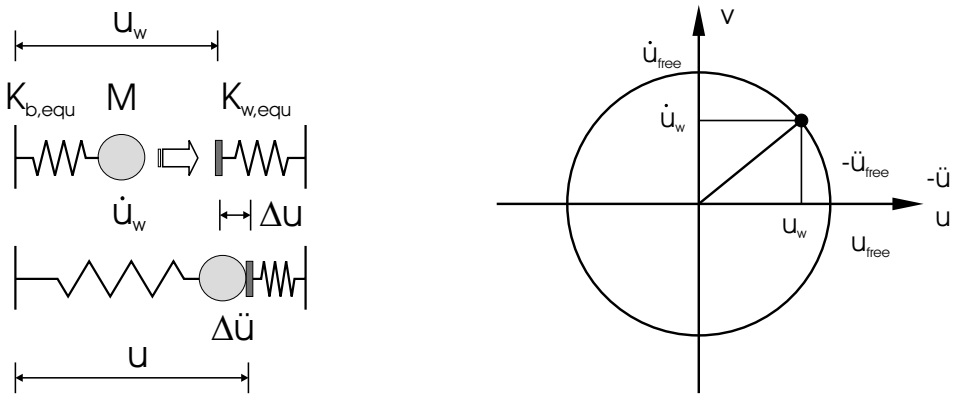

a.) Model configuration and parameters

b.) Phase diagram

$$\ddot{u}_w = \ddot{u}_{free} \sin\left(\frac{u_w}{u_{free}}\right) \tag{9-21}$$

Figure b.) in Tab. 9-18 shows this relationship, for stationary responses. Hence, for an SDOF system, the change in the acceleration as a result of the collision is

$$\Delta\ddot{u} = \dot{u}_w \sqrt{\frac{K_{b,equ} + K_{w,equ}}{M}} \tag{9-22}$$

The appropriate intrusion depth is

$$\Delta u = \dot{u}_w \sqrt{\frac{M}{K_{b,equ} + K_{w,equ}}} \tag{9-23}$$

The overall accelerations and deformations can be estimated as

$$\ddot{u} = \ddot{u}_w + \Delta\ddot{u} \tag{9-24}$$

$$u = u_w + \Delta u \tag{9-25}$$

9.3.4 Solution Strategy

The given problems are nonlinear and contain a considerable amount of design variables. Herein not only the determination of an optimal designed isolation layer is of interest, also necessary design or retrofit measures for the superstructure have to be considered. As for any design or retrofit a minimum of measures is demanded, optimization problems have to be solved. The utilization of computational approaches is beneficial, so means of the nonlinear mathematical programming are proposed for application.

As a result of the analysis the design parameters are given, such as the characteristic of the base isolation layer. These parameters have to be translated into device properties. Despite catalog devices usually provided by the manufacturers, nowadays industry is prepared to provide the devices with exact specified properties. Hence the calculation with continuous coefficients can be conducted. As seen in the parametric maps of Fig. 9-19 the parametric surfaces are dependent on the ground motion. These figures have been calculated for a 2DOF configuration by time history analysis using the Kobe near-fault set from Appendix Sec. 11.6. In the cases, that the calculations can be based on time history sets, all functions are practically convex as can be seen in the last figure. Thus, the use of convex, nonlinear optimization algorithms is mostly appropriate. Gradient solvers can be used conveniently for calculation. Suitable start vectors can be obtained by using simplified methods as described in Sec. 7.

Table 9-19 Plots for deformations, dependent on yield force and post-yield stiffness at base level for 2DOF example

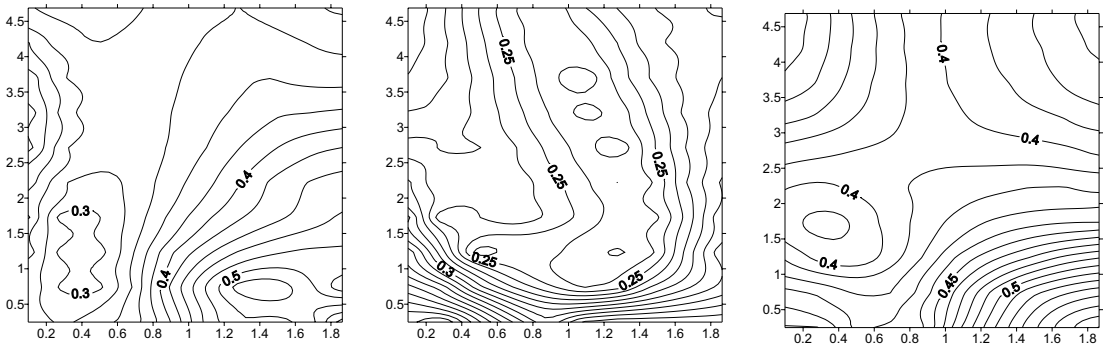

Kobe set component FN-AMC | Kobe set component FN-KOB | Kobe set mean

9.3.5 Optimum design strategies for buildings with potential collision

9.3.5.1 Strategy I: Prevention of collision

The first way is to prevent the collision by implementing additional devices that regulate the deformations due to the given limits. This option can be applied by adding stiffness, hysteretic or viscous damping to existing isolation components. This option seams best for cases in that the accelerations are determining the structural configuration, because any bumping will increase the accelerations dramatically. However, these measures are also influencing the responses in smaller earthquakes, because the accelerations are higher due to the accompanied increase in the effective stiffness.

Traditionally, the prevention of collision has to be considered as the primary objective. The retrofit task is closely related to the design of new buildings. The simplest way is the enlargement of the given clearance. However this is not always an option, because of given constraints in the vicinity. Moreover, device limits restrict possible deflections as well. The deformations can be restricted by reducing the flexibility of the layer and by incorporation of damping. Several measures or combinations are possible to consider, involving

- additional stiffness
- additional hysteretic damping
- additional viscous damping

It should be noted, that the addition of devices will commonly induce higher responses in the superstructure. This measure is often appropriate, if the superstructural accelerations are not the primary objective in the design.

To find an optimum combination is a challenging task in engineering. The design can be supported by optimization. The derivation of appropriate optimization schemes for the

design of base isolated structures is explained for structures that do not or only negligibly exhibit changes in the post-yield behavior. This case applies for the majority of projects that combine natural rubber bearings with hysteretic or viscous dampers or sliders. The simplest model of such a structure can be constructed by implementing a linear super-structure and a bilinear isolation system. As the super-structural parameters are typically unchanged the problem is only dependent on four parameters that are

- Post-yield stiffness K
- Ratio to the initial stiffness γ
- Elastic limit force F in the isolation interface
- Additional viscous damping ξ_v

contained in the vector of design variables.

Representing the maximum observed structural responses, the evaluation of the following parameters is of interest:

- Deformation u_s in the superstructure
- Deformation at base level u_b
- Acceleration $\ddot{u}_s$ in the superstructure
- Shear force F_s in the superstructure

that can be expressed as response functions dependent on the design variables.

$$r = r\left(u_s(x), u_b(x), \ddot{u}_s(x), F_s(x)\right) \tag{9-26}$$

Thus the following general optimization problem can be stated:

$$O(x, r) \rightarrow Min \tag{9-27}$$

$$g(x, r) \leq g_{lim} \tag{9-28}$$

The constraint functions are dependent on limit values g_{lim}.

9.3.5.2 Example Strategy I

The application of these problems is demonstrated with help of an example. A 2DOF model is applied with 1000t superstructural mass and 200t at the base level. The fixed base period is 1.3sec. The structure is subjected to mean Kobe set excitations according to Appendix Sec. 11.6. The maximum provided clearance is 40cm. Pounding has to be prevented.

Case a.): The objective is to find the appropriate stiffness K_b and yield force F_b of the isolation layer that minimize the accelerations in the superstructure $\ddot{u}_s$, while keeping a maximum deformations u_b at base level of 0.4m. The stiffness ratio is fixed to $\gamma_b =$

0.6. The design variables are restricted to lower limits to ensure the performance under serviceability conditions. The following optimization problem is solved:

$$O(K_b, F_b) = \ddot{u}_s \rightarrow Min \tag{9-29}$$

$$u_b \leq 0.4 \tag{9-30}$$

$$F_b \geq 200 \tag{9-31}$$

$$K_b \geq 1200 \tag{9-32}$$

The optimum solution is $K_b = 1557kN/m$ and $F_b = 252kN$, providing exactly the limit base deformation $u_b = 0.4m$, a roof deformation of $u_s = 0.42m$ and acceleration $\ddot{u}_s = 0.76m/s^2$.

Case b.): If Case a.) is changed in order to minimize the deformations, the following problem has to be solved:

$$O(K_b, F_b) = u_b \rightarrow Min \tag{9-33}$$

$$u_b \leq 0.4 \tag{9-34}$$

$$\ddot{u}_s \leq 1.0 \tag{9-35}$$

$$F_b \geq 200 \tag{9-36}$$

$$K_b \geq 1200 \tag{9-37}$$

In this case the acceleration have to be restricted as well. The optimal solution is $K_b = 1925kN/m$ and $F_b = 372kN$, having a base deformation $u_b = 0.38m$ and roof deformation $u_s = 0.40$. The acceleration is $\ddot{u}_s = 1.0m/s^2$.

The deformations and accelerations due to the Cases a.) and b.) are indicated in the contour plots of Tab. 9-20. Here a parameter area is given in dependence on the isolation layer parameters. Whereas the accelerations are monotonically changing in this parameter range, the deformations show a distinct minimum.

The introduction of additional viscous damping is another option to limit the deformations. As well this measure is increasing the effective stiffness of the structure as well, thus leading to higher accelerations for high level events. But compared to hysteretic damping the increase is velocity dependent. The calculation of an optimum amount of viscous damping can be determined by solving optimization problems.

Table 9-20 Example Strategy I: Deformations and accelerations for varied isolation stiffness K and yield force F, solutions to the design cases a.) and b.)

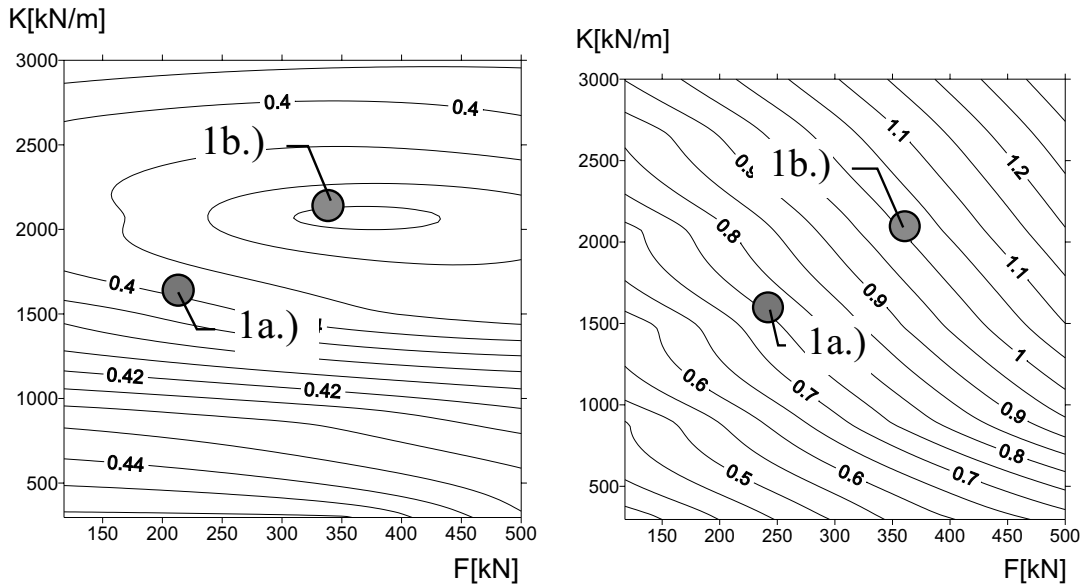

9.3.5.3 Strategy II: Acceptance of collision

In the traditional design, collision is completely prevented. However, recent events, like the Mid Niigata Prefecture (Chuetsu) Earthquake in Oct. 2004 show that ground accelerations can be far beyond design levels. Such rare events exceed the serviceability and security levels. The knowledge will influence new design but will lead to some review and retrofit requirements for existing structures. However, in the case of insufficient performance the means to prevent collision are limited. New design has better chances to consider extended levels of excitation.

However, basing the design on this load level will dramatically change the demands for the isolation interface. Furthermore, as device sizes and clearances cannot be scaled unlimited, more damping and stiffness is usually incorporated for control of the deformations, that increases costs. This is increasing the superstructural responses and therefore reducing the efficiency of seismic isolation for lower excitation levels. Considering the occurrence probability of such events, the influences on the design and the resulting costs can be significant. In those cases the consideration of an additional design option, the acceptance of collisions, can be beneficial.

But the collision has also positive effects. Firstly, limiting deformations that is important to maintain the operability of the isolation devices and secondly, during the collision additional energy is dissipated in the retaining wall and the soil.

The following principles for the design should be followed:

- Bumping against the surrounding walls should be as soft as possible
- Movement should stop before ultimate device limits are reached
- The superstructure has to survive without major damage
- The local strengthening effect in the corners, where the retaining walls merge, should be avoided. The joints between the walls should be movable.

From a mechanical point of view the pounding against surrounding walls can be similarly treated as hardening of a bearing in longer deflections. The response is not directly dependent on the frequency content of the earthquake. The velocity of the structure prior to collision, the mass of the structure and the characteristics of the wall-soil interaction determine the intensity of the impact.

Commonly the responses due to pounding are relatively high, compared with the responses without collision. It is of economical interest to know, what relation is received while comparing with a fixed-base design. In order to discuss the effects induced by pounding against surrounding walls a parametric study has been conducted. The objective was to explore given margins and to quantify the effectiveness of a collision-utilizing strategy, compared with an alternative fixed-base design.

In Tab. 9-21 the results for a 5-story building, with a fixed-base period of 1.0sec, 3.8sec base isolated period, and 1000t story masses are given. The structure was subjected either to the complete Kobe set (Appendix Sec. 11.6), or only to the FN-EKB component, that exhibit the large responses for this example. The load was varied between 0.5 and 1.0 times the original magnitude. The ratios between the responses due to base-isolation design with collision and responses of a fixed base design are compared. Values larger than 1.0 indicate the exceedance of the fixed-base values. The figures. a.) and b.) in Tab. 9-21 show the results for the inter-story drifts, in dependency of the retaining wall strength. For most records, the ratio is smaller than 1.0, as can be seen in the mean evaluation of a.). However, if the structure is subjected to the FN-EKB motion, advantages can be only gained for a limited parameter range. Considering the accelerations in c.) and d.), it becomes clear, that almost any colliding event produces high accelerations. The use of the proposed strategy should be weighed, if the structure contains acceleration sensitive equipment.

The response due to collision is dependent on the distance ratio between the clearance u_w and the deformation due to an freely moving system u_{free}:

$$\delta = \frac{u_{free}}{u_w} \tag{9-38}$$

In Tab. 9-22 the influence of changing distance factors and rising load intensity on the maximum superstructural inter-story drifts can be studied. They have been calculated for the previously described 5-storey example structure. The contour diagram contains again relative values to the corresponding fixed-base design. As can be seen, almost all values are smaller, so a wide region for possible acceptance of collisions is available.

Table 9-21 Parametric study for the influence of the Load intensity and strength in the retaining wall for the Kobe set and the FN-EKB ground motion

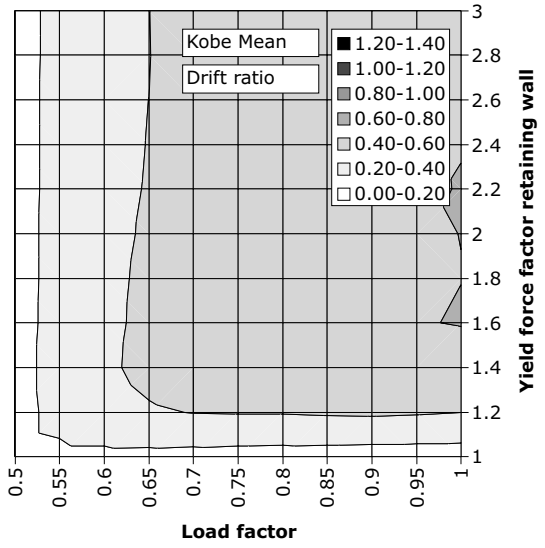

a.)

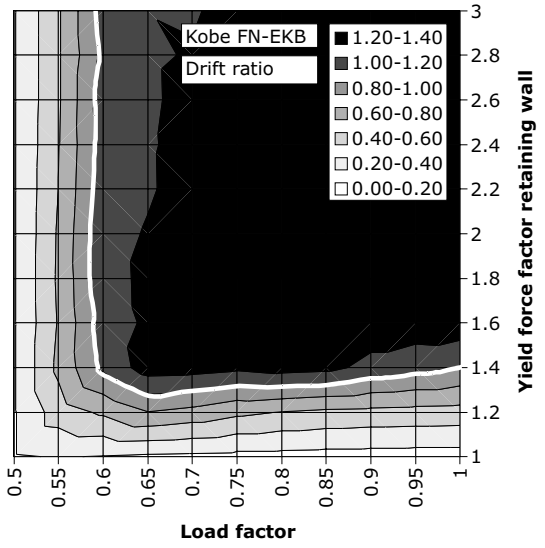

b.)

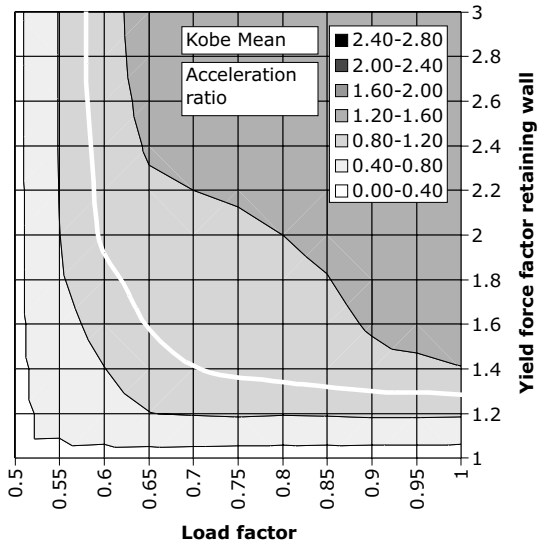

c.)

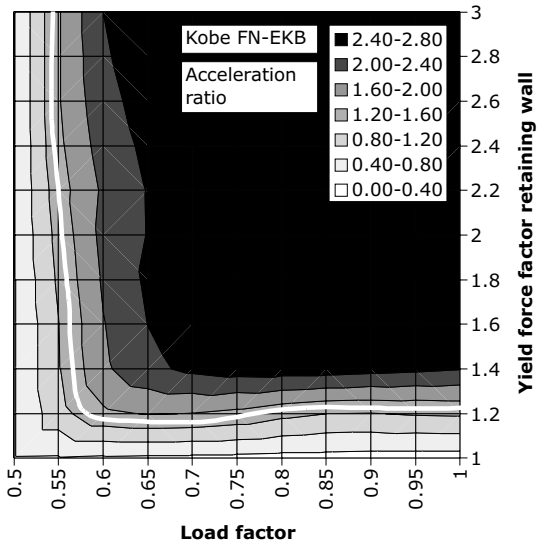

d.)

Table 9-22 Parametric study for the influence of the Load intensity and distance factor; for the Kobe ground motion set

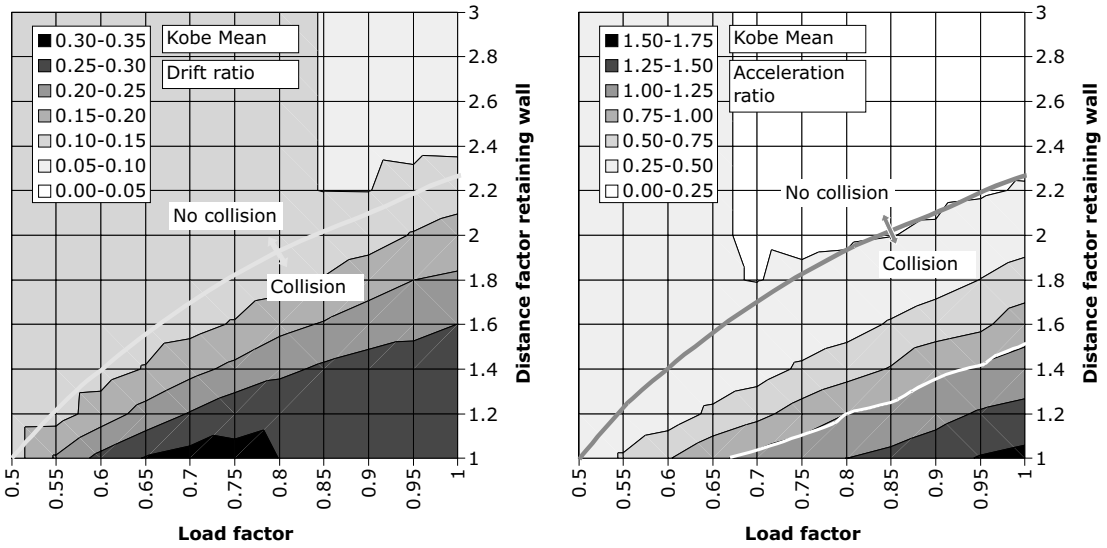

a.) b.)

Most attention has to be paid for the determination or definition of retaining wall/soil model parameters. The initial stiffness can be approximated from passive earth pressure calculations. If an elastic perfectly-plastic approximation is chosen, the yield force can be estimated from soil shear failure investigations. According to investigations of Kashiwa et al. [119], the model parameters can be conveniently determined by finite element analysis. This has the advantage, that surrounding foundations and facilities of neighboring structures can be included.

In limited bounds, the parameters can be influenced. One way is the change of the soil and the material of the wall. Another way is the modification of the failure mechanism. Penetrating the retaining wall for a defined shear failure can be an option to modify the failure line in the soil, as is illustrated in Fig. 9-6.

If the collision against retaining walls cannot be afforded, additional stops can be implemented as indicated in Fig. 9-7. Non-destructive versions can utilize any kind of stiffening or damping devices. Masonry infills, e.g. consisting of aerated concrete, which will be destroyed during crashes, can be an economic alternative.

For analysis any simplified method from Sec. 7 or even time history approaches from Sec. 8 can be used. The parameters of the system can be conveniently determined by application of nonlinear optimization routines.

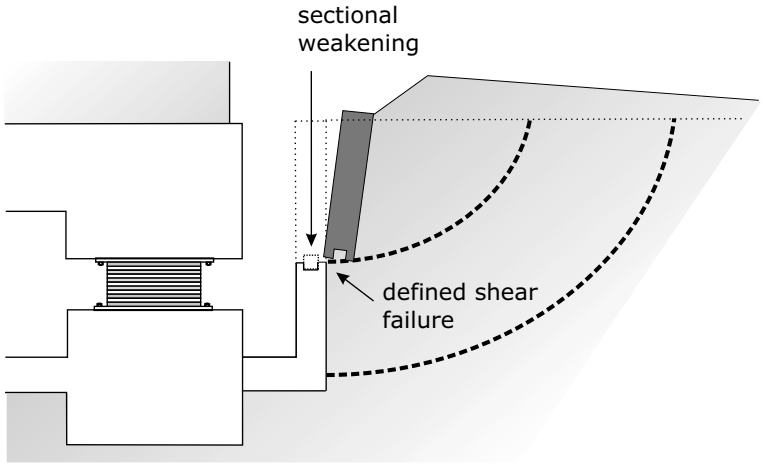

Figure 9-6 Penetration of the retaining wall for modification of the mechanical parameters

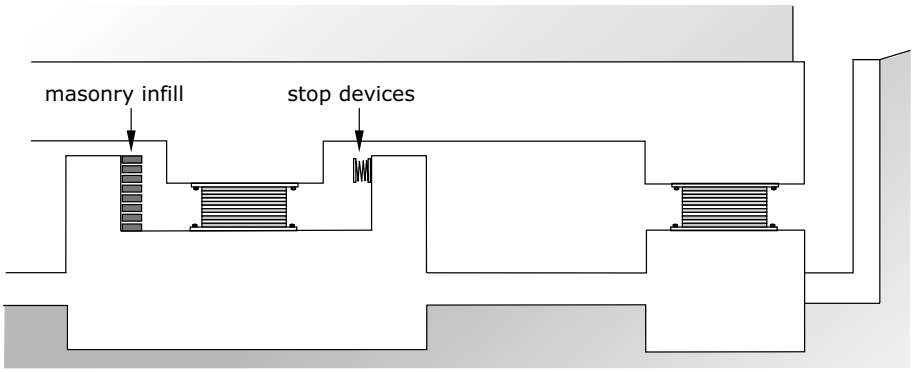

Figure 9-7 Pounding against stops, destructive or non-destructive variant

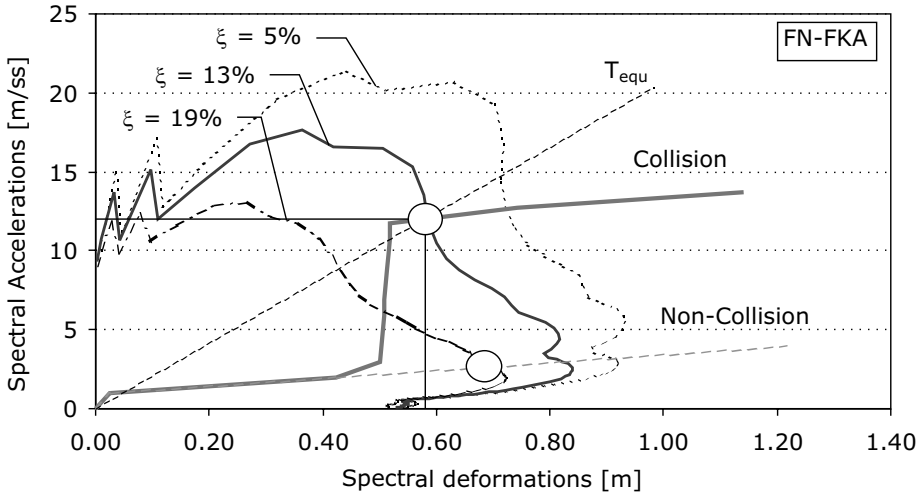

Figure 9-8 Example Pounding SDOF: Capacity spectrum analysis

9.3.5.4 Example Pounding SDOF

A SDOF model with a mass of $m = 1000t$ is examined. The base isolation parameters are: $F_b = 1000kN$; $K_b = 40000kN/m$; $\gamma_b = 1/16$, $u_{b,y} = 0.025m$. The clearance is $u_w = 0.5m$. The stiffness of the wall is $K_w = 500000kN/m$, the strength is $F_w = 10000kN$. The model is loaded by the FN-FKA ground motion from the Kobe set (Appendix Sec. 11.6).

First, the problem is solved by time history analysis. The solution is $u = 0.54m$ and $\ddot{u} = 12.37m/s^2$. This solution is provided for reference.

Second, a pushover analysis (Sec. 7.7) is utilized, leading to the results illustrated in Fig. 9-8. The deformations are $u = 0.58m$ and $\ddot{u} = 12.53m/s^2$.

Third, the approximate solution using the simplified pounding model of Sec. 9.3.3 is calculated. The calculation starts with the analysis of the non-colliding problem. The parameters of the equivalent system are: $T_{equ} = 3.22sec$, $K_{b,equ} = 12260kN/m$, $\xi_{equ} = 0.2$. The deformation is $u_{free} = 0.69m$, the acceleration is $\ddot{u}_{free} = 2.96m/s^2$ the velocity is $\dot{u}_{free} = 1.71m/s$ calculated with simplified linear analysis (Sec. 6). According Eqs. (9-20) and (9-21), the velocity and acceleration at the wall distance is $\dot{u}_w = 1.71\cos(0.5/0.69) = 1.28m/s$ and $\ddot{u}_w = 2.96\sin(0.5/0.69) = 1.96m/s^2$. The equivalent stiffness of the wall is $K_w = 71400kN/m$. The intrusion depth is $\Delta_u = 1.28\dot{1}000/(12260+71400) = 0.14m$. The increase in acceleration is $\Delta_a = 1.28\dot{(}12260 + 71400)/(1000) = 11.71m/s^2$. The resulting deformation is $u = 0.64m$ and the appropriate acceleration is $\ddot{u} = 13.67m/s^2$.

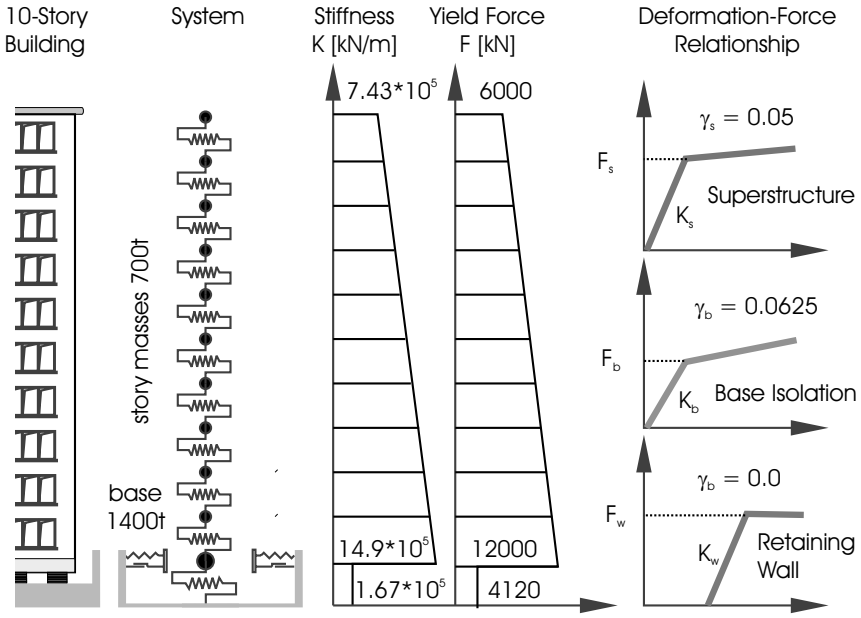

Figure 9-9 Example Pounding 10-DOF: System configuration

9.3.5.5 Example Pounding 10-DOF

A 10-story building, according to Fig. 9-9 is originally designed and constructed using the conventional time history set according Sec. 11.8. The fixed-base period of the structure is 1.0 second, the stiffness and yield force at the top are 80% of base stiffness, intermediate values are linear distributed. The post-stiffness ratio of the superstructure is 0.05. All story masses are 700t. The mass at isolation level is 1400t. In the original design, the superstructure was planed to remain elastic.

Because the building contains acceleration-sensitive equipment that can resist a maximum acceleration of $\ddot{u} = 3m/s^2$, it was base isolated, using a combination of rubber bearings and steel dampers. The isolation interface was designed for a fundamental period of around 3 seconds. The bearings provide a maximum design deflection of 50cm, the collapse deformation is $u_{crit} = 65cm$. The analysis results are given in Fig. 9-10. Based on the maximum observed deformation of $u = 33cm$, the retaining wall distance was chosen to $u_w = 50cm$, with intension to provide comfortable margin against pounding. The maximum acceleration is $\ddot{u} = 2.6m/s^2$.

After new evaluations, the location was considered as near-field area, and the design was reviewed using ground motions from Kobe set (Sec. 11.6). Under these excitations, the pounding of the building against the retaining wall cannot be excluded anymore. Three out of 11 ground motions exceed the clearance of 50cm. Two have the potential to exceed even the ultimate device deformation of 65cm. As the clearance is restricted to the given

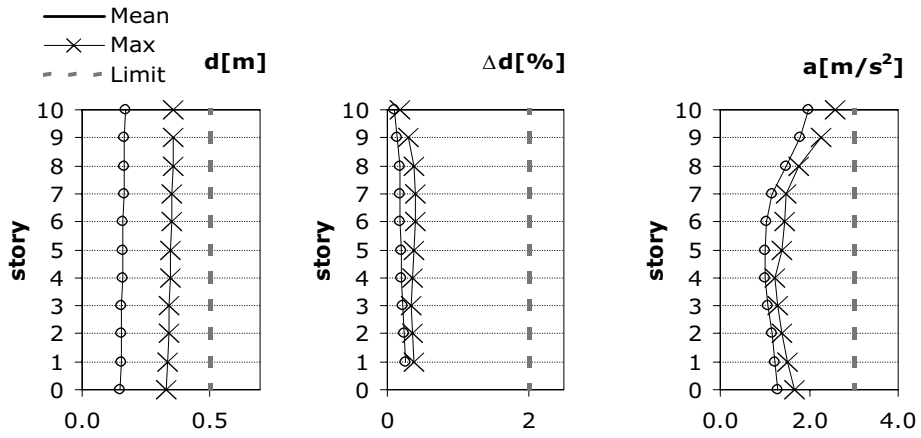

Figure 9-10 Example Pounding 10-DOF: Response for conventional time history set

distance, different strategies for retrofit are examined. All retrofit versions must utilize nonlinear reserves in the superstructure. Necessary strengthening in the superstructure is expressed by a vector of strengthening factors λ_s. The ductility supply in the superstructure is moderate, so drifts are limited to $\Delta_{d,lim} = 2\%$.

Case a.): This case is primarily for comparison. The retaining wall is not considered, the structure can move without collision using the original isolation configuration. The FN-FKA ground motion generates the largest deformation response. The results for this record from time history analysis are plotted in Tab. 9-23, the maximum deformation at base level is $u_b = 67cm$, exceeding the critical deformation of the bearings. The accelerations exceed the limit of $\ddot{u} = 3m/s^2$.

Case b.): The target is to avoid the collision by incorporation of additional stiffness $K_{b,add}$ and hysteretic damping $Q_{b,add}$. The necessary parameter configuration (including the strengthening vector) can be calculated by solving the following optimization problem

$$O(Q_{b,add}, K_{b,add}, \lambda_s) = \sum_{i=1}^{nstory} \lambda_{s,i} \rightarrow Min \tag{9-39}$$

$$u_b \leq u_w \tag{9-40}$$

$$\Delta u_s \leq \Delta u_{s,lim} \tag{9-41}$$

$$\lambda_{s,i} \geq 1.0 \tag{9-42}$$

The optimal solution is $K_{b,add} = 1.91K_b$ and $Q_{b,add} = 1.78Q_b$, this is nearly a triplication of the amount of devices. The maximum acceleration is increased up to $\ddot{u} = 8.2m/s^2$,

Table 9-23 Example pounding 10-DOF: a.) - c.) Comparison of maximum responses d.) Necessary strengthening of the superstructure

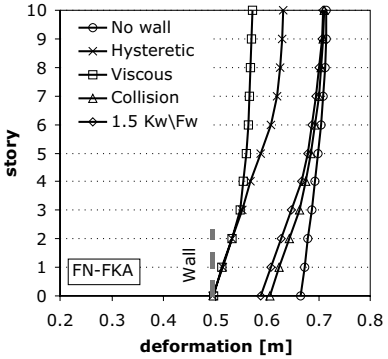

a.)

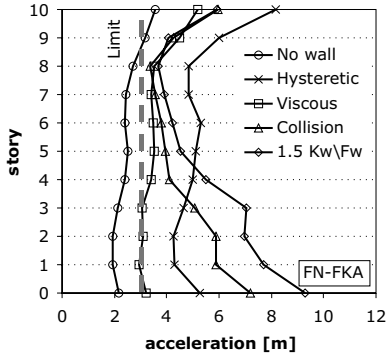

b.)

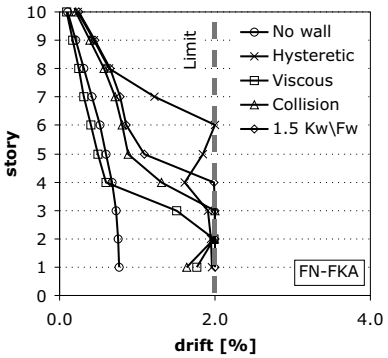

c.)

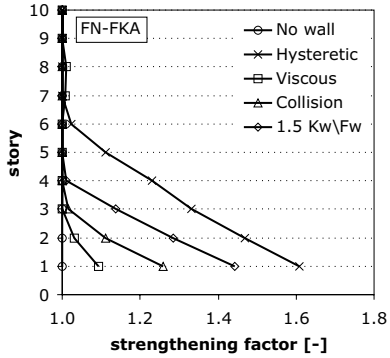

d.)

thus does not comply with the given limit. The strengthening factors are given in Tab 9-23 figure d.), thus the building needs to be retrofitted up to the 6th floor.

Case c.): The collision is avoided by incorporation of additional linear viscous damping devices. The optimal amount of damping and the appropriate strengthening of the superstructure can be determined by solving the following optimization problem

$$O(C_{add}, \lambda_s) == \sum_{i=1}^{nstory} \lambda_{s,i} \rightarrow Min \tag{9-43}$$

$$u_b \leq u_w \tag{9-44}$$

$$\Delta u_s \leq \Delta u_{s,lim} \tag{9-45}$$

$$\lambda_{s,i} \geq 1.0 \tag{9-46}$$

Table 9-24 Example pounding 10-DOF: Maximum responses for 86% excitation

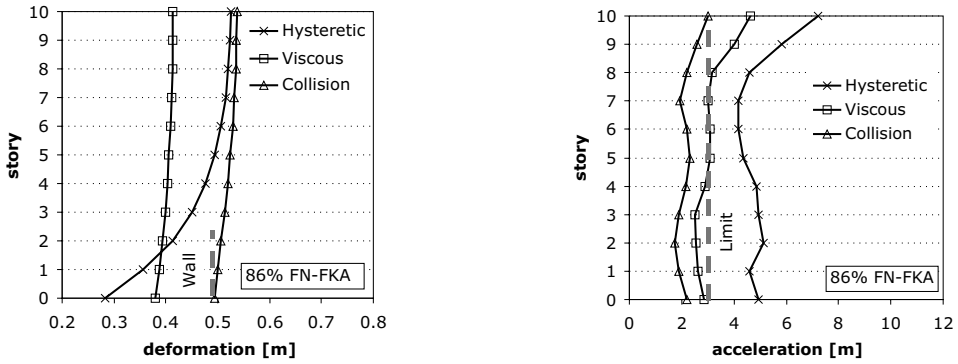

The deformations can be restricted to the given limit, if damping devices, providing a coefficient of $C_{add} = 7410kNs/m$, are installed. The results are given in Tab. 9-23. The responses are reduced compared with Case b.). The necessary strengthening of the superstructure is relatively small and concerns only the first two floors. However, the limit in the accelerations is not fulfilled.

Case d.): The original configuration is kept unchanged; collision is accepted. The wall is modeled as elastic-perfectly plastic. The parameters are $K_w = K_{s,1story}$ and $Q_w = 10000kN$. The maximum deformation has to be restricted to the collapse deformation of $u_{crit} = 65cm$. The strengthening is calculated by:

$$O(\lambda_s) == \sum_{i=1}^{nstory} \lambda_{s,i} \rightarrow Min \tag{9-47}$$

$$u_b \leq u_{crit} \tag{9-48}$$

$$\Delta u_s \leq \Delta u_{s,lim} \tag{9-49}$$

$$\lambda_{s,i} \geq 1.0 \tag{9-50}$$

The resulting maximum deformation at base is $u_b = 61cm$. The accelerations are increased up to $\ddot{u} = 7.2m/s^2$. The structure has to be strengthened in the first three floors according to Tab. 9-23.

Case e.): The system of Case d.) is tested for 50% increased stiffness and yield force of the retaining wall and the soil. The deformation at the base is reduced to $u_b = 59cm$. The accelerations are increased about 25%. Necessary retrofit is limited to the first three floors. The results are again plotted in Tab. 9-23.

Discussion of all cases: The safety of the structure can be ensured with either solution. In any case, retrofit measures are demanded. The least measures for the superstructure

can be obtained by incorporating viscous damping. However, the decision has to be made by comparing the overall costs for the project. All solutions fail for the objective to ensure a limited acceleration level. It is clear, that in the case of an earthquake with high magnitude, the safety of the structure requires that the limit cannot be reached at all. It is interesting to determine the solution that provides the highest excitation level possible, ensuring the operability of the building. It is clear that all measures provided for safety will influence the performance of the structure in lower excitation levels. If additional devices are incorporated into the isolation interface, the responses are increased. Hence the Case d.) and e.) should provide the best serviceability. Above a magnitude of 86%, the pounding occurs. Up to this level, the maximum acceleration is $2.94m/s^2$ using the original isolation configuration (see selected results in Tab. 9-24). For Case b.) the value is already $\ddot{u} = 7.2m/s^2$, for Case c.) up to $\ddot{u} = 4.6m/s^2$. The acceptance of collisions provides operability up to 86%. Only under extremely rare conditions, the operability has to be abandoned, but structural safety can be ensured through retrofit. Strengthening measures for the superstructure are necessary anyway.

Base isolation can be a beneficial alternative to the traditional fixed base concepts. Colliding is by all means avoided so far, but the potentials are shown and theoretical approaches are provided. It has been shown, that the risks can be managed. The acceptance of pounding has to be decided with consideration of the probability of the event. It was shown that collision is a worthwhile option to check during design. Nevertheless more research is needed, especially for the assessment of the wall and soil parameters under impact. In general, the application of optimization strategies has proved to be a valuable design measure for design of base isolated structures.

9.4 Graphical design of base isolated structures

9.4.1 Introduction

The design of base-isolated structures is commonly iterative and can be described as an optimization process (Tab. 9-25). The task is to appropriately combine several devices within isolation layers. Most of the concepts apply one of the following combinations

1.) rubber bearings/sliders and hysteretic damping

2.) rubber bearings/sliders and viscous damping.

3.) rubber bearings/sliders and hysteretic + viscous damping

4.) other systems and combinations

Combination 1.) is often preferred in engineering practice because of the well-understood behavior and the cost effectiveness [171]. As well combination 2.) gained recently increasing importance in design.

The analysis of such systems requires the dimensioning of the devices with respect to the overall structural behavior. The traditional analysis is based on simplified analysis methods, as indicated in Tab. 9-25. Recent publications show difficulties in realistic as-

Table 9-25 Iterative procedure for optimization of base-isolated structures

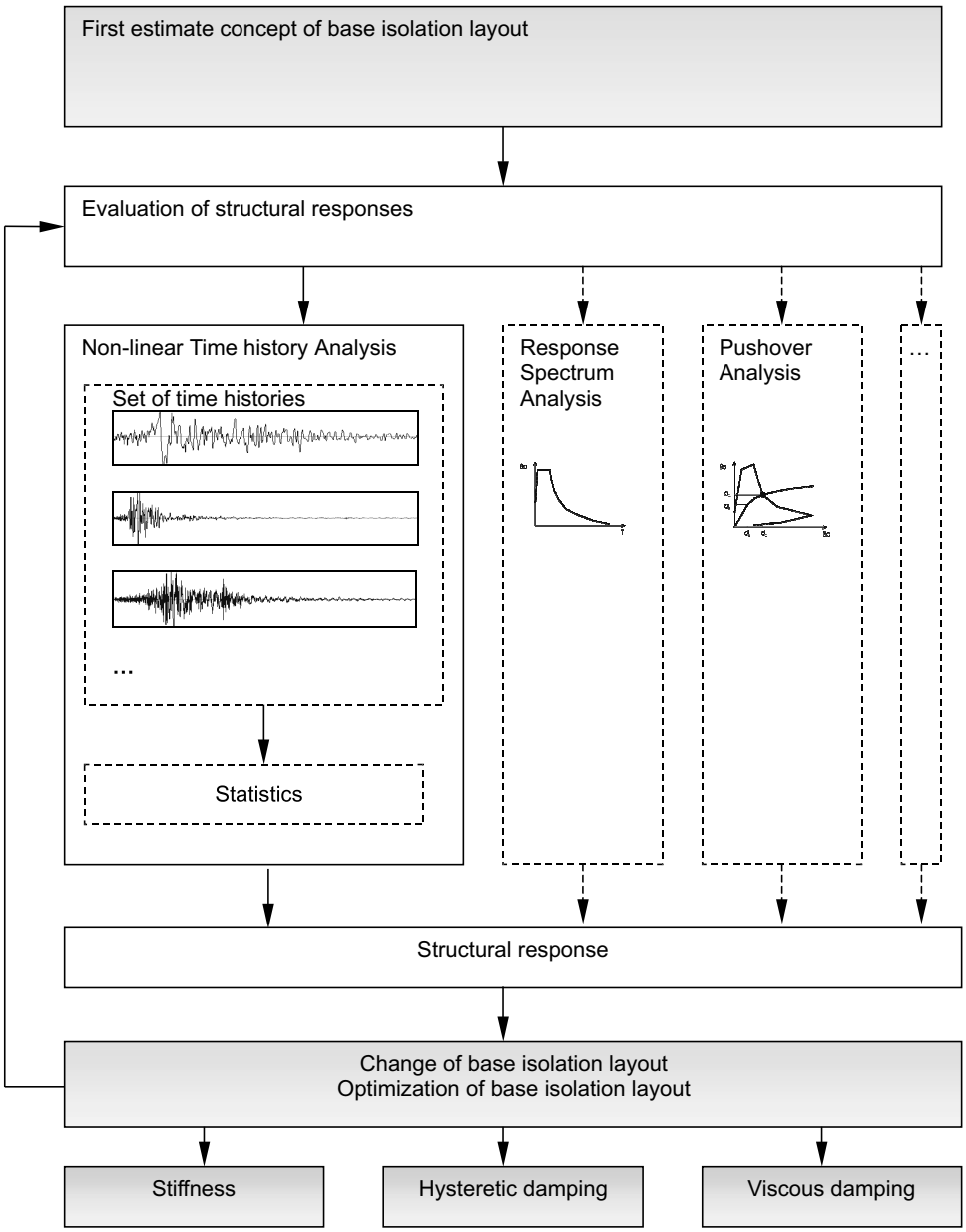

sessment of the actual structural behavior, e.g. [221]. Therefore the analysis of base-isolated structures is increasingly performed with time history approaches. The main problem is the costly and complex nonlinear analysis using appropriate sets of acceleration records. And, repeating the analysis for several times within an iterative design procedure.

However, the design can be simplified without refraining from the precision of time history analysis. The key is the simplicity of the structural behavior of base-isolated structures. This is illustrated in Fig. 6-15. Basically, superstructures show sufficient stiffness, so that the mechanical system can be simplified as a nonlinear 2-DOF system.

The following assumptions are made:

- Usage of 2-DOF models of base isolated structures provides sufficient accuracy for design
- Superstructure behaves elastically, all parameters are constant
- Base isolation behaves bilinear
- Initial stiffness of base isolation can be fixed or correlated to the model parameters
- Ratio of the superstructural to base-layer mass is constant
- Model can be used for device combinations 1.) and 2.)

Such assumptions are common in structural design of base-isolated structures. The differences from the reality are marginally [159]. Then the base isolation behavior can be described with a two-parametric model.

9.4.2 Base isolation with hysteretic damping

The mechanical background for the simplification of the model is illustrated in Tab. 9-26. As can be seen from device tests, the behavior of the rubber bearings can be approximately simplified to a linear behavior. As well, lead damper behavior is close to linear elastic perfectly plastic. Therefore the combined action is linear elastic plastic. As the initial stiffness is assumed to be fixed or dependent on the second slope in the material law, only two parameters are necessary to describe the device behavior in total. These two parameters are for device combination 1.)

- Second slope (or yield stiffness) K in the isolation layer
- Yield force Q in the isolation layer, indicating the yielding of the hysteretic damping component

Thus, the function of these two parameters can be graphically provided in maps. A design strategy can be established on a graphical basis that consists of two main parts:

- Preparation phase (established only once)
- Application phase, using prepared maps

Table 9-26 Derivation of a two-parametric model for base isolation layers (hysteretic damping)

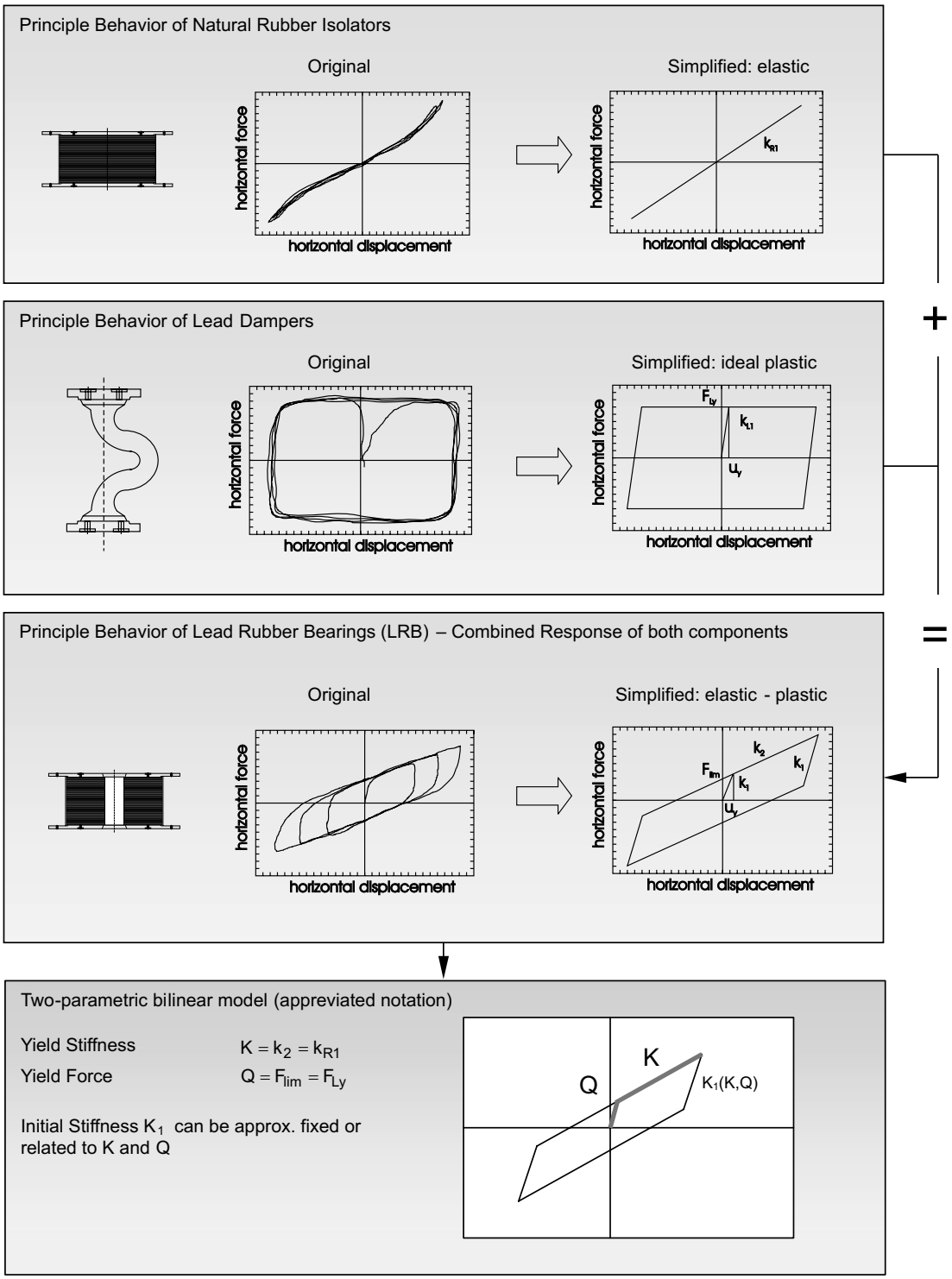

Table 9-27 Major preparation and application steps

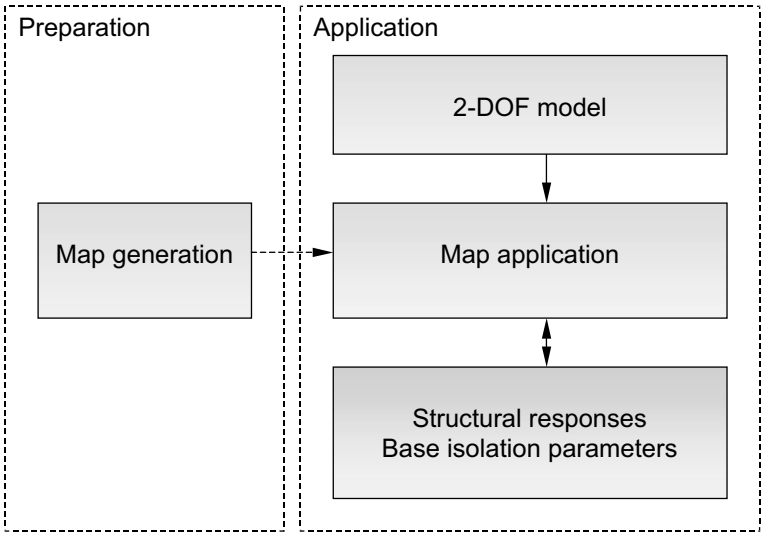

The steps are summarized in Tab. 9-27. The first part consists of the generation of design maps. These design maps consists of the two involved input parameters and one selected response parameter of the structure. The generation follows Tab. 9-28 for the hysteretic damping (combination 1.)).

It should be noted, that the maps are to be generated not for a single structure, but for a variety of structures having approximatelly the same:

- superstructural eigenperiod T
- ratio of initial stiffness K_i to yield stiffness of the base isolation layer (commonly determined by other service limit states, e.g. wind)
- superstructural to base-layer mass ratio μ
- same structural damping ξ (except hysteretic damping)
- loading sequence (Time history set), not magnitude

The calculation is commonly performed using computational support. The generation starts by choosing the previously listed parameters. Just for map generation, a basis mass for the generation must be arbitrarily chosen. Then, dependent parameters as the base mass m_B, the superstructural stiffness k_S and the total mass m are calculated. For the maps, an appropriate range of parameters K and Q needs to be specified. Then this range is divided into sufficient subdivisions, forming an analysis grid on the parameter map. Following, in a successive procedure all possible value combinations of K and Q in the parameter grid are used to perform a time history analysis. The recommendation is to use appropriate time history sets that are modified to meet appropriate statistical properties for the local situation. The intensity of loading can be scaled using the load intensity scaling

Table 9-28 Map generation using time history method

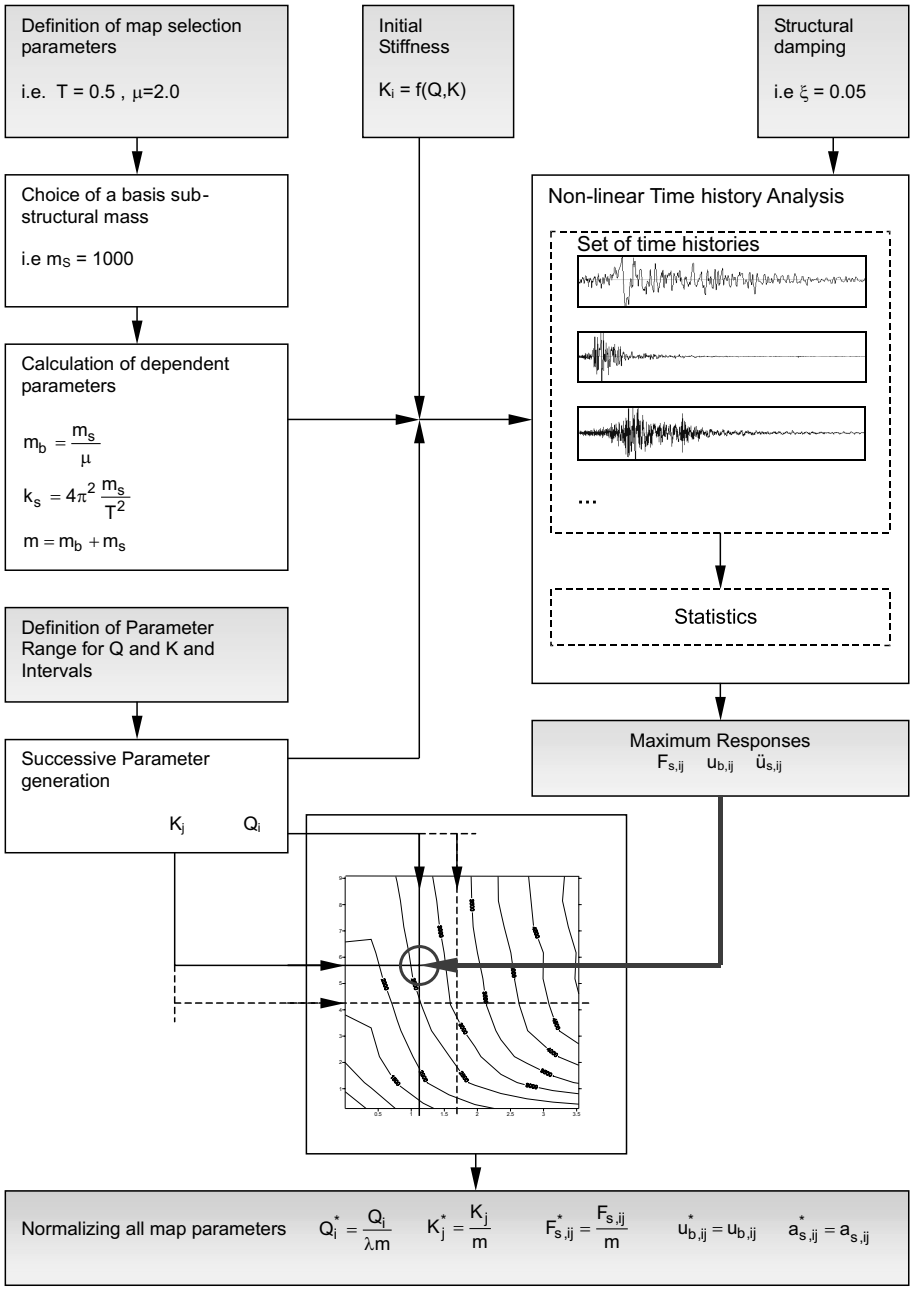

factor λ. All values must be normalized in order to eliminate the effect of the arbitrarily chosen basis mass.

The responses are introduced in the maps. For better readability, the map can be prepared to be a contour plot showing the response values. Such plots need to be provided once and can be collected in catalogs. Appendix Sec. 11.12 shows several example maps for the LA 10in50 time history set form the SAC-FEMA projects [200] that have been generated due to the described procedure.

The application of the maps in design of a new or review of an existing structure is now possible and simple. In Tab. 9-29 the necessary steps are given. First, the given structure must be transformed into an sufficiently equivalent 2-DOF system. The load level for analysis can be chosen (usually the maps are provided for load level $\lambda = 1.0$). With the calculation of the fixed base period T and the mass ratio μ the appropriate map is chosen from the catalog. Then with the normalized map parameters K^* and Q^* the normalized maximum responses (superscript *) can be read from the map. Afterwards the real response values can be determined. There is a wide variety of applications for these maps, that are illustrated next with help of examples.

It should be noted, that the method contains no simplifications other than listed in Sec. 9.4.1. The usage of the maps is identical to the application of a nonlinear time history analysis. The following advantages can be stated:

- Method is graphical, easy and fast
- Usage for pre-design, design and review, device selection
- Incorporates seismic loads, base isolation characteristics and maximum structural responses in one chart
- Avoidance of complex nonlinear calculations, while having the same precision
- Parameters can be easily scaled to consider different load levels
- No usage of abstract device parameters (like equivalent damping): Parameters in the map for the description of the base isolation layer behavior (Q,K) can be easily read from real test results
- Maps can be provided for any structural parameter of the model
- Maps can be generated using time history - or response- or pushover-analysis,...
- The proposed method of accessing data in maps is generally independent from the method of map generation (map generation can be more sophisticated)
- Maps can consider real or artificial earthquakes
- Maps can consider statistical representations of earthquake responses
- Maps can consider site depended characteristics
- Maps can be globally or locally adjusted for the consideration of other effects e.g. specific behavior of isolation devices (e.g. hyper elasticity in ultimate deformation state), special code provisions
- Different levels of overall structural viscous damping can be adjusted using the scaling factor for the seismic loads

A main advantage is the possibility of immediate change of device parameters, for optimization of the overall behavior. This simplifies optimization processes of isolation layers considerably, as the consequences for the changes can be visually pursuited. Some typical applications are illustrated in the following sections.

Table 9-29 Principle of map application

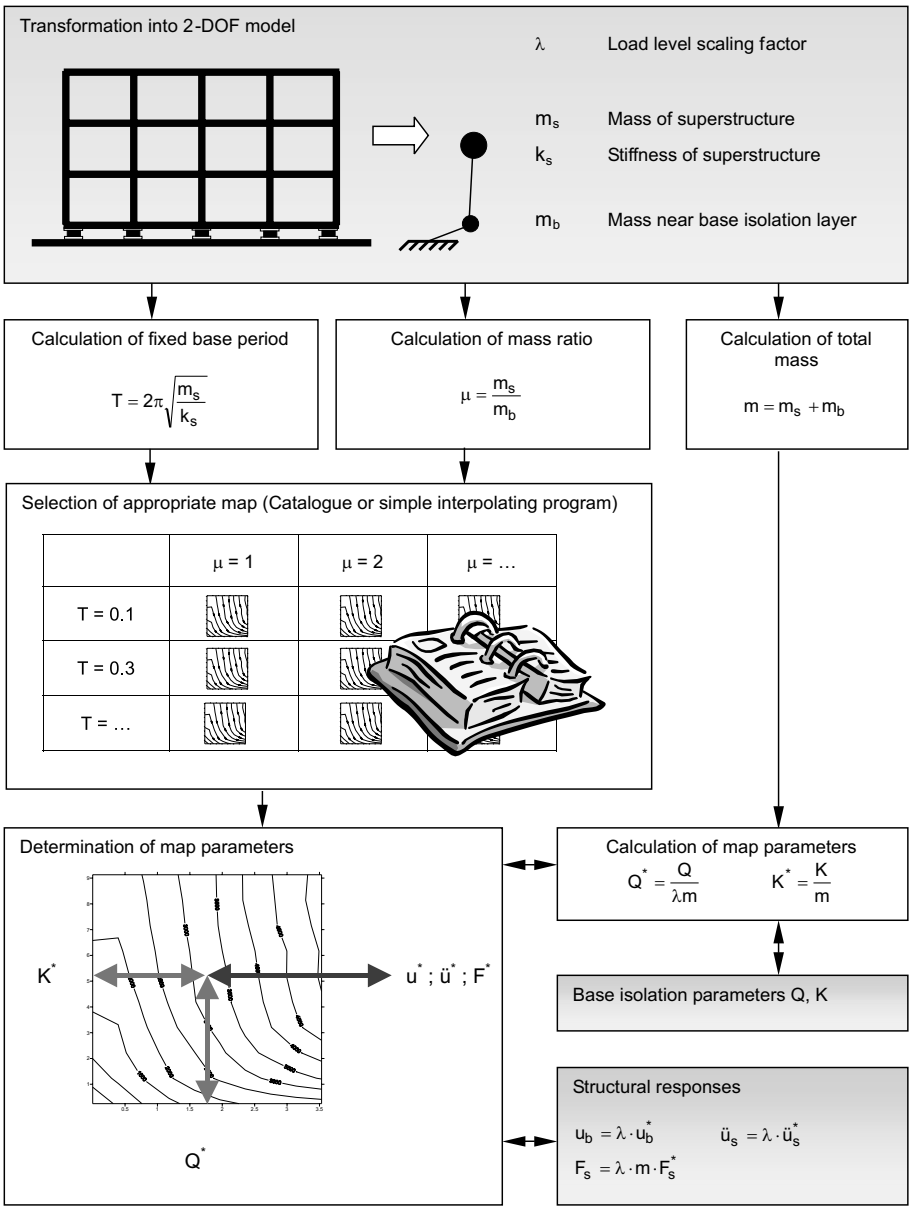

9.4.3 Examples for principle usage of maps

Example 1.): This example shows a basic application of the maps. For a known device configuration $K$and Q, the appropriate response values for the base-isolation deflection u_b and the superstructural acceleration $\ddot{u}_s$ can be taken from the map. This example is graphically illustrated in Fig. 9-11 for load level $\lambda = 1$. For better convenience, both response parameters have been plotted together in one contour plot.

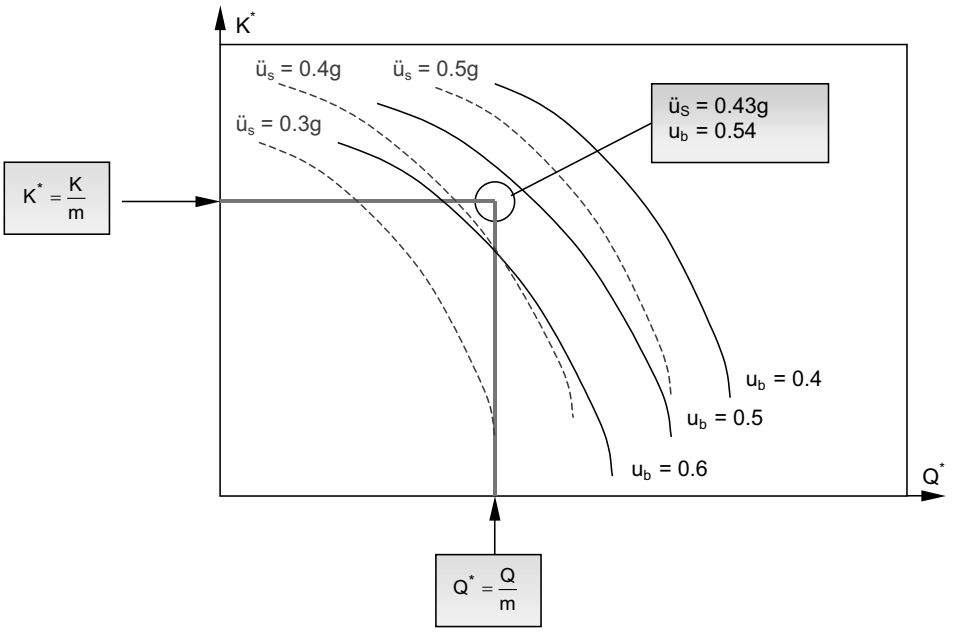

Figure 9-11 Example 1.): Determination of responses using given base isolation parameters K and Q

Example 2.): This example shows another basic form of application in Fig. 9-12, that is the determination of base isolation parameters Q and the necessary base isolation clearance u_b using a given K and a preferred maximum acceleration $\ddot{u}_s$ in the superstructure. The method is to find the appropriate isoline for the acceleration that will be crossed with the stiffness K. Following a vertical line from this intersection point will give the appropriate necessary yield force Q. As well at this point, the maximum deformation at base level can be determined.

Example 3.): The example in Fig. 9-13 illustrates an application corresponding to a solution of an optimization problem. It shows the determination of optimal parameters Q and K, while knowing the maximum given base isolation clearance u_b, the maximum acceleration $\ddot{u}_s$ and some known constraints for the choice of base isolation parameters. Within the map an area for choice of parameters is derived, from that a solution can be chosen.

Example 4.): This examples demonstrates the application of maps for calculation of the necessary amount of isolators of the same type (see Fig. 9-14). Knowing the specifications K and Q for one device, other numbers will be find on a strait line. Then according to given limits (here the maximum base deformation) the number can be determined.

Example 5.): This example illustrates sophisticated use of the maps, involving changing device parameters or different device characteristics in different parts of the deformation behavior (e.g. hardening in the rubber bearings, see Fig. 9-15). The behavior can be introduce in two ways

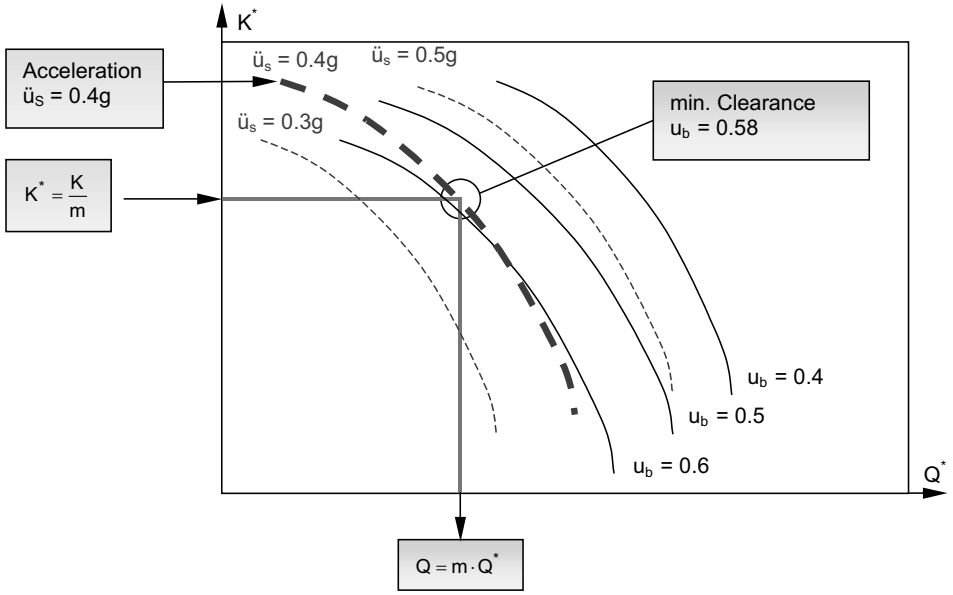

Figure 9-12 Example 2.): Determination of responses using given base isolation parameters K and acceleration $\ddot{u}_s$

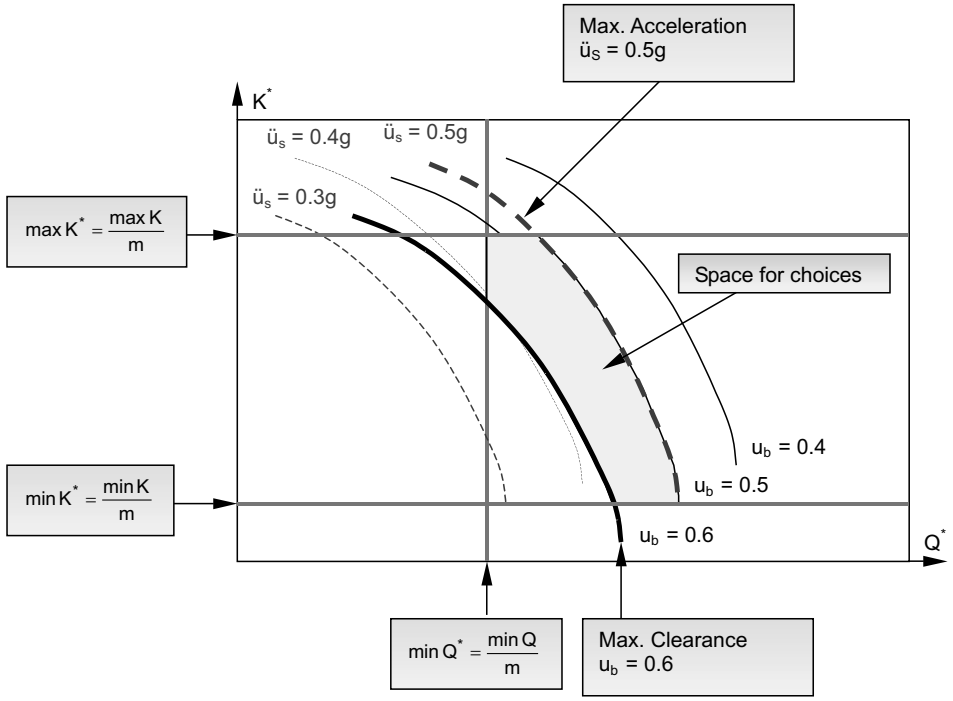

Figure 9-13 Example 3.): Determination of responses within a decision area

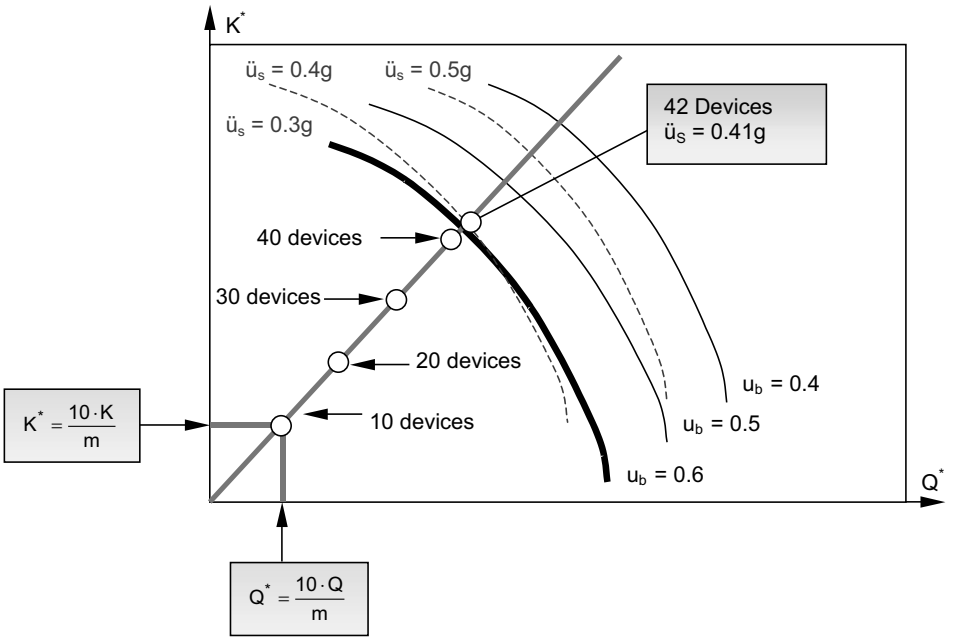

Figure 9-14 Example 4.): Determination of number of isolators

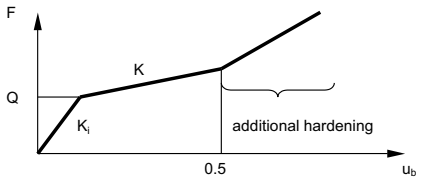

Figure 9-15 Example 5.): Different hardening characteristics for bearings

- Include behavior directly into the map (i.e. provided by manufacturer)
- Provide functions to adjust general map

The first variant is changing the map, whereas the second variant uses a basis map and applies some changes. In Fig. 9-16 such a modification is exemplarily illustrated.

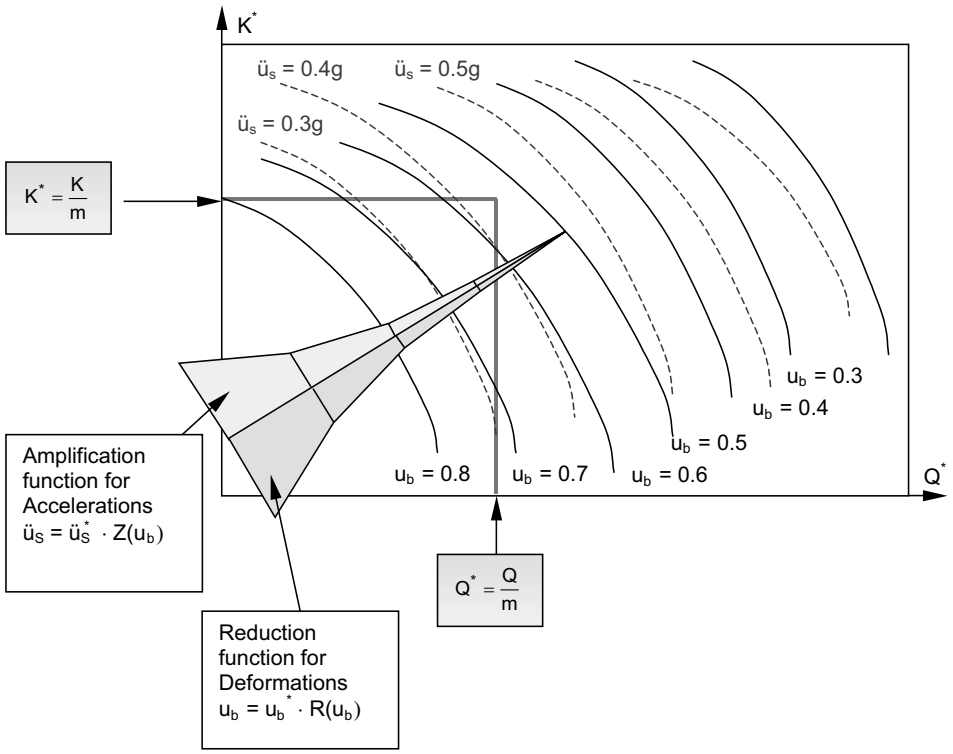

Figure 9-16 Example 5.): Involvement of hardening within maps

9.4.4 Base isolation with viscous damping and other device combinations

Generally, the visual design method presented in the previous chapters can be applied for other device combinations. The strategy for determining and usage of the maps remain basically the same. It should be considered, that the combination of three devices within one base-layer is possible while fixing one component or establishing the relation between two parameters. The application of rubber bearing together with viscous damping is straight forward. Example maps, for the LA 10in50 set [200] are given in the Appendix Sec. 11.13. Here the two independent parameters are the stiffness in the rubbers K and the sum of viscous damping C. Comparing the plots from hysteretic (Appendix Sec. 11.12) and viscous damping (Appendix Sec. 11.13), it can be seen, that the overall structural behavior of these systems is completely different.

10 Conclusion

10.1 Summary

The study provides insight into the basic theories and applications of optimization strategies in earthquake engineering, with a main focus on methods of shape optimization that relates to practical usage. The relations between design and optimization problems are discussed and utilized for derivation of appropriate mathematical formulations. It is obvious, that most engineering problems can be treated as optimization problems. And, the advantages using optimization strategies in comparison to traditional methods or in combination with established procedures can be noted.

For basic and special engineering tasks, the theoretical background is provided. The application is demonstrated with help of several examples throughout all sections. The basics of mathematical optimization are discussed and the main categories of algorithmic solution methods are introduced.

An overview is given on the mechanical background of solution strategies based on mathematical optimization. Means of variational calculus are applied for derivation and rearrangement of mechanical principles. Here intentionally, well know classical principles of mechanics have been chosen for demonstration. Their beneficial application particularly in seismic engineering is illustrated within several chapters.

In order to prepare the numerical treatment and to provide basic continuum mechanical background, some theoretical insight into the mechanics of elastic and elastic-plastic bodies is provided. It helps understanding important starting points for the formation of extremum principles, for geometrical and physical nonlinear problems. Their transformation into discrete formulations is the key issue to obtain optimization formulations. The underlying methods based on matrix notation are provided.

Much emphasis is given to the practical application of optimization strategies in earthquake engineering. One chapter is dedicated to modal analysis concepts. The analysis of eigenvalue problems with help of optimization algorithms illustrates the application also in classical topics. The derivation of new design tasks and the formulation of appropriate solution concepts is shown. New bases for practical stability analysis in dynamics of structures with elasto-plastic behavior are introduced.

The most important concepts of simplified linear and nonlinear analysis are assessed, with the provision of several optimization tasks. The application for elastic, plastic and base isolation design is demonstrated, always with reflection to the theoretical background and provision of examples. The well known response spectrum based analysis methods have been reformulated to fit into optimization concepts. Those chapters not only show classical design, but highlight new concepts of performance based design. Here the low damage design is emphasised with design alternatives based on shakedown theory and applications of the base isolation concept. With several examples, the variability of the analysis and design with help of optimization strategies is illustrated.

As well, analyses in the time domain using step-by-step numerical treatment can be supported by optimization strategies. Here the classical principles of dynamics are utilized for derivation of appropriate optimization formulations. The given formulations can be extended for dynamic limit state analysis.

The variety of applications of optimization strategies in seismic engineering is shown for specialized engineering tasks. Those tasks involve the generation of artificial accelerograms, the determination of spectral parameters, the design of base isolated structures using controlled impact and methods of graphical optimization.

10.2 Future work

The presented content points out the great potentials and benefits that can be gained by the application of optimization concepts in earthquake engineering. The discussed topics are to provide a basis for theoretical problem solution in mathematical optimization, possible applications are illustrated with selected examples. The natural compatibility of optimization strategies with design tasks of practical engineering enables to provide adopted methods for almost any other application. Therefore the following fields of investigation are worth studying.

One of the most interesting topics in structural optimization is topology optimization. This topic is characterized by non-convex problem classes that are difficult to formulate and solve even for statical problems. Involving seismic conditions will be a challenging task, as the time aspect in dynamics will considerably influence the outcome of the optimization process. The task will combine statical and dynamical load cases, that can be differently weighted, with a combination of different objectives in design.

Accordingly, the extension of the presented engineering problems for probabilistic assessment will be an interesting combination. The stochastic character of the seismic excitation can be better respected and evaluated. The presented problem classes can serve as deterministic cores for probabilistic analyses. All or selected design variables are given as probabilistic parameters. The objective and subsidiary functions are formulated as functions of these stochastic parameters.

The analysis of the sensitivity of design variables at the optimum point is always strongly related to structural optimization. This additional information can be obtained by gradient evaluations. Moreover, the sensitivity itself can be treated as a optimization target, in order to generate robust solutions.

This study focusses on elasto-plastic structures. The involvement of other (mainly nonlinear) material laws in combination with difficult path dependent behavior is challenging in solution. This category of analysis needs to embed time history procedures on a small step scale for a proper characterization of the structural behavior under optimization criteria.

11 Appendices

11.1 Appendix A: 3D-Tensor-Matrix transformation operators

To handle non-symmetric tensors, the following transformation operators are introduced.

The second order - three dimensional tensor

$$\hat{T} = \begin{bmatrix} T_{0,0} & T_{0,1} & T_{0,2} \\ T_{1,0} & T_{1,1} & T_{1,2} \\ T_{2,0} & T_{2,1} & T_{2,2} \end{bmatrix} \tag{11-1}$$

can be made symmetric

$$\mathrm{sym}(\hat{T}) = \frac{1}{2}\left(\hat{T} + \hat{T}^T\right) \tag{11-2}$$

or can be transformed into a vector

$$V = \mathrm{vec}(\hat{T}) = [\ T_{0,0} \quad T_{1,1} \quad T_{2,2} \quad T_{1,0} \quad T_{0,1} \quad T_{2,1} \quad T_{1,2} \quad T_{2,0} \quad T_{0,2}\ ]^T \tag{11-3}$$

The inverse operation for the vector V is

$$\hat{T} = \mathrm{ten}(V) = \begin{bmatrix} V_0 & V_4 & V_8 \\ V_3 & V_1 & V_6 \\ V_7 & V_5 & V_2 \end{bmatrix} \tag{11-4}$$

Furthermore, the tensor $\hat{T}$ can be transformed into a non-quadratic matrix with this spread operation

$$\mathrm{spr}(\hat{T}) = \begin{bmatrix} T_{0,0} & & \\ & T_{1,1} & \\ & & T_{2,2} \\ T_{1,0} & & \\ & T_{0,1} & \\ & T_{2,1} & \\ & & T_{1,2} \\ T_{2,0} & & \\ & & T_{0,2} \end{bmatrix} \tag{11-5}$$

or into a quadratic matrix with this spread operation

$$\mathrm{arr}(\hat{T}) = \begin{bmatrix} T_{0,0} & & & T_{0,1} & & & & T_{0,2} & \\ & T_{1,1} & & & T_{1,0} & T_{1,2} & & & \\ & & T_{2,2} & & & & T_{2,1} & & T_{2,0} \\ T_{1,0} & & & T_{1,1} & & & & T_{1,2} & \\ & T_{0,1} & & & T_{0,0} & T_{0,2} & & & \\ & T_{2,1} & & & T_{2,0} & T_{2,2} & & & \\ & & T_{1,2} & & & & T_{1,1} & & T_{1,0} \\ T_{2,0} & & & T_{2,1} & & & & T_{2,2} & \\ & & T_{0,2} & & & & T_{0,1} & & T_{0,0} \end{bmatrix} \tag{11-6}$$

The material pseudo-tensor D

$$D = \begin{bmatrix} D_{0,0} & D_{0,1} & D_{0,2} \\ D_{1,0} & D_{1,1} & D_{1,2} \\ D_{2,0} & D_{2,1} & D_{2,2} \end{bmatrix} \tag{11-7}$$

can be spreaded into matrix form

$$\mathrm{mat}(D) = \begin{bmatrix} D_{0,0} & D_{0,1} & D_{0,2} & & & & & & \\ D_{1,0} & D_{1,1} & D_{1,2} & & & & & & \\ D_{2,0} & D_{2,1} & D_{2,2} & & & & & & \\ & & & \frac{1}{2}(D_{0,0}-D_{0,1}) & \frac{1}{2}(D_{1,1}-D_{0,1}) & & & & \\ & & & \frac{1}{2}(D_{0,0}-D_{0,1}) & \frac{1}{2}(D_{1,1}-D_{0,1}) & & & & \\ & & & & & \frac{1}{2}(D_{1,1}-D_{1,2}) & \frac{1}{2}(D_{2,2}-D_{2,1}) & & \\ & & & & & \frac{1}{2}(D_{1,1}-D_{1,2}) & \frac{1}{2}(D_{2,2}-D_{2,1}) & & \\ & & & & & & & \frac{1}{2}(D_{0,0}-D_{0,2}) & \frac{1}{2}(D_{2,2}-D_{2,0}) \\ & & & & & & & \frac{1}{2}(D_{0,0}-D_{0,2}) & \frac{1}{2}(D_{2,2}-D_{2,0}) \end{bmatrix} \tag{11-8}$$

11.2 Appendix B: Simplified period dependent reduction coefficient for pseudo-acceleration spectra

The determination of the reduction factor according Sec. 9.2 can be simplified for practical use. If $R_\xi = R_{EC8}$ within Eq. (9-17) a physical meaning can be assigned to η_1 in representing a dominant velocity of the ground motion. Then the value is approximately determined by the dominant pseudo-acceleration $PSa_{5\%,dom}$ and the dominant period T_{dom}

$$\eta_1 \approx \frac{PSa_{5\%,dom} T_{dom}}{2\pi} \tag{11-9}$$

Herein $PSa_{5\%,dom}$ denotes the average value of the 5% damped pseudo-acceleration spectrum between the beginning of the sensitive part in the pseudo-acceleration spectrum (sometimes indicated as the plateau or constant part) at period T_a and the beginning of the sensitive part in the pseudo-velocity spectrum at period T_v. The appropriate dominant period T_{dom} is estimated from averaging the plateau periods

$$T_{dom} = \frac{T_a + T_v}{2} \tag{11-10}$$

In this equation, T_{dom} characterizes the center of the period region with high accelerations. Examples for the manual derivation of η_1 are provided in Fig. 11-1-11-3. In code spectra the ′corner periods′ can be used to derive $PSa_{5\%,dom}$ and T_{dom} (Fig. 11-1). Because of the smoothing effect, the reading of the appropriate values in the mean spectra becomes almost as easy as for code spectra, as illustrated in Fig. 11-2 and 11-3. Summarizing the simplified version, incorporating Eq. (9-17) leads to

$$R_{mod} = 1 + \left[\left(\frac{10}{100\xi + 5} \right)^{-0.5} - 1 \right] \frac{PSa_{5\%}(T)}{PSa_{5\%,dom}} \cdot \frac{T}{T_{dom}} \tag{11-11}$$

For further detail refer to [221].

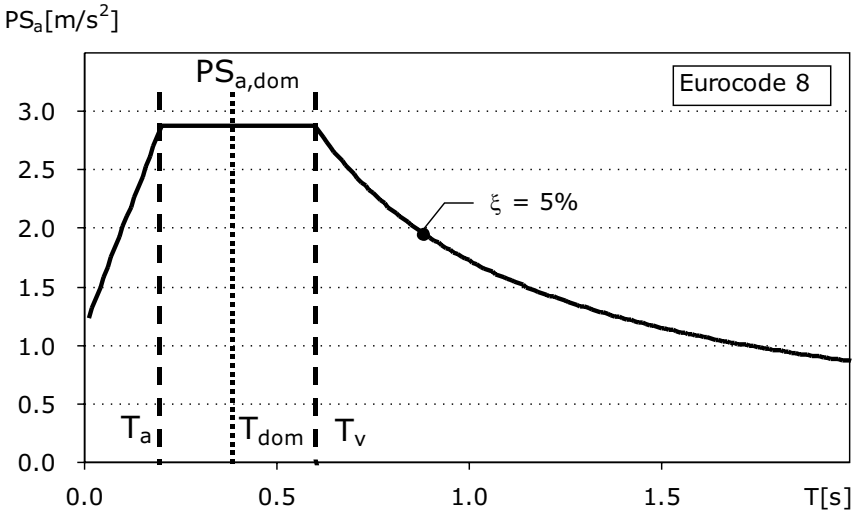

Figure 11-1 Example: Determination of plateau periods and η_1 for code spectra

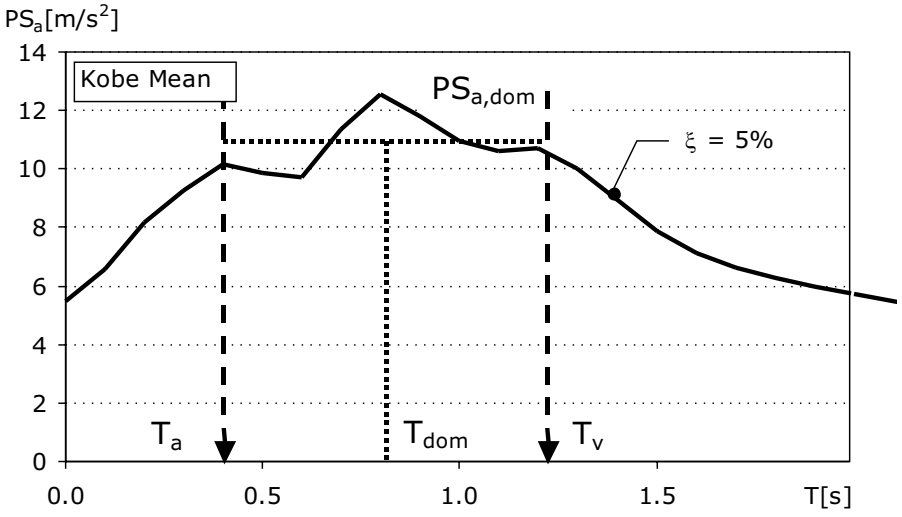

Figure 11-2 Example: Determination of plateau periods and η_1 for mean acceleration spectra

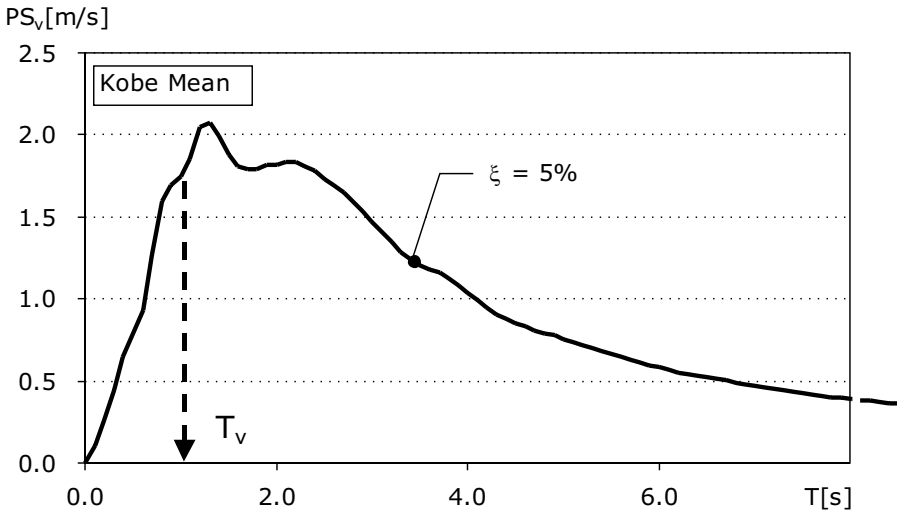

Figure 11-3 Example: Determination of plateau periods and η_1 for mean velocity spectra

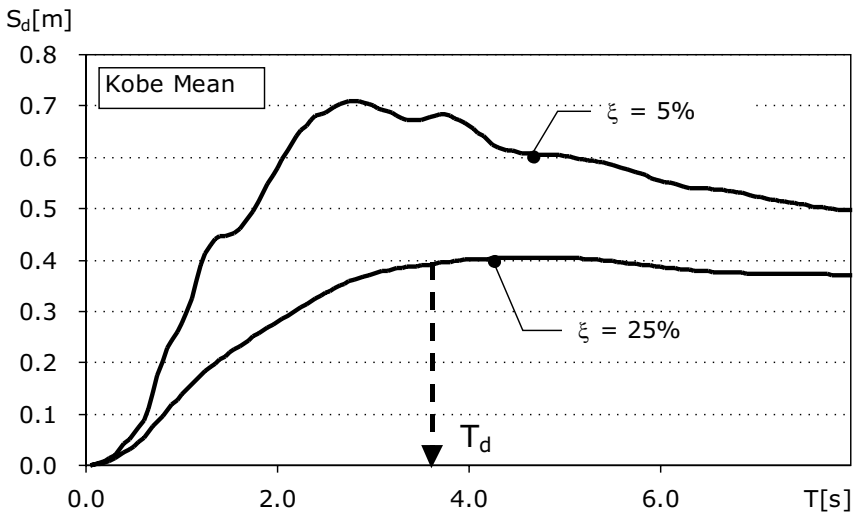

Figure 11-4 Example: Determination of plateau periods and η_1 for mean deformation spectra

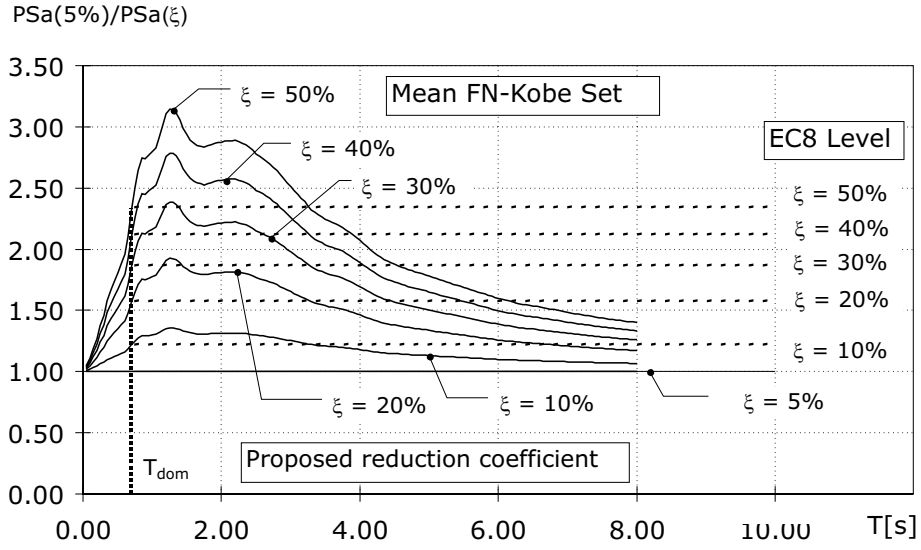

Figure 11-5 Example: Proposed simplified reduction concept spectra

11.3 Appendix C: Period dependent reduction coefficient for total acceleration spectra

In engineering practice, the differences in pseudo-accelerations PSa and total accelerations Sa are often neglected. As illustrated in Fig 11-6, however, the deviations become considerable in the long-period range if large damping is applied. Respecting this aspect is especially obligatory in base isolation design.

As can be confirmed from Fig. 11-6, the relation between the total and pseudo-accelerations in the long period range from 2 to 8s is nearly linear. So a linearized version for the long-period range is proposed

$$r = \frac{Sa_\xi(T)}{PSa_\xi(T)} = \eta_2 T\,(2\xi)^{5/3} + 1 \tag{11-12}$$

The coefficient η_2 is constant for each ground motion set. It provides an adjustment option using $r_{50\%}(T = 6sec)$ that is determined by time-history analysis at a period of 6 seconds and a damping ratio of 50%.

$$\eta_2 = \frac{1}{6\,\mathrm{sec}}\left[r_{50\%}(T = 6\,\mathrm{sec}) - 1\right] \tag{11-13}$$

For practical purposes, η_2 is approximately

$$\eta_2 \approx \frac{1}{3}\,\mathrm{sec}^{-1} \tag{11-14}$$

An example application is plotted in Fig. 11-7.

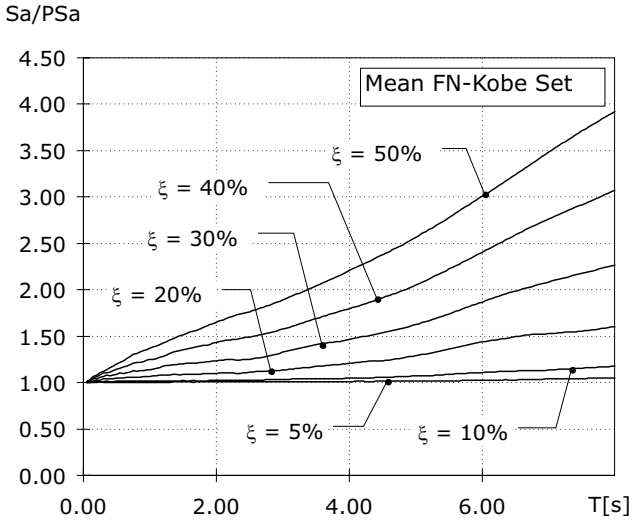

Figure 11-6 Ratio of mean total accelerations to pseudo-accelerations for different levels of damping calculated by time-history analysis

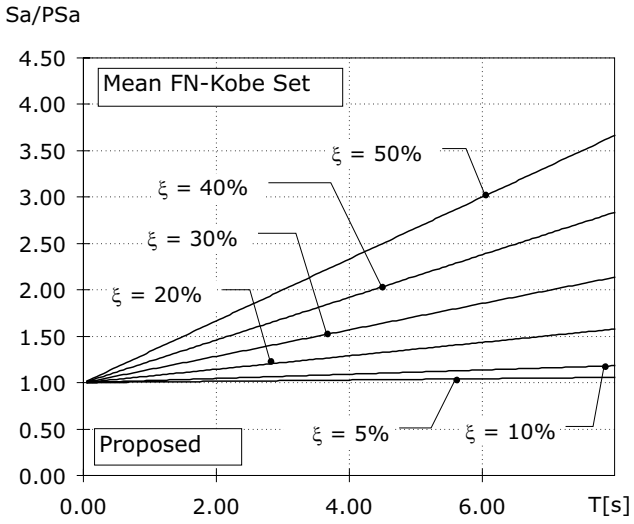

Figure 11-7 Ratio of mean total accelerations to pseudo-accelerations for different levels of damping calculated by the proposed approximation

11.4 Appendix D: Coefficients for modified equivalent linearization in the long period-high damping range

For flexible structures, the difference between the excitation period T_{exc} and equivalent period of a structure T_{equ} are increased. The viscous and hysteretic damping energy are not equivalent. The explicit consideration of a period dependency of the damping ratio is incorporated by the following damping modification factor

$$\nu_1 = \frac{T_{exc}}{T_{equ}} \tag{11-15}$$

Because the seismic response is non-stationary, a mixed influence of the dominant ground motion period T_{dom} and the structural eigenperiod T on the response is notable. The following weighted average formulation for the excitation period describes this influence

$$T_{exc} = \alpha_1 T + (1 - \alpha_1) T_{dom} \qquad 0 \leq \alpha_1 \leq 1 \tag{11-16}$$

From parametric studies, the contribution of the eigenperiod T is found to be greater than that of T_{dom}, so the interpolation coefficient $\alpha_1 \approx 0.6$ can be adopted. The dominant period is according to Eq. (11-10). The relation of the excitation period to the eigen- and dominant period within the acceleration spectrum is illustrated in Fig. 11-8.

The equivalent damping is commonly derived with the assumption of stationary response, establishing perfect hysteretic loops. It is known that cycles due to transient excitations are often incomplete and therefore develop less damping, thus larger responses. Figure 11-9 explains this effect, wherein the maximum deformation u_{max} is mainly dependent on the maximum deformation in the previous half-cycle u_pre. To account for reduced damping, resulting from incomplete cycles, adjustment factors for the damping ratio are utilized [140,115]. However, it can be shown that the formation of cycles is period dependent and so the accompanied damping reduction effect. At smaller periods, where the dominant ground period is close to the structural period, the damping ratio is reduced because the cycles are often interrupted by short elastic pulses. For longer periods this influence decreases, as high frequencies are filtered. However, the total amount of cycles and the transmitted energy are reduced. Consequently, the probability for a hysteresis completion is reduced as well, and the real damping is again smaller than estimated within the equivalent model. It can be observed, that the location of the maximum is close to the plateau period T_d, determined in the reduced deformation spectrum (see Appendix 11.2). At this period, where the sensitive part of the deformation spectrum begins, the response is characterized by large deformations accompanied by high energy, which increases the probability of full cycle responses.

The effect can be considered in the equivalent model by the modification of the damping ratio with a second factor. As in Fig. 11-9, the tendency for full cycles reduces with increasing distance of the structural period T from the period T_d, approximately according to a quadratic function with the maximum value at T_d. The following approach is applied

$$\nu_2 = 1 - \alpha_2 \frac{(T_d - T)^2}{T_d^2} \qquad with \qquad \alpha_2 \approx 1.0 \tag{11-17}$$

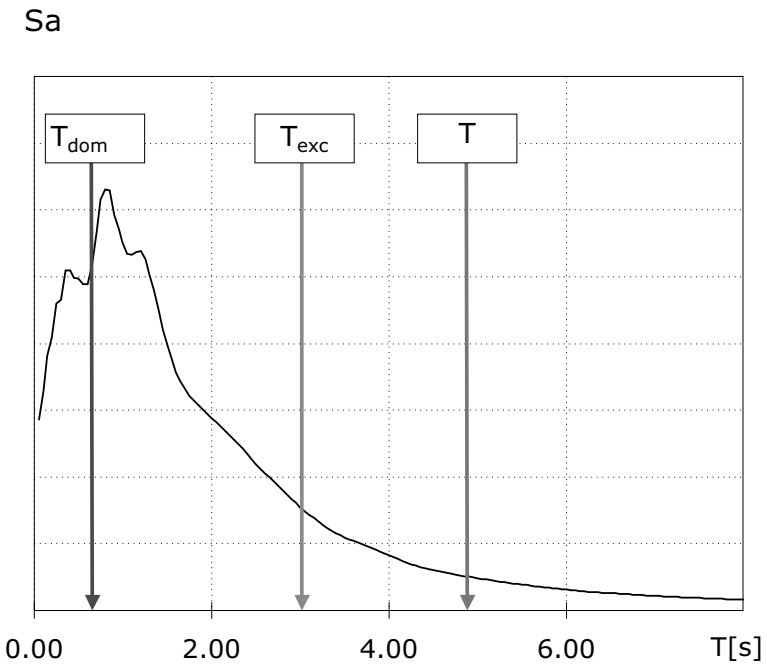

Figure 11-8 Definition of the excitation period

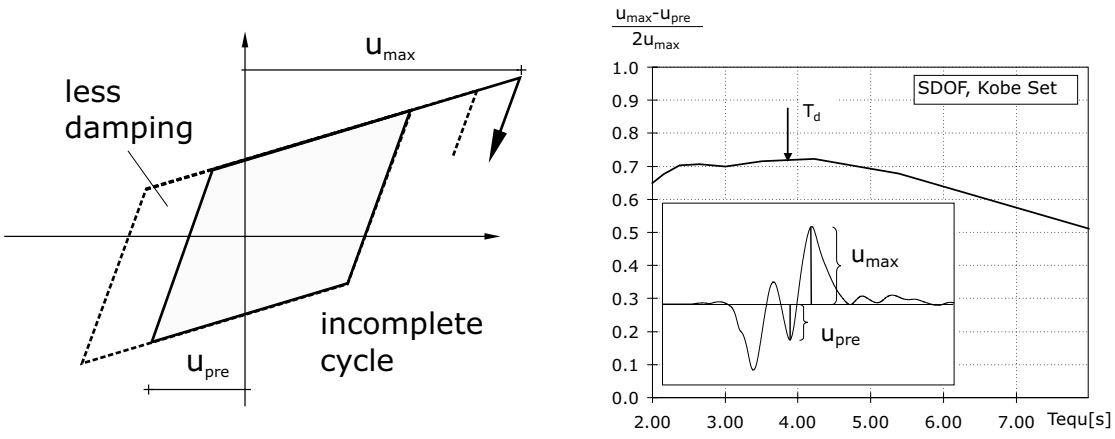

Figure 11-9 Deformations due to complete and incomplete loops and period dependency of cycle completion

11.5 Appendix E: Galerkin Method for solving Poisson differential equation

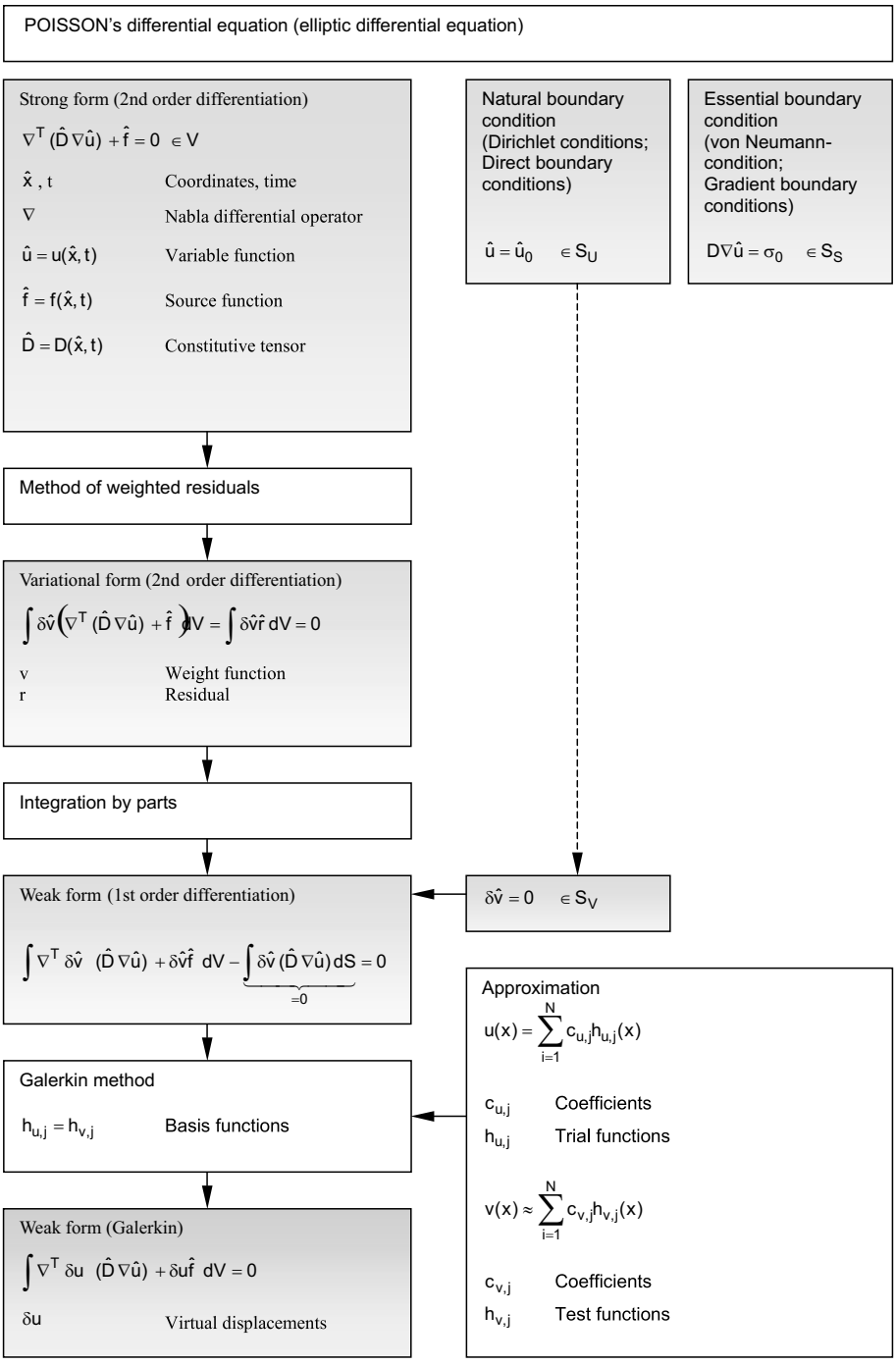

11.6 Appendix F: Kobe ground motion set

Table 11-1 Kobe near-fault set (fault normal) [164]

Record	PGA (m/s^2)	max Sv(m/s)	η_1 (2-8 sec) (m/s)
FN-AMC	3.45	1.72	4.40
FN-EKB	4.05	3.87	11.54
FN-FKA	8.28	3.30	19.23
FN-KB3	3.28	2.28	10.22
FN-KBU	3.22	1.72	3.94
FN-KOB	8.49	3.29	6.06
FN-KOJ	5.09	2.21	9.41
FN-PR1	6.80	1.45	5.29
FN-RKI	3.68	2.43	7.10
FN-TKT	7.41	4.89	16.60
FN-TKZ	6.38	1.97	7.57
KOBE-FN-MEAN	-	2.02	8.21

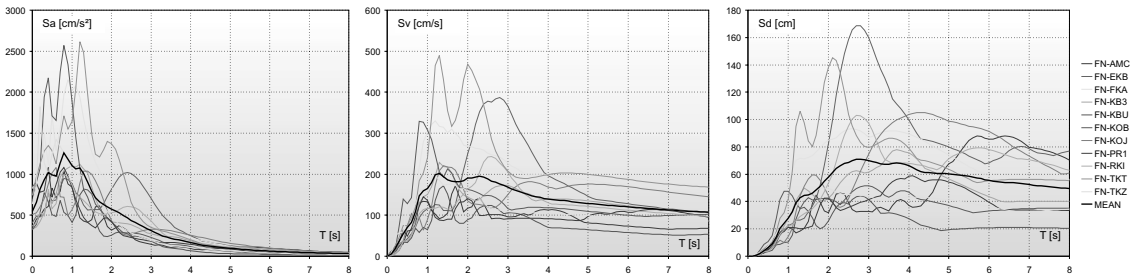

Figure 11-10 Spectra of Kobe ground motion set

11.7 Appendix G: SAC-FEMA project Los Angeles 10in50 ground motion set

Table 11-2 LA set (10% probability in 50 years) [200]

Record	PGA (m/s^2)	max Sv(m/s)	η_1 (2-8 sec) (m/s)
LA01	4.52	1.71	6.36
LA02	6.63	1.81	5.51
LA03	3.86	1.89	8.67
LA04	4.79	1.73	7.67
LA05	2.96	2.17	9.98
LA06	2.30	1.17	6.12
LA07	4.13	1.82	4.62
LA08	4.17	1.46	4.20
LA09	5.10	2.44	6.84
LA10	3.53	1.71	6.36
LA11	6.52	1.84	8.01
LA12	9.51	1.40	3.22
LA13	6.65	1.82	5.60
LA14	6.44	2.25	6.41
LA15	5.23	1.65	8.88
LA16	5.69	1.89	8.42
LA17	5.58	1.98	7.83
LA18	8.01	1.93	9.30
LA19	9.99	1.76	6.39
LA20	9.68	1.94	13.03
LA-MEAN	-	1.29	5.94

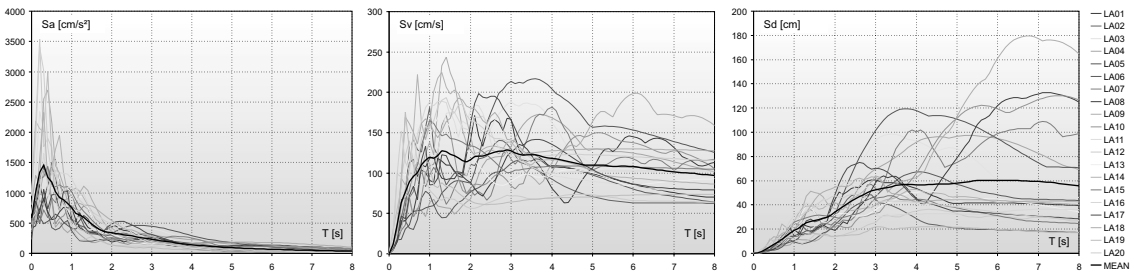

Figure 11-11 Spectra of SAC-FEMA project LA 10in50 ground motion set

11.8 Appendix H: Conventional ground motion set

Table 11-3 Conventional set

Record	PGA (m/s^2)	max Sv(m/s)	max Sd(m)
El Centro EW	2.10	1.09	0.56
El Centro NS	3.42	1.18	0.41
Hachinohe EW	1.83	2.93	1.62
Hachinohe NS	2.25	3.14	1.67
Miyagi EW	2.03	0.90	0.24
Miyagi NS	2.58	1.50	0.28
Taft EW	1.76	0.65	0.39
Taft NS	1.53	0.64	0.28
C-MEAN	-	2.02	0.59

11.9 Appendix I: Dissipation energy bounds (strategy Atkociunas/Norkus)

The strategy is according to Atkociunas/Norkus [12], for estimation of the upper and lower bounds of the dissipation energy at shakedown state.

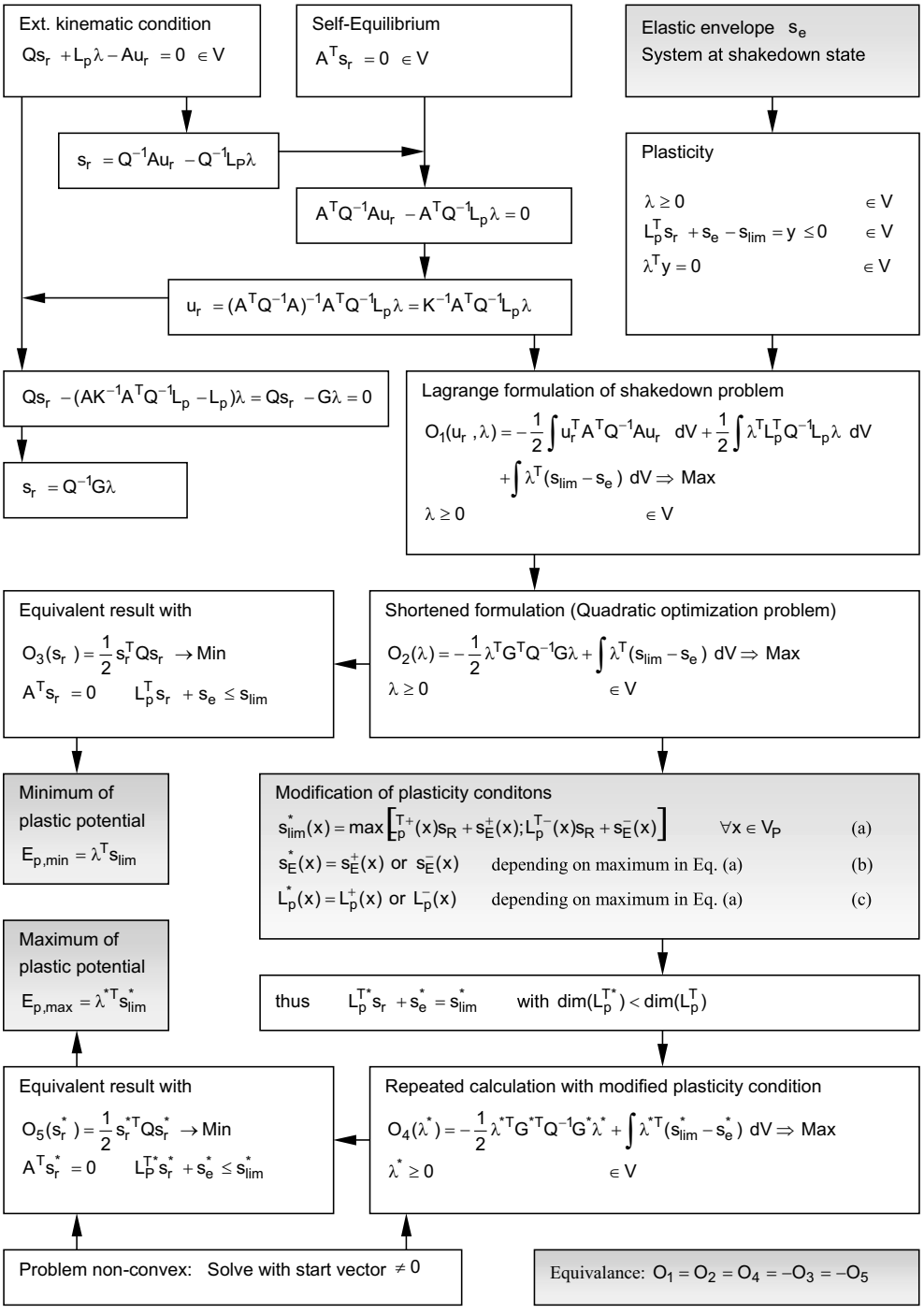

11.10 Appendix J: Displacement bounds (strategy Ponter)

The strategy is according to Ponter [178], for estimation of the upper and lower bounds of residual displacements at shakedown state.

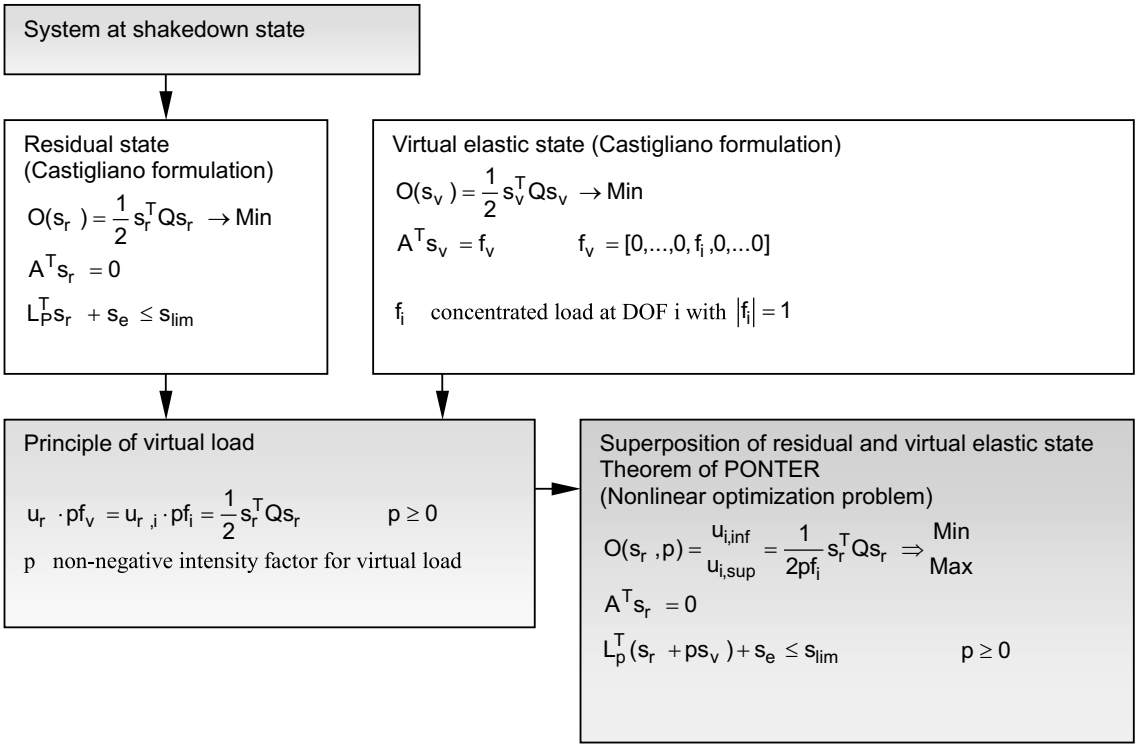

11.11 Appendix K: **Residual displacement bounds (strategy Atkociunas/Norkus)**

The strategy is according to Atkociunas/Norkus [12], for estimation of the upper and lower bounds of residual displacements at shakedown state.

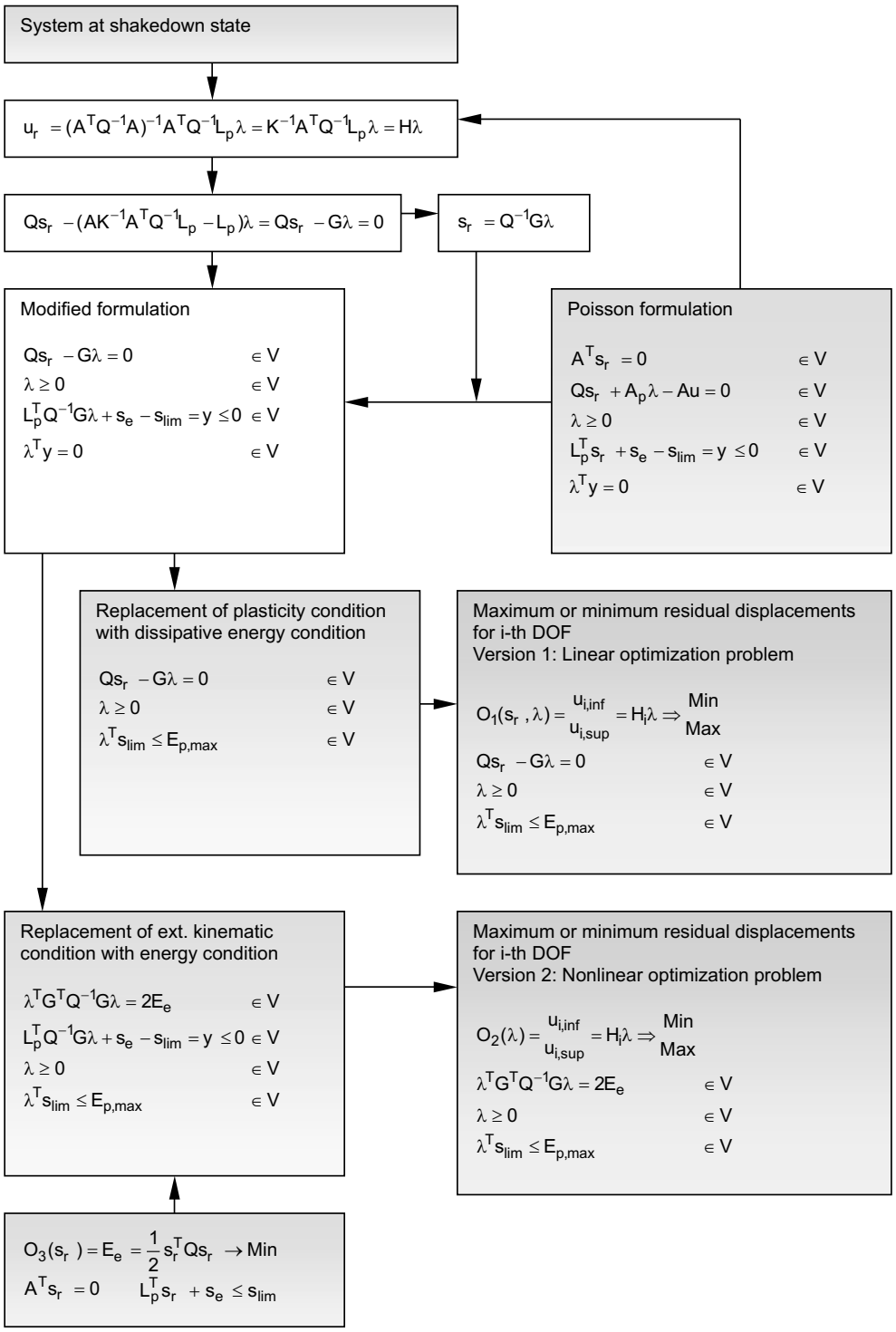

11.12 Appendix L: Example parameter maps (hysteretic damping)

The given maps are examples for the graphical design of base-isolated structures using a combination of rubber bearings and hysteretic damping (using LA 10in50 set [200]).

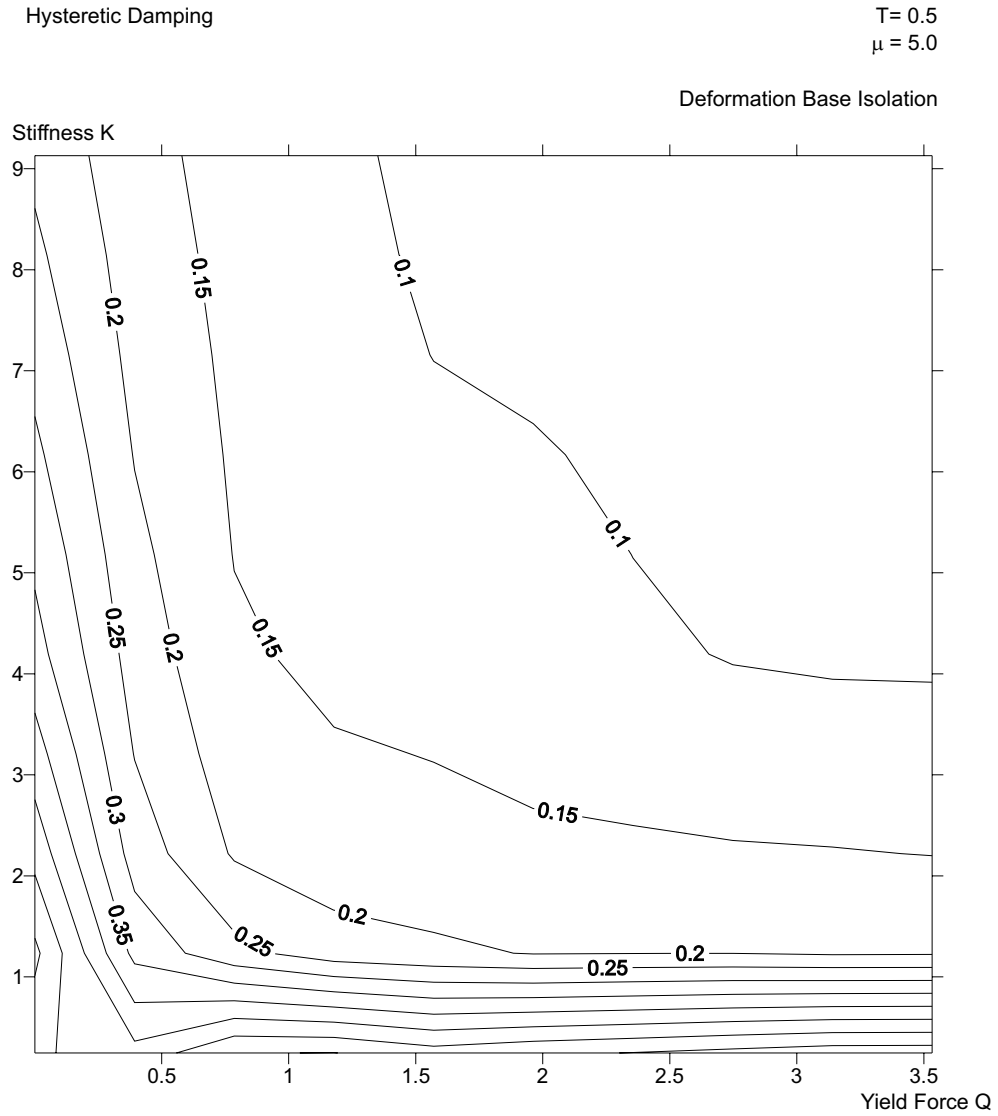

Figure 11-12 Design map for determination of the maximum deflection at base isolation layer height

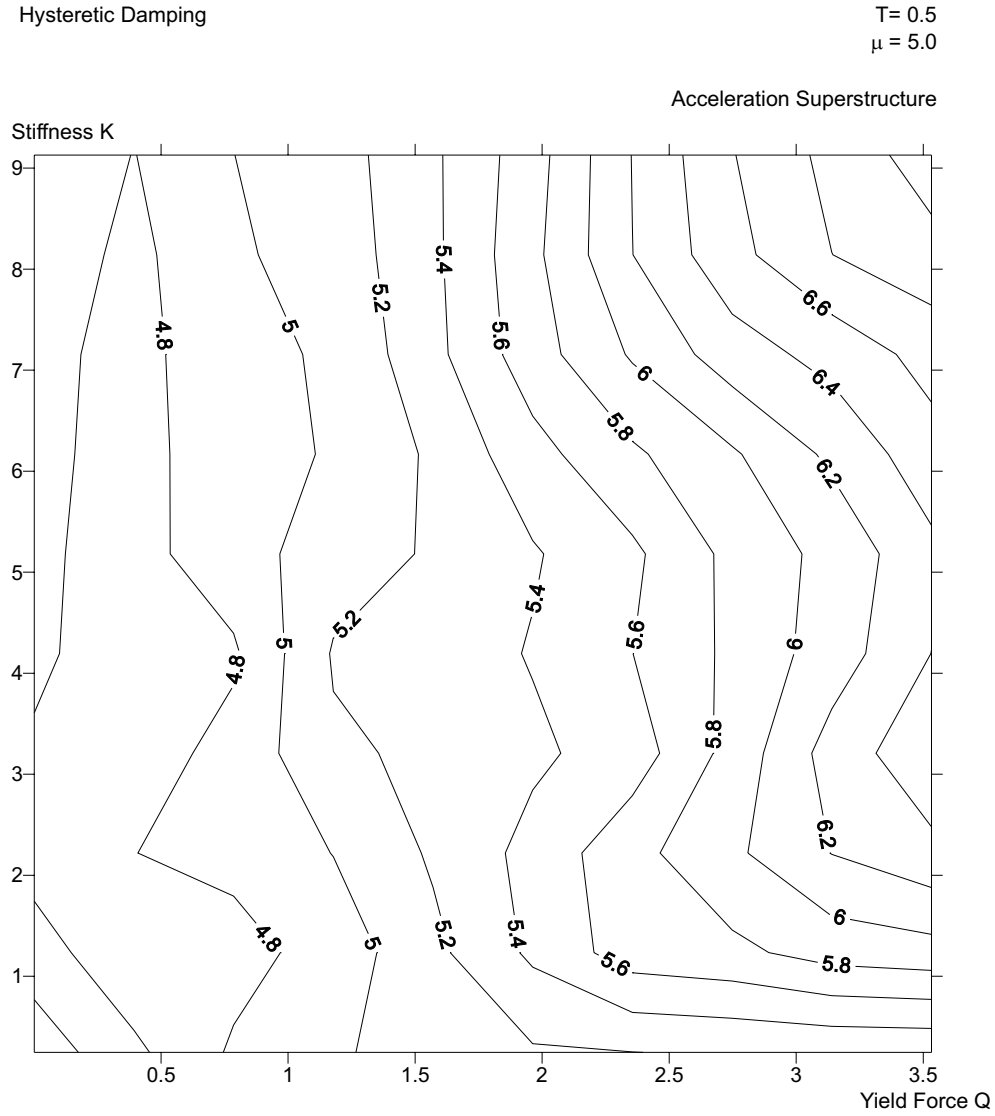

Figure 11-13 Design map for determination of the maximum acceleration at the center of gravity in the superstructure

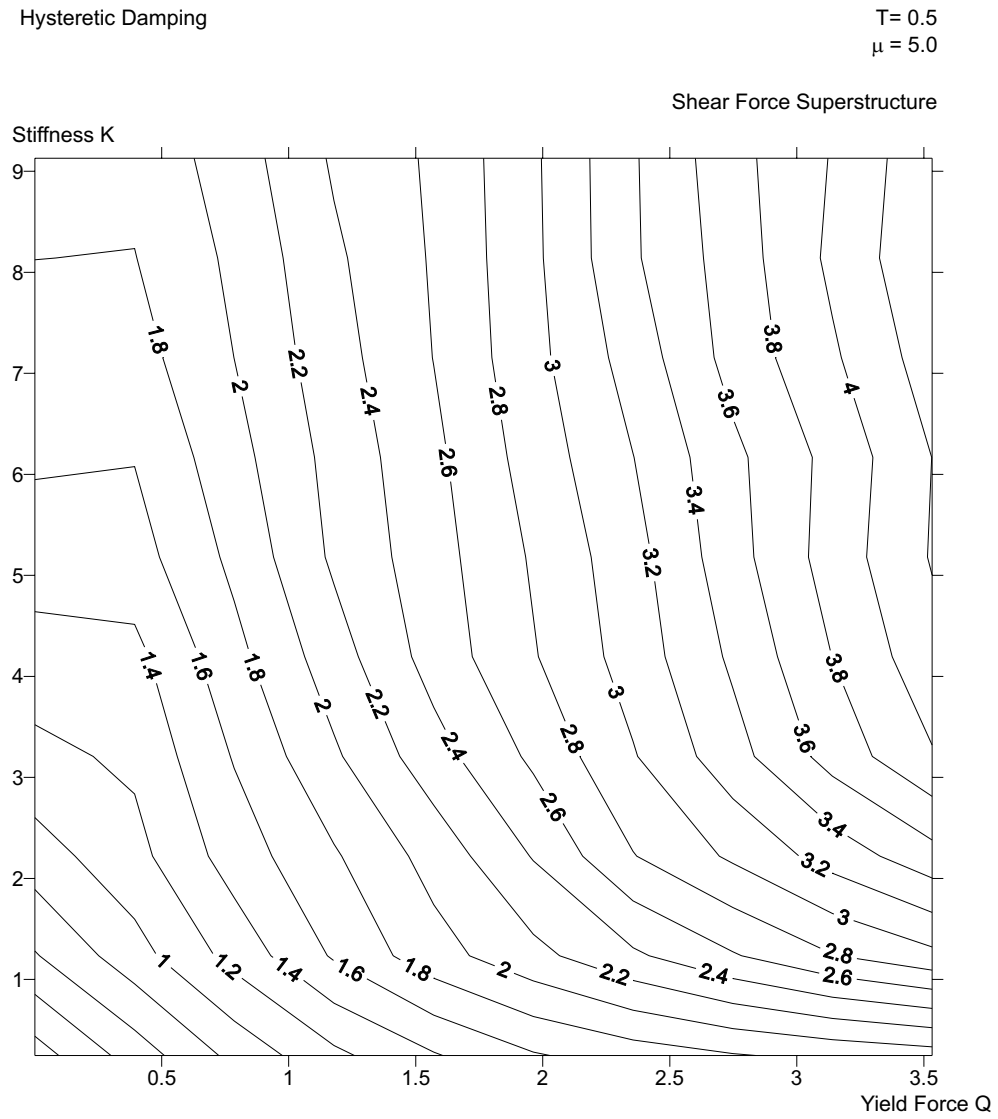

Figure 11-14 Design map for determination of the maximum shear force in the superstructure measured at the bottom

11.13 Appendix M: Example parameter maps (viscous damping)

The given maps are examples for the graphical design of base-isolated structures using a combination of rubber bearings and viscous damping (using LA 10in50 set [200]).

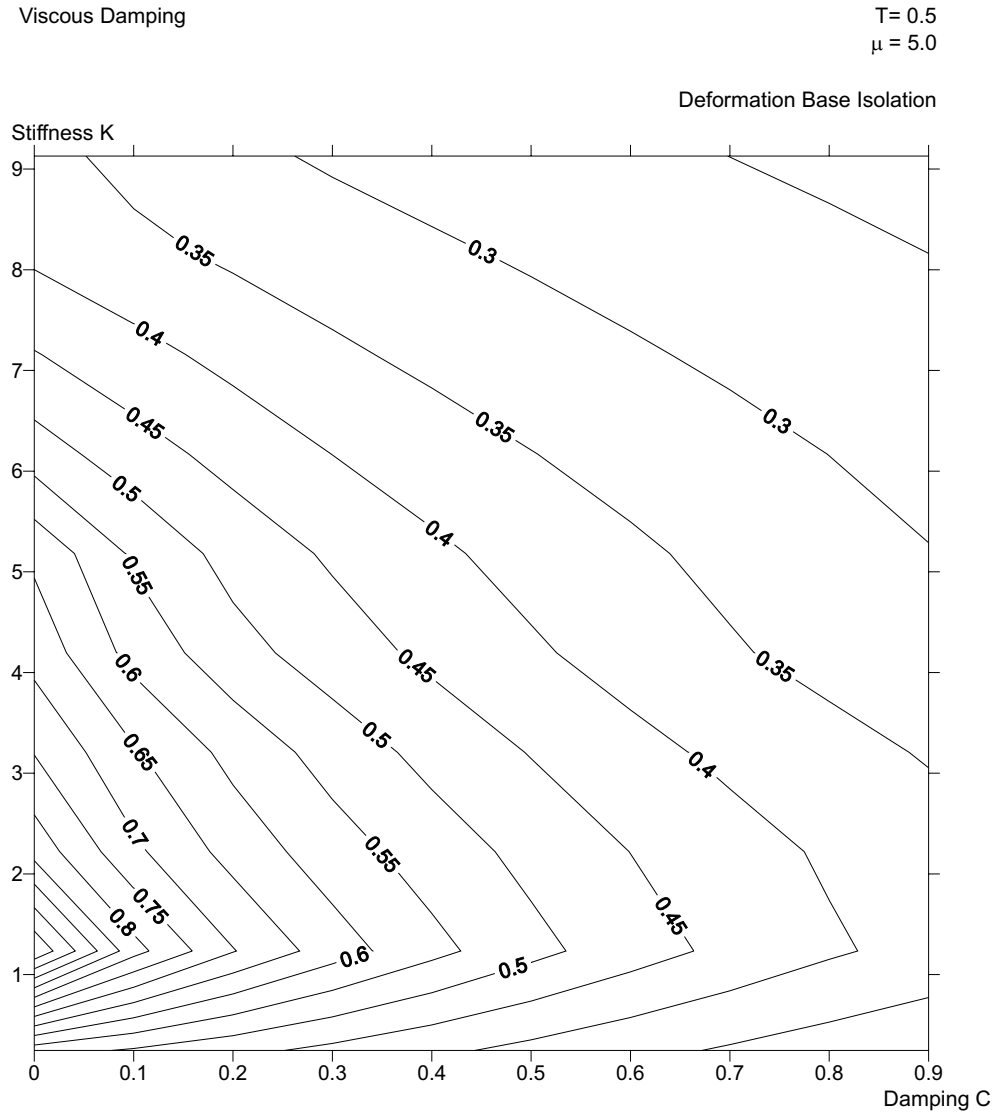

Figure 11-15 Design map for determination of the maximum deflection at base isolation layer height

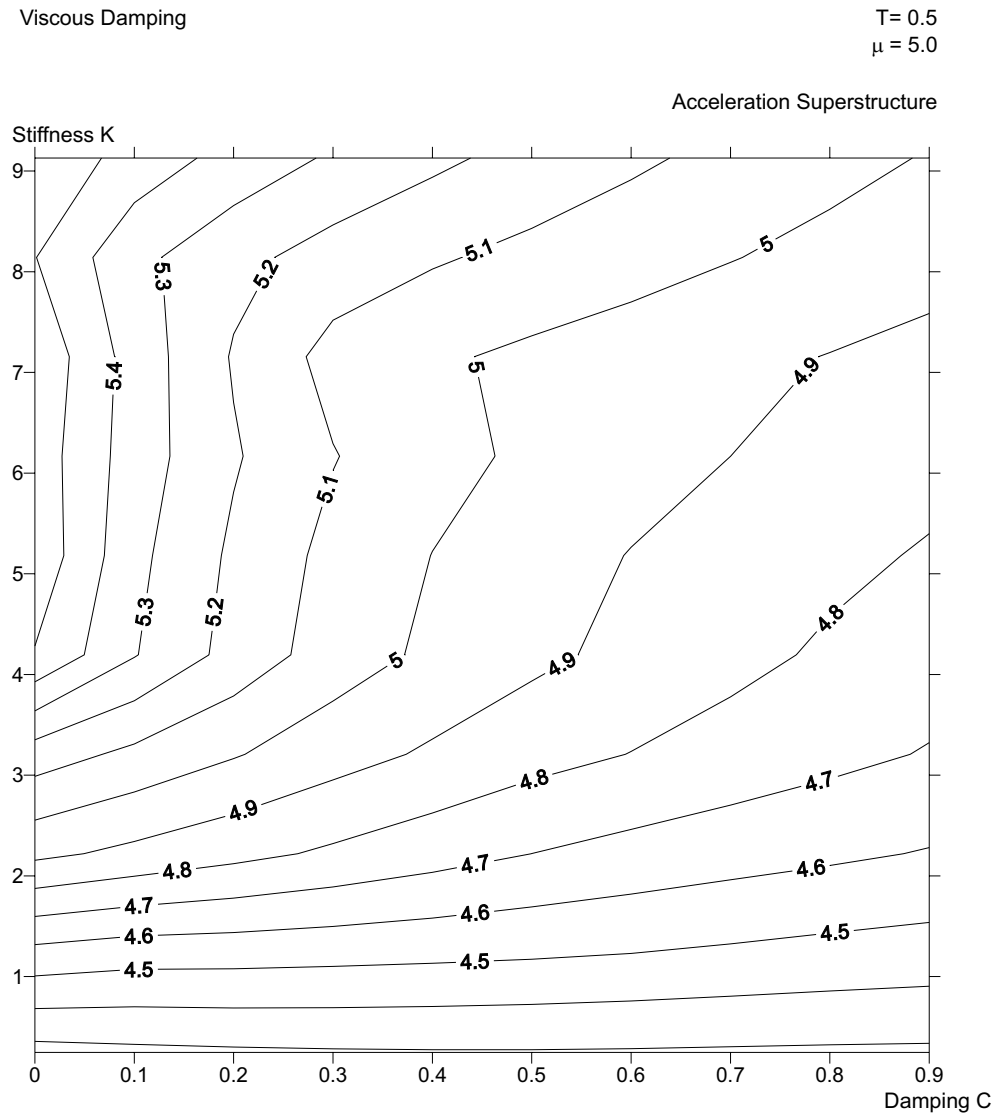

Figure 11-16 Design map for determination of the maximum acceleration at the center of gravity in the superstructure

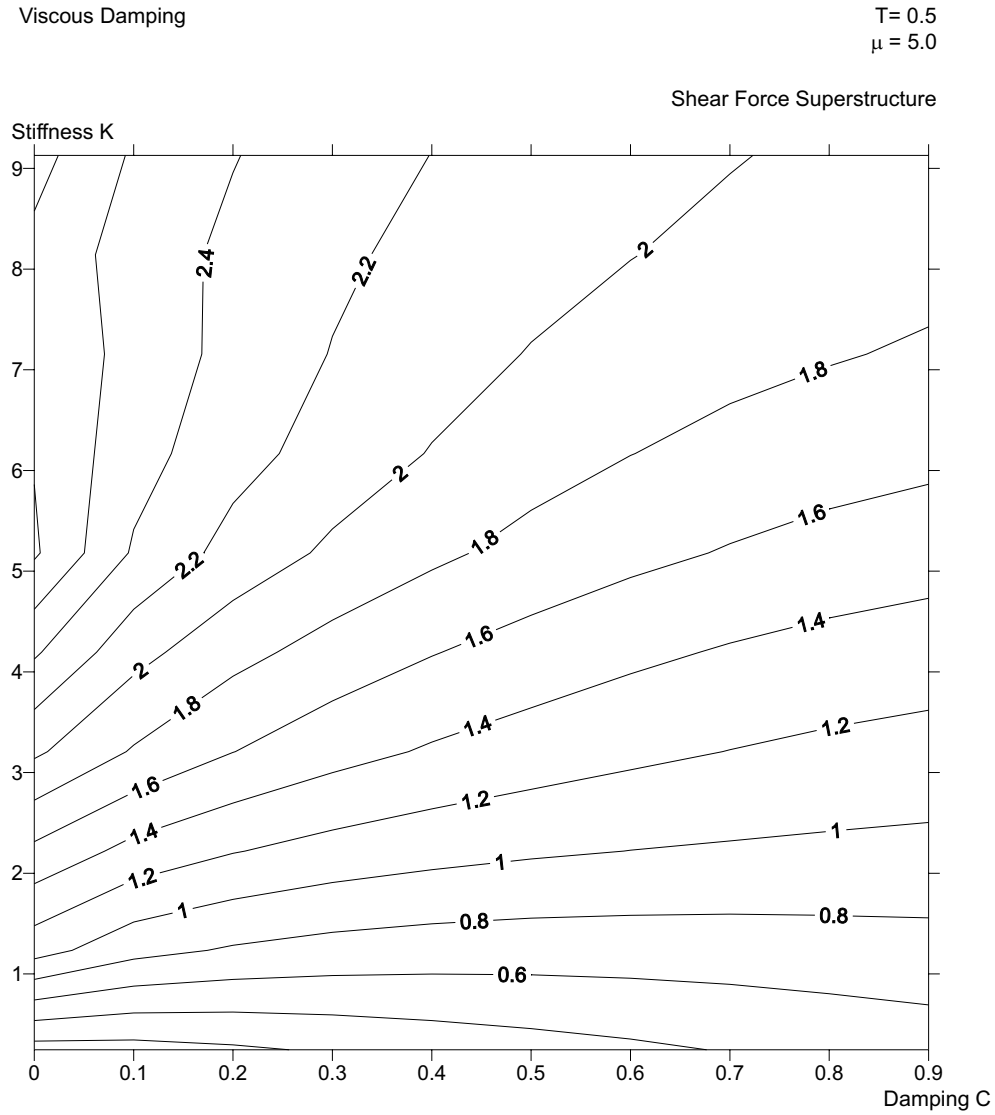

Figure 11-17 Design map for determination of the maximum shear force in the superstructure measured at the bottom

12 Notations and lists

12.1 Notation and abbreviation

If not otherwise stated in the text, the following notation is applied:

Table 12-1 General notation

Variable	Description
$\hat{a}$	Tensor notation
a_E	Element related, discrete value
a_N	Node related, discrete value
a	Matrix/vector/scalar notation
${}^t a$	Related to time t
a^T	Transposed value
a^{-1}	Inverse value

Table 12-2 Indices

Index	Description
0	Initial value
$1, 2, 3$	Counts or principal directions
a	Shakedown (adaptation) state related parameter
b	Base related parameter
C	Cauchy type or Damping related
cd	Conservative deformation limit state
cs	Conservative stress limit state related parameter
d	Deformation based limit state related parameter
DP	Drucker-Prager
e	Elastic behavior related parameter
E	Element edge related parameter
EFG	EFG related
eng	Used in engineering
ϕ	Force related parameter
g	Geometry related
G	Inequality condition related parameter Geometric nonlinear part
i	Count variable related
$intern$	Internal parameter
iso	Isotropic parameter
j	Count variable related
kin	Kinematic parameter
L	Linear plasticity condition
lim	Limit or ultimate value
log	Logarithmic or Hencky type
M	Inertia related

Table 12-3 Indices (conclusion)

Index	Description
$mode$	Mode related value
nom	Nominal or Biot type
N	Node related
NL	Nonlinear
O	Objective function related parameter
opt	Value at optimum point
p	Plastic behavior related parameter
P	1st Piola-Kirchhoff
PS	Plastic strain related
$quad$	Quadratic or Green-Lagrange/2nd Piola-Kirchhoff type
r	Residual state related parameter
s	Stress or equilibrium condition or Superstructural parameter
$stat$	Statical component
$total$	Total amount
u	Kinematic condition related parameter or ultimate value
v	Virtual state related parameter
vM	von Mises
x	Design variable or coordinate related value
YF	Yield function related

Table 12-4 Parameters and variables

Variable	Description
0	Zero value, vector, matrix
a	Variable, coefficient or Amplitude vector
α	Vvariable
A	Area or Coefficient matrix of kinematic and equilibrium conditions
A_h	Hardening coefficient matrix
b	Variable
B	Differential operator
c	Variable
C	Cauchy tensor or Damping matrix
c_s	Constant value of statical boundary conditions or Seismic coefficient
c_u	Constant value of geometric boundary conditions
d	Variable
D	Material tensor or Elasticity tensor
e	Variable, General strain parameter
E	Modulus of elasticity or Energy
ε	Strain
f	General function/variable or External forces vector
f_B	Base shear force
F	Field conditions or Shear force
φ_S	Surface force density
φ,φ_V	Volumetric force density
$\hat{\phi}$	Force tensor
Φ	Modal matrix or Matrix of phase angles
h	Equality condition or hardening coefficient
H	Hesse matrix

Table 12-5 Parameters and variables (conclusion)

Variable	Description
H_c	Interpolation matrix of damping distribution
H_m	Interpolation matrix of mass distribution
H_g	Interpolation matrix of geometry
H_s	Interpolation matrix of stresses/internal forces
H_u	Interpolation matrix of displacements
g	Inequality condition or variable
G	General inequality condition or boundary condition
G_g	Nodal polynomial function of geometry
G_s	Nodal polynomial function of stresses/internal forces
G_u	Nodal polynomial function of displacements
γ_S	Safety factor loading
γ_R	Safety factor resistance
Γ	Matrices of EFG method or Participation factor
i	Count variable
I	Identity matrix of vector
j	Count variable
J	Invariant
J_H	Hamiltonian potential
k	Counting variable
K	Stiffness matrix
K_{geo}	Geometric stiffness matrix
λ	Lagrange multiplier, plastic multiplier
l	Linear contact coefficient
L	Left rotational operator or Linear coefficient matrix
L_p	Linear plasticity coefficient matrix

Table 12-6 Parameters and variables (conclusion)

Variable	Description
L_u	Linear contact coefficient matrix
$\hat{\Lambda}$	Principal stretch tensor
Λ	Vector of eigenvalues
m	Modal mass
M	Mass matrix or Bending moment
n	Number or Normal tensor or Number of replastifications
N	Direction tensor/matrix
ν	Damping density or Poisson coefficient
o	Dual objective function
O	Objective function
Ω	Region
p	Load intensity factor
P	Polynomial interpolation function
Π	Potential
q	Behavior factor
Q	Quadratic matrix or Flexibility matrix
Q_P	Quadratic plasticity coefficient matrix
r	Resistance intensity factor or Radius
R	General resistance or Right rotation operator or Reduction coefficient
ρ	Mass density
s	Internal forces/stresses or Line segment length
S	General loading,excitation or Surface
S_f	Force related surface
σ	Stress
σ_{lim}	Limit stress

Table 12-7 Parameters and variables (conclusion)

Variable	Description
t	Time, current time
Δt	Time step
T	Transformation
T_C	Eigenvectors of Cauchy tensor
Θ	Temperature
τ	Surface related stresses
u	Displacement or eigenform
$\dot{u}$	Velocity
$\ddot{u}$	Acceleration
$\ddot{u}_g$	Ground acceleration
$\hat{U}$	Stretch tensor
v	Generalized coordinate
V	Volume or Extremum function
w	Weight function
W	Work or Weight
x	Coordinates or general design variable
X	Deformation gradient
Ξ	Transfer function
y	Slack variable or coordinate or general function
Y	Yield function
z	Coordinate

12.2 Abbreviations

Table 12-8 Often used abbreviations

Abbreviation	Description
CP	Performance level Collapse prevention
CP	Complementarity problem
CQC	Complete quadratic combination
DOF	Degree of freedom
EFG	Element Free Galerkin Method
FDM	Finite Difference Method
FEM	Finite Element Method
IO	Performance level Immediate occupancy
LP	Linear programming
LS	Performance level Life Safety
MDOF	Multi degree of freedom system
NLP	Nonlinear programming
QP	Quadratic programming
SDOF	Single degree of freedom system
SDP	Semi-definite programming
SLP	Sequential linear programming
SQP	Sequential quadratic programming
SRSS	Square root of sum of squares

12.3 Notation of optimization problems

12.3.1 Notation as formulas

All optimization problems can be noted in formula form. In the braces of the objective function the design variables of the problem are indicated

$$O(x) \rightarrow Min \tag{12-1}$$

As well, the subsidiary conditions are given as equations or inequalities

$$h(x) = 0 \tag{12-2}$$

$$g(x) \leq 0 \tag{12-3}$$

All involved functions can be generally nonlinear.

12.3.2 Tabular notation

For linear or quadratic functions a tabular form is applied within this study. This form enables to display symmetries and dual dependencies between variables.

Table 12-9 Tabular notation of optimization problems

		x_1	x_2	...	x_n	1		result
objective		a_z (	k_{z1}	k_{z2}	...	k_{zn}	c_z	) $\rightarrow$	Min
subsidiary 1	d_1	a_1 (	k_{11}	k_{12}	...	k_{1n}	c_1	) =	0
subsidiary 2	d_2	a_2 (	k_{21}	k_{22}	...	k_{2n}	c_2	) $\leq$	0
⋮		⋮	⋮	⋮	⋱	⋮	⋮	⋮	⋮
subsidiary m	d_m	a_m (	k_{m1}	k_{m2}	...	k_{mn}	c_m	) $\leq$	0

n	number of design variables
m	number of subsidiary conditions
$x_1...x_n$	vectors of primal optimization variables (design variables)
$d_1...d_m$	vector of dual optimization variables
$k_{z1}...k_{zn}$, k_{nm}	coefficients of the objective function or subsidiary conditions
a_z, $a_1...a_m$	multipliers of the objective function or subsidiary conditions
c_z, $c_1...c_m$	constant values of the objective function or subsidiary conditions

12.4 List of figures

The following figures are contained in this study:

1-1 Akashi-Keikyo Bridge, Japan 9
1-2 Base isolated high rise building at Tokyo Institute of Technology, Japan 10
1-3 Plastic design vs. isolation 13
3-1 General body motion 39
3-2 Motion of a line segment 39
3-3 Difference in the strain measure in the initial and current system 40
3-4 Elongation of a line element in current and initial coordinates 40
3-5 Differences in nominal and logarithmic strain measures for a linear force/displacement relationship 50
4-1 Example weight function 60
4-2 Hardening concepts 72
4-3 Linearization of plasticity conditions 73
4-4 Comparison of geometric linear and nonlinear calculation of an extremely loaded shell structure 80
4-5 Integration over bounds using coordinate rotations into the Bernoulli-plane 90
4-6 Model of a polygonally bounded cross section 92
4-7 Illustration of cross section discretization as a fiber or layer model, using rectangular shapes and averaged material properties 94
4-8 Example: Application of nonlinear material laws in layer models of composite cross sections 95
4-9 Derivation of segment models, using fiber or equivalent beam discretizations 97
4-10 Equivalent beam model for the analysis of wall structures 98
4-11 Examples for composite structures 103
5-1 Real and imaginary parts of complex modes 110
5-2 Example eigenvalue analysis (spatial model) 112
5-3 Example eigenvalue analysis (plane frame) 113
5-4 Example: Structural configuration 119
5-5 Example: Artificial accelerograms 119
5-6 Example: Differences in moment development calculated in a linear and nonlinear analysis at Load level 1 120
5-7 Example: Development of concrete strains in the considered beam end 121
6-1 Example: Tuned mass damper 126
6-2 Example: Tuned mass damper, Illustration of design space, minimum point 127
6-3 Example: Application of response spectrum method for the retrofit with cable braces 127
6-4 Comparison of equivalent displacement and energy approaches for the derivation of the reduction factor 129
6-5 Example: Application of the reduction coefficient method 129
6-6 Example: Results from linear calculation obtained with spectrum reduction (R=2.0) 130
6-7 Example: Cross-section behavior for a fixed reinforcement 132
6-8 Definition of equivalent stiffness 133
6-9 Equivalence of responses in viscously and hysteretically damped systems 135
6-10 Dependency of equivalent damping on ductility and stiffness ratio 135
6-11 Example: Design of MDOF structure using equivalent linearization 139
6-12 Example: Moment envelope for the elastic and inelastic systems 139
6-13 Example: Solution space; Dependency of the curvature and system ductility on the stiffness multiplier 140
6-14 Base isolation basic devices and combined reaction 141
6-15 Typical base isolation model assumptions 142
6-16 Elasto plastic analysis model for base isolated structures 142

6-17 Example: Comparison of maximum deformations and accelerations for SDOF obtained by time history analysis and simplified linear analysis, utilizing period-independent spectrum reduction coefficients 143
6-18 Example: Maximum deformations and accelerations for 10-DOF obtained by time history analysis and simplified linear analysis, utilizing period-independent spectrum reduction coefficients 144
6-19 Deformation-acceleration relationship at isolation level for: SDOF, MDOF example and principle of period shift 145
6-20 Example: Comparison of deformations and accelerations for SDOF and MDOF structure 147
7-1 Example: System and initial conditions 158
7-2 Example EFG-FEM: Structural system and parameters 171
7-3 Example EFG-FEM: Domains of different discretization 171
7-4 Behavior characteristics due to different load intensities of elastic-plastic structures 176
7-5 Elastic behavior after certain amount of plastic cycles 177
7-6 Principle of superposition of elastic and residual response components 178
7-7 Determination of the elastic envelope response for nonlinear yield conditions and simplification by polyhedron envelope 179
7-8 Illustration of possible differences in the residual state 189
7-9 Decreasing capacity due to cyclic action 200
7-10 Principle of signal reduction corresponding to the number of re-plastifications n 202
7-11 Example: Plastic rotations development for the design procedure based on the elastic limit load for $n = 0, 2, 4$ 203
7-12 Example: Elastic moments at beam 5 and levels of reduction according to $n = 0, 2, 4$ for an elastic basis 204
7-13 Principle of signal reduction corresponding to the number of re-plastifications n 205
7-14 Example: System, loads, masses, pre-design of stiffness 212
7-15 Example: Design steps D3/D4. 213
7-16 Example: Design steps D5/D6. Calculation of limit state: Fictitious residual state 213
7-17 Bending moment at point 3 for n=5 214
7-18 Plastic beam rotations at point 3 for n = 1,3 and 5; Marked: changes in plasticity direction 214
8-1 Example: Time history analysis, case 1.) impulsive load, case 2.) transient (seismic) load 236
9-1 Shape functions for artificially generated time history plots 241
9-2 Example: Compound envelope function 244
9-3 Comparison of different period-independent reduction coefficients 254
9-4 Comparison of reduction concepts for damping ratio of 30% 255
9-5 Composition of multi-linear material law out of several elastic perfectly-plastic bodies 259
9-6 Penetration of the retaining wall for modification of the mechanical parameters 268
9-7 Pounding against stops, destructive or non-destructive variant 268
9-8 Example Pounding SDOF: Capacity spectrum analysis 269
9-9 Example Pounding 10-DOF: System configuration 270
9-10 Example Pounding 10-DOF: Response for conventional time history set 271
9-11 Example 1.): Determination of responses using given base isolation parameters K and Q 282
9-12 Example 2.): Determination of responses using given base isolation parameters K and acceleration $\ddot{u}_s$ 283
9-13 Example 3.): Determination of responses within a decision area 283
9-14 Example 4.): Determination of number of isolators 284
9-15 Example 5.): Different hardening characteristics for bearings 284

9-16 Example 5.): Involvement of hardening within maps 285
11-1 Example: Determination of plateau periods and η_1 for code spectra 291
11-2 Example: Determination of plateau periods and η_1 for mean acceleration spectra 291
11-3 Example: Determination of plateau periods and η_1 for mean velocity spectra 292
11-4 Example: Determination of plateau periods and η_1 for mean deformation spectra 292
11-5 Example: Proposed simplified reduction concept spectra 293
11-6 Ratio of mean total accelerations to pseudo-accelerations for different levels of damping calculated by time-history analysis 295
11-7 Ratio of mean total accelerations to pseudo-accelerations for different levels of damping calculated by the proposed approximation 295
11-8 Definition of the excitation period 297
11-9 Deformations due to complete and incomplete loops and period dependency of cycle completion 297
11-10 Spectra of Kobe ground motion set 299
11-11 Spectra of SAC-FEMA project LA 10in50 ground motion set 300
11-12 Design map for determination of the maximum deflection at base isolation layer height 305
11-13 Design map for determination of the maximum acceleration at the center of gravity in the superstructure 306
11-14 Design map for determination of the maximum shear force in the superstructure measured at the bottom 307
11-15 Design map for determination of the maximum deflection at base isolation layer height 308
11-16 Design map for determination of the maximum acceleration at the center of gravity in the superstructure 309
11-17 Design map for determination of the maximum shear force in the superstructure measured at the bottom 310

12.5 List of tables

The following tables are contained in this study:

1-1 Basic performance levels according FEMA 356 and associated analysis concepts 14
1-2 Transformation of a design problem into an optimization problem 16
2-1 Selection of optimization categories 19
2-2 Lagrange function and Kuhn-Tucker conditions for optimality 23
2-3 Selection of algorithms for deterministic and heuristic optimization 26
2-4 Algorithmic concepts 29
2-5 Scheme of engineering model-optimization algorithm coupling 30
2-6 Concepts for solving variational problems 32
2-7 Principle for derivation of variational formulations from strong form via weak forms approach 33
2-8 Derivation for principle of stationary potential with weak forms approach 34
3-1 Structure of general differential equation system (DES) 37
3-2 Polar decomposition of deformation gradient (regular approach) 46
3-3 Polar decomposition of geometry gradient (Orthogonal transformation approach) 47
3-4 Polar decomposition of 2D-geometry gradient (Orthogonal transformation approach) 48
4-1 Discretization categories in structural dynamics 56
4-2 Derivation of engineering operator matrix of kinematic conditions 61
4-3 Linear/nominal strain measures 65
4-4 Use of nonlinear strain measures (nonlinear strains, stresses and forces) 65
4-5 Use of nonlinear strain measures (nonlinear strains and stresses) 66
4-6 Use of nonlinear strain measures (nonlinear strains) 66
4-7 Elastic material matrix D 69
4-8 Elastic isotropic material matrix D (plane special cases) 70
4-9 Derivation of operator matrix of equilibrium conditions 77
4-10 Detailed relation scheme of mechanical quantities for elastic-plastic structures 81
4-11 Reduced relation scheme of mechanical quantities for elastic-plastic structures (Strains eliminated) 82
4-12 Simplified relation scheme of mechanical quantities for elastic-plastic structures (Strains, slack variables eliminated, boundary conditions introduced) 83
4-13 Simplified relation scheme of mechanical quantities for elastic-plastic structures (Stresses and strains eliminated, boundary conditions introduced) 84
4-14 Gauss integration parameter derivation (2D example, trapezoidal object) 85
4-15 Integration of arbitrary volumes (2D example) 86
4-16 Direct coupling of systems with different pre-deformation state (elastic example) 100
4-17 Indirect coupling of systems with different pre-deformation state (elastic example) 101
5-1 Example: Real and complex eigenfrequencies using mass proportional damping 113
5-2 Example: Real and complex eigenfrequencies using stiffness proportional damping 113
5-3 Example: Real modes 114
5-4 Example: Complex modes mass proportional damping 114
5-5 Example: Complex modes stiffness proportional damping 115
5-6 Principle of a simplified stability estimation 118
5-7 Example: Comparison of real part eigenvalue differences 120
6-1 Classical response spectrum analysis 125
6-2 Iterative analysis of MDOF systems using equivalent linearization 137
6-3 Analysis of MDOF systems using equivalent linearization and nonlinear optimization 138

7-1 Determination of elastic limit resistance and limit load factor (Poisson formulation) 155
7-2 Steps for determination of elastic limit load factor (Lagrange formulation) 156
7-3 Steps for determination of elastic limit resistance factor (Castigliano formulation) 157
7-4 Example: First natural mode and quasi-static substitution load cases 159
7-5 Example: Moment distribution (Elastic limit resistance) 159
7-6 Example: Residual moment distribution (Elastic limit resistance) 160
7-7 Relation scheme for analysis of rigid plastic bodies (simple boundaries) 161
7-8 Derivation of the principle of conjugated potential (elasto-plastic material) 162
7-9 Derivation of the principle of total potential (elasto-plastic material) 163
7-10 Derivation of the principle of total potential (elasto-plastic material); continued 164
7-11 Optimization scheme for limit load analysis of rigid plastic structures (Static formulation) 165
7-12 Nonlinear optimization scheme for limit load analysis of rigid plastic structures (Kinematic formulation) 166
7-13 Linear optimization scheme for limit load analysis of rigid plastic structures (Kinematic formulation) 167
7-14 Example: Moment distribution (Plastic limit resistance) 169
7-15 Example: Residual moment distribution (Plastic limit resistance) 169
7-16 Optimization scheme for plastic limit load analysis for different domains EFG and FEM 170
7-17 Example EFG-FEM: Results of analysis 172
7-18 Example: Coupled shear wall: Structural system and parameters 173
7-19 Example coupled shear walls: System and deformation for case 2 elastic p= 1.0 and case 2 elasto-plastic p=1.835 173
7-20 Example coupled shear walls: Summary of results 174
7-21 Example coupled shear walls: Elasto-Plastic Response (case 2, p=1.0) 174
7-22 Example coupled shear walls: Elasto-Plastic Response (case 2, p=1.853) 174
7-23 Optimization schemes for shakedown limit state analysis of rigid plastic structures (Static formulation) 181
7-24 Optimization scheme for shakedown state analysis of elasto plastic structures (Static formulation) 182
7-25 Example: Cyclic behavior for plastic strains at plastic limit state for Load Sequence A and B 183
7-26 Example: Cyclic behavior for bending moments at plastic limit state for Load Sequence A and B 183
7-27 Example: a.) Envelope function b.) Residual moment distribution 184
7-28 Example: Moment distribution for load combinations (Shakedown limit resistance) 185
7-29 Example: Residual moment distribution for load combinations (Shakedown limit resistance) 185
7-30 Example: Cyclic behavior for shakedown strains at plastic limit state for Load Sequence A and B 186
7-31 Example: Cyclic behavior for moments at shakedown limit state for Load Sequence A and B 186
7-32 Example: Residual moment distribution after load sequence application (Shakedown limit resistance) 187
7-33 Classical optimization problems for determination of the lower bound for dissipation energy 188
7-34 Two step strategy for estimation of the upper bound of dissipative energy at shakedown state (Successive activation strategy) 190
7-35 Example: Load sequence analysis of dissipative energy at shakedown limit 191
7-36 Strategy for estimation of the upper and lower bound of residual displacements at shakedown state using virtual loads 193

7-37 Strategy for estimation of the upper and lower bounds of residual displacements and stresses at shakedown state using dissipative energy bounds 194
7-38 Example: Load sequence analysis of residual horizontal displacement (shakedown limit state) 195
7-39 Iterative calculation for geometrical nonlinear shakedown analysis (Limit load analysis) 197
7-40 Iterative calculation for geometrical nonlinear shakedown analysis (Limit resistance analysis) 198
7-41 Example: Residual moment distribution after load sequence application (Stress-based conservative limit resistance) 199
7-42 Example: Residual plastic strain distribution after load sequence application (Deformation-based conservative limit resistance) 199
7-43 Example: Resistance factors r for intended numbers of re-plastifications n_{design} and the obtained numbers n_{cal} (on basis of elastic limit state) 204
7-44 Design procedure "Verification" 207
7-45 Design procedure "Dimensioning" 208
7-46 Elastic analysis and derivation of the reduced envelope for strategy based on time history analysis 209
7-47 Elastic analysis and derivation of the reduced envelope for strategy based on response spectrum analysis 210
7-48 Limit state analysis 211
7-49 Example: Resistance factors r for intended numbers of re-plastifications n_{design} and the obtained numbers n_{cal} (on basis of adaptive limit state) 212
7-50 Concepts for deformation based limit state analysis 216
7-51 Optimization scheme for calculation of deformation based limit state according to the concept of shared plastic response 217
7-52 Example: Limitation of the total horizontal deformations using deformation based optimization strategies 218
7-53 Principle of capacity spectrum analysis 220
8-1 Selection of time integration methods in structural engineering 222
8-2 Time integration scheme for implicit one-step methods 224
8-3 Newmark time integration scheme 225
8-4 Optimization problem for implicit time integration (Lagrange approach, elasto-plastic material) 227
8-5 Optimization problem for implicit time integration (Lagrange approach, continued) 228
8-6 Quadratic optimization scheme for step-by-step analysis of elasto-plastic structures (implicit dynamic Lagrange formulation) 229
8-7 Optimization problem for implicit time integration (Castigliano approach) 231
8-8 Optimization problem for implicit time integration (Castigliano approach, continued) 232
8-9 Quadratic optimization scheme for step-by-step analysis of elasto-plastic structures (implicit dynamic Castigliano formulation) 233
8-10 Optimization problem for explicit time integration (Lagrange formulation) 234
8-11 Optimization problem for explicit time integration (Castigliano formulation) 234
8-12 Relation scheme of mechanical quantities for contact problems 235
8-13 Example: Case 1.) Impulsive load at elastic structure 236
8-14 Example: Case 1.) Example: Impulsive load at elastic-plastic structure 237
8-15 Example: Case 1.) Seismic load at elastic structure 237
8-16 Example: Case 1.) Example: Seismic load at elastic-plastic structure 238
8-17 Example: Dynamic limit load intensity factors 239
9-1 Classical artificial time history determination 242
9-2 Example: Time history generation in frequency domain 244
9-3 Example: Artificial time history results obtained by modification of the spectrum amplitudes 245
9-4 Statistically compatible phase function generation 246
9-5 Example: Input time history 247

9-6	Example: Phase function generation	247
9-7	Example: Artificial ground motion	248
9-8	Example: Generation in time domain using random start vector	249
9-9	Example: Generation in time domain	249
9-10	Example: Spectra for random and sinusoidal+random case	250
9-11	Example: Generation of time history set	251
9-12	Example: Spectra of ground motion sets	252
9-13	Mean acceleration spectra of ground motion sets with applied damping	253
9-14	Reduction coefficients calculated by time-history analysis	253
9-15	Pseudo velocity spectra	255
9-16	Proposed approximation	256
9-17	Pounding problem	257
9-18	Simplified pounding analysis	259
9-19	Plots for deformations, dependent on yield force and post-yield stiffness at base level for 2DOF example	261
9-20	Example Strategy I: Deformations and accelerations for varied isolation stiffness K and yield force F, solutions to the design cases a.) and b.)	264
9-21	Parametric study for the influence of the Load intensity and strength in the retaining wall for the Kobe set and the FN-EKB ground motion	266
9-22	Parametric study for the influence of the Load intensity and distance factor; for the Kobe ground motion set	267
9-23	Example pounding 10-DOF: a.) - c.) Comparison of maximum responses d.) Necessary strengthening of the superstructure	272
9-24	Example pounding 10-DOF: Maximum responses for 86% excitation	273
9-25	Iterative procedure for optimization of base-isolated structures	275
9-26	Derivation of a two-parametric model for base isolation layers (hysteretic damping)	277
9-27	Major preparation and application steps	278
9-28	Map generation using time history method	279
9-29	Principle of map application	281
11-1	Kobe near-fault set (fault normal) [164]	299
11-2	LA set (10% probability in 50 years) [200]	300
11-3	Conventional set	301
12-1	General notation	311
12-2	Indices	312
12-3	Indices (conclusion)	313
12-4	Parameters and variables	314
12-5	Parameters and variables (conclusion)	315
12-6	Parameters and variables (conclusion)	316
12-7	Parameters and variables (conclusion)	317
12-8	Often used abbreviations	318
12-9	Tabular notation of optimization problems	319

13 References

1. Abaqus Inc: Getting started with ABAQUS Version 6.5, Manual, Abaqus, Inc. 2004
2. Adami, K.: Physically nonlinear analysis of multi-storey buildings with methods of mathematical optimization (in German: Beitrag zur physikalischen nichtlinearen Analyse von Aussteifungssystemen mit Methoden der mathematischen Optimierung); PhD-Thesis. Bauhaus-University Weimar, 2002
3. Akkar, S.; Miranda, E.: Critical Review of Equivalent linear methods in ATC-40; Fifth International Conference on Earthquake Engineering; 16-30 May 2003; Instambul Turkey; 2003
4. Almansi, E.: Sulle deformazioni finite dei solidi elastici isotropi, I. Rendiconti della Reale Accademia dei Lincei, Classe di scienze fisiche, matematiche e naturali, v. 20, pp. 705-714. 1911
5. Alt, W.: Nonlinear Optimization (in German: Nichtlineare Optimierung - Eine Einführung in Theorie, Verfahren und Anwendungen); Vieweg Studium; Vieweg Verlag; 2002
6. Ansys Inc.: User manual Ansys 6.1; SAS IP, Inc, 2002
7. Arora, J.S.: Introduction to optimum design; Second Edition; Elsevier; 2004
8. Ascher, U.M.; Ruuth, S.J.; Wetton, B.T.R.: Implicit-Explicit Methods for Time-Dependent Partial Differential Equations;SIAM Journal on Numerical Analysis, Vol. 32, No. 3 (Jun., 1995) , pp. 797-823
9. Applied Technology Council ATC: Seismic evaluation and retrofit of concrete buildings, report ATC-40; Applied Technology Council; Redwood City; California; 1996
10. Atkociunas, J.; Borkowski, A.; König, J.A.: Improved bounds for displacements at shakedown. Comput. Meth. Appl. Mech: Engng, 28,365-376; 1981
11. Atkociunas, J.: Design of elastoplastic systems under repeated loading. Vilnius, Science and Encyclopedia Publishers (in Russian); 1994
12. Atkociunas, J.; Norkus, A.: Method of fictitious system for evaluation of frame shakedown displacements. Comput. Struct. 50 (4) 563-567; 1994
13. Atkociunas, J.: Compatibility equations of strains for degenerate shakedown problems; Comput. & Struct Vol. 63. No. 2. pp. 277-282; 1997
14. Atluri, S.N.:Alternate Stress and Conjugate Strain Measures, and Mixed Variational Formulations Involving Rigid Rotations, for Computational Analyses of Finitely Deformed Plates and Shells: Part-I: Theory; Computers & Structures, Vol. 18, No. 1, pp. 93-116, 1984
15. Bachmann, H.: Erdbebensicherung von Bauwerken (in German); Birkhäuser; 2nd Edition , 2002
16. Bajer, C.. Triangular and tetrahedral space-time finite elements in vibration analysis. Int. J.Numer. Meth. Engng., 23:2031-2048, 1986.
17. Bajer, C.. Space-time finite element formulation for the dynamical evolutionary process. Appl. Math. and Comp. Sci., 3(2)251-268, 1993.
18. Bajer, C.;Bohatier, C.: The soft way method and the velocy formulation. Comput. and Struct., 55(6):1015-1025; 1995
19. Baratta, A.; Corbi, I.: Optimal design of base-isolators in multi-story buildings; Computers and Structures, 82 pp. 2199-2209; 2004

20. Basar, Y.; Weichert, D.: Nonlinear Continuum Mechanics of Solids- Fundamental mathematical and physical concepts; ISBN 354066601X; Springer 2000

21. Bathe, K.-J.; Ramm, E.; Wilson, E.L. : Finite element formulations for large deformation dynamic analysis; International Journal for Numerical Methods in Engineering; Volume 9, Issue 2 , pp. 353 - 386; 1975

22. Bathe, K.-J. : Finite Elemente Methoden (in German); 2nd. Editon; Springer 2002

23. Bazant, Z. P., Adley, M. D., Carol, I., Jirasek, M., Akers, S. A., Cargile, J. D., Rohani, B., Caner, F. C. : Large-strain generalization of microplane constitutive model for concrete; J. Eng. Mech.; Vol. 126, pp. 971-980; 2000

24. BCJ: Structural Provisions for Building Structures. Building Center of Japan, Tokyo, 2000 (in Japanese).

25. Bleich, H.: Über die Bemessung statisch unbestimmter Stabtragwerke unter Berücksichtigung des elastisch-plastischen Verhaltens des Baustoffes; Der Bauingenieur, Berlin 13, 19/29, S.261; 1932

26. Belytschko, T.; Liu, W.K.: Computational mehods for impact and penetration. Impact: Effects of fast transient loadings, Balkema, Rotterdam; 1988

27. Belytschko, T.; Lu Y.Y.; Gu L.; (1994) Element Free Galerkin Methods; Int. J. Num. Meth. Eng. 37:229-256

28. Belytschko T.; Organ D ;Krongauz Y.(1995); A Coupled Finite Element - Element-Free Galerkin Method; Computational Mechanics

29. Belytschko T.; Krongauz Y.; Organ D.; Fleming M.; Krysl P.; (1996): Meschless methods:an overview and recent developments; Comp. Meth. Appl. Mech. Eng. 139:3-47

30. Belytschko, T., Liu, W., Moran, B.: Nonlinear Finite Elements for Continua and Structures, John Wiley & Sons; 2001

31. Bertram, A.: Elasticity and Plasticity of Large Deformations - An Introduction; Springer 2005

32. Betten, J.: Kontinuumsmechanik: Elasto-, Plasto- und Kriechmechanik; Springer 1993

33. Bommer, J.J.; Elnashai, A.S.; Weir, A.G.: Compatible acceleration and displacement spectra for seismic design codes. Proceedings of the 12th World Conference on Earthquake Engineering, Auckland; Paper No. 207, 2000

34. Bommer, J.J; Mendis, R.: Scaling of spectral displacement ordinates with damping ratios. Earthquake Engineering and Structural Dynamics 34:145-165; 2005

35. Bommer, J. J.; Pinho, R.:Adapting earthquake actions in Eurocode 8 for performance-based seismic design;Earthquake Engineering & Structural Dynamics, Vol.35; John Wiley & Sons Inc. DOI: 10.1002/eqe.530; 2006

36. Borkowski, A.; Atkoiunas, J.: Optimal design for cyclic loading. IUTAM, Optimization in Structural Design, Symposium Warszaw/Poland, Springer, Berlin, pp. 432-440; 1973

37. Borzognia, Y.; Bertero, V.V. (Eds.): Earthquake engineering - form engineering seismology to performance based engineering; CRC Press; ISBN 0-8493-1439-9; 2004

38. Wood,W.L.;Bossak, M.;Zienkiewicz, O.C: An alpha modification of Newmark′s method; Int. J. Num. Meth. Eng., 15:1562-1566, 1981.

39. Bronstein, I.N.; Semendjajew, K.A.: Taschenbuch der Mathematik; Teubner Verlagsgesellschaft, Leipzig, 1960

40. Bruhns, O.T.: Advanced Mechanics of Solids; Springer 2003

41. Bucher, C.; Most, T.: Approximate response functions in structural reliability analysis; 5th Conference on Computational Stochastic Mechanics; Rhodes; Greece; Millpress; 2006

42. Burns, S.A.(Ed.): Recent advances in optimal structural design; ASCE; 2002

43. Cacuci, D. G.; Ionescu-Bujor, M.; Navon, M.: Sensitivity And Uncertainty Analysis: Applications to Large-Scale Systems (Volume II), Chapman & Hall; 2005

44. M. Capurso, A displacement bounding principle in shakedown of structures subjected to cyclic loads. Int. J. Solids Struct. 10, 77-92; 1974

45. Capurso, M.; Corradi, L.; Maier, G.: Bounds on deformations and displacements in shakedown theory. Proc. Materiaux et Structures sous Chargement Cyclique, pp. 213-244, Palaiseau, France; 1978

46. Cartwright,J.H.E; Piro, O.:The dynamics of Runge-Kutta methods; Int. J. Bifurcation and Chaos, 2, pp. 427-449, 1992

47. Castigliano, C. A.: Théorie de l′équilibre des systèmes élastiques et ses applications, Turin; 1879

48. Ceradini, G.: Dynamic shakedown in elastic-plastic bodies; Journal of Engineering Mechanics; Division-ASCE 106: 481-498; 1980

49. Chatfield, Ch: Statistics for Technology; CRC Press;ISBN 0412253402; 1983

50. Chau, K.T.; Wei, X.X.: Pounding of structures modeled as nonlinear impacts of two oscillators; Earthquake Engineering and Structural Dynamics, 30, pp. 633-651; 2001

51. Chopra, A.K.: Dynamics of structures - Theory and application to earthquake engineering; Prentice Hall; Upper Saddle River; New Jersey; 2001

52. Chopra, A.K.; Goel, R.K. : Capacity-demand-diagram methods for estimating seismic deformations of inelastic structures: SDF systems; Pacific Earthquake Research Center Report PEER-1999/02; University of California; Berkeley; California, 1999

53. Chopra, A. K.; Goel, R. K.: A modal pushover analysis procedure for estimating seismic demands for buildings; Earthquake Engineering and Structural Dynamics 31 p561-582; 2002

54. Christensen, P.W.; Klarenberg, A.; Pang, J.S.; Strömberg, N.: Formulation and comparison of slgorithms for frictional contact problems. International Journal for Numerical Methods in Engineerin, Vol. 42 No. 1, pp. 145-174; 1998

55. Comartin, C.D.: ATC 55: Evaluation and Improvement of Inelatic Seismic Analysis Procedures; Phase I Research Summary, ATC Council, December 2001

56. Comartin, C.D.; Aschheim, M.; Guyader, A.; Hamburger, R.; Hanson, R.; Holmes,W.; Iwan, W.; Mahoney, M.; Miranda, E.; Moehle, J.; Rojahn, C.; Stewart, J.: A summery of FEMA 440: Improvement of nonlinear static seismic analysis procedures: 13th World Conference on Earthquake Engineering, Vancouver, B.C.,Canada; Paper No. 1476; August 1-6 2004

57. Constantinou, M.C.; Tadjbakhish, I.G.: Probabilistic optimum base isolation of structures; Journal of Structural Engineering, Vol. 109 (3), pp. 676-688; March 1983

58. Constantinou, M.C.; Tadjbakhish, I.G.: The optimum design of a base isolated system with frictional elements; Earthquake Engineering and Structural Dynamics, 12, pp. 203-214; 1984

59. Corradi, L.; Maier, G.: Inadaptation theorems in teh dynamics of elastic-plastic-work hardening structures; Ingenieur-Archiv, 43, pp. 44-57; Springer Verlag; 1973

60. Corradi, L., and G. Maier: Dynamic non-shakedown theorem for elastic perfectly-plastic continua; Journal of the Mechanics and Physics of Solids 22: 401-413; 1974

61. Corradi, L.; Nova, R.: A comparative study of bounding techniques in dynamic shakedown of elasto-plastic structures; Earthquake engineering and structural dynamics; Vol. 3, pp. 139-155; 1974

62. Corradi, L.; De Donato, O.: Dynamic Shakedown theory allowing for second order geometric effects. Meccanica, June, (2), 93-106; 1975

63. Corradi, L.: Deformation bounding techniques in elastoplastic analysis. In: Cohn, M.Z.; Maier, G. (eds.) Engineering plasticity by mathematical programming, pp. 495-516. New York: Pergamon Press; 1977

64. Cyras, A.A.: Matematiceskie modeli analiza i optimizacii uprugoplasticeskich sistem. Vilnius Mokslas Publishers, 1982 (engl.: Mathematical models for the analysis and optimization of elastoplastic structures. Ellis Horwood Limited, Chichester 1983)

65. Dantzig, G.B.: Linear Programming and Extensions, Princeton Univ. Press; 1963

66. De Donato, O.; Maier, G.: Bounds on dynamic deflections of elastoplastic structures allowing for second-order geometric effects; Mech. Res. Comm. 1, pp. 37-41; Pergamon Press; 1974

67. DesRoches, R.; Muthukumar, S.: Effect of Pounding and Restrainers on Seismic Response of Multiple-Frame Bridges; Journal of Structural Engineering, Vol. 128 (7), pp. 860-869; July 2002

68. Deutsches Institut für Normung (Hrsg .): DIN 1045 Tragwerke aus Beton, Stahlbeton und Spannbeton(in German); 2001

69. Deutsches Institut für Normung (Hrsg .): DIN 4149 - Bauten in deutschen Erdbebengebieten - Lastannahmen, Bemessung und Ausführung üblicher Hochbauten (in German); 2005

70. Dorosz, S.: An upper bound to maximum residual deflections of elastic-plastic structures at shakedown. Bull. Acad. Polon. Sci. Ser. Sci. Tech. 24, 167-174; 1976

71. Drucker, D. C.: A more fundamental approach to plastic stress-strain relations; in: Proceedings of the First US National Congress in Applied Mechanics, ASME, pp. 487-491; 1951

72. Drucker, D. C., Prager, W.: Soil mechanics and plastic analysis of limit design; Quarterly Appl. Math., Vol. 10, pp. 157-175; 1952

73. CEN: Eurocode 8: Design of structures for earthquake resistance, Part 1: General rules, seismic actions and rules for buildings;. European Committee for Standardization; April 2006

74. Engelhardt, M.;Schanz, M.; Stavroulakis G.E.; Antes, H.: Defect identification in 3-D elastostatics using a genetic algorithm; Optim Eng (2006) 7: 63-79 DOI 10.1007/s11081-006-6591-4

75. ETABS Integrated Building Design Software - Manuals; Computer & Structures Inc.; 2002

76. Faires,J.D,; Burden, R.L.: Nummerical Methods, PWS Publishing Company, Boston 1993

77. FEMA 450 - "NEHRP Recommended Provisions for Seismic Regulations for New Buildings and Other Structures"; National Earthquake Hazards Reduction Program; 2003

78. Ferris, M.C., Kanzow, C.: Complementarity and Related Problems: A Survey; Mathematical Programming Technical Report 98-17; November 1998

79. Fiacco, A.V.; McCormick, G.P.: Nonlinear programming: Sequential unconstrained minimization techniques; Philadelphia Society for Industrial and Applied Mathematics; 1968

80. Felippa, C.A.; Fluid-Structure Interaction, Course material; Aerospace Engineering Sciences; University of Colorado at Boulder; http://www.colorado.edu/engineering/CAS/courses.d/FSI.d/; 2004

81. Fleßner, H.: Derivation of cross section parameters using computers (in German: Ein Beitrag zur Ermittlung von Querschnittswerten mit Hilfe elektronischer Rechenanlagen); Der Bauingenieur 37-4; 1962

82. Fletcher, R.: Practical methods of optimization, vol. 1: unconstrained optimization, John Wiley & Sons, New York-Brisbane-Toronto; 1980

83. Fletcher, R.: Practical methods of optimization, vol.2: constrained optimization; John Wiley & Sons, Chichester-New York-Brisbane-Toronto; 1981

84. Gasparini, D.A.; Vanmarcke, E.H.: Simulated Earthquake Motions Compatible with Prescribed Response Spectra, Publication No. 76-4. Department of Civil Engineering, Massachusetts Institute of Technology.; 1976

85. Gill, P.E.; Murray, W.; Wright, M.H.: Practical optimization, Academic Press, London; 1981

86. Göldner, H. et.al.: Lehrbuch höhere Festigkeitslehre; Band 1 und 2, Fachbuchverlag Leipzig - Köln, 1991/92

87. Gosavi, A.: Simulation-Based Optimization; Springer; ISBN 1402074549; 2003

88. Green, G.: On the Propagation of Light in Crystallized Media. Trans. Cambridge Phil. Society, vol. 7, pp. 121-140; 1841

89. Greve, R.: Kontinuumsmechanik - Ein Grundkurs (in German); Spinger 2003

90. Grüning, M.: Die Tragfähigkeit statisch unbestimmter Tragwerke aus Stahl bei beliebig häufig wiederholter Belastung; Springer Verlag Berlin, 1926

91. Gupta, I.D.: A note on response spectra of peak amplitudes expected to be exceeded for a given number of cycles; Soil Dynamics and Earthquake Engineering; Vol 10, Issue 1, Pages 5-9; Jan. 1991

92. Hahn, S.; Weitzmann, R.: Non-linear analysis of hybrid structures with selectively coupled structural and cross-sectional models (in German: Nichtlineare Analyse von hybriden Konstruktionen unter Verwendung selektiv gekoppelter Tragwerks- und Querschnittsmodellen); International Colloquium for Applications of Information Science and Mathematics in Architecture and Civil Engineering (IKM) 2003, Bauhaus-University Weimar, Germany June 2003

93. Hahn, S.; Broßmann, M.: Bewertung von Verfahren zur Analyse von Stahlbetonbauteilen unter veränderlichen Lastkonfigurationen, 16. Forum Bauinformatik, CD zur Tagung, Braunschweig, 2004

94. Hancock,J; Bommer, J.J.: The effective number of cycles of earthquake ground motion; Earthquake Engineering & Structural Dynamics; Volume 34, Issue 6; Pages 637-664, 2005

95. Hencky, H.:Zur Theorie plastischer Deformationen und der hierdurch im Material hervorgerufenen Nachspannungen, ZAMM, Vol. 4, pp. 323-334; 1924

96. Hencky, Heinrich.(1885-1952): Über die Form des Elastizitätsgesetzes bei ideal elastischen Stoffen; Zeitschrift der Technischen Physik; Vol. 9, pp. 215-220, 457; 1928

97. Hencky, H.: Welche Umstände bedingen die Verfestigung bei der bildsamen Verformung von festen isotropen Körpern; Z. Phys. 55, 145-155; 1929

98. Hencky, H.: The law of elasticity for isotropic and quasi-isotropic substances by finite deformations. J. Rheology 2, 169-176; 1931

99. Hencky, H.: The elastic behavior of vulcanised rubber. Rubber Chem. Technol. 6, 217-224; 1933

100. Hilber, H.M; Hughes, T.J.R.; Taylor, R.L.: Improved numerical dissipation for time integration algorithms in structural dynamics. Earthquake Eng; And Struc. Dyn., 5:283-292; 1977

101. Himmelblau, D.M.: Applied nonlinear programming; McGraw-Hill; New York; 1972

102. Ho Hwa-Shan: Shakedown in elastoplastic systems under dynamic loading. Journal of Applied Mechanics, Vol. 39, 1972

103. Hwang, J.S.; Chiou, J.M.: An equivalent linear model of lead-rubber seismic isolation bearings: Engineering structures, Vol. 18 (7) pp. 528-536, 1996

104. ICBO: Uniform Building Code, International Conference of Building Officials, Whittier; 1997

105. ICC: International Building Code, 2003 Edition, International Code Congress, Whittier, California; 2003

106. Iwan, W.D.; Gates, N.C.: Estimating earthquake response of simple hysteretic structures", J. Eng. Mech. Dev. ASCE, June. 1979

107. Jacobsen, L.S.: Steady forced vibrations as influenced by damping", Transactions ASME, Vol. 52, Part 1, pp. APM 169-181, 1930

108. Jangid, R.S.: Optimum damping in a nonlinear base isolation system; Journal of Sound and Vibration, 189 (4), pp. 477-487; 1996

109. Jennings, P.C.; Housner, G.W.; Tsai, N.S.: Simulated Earthquake Motion Generation. EERL, California Institute of Technology; 1968

110. Jennings, P.C.: Equivalent viscous damping for yielding structures; J. Eng. Mech. Dev. ASCE, Feb. 1968

111. Johnson, A.R.; Quigley, C.J.: Frictionless geometrically nonlinear contact using quadratic programming. International Journal for Numerical Methods in Engineering; Vol. 28, pp 127-144; 1989

112. Kaczkowski, Z.: On the application of non-rectangular space-time elements. Mech. Teoret.i Stosow; 21(4):531-542, 1883.

113. Kaliszky, S.; Logo, J.: Plastic behaviour and stability constraints in the shakedown analysis and optimal design of trusses; Struct. Multidisc. Optim. 24, 118-124, Springer-Verlag; 2002

114. Kamogari,Y.; Tanabe, Y.; Kitagawa, Y.: Adaptive selection system of base-isoalation devices based on a soft computing method; JSSI 10th Anniversary Symposium on Performance of Response Controlled Buildings; Yokohama, Japan, Nov. 17-19, 2004

115. Kani, N.; Koshika, N.; Midorikawa, M.; Iiba, M.; Wada, A.: Technical background on the Japanese linearized equivalent method for seismically isolated buildings; Proceedings of Structural Engineering World Congress 2002; Yokohama, Japan; T2-1-b-2; 2002

116. Kantorowitsch, L.W.: Mathematical methods of organization and planning of production (in Russian); Leningrad; 1939

117. Kaplan, H.; Seireg, A.: Optimal design of a base isolated system for a high-rise steel structure; Earthquake Engineering and Structural Dynamics, 30, pp. 287-302; 2001

118. Karmarkar, N.: A new polynomial-time algorithm for linear programming; Combinatorica 4, 373-395; 1984

119. Kashiwa, H.; Nakayasu, N., Nakashima, M.: Response and damage of base-isolated buildings subjected to very large earthquakes; Journal of Structural Engineering, Architectural Institute of Japan, Vol. 51B, March 2005 (in Japanese)

120. Kaufmann, A,; Henry-Larbordere, A.: Integer and mixed-integer programming: Theorie and Application; Academy Press, New York; 1977

121. Kawashima, K.; Aizawa, K.: Earthquake response spectra taking account of number of response cycles; Earthquake Engineering and Structural Dynamics 14, 185-197; 1986

122. Kawashima, K; Aizawa, K: Modification of earthquake response spectra with respect to damping ratio; Proceedings of the Third U.S. National Conference on Earthquake Engineering; Earthquake Engineering Research Institute; Charleston, SC; 1107-1116; 1986

123. Kawashima, K.; Shoji, G.: Effect of restrainers to mitigate pounding between adjacent decks subjected to a strong ground motion; 12th World Conference on Earthquake Engineering, Paper-No. 1435; Auckland, New Zealand, 2000

124. Kelley, J.E.: The cutting plane method for solving convex programs; J. SIAM 8 703-712; 1960

125. Kelly, J. M.: The role of damping in seismic isolation; Earthquake Engineering & Structural Dynamics, Volume 28, Issue 1,3-20; January 1999

126. Kennedy, J.; Eberhart, R.: Particle swarm optimization, in Proc. of the IEEE Int. Conf. on Neural Networks, Piscataway, NJ, pp. 1942-1948; 1995

127. Khachiyan, L.G.: A polynomial algorithm in linear programming; Dokl. Ak. Nauk SSSR 244, 1093-1096; 1979

128. Kikuchi, M.; Oden, J.T.: Contact problems in elasticity: A study of variational inequalities and finite element methods; SIAM, Philadelphis; 1988

129. Kikuchi, M.; Aiken, I.D.; Kitamura, Y.; Ueda, M.: Seismic Response Of Isolated Structures Depending On Hysteresis Models For Isolation Devices; JSSI 10th Anniversary Symposium on Performance of Response Controlled Buildings; Yokohama Japan;November 17-19 2004

130. Kirsch, U.: Design-Oriented Analysis of Structures;Springer;ISBN 1402004435; 2002

131. Klarbring, A.: A mathematical programming approach to three dimensional contact problems with friction. Computer Methods in Applied Mechanics and Engineering; Vol. 58, pp. 175-200; 1986

132. König J.A.: Shakedown of elastic-plastic structures; PWN-Elsevier; Warsaw-Amsterdam; 1987

133. König, J.A.; Siemaszko, A.: Strainhardening effects in shakedown processes; Ingenieur-Archiv 58, 58-66; Springer-Verlag; 1988

134. Koiter,W.T.: General theorems for elastic-plastic solids; Progress in Solid Mechanics I; 6; 203-313; (Edited by I.N. Sneddon and R. Hill), North-Holland, Amsterdam; 1960

135. Kuhn, H.W.; Tucker, A.W.: Linear inequalities and related systems; Princeton Univ. Press, Princeton; 1956

136. Lancaster P.; Salkauskas K. (1981): Surface Generated by Moving Least Square Methods; Mathematics of Computation 37:141-158

137. Lange-Hansen, P.; Nielsen, S.M.: An improved upper bound on the residual deflection in elastic-plastic structures subject to variable loading; Department of Sztructural Engineering, Technical University of Denmark, Series R, No. 224; 1988

138. Lange-Hansen, P.: Comparative study of upper bound methods for the calculation of residual deformation after shakedown. Technical University of Denmark, Dept. of Struct.Engineering and Materials. Series R No. 49; 1998

139. Lee, T.Y.; Kawashima, K.: Effectiveness of supplemental dampers for isolated bridges under strong near-field ground motions; 13h World Conference on Earthquake Engineering, Paper-No. 138; Vancouver, Canada, 2004

140. Lin, Y.Y.; Chang, K.C.: Study on damping reduction factor for buildings under earthquake ground motions. Journal of Structural Engineering (ASCE); 129(2):206-214; 2003

141. Livesley, R.K.: Matrix methods of structural analysis; 2nd. edition; Pergamon Press, Oxford UK; 1975

142. Luenberger, D.: Linear and nonlinear programming. International Journal of Solids and Structures, Vol. 22, No. 12, pp. 1377-1398; 1986

143. Maier, G.: Complementary plastic work theorems in piecewise-linear elasto-plasticity. Int. J. Solids Struct. 5, 261; 1969

144. Maier, G.: On some issues in shakedown analysis; Journal of Applied Mechanics-ASME 68: 799-807; 2001

145. Mase, G.T.; Mase, G.E.: Continuum Mechanics for Engineers; 2nd Edition; CRC Press 1999

146. Maute, K.;Schwarz, S.; Ramm, E.:Adaptive topology optimization of elastoplastic structures; Structural and Multidisciplinary Optimization, Volume 15, Issue 2, Apr 1998, Pages 81 - 91

147. Melan, E.: Theorie statisch unbestimmter Systeme aus idealplastischem Baustoff; Sitzungsbericht der Akademie der Wissenschaften, Wien, Abt. IIa, 145, 195-218; 1936

148. Melan, E.: Der Spannungszustand eines Mieses-Henckischen Kontinuums bei veränderlicher Belastung. Vienna: Sitz. Berg Akad.Wiss., Abt. 11/a 147-173; 1938

149. Michalewicz, Z.; Fogel, D.B.: How to solve it: Modern Heuristics; Second Edition; Springer, 2004

150. Meskouris, K.: Moderne Baudynamik; Ernst & Sohn; 1999

151. Meskouris, K.: Structural Dynamics; Ernst & Sohn; 2000

152. Meskouris, K.: Hinzen, K.-G.: Bauwerke und Erdbeben; Vieweg; 2003

153. von Mises, R.: Mechanik der festen Körper im plastisch-deformablen Zustand, Nachrichten von der Königlichen Gesellschaft der Wissenschaften zu Göttingen, mathematisch-physikalische Klasse, pp. 582-592; 1913

154. Mohr, O.: Welche Umstände bedingen die Elastizitätsgrenze und den Bruch eines Materiales?; Zeitschrift des Vereins Deutscher Ingenieure, Vol. 46, pp. 1524-1530, 1572-1577; 1900

155. Moreschi, L.M.; Singh, M.P.: Design of yielding metallic and friction dampers for optimal seismic performance; Earthquake Engineering and Structural Dynamics, 32, pp. 1291-1311; 2003

156. Most, T.: Stochastic crack growth simulation in reinforced concrete structures by means of coupled finite element and meshless methods; PhD Thesis, Bauhaus-University Weimar, 2005, ISM-Bericht 1/2005, ISSN 1610-7381

157. Murtagh, B.A.: Advance linear programming: computation and programming; McGraw Hill; 1981

158. Myers, H.; Montgomery, C.: Response Surface Methodology: Process and ProductOptimization Using Designed Experiments; Wiley, New York, 1995

159. Naeim, F; Kelly, J.: Design of Seismic Isolated Structures - From Theory to Practice; Wiley New York; 1999

160. Naeim, F.; Alimoradi,A.; Pezeshk,S.: Selection and Scaling of Ground Motion Time Histories for Structural Design Using Genetic Algorithms; Earthquake Spectra, Volume 20, No. 2, pages 413-426, May 2004; Earthquake Engineering Research Institute; 2004

161. Program library NAG; The Numerical Algorithms Group Ltd.; Oxfort; 1998

162. Nguyen, Q.S: On Shakedown Analysis in Hardening Plasticity; Journal of the Mechanics and Physics of Solids 51: 101-125; 2003

163. Nakamura, Y.; Saruta, M.; Mase, S.; Hori, T. The Development Of An Isolated Balanced Structure: Seismic-Free System 21, JSSI 10th Anniversary Symposium on Performance of Response Controlled Buildings, Yokohama Japan; 2004

164. Nakashima, M.; Matsumiya, T.; and Asano, K.: Comparison in Earthquake Responses of Steel Moment Frames Subjected to Near-Fault Strong Motions Recorded in Japan, Taiwan, and the U.S.;International Workshop on Annual Commemoration of Chi-Chi Earthquake, Taipei, Taiwan; September 18-20,pp.112-123, 2000

165. NEOS Optimization Guide; Hosted by Optimization Technology Center; Northwestern University Enanston/Chicago IL; http://www.ece.northwestern.edu/OTC/; accessed: 16th Feb. 2007

166. N.M. Newmark. A method of computation for structural dynamics. Proc. A.S.C.E., 8:67-94, 1959.

167. Newmark, N.M.; Hall, W.J.: Earthquake Spectra and Design; Earthquake Engineering Research Institute, Berkeley,CA; 1982.

168. Norris, A.N.: Eulerian conjugate stress and strain; arXiv.org >cond-mat >arXiv: 0708.2736v2

169. Oden, J.T.; Pires, E.B.: Nonlocal an nonlinear friction laws and variational principles for contact problems in elasticity. Journal of Applied Mechanics, Vol. 50, pp. 67-76, 1983

170. Ogden, R.W.: Non-Linear Elastic Deformations; John Wiley & Sons Inc; 1984

171. Pan, P.; Zamfirescu, D.; Nakashima, M.; Nakayasu, N.: Base-Isolation design practice in Japan: introduction to the post-Kobe approach; Journal of Earthquake Engineering 9:147-171; 2005.

172. K. Park and J.M. Housner. Semi-implicit transient analysis procedures for structural dynamics analysis. Int. J. Num. Meth. Eng., 18:609-622, 1982

173. Plaschko, P.; Brod, K.: Nichtlineare Dynamik, Bifurkation und chaotische Systeme; Vieweg Verlag; 1995

174. C. Polizzotto, Upper bounds on plastic strains for elastic-perfectly plastic solids subjected to variable loads. Int. J. Mech. Sci., 21, 317-327; 1979

175. Polizzotto, C: A unified treatment of shakedown theory and related bounding techniques. J. Solid.Mech.Arch. 7, 19-75; 1982

176. Polizzotto, C.: On the conditions to prevent plastic shakedown of structures: part I-theory; Journal of Applied Mechanics-ASME 60: 15-19; 1993

177. Polizzotto, C: A study on plastic shakedown of structures: part I-basic properties. Journal of Applied Mechanics-ASME 60: 318-323; 1993

178. Ponter, A.R.S.: An upperbound on the small displacements of elastic, perfectly plastic structures. J. Appl. Mech. 39, 959-963; 1972

179. Powel, M.J.D: Algorithms for nonlinear constraints that use Lagrangian functions; Math. Progr. ; Vol. 14, 224-248; 1978

180. Prager, W.: The general theory of limit design; Procedings of the 8th International Congress on Theoretical and Applied Mechanics; Instanbul, 1952, Vol. 2. Faculty of Science, University of Istanbul, pp 65-72; 1955

181. Prager, W.: Einführung in die Kontinuumsmechanik; Basel; Stuttgart: Birkhäuser Verlag, 1961

182. Qin, Q.H.; He, X.Q.: Variational principles, FE and MPT for analysis of non-linear impact-contact problems; Computer Methods in Appleid Mechanics and Engineering, Vol. 122, pp 205-222; 1995

183. Rackwitz, R.(Ed.):Reliability and Optimization of Structural Systems; 6th Meeting IFIP Working Group 7.5; Springer; ISBN 0412636301; Assisi;Italy; Sep. 1994

184. Ramberger, G. et. al: Zeman Wellstegträger - Technischer Bericht; Institute for Steel Structures, Vienna University of Technologie; Vienna Austria; 2001

185. Ramm, Ekkehard: Geometrisch nichtlineare Elastostatik und Finite Elemente; Universität Stuttgart, Institut für Baustatik; Diss.; Januar 1976

186. Raue, E.; Weitzmann, R.: On dynamic analysis of elasto-plastic structures with methods of nonlinear mathematical programming; 5th International Conference "Modern building materials, structures and techniques", Faculty of Civil Engineering Vilnius Technical University; May 1997

187. Raue, E.: Alternative mathematical modeling in the analysis of reinforced concrete structures. In: The 8the International Conference Modern Building Materials, Structures and Techniques. Vilnius May 19-21 2004. Selected papers. Vilnius Gediminas Technical University Press "Technika": 2004

188. Raue, E.; Weitzmann, R.: Analysis and design of hybrid structures using optimisation strategies, Xth International Conference on Computing in Civil and Building Engineering (ICCCBE); Weimar, Germany, 2004

189. Richter C.: Optimization methods and BASIC programs (in German: Optimierungsverfahren und BASIC Programme); Akademie-Verlag Berlin; 1988

190. Ritz, W.: Über eine neue Methode zur Lösung gewisser Variationsprobleme der mathematischen Physik; Journal für die reine und angewandte Mathematik, Bd. 135; 1909

191. Ruangrassamee, A.; Kawashima, K.: Relative displacement response spectra with pounding effect; Earthquake Engineering and Structural Dynamics, 30, pp. 1511-1538; 2001

192. Ruangrassamee, A.; Kawashima, K.: Control of nonlinear bridge response with pounding effect by variable dampers; Engineering Structures 25 pp. 593-660, 2003

193. Scawthorn, C.; Chen, W.F.,Chen, C.: Earthquake Engineering Handbook; ISBN 0849300681; CRC Press; 2002

194. Schittkowski, K.; Zillober, C.: Sequential convex programming methods; In Stochastic Programming, K. Marti, P. Kall eds., Lecture Notes in Economics and Mathematical Systems, Vol. 423, Springer, 123-141; 1995

195. Schleupen, A.; Maute, K.; Ramm, E.: Adaptive FE-procedures in shape optimization; Struct Multidisc Optim 19, 282-302, 2000

196. M. Schön: Finite-Raum-Zeit-Elemente für die Modellierung der instationären Eulergleichung. Dissertation Universität Stuttgart, 1994

197. Schüler, H.: Zur Analyse und zur Bemessung adaptiver Tragwerke aus Stahlbeton unter dynamischen Einwirkungen; Dissertation at Fakulty of Civil Enginering, Bauhaus-University Weimar; 1997

198. SEAOC: Recommended Lateral Force Requirements and Commentary; Structural Engineers Association of California, Sacramento, California; 1999

199. Sinha, S.C.; Li, G.: Optimal design of base-isolated structures with dynamic absorbers; Journal of Engineering Mechanics, Vol. 120 (2), pp. 221-231; Feb. 1994

200. Somerville, P.; Smith, N.; Punyamurthala, S.; Sun, J.: Development of ground motion time histories for the Phase 2 of the FEMA/SAC Steel Project; SAC Background document, Report No. SAC/BD09/04, Sacramento California; 1997

201. Stander, N.;Craig, K.: On The Robustness of a Simple Domain Reduction Scheme for Simulation-Based Optimization; Eng. Comput.; Vol. 19 (4); pp. 431-50, 2002

202. Takemura, H.; Kawashima K.: Effect of loading hysteresis on ductility capacity of reinforced concrete bridge piers; Journal of Structural Engineering; Vol 43A, pp 849-858;1997

203. Takewaki, I.: Displacement-acceleration control via stiffness-damping collaboration; Earthquake Engineering and Structural Dynamics, 28, pp. 1567-1585; 1999

204. Tanabe, Y.; Kitagawa, Y.: An adaptive selection system of base-isolation devices evaluated by using a soft computing method that considers seismic performance; 13h World Conference on Earthquake Engineering, Paper-No. 1396; Vancouver, Canada, 2004

205. Tin-Loi, F.: Optimum shakedown design under residual displacement constraints; Struct. Multidisc. Optim. 19, 130-139; Springer Verlag; 2000

206. Tresca, M. H.:Sur l′ecoulement des corps solides a de fortes pressions; Comptes Rendus Hebdomadaires des S′eances de l′Academie de Sciences, Vol. 64, pp. 809-812; 1867

207. D.M. Trujillo. An unconditionally stable explicit algorithm for structural dynamics. Int. J. Num. Meth. Eng., 11:1579-1592, 1977.

208. Uniform building code; International Conference of Building Officials, Whittier, CA.; 1994

209. Unjoh, S.; Hoshikuma, J.; Nishida, H.; Shiojima, A.: Research and development on high seismic performance bridge structures; 36th Joint Meeting Panel on Wind and Seismic Effects, US-Japan Cooperative Program in Natural Resources (UJNR), 17-22 May 2004

210. Vanmarke E.H.: SIMQKE: A program for artificial motion generation; Civil Engineering Department, Massachusetts Institute of Technology; 1976

211. Vanderplaats, G.N.: Numerical optimzation techniques for engineering design; 3rd Edition; Vanderplaats Reserach & Development Inc.; 2001

212. Verhulst, F.:Nonlinear Differential Equations and Dynamical Systems; Springer 1990

213. Vitiello E.: Upper bounds to plastic strains in shakedown of structures subjected to cyclic loads; Meccanica 7, 205-213; 1972.

214. Washizu, K.: Variational Methods in Elasticity and Plasticity. Pergamon Press; 1982

215. Watanabe, G.; Kawashima, K.: Numerical simulation of pounding of bridge decks; 13h World Conference on Earthquake Engineering, Paper-No. 884; Vancouver, Canada, 2004

216. Weichert, D.; Maier, G. (Eds.): Inelastic analysis of structures under variable loads - Theory and engineering applications; Kluver Academic Publishers; Solid mechanics and its applications SMIA 83; 2000

217. Weichert, D.; Maier, G. (Eds.): Inelastic behaviour of structures under variable repeated loads. Vienna: Springer; 2001

218. Weitzmann, R.: Design concept for reinforced concrete structures using deformation based limit state analysis (in German: Bemessungskonzept für Stahlbetontragwerke auf der Grundlage deformationsbasierter Grenzzustandsbetrachtungen); PhD Thesis; Bauhaus-University Weimar; 2000

219. Weitzmann, R.; Raue, E.: Alternative analysis and design of r/c structures subjected to seismic loading using optimisation strategies; Twelfth European Conference on Earthquake Engineering ECEE; Elsevier; London; Great Britain; 2002

220. Weitzmann, R.: Limit state design of hybrid structures with meshless methods using mathematical optimisation; International Colloquium for Applications of Information Science and Mathematics in Architecture and Civil Engineering (IKM) 2003, Bauhaus-University Weimar, Germany June 2003

221. Weitzmann, R., Ohsaki, M.; Nakashima, M.:Simplified methods for design of base-isolated structures; 2005 John Wiley & Sons, Ltd. Earthquake Engng Struct. Dyn. 2006; 35:497-515

222. Wikipedia: Optimization (mathematics); http:// en.wikipedia.org/wiki/ Optimization_(mathematics); 19.Feb. 2007

223. Willner, K.: Kontinuums- und Kontaktmechanik; Springer 2003

224. Wolfe, P.: The simplex method for quadratic programming; Econometica, 27(3), 382-398; 1959

225. Wolfe, P.: A duality theorem for nonlinear programming; Quaterly Applied Mathematics; Vol. 19, 239-244; 1961

226. Wolkowicz, H.; Saigal, R.; Vandenberghe L. (editors): Handbook on Semidefinite Programming; Kluwer; 2000

227. Yamamoto, H.; Teramoto, T.; Takayama, M.; Kitamura, H.: Design of Seismic isolated building of 4 seconds natural period; Proceedings of Structural Engineering World Congress 1998; San Francisco, California, USA; 163-6; 1998.

228. Zhong, W.X.; Sun, S.M.: A finite element method for elasto-plastic structures and contact problems by parametric quadratic programming; International Journal for Numerical Methods in Engineering, Vol. 26, pp 2723-2738; 1988

229. Zhong, W.X.; Sun, S.M.: A parametric quadratic programming approach to elastic contact problems with friction; Computers and Structures, Vol. 32, pp 37-43; 1989

230. Zienkiewicz, O. C.;Taylor, R. L.:Finite Element Method; Vol. 1-3; McGraw-Hill Publ., New York, ISBN 0-07-084175-6, 1991